

AD-A074 469

AIR FORCE GEOPHYSICS LAB HANSCOM AFB MA
PROCEEDINGS OF THE AFGL SCIENTIFIC BALLOON SYMPOSIUM (10TH) HEL--ETC(U)
MAR 79 C L RICE
AFGL-TR-79-0053

F/G 1/3

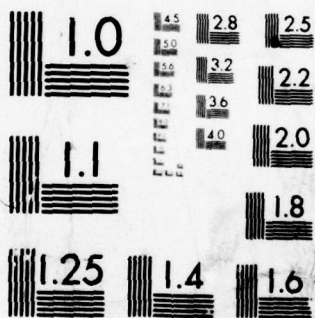
UNCLASSIFIED

NL

1 OF 6

AD
A074469





MICROCOPY RESOLUTION TEST CHART
NATIONAL BUREAU OF STANDARDS-1963-A

AD A 074469

053, AFGL-SK-
217

AFGL-SK-

12

LEVEL II



of the

(1st)

ings, Tenth AFGL
ic Balloon Symposium
st to 23 August 1978

held
Portsmouth, NH.

RICE Editor

Special rept.

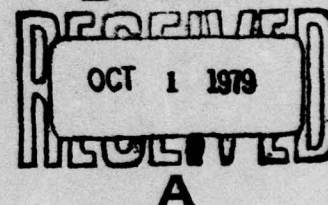
11

1 Mar 1979

12

530 p.

DDC



167659

1711

DDC FILE COPY

Approved for public release; distribution unlimited.

AEROSPACE INSTRUMENTATION DIVISION PROJECT 7659
AIR FORCE GEOPHYSICS LABORATORY
HANSCOM AFB, MASSACHUSETTS 01731

AIR FORCE SYSTEMS COMMAND, USAF



409578

79 10 01 027

Qualified requestors may obtain additional copies from the Defense Documentation Center. All others should apply to the National Technical Information Service.

Unclassified

SECURITY CLASSIFICATION OF THIS PAGE (When Data Entered)

REPORT DOCUMENTATION PAGE		READ INSTRUCTIONS BEFORE COMPLETING FORM
1. REPORT NUMBER AFGL-TR-79-0053	2. GOVT ACCESSION NO.	3. RECIPIENT'S CATALOG NUMBER
4. TITLE (and Subtitle) PROCEEDINGS, TENTH AFGL SCIENTIFIC BALLOON SYMPOSIUM, 21 AUGUST to 23 AUGUST 1978		5. TYPE OF REPORT & PERIOD COVERED Scientific. Biennial.
7. AUTHOR(s) Catherine L. Rice, Editor		6. PERFORMING ORG. REPORT NUMBER Special Reports No. 217 ✓
9. PERFORMING ORGANIZATION NAME AND ADDRESS Air Force Geophysics Laboratory (LC) ✓ Hanscom AFB Massachusetts 01731		8. CONTRACT OR GRANT NUMBER(s)
11. CONTROLLING OFFICE NAME AND ADDRESS Air Force Geophysics Laboratory (LC) Hanscom AFB Massachusetts 01731		10. PROGRAM ELEMENT, PROJECT, TASK AREA & WORK UNIT NUMBERS 62101F 76591100
14. MONITORING AGENCY NAME & ADDRESS (if different from Controlling Office)		12. REPORT DATE 1 March 1979
		13. NUMBER OF PAGES 543
		15. SECURITY CLASS. (of this report) Unclassified
		15a. DECLASSIFICATION/DOWNGRADING SCHEDULE
16. DISTRIBUTION STATEMENT (of this Report) Approved for public release; distribution unlimited.		
17. DISTRIBUTION STATEMENT (of the abstract entered in Block 20, if different from Report)		
18. SUPPLEMENTARY NOTES Conference held at Wentworth-By-The-Sea, Portsmouth, New Hampshire		
19. KEY WORDS (Continue on reverse side if necessary and identify by block number)		
Aerodynamics	Balloons	Conductivity
Aerosols	Balloon-design	Cryogenics
Air-launched balloons	Balloon-borne experiments	Materials
Airships	Cable	Plastics
Atmospheric constituents	Catenary	Stratosphere (Cont)
20. ABSTRACT (Continue on reverse side if necessary and identify by block number) → This publication contains the Keynote Address and twenty-nine papers presented at the Tenth AFGL Scientific Balloon Symposium, 21-23 August 1978, at Portsmouth, NH. The five sessions were entitled: Balloon Technology - Progress and Problems; Manned Flights; Stratospheric Measurements; Airship Design Concepts; and Methods and Models.		

DD FORM 1 JAN 73 1473 EDITION OF 1 NOV 65 IS OBSOLETE

Unclassified

SECURITY CLASSIFICATION OF THIS PAGE (When Data Entered)

Unclassified

SECURITY CLASSIFICATION OF THIS PAGE(When Data Entered)

Block 19 (Cont)

Stratospheric measurements
Test facilities

Superpressure balloons
Tethered balloons

Unclassified

SECURITY CLASSIFICATION OF THIS PAGE(When Data Entered)

Accession For	
NTIS GFA&I	<input checked="checked" type="checkbox"/>
DDC TAB	<input type="checkbox"/>
Unannounced	<input type="checkbox"/>
Justification _____	
By _____	
Distribution/ _____	
Availability Codes	
Dist.	Avail and/or special
A	

Summary

The Tenth AFGL* Scientific Balloon Symposium was held at Portsmouth, NH in August 1978. This document contains the Keynote Address and twenty-nine papers presented during the five sessions: Balloon Technology - Progress and Problems; Stratospheric Measurements; Manned Flights; Airship Design; and Methods and Models.

The session on balloon technology included superpressure balloons, heavy-lift balloon performance, cryogenic inflation, the Sky Anchor, computerized data-acquisition, a balloon-borne LORAN antenna system, current balloon development in France, balloon system design theory and analysis, and a tethered-balloon winch.

Five major, balloon-borne Stratospheric Measurements programs, recent flight histories for the manned, U.S. ATMOSAT and for several British, hot-air balloon expeditions, records of U.S. Navy rigid airships and concepts for advanced airship designs were presented.

Methods for predicting platform attitude, estimating subsonic aerodynamic characteristics of finned, axisymmetric bodies, computing pitch angle and other static data for an aerostat, controlling altitude using a compound aerostat, and a model for an elastic catenary were described.

* Air Force Geophysics Laboratory, formerly AFCRL, Air Force Cambridge Research Laboratories.

Preface

The Editor is sincerely grateful for substantial help, generously contributed by many busy colleagues. The Division Director, Mr. Thomas W. Kelly, and the other members of the balloon groups in the Aerospace Instrumentation Division, AFGL, gave invaluable assistance and encouragement in planning the program.

We are all very much indebted to the distinguished scientists who participated in the program: to Dr. Hans Mark, Undersecretary of the Air Force, who gave the Keynote Address; to Colonel Chester G. R. Czepyha, Vice Commander, AFGL, the Official Welcoming Remarks; and to the Session Chairmen: Professor Alvin H. Howell, Tufts University; Mr. James F. Dwyer, Air Force Geophysics Laboratory; Mr. Thomas J. Gross, U. S. Department of Energy; Mr. Norman J. Mayer, NASA Headquarters; and Professor James DeLaurier, University of Toronto.

Special thanks are due to Mrs. Charlotte Stankiewicz for so efficiently handling announcement and registration matters, to Chief Master Sergeant Harold W. Greenlee and Miss Margo Cross for help with arrangements during the meetings, and to Airman First Class Ivan Thomas for working long hours in operating the audio-visual equipment with exceptional skill and courtesy.

Contents

Keynote Speech - Balloon Symposium	11
Dr. Hans M. Mark, Undersecretary of the Air Force	
SESSION I. BALLOON TECHNOLOGY - PROGRESS AND PROBLEMS - PART 1.	17
Chairman: Dr. Alvin H. Howell, Tufts University	
Development of a Balloon-Borne LORAN Antenna	19
A.O. Korn, AFGL	
Up to Date CNES Balloon Studies	39
M. Rougeron, CNES, Toulouse, France	
A Review of Heavy Lift Balloon Failures	57
W.F. Cuddihy, A.D. McHatton, NASA-Langley Research Center	
R.L. Golden, New Mexico State University	
Development of the Sky Anchor Balloon System	81
I.S. Smith, Jr., National Scientific Balloon Facility, NCAR	
Large Superpressure Balloons - Here and Now State of the Art	103
J. Lehmann, National Scientific Balloon Facility, NCAR	
The Air Launched Balloon System (ALBS) Flight Test Program	105
A.S. Carten, Jr., AFGL	
A System for Inflating an Air Launched Balloon	149
C.F. Sindt, NBS	
Facilities for Real-Time Flight Support of Scientific Balloon Experiments	161
J.C. Erickson, New Mexico State University	
SESSION I. BALLOON TECHNOLOGY - PROGRESS AND PROBLEMS - PART 2.	163
Chairman: James F. Dwyer, AFGL	
Required, A New Zero Pressure Free Balloon Shape	165
J.F. Dwyer, AFGL	
Analysis of Balloons in Off-Design Configurations	171
J.L. Rand, Texas A&M University	

Contents

On Determining Poisson's Ratio for Thin Plastic Films K. H. Hazlewood, Winzen Research, Inc.	185
A New Thermal Analysis Model for High Altitude Balloons L. A. Carlson, Texas A&M University	187
SESSION II. MANNED FLIGHTS	207
An Update on the Atmosat Project T. F. Heinsheimer and P. C. Neushul, Aerospace Corporation	209
Sport Ballooning - A Scientific Approach J. R. P. Nott, The Hot-Air Balloon Company Ltd.	241
SESSION III. STRATOSPHERIC MEASUREMENTS	255
Chairman: Thomas J. Gross, U.S. Govt., Dept. of Energy	
Stratospheric, Trace Gas Studies Using a Balloon-Borne, Cryogenic, Whole Air Sampler C. C. Gallagher, R. V. Pieri, C. A. Forsberg, G. A. Faucher, AFGL	257
Cassette Sampler for Stratospheric Aerosols and Vapors B. W. Gandrud, A. L. Lazrus, E. V. Lambdin, P. H. Johnson, and L. W. Beaman, NCAR R. H. Cordella, NOAA	267
Stratospheric Electrical Conductivity Measurements by Balloon-Borne Blunt Probes J. D. Mitchell, University of Texas at El Paso, L. C. Hale and C. L. Croskey, Pennsylvania State University	281
Stratospheric Composition Balloon, Aircraft, and Rocket-Borne Experiments, 28-30 September 1977 (STRATCOM VIII). (Systems, Instruments, Trajectories, Supporting Measurements) H. N. Ballard, U. S. Atmospheric Sciences Laboratory, M. Izquierdo, University of Texas at El Paso, A. O. Korn, AFGL, D. Murcray, University of Denver, W. Page, NASA Ames Research Center	293
The Measurement of Optical Scattering From Atmospheric Aerosols As A Function of Altitude F. N. Gibson, AFGL, N. C. Poirier, Northeastern University	315
Automatic Low Tension Inhaul Winch System for Slack Line Abatement W. C. Lane, Otis Engineering Corporation	333
SESSION IV. AIRSHIP DESIGN CONCEPTS	343
Chairman: Norman J. Mayer, NASA Hqs.	
Records of Maintenance and Repair of Rigid Airships D. E. Woodward and H. Walker, Jr., Association of Balloon & Airship Constructors	345
NASA Studies of a High Altitude Powered Platform (HAPP) N. J. Mayer, NASA and H. C. Needleman, NASA Wallops Flight Center	379
A Predictive Steering Control System for Dirigibles R. O. Hookway, Martin Marietta Aerospace Corp.	401

Contents

Applications for a High Altitude Research Dirigible (HARD) K. R. Stehling, NOAA	427
SESSION V. METHODS AND MODELS	431
Chairman: Dr. James DeLaurier, University of Toronto	
Improved Method for Predicting Attitude of Balloon Gondolas N. J. Nigro, P. Nimityongskul, Marquette University, D. E. Hinton, NASA Langley Research Center	433
A Semi-Empirical Method for Estimating the Subsonic Aerodynamic Characteristics of Finned Axisymmetric Bodies J. DeLaurier and S. Podleski, University of Toronto	461
Computation of Tethered Aerostat Pitch Angle and Vent Ceiling From Standard Curves S. P. Jones, TCOM Corporation	489
Mathematical Model of an Elastic Tether With Catenary for Static and Stability Analysis N. A. Dresner and S. P. Jones, TCOM Corporation	511
A Compound Aerostat of Controllable Altitude R. M. Dunlap, U.S. Naval Underwater Systems Center	525
LIST OF REGISTRANTS	539

KEYNOTE SPEECH - BALLOON SYMPOSIUM

Hans M. Mark
Dept. of the Air Force
Washington, DC 20330

It is a great pleasure for me to be here and to have the opportunity to give the keynote address for this important conference. It is a rare occasion. When I am asked to make a speech now, I generally am talking to groups with whom I have no connection and whose activities are outside my own experience. This is perhaps a polite way of saying that many times now I only have a vague idea of what I am talking about. All of which seems to be the fate of bureaucrats eventually, so I guess I am living proof that the "Peter Principle" really describes our condition!

This occasion is different. I do know something about balloons and the art of ballooning. I have flown many myself and thus I hope you will forgive me if I begin with some war stories. I began flying balloons almost 20 years ago, in 1960. I was at the time interested in atmospheric x-rays and it seemed to us that balloons would be the best way to get sensitive x-ray detectors into the upper reaches of the atmosphere. I remember the first flight we made was from a little airfield north of Minneapolis, Minnesota sometime in the middle of the winter. It was cold but there were no ground winds early in the morning so from the point of view of ballooning it was an excellent place. We did get off some beautiful flights but I don't think I have ever been so cold again. We then moved south, first in the New Mexico mountains near the little town of Socorro. We had a launch site on top of a fairly high mountain and we trucked our helium and our equipment to the launch site before the series of flights started. Now you know that region of the world is famous for thunder storms, and it is in one of those thunder storms that I first saw a balloon fly horizontally. We launched the balloons by hand as they were quite small - about 100,000 cu. ft. I remember one day one of them disappeared into a thunderhead. We lost the telemetry and therefore we went outside of our communications shack and looked up to try to find it. A minute later we saw it shooting out of the cloud almost horizontal, and

moving at quite a clip. This really was a sight to behold. The balloon and its payload looked for all the world like a Squid escaping from the mouth of a large shark.

Needless to say, I also wound up flying from the "Holy Land" of all ballooning, Palestine, Texas. You all know, of course, that in Texas, Palestine is pronounced "Palesteen." I found that out one day in Tyler, Texas when I was driving to Palestine with a pickup truck and a trailer with a load of equipment. We stopped and asked a gas station attendant where Palestine was. He said: "Palestine is in the mid-East, but Palesteen is about 40 miles down the road and here's how you get there." So, I am now one of the initiates. Looking back, I must say that I always very much enjoyed my trips to East Texas for balloon flying. It was somehow an important thing to do.

Finally we had some interesting experiences at an airfield near Chico, California where the Air Force once had a small ballooning station. I remember once we lost a very large balloon, I think it was perhaps a three million cubic footer, and this was the only time I have ever seen one balloon grow a second one. It was a very hot day, well over a 100⁰F. The day was very dry and the sun was brilliant. Something happened to the plastic on top of the balloon and it bulged out in the most obscene way. After a few seconds, the top blew out and the balloon sank gracefully back to earth. Fortunately the payload was only a few feet above the ground at the time so that it was undamaged and the next day we could fly again.

We finally did publish some results of our work and those of you who are familiar with the more obscure and esoteric literature will remember some papers in 1964 and 1965 dealing with the subject of soft x-rays in the upper atmosphere. These are all stories that describe things which were good fun to us in those days and we thoroughly enjoyed ourselves. Ballooning has the advantage that it is much more casual and relaxed than the sterner disciplines of space flight. Perhaps so, but even at that, balloons have had important scientific uses. At least two Nobel prizes have been awarded in part for work done with balloons. One was to Victor Hess in 1936 who discovered cosmic rays in 1913 by flying a small electrometer on very primitive balloons to altitudes in excess of 15,000 feet.

The other was awarded in 1948 to Cecil Frank Powell, who discovered mesons by flying stacks of sensitive photographic emulsions on balloons. He was the first to determine the mass of the pi and mu mesons and thus was the first man to confirm the brilliant insight of Hideki Yukawa that nuclear forces imply the existence of particles having intermediate mass between electrons and nucleons.

I must say that I am very impressed by the papers that will be presented at this meeting. Much progress has obviously been made since I gave up the business in 1966. From a scientist's viewpoint, I think the notions that controllable, long duration, high altitude platforms can be developed using balloons are the most interesting ones that will be discussed. There is no doubt that many important scientific experiments can be conducted with such balloons and I believe this particular technology should be strongly encouraged. I am also interested in experimental programs designed to measure the properties of the upper atmosphere. I doubt, for example, whether the flap over the ozone layer a few years ago would have occurred if we had at that time had cheap and easy ways of making accurate measurements of the minor constituents of the upper atmosphere. In the future, measurements of minor constituents of the upper atmosphere will become more important. We will be doing things that will have, or may have, macroscopic effects on our environment and we need to know with much greater precision what is happening than is now possible. Balloons probably are among the best platforms for this kind of work. I am also still optimistic about doing more astronomy in astrophysics using balloons, although I know from personal experience how difficult this particular effort can be. I would eventually like to see large, super-pressure balloons orbit the earth in the upper atmosphere just the way satellites do above the atmosphere. Much can be done with these.

Let me conclude by laying a challenge before this group. I believe that perhaps the most important and interesting scientific applications of balloons will be made by flying balloons in the atmospheres of Venus and Mars. As you know, I had something to do with the Pioneer Venus flights that have recently been launched. (The spacecraft carrying the atmospheric entry probes to Venus was launched just two weeks ago.) Venus balloons

could be deployed from an entering spacecraft and this may be the best way to obtain accurate information about the behavior of the strange atmosphere of that planet. The atmosphere of Venus is dense, so that it will be relatively easy to get lift. On the other hand, we have some evidence that there may be some very corrosive materials in the atmosphere as well. Designing a balloon to fly in that environment will be very challenging. I would like to see a balloon in the atmosphere of Venus that could stay there for some months and that could give us good information on the circulation patterns of the Venus atmosphere. If at all possible, one might think of putting an imaging radar on the balloon as well. We now have plans for an imaging radar satellite and better imagery could be obtained from a balloon. The technical problems that would have to be solved are formidable but I do believe that the enterprise of flying balloons on Venus is worth serious consideration. I hope very much that an experiment of this kind will eventually be conducted.

In the case of Mars, the balloon would have to be quite different since the atmosphere is very tenuous. The surface pressure on Mars is approximately 7mm so that one can at least think of flying large balloons. If I remember correctly, large balloons can be flown at pressure altitudes to 2-3mm so that it should be possible to do something such as this. In the case of Mars, the taking of pictures of the surface is most important. Good pictures have been obtained from spacecraft in orbit around Mars but much better ones could be obtained from platforms that are closer to the surface of the planet. The smaller gravity on Mars would help, but the engineering problems connected with deploying a balloon from a landed spacecraft would be formidable indeed. Even here, however, I believe it is possible to think about doing something valuable with such a balloon. I know there have been proposals to fly a small drone aircraft in the Martian atmosphere, and it should be a challenge to us to see whether one can do something with balloons as well. Perhaps the most important consequence of trying to fly balloons on Venus and Mars will be to stretch our imaginations and thus to advance the technology and engineering of ballooning.

Lest I get too serious, however, I note that the old balloonist devil is still with us. One of the papers here carries the title, would you

believe, "A Review of Heavy Lift Balloon Failures." Now in what other scientific conference could you find a paper describing failures? Only among us old balloonists would such a paper be possible. Good luck, best wishes, and I look forward to listening to the papers today.

Session I
BALLOON TECHNOLOGY — PROGRESS AND PROBLEMS
Part 1

Chairman, Dr. Alvin H. Howell
Tufts University

Contents

1. Summary
2. Background
3. System Description
4. Antenna Tethers
5. Antenna Design
6. Antenna Hardware
7. Balloon Hardware
8. Antenna Tests
9. Conclusion

Proceedings, Tenth AFGL Scientific Balloon Symposium, 21 August to 23 August 1978

Development of a Balloon - Borne LORAN Antenna

Arthur O. Korn
Aerospace Instrumentation Division
Air Force Geophysics Laboratory

Abstract

The Electronic Systems Division Tactical LORAN System Program Office (SPO) is developing a mobile LORAN navigation ground installation. A requirement exists for an emergency replacement for a 400 foot LORAN tower should it be destroyed by severe weather or enemy action. This paper describes the design, development and test of a balloon-borne antenna as a replacement for a downed tower. The system uses a 45,000 cubic foot, aerodynamically shaped balloon, tethered at 1,000 feet to lift a 500-foot antenna and tri-tether system. The tri-tethers also serve as top loaders for the antenna. The tethered balloon antenna system was erected and successfully tested in June 1978 at the Anniston, Alabama LORAN Site. Further testing is planned in FY79.

1. SUMMARY

In Nov 1975, the ESD Tactical LORAN SPO requested that the Aerospace Instrumentation Division of AFGL investigate the feasibility of using a tethered balloon to support a LORAN (Long Range Navigation) antenna. Their desire was to have a backup antenna system for a 400-foot tower in case the tower should be destroyed by sabotage, hostile action, or violent weather. A pictorial of the system is shown in Figure 1. A LORAN station or "chain" is made up of 3 of these towers. One of these chains under development is located in the southeastern United States with towers located in Anniston, Alabama; Alexandria, LA; and Stark, FL. When this portable LORAN navigation system is developed, it is planned to have them available for world wide deployment. Because of this, the balloon-borne backup antenna system must be air transportable and rapidly deployed. Also, since the tower sites are maintained and operated by Air Force Communication Service personnel, the balloon antenna must be kept uncomplicated so that people not experienced with balloons could erect the system in an emergency situation.

With these ground rules in mind, the Aerospace Instrumentation Division initiated a program to design and test such a system. This paper describes the development and test of the evolved balloon antenna system.

2. BACKGROUND

The Division has been flying tethered balloons for 10 years from remote and fixed locations. Depending upon project requirements, either single or multiple tether lines are used. Because the SPO indicated that it was desirable to have the vertical element of the antenna remain as stable as possible, it

was decided to use a tri-tether system. Use of the tri-tether configuration had the added advantage that it allowed the tethers to serve a second function, that of the supports for the antenna "top loaders". An early antenna design had these top loaders suspended along the tether lines, but this was found to be susceptible to corona discharge. The final top loader configuration used a wire overbraid integral with the Kevlar tether, as will be described later.

Stability of the vertical element would be maintained during windy conditions as long as the face angles of the pyramid formed by the tri-tethers remain intact. If a face angle is allowed to collapse, (caused by wind on the balloon), the antenna moves downward and could strike the ground -- a very dangerous situation if the antenna is under power.

In order to maximize antenna stability, the optimum distance that the balloon should be above the tri-tether confluence point had to be determined. Previous work by Division scientists (Ref 1 & 2) attacked this problem but with different balloon shapes and tether configurations. It was therefore necessary to conduct further testing using the actual balloon and tether line configuration to be used on the Tactical LORAN antenna. This work was accomplished at Det 1, Holloman AFB during several field experiments. The conclusion was that a 500-foot long balloon tether above the antenna confluence point was more stable than the 100-foot tether. The 1000-foot tether was only slightly better than 500-foot length so the decision was made to use the 500 foot tether. This tether would be non-conductive so as not to influence the electrical characteristics of the antenna.

3. SYSTEM DESCRIPTION

BALLOON

The tethered balloon antenna system as designed uses a 45,000 ft³ British BJ balloon. It is admittedly of World War II vintage - very heavy and ram air-pressurized, but it is in the inventory and considered adequate for this feasibility demonstration. A lighter weight, blower-pressurized 45,000 ft³ balloon is under development and would probably be used on an operational antenna system. The balloon characteristics are as follows:

Volume	45,000 ft ³
Length	90 feet
Diameter	33.5 feet
Type	BJ
Manufacturer	Lea Bridge, Inc.
Material	Rubberized cotton
Weight	930 lbs

4. ANTENNA/TETHERS

The balloon-borne antenna has an aluminum center element and 3 top loaders. The center element is made up of size #1/0, 19-strand wire coated with 2 heavy coats of corona dope and covered with shrink tubing. The coatings and covering were added to prevent corona discharge. The 3 top loaders were fabricated by overbraiding 2 layers of 6-mil diameter aluminum wire on the 3 balloon tethers. This overbraiding was applied over 700 feet of the tether's 788-foot length. (See Fig 2). The tri-tethers are made of Kevlar and have a break strength of 12,000 lb and weigh 35 lb/1000 ft. The 500-foot balloon tether is also Kevlar with a break strength of 11,000 lb.

The antenna ground radial system is comprised of 6 ea. 300-foot long, 3/16 in. diameter, solid aluminum wires. These radials are clamped together at one end at ground zero, using a special adapter as shown in Fig 3. The adapter ends are grounded to a 12-foot, copper ground rod, and the outer ends are grounded to a 2-foot copper ground rod.

5. ANTENNA DESIGN

The LORAN C/D TRN 39 transmitter to which the balloon-borne antenna was to be connected operates at 78,000 volts and at a frequency of 1000 KHz. Therefore, a careful analysis had to be made before the antenna was built to insure that it would be corona free. (Ref 3). Not only would substantial corona result in a high loss and therefore an ineffective antenna but the corona could threaten the safety of the system by degrading or burning the Kevlar cables to which the top loaders are attached and which hold the balloon in position.

The LORAN system frequency of 100 KHz is 1667 times higher than the frequency where corona loss calculations are usually made. A situation that would produce a single watt of loss on a power system, an amount that would be trivial in that application, produces 1.67 kW on the LORAN antenna. Since the power from the Loran transmitter is limited for supplying both the useful output and the losses, the antenna should have large diameter conductors terminated in smooth surfaces of considerable size, but this approach can't be completely managed with the balloon-supported antenna because of weight and flexibility considerations.

A basic requirement in the design was to establish a way to correctly predict the corona loss on an uninsulated balloon-supported antenna, and for this it was necessary to develop a procedure for properly handling the peculiar antenna configuration. The goal is to find the charge distribution throughout the system when the voltage everywhere has a specified value. Then the corona loss can be calculated because it depends on voltage gradient, which in turn depends on charge density. But finding the charge distribution is essentially a cut-and-try process for a structure like the antenna. It involves first assuming a uniform distribution, then calculating the potential at all positions due to the assumed distribution, and from this computing a new distribution to be used in the next calculation. It turns out that ten or twenty iterations give the correct charge distributions with good accuracy.

After the corona study was completed the computer program was further modified to calculate current distribution throughout the system, and ohmic losses in all segments as well as total ohmic loss.

The LORAN tower arrangement was also analyzed to find how the voltage gradients on the balloon-supported antenna compared with those on a system that has been operating for more than a year. Output from this comparison indicates that corona problems on the balloon-supported top loaders are similar to those on the top loaders now being used. The tower, however, is far superior to the vertical member of the balloon-supported substitute because of its large diameter. Ohmic losses for the two systems were also compared. Again the tower structure was shown to be superior because of the large mass of metal in the tower.

6. ANTENNA HARDWARE

In addition to the theoretical calculations of antenna performance, practical antenna hardware that would be compatible with a balloon operation had to be designed and fabricated. All elements of the antenna carrying high voltage should be as large in diameter as practical, and all end points and corners should be rounded and smooth. A tetrahedron structure was chosen for the apex of the antenna. (See Fig 4). It is physically large enough to prevent twisting of the top loaders/tether cables during reel up and provides a good junction structure for all of the cables. It also carries full antenna current and is the connector between the vertical antenna element and the three top loaders. Special spring-loaded cable ends were devised that would insure good electrical contact with the tetrahedron but still allow for flexibility of the connecting joint.

Six-inch diameter hollow spheres were designed that could be clamped at the bottom of the top loaders in order to prevent corona at the otherwise abrupt high voltage end point. These spheres had to be removable so that the cables could be stored on spools when not deployed.

The lower end of the vertical element is the antenna feed point. It is fed with a flexible wire so as to allow some vertical movement of the element in a windy situation. The vertical element cannot be allowed to twist, however, since the feed wire would be wrapped around the element. To prevent this twisting, it was necessary to provide at the base of the vertical element a T-bar structure that could be tied to tensioning devices that keep a constant tension on the element and also prevent twisting. To protect the high voltage termination from corona buildup, 6-inch diameter spheres were added to the ends of the cross of the tee. This configuration is shown in Fig 5.

Another concern that had to be dealt with was lightning. Balloon antenna testing was to take place in the southeastern United States during the summer where the afternoon thunderstorm can be nearly a daily occurrence. If the balloon or balloon-borne antenna were to be struck by lightning, the resulting effect on the LORAN transmitter could be catastrophic. It was therefore necessary to build a ball spark gap protection device into the antenna power feed system as shown in Fig 6. This spark gap is adjustable as are all of the other feed elements. The supporting insulator has a rating of 80,000 volts. The longer horizontal arm shown in Figure 6 is connected to the antenna matching unit to supply power to the balloon-borne antenna.

7. BALLOON HARDWARE

Normally, on tethered balloon flights a UHF instrumentation package is flown to control operation of valves and experiments and to telemeter data. (It was realized that such a control package could not be flown on this balloon antenna configuration because the sensitive receiver would almost certainly be jammed by the strong radiation and inductive fields from the antenna. Accidental balloon-valve operation and tether-cable release might also be expected because diodes in the circuitry could rectify the strong signals that are picked up and cause relay closures.) In addition to the command receiver, the safety package includes a differential pressure switch to automatically open the balloon valves if the internal pressure exceeds a preset level, and to close them again when the overpressure was relieved. It was decided that this overpressure feature was still required

along with a feature to latch the valves open in case of balloon break-away. What was finally designed to provide these features was a "Smart" valve as shown in Fig 7. (cover removed). This is a modified, conventional EV-13 valve equipped with its own battery power source. An integral, aneroid-operated switch locks the valve open if the balloon breaks away and exceeds a preset altitude, and a differential pressure switch senses internal balloon pressure and momentarily opens the valve until the overpressure is relieved. Building the instrumentation into the valves eliminates the cumbersome safety package altogether, and thereby simplifies the rigging by removing both the long electrical cables and the pressure-sensing tube that tie the safety package to the valves and balloon. Removing the long wires also eliminates the possibility of induced voltage in the wires from the strong electromagnetic fields from the antenna. Design of the smart valve is such that either the aneroid-operated or the differential switch can be easily removed for checking or setting in the laboratory. Test buttons are provided that allow for a simple checkout prior to flight. Button operation simulates the aneroid or differential pressure switch and the circuitry is so arranged that the test fails if either of these items is unplugged. The Smart valve is also equipped with a lanyard-operated switch, Fig 8 (lower right), that is activated from the ground for balloon deflation.

Another item that was redesigned mainly for convenience and time saving was the balloon confluence hardware. This hardware is shown in Fig 9. The hardware on the left is "before", and "after" is on the right. In the original system, many shackles were used to collect the balloon flying lines so that a single point of attachment was formed. These shackles were all

wrench-tightened and safetied with cord, which consumed considerable time and resulted in an aesthetically poor system. The new system uses the bail and yoke from a Reliable Electric potting head. This type of hardware is commonly used as cable ends for guying telephone poles. After unscrewing the securing eye nut, the bale is removed from the yoke by applying hand compressive force, springing the bale inward and releasing its ends from the keepers. The improved hardware can be rigged in less than a minute, while the shackle system required twenty minutes.

8. ANTENNA TESTS

In March 1977, the prototype tethered antenna system was deployed at Holloman AFB, New Mexico for measurement of the antenna electrical properties and test of the mechanical integrity of the antenna system parts. Electrical parameters measured included input impedance, radiation resistance, and effective antenna height. Results of these tests are reported in reference 4.

On 20 and 21 June 1978, the balloon antenna system was fully deployed at the Master TRN-39, LORAN C/D ground transmitter site, located at Fort McClellan, Anniston, Alabama. (Ref 5). The objectives of the test were:

- A. To demonstrate the deployment of the Balloon Supported Antenna and its mechanical compatibility with the AN/TRN-39.
- B. To electrically match the Balloon Supported Antenna to the AN/TRN-39 LORAN Transmitter.
- C. To measure the signal characteristics of the LORAN signal radiated by the AN/TRN-39 using the Balloon Supported Antenna.
- D. To determine time lines for Balloon Antenna erection, transmitter set up and tuning.

The balloon antenna site was located in a field across the road from the tower facility. The LORAN tower is shown in Fig 10. The field had

to be graded and filled and have anchor points installed for balloon inflation and tethering. The prepared site is shown in Fig 11. Launch preparations began at midnight on 30 June. The balloon is shown being inflated in Fig. 12. The fully inflated balloon is shown in Fig 13. The antenna was then erected and was ready for test. The lower 10 feet of the 500-foot antenna is shown in Fig. 14. From beginning to end, the erection time had been 6 hours. It is felt due to the learning process that the antenna could now be erected in four hours. After the system was erected, the antenna impedance measurement was made. Five measurements were made and the following average capacitance and inductance values established:

$$CA = 4085 \text{ PF}$$

$$LA = 310.4 \text{ uH}$$

Knowing the antenna impedance value, the load coil inductance for the antenna matching unit (AMU) was calculated. The proper coil was selected on the AMU and the antenna was fine tuned. The balloon antenna was then powered with the tower transmitter and current and signal strength measurements made. These measurements have been analyzed and preliminary results indicate a power output of 10 kilowatts that was monitored and locked in on by the evaluation station at Eglin AFB, Florida. More detail as to results can be found in Ref 6 & 7. Sixteen hours of measurements and testing were completed on the first day. On the following day the system was recovered and packaged in four hours. During the time from launch to recovery, the weather was good with winds never exceeding 10 knots.

9. CONCLUSION

A relatively simple, quickly deployable balloon-borne antenna system has been built and tested. The system is capable of replacing a damaged 400-foot LORAN tower and keeping an otherwise down "chain" in operation. A special valve was designed and built to operate in the hostile antenna radiation environment. Special rigging was devised to keep the erection operation as simple as possible. The tethered balloon antenna was tested at the LORAN site in Anniston, Alabama in June 1978 and signal measurements made. Preliminary results indicate that output power was adequate, although changes in the system could be made to improve performance. Funds have been requested to continue testing of the system.

REFERENCES

1. Leclaire, R.C., Rice, C.B., "The Local Motions of a Payload Supported by a Tri-tethered Natural Shape Balloon", AFCRL-TR-73-0748, 12 Dec 1973.
2. Jackson, E.D., Rice, C.B., "Motions of a Payload on a Tethered, Aerodynamic Shape Balloon Using Various Cable Lengths" AFCRL-TR-75-0148 17 March 1975.
3. Howell, A.H., "Quarterly Status Reports," Contract F19628-77-C-0047, Numbers 1-4, 1 Nov 76-31 Oct 77.
4. Heckscher, J.L., Whidden, R.W., "Loran-D Prototype Tethered Antenna Impedance and Radiation Measurements," RADC-TR-77-280, August 1977.
5. Rustenburg, W., "Balloon Supported Antenna Test Procedure," June 1978.
6. Rustenburg, W., "Balloon Supported Antenna Test", July 1978.
7. Applied Physics Laboratory, Johns Hopkins University, "Spectrum Analyzer Photographs from Single AN/TRN-39 Transmitter Test", July 1978.



Figure 1. Pictorial of Balloon-Borne Antenna System

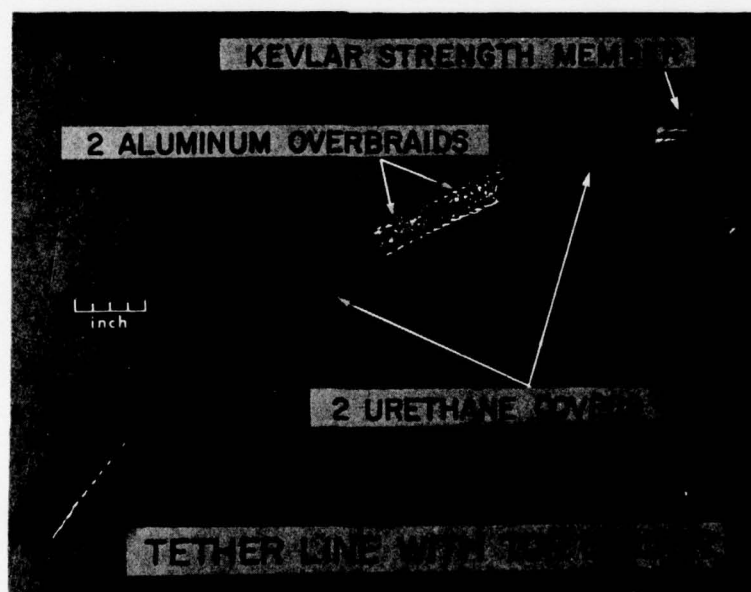


Figure 2. Kevlar Tri-Tether Line Construction



Figure 3. Ground Radial Clamp



Figure 4. Antenna Apex Structure

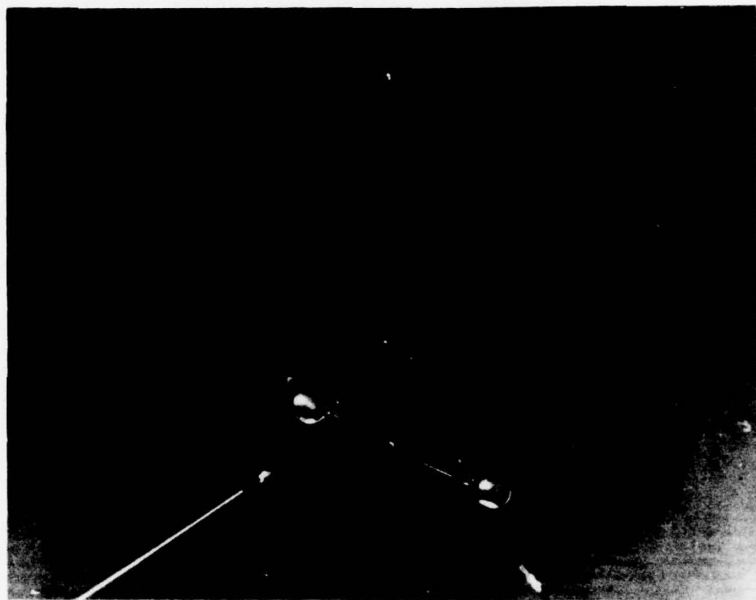


Figure 5. Center Element Lower Structure

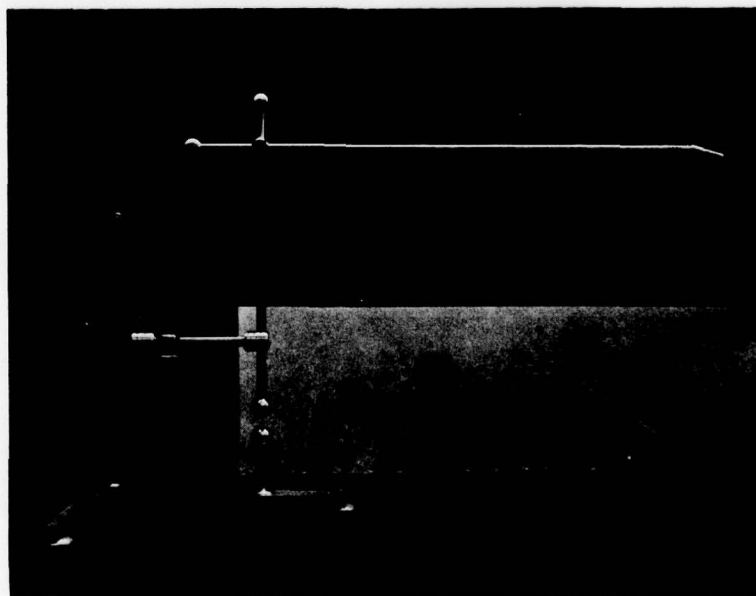


Figure 6. Ball Spark Gap Lightning Protection Device

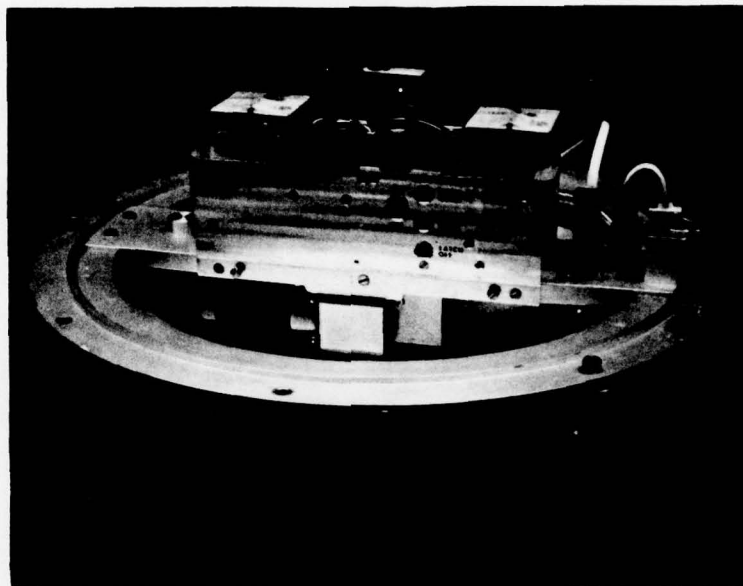


Figure 7. Smart Valve

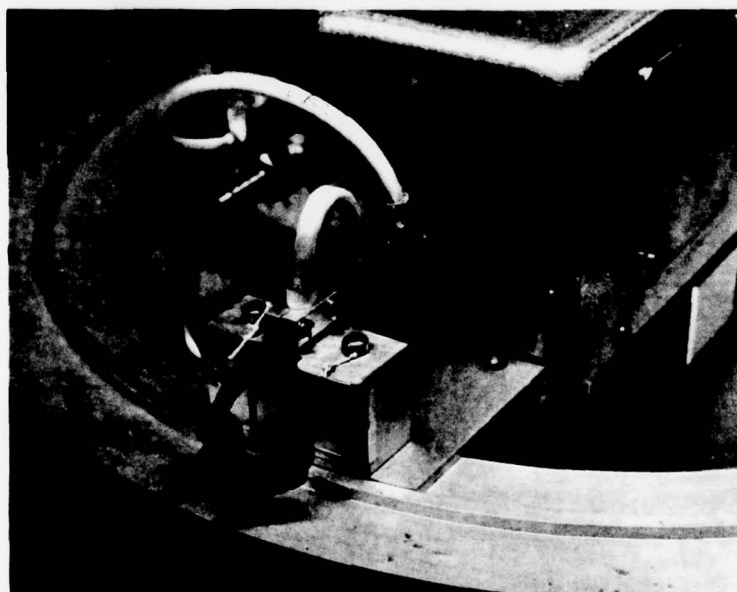


Figure 8. Lanyard Balloon Deflation Switch

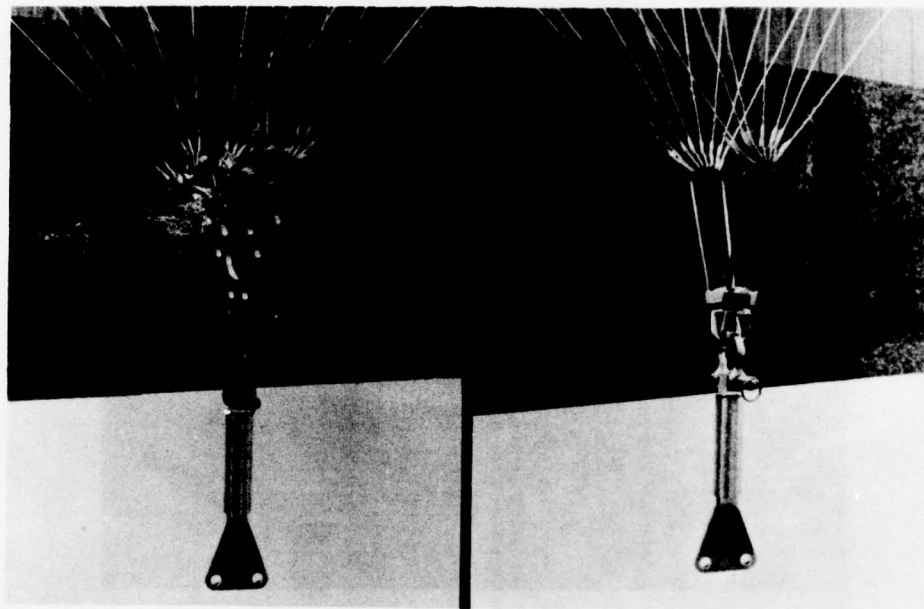


Figure 9. Balloon Confluence Point Hardware

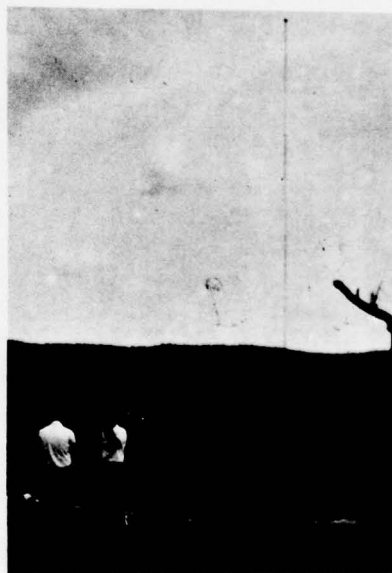


Figure 10. 400 Foot LORAN Tower

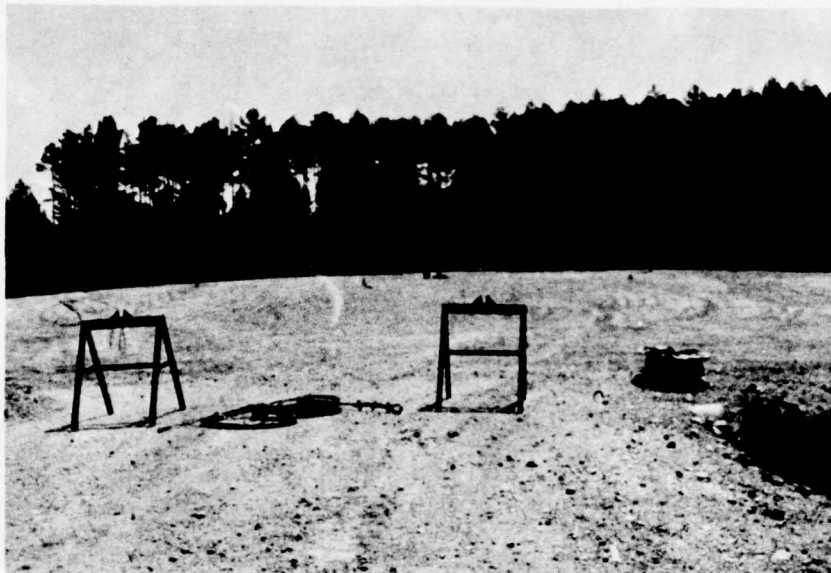


Figure 11. Balloon Antenna Site



Figure 12. Balloon Inflation



Figure 13. Fully Inflated Balloon



Figure 14. Lower End of
Erected Balloon Antenna

Contents

1. Introduction
2. Superpressure pumpkin balloons
3. Kevlar cloth reinforced superpressure balloons
4. Infra-red hot air balloons

UP TO DATE CNES BALLOON STUDIES

M. ROUGERON
CENTRE NATIONAL D'ETUDES SPATIALES
Centre Spatial de Toulouse
Division des Systèmes et Projets Ballons
18, Avenue E. Belin

31055 TOULOUSE CEDEX - FRANCE -

I. INTRODUCTION

Open stratospheric balloons constitute for the scientific community a platform having few constraints on the technical plan, low cost and ease of access. They make it possible to accomplish experiments of a spatial nature, in very diverse domains, without being confronted with difficult problems of utilization of satellites. As in the United States, their success is never denied in France, and the operational activity of CNES in this sector continues at a high level, particularly with some important programs outside France (Brazil during the winter 76/77), and a new activity with transmediterranean flights during the summer period in cooperation with Italy and Spain.

Musing about the future however leads to the thought that the coming of the space shuttle will facilitate access to space for experimenters, and that open stratospheric balloons will lose a part of their interest, unless it is possible to foresee precisely the extent of this backward trend.

However that may be, there exists a domain of science, still new despite its importance, for which the balloon constitutes an irreplaceable tool ; this is the study of the dynamics, physics and photochemistry of the atmosphere. Capable of effecting in-situ measurements in vast range of altitudes, the balloon can be utilized either independently or paired with remote sensing satellites.

But the open balloon for which the flight duration is very limited is poorly adapted to this type of experiment. That is why the CNES prefers, for the future, studies of balloons having a long-life duration.

In the past, and still today, flotillas of pressurized, spherical balloons of some meters in diameter, fabricated from polyester film, have been used with success by France in the area of meteorological experiments (general circulation at the 200 mb level, Indian monsoon ...).

But these balloons called upon an already old technology for which range of application was found to be quite narrow. It is to accomodate a very great variety of missions, in particular, exploration and surveillance of the stratosphere, that the CNES has undertaken to develop some new types of pressurized balloons, the mechanical structure of which is based upon aramide fiber (kevlar). This fiber appears either in two-dimensional form (grids or cloth) or in mono-dimensional form (cables or tapes). In the latter case, the envelope is no longer homogeneous and spherical but presents the appearance of a pumpkin.

It is also interesting to note that this latter family of balloons, which appeared to present almost unlimited possibilities for extrapolation, should eventually give birth to vehicles of very great volume, veritable "atmospheric satellites" ; their missions, rediscovering the variety of those of existing open stratospheric balloons, will have a much longer duration.

The pressurized balloon, however, suffers a fundamental limitation : it flies at an iso-density level. Now, the study of the atmosphere requires, most often, a three-dimensional description, and therefore the possibility of excursions in altitude.

The first endeavors in this regard made use of pressurized balloons with air ballast. To make the system descend, a pump fills a ballonet with air taken in the ambient surroundings. To initiate ascent, this air is simply evacuated through a valve. But the performance obtained remains very modest.

This is why the CNES prefers, in fact, to study an entirely new vehicle for which the concept was born a little more than a year ago at the Service d'Aeronomie of CNRS : la Montgolfière infra-red (MIR), Figure 1.

II. PRESSURIZED "PUMPKIN" BALLOONS

II.1. History

After having consulted the potential users of this type of vehicle, the CNES decided three years ago to develop pressurized balloons of great size, capable of exploring the stratosphere. The first objective was defined thus : altitude 30 km ; useful payload 30/50 kg (ultimately 100/150 kg) ; flight duration 3 months.

To fabricate the balloon suitable for this mission from a light, biaminated polyester film was a risky solution because of the fragility of this material.

Instead of trying to find a simple plastic film having several opposing qualities, we have now tried to use composites, each element of which possesses its own function :

- . mechanical strength : kevlar grid
- . gas barrier : thin polyester film
- . external protection (to avoid creation of microholes due to handling, transport, ascension) : flexible coating (for example, polyethylene or EVA).

This technique offers a supplementary advantage, that of permitting, within certain limits, adjustment of the mechanical strength of the composite (by modifying the structure of the grid), according to the possible mission evolutions, without changing the other characteristics (flexibility, in particular).

After many efforts, in a difficult industrial context, there was developed a complex :

EVA - P6 - Grid K - P6 - EVA

the laboratory characteristics of which are in every regard satisfactory :

- . surface mass : 42 g/m²
- . rate of diffusion at 20° C : 21/m²/24 h
- . resistance to rupture (multidirectional test) : 7 daN/cm
value reduced to 5 daN/cm after aging for 3 months in flight conditions
- . "long duration" tenacity (multidirectional test) : greater than 3.5 daN/cm
- . solar absorptance 4 % on virgin material ; 13 % after aging.

Concurrently, methods have been defined for assembly, thanks to a wide, overlapping gore tape, to obtain a mechanical strength of the joint better than 80 % of that of the material.

Unfortunately, the results of ground tests on balloons of 3,70 m (afterward 7,80 m) in diameter consistently proved to be disappointing.

It seems that the kevlar grid prevents complete local, plastic adaptation of the material and induces considerable overstresses in zones presenting the slightest flaw, whether with regard to the material or in fabrication (imperfect geometry).

It was decided in mid 1977 to abandon this approach, at least temporarily, and to direct all effort to the study of the pumpkin, the first results of which were promising.

II.2. Calculation of the "pumpkin" shape

The initial concept rests on 3 fundamental considerations :

- . the mono-dimensional structures in kevlar (cables or tapes) present a quality factor (strength/weight) greater than that of the bi-dimensional grids ; their technology is better controlled ; their assemblies are relatively easy ; the effect of aging under solar radiation remains limited, even without protection.
- . the envelope of a balloon can be really flexible only if the mechanical resistance provided by the plastic films of which it is composed remains relatively low.
- . the material of the envelope should present capabilities for plastic adaptation to avoid too high localized stresses (inevitable geometric defects).

One should try, therefore, to carry the greatest part of the stresses of superpressure onto a structure formed by the assembly of mono-dimensional elements, while taking care that the induced deformations of the skin remain less than an acceptable limit.

The dimensions of the "mesh" on which the skin is supported should be much smaller than that of the material of the envelope :

- . less tough
- . less deformable (for equal mechanical strength, a greater capability for deformation allows decrease of the local radius of curvature, hence the stresses).

For reasons of simplicity, with regard to fabrication, one is limited for the moment to considerations of a strong structure formed by meridional tapes, terminating on the toroidal polar attachments. The "mesh" is thus formed by the gores themselves.

This mesh, very elongated, leads us to investigate a general shape of balloon in which the circumferential stresses should be as small as possible. This shape is flattened ; it is that of a pumpkin.

Inside the "mesh" the skin behaves in the following manner :

- . in the meridional direction, it is stretched and transfers the greater part of the meridional stresses to the tapes.
- . in the circumferential direction it supports the stresses, which remain moderate, thanks to the general shape of the balloon and to the low value of the local radii of curvature (deformation capacity of the material).

A semi-empirical computation program has been developed in order to optimize the shape of the gores for a given envelope material.

Numerous ground tests have made it possible progressively to improve this program, which today can be considered to be perfectly realistic.

Inputs : superpressure ; number of gores ; radius at max diameter ; simplified curves of stress/deformation of the envelope material and the tapes (at the temperature of utilization) ; difference in initial length, tape vs. gore.

Hypotheses : circumferential tensions on the skin, constant and equal to the elastic limit in the transverse direction of the material ; meridional tensions a linear function of the elongation up to the elastic limit in the longitudinal direction, constant beyond ; flow from shearing, none.

Outputs : gore shape ; elongation in the longitudinal direction ; stress in the tapes.

The computation is iterated until the outputs are compatible with the elongation capability of the skin and the mechanical strength of the tapes.

It is planned for the future to attack the problem using a more theoretical approach, by adapting a general program for computation of structures by finite elements.

II - 3. The supporting structure

II - 3.1. Tapes

The meridional structural elements are made up of kevlar 29 tapes having a very high modulus of elasticity. Tapes were preferred to cables for several reasons : ease of attachment to the skin ; the tapes are impregnated by pressure, hot, with a plastic resin which then can be welded onto the envelope ; possibility of joining to the polar attachments by the use of simply sewn loops, hence very flexible.

On the other hand, they have one fault, that of elongating appreciably under low stress and consequently of demanding even greater capability for elongation of the skin (+ 2 % approximately).

The tapes actually used, with sewn loops at the extremities, have the following characteristics :

- . mass/unit of length : 14 to 23 g/m
- . width : 17 to 25 mm
- . resistance to rupture : 1400 to 2300 daN
- . "long duration" tenacity (1 week) in cycles of traction to 55 % of the rupture resistance
- . very low increase in resistance to rupture at cold temperature (- 30° C)

In flight, the traction on the tapes will not surpass 45 % of their resistance to rupture.

In the future these tapes will be coated with an aluminized film in order to reduce the global solar absorptance of the balloon, and protect the kevlar fibers from ultraviolet radiation.

II - 3.2. Polar fittings

They are formed by the assembly of two demi-toruses on which are threaded the loops at the extremity of the tapes. Mechanically the polar fittings work essentially in traction. The force sustained is equal to :

$$\frac{n \text{ (number of tapes)} \times T \text{ (traction in the tape)}}{4}$$

One makes sure, moreover, that the cross section of the torus is not too small, for the winding radius of the tapes must be sufficient not to cause diminution of the mechanical characteristics in the region of the loop. For the tapes described above (III - 3.1.) this diameter should be greater than 25 mm.

The mass of each polar fitting, for a fabrication from a light alloy, in the case of a balloon enforced with 36 tapes, having a rupture resistance of 1400 to 2100 daN, is from 750 to 1100 g.

II - 4. The envelope material

II - 4.1. Triplex

The plastic films currently utilized in the balloon industry are polyethylene or polyester. For the fabrication of pressurized balloons, even in the pumpkin structure, the mechanical properties of polyethylene are not good enough.

The first developments, accordingly, were undertaken using polyester film, very strong and having moderate capability for elongation, but still satisfactory at very low temperature. The thickness of this film should not be greater than 23 μ so that the material will remain sufficiently flexible and easily pliable. To limit the risks of seeing microholes created before pressurization of the balloon, the polyester film is coated on its two faces with about 10 μ of polyethylene which prevents abrasion and the formation of too pronounced folds. Moreover, the "triplex" thus obtained can be assembled by welding, which ameliorates the reliability of the bond.

An identical material had been ground tested by the CNES several years ago, in anticipation of the realization of large pressurized spherical balloons. The results were excellent in regard to gas tightness; but the dead weight of the polyethylene coating too greatly limited the performance of this type of balloons and made them unable to withstand extreme thermal conditions.

This is no longer the case for the triplex pumpkin balloons, which, although relatively heavy, have, after all, appreciably better performance than the classic spherical balloons, Figure 2.

Thus, the 214 m³ balloons actually tested for flights at 100 mb level weigh 19 kg. Ground tests, at ambient and cold temperatures, show 50 mb to be the admissible value of superpressure in flight, and this with a good margin of security. Actually, if, within certain limits, this value is surpassed, the triplex deforms in its plastic zone, but returns to a state of stable equilibrium. Moreover, the burst superpressure reaches 65 mb in ambient, 80 mb in cold conditions.

These balloons are comparable to spherical balloons of 7,42 m in diameter made from polyester $2 \times 30\mu$, for which the maximum permissible superpressure in flight is at best 35 mb.

Although the pumpkin balloon absorbs solar radiation more strongly than the equivalent spherical balloon (increased mid-diameter, presence of opaque tapes) - evidenced by an increase in superpressure, in extreme conditions, of the order of 7 to 9 mb - it still, in the aggregate, has better performance than the spherical balloon (gain of at least 15 to 20 %).

II - 4.2. Polyamide 12

The characteristics of polyamide 12 films correspond particularly well to the ideal specifications which one would establish for envelope materials for pumpkin balloons of large volume.

These films are, in fact, the object of exhaustive studies in thicknesses from 25 to 30μ .

Numerous positive observations have already been acquired :

- . suitable mechanical strength
- . very great capacity for elongation for temperatures higher than -40°C
- . minimum aging in flight environment both with regard to mechanical and thermo-optical properties
- . easily achievable assembly by heat welding, even in peel.

Studies are being carried out on the formulation of the resin, which must be optimized to lower the temperature of vitreous transition of the film.

II - 5. Perspectives of development - FIGURE 3, FIGURE 4.

II - 5.1. Triplex

The first tests of 214 m³ balloons will take place next August in the southern hemisphere. The useful payload is from 12 to 13 kg, the flight level 100 mb. This size of balloon was chosen because, on the one hand, it is sufficiently small so that it should be possible to carry out numerous preliminary tests on the ground, and on the other hand it lends itself to scientific possibilities interesting even now.

Eventually it will be possible to grow toward useful loads of 30 to 150 kg at levels between 70 and 30 mb (balloons of 1000 to 12000 m³).

II - 5.2. Polyamide 12

This concerns a method of "high altitude" development calling for balloons of large size, but for which the fabrication is as simple as that of open stratospheric balloons made of polyethylene.

A range of volumes from 8000 to 120 000 m³ should make it possible to cover a wide domain of performance ; useful load 30 to 150 kg ; level of flight 15 to 6 mb.

III - PRESSURIZED BALLOONS REINFORCED BY KEVLAR FABRIC

In the category of traditional pressurized balloons of spherical shape, or rather quasi-spherical, with optimization of shape for hanging the gondola at the lower pole, we have seen in para. II - 1, the reasons which led the CNES to study the use of composites.

The kevlar grids, more or less close together, make it possible, at least theoretically, to cover a certain range of performances - moderate payload in the middle stratosphere - but they must be replaced by a fabric since one wishes to fly at lower altitudes and (or) with higher payloads. The material then being opaque, it becomes necessary to aluminize the gas-tight film on its internal surface, in order to limit the solar absorptance of the balloon while preserving a good infra-red emissivity.

III - 1. Balloon for exploration of the VENUS atmosphere

It is a vehicle of this type which was actually developed by the CNES in the framework of the Franco-Soviet project for the balloon on Venus.

The flight level chosen corresponds to a density 1 kg/m³; the payload approaches 250 kg. The balloon diameter is about 9 m. The material is made up of (from inside toward outside) :

- . kevlar fabric 440 dtex, plus or minus thickness (110 to 160 g/m²)
- . gas barrier film of 12 μ -thickness aluminized (film polyester or polyamide)
- . coating capable of protecting the envelope from aerosols of concentrated sulfuric acid present in the Venusian clouds ; this is a film FEP 25 μ , aluminized on its inside surface so as to give the balloon correct thermo-optical properties ($\alpha = 0,20$; $\epsilon = 0,50$).

The mechanical assembly is made in the interior with the aid of a band : kevlar (transverse direction) / nomex (longitudinal direction), glued with an adhesive which must be thermostable due to the elevated temperatures which the balloon skin can attain on the bright side of the planet.

Gas-tightness is obtained by welding or gluing with an exterior band.

The polar fittings, rigid (metallic) are of large diameter (\varnothing 0,60 m) and achieve a self-tightening locking of the ends of the gores, without the intermediary of a flexible cap.

III - 2. Terrestrial balloons

The first balloon studies (in particular, of structure definition and evaluation of fabrication tolerances) were made without taking into account the specific constraints of the VENUS mission, hence, with a non-coated material of FEP, but simply made up of 2 layers : kevlar fabric ; polyester film 23 μ , aluminized on its internal face ; with classic adhesives.

Many tests made it possible to define the pressurization limits of the envelope, which is directly useable in the earth's atmosphere. Most of the tests were made in a tank, then in the ocean, the balloon itself being filled with water. This technique, by using an incompressible fluid for pressurization, allows one to limit the propagation of initial tears and hence to reveal their cause.

The main conclusions are the following :

- . the junction of gore/polar fitting and the joining of one gore to another are not the weak points of the balloon, if they are correctly made
- . the local overstresses due, in particular, to defects of fabrication, are quite well absorbed thanks to the possible deformations of the fabric, and in any case do not surpass 50 % of the average stress on the envelope
- . in long duration pressurization, the kevlar fabric cannot support a stress greater than 50 % of its rupture stress (measured in a test under traction),

Thus a balloon of 9 m, made from a composite : kevlar fabric 120 g/m² (95 daN/cm at rupture), adhesive 40 g/m², 23 μ -polyester film aluminized, of surface mass 192 g/m², weighs about 80 kg (of which 60 kg is flexible envelope, and 20 kg polar fittings) and is capable of withstanding a maximum superpressure of 140 mb.

With a suitable factor of safety, ($f = 1,3$ for example) its limit of useful superpressure in flight can be fixed at 110 mb while it carries a payload of 25 kg at 200 mb level.

One sees, therefore, that this balloon has mechanical characteristics that largely compensate for the increase of thermal effects, due to the opacity of the envelope.

III - 3. Perspectives for development

If this balloon can give birth to the ideal heavy platform for surveillance of the lower stratosphere (gondola of 250 kg at 100 mb level - balloon 20 m), with the possible life duration of several months, there remains a problem difficult to manage : that of flight safety with respect to supersonic aircraft traffic.

IV - INFRA-RED MONTGOLFIERES (MIR)

In 1976, the Service d'Aeronomie of CNRS, until then the user of superpressure balloons, proposed to analyze the possibilities offered by Montgolfier s for exploration of the stratosphere. This vehicle presents a fundamental advantage, that of being pilotable at altitude by opening or closing a valve.

This certainly is not a matter of classic Montgolfiers with a burner, but rather of a vehicle which transforms the thermal energy available in the atmosphere into energy of lift (Archemedes) ; the air enclosed in the Montgolfier being heated by the intermediary of the thermally absorbing envelope itself.

A first step was taken at the beginning of 1977 with two flights of solar Montgolfiers made of black fabric, made by the Service d'Aeronomie, from Pretoria. The effectiveness of heating by solar energy is considerable (ΔT of the order of 80 to 100° C at 70 mb) and permits excursions in altitude of wide amplitude, and if necessary, at rapid speed. The reaction time (for example, after closing the valve, at the end of descent) is extremely rapid.

Unfortunately the solar Montgolfier cannot survive the night.

Some relatively complex systems of three balloons can be envisaged for missions of long duration, with excursions in altitude by day : open carrier of transparent film, solar Montgolfier, pressurized stabilizer strengthened by kevlar fabric.

But it is evidently simpler to conceive of one infra-red Montgolfier (MIR) capable of stabilizing itself by night at a floor level, in the worst conditions of radiation. This would be a balloon having very little emissivity in its upper portion and absorbing in its lower portion, by way of making a radiative coupling with the lower layers of the atmosphere (warm in rapport with the surroundings) without re-emitting out into space the energy thus captured.

The nighttime heat thus obtained is surely very much less than the daytime heat from solar radiation, but it attains, however, 20 to 30° C in clear weather. Yet, in the presence of high level clouds ("anvils" of cumulo nimbus, thick cirrus ..) one can hardly hope for supertemperatures higher than 5/10° C. It is thus necessary to conceive of a MIR made from ultra-light material, and of large volume.

Taking account of these characteristics, the MIR is thus found to be "overdimensioned" by day and capable of making large excursions in altitude even if it absorbs solar energy only poorly.

IV - 1. Flights of feasibility

In order to demonstrate the validity of the concept of the infra-red Montgolfier and before entering into a more ambitious program of development, the Service d'Aeronomie of CNRS and the CNES felt it mandatory to make some feasibility flights very quickly.

The vehicle specified for this preliminary phase calls for known technologies but evidently does not present a very great reliability.

The envelope is composed of two parts : the upper part made of 12 μ polyester film externally aluminized, the lower part of 15 μ polyethylene.

It is open at the lower pole (a short sleeve stiffened by two pieces of fibreglas) and eventually fitted with a valve at the upper pole (flexible disk stiffened by a fibreglas hoop coming to lie flat on the internal face of the pole).

Release is made either under an open balloon inflated with hydrogen or helium and floating in the lower stratosphere (the Montgolfier then inflates spontaneously and is set free when its ascensional force is

no more than barely negative); or, in autonomous fashion by introducing into the Montgolfier a bubble of helium which is afterward expelled at the time of the first opening of the valve.

Four flights were made with diverse fortunes from Aire sur l'Adour and from Pretoria, using MIRs of 6000 and 13000 m³, carrying a useful load of 10 to 20 kg, FIGURE 5. The principal results were the following :

- . the principle of heating the Montgolfier by capture of the IR energy coming from the ground and lower layers of the atmosphere was demonstrated. The average temperature of the air enclosed in the envelope agreed with the predicted value. The lift obtained was in every case greater than 6 to 8 g/m³.
- . excursions of about 10 km in amplitude (18 to 28 km) are possible during the daytime. One can determine the optimum cross sections of opening permitting excursions in altitude at the same time ample and reliable (no diminution in volume of the Montgolfier during descent).

On the other hand, a certain number of problems were apparent which prevented us from obtaining flights of very long duration : risk of tumbling of the MIR around a horizontal axis during rapid descent ; in effect, the useful load is always light with respect to the envelope, hence a center of gravity close to the center of thrust ; sensitivity of the envelope to vertical gradients of the winds (considerable inertia of the MIR) and possibilities of vitreous tearing of the lower part made of polyethylene, in the cold surroundings of the tropopause ; technological difficulties in achieving a valve which in its initial conception must reconcile rigidity and lightness.

IV - 2. Perspective of development

The first phase of demonstration of the concept of the MIR is now considered to be terminated. A program of development has been defined having for its objective possibilities of operational utilization after the mid-1980's. Three types of mission can be envisaged :

- . platforme : no valve ; flight level by day (15 to 30 mb) and by night (50 to 90 mb) quite different and variable according to ambient conditions ; but very long duration due to the insensitivity of the MIR to leakage.
- . sounder : very simple pilotage by opening and closing of the valve.
- . tracer : pilotage following some law (isentropie ..) or again telecommanded ; it is thus possible, for example, to choose an optimum trajectory by variation of the level of flight (possibility of recovering the payload at the end of the mission, stationary flight ...).

In every case, the loads transported remain moderate (less than or equal to 150 kg for MIRs of some tens of thousands of cubic meters), the maximum altitudes attained lower than 30 km, and the minimum altitudes limited by level of the tropopause.

The reference version chosen for this vehicle is the following:

- envelope entirely fabricated from polyester 6 to 12 A reinforced with a textile grid and aluminized on the upper portion of the balloon (a solution a little less efficacious than the experimental one just above, but more reliable). The polyester film could eventually be tinted to augment the efficacy of the Montgolfier by day, and consequently, the maximum altitude attained.

- flexible valve

- tropospheric inflation by day under an auxiliary balloon of small volume.

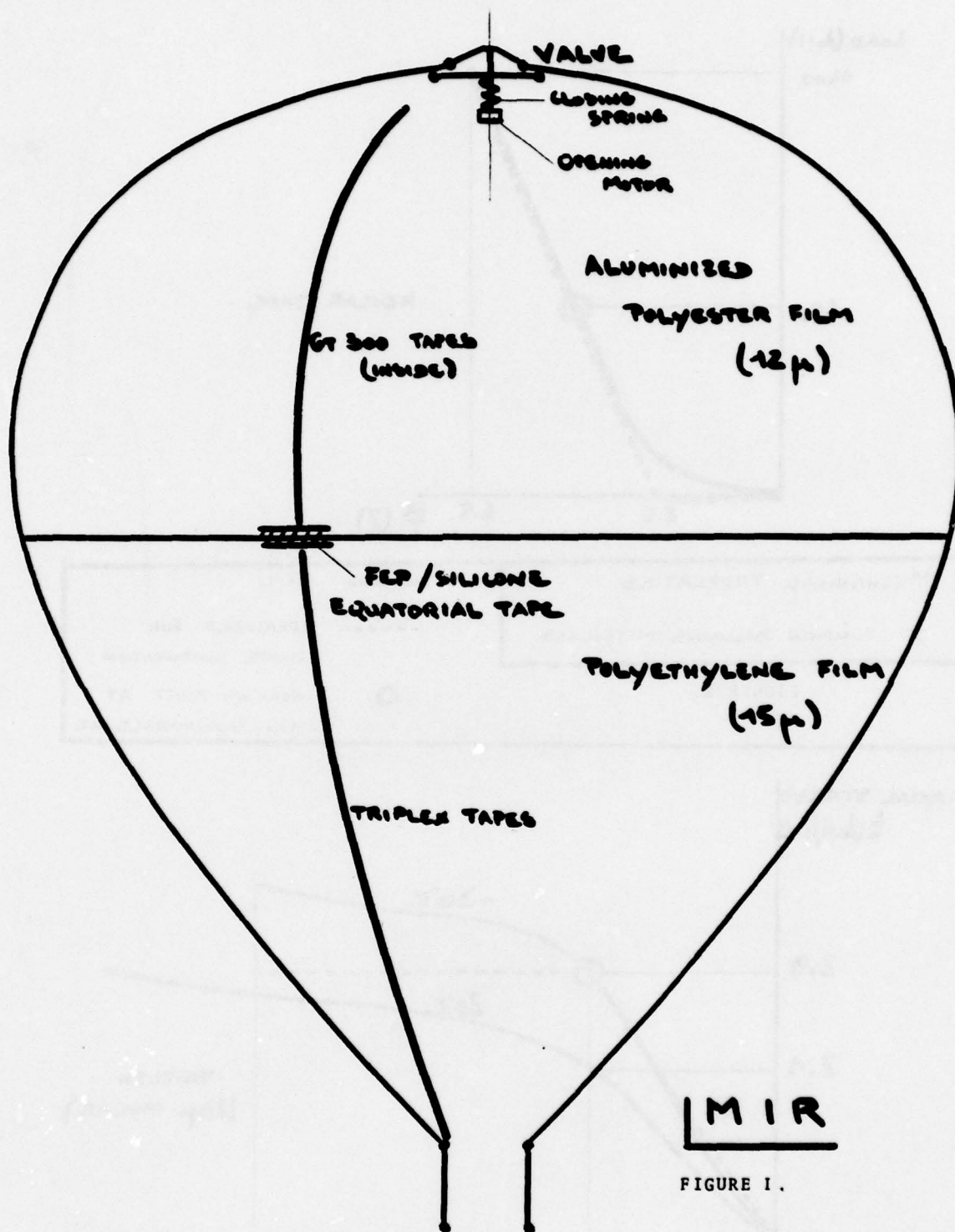
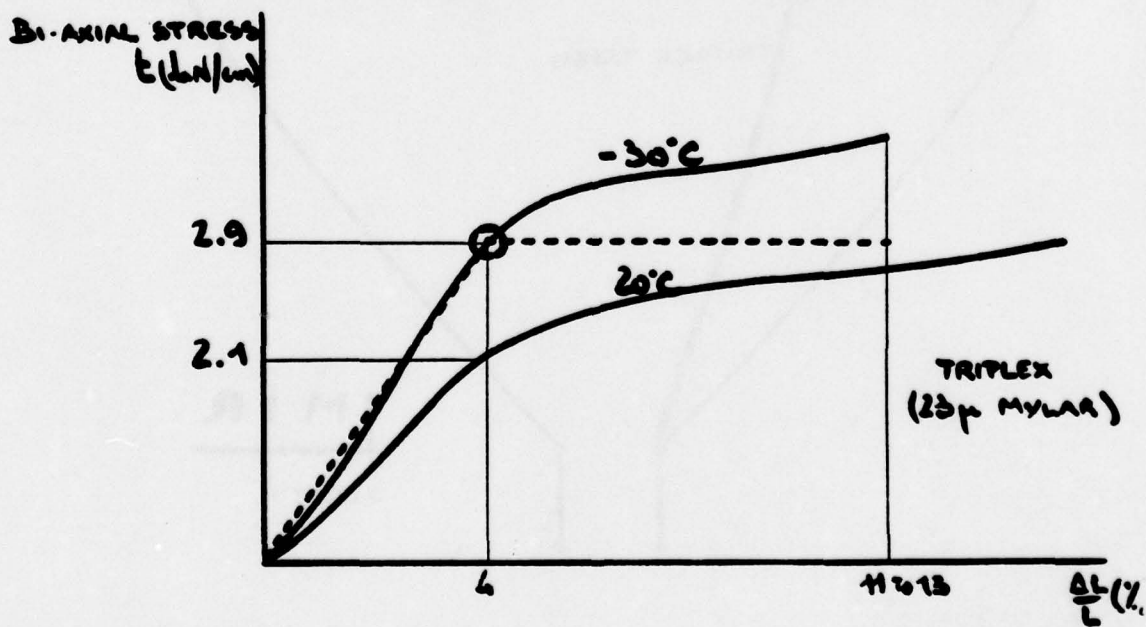
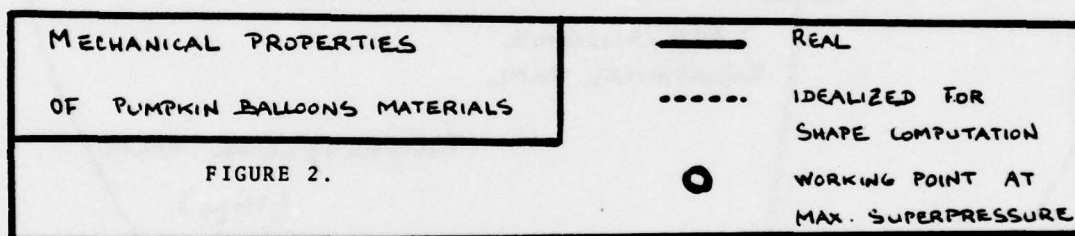
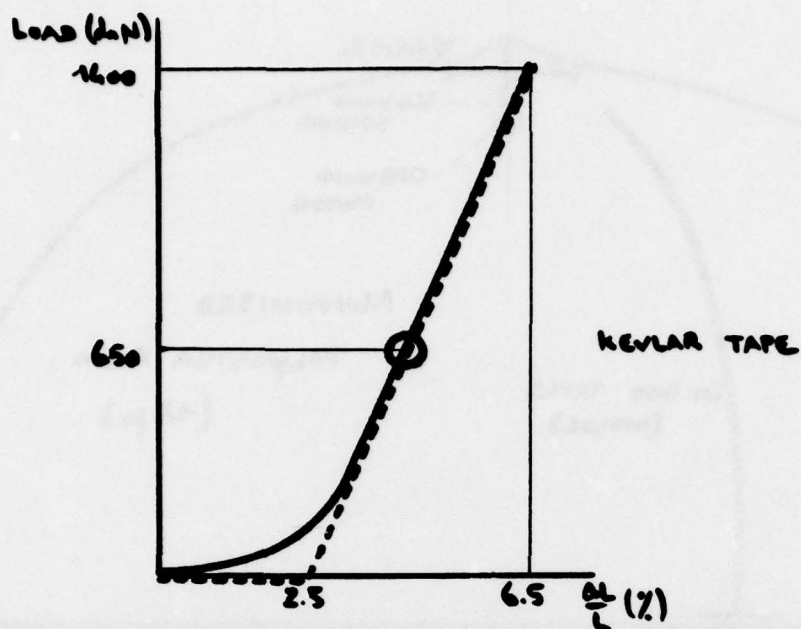


FIGURE 1.



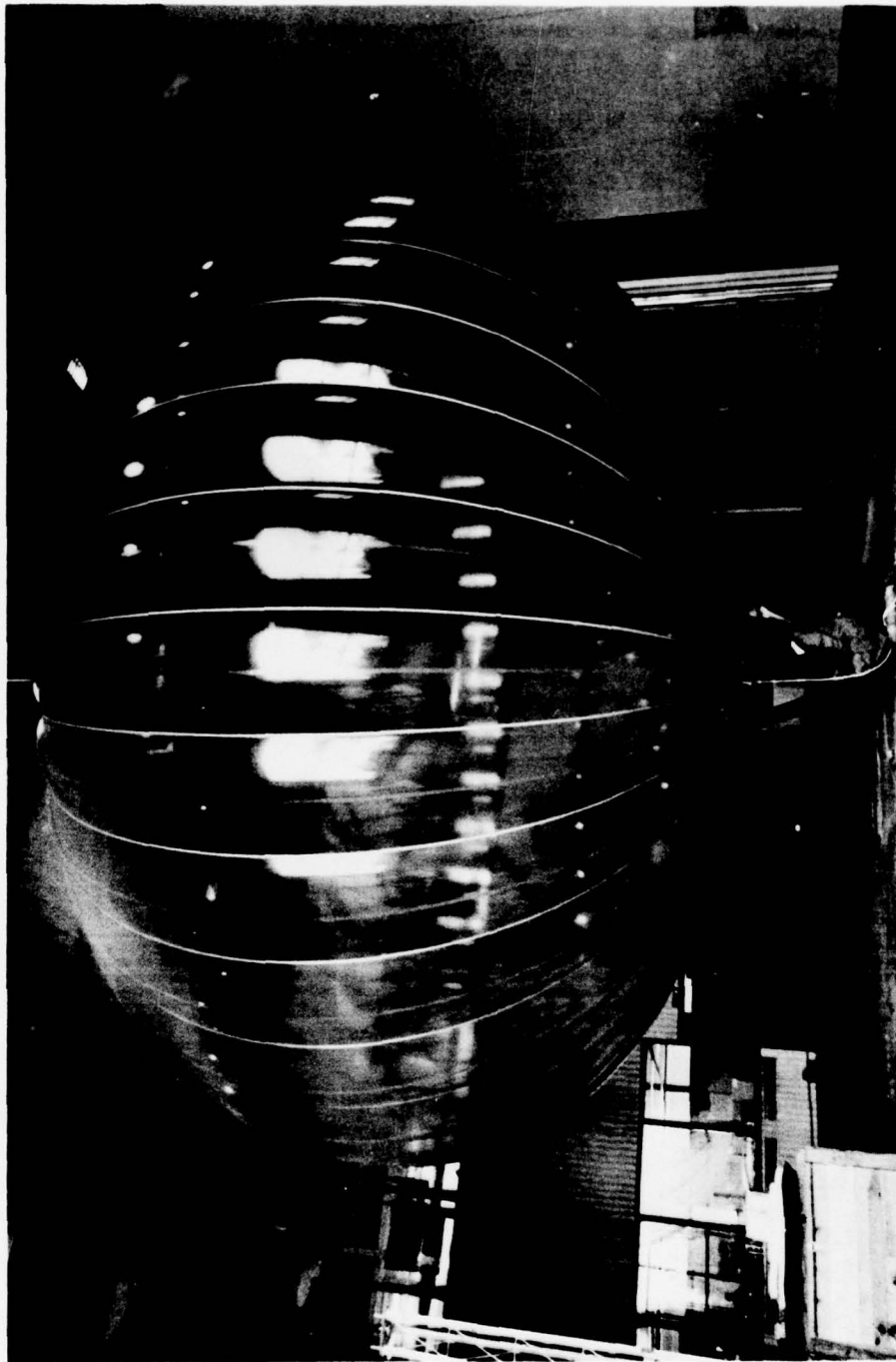
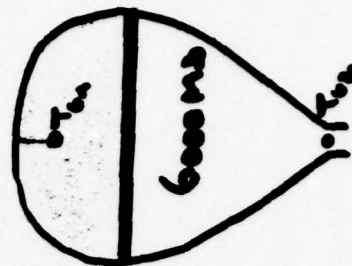
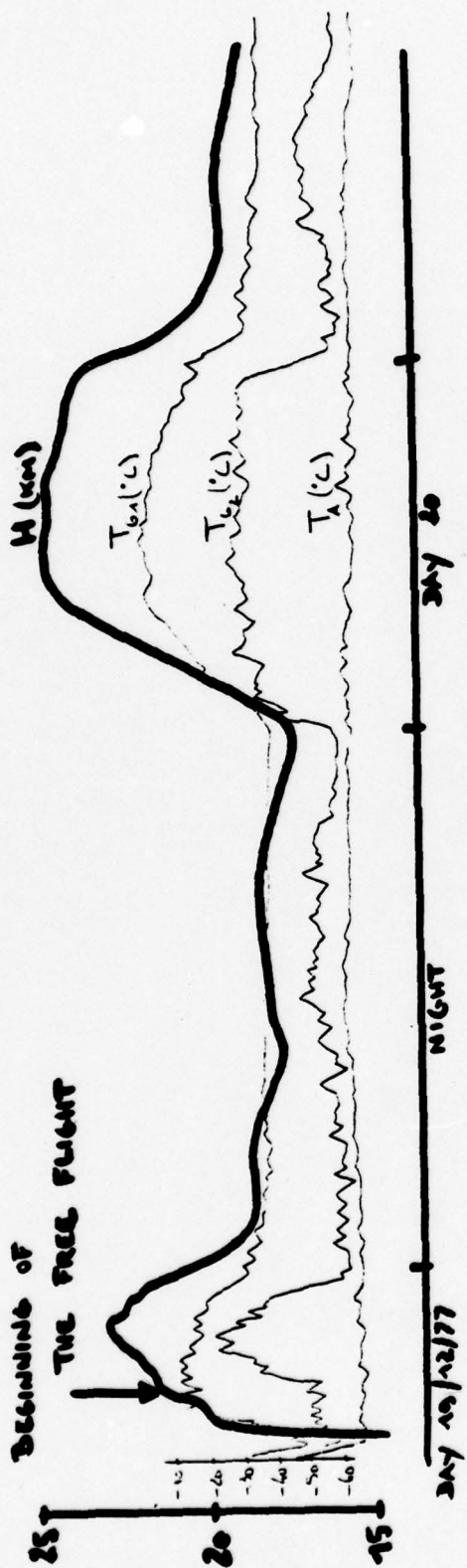


Figure 4. 200 M3 "Pumpkin Balloon"



3 DAYS FLIGHT FROM AIRCRAFT ABOVE
(EXPERIMENTAL MIA)

FIGURE 5.

Contents

1. Introduction
2. Recommendations
3. Flight Histories
4. Failure Analysis
5. Success Record
6. Conclusions

A REVIEW OF HEAVY LIFT BALLOON FAILURES

W. F. Cuddihy
NASA, Langley Research Center

A. D. McHatton
NASA, Langley Research Center

R. L. Golden
New Mexico State University

ABSTRACT

A study has been conducted of the Heavy Lift Balloon Technology in view of the recent failure history of these flights. The failures for the period from 1969 to present have been analyzed and statistical data are presented. Launch operations and balloon manufacturing are examined. It is concluded that heavy lift launch techniques are marginal with existing systems. It is also shown that there is a high probability that some change in the balloon manufacturing or launch technique has adversely shifted the margin for success since about the first quarter of 1977.

1. INTRODUCTION

As a result of a number of heavy lift balloon failures, the NASA Office of Space Science suspended further NASA heavy lift balloon flights in October of 1977. A review committee was convened to examine the heavy lift balloon program and to recommend possible corrective actions. Figure 1 lists the committee members and consultants.

The review committee examined all phases of the balloon program including polyethylene film production, balloon fabrication, quality assurance, shipping and storage, launch operations, and associated research efforts. With the aid of the National Scientific Balloon Facility (NSBF), flight histories for all launches from 1972 through 1977 were examined (Table 1). Out of 468 flights there were 402 successes for an 86% success rate. Figure 2 shows the success rate for each year. There is no trend indicated.

A payload weight of 1600 kg was arbitrarily selected as the dividing point between light and heavy payloads and the data examined for light vs heavy loads (Figure 3). The heavy payloads were further examined for remote vs home base launches (Figure 4). As might be expected, there is a lower success rate for heavier launches and for remote operations. At the time of this review (fall '77) the higher failure rate for heavy payloads in 1977 from Figure 3 did not strike us as statistically significant.

The failures modes were examined as a function of Mission Mode (Figure 5). It is seen that while there is a variety of causes for failure, there are two predominant classes:

1. Damage to, or defects in, the balloon at inflation and release.
2. Leak or burst during ascent.

A change in these two categories could significantly increase the success ratio. It was also noted that some of the failures, which manifested themselves in the ascent phase, may have been induced by launch dynamics.

The recommendations of the Review Committee, as reported to the Office of Space Science in January 1977, are given below.

2. RECOMMENDATIONS

2.1 Science Requirements

The OSS Program Offices should interact with the experimenter for each proposal submitted to trade off such factors as cost, float time and altitude requested, and maximum suspended weight. The objective here is to drive the balloon size to the minimum required to accomplish the mission, thus increasing the probability of success.

Each NASA-supported experiment should be required to establish minimum mission success criteria before the start of launch operations. These criteria can serve as go, no-go decision guides during actual operations.

The Panel endorses the NSBF plans to control remote operations in the U.S. with only two semi-permanent launch sites (one northern and one mid-latitude). Any NASA experiment that requires use of another location should be critically reviewed by the OSS Program Office for added science versus increased probability of failure.

2.2 Operations

Heavy payload NASA flights should be confined to Palestine to the extent that is feasible. Exceptions should require Headquarter's specific approval, and concurrence for added risk. Each exception should require a Remote Station Operation Plan with launch criteria pre-established.

Adequate crane facilities should be provided at the two semi-permanent remote sites.

Adequate meteorological coverage should be provided at the two semi-permanent remote sites.

All NASA heavy payload balloons should be provided with vent valves to enhance control.

Review balloon packing and storage procedures, establish additional requirements as needed.

2.3 Heavy Payload Launch Techniques

NASA long range R&D effort should be directed at improved launch techniques for heavy payloads. Several suggestions for use of sleeves and winches during balloon erection have been considered. Although least developed, the single cell "soft collar" approach appears to be most promising and most cost effective.

2.4 Failure Reviews

Each unsuccessful NASA balloon experiment should have a failure analysis conducted to determine most likely cause of failure and to recommend corrective action. The report should be submitted to the Project Office for formal review.

For each heavy payload launch, adequate high speed camera coverage should be provided to analyze and isolate problems associated with launch dynamics, balloon material, and launch operations.

2.5 Balloon Manufacturing

Provide NASA material and fabrication consultant to work with Winzen at Sulphur Springs plant. Minor changes in handling might result in improved material performance during launch dynamics stage.

The Project Office consider items listed in Alley and McHatton memos (memos discussing polyethylene handling, testing, and processing) for possible research and development programs.

2.6 Information Exchange

It is recommended that a Balloon Working Group be established with NASA, AFGL, NSF, and ONR participating. This group would provide a means of information exchange, failure reporting and specification review. It would provide a means of coordinating R&D effort and a forum for such questions as the possibility of developing a second source for balloon supply.

2.7 University Research Program

It is recommended that the NSBF research contract at Texas A&M be coordinated with other agencies, and that it be directed more to the solution of problems associated with heavy payload balloons.

3. FLIGHT HISTORIES

3.1 Flight 1063P

Following the heavy lift review committee report, the Office of Space Science decided to waive the moratorium on heavy lift launches on an individual basis. The first heavy payload attempted was Flight 1063P, a $1.33 \times 10^6 \text{M}^3$ balloon with a 2416 kg payload. This balloon failed in the launch phase, and a failure review panel (as listed on Figure 6) was able with the aid of high speed movies to pin point the failure to ripping of the material induced by sailing. The rip appeared a few seconds before payload release. While it is not known if the rip was due solely to the high stress or if it originated in a balloon flaw, the failure, under ideal wind and weather conditions, confirmed the previous finding that the launch of a large balloon with a payload as heavy as this strains the single cell dynamic launch technique.

3.2 Flight 1065P

A second launch attempt was made with a payload considered to have a high probability of success. The flight was 1065P with a 2362 kg payload and a $1.60 \times 10^5 \text{M}^3$ balloon. This flight failed due to a burst at 18.6 km. A thorough failure analysis was conducted on this balloon by the panel listed in Figure 6, including a detailed examination of the recovered balloon. It was found that there was extensive cold-brittle shattering and cold-ductile ripping in the cap region. One example of a cold-brittle shattered area is shown in Figure 7. The most probable cause of failure was judged to be due to one or both of the following causes:

- a. A combination of pre-strain during launch and ascent, heavy loading, and cold tropopause temperature.
- b. Possible local damage to the polyethylene material during fabrication, launch preparation, or the dynamics of launch.

3.3 Flight Summary

Flight 1065P was one of a series of seven balloons of this size, with the first five being successful and the last two being failures. Table 2 summarizes the seven flights and suggests a trend from success to failure for supposedly similar conditions. The review panel expanded the heavy-lift data base by collecting data on all NSBF heavy lift flights from 1966 to the present time (Table 3).

4. FAILURE ANALYSIS

Failures were plotted as a function of balloon manufacture date. The plot was limited to failures related to balloon performance during launch and ascent, i.e. if a failure could be attributed to an operational problem or unexpected weather conditions, it was not counted. The results are given in Figure 8 and show a strong trend from success to failure starting in the first quarter 1977. It is important to note that in this same time frame, (from Jan. '77 thru May '78) NSBF has launched approximately 72 payloads below 1600 kg with only one failure. From the above we conclude that some of the heavy-payload failures may be due to a subtle change in balloon material production, manufacturing, or launch technique.

All failures (both heavy and light payloads) occurring during ascent and float, listed on Figure 5, were plotted in Figure 9 as a function of altitude of failure vs date. It is noted that a few leakers failed to reach the tropopause, but the majority of failures were at cold temperatures.

The failure at cold temperature of the last two $1.60 \times 10^5 \text{M}^3$ balloons in the series of seven launches (Table 2) indicates that the change allowing the failure could manifest itself under conditions of cold temperature and heavy loading. A review of the literature (Ref. 1-3) would also indicate that cold-brittle failure is a function of pre-strain. That is, if the material is loaded at ground temperature sufficiently to impart a permanent deformation, subsequent loading will cause brittle behavior at warmer temperature than that found for virgin material. It is obvious that the onset of brittle behavior is, therefore, a function not only of the cold temperature in the tropopause, but also of high temperatures at launch, since the modulus of elasticity and yield stress drop rapidly with increasing temperature.

5. SUCCESS RECORD

The overall heavy-payload success record prior to the beginning of 1977 indicates that, while the pre-strain of launch followed by heavy loading at cold temperature can induce the present failure mode, there must have been a change in the system that now allows it to exceed previous margins. From the data base of heavy lift flights, Table 3, the 12 single cell heavy lift polyethylene flights that failed due to a balloon-associated problem were examined for trends. Figures 10 through 19 provide success ratio vs payload wt., gross wt., balloon volume, percent free lift, shell thickness, top thickness, number of caps, serial number, flight date, and manufacture date.

6. CONCLUSIONS

Conclusions drawn from this small sample should be suspect, but the best correlation appears to be with manufactured date. There is a 15% chance that success is independent of launch date and a 2.7% chance that success is independent of manufacturing date. If one calculates the odds that the 1977-1978 manufactured date success ratio is unchanged from the previous years, the odds drop to 0.5% that nothing has changed.

Examination of launch techniques and manufacturing procedures has not identified any changes that appear significant. A correlation was noted in Table 2 in the change to radar tape with reflective threads and rate of failure. However, the investigation has not provided any clue as to how this change could affect the performance of the balloons. A test program on Winzen Research, Inc. StratoFilm® produced pre- and post-1977 is being conducted at Texas A&M for the NSBF to determine if a change in material properties has occurred. As of this date, the results are too preliminary to report any discernable change.

In conclusion, the heavy lift balloon program failure rate has resulted in an examination of the program. It has been concluded that the heavy-lift single-cell launch technique is marginal, and that there is a reasonable probability that a subtle change has occurred in the system that has worsened the case for heavy lift flights without affecting lighter payloads. Investigation of balloon material properties, plans for engineering flight tests, and consideration of new heavy lift launch techniques are underway.

REFERENCES

1. Alexander, H., and Weissmann, D. (1972) A compendium of the Mechanical Properties of Polyethylene Balloon Films, Stevens Inst. of Tech., Contract F19628-69-C-0069, Scientific Report 2.
2. Webb, L. Dale (1974) Balloon Strength and Failure Analysis Presented at Eighth AFCRL Scientific Balloon Symposium.
3. Dwyer, James F. (1978) Zero Pressure Balloon Shapes, Past, Present, and Future. AGARD Presentation.

Acknowledgement:

This report is the result of the efforts of the review committee, the failure review panel, and the consultants listed in Figure 1 and Figure 6. The current authors have merely summarized the work of these groups.

H. K. Clark, Chairman
W. F. Cuddihy, Vice Chairman
F. R. Sawyer
W. R. Nagel
R. L. Golden
M. J. Long

NASA, Langley Research Center
NASA, Langley Research Center
NASA, Wallops Flight Center
NASA, Goddard Space Flight Center
NASA, Johnson Space Center*
NASA, Langley Research Center

Consultants:

V. L. Alley
V. L. Bell
A. D. McHatton
J. W. Grey
J. F. Dwyer
W. Martin
A. Shipley
G. Tesi
J. R. Holtz

NASA, Langley Research Center (Ret.)
NASA, Langley Research Center
NASA, Langley Research Center
NASA, Wallops Flight Center
Air Force Geophysical Laboratory
Office Naval Research
National Scientific Balloon Facility
National Science Foundation
NASA Headquarters, Washington, D. C.
*Now at New Mexico State University

Figure 1. Heavy Lift Balloon Review Committee

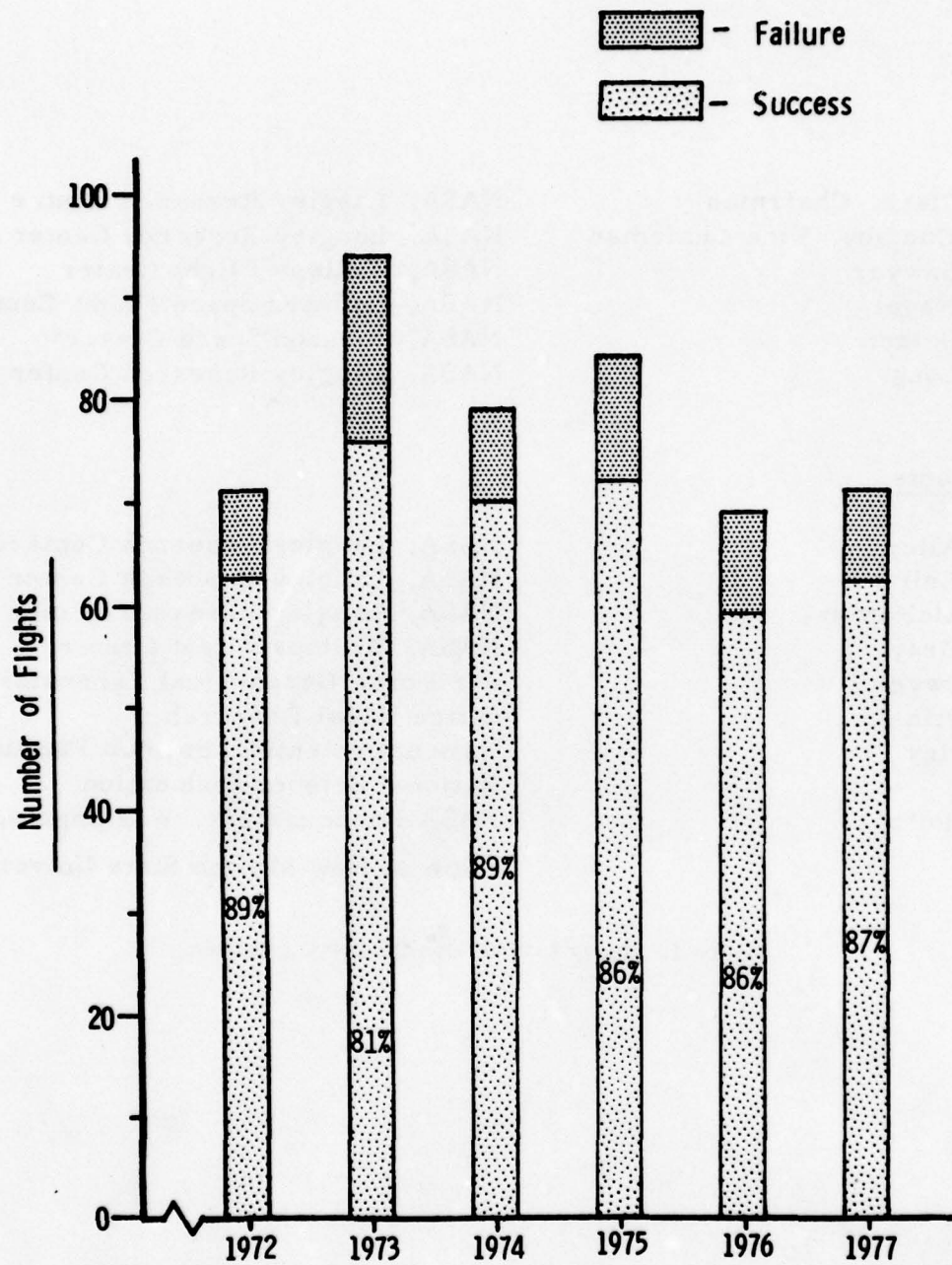


Figure 2. Success Rate vs Year—All Balloons

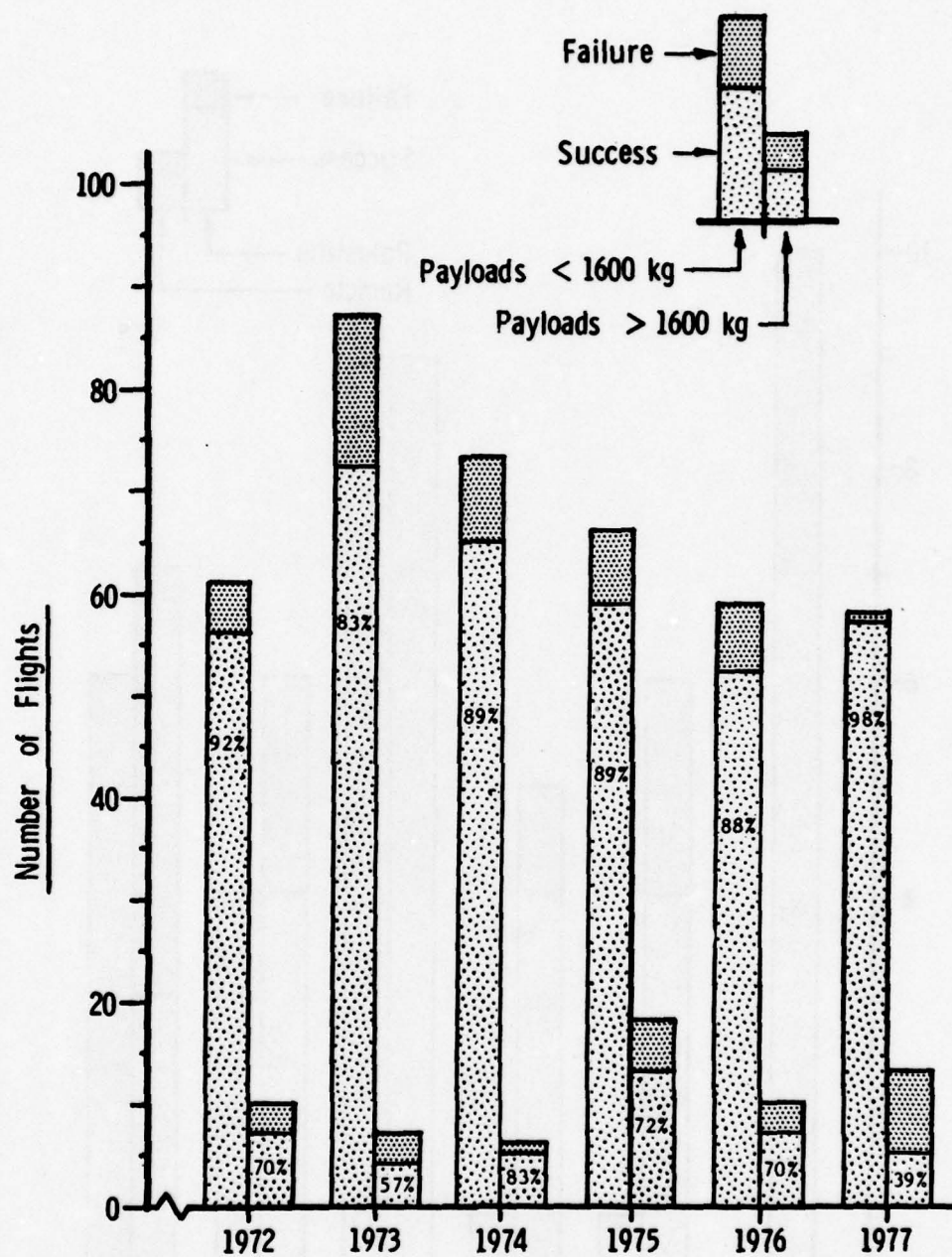


Figure 3. Success Rate vs Year, Light and Heavy Payload Flights

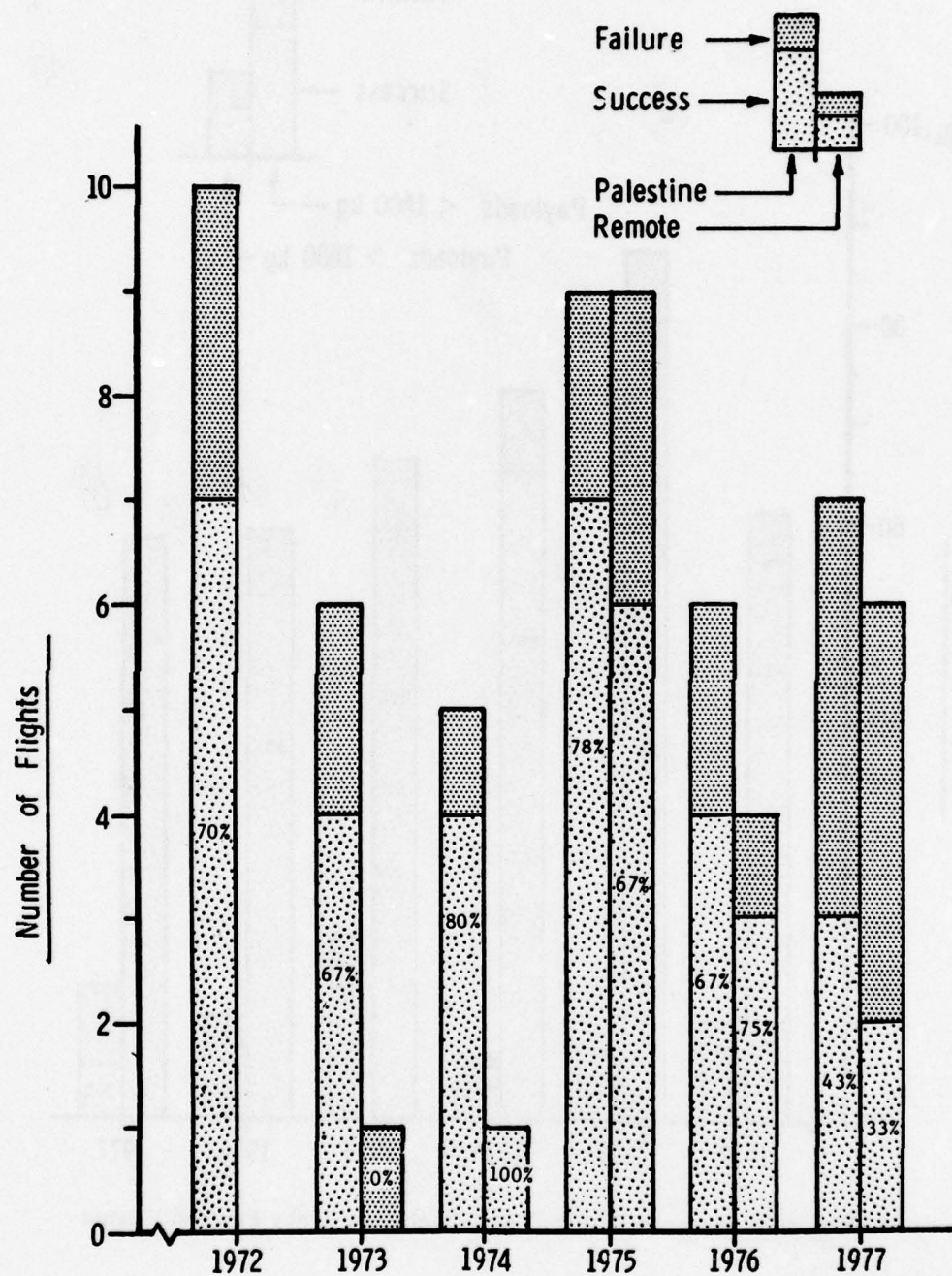



Figure 4. Success Rate vs Year, Heavy Payloads-Remote and Palestine

NSBF BALLOON FAILURES 1972-1978

NSBF BALLOON FAILURES 1972-1978

Remote  Flt. No. > 1600 kg

FAILURE MODE						
MISSION PHASE	ELECTRONICS	METEOROLOGY	OPERATIONAL	Balloon Leak or Burst		OTHER
				Before Launch	After Launch	
INFLATION AND RELEASE	<div>109</div> <div>1040</div>	<div>107</div> <div>129</div> <div>130</div>	<div>798</div> <div>96</div> <div>803</div> <div>816</div> <div>847</div> <div>115</div> <div>123</div>	<div>664</div> <div>695</div> <div>84</div> <div>86</div> <div>762</div> <div>768</div> <div>779</div> <div>99</div> <div>874</div> <div>877</div> <div>904</div> <div>918</div> <div>922</div>	<div>944</div> <div>957</div> <div>989</div> <div>134</div> <div>1023</div> <div>1043</div> <div>1063</div>	
ASCENT	<div>706</div> <div>954</div>		<div>744</div> <div>850</div>		<div>661</div> <div>697</div> <div>704</div> <div>712</div> <div>742</div> <div>747</div> <div>756</div> <div>772</div> <div>781</div> <div>787</div> <div>90</div> <div>796</div> <div>797</div> <div>94</div> <div>800</div> <div>871</div> <div>888</div> <div>926</div> <div>950</div> <div>971</div> <div>1041</div> <div>1065</div>	
FLOAT					<div>85</div> <div>849</div> <div>987</div> <div>123</div> <div>1023</div>	
TERMINATION	<div>920</div>					<div>714</div> <div>996</div>
OTHER						<div>727</div> <div>952</div>



Figure 5. Mission Phase vs Failure Mode

W. F. Cuddihy, Chairman
C. W. Ballance
R. L. Golden
W. R. Nagel

NASA, Langley Research Center
NASA, Wallops Flight Center
NASA, Johnson Space Center*
NASA, Goddard Space Center

Consultants:

M. J. Long
A. D. McHatton
J. F. Dwyer
R. S. Kubara
J. Lehmann
L. D. Webb
J. R. Nelson
C. Foster

NASA, Langley Research Center
NASA, Langley Research Center
Air Force Geophysical Laboratory
National Scientific Balloon Facility
National Scientific Balloon Facility
Texas A&M
Winzen Research Incorporated
Winzen Research Incorporated

*Now at New Mexico State University

Figure 6. Review Panel for 1063P and 1065P Failure Analyses

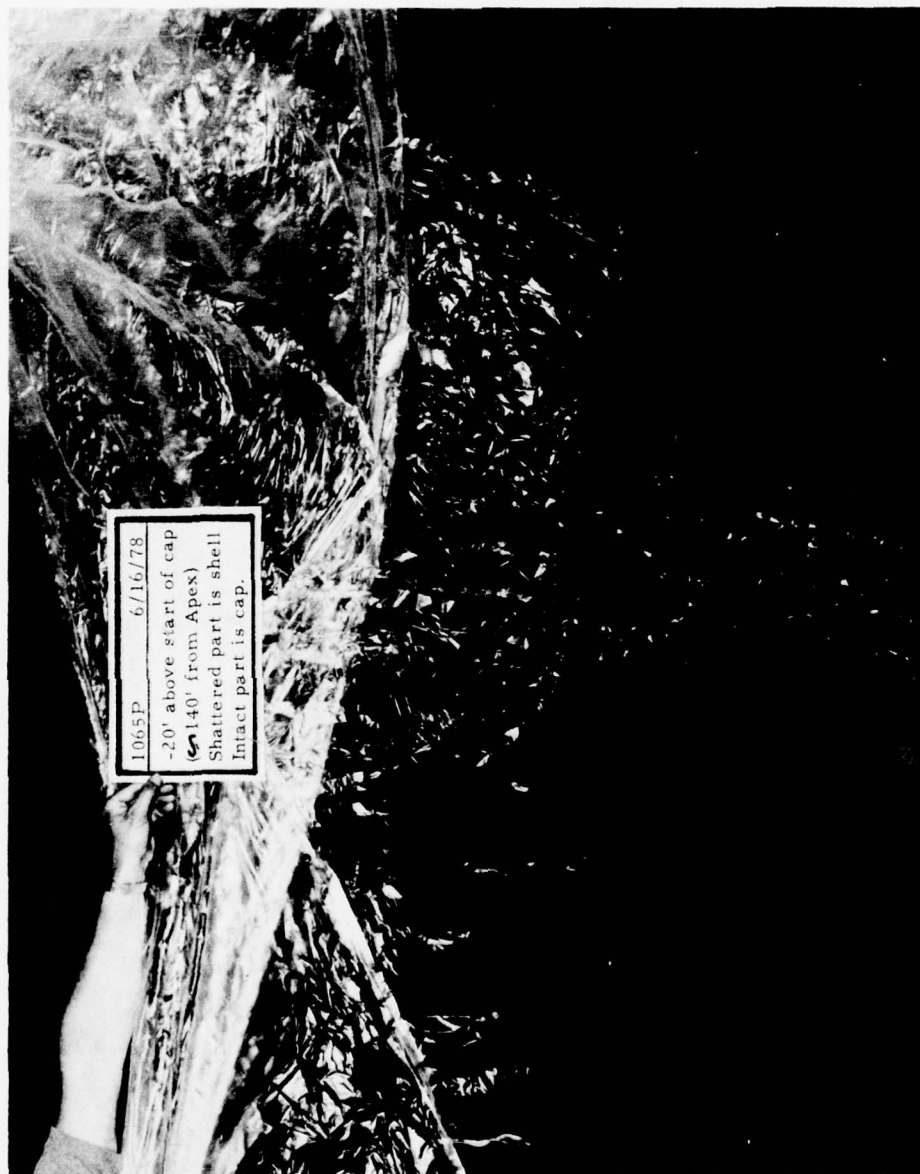


Figure 7. Cold Brittle Failure Area, 1065P

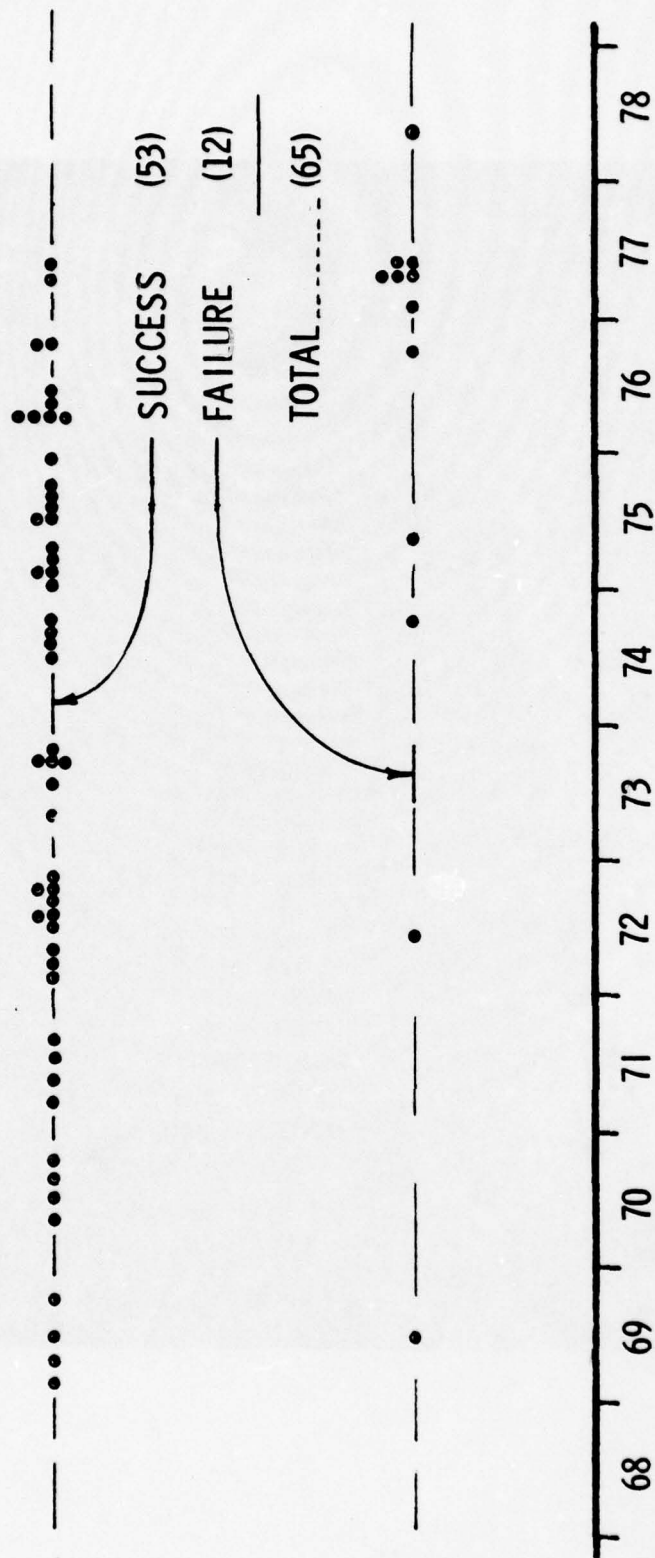


Figure 8. Heavy Lift Flights; Successes and Balloon Related Failures vs Balloon Manufacturing Date

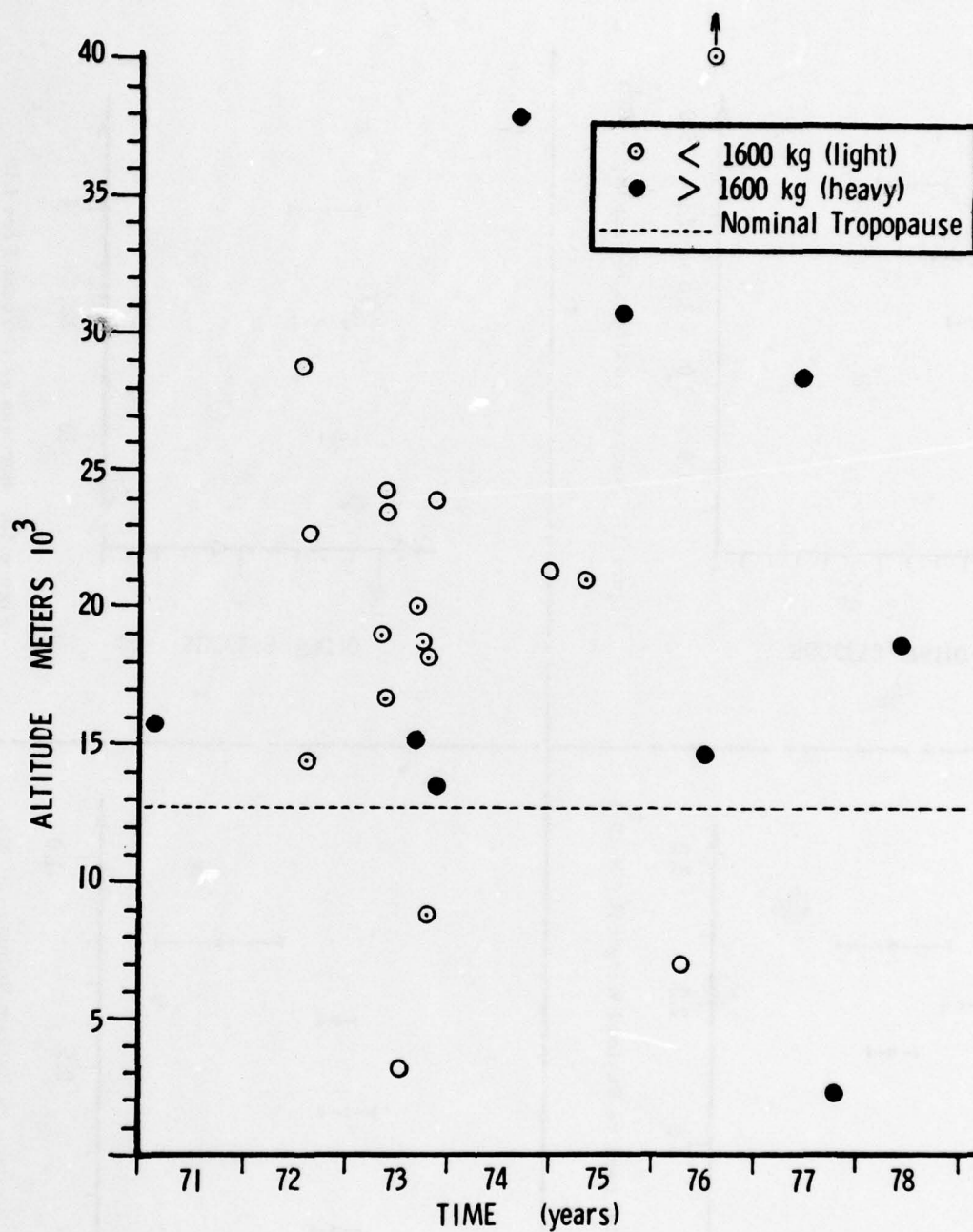


Figure 9. Balloon Failures, Altitude vs Time

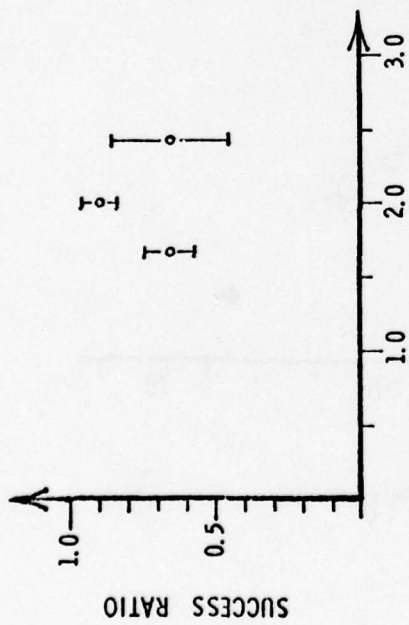


Figure 10. Success vs Payload Weight ($\text{Kg} \times 10^3$)

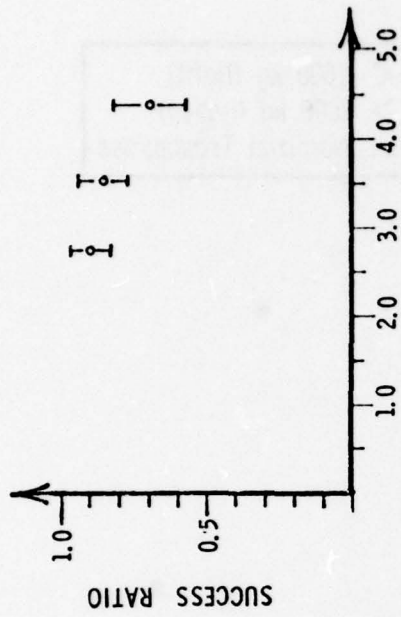


Figure 11. Success vs Gross Weight ($\text{Kg} \times 10^3$)

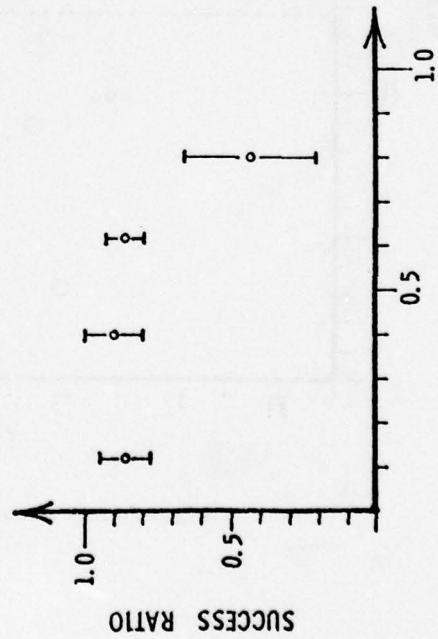


Figure 12. Success vs Balloon Volume (MCM)

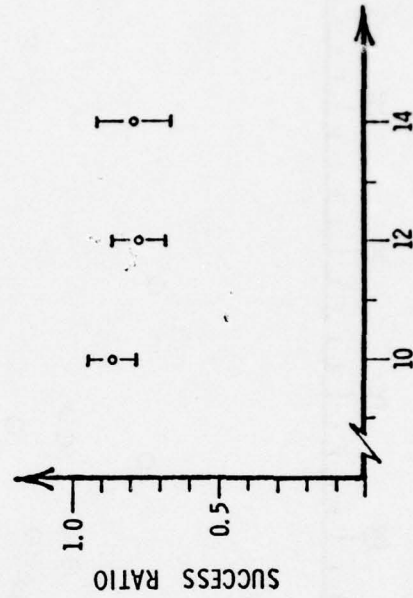


Figure 13. Success vs Percent Free Lift

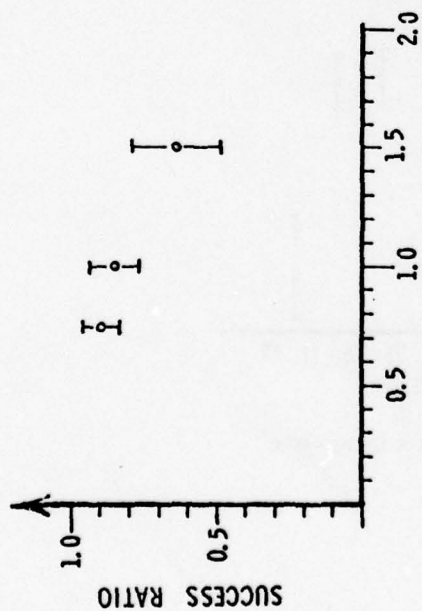


Figure 14. Success vs Shell Thickness (mil)

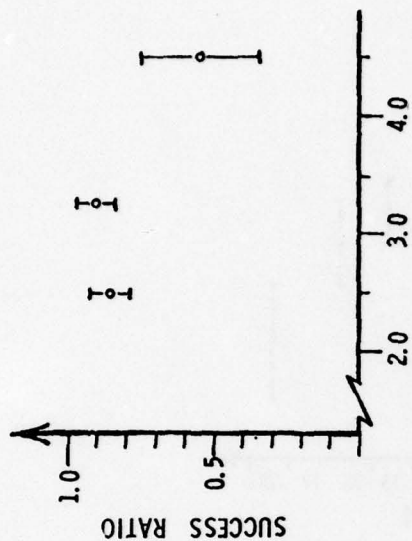


Figure 15. Success vs Top Thickness (mil)
(top equal shell plus all caps)

NO TEST; 75 PERCENT OF ALL HEAVY LIFT
HAD 2 CAPS SO NOT ENOUGH EXAMPLES
OF 1 OR 3 EXIST

NUMBER OF CAPS	SUCCESS			FAILURE		
	3	2	1	3	2	1
3	(1)	—	—	—	—	(1)
2	—	(39)	—	—	—	(9)
1	—	—	(11)	—	—	(1)
0	—	—	(3)	—	—	—

Figure 16. Success vs Caps

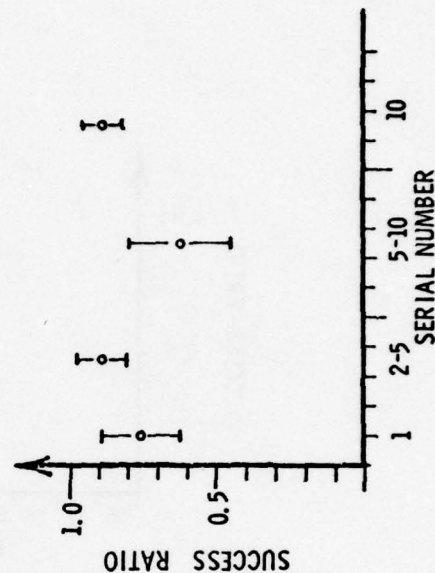


Figure 17. Success vs balloon Serial Number

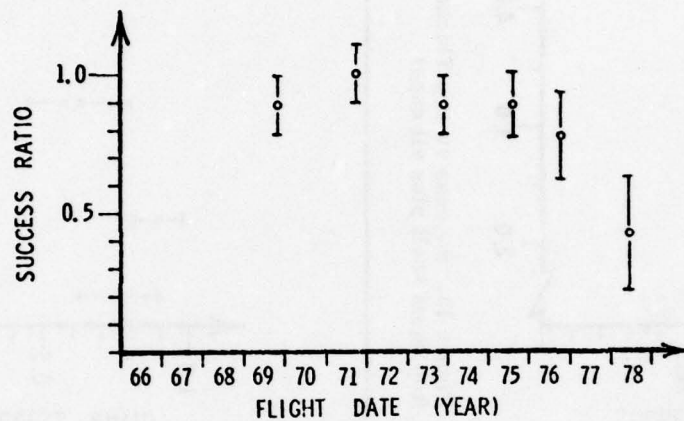


Figure 18. Success vs Flight Date

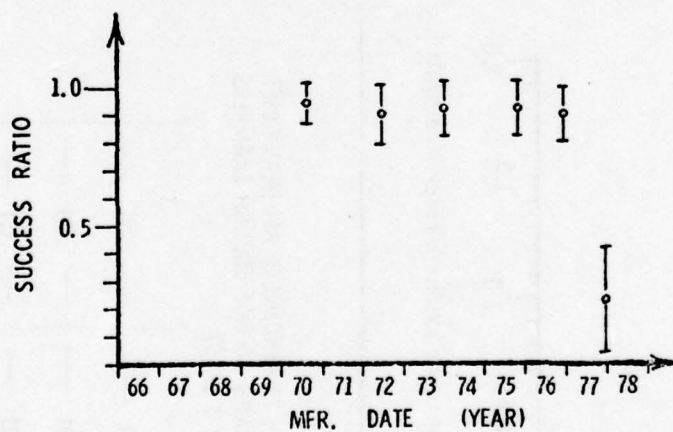


Figure 19. Success vs Manufacturing Date

Table 1. NSBF Balloon Success Record

Year	Total Flights			Payloads > 1600 Kg.			Payloads < 1600 Kg.		
	Total No.	Success No.	Success %	Sub-total No.	Success No.	Success %	Sub-total No.	Success No.	Success %
1972	71	63	89	10	7	70	61	56	92
1973	94	76	80	7	4	57	87	72	83
1974	79	70	89	6	5	83	73	65	89
1975	84	72	86	18	13	72	65	59	89
1976	69	59	86	10	7	70	59	52	88
1977	71	62	87	13	5	39	58	57	98
Totals	468	402	86	64	41	64	404	368	91

Table 2. Flight History of $1.60 \times 10^5 \text{ m}^3$ Fazio Series Balloons

		Fazio Series Balloons						
		1	2	3	4	5	6	7
Flight History	Success	yes	yes	yes	yes	yes	no	no
	Manf. Date	2/75	2/75	3/76	3/76	3/76	3/77	5/77
	Flight Date	6/75	5/75	5/76	4/76	4/77	6/77	5/78
	Flight #	899P	890P	970P	956P	1013P	1023P	1065P
	Payload Wt. (Kg)	2234	2126	2239	2224	2236	2249	2362
	Gross Lift (Kg)	3402	3395	3411	3401	3343	3419	3501
	% Free Lift	14	14	14	14	12	14	12
	Radar Tapes	no	no	no	no	no	yes	yes
	Tropopause Alt. (Km)	14.6	17.6	17.9	19.2	16.5	17.4	18.0
	Trop. Temp. (°C)	-71	-66	-64	-66	-64	-70	-70
	Launch Temp. (°C)	28	23	19	20	18	28	25
	Balloon Wt. (Kg)	750	762	753	760	749	750	763
Ascent Rate (Meters/Min.)	Below 18 Km	356	301	219	258	208	343	261
	Above 18 Km	200	149	146	177	118	154	—

Table 3. NSBF Heavy Lift Balloon History

FLIGHT DATE (Y/M/D)	FLIGHT NO. (P/PALISTONE S/RENOTE)	MANF. (S)SHELDHAHL (R)RAVEN	SER. NO.	MANF. DATE (mm/Yr)	BALLOON VOLUME M ³ × 10 ³	SHELL THICK MIL.	CAP THICK MIL.	PAYLOAD WEIGHT (kg)	PERCENT FREE LIFT	GROSS WEIGHT (kg)	NASA SUPPORT	SUCCESS	FAILURES		COMMENTS	
													MISSION PHASE	FAILURE MODE		
23/3/74	1063-P	W	7	4/77	160.2	1.0	1.5	2362.3	12	3501	yes	—	Ascent	Balloon Burst	Max. alt. 18.6 km	
5/3/75	1063-P	W	6	4/77	1.331.0	0.5	1.2/1.5	2416	12	4749	yes	—	Ground	Launch Dynamics		
19/7/77	1043-P	W	2	1/77	965.2	0.8	1.0/1.0	2232	10	4434	yes	—	Ground	Launch Dynamics		
10/7/77	1041-P	W	6	5/77	612.1	0.9	1.2/1.0	2956	10	5177	yes	—	Ascent	Balloon Leak	Max. alt. 2.1 km	
17/7/77	1040-P	W	5	4/77	612.1	0.9	1.2/1.0	3012	10	5165	yes	—	Ground	Electronics		
19/7/77	142-N	W	4	4/76	594.6	0.6	0.8/0.9	1761	14	3196	yes	yes				
19/7/77	1038-P	W	1	10/76	965.2	0.8	1.0/1.0	1982	12	4346	yes	yes				
5/7/77	140-N	W	2	3/77	1.121.2	0.8	0.9/0.9/0.9	2862	10	5700	yes	yes	Ascent	Balloon Leak	Max. alt. 28.3 km	
1/5/77	1023-P	W	6	3/77	160.2	1.0	1.5	2249	14	3419	yes	—	Float	Balloon Burst	8.5 hours at float	
25/3/77	133-N	W	4	3/77	612.1	0.9	1.2/1.0	2359	12	4502	yes	yes	—			
5/7/77	1018-P	W	3	5/77	628.6	0.8	0.7/0.7	2805	12	4976	yes	yes	Ground	Launch Dynamics		
25/5/77	138-N	W	1	4/77	884.0	0.5	0.6/0.6/0.6	1701	12	3344	yes	—	Ground	Meteorology		
5/5/77	130-N	W	2	3/77	628.7	0.8	0.7/0.7	2389	10	4406	yes	—	Ground	Meteorology		
25/4/77	129-N	W	1	3/77	628.7	0.8	0.7/0.7	2352	12	4486	yes	—	Ground	Meteorology		
4/7/77	1013-P	W	5	3/76	160.2	1.0	1.5	2236	12	3343	yes	yes	—			
10/7/77	222-P	W	1	9/76	696.5	0.9	1.5/1.5	3460	12	6336	yes	yes	Ground	Launch Dynamics		
35/5/76	240-P	W	1	9/76	860.6	0.9	1.5/1.5	3117	14	5938	yes	—	Ground	Launch Dynamics		
4/7/76	126-N	W	2	12/75	594.6	0.6	0.8/0.9	1770	14	3173	yes	yes	Ground	Meteorology		
7/7/76	125-N	W	5	5/76	594.6	0.6	0.8/0.9	1814	12	3193	yes	yes	Ground	Meteorology		
17/5/75	124-N	W	3	-72	753.1	0.7	0.8/0.8	1630	12	3198	yes	yes	Ground	Operations	Max. alt. of good	
5/7/76	123-N	W	3	10/74	735.7	0.6	0.8/0.9	1766	12	3248	yes	yes	Ground	Operations	Max. alt. of good	
10/7/75	117-N	W	2	9/75	593.1	0.5	0.8/0.8	1692	14	2946	yes	yes	Ground	Operations	Max. alt. of good	
9/7/75	116-N	W	1	8/75	593.1	0.5	0.8/0.8	1719	14	2981	yes	yes	Ground	Operations	Max. alt. of good	
7/5/75	115-N	W	25	9/75	587.9	0.8	0.9/0.9	2215	14	4011	yes	—	Ground	Operations	Car Run Up Rain	
9/7/75	114-N	W	50	8/74	328.4	0.7	1.0	1600	14	2623	yes	yes	Ground	Operations	Car Run Up Rain	
9/7/75	112-N	W	4	7/75	435.9	0.7	0.9/0.9	1699	10	2882	yes	yes	Ground	Operations	Car Run Up Rain	
8/7/75	110-N	W	2	6/75	435.9	0.7	0.9/0.9	1782	10	3085	yes	yes	Ground	Operations	Car Run Up Rain	
2/4/75	109-N	W	3	7/75	435.9	0.7	0.9/0.9	1778	10	3128	yes	yes	Ground	Operations	Car Run Up Rain	
9/7/75	108-N	W	1	6/75	594.6	0.6	0.8/0.9	1643	12	2962	yes	yes	Ground	Operations	Car Run Up Rain	
3/5/75	971-P	R	131-R	-72	311.4	1.0	1.0	1681	12	2867	yes	—	Ground	Operations	Car Run Up Rain	
2/5/75	970-P	W	3	3/76	160.2	1.0	1.5	2239	14	3411	yes	yes	Ground	Operations	Car Run Up Rain	
5/7/76	962-P	W	3	3/76	612.1	0.9	1.2/1.0	3097	12	5235	yes	yes	Ground	Operations	Car Run Up Rain	
4/7/76	960-P	W	4	3/76	160.2	1.0	1.5	2264	14	3410	yes	yes	Ground	Operations	Car Run Up Rain	
10/7/75	929-P	W	24	3/75	586.9	0.8	0.9/0.9	2218	14	4019	yes	yes	Ground	Operations	Car Run Up Rain	
31/4/75	926-P	W	23	4/75	587.9	0.8	0.9/0.9	2259	12	3979	yes	—	Ascent	Balloon Burst	Max. alt. 30.8 km	
9/7/75	923-P	W	22	4/75	587.9	0.8	0.9/0.8	2332	12	4067	yes	yes	Ground	Operations	Car Run Up Rain	
23/4/75	922-P	W	2	9/75	612.1	0.9	1.2/1.0	3022	12	5040	yes	yes	Ground	Operations	Car Run Up Rain	
9/7/74	105-N	W	1	8/74	735.6	0.6	0.8/0.9	1652	12	3132	yes	yes	Ground	Operations	Car Run Up Rain	
5/7/75	921-P	W	1	2/75	160.2	1.0	1.5	2234	14	3402	yes	yes	Ground	Operations	Car Run Up Rain	
5/7/75	920-P	W	19	10/73	587.9	0.8	0.9/0.9	2259	14	4012	yes	yes	Ground	Operations	Car Run Up Rain	
5/7/75	919-P	W	2	2/75	160.2	1.0	1.5	2126	14	3395	yes	yes	Ground	Operations	Car Run Up Rain	
5/7/75	918-P	W	1	-75	162.5	1.0	1.0/1.0	2461	10	3688	yes	yes	Ground	Operations	Car Run Up Rain	
5/7/75	917-P	W	1	8/74	612.1	0.9	1.2/1.0	3022	12	5211	yes	yes	Ground	Operations	Car Run Up Rain	
12/7/74	916-P	W	4	9/73	591.7	0.7	0.8/0.8	1730	12	3101	yes	yes	Ground	Operations	Car Run Up Rain	
9/7/74	915-P	W	6	9/73	592.3	0.7	0.8/0.8	1727	12	2855	yes	—	Float	Balloon Leak	13 hours at float	
7/7/74	914-P	W	20	7/74	587.9	0.8	0.9/0.9	2085	8	3682	yes	yes	Ground	Operations	Car Run Up Rain	
2/7/74	910-P	W	18	8/73	587.9	0.8	0.9/0.9	2244	12	3817	yes	yes	Ground	Operations	Car Run Up Rain	
2/7/74	909-P	W	1	6/72	145.5	1.0	1.2	2064	12	3023	yes	yes	Ground	Operations	Car Run Up Rain	
12/7/73	900-P	W	1	-73	151.9	1.0	1.2	2185	12	3324	yes	—	Ascent	Meteorology	Max. alt. 13.4 km	

Table 3. NSBF Heavy Lift Balloon History (Cont)

FLIGHT DATE	FLIGHT NO.	MANF.	MANF. (W) WINZEN (S) SHELDAHL (R) RAVEN	MANF. DATE	BALLOON VOLUME M ³ x 10 ³	SHELL THICK MIL.	CAP THICK MIL.	PAYLOAD WEIGHT (kg)	PERCENT FREE LIFT	GROSS WEIGHT (kg)	NASA SUPPORT	SUCCESS	MISSION PHASE	FAILURE MODE	COMMENTS
10/73	732-P	W	1	9/73	189.1	1.0	1.0/1.5	2867	10	4393	Yes	Yes	Ascent	Burst	Max. alt. 21.1 km
4/73	772-P	R	150	1/73	314.3	1.0	1.5	1610	12	2869	Yes	Yes	Ascent	Burst	Max. alt. 21.1 km
5/73	767-P	W	17	2/73	587.9	0.8	0.9/0.9	2160	10	3783	Yes	Yes	Ground	Operations	
5/73	84-N	W	1	2/73	747.6	0.7	0.8/0.9	1621	12	3175	Yes	Yes	Ground	Operations	
5/73	748-P	W	15	7/73	587.9	0.8	0.9/0.9	2337	12	4054	Yes	Yes	Ground	Operations	
4/73	739-P	W	7	7/73	145.5	1.0	1.2	2032	12	2988	Yes	Yes	Ground	Operations	
11/72	720-P	W	11	2/72	587.9	0.8	0.9/0.9	2384	12	4111	Yes	Yes	Ground	Operations	
10/72	714-P	W	1	3/72	559.5	1.0	1.5/1.5	2792	10	4938	Yes	Yes	Ground	Operations	Parachute Failure
10/72	713-P	W	8	7/72	145.5	1.0	1.2	2117	10	3037	Yes	Yes	Ground	Operations	
10/72	709-P	W	13	8/72	587.9	0.8	0.9/0.9	2101	12	3798	Yes	Yes	Ground	Operations	
9/72	707-P	W	7	7/72	587.9	0.8	0.9/0.9	2223	12	4019	Yes	Yes	Ground	Operations	
9/72	706-P	W	14	9/72	589.0	0.8	0.9/0.9	2063	12	3743	Yes	Yes	Float	Electronics	Parach. Com. Failed
9/72	698-P	W	12	7/72	589.0	0.8	0.9/0.9	2058	9	3681	Yes	Yes	Ground	Operations	
7/72	663-P	W	3	7/72	535.1	1.5		3368	10	6352	Yes	Yes	Ground	Operations	
2/72	661-P	W	10	7/72	589.0	0.8	0.9/0.9	2028	8	3597	Yes	Yes	Ascent	Reeling Sleeve	Max. alt. 15.8 km
2/72	660-P	W	2	7/72	194.5	1.8	1.8/1.8	4264	10	7258	Yes	Yes	Ground	Operations	
5/71	612-P	W	1	7/71	194.5	1.8	1.8/1.8	3801	11	6971	Yes	Yes	Ground	Operations	
9/71	629-P	S	12	7/71	158.0	GT - 11	G.T. 12	4845	14.2	7259	Yes	Yes	Ground	Operations	
5/71	615-P	W	2	7/71	753.1	0.7	0.8/0.8	1787	12	3381	Yes	Yes	Ground	Operations	
5/71	614-P	W	8	7/71	589.0	0.8	0.9/0.9	1773	12	3510	Yes	Yes	Ground	Operations	
5/71	609-P	W	4	7/71	589.0	0.8	0.9/0.9	2245	10	3960	Yes	Yes	Ground	Operations	
5/71	607-P	W	323	7/71	300.1	1.0	1.5	1764	10	3026	Yes	Yes	Ground	Operations	
10/71	637-P	W	9	7/71	589.0	0.8	0.9/0.9	2046	8	3654	Yes	Yes	Ground	Operations	
2/71	594-P	W	330	6/71	300.1	1.0	1.5	1860	8	3060	Yes	Yes	Ground	Operations	
3/70	536-P	W	2	7/70	300.1	1.5	1.0	1983	10	3514	Yes	Yes	Ground	Operations	
3/70	517-P	S	70	7/70	148.8	GT - 11		3538			Yes	Yes	Ground	Operations	
7/70	512-P	W	3	7/70	300.1	1.5	1.0	2080	10	3623	Yes	Yes	Ground	Operations	
9/70	590-P	W	5	7/70	589.0	0.8	0.9/0.9	2208	10	3924	Yes	Yes	Ground	Operations	
9/70	535-P	W	6	7/70	589.0	0.8	0.9/0.9	2329	10	4108	Yes	Yes	Ground	Operations	
6/69	486-P	W	58	6/69	82.1	2.0		1918	8	2689	Yes	Yes	Ground	Operations	
8/62	493-P	W	331	6/69	300.1	1.0	1.5	1674	10	2916	Yes	Yes	Float	Balloon Leak	2-hr. at float
9/69	498-P	W	1	6/69	57.4	1.5	1.5	1592	10	2406	Yes	Yes	Ground	Operations	
9/69	492-P	W	329	6/69	300.1	1.0	1.5	1701	10	2954	Yes	Yes	Ground	Operations	
11/68	440-P	S			86.4	GT - 11		2225	12	3418	Yes	Yes	Ground	Operations	
10/67	363-P	W	1	6/7	3.1	2.0		1803	15	2762	Yes	Yes	Ground	Operations	
10/66	261-P	S			90.6	GT - 11		2032	15	3460	Yes	Yes	Ground	Operations	
11/66	265-P	S			90.6	GT - 11		2036	15	3460	Yes	Yes	Ground	Operations	
10/66	255-P	W			4.2	GT - 12		2004	15	2971	Yes	Yes	Ground	Operations	

* Mission completed, lost payload

Contents

1. Introduction
2. Vehicle Development
3. Sky Anchor Balloon History
4. Sky Anchor System
5. Test Flights
6. Summary

DEVELOPMENT OF THE SKY ANCHOR BALLOON SYSTEM

I. Steve Smith, Jr.*
National Scientific Balloon Facility
Palestine, Texas

ABSTRACT

With the development of large plastic balloons in the early 1950's, the scientific research balloon has become the "poor man's" satellite platform. Zero pressure balloons, fabricated from polyethylene materials, offer good load carrying capability, however, due to ballasting requirements, have limited flight durations of hours or a few days. The demand for exposure periods of several days, weeks, or months for many scientific experiments has prompted the development of globe-circling balloons capable of floating for extended periods of time. Large unreinforced super pressure balloons, although very stable, have lower payload-carrying capabilities and little

* The National Scientific Balloon Facility is operated by the University Corporation for Atmospheric Research under sponsorship of the National Science Foundation.

safety factor for surviving for extended periods of time. The work of the National Scientific Balloon Facility (NSBF) towards the development of a tandem zero pressure - super pressure balloon system (Sky Anchor) that will accomplish the goal of sustaining a 500 lb payload at 130,000 feet for 100 days is discussed.

1. INTRODUCTION

Surveys conducted by the National Scientific Balloon Facility (NSBF) of the scientific community have shown that nearly all balloon-borne scientific investigations could benefit from longer exposure at altitude. Since present zero pressure (ZP) balloons allow an average time at float of only several hours, a great deal of information could be gained by extending the flight time. The polls taken of the scientific users revealed that a vehicle should be developed with the capability of supporting a 500 lb payload at 130,000 ft for a minimum of 100 days duration.

From these requirements, a proposal was written to the National Science Foundation (NSF) which resulted in a contract being awarded for a two year study program. Funding for this program officially started at the start of FY 1975.

There are two basic techniques for extending the float duration of a balloon. One method is the use of the normally flown "natural shape" unpressurized balloon or ZP balloon, utilizing its heavy lift capability to support a heavy ballast load. The ZP balloon is vented to the atmosphere to valve off excess lifting gas to prevent overpressurization of the balloon, thus requiring the dropping of ballast each night, (approximately 7% of the gross system's mass), to compensate for descent caused by the nighttime cooling of the gas. However, flight durations using this method are only

feasible for 5-8 days, soon becoming unfeasible due to the large ballast requirements.

The second method of achieving increased flight duration is to fly a pressurized balloon capable of withstanding high skin stress caused by over-pressurization from warm daytime gas temperatures. Balloons of this type require no diurnal ballasting, and, due to the material properties which enable the balloon to withstand the high skin stress, very good altitude stability results as long as enough overpressure is maintained in the balloon to prevent going slack at night.

Based upon the experience, knowledge, and success which had been achieved by the NCAR GHOST program, the initial NSBF approach was to scale up the already existing smaller unreinforced polyester super pressure spheres. Preceding the official start of the program in FY 1975, several scaled-up versions of unreinforced polyester spheres were attempted with varying degrees of success. The purpose of these flights was to establish design parameters for which larger balloons could be built.

2. VEHICLE DEVELOPMENT

With the start of funding in FY 1975, test flights were continued utilizing unreinforced polyester spheres. Several design changes were incorporated with each successive flight to improve the structural integrity of the system. Tremendous amounts of data were taken including such parameters as load-line loads at launch, ascent, and float, balloon gas temperatures, balloon skin temperatures, balloon strain, balloon pressure, earth albedo measurements, black ball temperatures, ambient air temperatures, altitude stability, and various other parameters. Four unreinforced polyester super-pressure sphere test flights were conducted, again with varying degrees of

success. In addition to these test flights, various other test flights were conducted utilizing ZP balloons to obtain additional radiometric data and design changes.

A great wealth of information was obtained from these test flights regarding balloon design and fabrication, thermodynamics and balloon loads. However, from these flights and various study contracts that were on-going at the same time, one major problem area became evident: the use of unreinforced polyester film (Mylar-Celanar) as the material in large super pressure balloons.

Unreinforced polyester film has been used in various applications in ballooning for many years, the most significant use being in the NCAR GHOST program. However, most balloons fabricated from this material were small in size and the film gauge was fairly large compared to gauges that would have to be used to meet long-duration program goals if a single cell super pressure balloon were used. The thicker film previously used is a significant factor when it is considered with present methods of fabrication, shipping, and handling. The reason why most failures occur in the lighter gauge film can be explained if we consider just the handling or fabrication of a balloon. During fabrication, the film is handled extensively, which causes damage to the film and a decrease in film strength. The thicker the material, the less damage in the form of cracks and holes occurs, because due to the greater thickness the induced stresses from handling are lower. It would take a much greater force to cause the same damage as the lighter gauge film sees. This reasoning can also be applied to launch, ascent, and pressurization, which would explain why the heavier gauge film is more likely to survive. However, due to the large balloon sizes that are

required to meet program objectives, thicker gauge films are unfeasible for single cell super pressure balloons.

Another major drawback which enters in results from the thermodynamics of the balloon system at float. In order for a "super pressure" to achieve long duration, it must survive the worst possible environmental conditions that it may fly over during the mission, and maintain overpressure. In order to do this, large daytime stresses result which closely approach the yield point of polyester film. Anytime there is a discontinuity in the film, cut-out, crack, or hole, higher stresses result in that region. Often, this stress is then beyond the yield point of the material if the envelope is already highly stressed. Therefore, failure will occur. This is very significant when considering a very large sphere with a very large surface area. The chances of a flawless balloon are astronomically low.

There are various methods that can be used to possibly remedy this situation. One method is to use a system which will allow lower operating pressures and allow thicker gauge polyester which is more resistant to damage. Such a method can be utilized in the Sky Anchor System which will be discussed later. Another method is to use a completely different material which has better handling characteristics and crack-propagation resistance. This could be in the great circle load-tape design which utilizes nylon-12, stemming from the Winzen study that is currently being conducted. One other method which is also being pursued is the fabrication of a composite material utilizing a thin-gauge polyester film with an aramid fiber net bonded to it. However, much work is still required in understanding aramid fibers. Presently the major developmental emphasis is on the Sky Anchor System with the Sheldahl Kevlar-polyester composite material, -- the Winzen approach being a longer term approach.

3. SKY ANCHOR BALLOON HISTORY

As the Boomerang test flights progressed, it became increasingly evident that unreinforced polyester film could not be fabricated into a single-cell super pressure spherical balloon to achieve long-duration program goals and still have a high degree of reliability. This therefore necessitated a different approach to the problem.

In December 1975, instigated by a request from Britain's Science Research Council (SRC), the NSBF undertook a more detailed study of the possibility of a hybrid zero-pressure - super pressure balloon system which would require no diurnal ballasting. Upon further investigations by the NSBF, it was found that various air-ballast systems have been devised over the years, many requiring a variety of motors, blowers, winches, ducts and high-pressure containers which are used to counter the effects of sunset and the subsequent loss of gas from a zero pressure balloon if the suspended payload is changed. Due to the need for power on these systems and the requirement to remain aloft for an indefinite period of time, a passive system is very attractive. The survey of these various techniques by Davidson (1967) contained a great deal of information on the performance of these various systems.

The Sky Anchor concept has been credited to NCAR (1963) with this being the only successful flight until recently. On August 5, 1963, a Sky Anchor flight was launched from the NCAR grounds at Boulder, Colorado. The top balloon was a 0.5 mil polyethylene balloon 18 feet in diameter and weighing 4 lbs. The "anchor" balloon was an 8-foot diameter, bi-laminated Mylar sphere weighing 2.5 lb. The payload was a .8 lb timer set for 72 hours. The Mylar balloon by itself could carry this payload only to an altitude of 47,000 feet. However, the amount of air sealed into the Mylar balloon was metered to provide

super pressure at 56,000 feet, with flight altitude computed to be 63,000 feet in the daytime and 58,000 feet at night. The balloon system flew for two days at the design altitudes through two sunsets - a remarkable achievement for an "unballasted" zero pressure balloon. Failure to achieve the full 72 hours flight time was attributed to gas loss in the zero pressure balloon, since it evidenced some gas loss prior to flight when held inflated overnight.

The next two attempts utilizing a Sky Anchor System were undertaken by the Air Force Cambridge Research Laboratories in 1968. The first flight utilized a .75 mil polyethylene main balloon, 39,300 ft³ in volume. The ballast balloon was a 24.4-foot diameter "super pressure" constructed from 3-mil tri-laminate Mylar. Launch of the system went very smoothly. However, ascent of the system was faster than expected, reaching 1,320 feet per minute after initially passing through the tropopause at 43,000 feet. It was calculated for this flight that with the proper amount of helium in the anchor balloon, the anchor balloon would begin pressurization at 61,900 feet and reach full pressure at 70,000 feet. However, the anchor balloon had been overfilled and began pressurization at approximately 52,000 feet at a much faster rate than anticipated. At 58,400 feet, the anchor balloon over pressurized and burst.

The second flight consisted of a 15.6-foot diameter, 3-mil thick tri-laminated Mylar super pressure anchor balloon. The main balloon was a 2-mil polyethylene cylinder balloon with a gore length of 99.75 feet. Because of the experience with the first flight, the helium was metered into the anchor balloon so that a more accurate quantity of helium was in the balloon at launch. In addition, a lower amount of free lift was used in the main balloon allowing for a slower ascent rate. Launch and ascent were nominal with a 57,000-foot calculated fill altitude being achieved. It was discovered,

shortly after the anchor balloon began pressurization, that the pressure was not holding, indicating that the anchor balloon was leaking. After reaching a ceiling altitude of 69,600 feet and the anchor balloon depressurizing, the flight was terminated.

4. THE SKY ANCHOR SYSTEM

The Sky Anchor System is a super pressure balloon carried aloft by a zero pressure main balloon to its operational altitude during the day as shown in Figure 1. On the way to the main balloon's operational altitude, the "super pressure" becomes filled and pressurizes. As the "super pressure" continues to be carried upward it loses more and more lift. When sunset occurs the entire system descends to a new equilibrium altitude where the increase in lift on the super pressure balloon just equals the sunset effect on the main balloon. Although its volume is decreased, no gas is lost from the main balloon. At sunrise, the main balloon will expand and the system will once again rise. In so doing the super pressure balloon will lose the lift that it gained at sunset and the system should stabilize at the same altitude as the preceding day. Since there is no change in suspended weight on the main balloon, it should not overshoot and again there will be no loss of gas. As in the pure super pressure system, the flight duration will be limited only by creep, gas diffusion and ultraviolet degradation, assuming there are no leaks.

During the early stages of investigation of the Sky Anchor System a design feasibility program was developed by Rand (1976) at Texas A & M University under its contract with the NSBF. From this study, the advantages of a Sky Anchor System over a single-cell super pressure balloon becomes obvious as can be seen in Figures 2, 3 and 4. Although these results are for anchor balloons that are stressed up to 10,000 psi and are optimized, the effects of a lower operating skin stress can be seen in Figure 5. The ballast effect

produced is the entire amount required to maintain constant altitude. Since the balloon system must drop some in altitude to obtain this effect, it therefore means that these numbers are somewhat conservative since, by dropping in altitude, less ballast is required. It should be noted that the size of anchor balloons required for a daytime float at 120,000 feet and a 2-mb excursion at night is already within the state-of-the-art. It should also be noted that for operations up to 140,000 feet, these balloons are also within the state-of-the-art.

With the results obtained from the various studies conducted on the system during 1976, it was decided to conduct test flights of the system. The following are flights which have been conducted by the NSBF to date (see Table 1).

5. TEST FLIGHTS

5.1 Sky Anchor I

In January 1977, the test flight of Sky Anchor I was conducted from Page, Arizona. The system consisted of a 4.13-MCF zero pressure balloon, a 540-lb payload, and a 1.25-MCF super pressure*. The launch and initial ascent went as expected except for a slightly higher ascent rate than desired. The reefing system had started to deploy properly and at approximately 33,000 feet visual was lost due to clouds. At approximately 52,000 feet a sudden drop in altitude was registered. The system then continued to ascend to a float altitude of 119,000 feet. After obtaining several visual sightings that the super pressure had failed, the flight was terminated in Colorado. Down cameras revealed that the reefing sleeve slit all the way down the balloon thus allowing the sphere to open up into a gigantic sail. At this altitude a shear was encountered which, due to the sailing balloon, probably caused severe loading and failure.

*balloon

After the test flight of Sky Anchor I, theoretical work continued on the system. Studies were conducted to correct the system-dynamics computer programs already developed and take into account the fact that for normal conditions, 7-8% ballast is not required if the system is allowed to drop some in altitude at night. Preliminary results have indicated, depending upon the excursion requirements, that 4-5% is sufficient. The impact is very important since the ballast sphere size decreases significantly.

Several design changes were made stemming from the Sky Anchor I flight which were applied to future Sky Anchor flights. Some of the basic changes are as follows:

- A. Shorten the ballast sphere-payload tether line so that there is a smaller shear velocity gradient between the ballast sphere and the main zero pressure balloon.
- B. Utilize a bottom load attachment harness with some pressurization ballast to help "string out" the sphere to prevent sailing (rather than a reefing system).
- C. Utilize a valve in the top of the main zero pressure balloon to valve off some free lift so that a slow ascent rate can be maintained.
- D. Use a lower percentage of free lift in the main balloon.

5.2 Sky Anchor II

In May 1977, the test flight of Sky Anchor II was conducted from Palestine, Texas. The system consisted of a 0.5-MCF zero pressure balloon, a 320-lb payload, and a 70.2-foot diameter super pressure balloon. Instrumentation included altitude monitoring, two (2) super 8-mm surveillance cameras, one (1) super pressure strain gauge, and one television camera on the main package for live, on-board coverage of the balloon system and cloud cover.

The launch and ascent were as expected with an average ascent rate of 500 feet/second. The balloon system achieved a float altitude of 94,400 feet. The system was allowed to float for 47 hours, through two nights, without ballasting, before being terminated, with the package being recovered in excellent condition. The flight was very successful, thus making it the largest system of its kind ever to have successfully flown.

5.3 Sky Anchor III

In June 1977, the test flight of Sky Anchor III was conducted from Grenada, Mississippi. The remote site was chosen due to the high winds at the float altitude which would not allow sufficient float time from Palestine. The balloon system consisted of a 4.13 MCF zero pressure balloon, a 514 lb payload and a 1.25 MCF super pressure balloon.

The launch of the system went smoothly. However, when the tow balloon, above the super pressure balloon, was cut away at approximately 3,000 feet the ascent stopped. Ballast was then dropped to aid the ascent. The pilot reported a large hole in the wall of the super pressure balloon. The flight was then terminated when the balloon system was over a satisfactory recovery zone. Investigations revealed that when the tow balloon was cut away, the primer cord destruct was activated thus destroying the super pressure balloon. Instrumentation included 2 super 8-mm movie cameras, a load cell, altitude monitors, differential pressure gauge, and a television camera for real time visual monitoring of the system.

Investigation into the failure yielded two possibilities of failure. One was the possibility of a short to the PCM Command Package located between the tow balloon and the top of the super pressure balloon. The other possibility was that of a static discharge. To correct the problem for future flights the command box was moved to the base of the super pressure balloon along with

the bottom ballast container.

5.4 Sky Anchor IV

In September 1977, a test flight from Palestine, Texas, of another small Sky Anchor balloon system was attempted utilizing a 0.5 MCF zero pressure balloon, a 346 lb payload, and a 70.2 foot diameter super pressure balloon. The purpose of the flight was to provide more launch experience for the launch crews and to obtain more system dynamic behavior to verify changes in the Sky Anchor models. Instrumentation included altitude monitoring, two (2) super 8-mm surveillance cameras, one (1) super pressure strain gauge, one (1) television camera, and one (1) Satellite Transit Receiver for position.

The layout and inflation of the balloons went very smoothly. A wind direction change occurred approximately 10 minutes prior to launch. Then, when the main balloon was launched, the cross wind carried the payload and tether in a direction different from that the system was laid out for. The tether line then snagged on the corner of the super pressure spool trailer which was protruding several feet out. The flight was then terminated. Steps to remedy the fouling of the tether line resulted in the fabrication of a low profile launch spool and the addition of PIBALS to aid in the lifting of the tether line.

5.5 Sky Anchor V

In October 1977, the test flight of Sky Anchor V was conducted from Palestine, Texas. The system consisted of a 4.13 MCF zero pressure balloon, a 516 lb payload, and a 1.25 MCF super pressure balloon. Instrumentation included altitude monitoring, two (2) super 8-mm surveillance movie cameras, a differential pressure gauge, air temperature monitoring, and video camera for real-time visual monitoring of the system.

The launch of the system went very smoothly. Shortly after launch the balloon system slowed due to an inversion, but after breaking through it started ascending at the planned 500 feet/second. At approximately 19,000 feet it was noticed that the super pressure balloon was being destroyed. Shortly after this the system failed and the flight was terminated.

After reviewing the video tapes and down camera film it became obvious that the balloon destruct had prematurely activated itself. The electronics were then inspected and it was found that damage had occurred to the terminate electronics and the main electronics package above. After reviewing a large number of possible causes it was concluded that a static discharge was the only cause that could generate enough voltage to cause the damage that had occurred. Steps have since been taken to help try to eliminate the problem by electrically isolating the destruct electronics from any other electronics.

5.6 Sky Anchor VI

In May 1978, the test flight of Sky Anchor VI was conducted from Malden, Missouri. The system consisted of a 4.13 MCF zero pressure balloon, a 578 lb payload, and a 1.25 MCF super pressure balloon. Instrumentation included altitude monitoring, a differential pressure gauge, air temperature monitoring, down radiometer, transit receiver, and GOES satellite platform.

The launch of the system occurred just prior to sundown. Shortly after launch the bottom pressurization ballast had to be dropped to counteract an inflation error. The balloon then continued to altitude. The super pressure anchor balloon started over-pressuring at 111,000 feet as predicted and the system continued to climb to a ceiling of 114,000 feet. The system was allowed to float at this altitude during the night with plans to continue slowly pressurizing the system after sunrise the next day. After sunrise the skin stress

in the anchor balloon reached approximately 4,000 psi and started to stabilize. The dropping of the top liquid ballast was then initiated to bring the anchor balloon up to a calculated skin stress of 7,500 psi. However, at the start of the third drop, the anchor balloon catastrophically failed at a skin stress of approximately 4,200 psi. The system then climbed to an altitude of 119,000 feet and was later terminated.

Upon inspection of the remnants of the balloon it was found that one of the 36-inch diameter load rings had become shifted at some point in time. It was reasoned therefore, that this would have possibly loaded one side of the "super pressure" highly, thereby possibly causing failure. Steps were taken to prevent further occurrence of this problem, and another flight was sheduled approximately two weeks later.

5.7 Sky Anchor VII

In May 1978, the test flight of Sky Anchor VII was conducted from Palestine, Texas. The system consisted of a 4.13 MCF zero pressure balloon, a 550 lb payload, and a 1.25 MCF super pressure anchor balloon. Instrumentation included altitude monitoring, a differential pressure gauge, air temperature monitoring, down radiometer, one video camera, and two super 8-mm surveillance cameras.

The launch of the system was conducted at sunrise and went smoothly despite a 90-degree cross wind to the layout direction of the system. Ascent averaged around 600 feet per minute to a fill altitude of the anchor balloon of approximately 111,000 feet. The system then leveled off at approximately 112,000 feet. The bottom pressurization ballast was then dropped to slowly bring the anchor balloon up to a skin stress of approximately 4,800 psi. With this completed, the balloon system was allowed to stabilize and once having done so, the top liquid ballasting was started. However, on the very first

drop, the anchor balloon catastrophically failed. The system then climbed to approximately 119,000 feet and was later terminated. Figures 6 and 7 show the pressurization and altitude plots for the flight.

After recovery of remnants of the balloon, the prime cause of failure is suspected to be the liquid ballast. When taken together with the failure of the Sky Anchor VI system it is a very probable cause. To correct this problem future flights will carry no top liquid pressurization ballast. This will necessitate a slight increase in the bottom pressurization ballast located at the base of the "super pressure."

6. SUMMARY

Three more large systems will be flown beginning this fall with one or two smaller systems also. It is felt that by correcting the ballast problem on the large systems, the prospects for success are very promising. The NSBF feels that although the Sky Anchor System provides a slightly higher degree of difficulty in launching, the system should offer a higher reliability and greater payload-carrying capability over single-cell super pressure balloons. Coupled with current developmental programs in materials and super pressure design, a more reliable and larger single-cell super pressure balloon should become feasible. It is currently within the state-of-the-art of super pressure balloons to fly a 2,000 lb payload to 120,000 feet. With further advances in super pressure design and materials, this goal can soon be realized. The NSBF will pursue these goals of providing larger long-duration balloon vehicles.

References

- Davidson, Allen R., Jr. (1967) A Survey of Methods for Controlling the Altitude of Free Balloons with Air Ballast Systems, AFCRL-67-0372, Scientific Report No. 1, Contract F19628-67-C-0192, Vitro Laboratoires.
- Davidson, Allen R., Jr. (1968) Development and Testing of Air Ballast Systems, AFCRL-68-0556, Final Report, Contract F19628-67-C-0192, Vitro Laboratories.
- Lally, Vincent E. (1967) Super Pressure Balloons for Horizontal Soundings of the Atmosphere, NCAR-TN-28, National Center for Atmospheric Research, Boulder, Colorado.
- Munson, James B. (1975) Preliminary Design Report for the Long Duration Platform Vehicle, NCAR Subcontract No. S5007, Sheldahl, Inc.
- Rand, James L. (1976) Long Duration Balloons, Report 7, Proceedings, Ninth AFGL Scientific Balloon Symposium, AFGL, Hanscom Field, Mass.
- National Center for Atmospheric Research (1963), Air is Ballast in "Sky Anchor" Concept NCAR 1-73, Texas Engineering Experiment Station.
- National Scientific Balloon Facility (1974), Technical Proposal - Long Duration Ballooning Development, National Scientific Balloon Facility, Palestine, Texas.

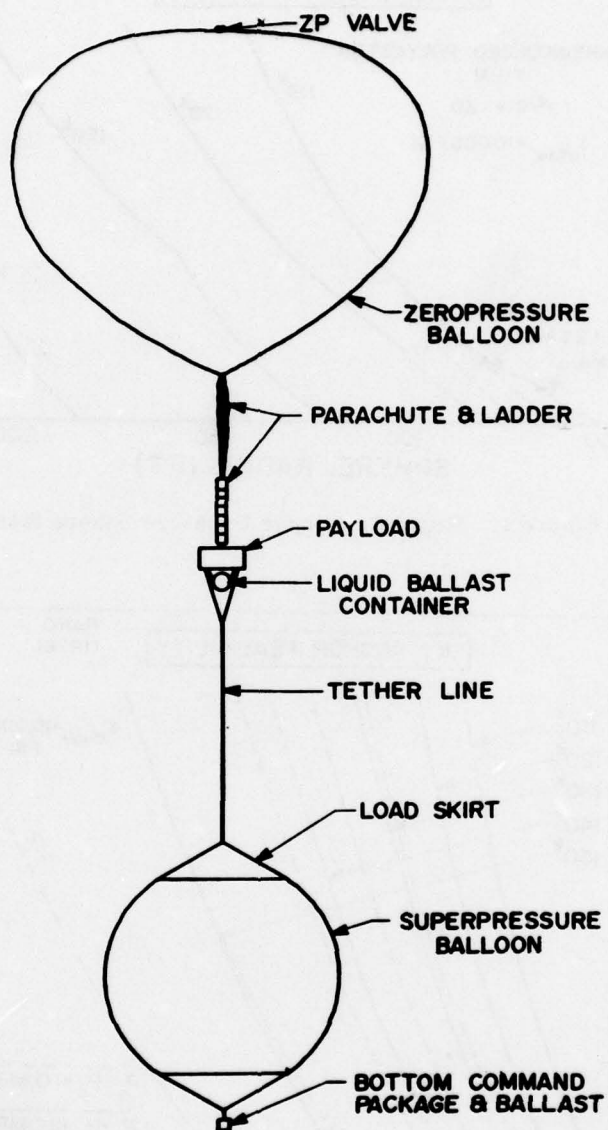


Figure 1. Sky Anchor Profile

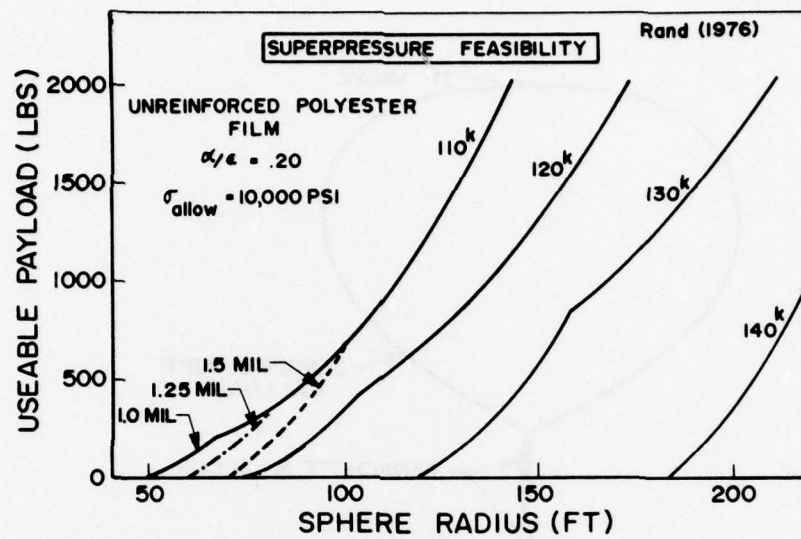


Figure 2. Single Cell Super Pressure Sphere Size

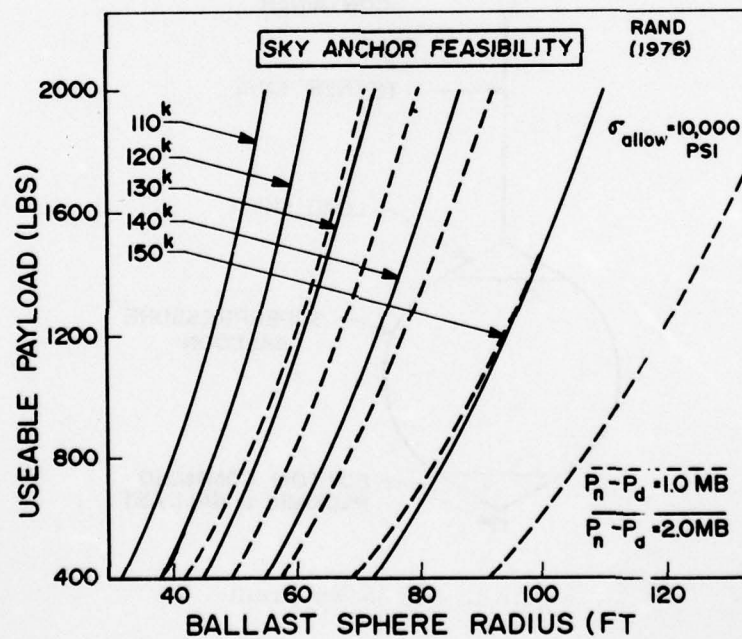


Figure 3. Sky Anchor Ballast Sphere Size

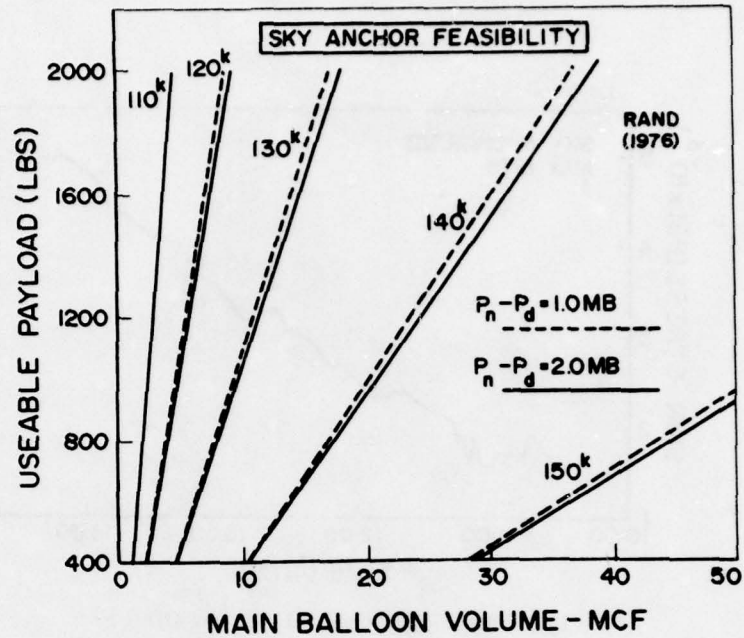


Figure 4. Sky Anchor Main Balloon Size

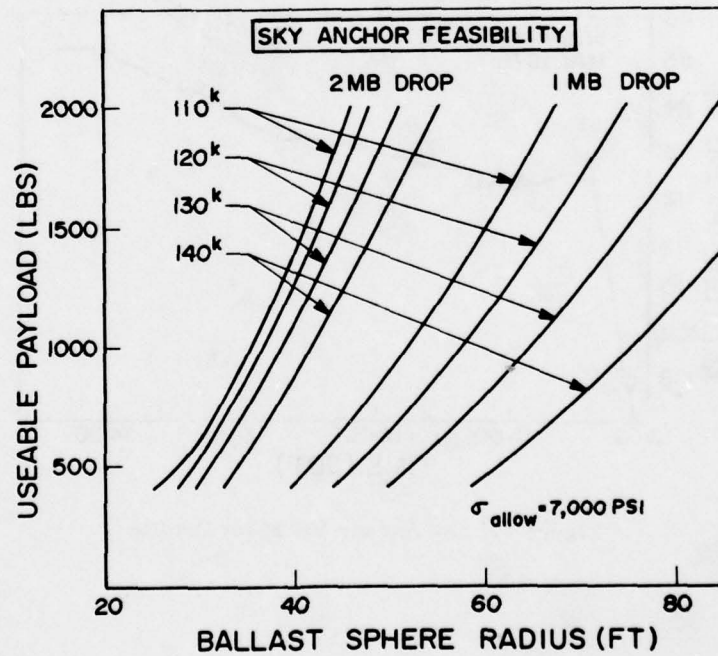


Figure 5. Sky Anchor Ballast Sphere Size - 7,000 PSI Allowable Stress

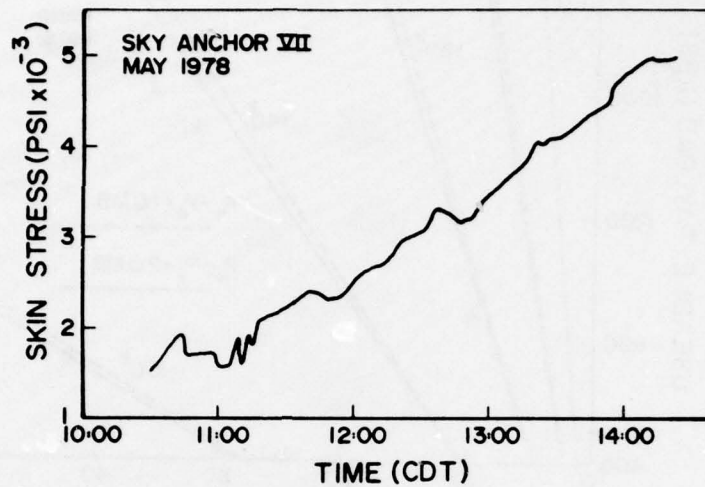


Figure 6. Sky Anchor VII Stress History

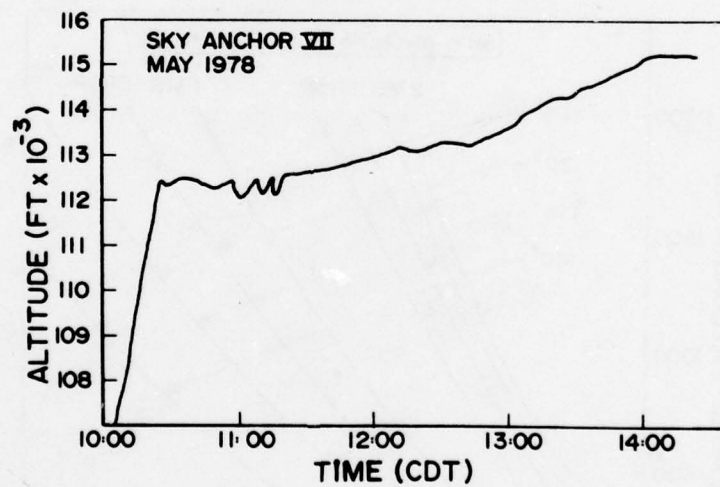


Figure 7. Sky Anchor VII Float Profile

AD-A074 469

AIR FORCE GEOPHYSICS LAB HANSCOM AFB MA
PROCEEDINGS OF THE AFGL SCIENTIFIC BALLOON SYMPOSIUM (10TH) HEL--ETC(U)
MAR 79 C L RICE

F/G 1/3

UNCLASSIFIED

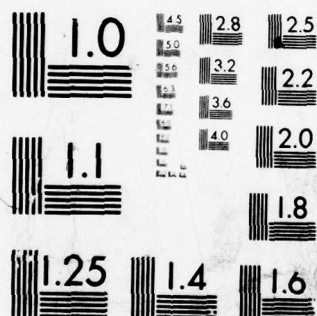
AFGL-TR-79-0053

NL

2 OF 6

AD
A074469





MICROCOPY RESOLUTION TEST CHART
NATIONAL BUREAU OF STANDARDS-1963-A

FLIGHT	ZP MAIN BALLOON				TOW BALLOON		SP ANCHOR BALLOON			Payload LBS.
	VOL. (MCF)	T, SHELL	T, CAP	MAT'L.	VOL. (MCF)	T, SHELL	VOL. (MCF)	T, SHELL	MAT'L.	
SA I	4.13	0.5	0.6	STRAT.	.006	1.5	1.25	1.5	.75 x .75 Celanar	540
SA II	0.5	.75	—	X-124	.006	1.5	.181	2.0	1 x 1 Celanar	320
SA III	4.13	0.5	0.6	STRAT.	.014	1.5	1.25	1.5	.75 x .75 Celanar	514
SA IV	0.5	.75	—	X-124	.006	1.5	.181	2.0	1 x 1 Celanar	346
SA V	4.13	0.5	0.6	STRAT.	.014	1.5	1.25	1.5	.75 x .75 Celanar	516
SA VI	4.13	0.5	0.6	STRAT.	.014	1.5	1.25	1.5	.75 x .75 Celanar	578
SA VII	4.13	0.5	0.6	STRAT.	.014	1.5	1.25	1.5	.75 x .75 Celanar	550

Table 1. NSBF Test Flights of the Sky Anchor Balloon System

ABSTRACT

LARGE SUPERPRESSURE BALLOONS - HERE AND NOW STATE OF THE ART

Jarvis Lehmann
National Scientific
Balloon Facility
PO Box 1175, Palestine
Texas 75801

A brief history of superpressure balloons up to the initiation of the long duration program in 1974, and a chronological listing of the development of the superpressure balloon as a long duration platform vehicle are presented. Initial design decisions, design configurations, material, manufacturing, packaging, launching, flight data and performance are also discussed.

Test flights of superpressure balloons as large as 60 meters in diameter, payloads up to 160 kg and altitudes of 36.5 kilometers have been conducted. Evaluation of this flight data indicates that present day superpressure balloons are capable of supporting 160 kg payloads at an altitude of 30 kilometers.

Contents

1. Introduction
2. Background
3. ALBS Prototype Test Configuration
4. The Parachute System Test Program Results
5. The Holloman AFB White Sands Missile Range Drop Test
6. Summary and Conclusions

The Air Launched Balloon System (ALBS) Flight Test Program

Andrew S. Carten, Jr.
Air Force Geophysics Laboratory
Hanscom AFB, MA 01731

Abstract

The background and previous development history of the ALBS project are reviewed briefly. The fourteen test flights carried out at the National Parachute Test Range (NPTR) in 1977 to qualify the parachute subsystem are described in some detail with emphasis on configuration changes resulting from problems experienced at the NPTR. Preparations for the key test of the complete, "live" ALBS system over the White Sands Missile Range in January 1978 are then outlined and the rationale for the chosen system configuration is given. The events surrounding the launch of the test system from Truth or Consequences, NM, including the malfunction of the carrier balloon and the subsequent destruction of the cryogenic unit are recounted. A discussion of plans for future work on the project closes out the presentation.

1. INTRODUCTION

NOTE

This paper has been abstracted from the final technical report IHWU66651101.¹

1. Carten, A.S., Jr. (1978) Flight Tests of the Air-Launched Balloon System (ALBS) Prototype Model, AFGL-TR-78-0074.

At the Ninth AFGL Scientific Balloon Symposium, the author presented a paper² which outlined the goals of the ALBS development program, revealed its past history and accomplishments to date and described plans for forthcoming flight tests of system prototype models. Considerable attention was given to the projected dynamic performance characteristics of the dual parachute array selected for mid-air deployment of the ALBS balloon, and to the predicted behavior of the descending system during the balloon inflation process.

Now, two years later, it is possible to report on the actual results of the planned tests, the triumphs and the failures, the lessons learned and the future direction of the program. There will be a brief restatement of goals and development history, for the benefit of persons not previously familiar with the program. The remainder of the paper will be given over to reporting the test results.

2. BACKGROUND

2.1 Basic Requirement

The Air-Launched Balloon System (ALBS) under development at AFGL is aimed principally at the requirement for a quick-reaction capability to put a lighter-than-air, tactical communications relay platform into position at high altitudes. Such a requirement is called out in TAC ROC 305-75 entitled A Satellite Airborne Communications Relay System for Tactical Air Forces.

For the purposes of the test program reported on here it was envisioned that the packaged ALBS would be extracted from a C-130 aircraft at 25,000 ft (7.62 km). When the system was properly deployed in midair by a tandem parachute array, the stored ALBS balloon would be extended vertically and filled from an attached helium storage unit. The inflated balloon would then carry the communications relay (approximately 200 lbs to its assigned altitude [$\approx 70,000$ ft (21.34 km)] while the inflation hardware floated to the ground (see Figure 1).

2.2 Previous Development History

In an earlier report³ the author proposed that a cryogenic gas storage and heat transfer subsystem be used in the ALBS to overcome the severe weight penalties associated with conventional compressed gas storage cylinders. Subsequently, the

2. Carten, A.S., Jr. (1976) The air-launched balloon system development program, Proceedings, Ninth AFGL Scientific Balloon Symposium, 20 October to 22 October 1976, pp 393-423, AFGL-TR-76-0306.

3. Carten, A.S., Jr. (1973) An Investigation of Techniques for Launching Large Balloon Systems for Aircraft or Rockets in Flight, AFCRL-TR-73-0633.

Cryogenics Division of the National Bureau of Standards (NBS), Boulder, Colorado, designed and fabricated for the ALBS program a heavy, ground-based prototype cryogenic storage and heat transfer unit.⁴ It was successfully used at Holloman AFB, New Mexico to inflate a 145,000-ft³ (4106-m³) balloon which, upon being released, carried a payload of 300 lb (1334.4N) to 75,000 ft (22.86 km). This was the first known flight of a large balloon inflated directly from a cryogenic source.

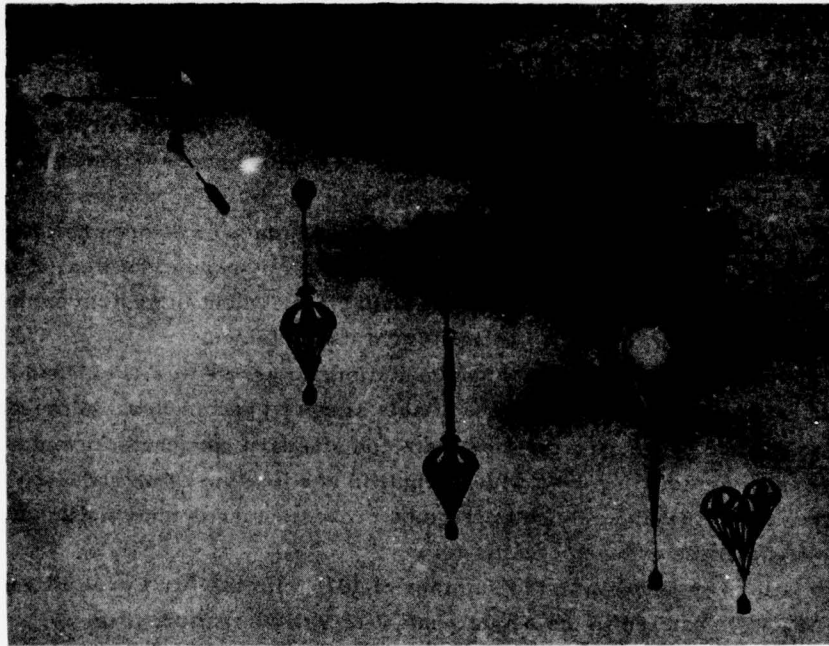


Figure 1. ALBS Air-Launched Balloon System (ALBS) Drop

With the basic development tests of the cryogenic unit successfully accomplished, the way was opened for flight tests of the complete system, that is, the dropping of the ALBS "module" or "package" from a suitable vehicle at the envisioned operational altitude, 25,000 ft (7.62 km), followed by mid-air inflation of the system's balloon. It was clear from the start that it would be an ambitious undertaking. A special balloon had to be designed and procured, a flight-weight version of the demonstration cryogenic gas storage and heat transfer subsystem had to be

4. Sindt, C. F., and Parrish, W. R. (1976) A System for Inflating a Balloon Using Helium Stored in the Liquid Phase, AFCRL-TR-76-0012, NBSIR 76-834.

constructed and the complicated parachute subsystem had to be tested and qualified. Despite the known problems, plans were initiated in December 1975 for the flight test program.^{2, 5}

A scientific balloon was chosen as the initial drop vehicle for the demonstration ALBS module, even though the ALBS was intended for eventual deployment from an aircraft. The overriding factor in this decision was the design adopted for the prototype flight-weight cryogenic unit under the dictates of project funding and available time. (It was adequate for a balloon drop but did not meet the standards for equipment carried aboard Air Force aircraft.) Thus, the planned tests had to be viewed as proof-of-concept testing, with the understanding that additional drops from a C-130 transport would be conducted at a later date, using a third, aircraft-qualified version of the system.⁵

Construction of the balloon-qualified version of the cryogenic unit was begun in the spring of 1976 by the NBS. (It is described in another paper in these Proceedings.⁶) The special balloon design needed for mid-air inflation was worked out at AFGL during the same time period and an order was placed for three balloons incorporating this design. The parachute subsystem then became the item of major concern because of its key role both in the aerial deployment of system components and in the extraction of the folded balloon from its container.

The author had carried out many computations to arrive at a preferred parachute subsystem which could employ available standard parachutes. Although these computations were based, for the most part, on standard parachute formulas, there were some assumptions involved which required verification by actual test. It was imperative, then, that the selected design be proven, using dummy units, prior to risking the expensive cryogenic unit.

Negotiations undertaken in the summer of 1976 with the Air Force Flight Test Center (AFFTC) resulted in the establishment of a flight test program at the National Parachute Test Range (NPTR), El Centro, CA under the auspices of the 6511th Test Squadron, with aircraft support from the 6514th Test Squadron at Hill AFB, Utah.

5. Carten, A.S., Jr. (1976) The Flight Test Aspects of the Air-Launched Balloon System Development Program, AFGL-TR-76-0196.
6. Sindt, C.F. (1979) A system for inflating an air-launched balloon, Proceedings, Tenth AFGL Scientific Balloon Symposium, 21 August to 23 August 1978, pp 149-159, AFGL-TR-79-0053.

Preparations for the parachute test program were begun at El Centro in the fall of 1976, but actual test flights did not get underway until February 1977.* As reported in the main body of this paper, they continued through October 1977 and were followed by the balloon drop test at Holloman AFB in January 1978.

2.3 Aircraft Test Impact

During the time period of the NPTR flight tests covered in this paper a gradual shift in program emphasis occurred. At the start, the stress was on the balloon drop test aspects, while the aircraft-oriented parachute subsystem tests were perceived as having an important secondary impact on overall system plans. Then, as the tests proceeded at the NPTR, a role reversal took place. The experience gained from deployments of the dummy system from C-130 aircraft pointed up several inadequacies in the original system design. As a result, the configuration of the prototype to be dropped from a balloon was refined considerably.

The aircraft drops at the NPTR also introduced a major change in the overall ALBS flight test program. Originally, only a dummy ALBS balloon was to be deployed ("extracted") at the NPTR. Real balloon extractions were to occur later, in preliminary balloon drops at Holloman AFB. (Those drops were to be dress rehearsals for the crucial "live" drop, also at Holloman, in which the cryogenic unit was to be deployed for the first time.) As things turned out, it proved both feasible and highly advantageous to prolong the NPTR tests to include real ALBS balloon extractions and even to attempt partial balloon inflations. Consequently, the scheduled preliminary balloon drops at Holloman AFB were cancelled, and the remaining live drop was rescheduled for a later date.

Test data obtained from the flights involving real balloon extractions at the NPTR were most helpful in planning for the January 1978 balloon drop at Holloman AFB. The aerial delivery program at the NPTR also provided a large amount of "hands-on" experience with ALBS aerial deployment hardware and techniques under semi-operational conditions.

*NOTE: The 6511th Test Squadron had begun construction of a test vehicle in which the simulated payload would be placed at the apex of the main canopy, along with the packed balloon. Then, in December 1976, the decision was made at AFGL to put the payload at the base of the main chute thus causing a delay for redesign and reconstruction of the test vehicle. (See the addenda to the 1976 reports^{2, 5} for the rationale behind the decision.) Although this decision solved a pressing technical problem, it necessitated the carrying of the collapsed main chute to altitude after balloon inflation. This in turn, reduced available payload weight significantly (see paragraph 5.4).

3. ALBS PROTOTYPE TEST CONFIGURATION

3.1 Initial Version

At the start of the flight test program, the envisioned ALBS prototype configuration was as described in the 1976 reports.^{2,5} It consisted of:

- (a) A flight-weight cryogenic unit (Figure 2),
- (b) A special 158,000-ft³ (4446-m³) balloon (Figure 3) and its associated container,
- (c) A lightweight 32-ft (9.8-m) ring slot upper or "drogue" parachute,
- (d) A 42-ft (12.8-m) ring sail lower or "main" parachute,
- (e) A 200-ft (61-m) extension line,
- (f) A simulated electronics payload, and various items of command and control equipment.

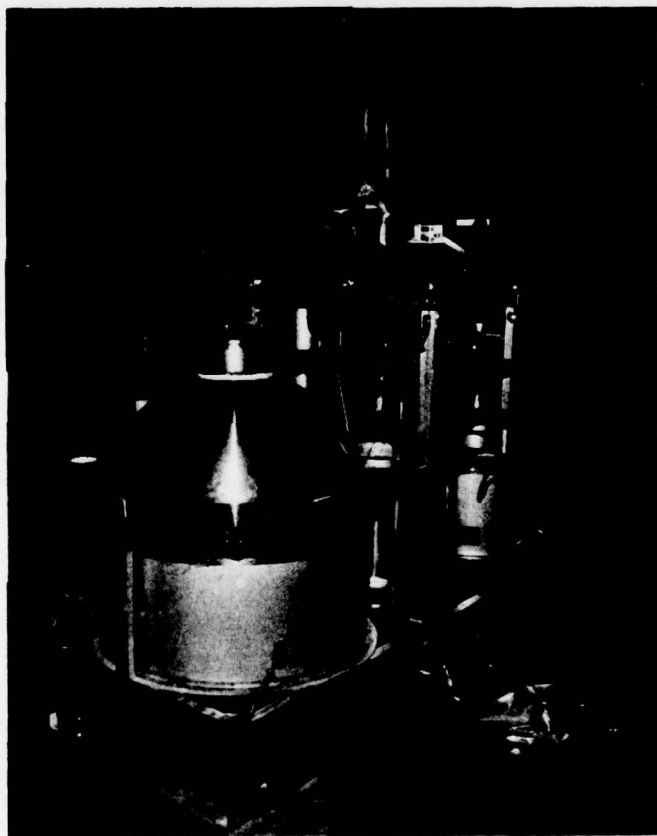
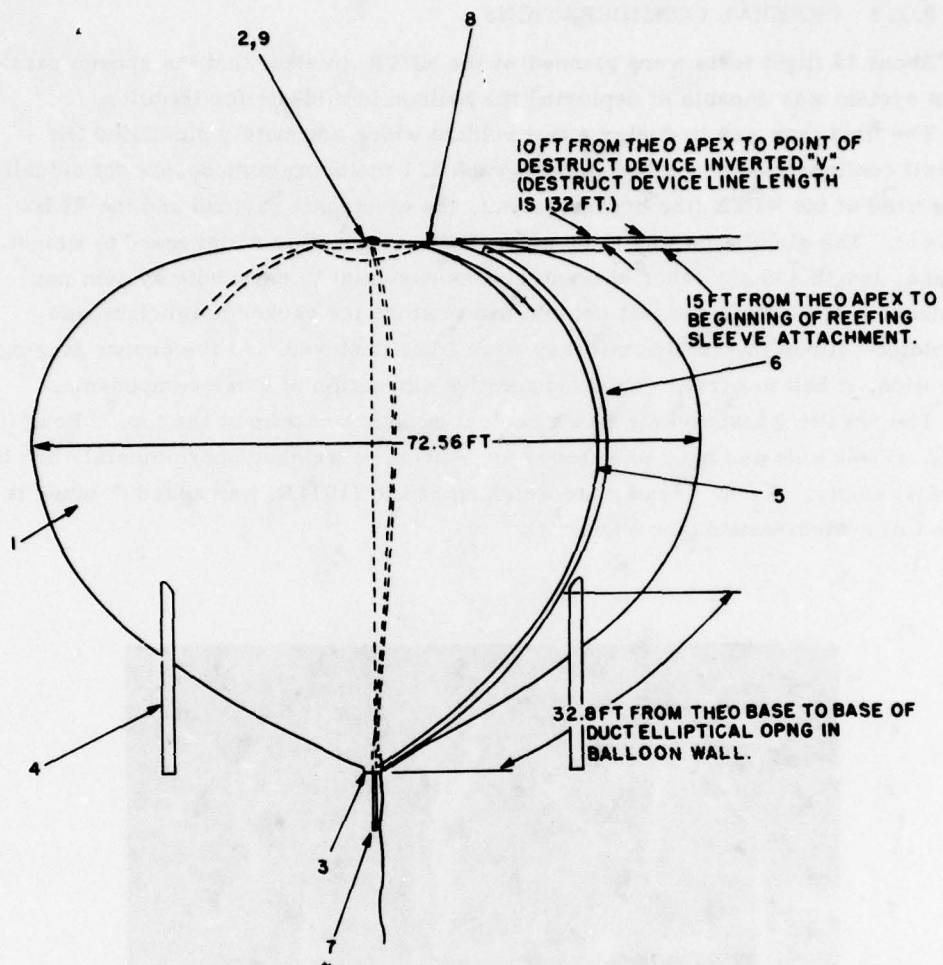


Figure 2. ALBS Cryogenic Inflation Unit, Less Superstructure



SYM	QTY	DESCRIPTION
9	1	NAMEPLATE
8	1	DESTRUCT DEVICE ASSY, GORES 13 & 27
7	1	INFLATION TUBE, 107.7 FT LONG, GORE SEAM 20
6	1	REEFING SLEEVE ASSY, GORE SEAM 28
5	1	VALVE CABLE ASSY, GORE SEAM 28
4	4	DUCT ASSY
		DUCT ATTACH, GORES 1, 8, 15 & 22
3	1	BASE FITTING ASSY
2	1	APEX FITTING ASSY
1	1	BALLOON SHELL ASSY (1.5 MIL MAT'L, NO LOAD TAPES)

Figure 3. ALBS Balloon Assembly

3.2 Parachute Subsystem Test Configuration

3.2.1 GENERAL CONSIDERATIONS

About 11 flight tests were planned at the NPTR to show that the chosen parachute system was capable of deploying the balloon in mid-air for inflation.

The first task was to design a test vehicle which adequately simulated the overall configuration described in paragraph 3.1 including components not actually to be used at the NPTR (the cryogenic unit, the electronic payload and the ALBS balloon). The simulation was to be as realistic as possible with regard to weight, volume, length and any other characteristics essential to parachute system performance. Moreover, the test vehicle had to store the packed main chute and simulated balloon internally until they were to be deployed. At the proper staging operation, it had to permit rapid and positive extraction of these components.

The resulting test vehicle was a cubical wooden box open at the top.⁷ Four ft (1.22 m) to a side and framed in heavy angle iron, it weighed approximately 665 lb (2958 N) empty. A heavy lead plate weighing 365 lb (1624 N) was added to bring it up to full system weight (see Figure 4).

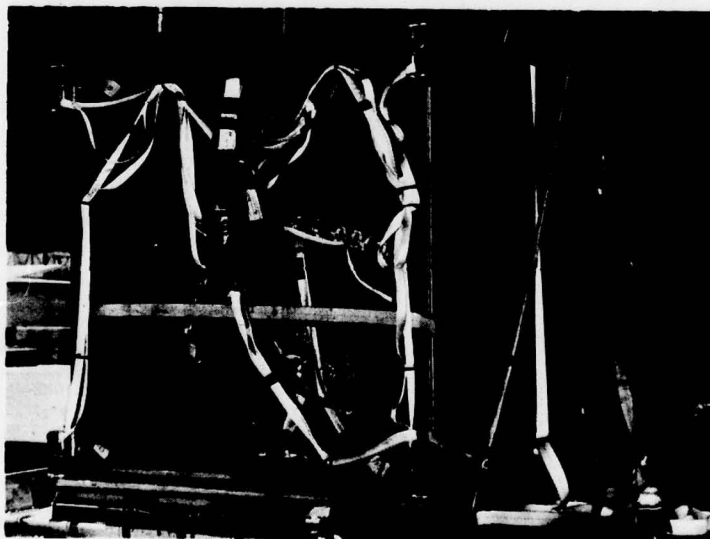


Figure 4. ALBS Test Vehicle Secured to Ramp of C-130; 28-ft Drogue Mounted on Pendulum (not shown)

7. Massey, W., and Wuest, M. (1978) The Air-Launched Balloon System, AFFTC-TR-77-42.

3.2.2 LOAD EXTRACTION AND DEPLOYMENT STAGES

The launch of the test vehicle from a C-130 aircraft and the deployment of the system components was planned as a three-stage operation (see Figure 5). The first stage was to be the load extraction (that is, the pulling of the test vehicle from the aircraft) and the transition to a vertical attitude. The second stage was to be the deployment of the main chute, 200 ft beneath the drogue chute. The third stage was to be the extraction of the simulated balloon from its container on top of the open main chute and the full extension of that balloon, as would be required for mid-air inflation. (The drag forces exerted on the packed balloon by the drogue chute were to be extraction mechanism.) After completion of the third stage, the array was to descend to the ground.

NOTE

In the deployment of the real balloon in a live operation there would be additional stages: the filling of the balloon, the cutting away of the drogue, the dropping away of the cryogenic unit, and so on (see Figure 1).

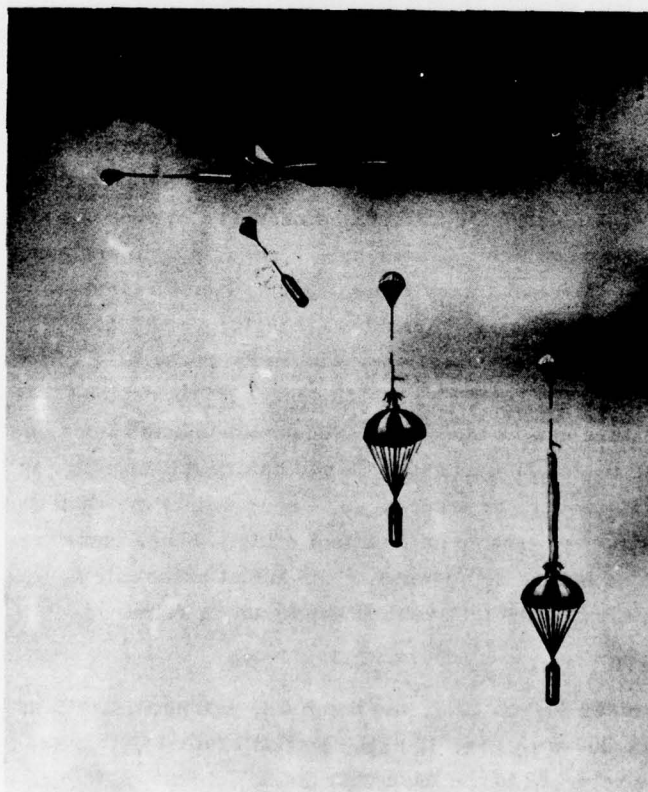


Figure 5. ALBS Test Vehicle Drop at the National Parachute Test Range

3.2.3 USE OF THE 32-ft (9.8-m) DROGUE CHUTE FOR LOAD EXTRACTION

The 32-ft light-weight drogue chute had been selected for the ALBS tests primarily for its drag characteristics. The author's chief concern was with the drag force needed to pull the folded ALBS balloon from its container on top of the main parachute, and with the dynamic pressure "q", which the exposed balloon would experience. Calculations showed that the 32-ft ring sail drogue chute, when deployed above the 42-ft main chute, would easily provide both the needed minimum drag force and the desired q of 0.5-1.0 psf (23.94 (23.94 - 47.88 N/m²).

To reduce system complexity, the drogue chute was also chosen to pull the ALBS module out of the aircraft, a role which would subject it to forces of approximately 10,000 lbf (44,480N). In evaluating the 32-ft chute for this additional role, the 6511 T.S. relied on a previous test where this chute had successfully withstood an extraction force of 11,400 lbf (50,707 N). Thus, it seemed reasonable to employ it in the ALBS extraction.

3.2.4 THE FIRST ALBS DROP TEST (Test No. 1)

The first extraction of the test vehicle from a C-130 took place over the NPTR on 2 February 1977. The aircraft was at 10,000 ft (3048 m), flying at an equivalent air speed of 130 knots. (True air speed = 255.5 ft/sec, 77.8 m/sec). Within seconds the suspension lines of the 32-ft chute failed and the chute separated from the load. In the resulting free-fall, the test vehicle was damaged beyond repair, thus introducing a month's delay into the program for rebuilding of the test vehicle.

Post-flight examination revealed that the failure had occurred in sections of the suspension lines, near the skirt, which had been dyed black approximately one year earlier to enhance contrast in documentary photography. Tensile strength tests revealed a marked deterioration in their breaking strength.

Although this failure did not bring into question the capacity of the 32-ft chute when not dyed, it instilled an attitude of caution nevertheless. It was decided that the next test would not only feature new, undyed and stronger suspension lines, but also would have the 32-ft chute reefed 50 percent for 8 sec before full opening, to reduce the extraction force. Moreover, an inert bomb, whose weight matched that of the test vehicle would be extracted first on an identical chute. Thus, chute capability would be demonstrated before deployment of the actual test vehicle, and if the chute failed again, rebuilding of the test vehicle would not be required.

3.2.5 TEST NUMBER TWO

In the second test flight, on 29 March 1977, the bomb was extracted first, as planned, from an altitude of 10,000 ft (e. a. s. 130 kt). Its chute failed immediately. Needless to say, the C-130 returned to the base with the ALBS test vehicle.

This time the failure was traced to the canopy apex area and had been triggered by an unexplained premature activation of the reefing line cutter after 1 second. The canopy "blew" when the parachute went from 50 percent open to fully open before the system had decelerated significantly. It was now decided to abandon the 32-ft light weight ring slot chute in favor of a heavier 28-ft (8.53 m) ring slot extraction chute routinely used by Air Force and Army operation elements. (Parachute, cargo, extraction, 28-ft FSN 1670-00-687-5459; Rated Load Capacity: greater than 25,000 lbf (1.112×10^5 N)).

Table 1. shows the calculated values of area drag and dynamic pressure for the 28-ft drogue chute and 42-ft main chute combination. Maximum calculated drag at the drogue (362.69 lbf, 1613.2 N) is almost exactly equal to the minimum required value (362 lb, 1610.2 N) while the dynamic pressure (1.071 psf, 51.28 N/m^2) slightly exceeds the specified range. Although these values suggest marginal extraction capability and a higher-than-desired force per unit area on the balloon film, no serious performance degradation occurred in actual tests.

3.2.6 FINAL PARACHUTE SYSTEM TEST CONFIGURATION

The use of the 28-ft drogue chute both restored the test program's momentum and fixed the system parachute sizes. All subsequent tests were conducted with a 28-ft drogue chute and a 42-ft main chute. Some changes were required later in minor system components (break-ties, line-cutting devices, and so on) which will be mentioned briefly in this paper and which are covered in detail in the 6511 Test Squadron report.⁷ Figure 6a and Figure 6b show major details of the parachute system test configuration in the first and second stages of deployment.

Table 1. Area, Drag and q Values for the 28-ft Ring Slot Drogue Chute and 42-ft Ring Sail Main Chute Combination

System Weight = 1520 lb (6761 N) Altitude = 9200 ft (2804 N)

$\sigma = .75732$

Minimum Required Drag (Drogue) = 362 lb (1610 N)

Parachute	Type	Dia	C_D	Reference Area (S_o)	Drag Area ($C_D S_o$)
Drogue	Ring Slot	28 ft	0.55	615.752 ft ²	338.664 ft ²
		8.52 m		57.21 m ²	31.46 m ²
Main	Ring Sail	42 ft	0.78	1385.442 ft ²	1080.645 ft ²
		12.8 m		128.71 m ²	100.4 m ²
Array	---	50.48 ft*	0.709*	2001.19 ft ²	1419.309 ft ²
		15.39 m		185.92 m ²	131.86 m ²

Dynamic Pressure, q , = 1.071 psf (51.28 N/m²)

Equilibrium Velocity, Ve_H = 34.49 ft/sec (10.51 m/sec)

Drag of Drogue at Ve_H = 362.69 lb (1613.2 N)

Drag of Main Chute at Ve_H = 1157.31 lb (5147.7 N)

Drag of Array at Ve_H = 1520 lb (6761 N)

NOTE: The drag of the drogue and the drag of the main chute will remain constant, regardless of the altitude (0-25,000 ft) provided that the calculation is made at equilibrium velocity. Drag is a function of dynamic pressure and effective drag area. Under equilibrium conditions, both are essentially constant.

*Theoretical

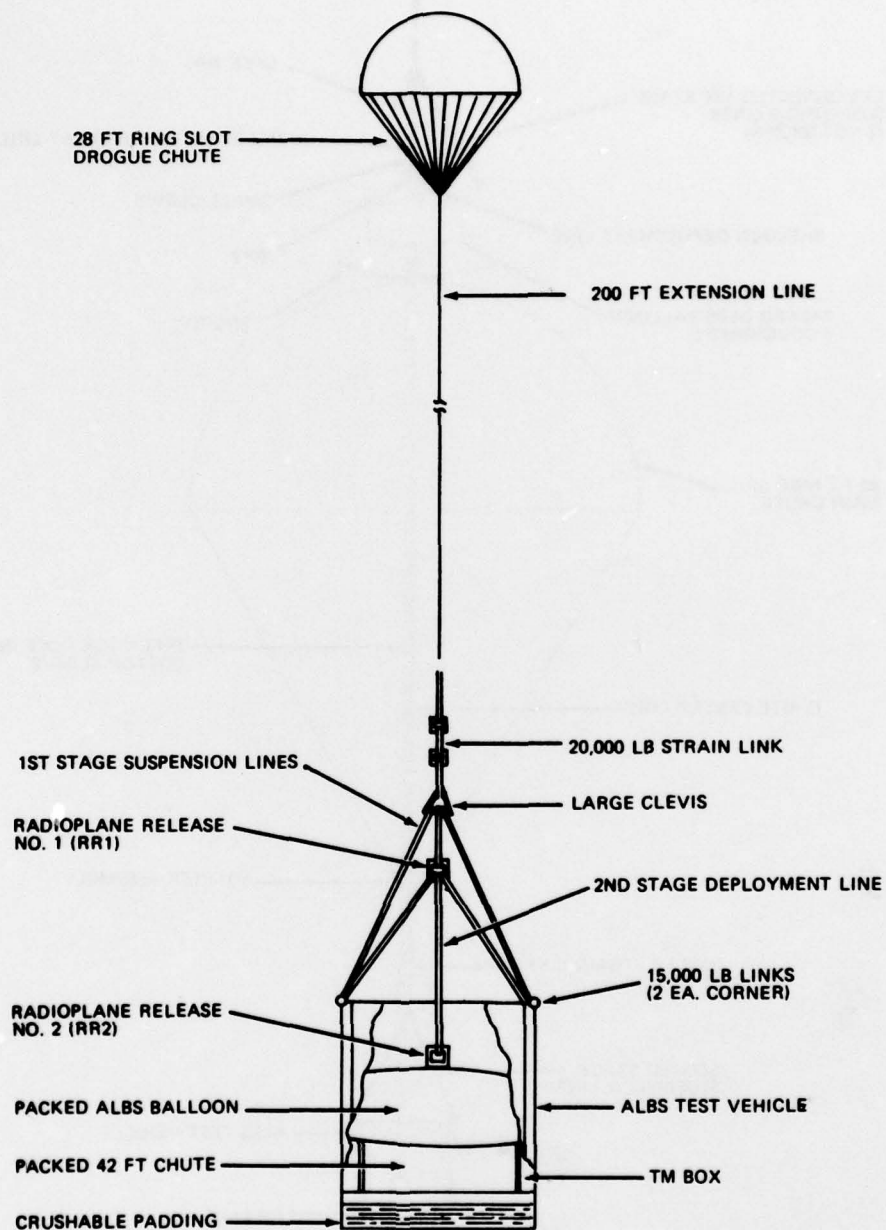


Figure 6a. Parachute System Test Vehicle, First Stage Configuration

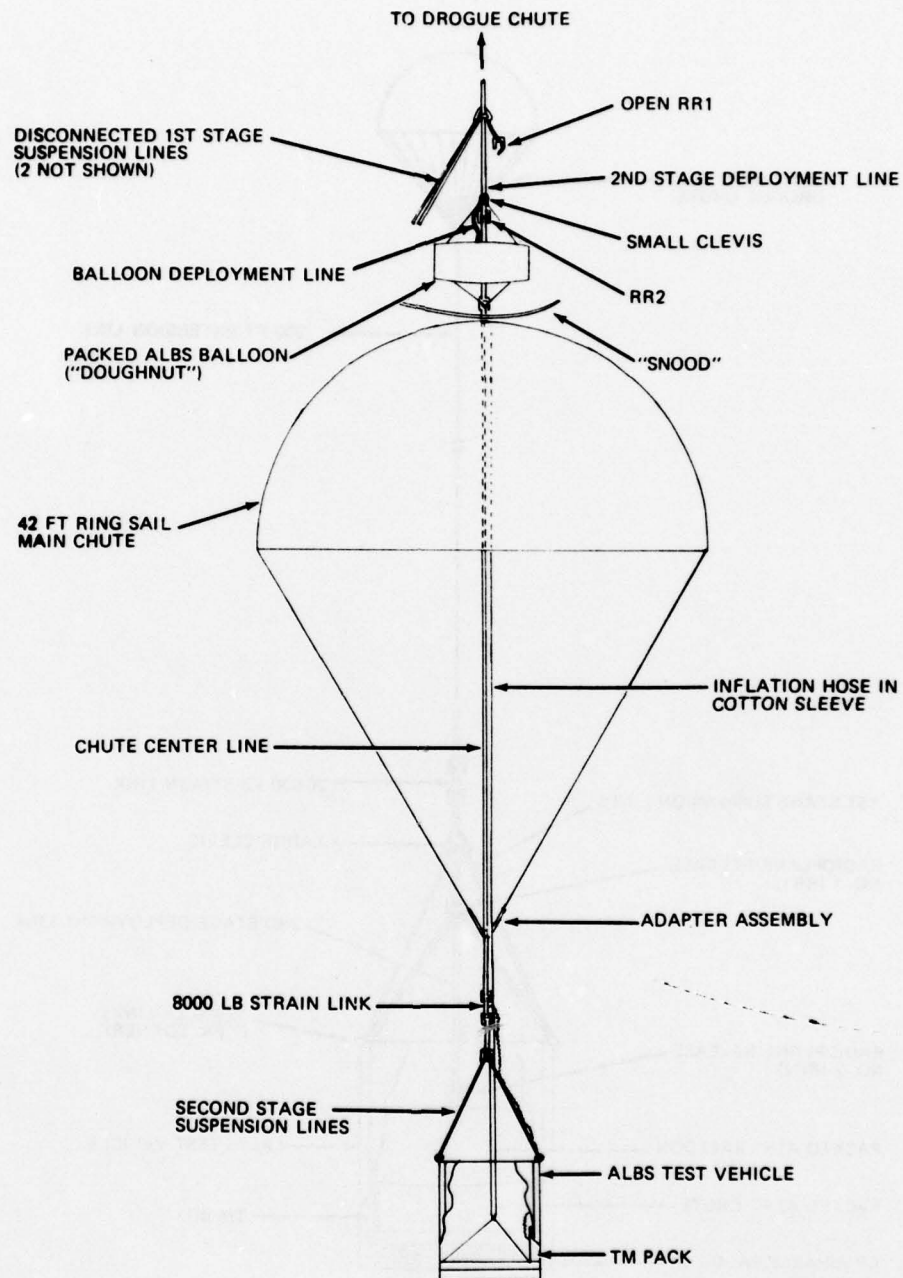


Figure 6b. Parachute System Test Vehicle, Second Configuration

3.3 Balloon Drop Test Configuration (Preliminary Discussion)

The parachute test configuration discussed above was selected to meet a more limited set of requirements than that of the live drop test planned for Holloman AFB, where a carrier balloon would be the launch vehicle.

Because it was not necessary to inflate the ALBS balloon to verify the dynamics of both the parachute deployment and the balloon extraction steps, a dummy ALBS balloon could be employed in the NPTR tests if it simulated the length and linear weight distribution of the real balloon (see note). Moreover, there was no requirement to separate the dummy balloon from the parachute system during the NPTR tests, even though separation of the real ALBS balloon (after inflation) would be necessary in the Holloman test.

As a consequence, the NPTR system test configuration could not be used directly in the Holloman carrier balloon drop test. However, in addition to qualifying the basic parachute system design, the NPTR test configuration provided the engineering foundation for the carrier balloon drop test configuration. As might be expected, the carrier balloon drop test configuration actually employed in January 1978 incorporates several additional features not found in the NPTR test vehicle. It is described in Section 5. The reader might better appreciate the subtleties of that configuration after reviewing the narrative account of the NPTR parachute system test program which follows.

NOTE

To simulate the real ALBS balloon, which weighs 200 lb (889.6 N) and is 102 ft (31 m) long, a dummy balloon was constructed of a double thickness of 9-ply Type XXVI Nylon riser material.

4. THE PARACHUTE SYSTEM TEST PROGRAM RESULTS

4.1 An Abortive Start

Paragraphs 3.2.3, 3.2.4, and 3.2.5 discussed the shortcomings of the 32-ft ring slot drogue chute and described the first two parachute system tests.

4.2 A Partial Success (Test No. 3)

On 8 April 1977 the first deployment of the parachute test system configuration with the 28-ft ring slot drogue chute was carried out. The aircraft was at 10,000 ft, e. a. s. 120 kt. * At zero time, T_o , load extraction was initiated and took place

*The early flights were performed at 10,000 ft for crew safety purposes. The launch crew could gain proficiency with this new system more readily if unhampered by the harsh environment at 25,000 feet. Also, the propeller-driven photographic chase plane (T-28) performs better at lower altitudes. Since this plane would have to bank sharply and continuously to follow the ALBS module down after its extraction, it seemed desirable to work out this maneuver first at an altitude of maximum aircraft response.

flawlessly. At $T_0 + 19$ sec, main chute staging was initiated. Six sec later, the packed dummy balloon was riding on top of the fully inflated main chute (as shown in Figure 6b), waiting to be extracted from its canvas container by the drogue chute. However, when the timer-initiated command for this function was given (at $T_0 + 39$ s) there was no extraction. The system floated to earth and landed without damage. Post flight inspection revealed that the wires leading to the explosive squibs on the number two Radioplane Release (RR2) had been broken during the deployment of the main chute.*

Although not completely successful, this test had several positive aspects; the perfect performance of the 28-ft extraction chute, the rapid (3 sec) inflation of the main parachute and the lack of damage to the 3-mil (0.0076 cm) thick polyethylene balloon inflation tubing during and after the main chute deployment

4.3 A Change in the Method of Activating the Radioplane Releases

It was decided to try the experiment again with a less vulnerable method of activating the Radioplane Releases. The battery-powered, timer-controlled explosive squibs would be replaced with lanyard-initiated, percussion-fired cartridges with a built-in delay of 10 sec (see Figure 7). Although reliable and quite commonly used in the aerial delivery of military cargos, these cartridges were not used in the earlier tests because of the original, long staging times. The test just concluded showed that shorter time stages were possible, thus permitting use of the 10-sec delay cartridges. The incorporation of this change fixed the initiation times for the second and third stages at $T_0 + 10$ sec and $T_0 + 20$ sec, respectively, for the remainder of the test series.

4.4 The Knife That Did Not Cut (Test No. 4)

The next test was conducted on 21 April 1977 (10,000 ft, 120 kt). Load extraction and main chute deployment were excellent. Balloon extraction still did not take place however, even though the percussion cartridges had initiated the extraction step as planned.

* Appendix C of the report¹ from which this paper was extracted contains calculations of main chute opening parameters, and shows that very powerful forces are involved. That the electrical lead wires had failed to survive the moment of violence when the main chute was deployed was rightly considered a correctable system design flaw, as later events proved.

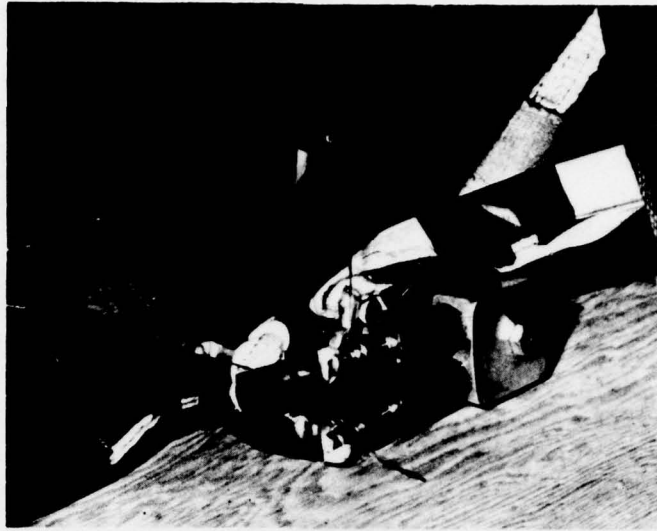


Figure 7. Radioplane Release With Lanyard-Initiated, 10-sec Delay Percussion Cartridges

When RR2 disconnected the drogue line from the apex of the main parachute, the drogue's residual drag force was supposed to pull two cutting knives across the drawlines of the balloon containment bag ("doughnut"). The severed lines would then be pulled from the bag, releasing the cover and allowing the drogue to pull the balloon upward. What actually happened was that only one knife cut completely through its drawline. The cover was not released and the balloon was not pulled upward. The array descended to the ground without damage, with the weight of the packed balloon apparently suspended by the non-functioning knife's cutting edge.

The response here was to replace the two cutting knives with four explosive reefing line cutters. A 6-sec delay time was included to allow them to be lanyard-initiated during main-chute deployment. In addition, nylon loops at the top of the doughnut were replaced by metal rings to reduce drawline friction.

4.5 The Retaining Ring Problem (Test No. 5)

On the next test flight (4 May 1977) a new "glitch" came to light: The load extraction force developed a transverse component which caused the retaining ring on Radioplane Release No. 1 (RR1) to fly off. The unrestrained RR1 pivot pin then fell out prematurely initiating main parachute deployment while the drogue chute and the 200-ft line were still in a horizontal attitude. The deceleration forces broke the doughnut's restraining straps allowing it to slide over the uninflated main

parachute. When the array swung into a vertical attitude, the doughnut kept the main chute from opening. The fouled lines inhibited balloon extraction also. The array descended on the drogue chute alone, landing at approximately 61 ft/sec, (18.6 m/sec). The impact was cushioned by the crushable padding but there was some damage to the rugged test box.

4.6 Success at Last (Test No. 6)

A repeat test was conducted on 11 May 1977, with the faulty retaining ring replaced by a threaded bolt and self-locking nut. Patience was finally rewarded on this occasion. All events occurred exactly as planned. The dummy balloon was stretched out vertically to its full length in approximately 8 seconds. The aircraft speed was 130 kt this time, but the higher load extraction forces caused no problem.

Moderate "coning" of the 42-ft parachute was observed for the first time on test No. 6. This motion, in which the lower part of the main chute and its load rotate through an included arc of about 30 degrees, was quite noticeable as the array descended to the ground. It gave rise to another system modification described in paragraph 4.7.

With the successful completion of all scheduled events at 10,000 ft the way was now clear for a test at 25,000 feet. The experience gained in the preceding tests had eased earlier concerns about operating under the harsh, open-cargo-deck environmental conditions at 25,000 ft, and as it turned out, the loadmaster, photomate, and other cargo deck personnel were able to function quite well at the higher altitude.

4.7 The First High-Altitude Drop (Test No. 7)

The first drop at 25,000 ft was conducted on 25 May 1977 (air speed: 130 kt). All stages deployed properly, with no adverse effects due to increased altitude. In an attempt to reduce or eliminate coning, the hardware at the apex of the 42-ft chute had been changed to allow fuller opening of the apex. Also, the inflation tubing, which had been attached to the center line heretofore, was routed up one of the main chute suspension lines and over the top of the canopy, in the belief that it could not survive the new harsher environment at the apex. (This new routing was employed in all later tests.) A swivel was added to the balloon deployment line to isolate drogue twisting action.

The fuller opening of the apex did not alleviate the coning problem, unfortunately, and it continued to be a worrisome item, eventually leading to the specialized coning tests described under tests Nos. 12 and 13.

Some damage occurred in test No. 7 at the base of the doughnut, although it did not interfere with balloon extraction. The culprit was the measured 7000-lbf shock loading developed during the exchange of momentum between the recoiling doughnut

and the suddenly decelerated test vehicle at the time of main chute deployment. It was decided, therefore, to reinforce the doughnut for the next test. In addition, 18 nylon loops, evenly spaced, were added to the centerline of the main chute. They were secured to a restraining steel eye by 350-lbf breaking strength ties. This change was made in the belief that sequentially-interrupted deployment of the centerline folds would attenuate the 7000-lb shock.

4.8 A Change of Scope

The NPTR test series had been planned to test the dynamics of the parachute system with the understanding that mid-air deployment of the real ALBS balloon would be carried out for the first time at Holloman AFB. (A scientific balloon would be the deployment vehicle for that test.) However, as the tests at the NPTR progressed, the idea of carrying out the first balloon deployment test there became increasingly attractive. Permission was obtained to add this test to the NPTR series and plans were made accordingly, even while the original test series with the dummy balloon was being carried out. One of the three special ALBS balloons at AFGL was shipped to El Centro for the newly established test. It quickly became apparent that the doughnut would have to be enlarged lightly to accommodate the bulk of the real balloon and its large end fittings.

4.9 The Final Test of the Dummy Balloon (Test No. 8)

On 17 June 1977, the dummy balloon was deployed for the last time (25,000 ft, 130 kt). All stages functioned properly. The reinforced doughnut was not damaged. The measured deployment shock stayed at 7000 lbf, however, indicating that the 18 Nylon loops were ineffective. They were dropped from the configuration and were not used again.

4.10 The Inflation Tubing Question

Tests to date with the dummy balloon had shown that the dynamic performance of the parachute subsystem matched the requirements laid down for mid-air balloon deployment. However, as plans were being made to use a real balloon, to test its survivability in the established environment, another likely problem area came under close review: the adequacy of the inflation subsystem.

The 3-mil (0.0076 cm) thick, inflation tubing, enclosed in a protective canvas sleeve, had been repeatedly deployed without damage when attached to one of the suspension lines of the main chute. This did not prove, however, that gas from the cryogenic unit would actually pass smoothly up through the deployed tubing and through the interior filling tube in the ALBS balloon. Twisting and kinking of the inflation tubing were feared, with possible tubing rupture. Clearly, demonstration testing was required to establish confidence in the overall inflation process.

Gradually, a plan evolved whereby a "mini" inflation system would be assembled by the NBS and added to the NPTR test vehicle so that a small amount of gas could be passed up to the extended balloon to verify the suitability of the inflation tubing. This would not be attempted however, until the real balloon had had at least one successful deployment (see Tests 9 and 10).

NOTE

The "mini" inflation system was to consist of two standard "K" bottles of compressed Helium gas (220 SCF each) which, along with appropriate valves and regulators, would be strapped to the underside of the test vehicle. This system was to match as closely as possible the gas output characteristics of the much larger ALBS cryogenic unit (which could not be deployed from a C-130).

4.11 First Deployment of the Real Balloon (Test No. 9)

On 29 June 1977, the first deployment of a real ALBS balloon was attempted (25,000 ft, 130 kt e. a. s.). Only about a 6-ft length of balloon was actually pulled out of the doughnut however, due to an interfering line. The system floated to earth with no damage to the balloon or test vehicle.

4.12 A Successful Balloon Extraction (Test No. 10)

The above test was repeated on 7 July 1977 with the offending line removed. The results were very gratifying. The entire balloon was extracted readily and suffered no damage either in the extraction or during the descent to the ground. The uninflated balloon material had tolerated the maximum dynamic pressure very well. Inflation tubing twisting was observed however, confirming earlier apprehensions.

In this test, the top end of the inflation tubing was attached to the flanged inflation port on the bottom end fitting of the balloon. (This connection had not been possible in earlier dummy balloon tests.) It clearly showed up the twist problem now and called for immediate remedial action, since twisting of the inflation tubing would cripple the planned mini-inflation test.

Lt. Warren Massey of the 6511 T.S. suggested a hardware change to alleviate the problem. It involved a flexible no-twist metal linkage system which could be folded in the packed doughnut and which would allow only a quarter-turn of twist. This linkage was fabricated for test flight No. 11. It is depicted in Figure 8, which is a sketch of the items required at the base of the ALBS balloon for a live flight test. (This is the configuration actually assembled for the Holloman AFB live drop test.)

4.13 The First Attempted In-Flight Inflation (Test No. 11)

On 26 July 1977, the ALBS test vehicle, modified to incorporate the mini-inflation system (see Figure 9), was extracted over the NPTR (25,000 ft altitude, 130 kts e. a. s.). Inflation was begun at $T_0 + 40$ sec via a timer-opened solenoid valve.

At first, it was not clear whether the gas had or had not gone into the balloon. Because the balloon was slightly damaged upon landing no verification was possible immediately. (A hole found near the apex would have released any gas which might have gone into the balloon. Later, when the recovered inflation tube was examined, several long burst-caused tears were noted in the area at the base of the 42-ft parachute, thus indicating that no inflation had taken place. The test films showed that the inflation tubing might have been stretched taut in that location, obstructing the flow of gas and allowing a quick build-up of pressure.

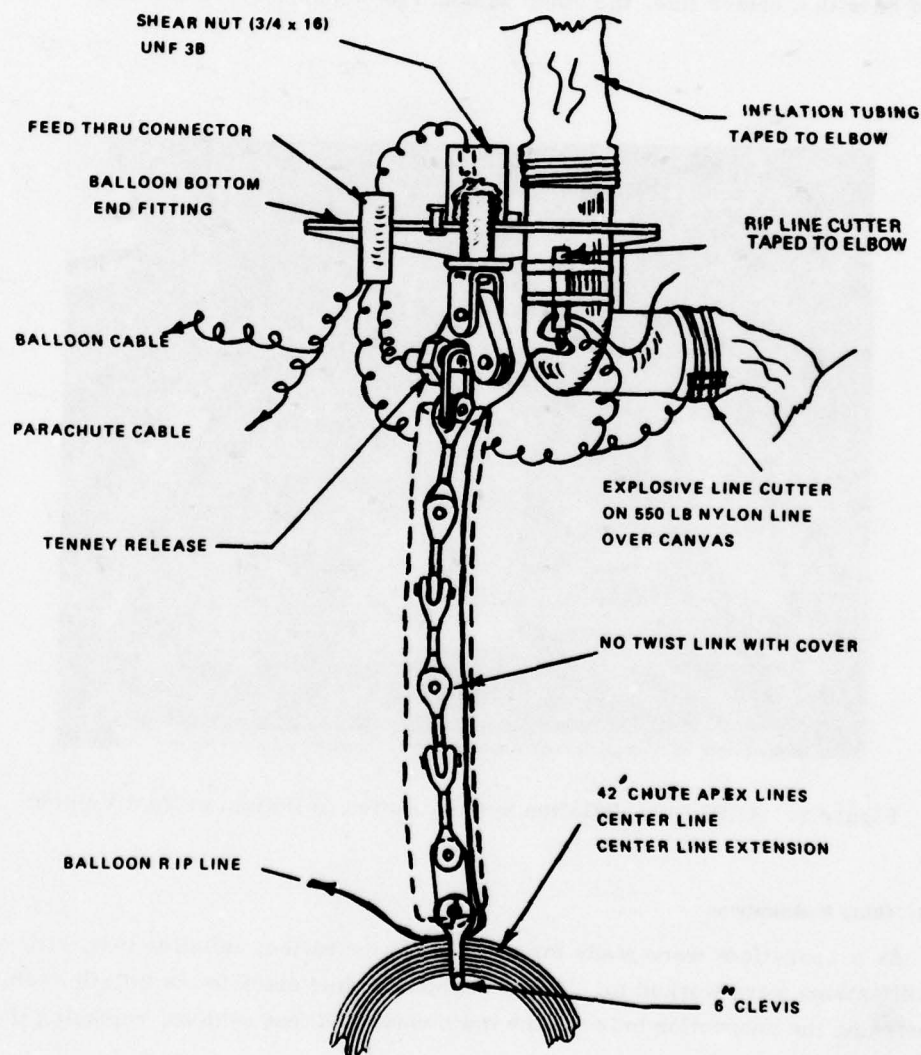


Figure 8. Base of Balloon

Tests conducted later at NBS, Boulder, CO, showed that the build-up of pressure in the mini-system was, indeed, very rapid and that almost any obstruction in the tubing would have led to a burst. The mini-inflation system was then modified, to provide a gradual pressure buildup which the tubing could tolerate, and was returned to the NPTR for a repeat flight test (see test No. 14).

The no-twist link between the apex of the 42-ft chute and the base of the balloon was very effective in Test No. 11 and became a permanent part of the system. Coning of the 42-ft chute was noted again in this test. The chute center line was suspected to be the chief cause and plans were made to fly two tests of the 42-ft chute alone, using a 1500-lb weight bomb to simulate the test vehicle. One test would be with a center line, the other without (see tests Nos. 12 and 13).

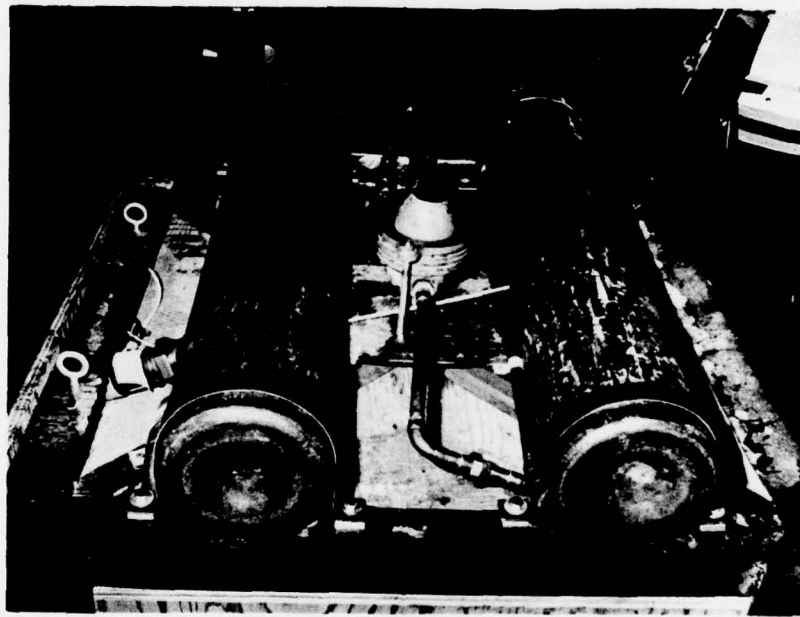


Figure 9. ALBS Mini-Inflation System Bolted to Bottom of Test Vehicle

4.14 Other Modifications

As preparations were made for a repeat of the balloon inflation test, still other modifications were worked in. These included adding slack to the inflation tubing, shortening the connection between the main chute and test vehicle, replacing the

straight gas inlet pipe on the bottom end fitting with a large elbow and fabricating a new, smoother protective sleeve for the inflation tubing. In addition, balloon damage was repaired.

The balloon drop planned for Holloman AFB (after the completion of the NPTR tests) had been receiving considerable attention during this same time period, and it was decided to incorporate in upcoming test No. 14 some of the items to be used at Holloman. (This was to test physical compatibility. The items would not be functional.) They included an 8-conductor cable attached to the 42-ft chute and explosive separation devices as would be required for termination of the ALBS balloon flight at Holloman AFB (see Figure 8).

4.15 The Final NPTR Flight Tests

The two tests to investigate coning were scheduled for the same date as the repeat of the balloon inflation test. The C-130 would carry all three drop vehicles simultaneously, releasing the 42-ft chute/weight bomb test packages at 10,000 ft (two passes) and climbing subsequently to 25,000 ft to release the ALBS module. This series of drops (tests 12, 13, 14) took place on 27 October 1977. The results are described below.

4.15.1 THE CONING INVESTIGATION TESTS (Tests 12, 13)

On the first test (No. 12) the 1500-lb weight bomb was dropped on a 42-ft ring sail chute equipped with a center line. Definite coning was noted. Unfortunately, in the second drop (test No. 13), several suspension lines of the 42-ft chute (no center line) failed, causing the chute to drift. The test was not considered meaningful because of the resultant parachute distortion. These tests proved that the 42-ft chute did indeed cone with a center line in place but the parachute's behavior with a heavy load in the absence of that line was not established. The tests were not repeated and the question has not yet been resolved.

4.15.2 THE SECOND BALLOON INFLATION TEST (Test No. 14)

The second attempt to achieve partial inflation was initiated after the above coning tests. However, a problem developed, just as the ALBS module was leaving the ramp of the C-130 (25,000 ft, 130 kt) which doomed the test to failure; main chute deployment was initiated prematurely and that chute opened in a horizontal attitude and at a much higher velocity than planned. The shock broke the center line, damaged several panels and suspension lines, and tore open a large hole in the balloon. Remarkably, the normal, two-parachute configuration was subsequently achieved and the balloon was even extracted to full length. The system descended to the ground on both chutes, with the tattered balloon fully deployed.

Post-flight examination showed that the gas inflation system had discharged properly. There was no way of telling whether gas had gone into the balloon, however, because of the many rips in the balloon film. Moreover, several long tears were found in the inflation tubing, just below the point of attachment to the badly damaged lower end fitting. It was not clear whether excessive main chute opening forces or gas pressure had split the tubing.

The cause of failure was a matter of speculation. Damage marks inside the test box indicated that Radioplane Release RR1 had struck the bottom side of the box as it was being pulled forward by the taut 200-ft drogue line (see Figure 10). The impact was severe enough to break or prematurely discharge the release. (It was never recovered.)

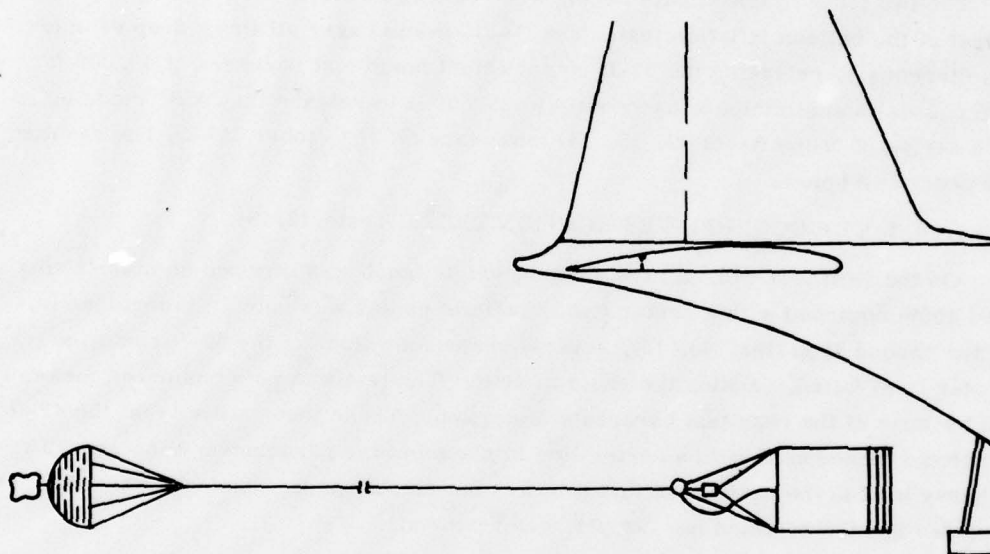


Figure 10. ALBS Load Extraction

4.16 Termination of the NPTR Tests

The latest failure introduced a new uncertainty into the air launch process. It was feared that the failure could reoccur on a random basis, and thus, any attempt to repeat the balloon inflation test without prior reengineering and testing, would be counter-productive. It was agreed, therefore, that the NPTR test flights would be terminated immediately, even though the coning issue had not been resolved and the inflation system had never really been successfully tested. This decision was

influenced by a shortage of funds to expand the effort at the NPTR and by a desire to avoid further major slippage of the long-delayed balloon drop test at Holloman AFB. The development of more reliable aircraft extraction techniques was left for a later date.

Emphasis was now shifted to preparations for the Holloman launch. The 6511th T.S. participated actively in these preparations and arranged both to furnish many of the components needed for the drop and to be present at Holloman.

With the termination of the NPTR test program, there was regret that not all of the questions had been answered. Nevertheless, there was a feeling of solid achievement in that the original test objective (see para. 3.2.1) had been met and that important data had been developed beyond the information originally sought. Also, plans for the Holloman drop were formulated with a degree of confidence in the parachute system which would otherwise have been impossible.

5. THE HOLLOMAN AFB/WHITE SANDS MISSILE RANGE BALLOON DROP TEST

5.1 Prior Preparations

With the termination of the NPTR tests in November 1977, a firm time period for the Holloman test was finally established; 17-20 January 1978.

The broad spectrum of preparations required for this test could not possibly be completed solely within the November to January time period. The January date was chosen only because most of the preparations had been started several months earlier and were actively in progress while the NPTR tests were being conducted. By way of illustration:

(a) The lightweight cryogenic unit had been built and was fully tested by the spring of 1977,

(b) Three (3) of the special ALBS balloons had been procured in 1976 and one of the three had already been deployed in mid-air several times by the end of the NPTR tests,

(c) The parachute subsystem had been fully qualified at the NPTR, both with a dummy and a real balloon,

(d) An S-Band telemetry module with UHF command and control functions and appropriate sensors had been made up at AFGL for the Holloman flight,

(e) The inflation tubing assembly had been fabricated and had been flown without harm on most of the NPTR tests,

(f) The remaining major item was the interface component to tie parachute, balloon, cryogenic unit and payload together. Key meetings held in July 1977, on the subject of interface design, resulted in the plan for a box-like superstructure

which would be attached to the cryogenic unit.* NBS undertook the construction of the superstructure and mated it with the cryogenic unit at Boulder. By late November it was ready for shipment to Holloman AFB.

Figures 12a and 12b show the components of the descending ALBS at the completion of the third stage balloon extraction. Details are consistent with the configuration chosen for the Holloman AFB drop test.

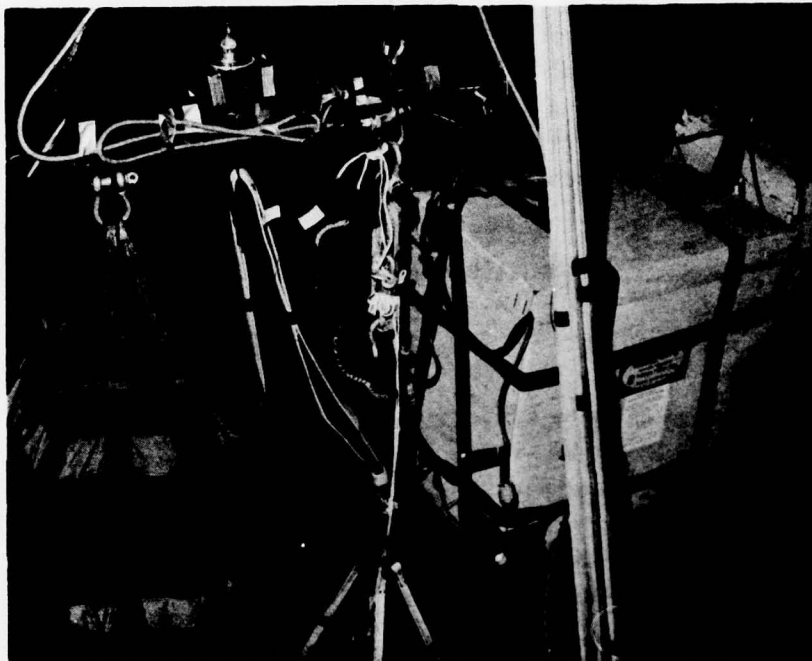


Figure 11. 28-ft Drogue Chute Attached to Carrier Balloon Load Bar

* With this design, main chute deployment and balloon extraction would occur essentially as they had during the NPTR tests using the same staging times. After drogue release and balloon inflation had been accomplished, a new staging operation would be accommodated: the cutting away of the cryogenic unit to permit the balloon to ascend.

It is to be remembered that in the NPTR tests, the 28-ft extraction chute was released to the airstream by the pendulum on board the C-130 (see Figure 10). As the chute moved out, it deployed the 200-ft extension line and then, as it began to open, it developed enough force to pull the ALBS test vehicle off the aircraft ramp. Subsequently, the system swung through a 90° arc to complete the transition from horizontal to vertical altitude.

In the balloon drop test, the ALBS unit stays vertical at all times. As it falls freely it deploys the 200-ft extension line above it which, when taut, pulls the 28-ft chute out of its pack, which is secured to the carrier balloon's load bar (see Figure 11). When the 28-ft chute opens, the balloon-dropped system is in the same configuration as the aircraft-dropped system at the completion of the first staging operation (see Figure 6a). In both cases deployment of the main chute (second stage) occurs at $t_0 + 10s$.

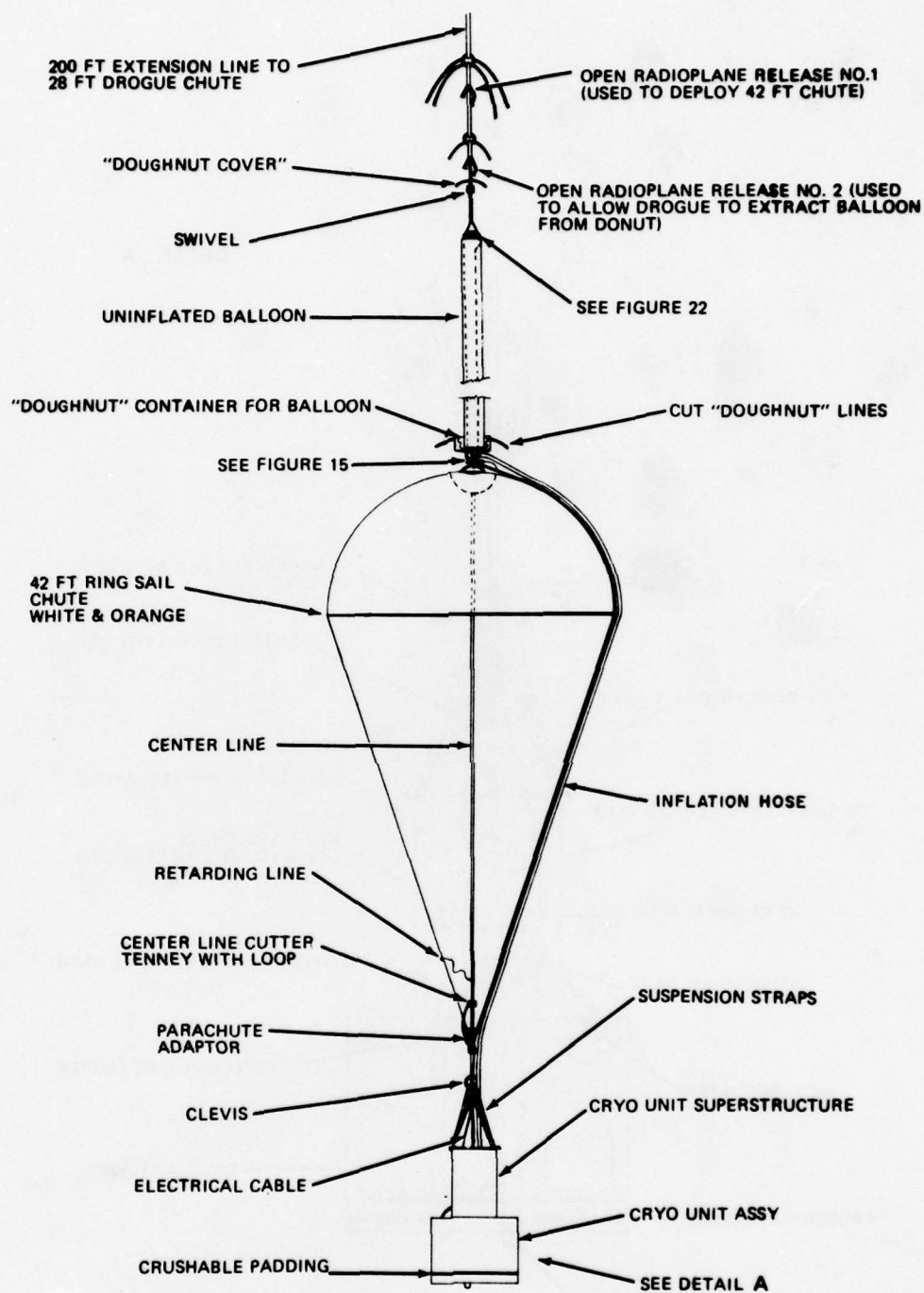


Figure 12a. Outline Drawing ALBS Prototype Configuration for January 1978 Test at Holloman AFB, NM

DETAIL A

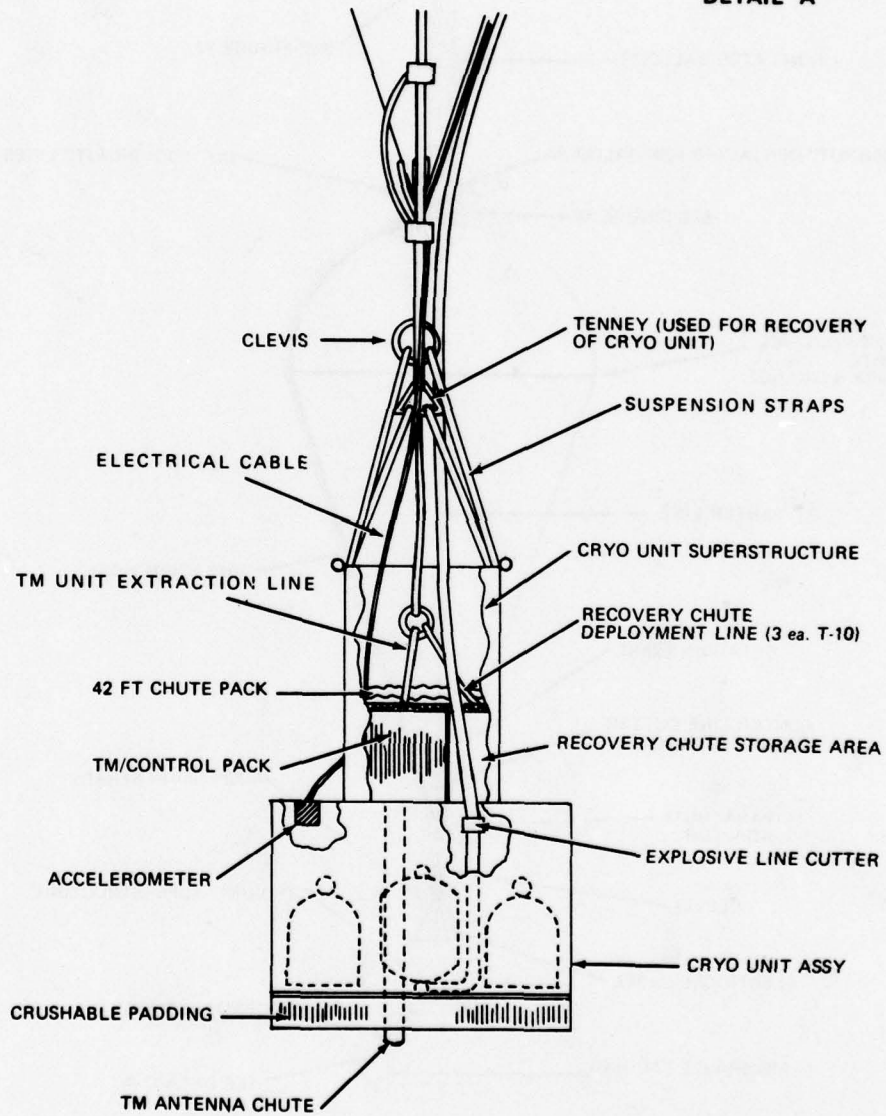


Figure 12b. Outline Drawing ALBS Prototype Configuration - Detail A

5.2 Flight Planning Meetings

5.2.1 GENERAL

The author conducted a series of planning meetings at Detachment 1, AFGL, Holloman AFB, NM during the week of 9 December 1977. A broad range of topics was covered, including test objectives, event sequences and times, potential launch sites, preferred target area, range support requirements, load bar configurations and Detachment 1 logistical operations in support of a remote launch, if so decided.

5.2.2 THE CHOICE OF LAUNCH SITE

A principal determinant in the choice of launch site was the requirement that the ALBS release be made over a test range. (This requirement arose from the experimental nature of the ALBS deployment process which, in case of failure, would allow the heavy cryogenic unit to impact at a high terminal velocity, and from the potentially hazardous pressure buildup in the cryogenic unit, if it should land intact and undischarged, with the pressure relief valve jammed.

Because Holloman AFB is at the eastern edge of the White Sands Missile Range and because the prevailing winds at 25,000 ft over the WSMR in January have a strong west to east component, a launch west of the usual site was initially indicated. Probable flight trajectories, using January wind fields, showed that only an off-range launch site would provide the required flight path for an acceptable percentage of the time as well as positioning the target area more favorably with regard to normal range camera locations.

The disadvantages of the remote launch were only too obvious: heavy per diem costs; the complicated logistics associated with gathering and transporting all the necessary vehicles, supplies and equipment 150 miles to the preferred remote site; the cost of renting temporary facilities; the inability to man recovery crews adequately with the personnel staying at Holloman, and so on.

The planning meetings resulted in the decision to launch off-range despite the disadvantages. The municipal airport at Truth or Consequences, NM (T. or C.) was chosen as the remote site. Because it had been used previously by Detachment 1, preparations for the remote launch were able to benefit from prior experience.

5.2.3 RANGE REQUIREMENTS DOCUMENT

As a result of the planning meetings, Detachment 1 was able to prepare the Range Requirements document needed to enlist the support of the WSMR photographic, tracking, and communication resources in connection with the planned ALBS drop test. That document, in turn, spawned a WSMR Operational Directive (OD41418A) which outlined the support actually to be provided.

The Range Requirements document (Operation Requirement No. 41418) is reproduced in part here:

5.2.3.1 Program and Mission Information

- (a) **Test Objectives:** The purpose of this program is to air-launch a high altitude research balloon. This will be accomplished by carrying the system to an altitude of 25,000 ft on a carrier balloon. When in position over WSMR a ground command will initiate the drop sequence. It is anticipated that launch of the carrier balloon will be from Truth or Consequences, NM so that prevailing winds will drive the system over WSMR for the test.
- (b) **Drop Sequence:** It will take approximately 1 hr from launch at Truth or Consequences for the carrier balloon to be in position over the 50 mile area of WSMR at 25,000 feet. When in proper position for optical coverage a drop command will be issued from the Balloon Control Center at HAFB. The ALBS package consisting of a cryogenic helium unit, a packed 42-ft parachute, packed air launched balloon, and electronic control package will fall from the carrier balloon deploying a 28-ft chute in the process. At T+10 sec, the packed 42-ft parachute is pulled from the container above the cryogenic unit by the 28-ft drogue chute. At T+20 sec the air-launched balloon (ALB) is pulled from its container atop the 42-ft chute by the 28-ft drogue chute. After the ALB is fully deployed as verified by Detachment 1 airborne observer and/or range TV coverage a start inflation command will be issued by the Balloon Control Center. Inflation will take approximately 5 minutes. Thereupon, commands will be issued to release the 28-ft drogue chute and drop the cryogenic unit on three 32-ft chutes. Both the carrier balloon and the ALB will float at approximately 70 Kft and will be terminated off range, probably east of the Sacramento Mountains. Using standard balloon recovery techniques all recoveries will be accomplished by Detachment 1, AFGL.

5.2.3.2 Vehicle and Payload Information

- (a) **Air Launch Balloon System (ALBS) description.** The ALBS consists of a carrier balloon (0.803 MCF) and associated HF control package. Suspended below the load bar by a nylon strap and dual separation devices will be a large wooden box containing the packed air launched balloon, 42-ft parachute, UHF balloon control system for airborne inflation and three 32-ft parachutes for cryogenic unit recovery. WSMR supplied C-band transponders will be flown on both balloon systems. A packed 28-ft drogue chute will be attached to the load bar and will be deployed at the initiation of the system drop. After ALB inflation, this drogue will be released by command. The cryogenic unit will also be dropped after inflation and be recovered on three 32-ft chutes. These two items will be recovered on range by Detachment 1, AFGL personnel.
- (b) **ALBS system weights:**

Total system weight:	3023 lb
ALBS weight:	1770 lb
- (c) **Instrumentation:** The carrier balloon will utilize an HF command and balloon control package. Telemetry, downlink will also use an HF system. The ALBS will utilize a UHF (420-440 MHz) command package with an S-band (2200-2300 MHz) telemetry system. All balloon commands and telemetry will be accomplished by the Balloon Control Center, Bldg. 850, HAFB, NM.
- (d) **Vehicle description:** Both balloons are constructed of 1.5 millimeter thick polyethylene. The carrier balloon has a maximum inflated diameter of 128 ft and weighs 614 lb. The ALB has a maximum inflated diameter of 72.6 ft and weighs 190 lb.

5.2.3.3 Vehicle Instrumentation Systems

- (a) Each balloon vehicle will be equipped with standard command, control, telemetry, and destruct systems. These systems are provided by AFGL, and operated by the AFGL Balloon Control Center at Bldg. 850, Holloman AFB. In addition to providing the routine balloon altitude control functions (ballast drop or helium release), AFGL provides certain command functions to facilitate system drop, inflation start, chute release and cryogenic unit drop. A command and telemetry van, user supplied, will be used at the launch site, T or C airport.

5.3 Choice of Carrier Balloon

The carrier balloon was chosen from the SF128-200-TT series, with a nominal expanded volume of 0.803 million ft³ (22741 m³) and a recommended maximum payload capacity of 2200 lb (9786 N). These balloons weigh approximately 600 lb (2669 N).

In the planning meetings at Detachment 1, the weight of the carrier balloon's load bar, ballast hoppers, range communications packages and the like were added to the new weights of the ALBS module* and it appeared that the estimated total weight would be more than 10 percent over the recommended payload (see Table 2). This raised the spectre of carrier balloon failure and prompted a quick survey of previous flight histories of the 128-200-TT balloon using heavy payloads. The findings are tabulated below (all flights successful).

Flight No.	Payload (lb)	N	Free Lift (lb)	N
H 76-052	2275	10119	283	1259
H 72-077	3800	16902	352	1566
H 68-007	2000	8896	153	681
C 68-001	2996	13326	179	796
C 67-018	2996	13326	178	792
C 67-026	2995	13322	143	636
C 67-034	2496	11102	154	685

As a result of the above histories the 128-200-TT balloon was retained as the carrier balloon for the ALBS drop.

*The ALBS module had acquired approximately 250 extra pounds (1112 N) of weight as various contingency modifications and reinforcements were added. It was now "grossing out" at approximately 1770 lb (7873 N) (see Table 3).

Table 2. Overall System Weights, ALBS Balloon Drop Test White Sands Missile Range, NM January 1978 (Estimated Weights vs Measured Weights)

Item	Estimated Weight		Actual Weight Measurements Before Launch	
	(lb)	(N)	(lb)	(N)
ALBS Module and 28-ft Chute	1770	7873	1812	8060
Load Bar, Double Unistrut, (Including All Hardware)	90	400	92	409
Ballast Hoppers (2 ea)	32	142	30	133
Range Pack II, (Minimum Batteries) and Backup Pack	120	534	115	512
C-band Transponder	10	44.5	25	111
Parachute, f. c., 100-ft dia.	201	894	190	845
Durable Ballast, Glass Beads	200	890	200	890
ALBS Release Mechanism	---	---	10	44.5
EV-13, Strobe	---	---	9	40.0
Subtotal a. (Total Payload on Carrier Balloon)	2423	10778	2483	11044
plus Weight of Carrier Balloon	<u>+600</u>	<u>2669</u>	<u>+609</u>	<u>2708</u>
= Subtotal b. Gross Weight at Launch	3023	13446	3092	13753
× 110 percent (10 percent Free Lift) = Gross Inflation	3325.3	14790	3401.2	15129
× 0.97 Correction Factor = Corrected Gross Inflation	3225.5	14347	3299.2	14675

Table 3. ALBS Module Weights, Balloon Drop Test White Sands Missile Range, NM January 1978 (Estimated Weights vs Measured Weights)

Item	Estimated Weight		Measured Weight at Launch	
	(lb)	(N)	(lb)	(N)
1. 28-ft Droque Chute	46	205	46	205
2. 200-ft Extension Line	36	160	36	160
3. Misc. Hardware on Line	20	89	24	107
4. Balloon and Associated Hardware	200	890	230	1023
5. Balloon Pack and Linkage	20	89		
6. 42-ft Main Chute Assembled	125	556	130	578
7. Simulated Comm. Relay	200*	890	200	890
8. Cryogenic Unit, Including Box and Liquid Helium	1003	4461	1079**	4799
9. Recovery Chutes for Cryo Unit	90	400	67	298
10. Ballast	<u>30</u>	<u>133</u>	<u>0</u>	<u>0</u>
	1770	7873	1812	8060

* See para 5.4.

** Includes three Layers of Crushable Padding at Base.

5.4 The Simulated Tactical Communications Relay

The ALBS balloon (Figure 3) was to take a gross load of 575 lb (2558 N) to 70,000 ft (21.34 km). This load was originally apportioned as follows:

Balloon and end fittings	200 lb	890 N
Tactical communications relay (dummy)	200 lb	890 N
Expendable ballast	60 lb	267 N
Recovery chute	35 lb	156 N
TM/Control pack	<u>80 lb</u>	<u>356 lb</u>
	575 lb	2559 N

Lift available from the cryogenic unit during mid-air inflation was fixed at approximately 633 lb (2816 N) to allow the balloon to support its own weight (200 lb) plus 375 (1668 N) of payload and to have 10 percent excess lift to insure a normal rate of rise.

As hardware was assembled for the January flight, however, it became necessary to revise the above apportionment drastically. For example, the balloon, strobe light, EV-13 valve, termination devices, end linkage and canvas balloon container—all of which had to be taken to altitude—totalled 230 lb (1023 N) thus reducing the available payload by 30 lb (133 N). A further major reduction had occurred earlier (see footnote page 109) as a result of the need to take the hardware-laden 42-ft main chute to altitude. Its weight was now measured at 130 lb (578 N) as opposed to the 35 lb (156 N) originally allocated for a recovery chute. Also, the ALBS TM/Control pack weighed 125 lb (556 N) vs 80 lb (356 N) estimated. These changes led to a tentative new weight apportionment:

Balloon and attached hardware	230 lb	1023 N
42-ft main chute*	130 lb	578 N
TM/Control pack	125 lb	556 N
Ballast	<u>90 lb</u>	<u>400 N</u>
	575 lb	2557 N

It was clear that, even with the ballast eliminated, there was no capacity left for a separate 200-lb (890 N) dummy communications relay. On the other hand, it was not certain that the sophisticated TM/Control pack required for an R&D flight would be needed operationally, at least as a separate item. Thus, for this test, it was decided to "create" a 200-lb dummy communications relay by adding 75 lb (334 N) of ballast to the TM/Control pack and to fly the following configuration:

Balloon and attached hardware	230 lb	1023 N
42-ft main chute attached hardware	130 lb	578 N
Misc. hardware	5 lb	22 N
Simulated comm. relay	<u>200 lb</u>	<u>890 N</u>
	565 lb	2513 lb

The resultant gross load was kept 10 lb (44.5 N) under the planned gross of 575 lb (2558 N) to allow for possible minor lift deficiencies in the mid-air inflation process.

5.5 The Need to Recalculate

5.5.1 GENERAL

The increase in the weight of the ALBS module discussed in paragraph 5.3 cast doubt on the continued validity of system deployment planning figures which had been

* Includes inflation tube and 8-conductor cable.

calculated in the summer of 1977 on the basis of a 1520-lb ALBS module weight. Consequently, in November and December 1977, a new set of calculations was carried out by the author.

5.5.2 MAIN CHUTE DEPLOYMENT SHOCK

The 7000-lb main chute deployment force was the first item checked, using a module weight value of 1769 lb. The resulting force value was 8184 lb. Although the g force on the cryogenic unit remained essentially the same (6 g) the shock on the doughnut was increased from 21.1 g to 24.2 g. Assurance was given by the 6511th Test Squadron that the balloon containment bag fabricated for the January test had been reinforced and should be able to withstand the increased g load.

Recomputations were then accomplished for the completion times, forces, and altitudes of the many steps in the ALBS deployment sequence. The changes were not major. The velocities and dynamic pressures were a little higher because of the added system weight but no change appeared capable of affecting the planned deployment significantly. The revised figures were incorporated in the Range Requirements Document.

5.6 Pre-Launch Preparations

The week of 9 January 1978 was selected as the make-ready period for the launch. The goal was to have the assembled payload, all vehicles and all personnel at Truth or Consequences not later than Saturday, 14 January. This would allow two days (Sunday and Monday) for final preparations, a period which would eliminate the need for last minute haste. It would also allow work to be terminated by noon on Monday to permit personnel rest prior to rising at 0100 - 0200 on Tuesday. This goal was met and all was in readiness for the scheduled Tuesday launch.*

A two-day weather delay then followed. On Wednesday, the forecast for the following day was favorable and the waiting crew was told to initiate launch preparations the next morning.

*

The final assembly of the ALBS module required a maximum effort. Just the preparation of the 42-ft main chute was very time-consuming. In addition to attaching the electrical cable and the inflation tubing assembly to the suspension lines, there was the new task of incorporating Tenney releases for severing the centerline and for effecting cryogenic unit release at the end of inflation. The packing of the balloon in the doughnut was more straightforward, but the details at the bottom and top of the balloon, as seen in Figures 8 and 13, required much time and patience. The most difficult chore was the assembly (for the first time) of the packed balloon and main chute to the cryogenic unit superstructure along with the TM/Control Pack and the 3 T-10 recovery chutes. This turned out to be a measure-and-cut operation, particularly with respect to the installation of the many required restraining lines and deployment lines. Figures 14, 15, and 16 illustrate some of the assembly operations.

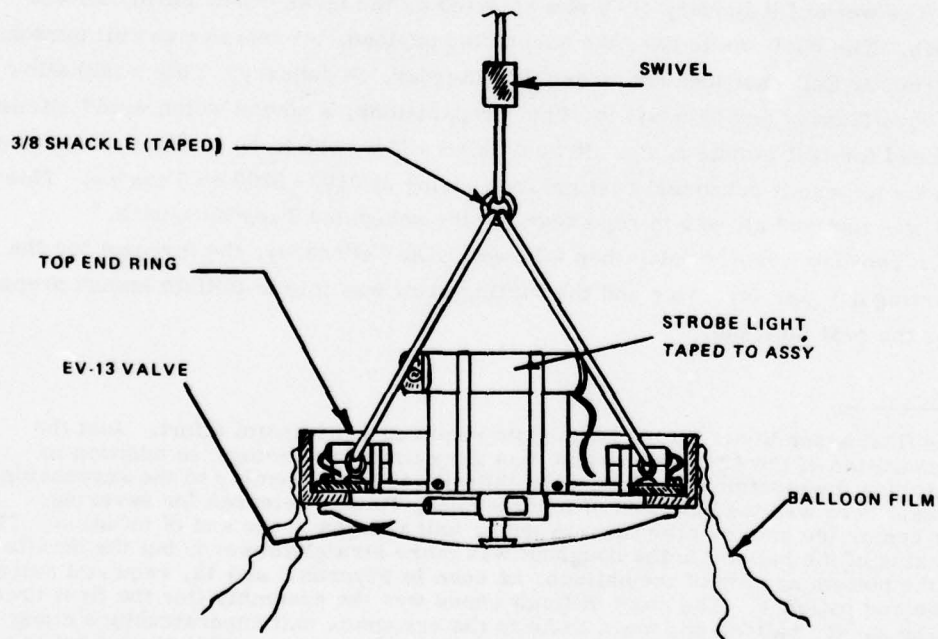
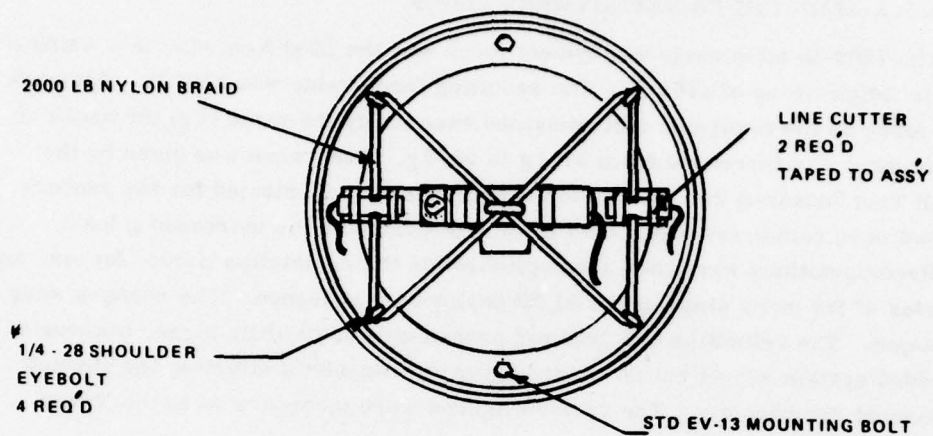


Figure 13. Top of Balloon



Figure 14. Assembly of Components at Base of Balloon



Figure 15. Packing of
ALBS Balloon in
Containment Bag
(Doughnut)

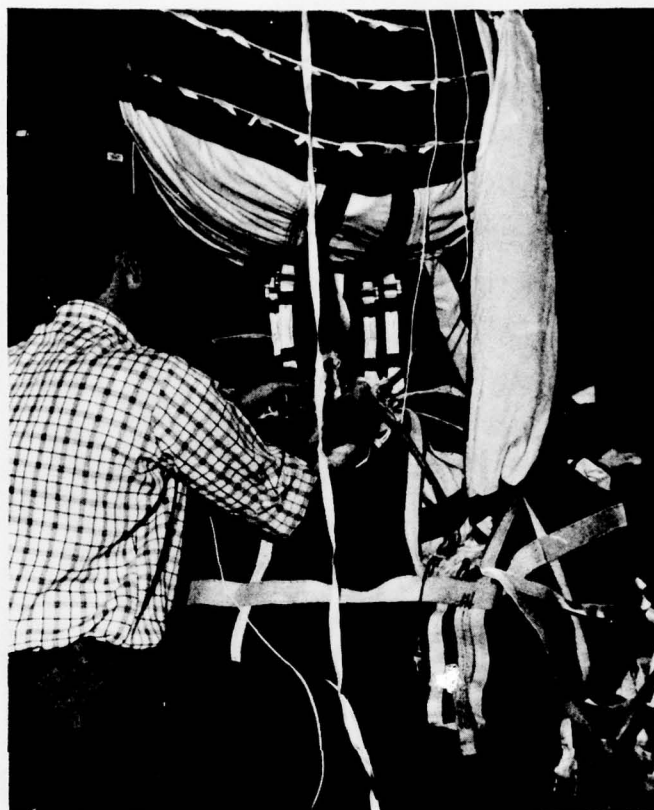


Figure 16. Attachment of Packed Balloon Containment Bag (Doughnut) to Packed 42-ft Main Chute Assembly

5.7 Launch of the Carrier Balloon

The launch site was manned by 0145 on the morning of 19 January 1978 (scheduled launch time was 0700). The ALBS module and all of the other flight components were hung on the load bar and suspended from the crane. [Allowing for 5 ft (1.52 m) of clearance under the payload, the distance to the attachment point on the crane was approximately 30 ft (9.14 m)] (see Figure 17). Normal equipment checks and command checks were carried out successfully. The dewars of the cryogenic unit were filled (Figure 18). Gas computations were made and checked for a gross load of 3092 lb (13,753 N) (see Table 2). Inflation of the balloon was delayed somewhat, commencing at 0643. At 0704, the inflation was interrupted to repair a tear in the inflation tube. Inflation was completed at 0729 (Figure 19). Launch occurred at 0734.

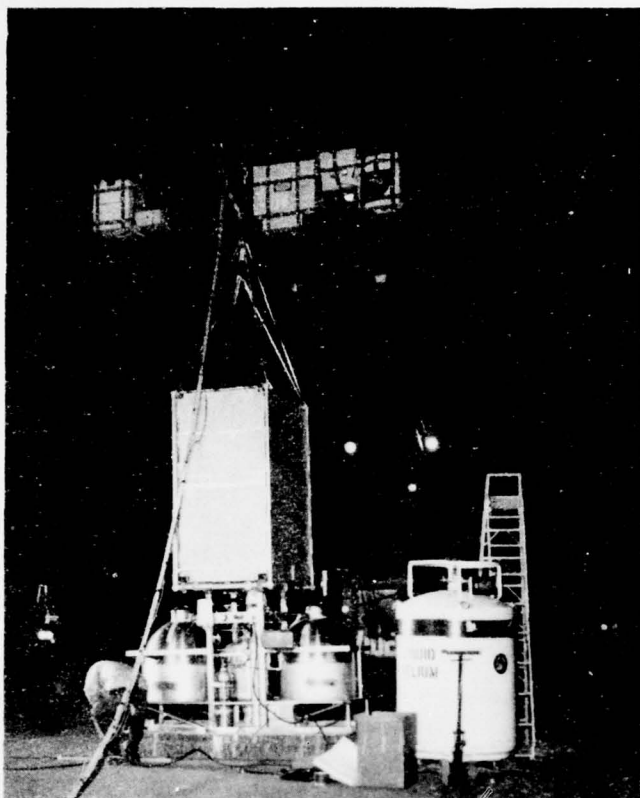


Figure 17. ALBS
Module Suspended
From Carrier
Balloon Load Bar

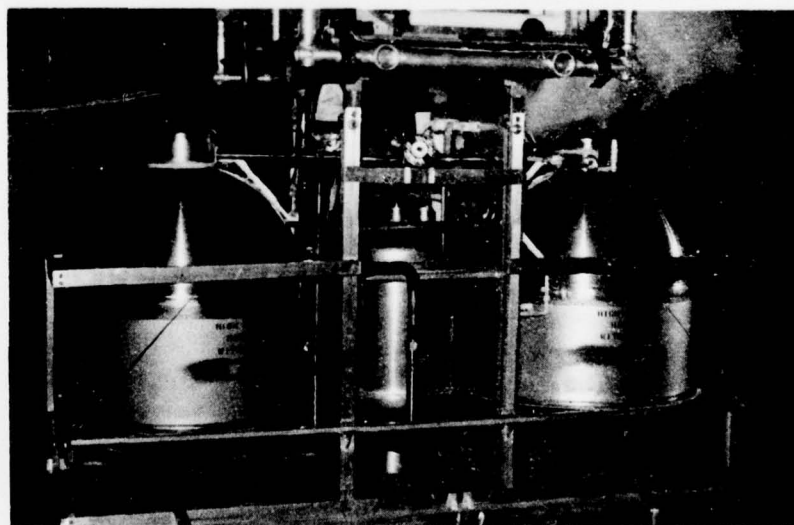


Figure 18. Venting of Filled Cryogenic Unit

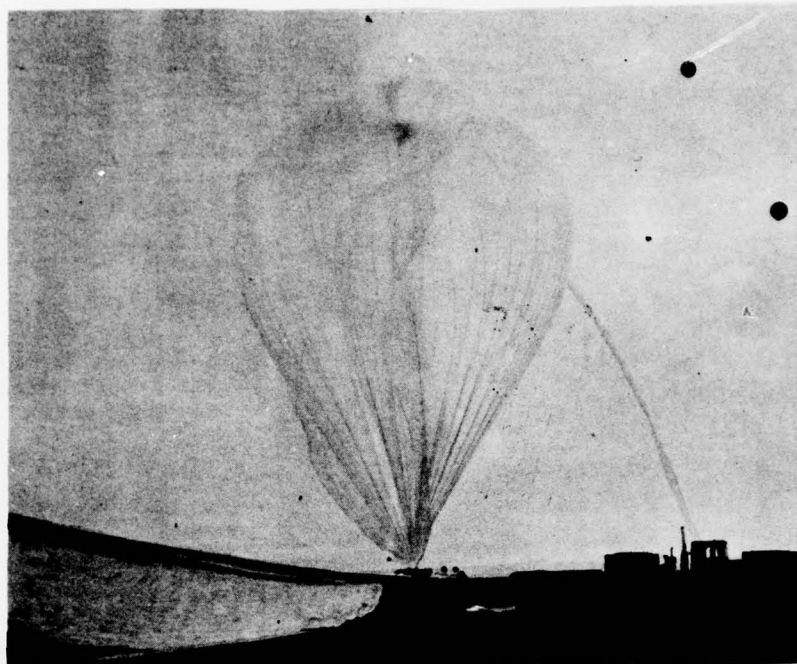


Figure 19. 128-200-TT Carrier Balloon at Inflation

At first the balloon started to rise normally. Then it settled down (Figure 20) and the payload bumped along the ground. Ballast was released for 45 sec at a rate of 34 lb (151 N) per min but the balloon was still only 3 to 5 ft (0.9 to 1.2 m) off the ground. The launch officer suspecting that he had a leaking balloon, and fearing that the payload would be carried down into a deep gulley at the edge of the T or C airport, commanded that the flight be terminated. This caused a double action to occur:

- (1) The residual ballast [approximately 175 lb (778)] was dumped all at once, restoring positive buoyancy to the carrier balloon which began to rise quickly.
- (2) Twenty seconds later, the carrier balloon and the unopened in-line 100-ft dia (30.5 m) safety parachute were separated at the apex of the parachute.

The ALBS module was approximately 70 ft (21.3 m) off the ground when separation occurred. There was insufficient time or space for the 100-ft chute to be effective and the ALBS module essentially fell freely to the ground. The compressive loading of 17-20 g was too much for the vertical support members of the cryogenic unit and they buckled under the weights of the loaded superstructure [approximately 850 lb (3789 N)] and the load bar [approximately 375 lb (1668 N)]. Figure 21

shows the damage to the cryogenic unit. The dewars were crushed so badly that they had to be scrapped. Incidentally, the crash ruptured the dewar connections and the helium vented off through the broken lines for about 50 min after impact. All personnel stayed clear until venting had stopped.

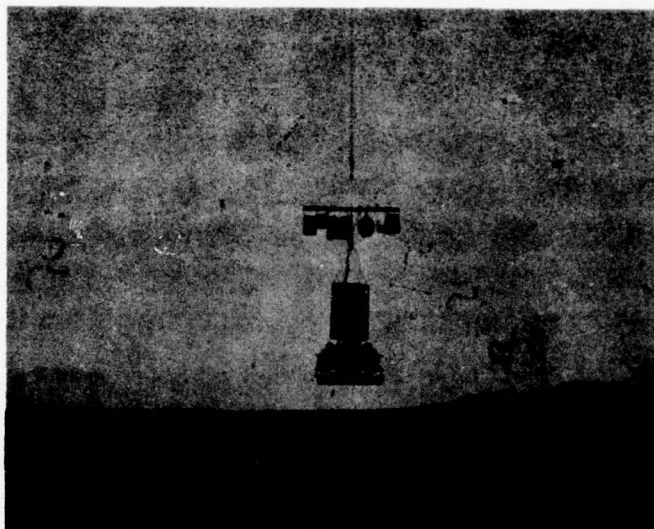


Figure 20. ALBS
Module and Load
Bar Components
Settling to Ground



Figure 21. Crushed
ALBS Cryogenic Unit

The load bar was badly bent but the components hung from it were salvageable (Figure 22). The cryogenic unit superstructure was moderately damaged but repairable. The components mounted inside the superstructure (42-ft main chute, balloon, TM pack, T-10 recovery chutes) survived surprisingly well and in many cases suffered no apparent damage.

It was later determined that the balloon was not leaking at the time of launch. It had simply been underinflated.

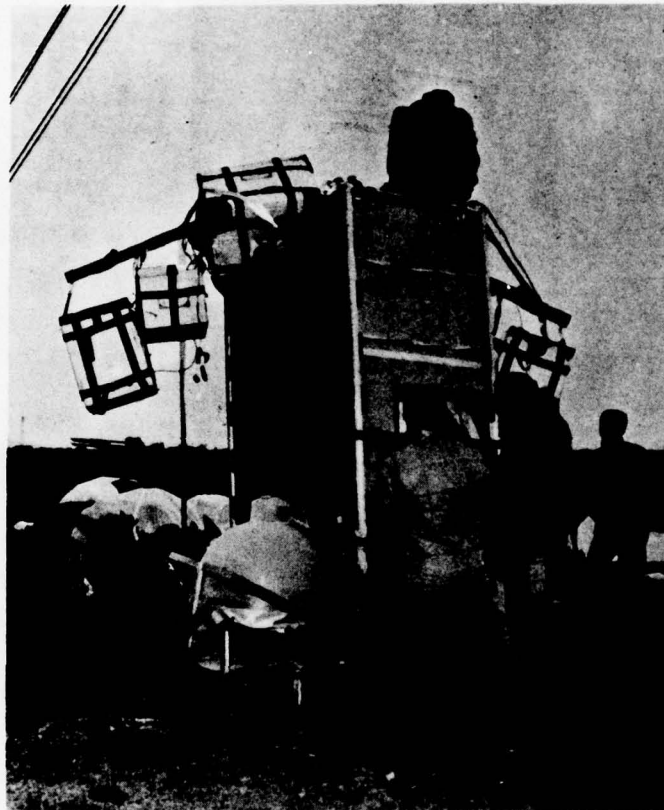


Figure 22. Bent Load Bar Atop ALBS Module

5.8 Impact of the Launch Failure

The unexpected and catastrophic loss of the cryogenic unit closed out the current flight test series abruptly, leaving many questions unanswered. All milestones, subsequent to the January flight test date, had to be cancelled, pending the making up of a new plan of action

In the months following the unsuccessful test, proposals to continue the program were adopted and are being implemented. Action is now underway to develop a follow-on ALBS module suitable for an aircraft drop. The details of this new phase of the development program will be the subject of another report.

6. SUMMARY AND CONCLUSIONS

This paper has described the preparations for and the results of the successful ALBS subsystem qualification tests at the National Parachute Test Range in 1977. It has given the details of the complicated configuration selected for the live drop of the complete ALBS prototype over the White Sands Missile Range in January 1978. The events leading up to the WSMR test are related and the unfortunate launch incident which led to destruction of the ALBS prototype is recounted.

It is concluded that much useful knowledge relevant to the stated goal of the ALBS program has been acquired in the testing accomplished to date. Not all of the questions were answered but there were no indications that the original goals cannot be met with continued development and testing.

References

1. Carten, A.S., Jr. (1978) Flight Tests of the Air-Launched Balloon System (ALBS) Prototype Model, AFGL-TR-78-0074.
2. Carten, A.S., Jr. (1976) The air-launched balloon system development program, Proceedings, Ninth AFGL Scientific Balloon Symposium, 20 October to 22 October 1976, pp 393-423, AFGL-TR-76-0306.
3. Carten, A.S., Jr. (1973) An Investigation of Techniques for Launching Large Balloon Systems for Aircraft or Rockets in Flight, AFCRL-TR-73-0633.
4. Sindt, C.F., and Parrish, W.R. (1976) A System for Inflating a Balloon Using Helium Stored in the Liquid Phase, AFCRL-TR-76-0012, NBSIR 76-834.
5. Carten, A.S., Jr. (1976) The Flight Test Aspects of the Air-Launched Balloon System Development Program, AFGL-TR-76-0196.
6. Sindt, C.F. (1979) A system for inflating an air-launched balloon, Proceedings of Tenth AFGL Scientific Balloon Symposium, 21 August to 23 August 1978, pp 149-159, AFGL-TR-79-0053.
7. Massey, W., and Wuest, M. (1978) The Air-Launched Balloon System, AFFTC-TR-77-42.

Contents

1. Introduction
2. Experimental Program

A SYSTEM FOR INFLATING AN AIR LAUNCHED BALLOON

Charles F. Sindt
Thermophysical Properties Division
National Engineering Laboratory
National Bureau of Standards
Boulder, Colorado, 80302

ABSTRACT

This paper describes a technique for inflating a balloon with helium as the balloon, its payload and the inflation system descend on a parachute. The helium used for inflation is stored in the liquid state and subsequently converted to gas using a hot bed heat exchanger. Two systems using this technique were tested. The first used a commercial liquid helium dewar and a heavy heat exchanger which was designed to prove the concept and not intended for flight. The second system, which was to be taken to the launch altitude by a carrier balloon, provided 48.5 kg of helium gas at an average temperature of 248°K in five minutes. This system, which weighed 363 kg, including helium, was self contained and required a single electrical signal for activation.

1. INTRODUCTION

The purpose of the air launch balloon system (ALBS) is to fill a balloon with helium gas while the system is descending on a parachute at some altitude. The ALBS is designed to be extracted from a flying aircraft by a small parachute. The system descends briefly before a larger parachute is deployed, after which the small parachute extracts the balloon from a bag secured to the canopy of the large parachute and extends it vertically. The balloon is ready to be inflated with gaseous helium at that point. The system is described in detail by Carten (1978).

The purpose of this paper is to describe the method by which mid-air inflation of the ALBS balloon is accomplished, prior to the balloon's ascent to floating altitude. This method has been developed by the Thermophysical Properties Division of the National Bureau of Standards under a support agreement with the Air Force Geophysics Laboratory. Two working models incorporating this inflation method have been constructed at Boulder to date and a third model is to be built over the next nine months. Tests of the first two models at Boulder and at Holloman AFB are described below, in Section 2.

In the ALBS inflation unit the helium is stored in the liquid state. The principle of operation of this unit is to convert part of the liquid helium flowing from the attached liquid helium dewar to high temperature gas then to mix this high temperature gas with a very cold gas in the correct proportion to get the desired final gas temperature for inflating the balloon. The hot gas is heated in a hot bed heat exchanger; the cold gas is converted from liquid by heat exchanging with ambient air. Figure 1 is a schematic drawing of the system.

Mid-air inflation of the ALBS balloon with this method requires approximately five minutes. The system descends about 12,000 ft (3.658 km) during this time period. After filling the balloon, the inflation unit separates from the rest of the system and descends to the ground on a three-parachute cluster. The filled balloon ascends to the desired altitude carrying the payload and the large parachute which is later used to recover the payload.

2. THE EXPERIMENTAL PROGRAM

2.1 Proof of Concept Experiment

The first experimental system tested the concept of using liquid helium and a hot-bed heat exchanger to produce helium gas for inflating a balloon on the ground. This system is described in detail by Sindt (1976). Liquid for this system was supplied from a commercial liquid helium dewar that was pressurized with helium gas from a commercial high pressure gas cylinder. The hot bed heat exchanger, which contained 3/8 inch diameter aluminum oxide balls that were used as the heat storage media, was designed to stand on a truck bed.

Two balloons were filled with the system; one balloon was filled at NBS, Boulder, Colorado; the second balloon was filled at Holloman Air Force Base, New Mexico. The 300 m³ balloon that was filled at Boulder was not launched. It was filled in 407 seconds with 45.8 kg of helium gas at an average temperature of 265 K. This system is shown in figure 2 and the balloon is shown in figure 3. The 4106 m³ balloon filled at Holloman Air Force Base was launched and subsequently ascended to 22,000 meters altitude. This balloon was filled with 46.2 kg of helium gas at 270 K. Figure 4 shows the system and the balloon. The successful filling of two balloons opened the way for the design and fabrication of a follow-on inflation unit constructed of lighter materials and suitable for flight tests.

2.2 Balloon Launched Flight Experiment

The second experimental system which was part of an ALBS prototype model was to be carried to the launch altitude of 7600 m by a large, ground-launched balloon. This launching of the ALBS was similar to the design objective of launching the balloon from a flying aircraft. The difference was that the small parachute was suspended from the load bar of the carrier balloon and was to be deployed upon the release of the ALBS from the load bar. This method of air launching the system does not impose high loads at the launch; therefore, the system was designed to accommodate only those peak loads that occur when the large parachute opens after the system is released from the carrier balloon. Also, the system did not need to be aerodynamically clean nor compact as would be desired for a unit that was to be launched from a flying aircraft.

2.2.1 EXPERIMENTAL BALLOON INFLATING SYSTEM

Since compactness of the system was not required, two existing dewars were used as the liquid helium containers instead of purchasing one new vessel.

Using the two dewars instead of one, complicated the system plumbing but was less expensive and time consuming than purchasing one new dewar designed for this application. Also, since they were made of titanium, the two existing dewars weighed less than any one available dewar of the correct size. The dewars each held 24.5 kg of liquid helium; with five percent ullage, the dewars held a total of 46.6 kg of liquid helium, the mass of gas desired for filling the balloon in mid-air.

The two dewars were mounted one on each side of a hot-bed heat exchanger. This arrangement resulted in a balanced system weight about the heat exchanger. The dewars were connected in series by a vacuum insulated line, so they emptied consecutively. No additional valves or controls were needed between the dewars. Each dewar required modification since they were designed originally to provide supercritical hydrogen for the Apollo life support system. The flow diagram for this system is the same as is shown in figure 1.

The hot bed heat exchanger contained 73.4 kg of 3/8 inch diameter aluminum oxide balls. This bed was designed to store the heat required to convert 46.3 kg of liquid helium to gas at 260 K. The design bed temperature was 1005 K with a maximum operating limit of 1080 K. A 2000 watt electrical heater heated the bed and temperature was maintained with a thermostat control. The heat exchanger was insulated with a 6.4 mm thick blanket and a 57 mm annulus of evacuated powder. The estimated heat loss of the heat exchanger at 1005 K was 400 watts.

The system used gas pressure to force the liquid helium from the dewars at a mass flow rate of 0.16 kg/s. The helium gas used for pressurization was stored at 32.4 MPa pressure in a 0.011 m³ aluminum cylinder which was reinforced with a glass fiber, epoxy wrap.

Valves used in the system for controlling the liquid and gas flow were industrial weight, solenoid valves designed for cryogenic service. The valve used in the helium gas pressurization line was a "flight weight" solenoid valve.

An electric timer with switches controlled the valve opening sequence. The timer and the valves were powered by a 24 volt battery.

The system components were mounted on an aluminum frame which was designed to support the components under a seven g load. To assure that the frame was strong enough to withstand these forces, the mounting pads for the dewars and the hot bed were loaded with lead weights equivalent to the loads expected. A

small additional dynamic load was then applied to each pad. A four foot by eight foot by one-half inch thick piece of plywood was attached to the base of the frame to provide a surface for installing several layers of crushable pad. The crushable pad was to cushion the landing of the cryogenic unit as it descended on the recovery parachutes. A small aluminum rail extended around each dewar to protect them during the ground launch. The cryogenic system weighed 314 kg without liquid helium.

The ALBS inflation unit was designed to operate independently of controls other than a 10 second switch closure which initiated the clock timer. The final sequence of system events were established as follows. The system started functioning 10 seconds after the timer switch closure when the dewar pressurization valve opened and the dewars were pressurized to 338 kPa. Twelve seconds later the liquid valve at the dewar exit opened and helium started flowing into the mixing area at the base of the heat exchanger. The secondary bypass valve opened two seconds later to increase the cold gas flow. At nine seconds after the liquid flow started the valve to the heat exchanger opened. Full flow was established 20 seconds after the start of liquid flow. One hundred and seventy seconds after the start of liquid flow the first dewar emptied. This resulted in less flow resistance in the liquid system and a higher liquid flow rate. To help compensate for an unbalance in the flow split between the heat exchanger and the cold bypass that occurred with higher flow rate, the secondary bypass flow was terminated. Even with the closing of the secondary bypass, the flow rate increased 15 to 20 percent and this increased flow rate continued until the second dewar emptied at about 300 seconds.

From the mixing chamber at the base of the hot bed heat exchanger the gas flowed through a 10 cm diameter tube into a 2.4 kg bed of 3/8 inch diameter balls of aluminum oxide. This second bed was not heated but served to increase the mixing of the hot and cold gas streams and to reduce the maximum temperature spike which occurred at the opening of the valve to the heat exchanger. From this mixing bed the gas flowed into a 16.5 cm diameter tube. This tube which terminated at the top of the frame was the gas supply tube for the balloon.

All of the flow paths from the liquid helium dewar contained replaceable orifices which were used to adjust the flow rates. Openings in these orifice

plates were sized during a test program in which a number of tests were conducted to establish the correct dewar pressure and flow rates to get an average mass flow rate of 0.16 kg/s at an average gas temperature of 260 K.

2.2.2 TEST OF THE EXPERIMENTAL BALLOON INFLATING SYSTEM

For the final test at Boulder both dewars were cooled for 24 hours, then the dewars were filled with liquid helium one hour prior to the run of the system. One half hour before the run the dewar vents were closed. The dewar pressure rose to 75 kPa before the run started. When the vents were closed the dewars contained 48.5 kg of liquid helium which was about five percent over the required mass. The run lasted 295 seconds. The peak gas temperature was 355 K with the temperature remaining above 320 K for less than 15 seconds. The minimum gas temperature was 176 K with the temperature remaining below 220 K for less than 20 seconds. The maximum flow rate was about 0.2 kg/s. The average flow rate was 0.165 kg/s and the average discharge gas temperature was 248 K. The discharge gas from this test flowed through five meters of the polyethylene fill tube that was to be used for the flight tests. The system delivered five percent more mass than required but the average gas temperature was five percent low. Since the larger than design mass would nearly offset the loss of lift in the balloon due to the low gas temperature, the system was accepted as ready for the flight test in this configuration.

2.2.3 THE FRAME FOR THE ALBS

In addition to building the ALBS inflation unit, the Thermophysical Properties Division provided further support to the Air Force by building an enclosed superstructure to hold the main parachute, the air launched balloon, the balloon's payload and the parachutes for recovery of the cryogenic unit. The enclosure of the superstructure was 96 cm by 137 cm by 198 cm high. The frame of the superstructure had four lugs at the base for attaching it to the cryogenic unit with four 1/2 inch bolts. The superstructure frame carried clevis mounts for attaching all of the parachutes; therefore, it was designed to carry the loads that were generated when the main parachute opened. The cryogenic system with the superstructure attached is shown in figure 5.

2.2.4 FLIGHT TEST OF THE ALBS

The ALBS was completely assembled at Holloman AFB in January 1978 and was taken to Truth or Consequences, New Mexico for the demonstration flight test. On January 18, 1978, about 18 hours prior to the flight time, the dewars were cooled to liquid helium temperature. One dewar was filled to 100 percent full. The second dewar was filled to about 25 percent full. The dewars were completely filled with liquid helium about 2-1/2 hours prior to the ground launch. The vents were closed at about 75 minutes before the launch at which time the system contained 46.2 kg of liquid helium. The dewar pressures rose to about 120 kPa gauge by launch time. This pressure rise rate was acceptable if the system was to function within 70 minutes from the ground launch. Figure 6 shows the system after the dewars were filled. As is explained by Carten (1978), the flight of the carrier balloon was terminated shortly after launch, for reasons unrelated to the ALBS, and the inflation unit was damaged beyond repair. Because of this accident no test data were obtained relative to the planned mid-air inflation and the usefulness of the configuration flown was not demonstrated.

2.3 Aircraft Launched ALBS

A third system which is now being constructed is the experimental model that will be extracted from a flying aircraft. Figure 7 shows a skeleton drawing of this system which is enclosed in a 1.2 meter cube. The system is designed to operate at a higher pressure than the other systems since the fill tube from the cryogenic unit to the balloon is to be smaller in diameter and constructed of a stronger material than the conventional 3 mil polyethylene fill tube. This system is to be tested next year.

REFERENCES

- Carten, A. S., Jr., (1978) The Air Launched Balloon System (ALBS) Flight Test Program, Proceedings of the 10th AFGL Scientific Balloon Symposium, pp. AFGL-TR-78- .
- Sindt, C. F. and Parrish, W. R. (1976), A system for inflating a balloon using helium stored in the liquid phase, Nat. Bur. Stand. (U.S.) Interagency Report 76-834, AFCRL-TR-76-0012.

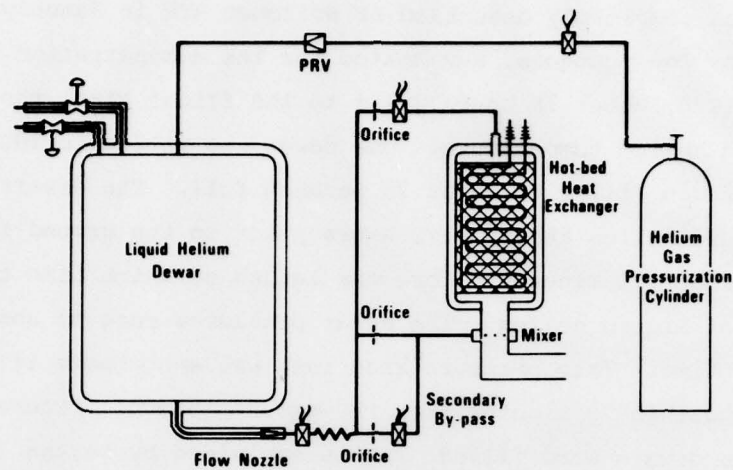


Figure 1. Air Launched Balloon System - Schematic

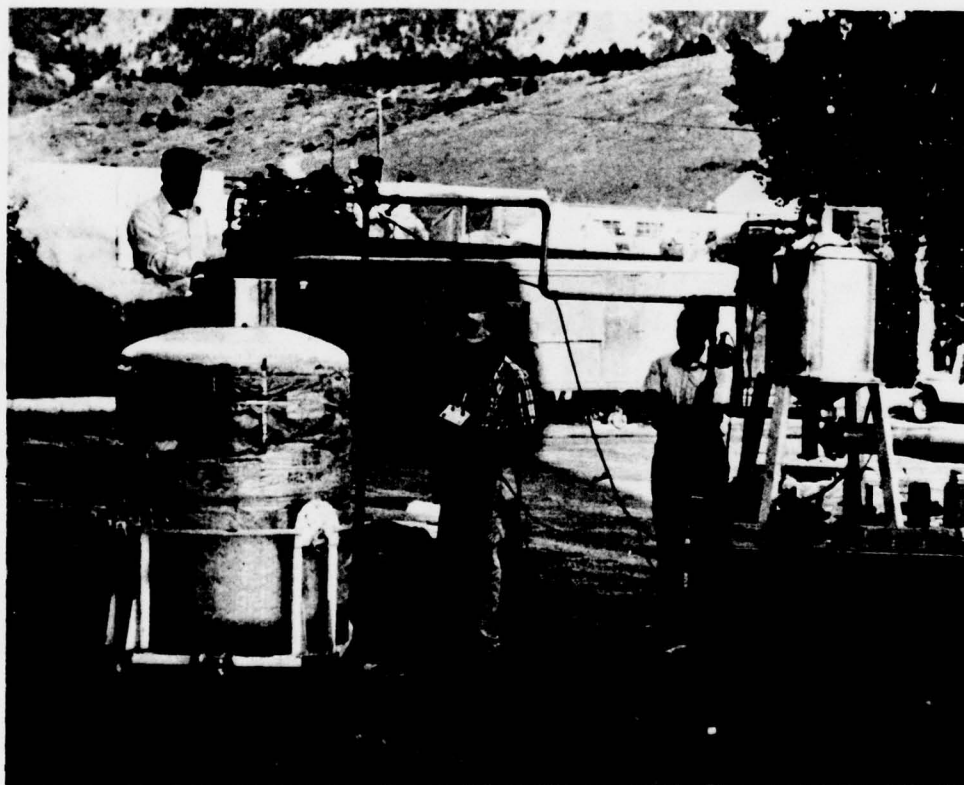


Figure 2. Ground Test System at Boulder, Colorado



Figure 3. Balloon Filled at Boulder, Colorado

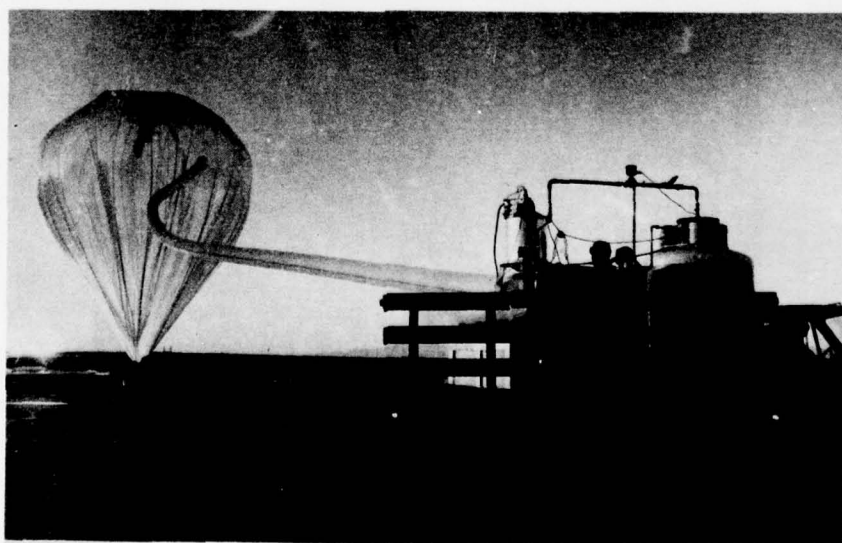


Figure 4. Filling the Balloon at Holoman Air Force Base, New Mexico

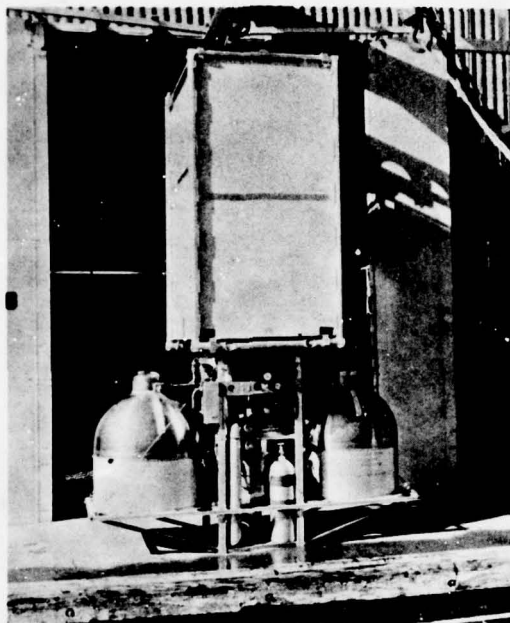


Figure 5. The Cryogenic Unit With the Superstructure Attached

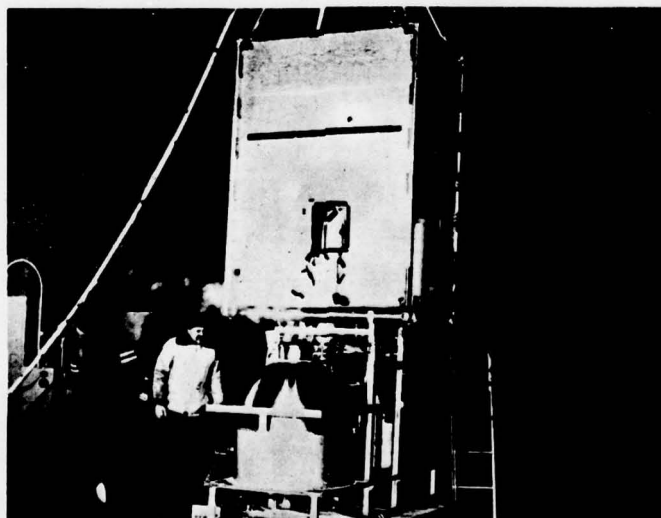


Figure 6. The Air Launched Balloon System at the New Mexico Launch Site

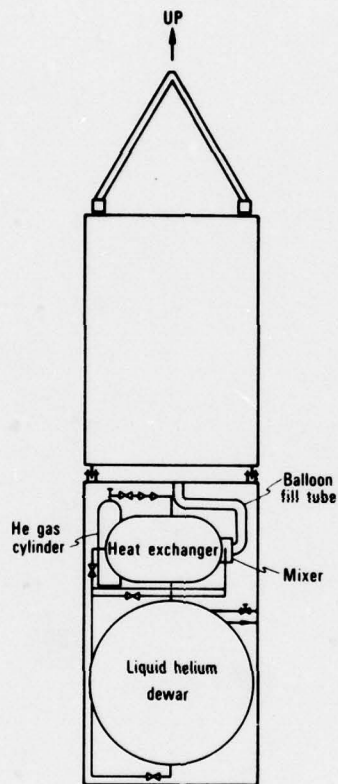


Figure 7. Skeleton Drawing of the
Air Launched Balloon System

ABSTRACT

FACILITIES FOR REAL-TIME FLIGHT SUPPORT OF SCIENTIFIC BALLOON EXPERIMENTS

J. Craig Erickson
Physical Science Laboratory
New Mexico State University

There are only two balloon-launch facilities in the United States: the Air Force Geophysics Laboratory (AFGL) Detachment 1 at Holloman Air Force Base, N.M., and the National Scientific Balloon Facility in Palestine, Texas. This paper describes the program for improving the ground support facilities at AFGL Det 1 to accommodate scientific users. The modernization program, underway for two years, includes improving the base support system and remote mobile facilities used either in conjunction with the base, or as stand-alone units in the field. The work is being performed by the Physical Science Laboratory of New Mexico State University.

An experimenter having unlimited resources - an exception rather than the rule - can afford to configure his onboard payload to optimize performance, and can usually provide his own ground support system. The average experimenter does not enjoy this luxury. His primary concern is for the balloon-borne scientific apparatus that is the basis of his mission. He depends upon AFGL Det 1 for data collection, telemetry, recording, display, command and control. The AFGL improvement program seeks to minimize the cost of these support functions to resource-limited experimenters. Economies can be realized through commonality and standardization of support hardware and software. The unique requirements of each experiment are not constrained and are actually enhanced by taking advantage of the extensive equipment and experience available.

This paper discusses real-time facilities primarily associated with reception, collection, manipulation and display of transmitted PCM telemetry data. The ground system operates with either an AFGL-provided, standard PCM data encoder, or encoders supplied by the experimenter. Multiple displays present real-time information about the on-board scientific apparatus. Collected data are recorded on analog and digital magnetic tape for analysis at the ground station, or later at the user's home station. The ground station is configured about a Digital Equipment Corp. PDP-11/40 computer and peripherals and EMR telemetry equipment.

Standard software is available for the "standard" data set, and special programs can be developed for users with special requirements. An example cited is the program of Dr. Earl Good, AFGL, who is seeking information for modeling upper atmosphere turbulence. Special manipulation, or special programs were generated together with special displays enabling him to continuously monitor status of the experiment and to make real-time decisions.

The paper concludes with a discussion of other techniques available to further increase the effectiveness of experimenter/payload interaction and optimization of the balloon flight profile.

The contents of this paper will appear in the Final Report for USAF Contract F19628-78-C-0070 with New Mexico State University.

Session I
BALLOON TECHNOLOGY — PROGRESS AND PROBLEMS

Part 2

Chairman, James F. Dwyer
AFGL

REQUIRED, A NEW ZERO PRESSURE FREE BALLOON SHAPE

J.F. Dwyer/AFGL

The historical background of the case for a neo-natural shape balloon design presented at this symposium is being published under the title, "Zero Pressure Balloon Shapes, Past, Present and Future." It will appear in the "Proceedings, Symposium on the Scientific Use of Balloons" (COSPAR 1978). This text restates some of the justification, but with additional supporting documentation.

Today's balloons, for the most part, utilize the natural shape design attributed to Upson (1) and further clarified by the University of Minnesota (2) and Smalley (3). The most advanced versions of this design concept - those that seem to be pacing technological growth - incorporate loadcaps according to the design and fabrication procedures of Winzen Research, Incorporated. These loadcaps are constructed from identical meridional gores which are most apt to be fully tailored, except at the base end, where a surplus of gore width is required for installation of the end fitting. They incorporate meridional load tapes which are secured to each gore seam as shown in Figure 1. The load tapes serve a two-fold purpose. First, they provide a means of transferring the load into the film, and second, they restrict the meridional straining of the seam, an action which apparently improves the transverse seam strength (at least in the case of cylindrical models). In this regard it is interesting to note that a variety of loadtape materials (with widely different properties) have been used successfully. They range from nylon fibers with an ultimate elongation of 18 percent to glass fibers with only 3.2 percent ultimate elongation. The assorted gore patterns (Fig 2) used with these tapes most surely played

an important part in accommodating the noted disparity in "room temperature" ultimate strain.

Figure 3 depicts schematically the general features of the modern polyethylene balloon. It is expected that a neo-natural shape design will be similarly constructed, but will have improved capability and efficiency.

Capability has been defined in different ways, but a comprehensive measure of capability, λ , has been rigorously defined by the author (4) as the cube root of the ratio of the payload weight to the specific lift of the inflatable at float altitude. Figure 4 shows values of λ versus the year in which the value was first achieved. It is clear from this figure that improved capability using contemporary design criteria will be achieved very slowly.

Another popularly suggested measure of capability (specific rather than comprehensive) is float altitude, the major technological influence on which is film weight, and thus film thickness. As a general rule, these measures (altitude and thickness), like those of many technologies, are believed to follow a trend characterized by a slow start, a rapid change stage and finally a mature state in which change is quite slow, and progressively much slower: such a trend was dramatically evident in the aforementioned comprehensive capability analysis (4). The quality of the fit for both of these specific measures seems to justify the selection of the same trend type for this analysis. Figure 5 shows that the correlation between the altitude and film thickness for the given time span is as expected. Further, the greatly reduced tendency toward achievement of even thinner films suggests that higher altitudes will result, not so much from thinner film as from an ability to use the strengths inherent in presently achievable film thicknesses. This ability will depend largely upon our developing advanced design criteria which will take into account

the actual load-deformation characteristics not only of the envelope material but also of the meridional reinforcement tapes, as well as the influence of the use environment on both.

Capability growth, whether measured comprehensively or specifically, appears to be strongly related to film technology. In balloon technology, the film quality required is high, but the annual tonnage used is low. Selection is thus economically restricted to those resins (if not those actual films) that are commercially available. Because there appears to be no economically competitive candidate film or resin at this time, we must strive to better understand the load-deformation characteristics of our present film, and to develop design criteria to enable us to make better use of it.

It is expected that any new design criteria will be based on a shape which yields an essentially constant volume over the total range of payload capability of a given balloon. This reasonably assumes that the material strains have a negligible effect on the volume. The analogous case for the present natural shape balloon demonstrates the expected advantage. In this case the balloon would be designed to carry a specific maximum payload at a specified altitude, and it would be fabricated so as to have no surplus circumferential material when flown with the design load. Under these circumstances, any other payload within the design range will be smaller, and the balloon volume will remain essentially constant with only a small, but tolerable, variation in the envelope stress field. The limiting case for this analogy would be the natural shape characterized by $\Sigma = 0$ (3), a shape which presumes a weightless envelope, and is thus theoretically invariant with payload.

Because the relationship between the natural shape balloon surface area (A) and volume (V) (accurate to within 0.25 percent over the range

of useful Σ values) is

$$A = 4.925V^{2/3},$$

obviously there is no envelope weight penalty. Further, since the shape for $\Sigma = 0$ is the least oblate natural shape, and since gores are made from a fixed width of lay-flat tubing, there will be a minimum number of gores to seal, and thus reduced labor cost and greater potential reliability. Finally, use of a constant volume balloon can increase the gross lift by up to 10 percent by eliminating the volume reduction resulting from shape changes at higher than design payloads.

Improved balloon design criteria are needed not only to provide improved capabilities, but also to assist in adequately specifying the critical properties of balloon structural materials. Adequate specification of critical material properties is most important when the normally used commercial materials are removed from the market and substitute materials must be found. (The polyester fibers now used in balloon load tapes present a case in point: they replace Fortisan fibers which are no longer manufactured.) Further, these criteria will form the basis for analytical techniques applicable to the evaluation of structural loads and failures in the flights of balloons made in accordance with contemporary design standards.

In summary, there are direct and indirect advantages to be gained through the development of a neo-natural shape balloon design. As shown, both here and in the 1978 COSPAR presentation, such a design should consider at least:

- (A) Elimination of volume defect by designing for full deployment at maximum payload.
- (B) Definition of pertinent mechanical properties of the synthetic material structural members which depend upon their load-strain-temperature histories.
- (C) Accommodation of the variability and effects of the intended use environment.

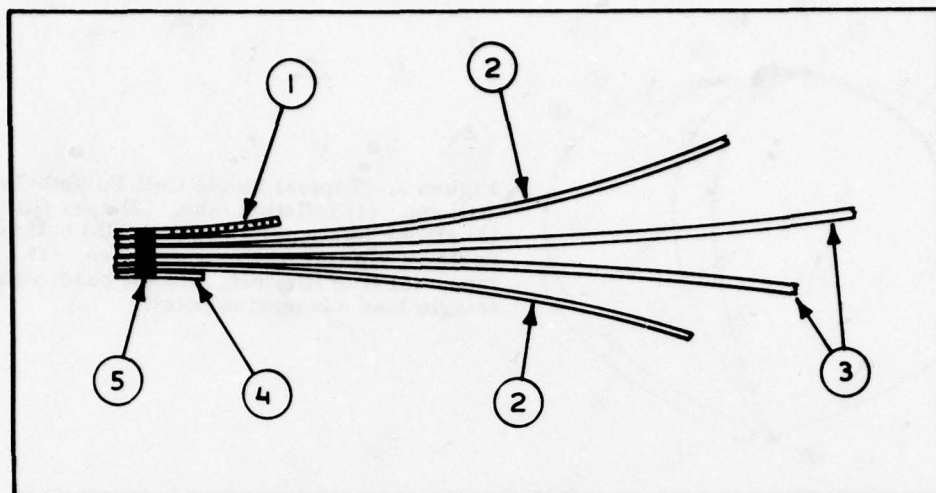


Figure 1. Modern Polyethylene Balloon Gore Seam. (1) Load tape, (2) balloon gores, (3) load cap gores (if any), (4) back-up tape, and (5) heat sealed region

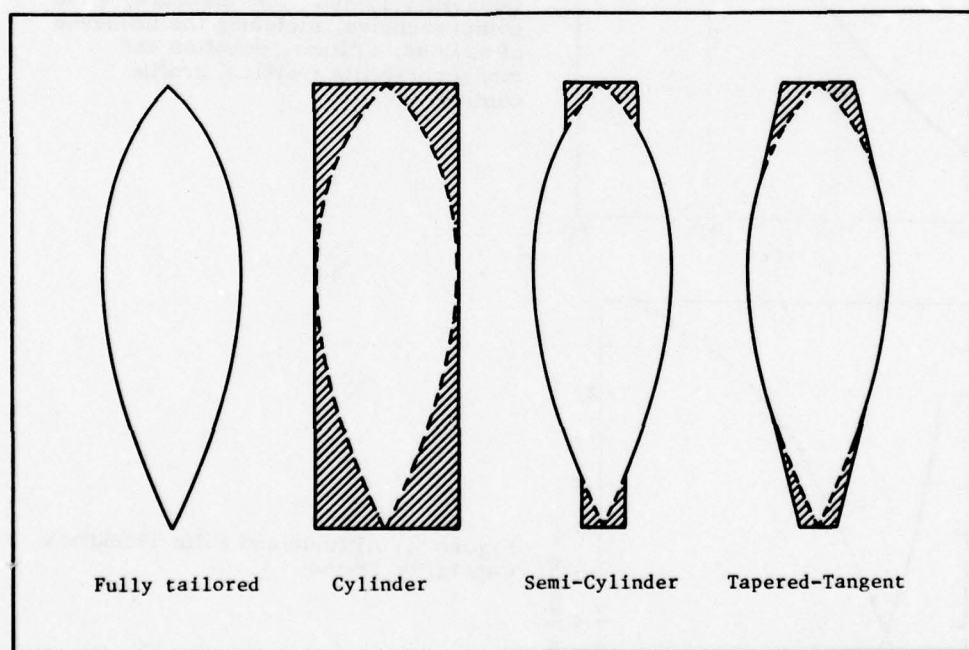


Figure 2. Historical Gore Patterns for Polyethylene Balloons

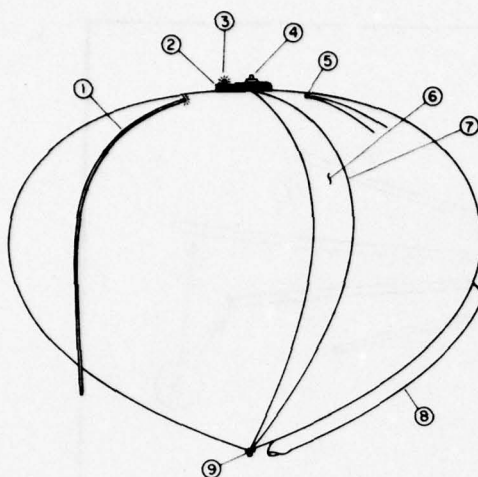


Figure 3. Typical Single Cell Polyethylene Balloon. (1) Inflation tube, (2) apex fitting, (3) strobe light, (4) gas valve, (5) balloon destruct rip line system, (6) gore, (7) load tape, (8) free lift duct, and (9) base fitting (single load suspension point)

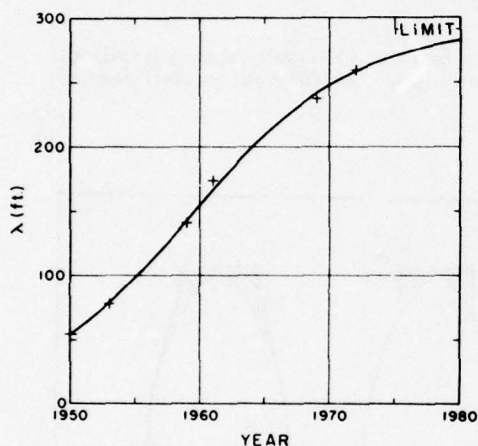


Figure 4. Zero Pressure Free Balloon Capability Trend. The measure, λ , is comprehensive, including the influence of payload, altitude, duration and maneuverability (vertical profile control)

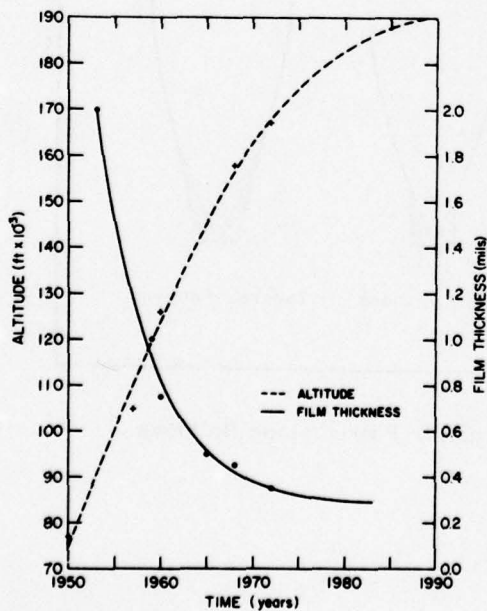


Figure 5. Altitude and Film Thickness Capability Trends

Contents

1. Introduction
2. Theoretical Model
3. Solution Technique
4. Results and Discussion
5. Conclusions

ANALYSIS OF BALLOONS IN OFF-DESIGN CONFIGURATIONS

J. L. Rand
Texas A&M University
College Station, Texas

Abstract

This paper presents the detailed formulation of a new physical model for determining the shape and stress distributions in a balloon operating in an environment for which it was not designed. Limited results are presented which indicate the presence of circumferential stresses and lobing in a natural shape balloon. Although the stresses are reasonable in value the distribution bears little resemblance to those computed using the design shape even at the design altitude.

1. INTRODUCTION

A balloon system is routinely designed to a shape which is dictated by a specific design payload and altitude. However, when placed in service, the system must operate under a variety of conditions which could cause significant departures from the design shape. Since even small departures from this shape cause the material to strain in the circumferential direction, an effort has been made to incorporate material deformation into both the design and analysis process. The original natural shape design was developed on the premise that seam strength was low relative to the film strength. However, manufacturing techniques have improved to such a point that it is now considered feasible to operate these systems with a moderate amount of circumferential stress. In particular, one laboratory is interested in operating balloons above the design altitude, since this would be a relatively constant volume system. Another laboratory is interested in the state of stress when a heavily loaded balloon operates below the design altitude.

A number of other problems exist which can only be explained by the presence of a predictable state of circumferential stress.

In the design of a zero pressure single cell balloon, the inclusion of material deformation is relatively straight forward provided the natural shape is desired. The assumed absence of circumferential stress, uniform meridional strain and developable surface of revolution produces a design shape which yields not only the usual shape and total load parameters, but also the distribution of both tape forces and film stresses along the gore. In addition, the circumferential strain distribution may be used to compute the difference between the deployed shape and the manufactured shape of each gore. This work was performed at Texas A&M University under my supervision and was presented earlier this year by Keese at the AIAA National Student Paper Competition.

The stress analysis of a flexible structure is significantly different from the design problem. Once the balloon has been manufactured, the available material at each gore position is fixed and the solution must be obtained as a boundary value problem. In addition, the simplifying assumptions of zero circumferential stress and a surface of revolution can no longer be made, which alters the formulation of the governing differential equations. This problem has been recognized for several years and various researchers have obtained solutions with varying degrees of success.

Gilbert was able to successfully model a parachute structure utilizing finite element techniques and assuming zero circumferential stress in order to optimize the aerodynamic drag characteristics of the system. Although the formulation of the differential equations is quite similar to those presented here, the radically different boundary conditions due to free surfaces at each end of the gore prevents the use of this program directly. Alexander solved this problem for several balloon systems by assuming that the load tapes assumed the design shape of the balloon. The film was permitted to bow out between the tapes and the stresses were computed. This approach permitted the meridional radius of curvature to change across the gore but this in turn prevented the equilibrium equation in the meridional direction from being satisfied.

The formulation to be presented here will postulate a mechanism by which loads are transferred between the load tapes and the film. The combination of shear stress in the film and lobing between load tapes allows the load to be transferred back and forth between the load carrying members in a manner which is easily visualized.

2. THEORETICAL MODEL

2.1 FORMULATION OF PROBLEM

In developing the theoretical model to determine the state of stress in a balloon system, a number of features will be introduced here for the first time. In order to eliminate as much confusion as possible, Lagrangian coordinates will be used throughout

this formulation. Lagrangian coordinates are routinely used in time dependent problems in the area of fluid and solid mechanics to denote the position of the particles initially. However, this system of coordinates is ideally suited to problems in elasticity where material properties have been defined with respect to the undeformed dimensions. All balloon material properties now being developed at Texas A&M University utilize "engineering" stress and strain rather than "true" stress and strain. Therefore, in this system of coordinates, the stress is defined as the load per unit initial (as manufactured) area rather than the actual area. The Lagrangian gore length remains the manufactured length, regardless of the actual deformed length of the gore. Another important quantity which is simplified by this technique is the increment of balloon film or tape weight between any two gore positions. This increment is known from the manufactured shape and remains fixed regardless of deformation.

In general, it will be assumed that each balloon gore deploys in an identical manner about the balloon centerline. All deformations will be assumed to be linearly elastic and orthotropic although numerical results have been obtained only for the isotropic case. The film will be permitted to lobe between the load tapes resulting in a surface which is not a surface of revolution. Due to the assumed symmetry of deployment, equilibrium equations will be written for a single differential element of tape and an adjacent element of film at an arbitrary gore position.

The usual deformed-balloon coordinate description as shown in Figure 1 will be used to demonstrate the compatibility of this formulation with the familiar design equations. The film is assumed to lobe in a direction perpendicular to the load tape or in the direction of the meridional radius of curvature, R_m . The deployed distance of the load tape from the centerline in the horizontal plane is designated r .

2.2 Tape Equilibrium

Consider a differential length of tape at some arbitrary point on the balloon as shown in Figure 2. The forces acting on this element include a changing tape force, F , as well as forces due to the film stresses, τ and σ_c , and the tape weight. It may be noted at this point that the actual length of the element is ds whereas the original length was ds_0 . Since "engineering" stress will be used consistently, the original film area will be $t_0 ds_0$ where t_0 is the undeformed film thickness. Therefore, the stress will always be multiplied by t_0 so that the units of stress may simply be considered to be load per unit original length.

Summing forces in the vertical direction it can be shown that:

$$(F+dF)\cos(\theta+d\theta) - F\cos\theta - W_T ds_0 - 2\tau \cos\theta ds_0 - 2\sigma_c \sin\beta \sin\theta ds_0 = 0$$

The circumferential stress term arises from the fact that β is defined in a plane containing the meridional radius of curvature and not the horizontal plane. This

equation may be rewritten by taking the limit as ds_0 and $d\theta$ approach zero as:

$$\frac{d(F\cos\theta)}{ds_0} = W_T + 2\tau\cos\theta + 2\sigma_c\sin\beta\sin\theta \quad [1]$$

A second differential equation may be obtained by summing forces in the horizontal plane. The resulting differential equation after taking the limit as above becomes:

$$\frac{d(F\sin\theta)}{ds_0} = 2\tau\sin\theta - 2\sigma_c\sin\beta\cos\theta \quad [2]$$

Equations [1] and [2] express the equilibrium of forces acting at any point along the load tape.

2.3 Film Equilibrium

Consider now a differential length of film that runs between two adjacent load tapes at the same gore position as shown in Figure 3. Here it will be assumed that some sort of constant meridional stress will be uniformly distributed across the gore width which is $2\pi r_0/N$ where N is the number of gores and r_0 is the manufactured radius of the balloon. The meridional stress is permitted to change in the meridional direction as shown. In addition there will be forces due to the shear stress, τ , the circumferential stress, σ_c , the film weight which is expressed in Lagrangian coordinates and the force due to pressure. This last force is obtained by using the actual projected area which may then be expressed in the original coordinates by observing the definition of meridional strain, i.e.,

$$\frac{ds}{ds_0} = 1 + \epsilon_m \quad [3]$$

Summing forces in the vertical direction it can be shown that:

$$\begin{aligned} \frac{2\pi}{N}(r_0\sigma_m + d(r_0\sigma_m))\cos(\theta + d\theta) - \frac{2\pi}{N}r_0\sigma_m\cos\theta - \frac{2\pi}{N}r_0W_f ds_0 + 2\tau\cos\theta ds_0 \\ - 2pr\sin(\frac{\pi}{N})\sin\theta ds + 2\sigma_c\sin\beta\sin\theta ds_0 = 0 \end{aligned}$$

Utilizing equation [3] and taking the limit as ds_0 and $d\theta$ approach zero, this equation becomes.

$$\frac{d(r_0\sigma_m\cos\theta)}{ds_0} = r_0W_f + pr(1 + \epsilon_m)\frac{N}{\pi}\sin(\frac{\pi}{N})\sin\theta - \frac{N\tau}{\pi}\cos\theta - \frac{N}{\pi}\sigma_c\sin\beta\sin\theta \quad [4]$$

A second differential equation for the film may be obtained by summing forces in the horizontal plane and taking the limit as before. The resulting equation is:

$$\frac{d(r_0\sigma_m\sin\theta)}{ds_0} = -pr(1 + \epsilon_m)\frac{N}{\pi}\sin(\frac{\pi}{N})\cos\theta - \frac{N\tau}{\pi}\sin\theta + \frac{N}{\pi}\sigma_c(\sin(\frac{\pi}{N})\cos\beta + \cos\frac{\pi}{N}\sin\beta\cos\theta) \quad [5]$$

2.4 Governing Equations

In working with these equilibrium equations it is a simple matter to rotate the system in such a way that the equilibrium equations in the meridional and normal directions are obtained. When this is accomplished the equations become:

Meridional Tape Equilibrium

$$\frac{dF}{ds_0} = 2\tau + W_T \cos \theta \quad [6]$$

Normal Tape Equilibrium

$$F \frac{d\theta}{ds_0} = -(W_T \sin \theta + 2\sigma_c \sin \beta) \quad [7]$$

Meridional Film Equilibrium

$$\frac{d(r_0 \sigma_m)}{ds_0} = r_0 W_f - \frac{N}{\pi} \tau + \frac{N}{\pi} \sigma_c \sin \theta [\sin \frac{\pi}{N} \cos \beta + \cos \theta \sin \beta (\cos \frac{\pi}{N} - 1)] \quad [8]$$

Normal Film Equilibrium

$$r_0 \sigma_m \left(\frac{d\theta}{ds_0} \right) = -r_0 W_f \sin \theta - pr(1+\epsilon_m) \frac{N}{\pi} \sin \frac{\pi}{N} + \frac{N}{\pi} \sigma_c [\sin \frac{\pi}{N} \cos \beta \cos \theta + \sin \beta (\cos \frac{\pi}{N} \cos^2 \theta + \sin^2 \theta)] \quad [9]$$

It may be noted that the governing equations in the normal direction, equations [7] and [9], are not influenced by the shear stress. However, at this point no distinction has been made between the angle θ when referred to the tape or the film. A discussion of this critical feature will be deferred to the next section of this paper.

Several additional equations are required to form a complete set. If the circumferential strain is defined as the change in gore width per unit original gore width, it may be expressed as:

$$1+\epsilon_c = \frac{r \sin \pi/N}{r_0 \sin(\alpha+\beta)} \frac{(\alpha+\beta)}{\pi/N} \quad [10]$$

where

$$\alpha \equiv \sin^{-1} [\sin \pi/N \cos \theta]$$

The material is assumed to be linearly elastic and orthotropic so that:

$$\epsilon_m = D_m \sigma_m + D_{mc} \sigma_c \quad [11]$$

and

$$\epsilon_c = D_{mc} \sigma_m + D_c \sigma_c \quad [12]$$

Finally, the geometric relationships are employed such that:

$$\frac{dr}{ds_0} = (1+\epsilon_m)\sin\theta \quad [13]$$

and

$$\frac{dz}{ds_0} = (1+\epsilon_m)\cos\theta \quad [14]$$

It is now a matter of arranging these equations into a suitable form which will be tractable for solution.

3. SOLUTION TECHNIQUE

In order to solve the set of equations just developed it is necessary to make some additional assumptions regarding the stress field and the tape angle. Since the tape force, F , appears in both tape equilibrium equations it is necessary to employ some sort of relationship between this force and the film forces. Therefore, it is assumed that the tape force is proportional to the meridional strain in the film. Therefore,

$$F = K_T \epsilon_m = K_T D_m \sigma_m + K_T D_{mc} \sigma_c \quad [15]$$

where K_T is the "tape modulus".

Although this assumption is reasonable at the interface between the tape and film, the assumption of a uniformly distributed stress across the gore will result in a uniform strain which will dictate the tape force. The alternative to this approximation is to allow the meridional strain to vary across the gore. This would result in a set of partial differential equations which would increase the computational time considerably.

3.1 The Design Equations

The equations of equilibrium may be arranged in a more familiar form if the total meridional load is defined as the sum of the tape forces and the film forces. Specifically,

$$T \equiv r_0 \sigma_m + \frac{NF}{2\pi} \quad [16]$$

The two meridional equilibrium equations [6] and [8] may be added together to finally yield,

$$\frac{dT}{ds_0} = \left(\frac{NW}{2\pi} + r_0 W_f \right) \cos\theta + \frac{N}{\pi} \sigma_c \sin\theta \left[\sin\left(\frac{\pi}{N}\right) \cos\beta + \sin\beta \cos\theta \left(\cos\frac{\pi}{N} - 1 \right) \right] \quad [17]$$

It may be noted that the shear stress which appeared in both of the contributing

equations is self equilibrating and does not appear in equation [17]. In addition, if the circumferential stress is assumed to be zero, this equation will reduce to the design equation for a natural shape balloon as reported by Smalley.

In a similar manner the equilibrium equations in the normal direction, equations [7] and [9] may be combined. However, in doing so it is necessary to assume that the tape and film are deployed at the same angle. When added together the following equation is obtained:

$$\begin{aligned} T \frac{d\theta}{ds_0} = & - \left(\frac{NW_T}{2\pi} + r_0 W_f \right) \sin\theta - pr(1+\epsilon_m) \frac{N}{\pi} \sin \frac{\pi}{N} + \frac{N}{\pi} \sigma_c \left[\sin \frac{\pi}{N} \cos\beta \cos\theta \right. \\ & \left. + \sin\beta \left(\cos \frac{\pi}{N} \cos^2\theta - 1 + \sin^2\theta \right) \right] \end{aligned} \quad [18]$$

This equation will also reduce to the familiar design equation if there is no circumferential stress and if $\sin \frac{\pi}{N} = \frac{\pi}{N}$. It must be observed that in order to obtain this equation no distinction may be made between the tape and film angles. This approximation is quite reasonable over the majority of the gore length; however, near the ends θ must be thought of as the average of two different angles.

A third useful relation may be obtained if it is assumed that the derivatives in equations [7] and [9] are equal. If the difference between these two derivatives is set equal to zero then the following algebraic equation will result:

$$\begin{aligned} r_0 W_f \sin\theta + pr(1+\epsilon_m) \frac{N}{\pi} \sin \frac{\pi}{N} - \frac{N}{\pi} \sigma_c \left[\sin \frac{\pi}{N} \cos\beta \cos\theta + \sin\beta \left(\cos \frac{\pi}{N} \cos^2\theta + \sin^2\theta \right) \right] \\ - \frac{N}{2\pi} \frac{r_0 \sigma_m}{(1-r_0 \sigma_m)} (W_T \sin\theta + 2\sigma_c \sin\beta) = 0 \end{aligned} \quad [19]$$

This equation places a very severe limitation on the shape of the deployed balloon since it effectively requires the tape angle to be identical to the film angle. Although this assumption appears to be reasonably valid over most of the gore length, it is obviously in error near the end points. However, since this is an algebraic equation rather than a differential equation, it may be used to determine the lobing angle for any set of shape variables without integration. This equation has no counterpart in the design procedure since no distinction is made between the tape and film angles.

Since equations [17], [18], and [19] do not involve the shear stress, this variable need not be evaluated to determine the shape. However, once the shape is found equation [6] may be used to evaluate the shear stress and ultimately the principal stresses and tension field patterns.

3.2 Method of Solution

Equations [13], [14], [17], [18] and [19] must be solved simultaneously in order to insure a compatible shape. An attempt was made to solve this set of equations utilizing the same modified Runge-Kutta numerical technique which is routinely used for the design of balloon shapes. However, the technique is best suited for initial value problems rather than boundary value problems. This so called "shooting" method is unable to impose a final boundary condition and must rely on the proper adjustment of initial conditions until the desired solution is obtained at the final boundary. In this particular case, the solution of five differential equations simultaneously is stable for only certain values of circumferential stress. As sufficiently large stresses are developed the integration scheme becomes divergent and a solution is unobtainable. It must be emphasized that this is a difficulty with the numerical technique and not in the formulation of the problem.

In an effort to obtain a stable solution with implicit control of the boundary conditions, the differential equations were rewritten in finite difference form to form a set of nonlinear algebraic equations. The boundary conditions may also be written as nonlinear algebraic equations and included in the set. The balloon gore is divided into a large number of points and the five equations written at each point. This results in a very large set of simultaneous equations which can be efficiently handled because of the banded nature of the problem. A Newton-Raphson technique was attempted but did not yield a convergent solution. It is difficult to ascertain the reason for this lack of convergence but it is suspected that the derivatives of the nonlinear function obtained from [14] near the top of the balloon approach zero which causes the coefficient matrix to become singular.

A direct iteration technique was employed to eliminate the instability associated with the inversion of a singular matrix that appeared in the Newton-Raphson technique. In the direct iteration technique an equation is written for each variable. For example, equation [13] may be used to evaluate the radius, r_i , for the next iteration according to the equation:

$$r_i = r_{i+1} - \Delta S_o (1 + \epsilon_m)_i \sin \theta_i$$

A similar equation may be written for each variable. An initial guess is required to evaluate the variable at the next step. Each variable is updated until the changes become negligibly small. As in the case of the Newton-Raphson technique, the direct iteration method was found to be divergent when applied directly. However, the use of under relaxation techniques in conjunction with direct iteration produced a convergent solution after 13 iterations when the design shape is used for the initial shape estimate.

4. RESULTS AND DISCUSSION

The formulation presented here was applied to a 20.8 MCF capped natural shape balloon with 2700 pounds of payload at 126,000 feet. This balloon was designed using the routine design equations which assume no circumferential stress. The manufactured radius, incremental film weights and tape weights were determined at 202 discrete points. The system consists of 140 gores, made of 0.8 mil polyethylene with a 0.9 mil cap starting 164.5 feet from the apex. The manufactured gore length is 527.4 feet.

The results of this analysis are shown graphically in Figure 4. For comparison purposes, the stress distributions predicted by making various assumptions regarding the state of stress is also shown. If it is assumed that the film carries the entire meridional load, which is the usual assumption, then the upper curve is obtained. This is a familiar curve where the meridional stress approaches infinity near the top of the balloon. If the effects of the load tapes are considered, as was done by Keese, then the lower curve will result. However, as the shape is allowed to change to accomodate the lobing between load tapes, the intermediate curve is obtained. Except for the present analysis, the other two states of stress assume no circumferential stress.

The stress distributions predicted by the present analysis are shown in Figure 5. It should be noted that the circumferential stress is not zero but of the same order of magnitude as the meridional stress except near the ends of the balloon. The normalized stress magnitudes revealed by this analysis are not particularly severe in this case; however, they bear very little relation to the stresses predicted by the design shape such as those reported by Alexander.

This new formulation may now be used to evaluate the realistic state of stress in other off-design configurations. Results have already been obtained for this balloon at a variety of altitudes. Figure 6 was prepared from computations using this new technique at a variety of altitudes, both above and below the design altitude. Only the limits of the meridional stress are shown since all meridional stresses calculated fall between the two curves shown. The significance of the curves for b/b_0 greater than one lies in the observation that circumferential stresses increase in value at altitudes below the design altitude. This is contrary to the normally assumed state of stress which assumes that since the load tapes are pulled toward the centerline of the balloon, more excess material will reduce whatever circumferential stress is present. This analysis indicates that shape changes occur of sufficient magnitude to alter the radius of curvature in such a way that the stress increases rather than decreases. It now appears feasible to obtain an accurate load-altitude curve both above and below the design altitude as well as the state of stress (and shape) at each point.

5. CONCLUSIONS

The study of balloons in off-design configurations presented here has produced a number of significant advancements in the determination of a realistic state of stress. In particular:

- a. The problem has been formulated in a manner which suggests a plausible explanation for the transfer of loads between load carrying members.
- b. The direct iteration technique with under relaxation has produced a convergent solution for a boundary value problem that has eluded solution until now.
- c. Results cannot be generalized, due to the nonlinear nature of all equations; however, results have been presented for a typical "heavy load" balloon system which revealed:
 1. The existence of circumferential stress and lobing between tapes significantly alters the state of stress even at the design altitude.
 2. All stresses increase at altitudes below the design altitude.
 3. The circumferential stress is a maximum at the base of the cap and exceeds the meridional stress below the design altitude.
 4. The balloon will float slightly below the load-altitude curve normally computed.

The results presented in this paper have only recently been obtained. These results are encouraging and work will continue to explore the state of stress under a variety of conditions. The effects of superpressure and subpressure regions have yet to be examined as well as heavy load balloons below their design altitude. The use of balloons above the design altitude may now be undertaken with some degree of confidence. A variety of observed phenomenon, such as stress bands, slack load tapes, etc., may now be predictable events. In any event, experimental results are now required in order to develop confidence in this analysis technique.

Acknowledgements

This work was supported in part by the Air Force Geophysics Laboratory under Contract No F19628-76-C-0082 and by the University Corporation for Atmospheric Research which is sponsored by the National Science Foundation. UCAR's technical representatives for the work contained in this paper are Mr. Alfred Shipley, manager, National Scientific Balloon Facility and Mr. I. Steve Smith, Head of the Engineering Department

References

- Alexander, H. (1974) Gore Panel Stress Analysis of High Altitude Balloons, AFCRL-TR-74-0597.
- Gilbert, J. L. (1974) Optimization Parameters for a Membrane Polygonal Body of Revolution with Zero Meridional Stress and Its Application to Parachutes, Unpublished Ph.D. Thesis, Virginia Polytechnic Institute and State University.
- Keese, D. L. (1978) Zero Pressure Balloon Design, AIAA Paper No. 78-314, presented at the AIAA 14th Annual Meeting and Technical Display, Washington, D.C.
- Smalley, J. H. (1965) Determination of the Shape of a Free Balloon, AFCRL-65-92.

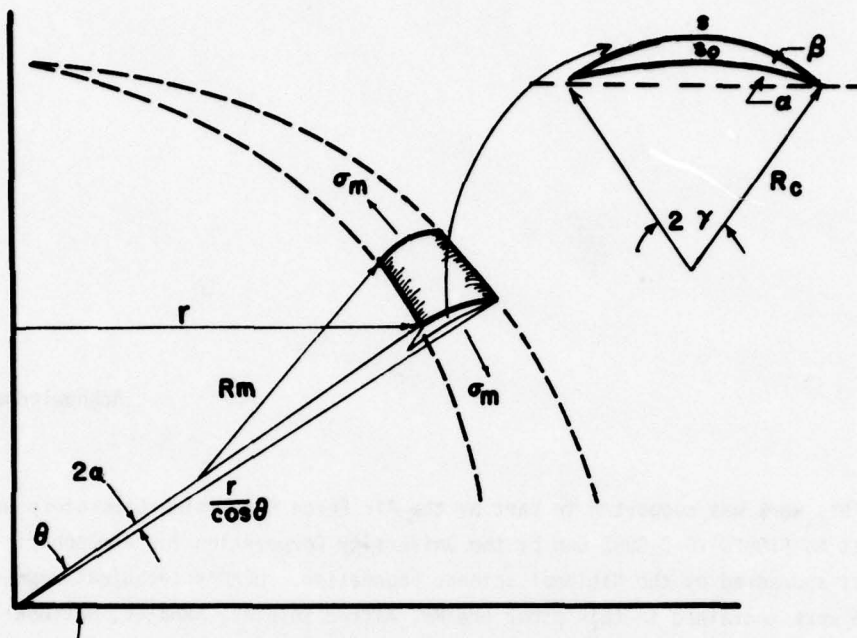


Figure 1. Balloon Coordinates at an Arbitrary Gore Position

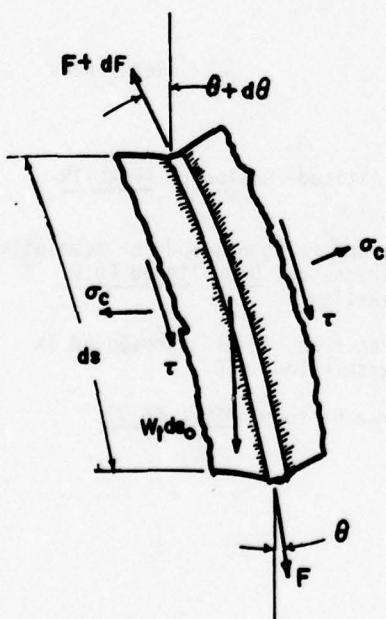


Figure 2. Differential Tape Element

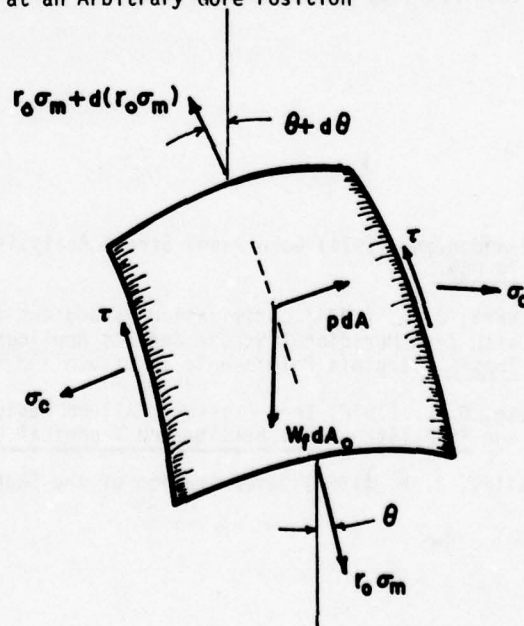


Figure 3. Differential Film Element

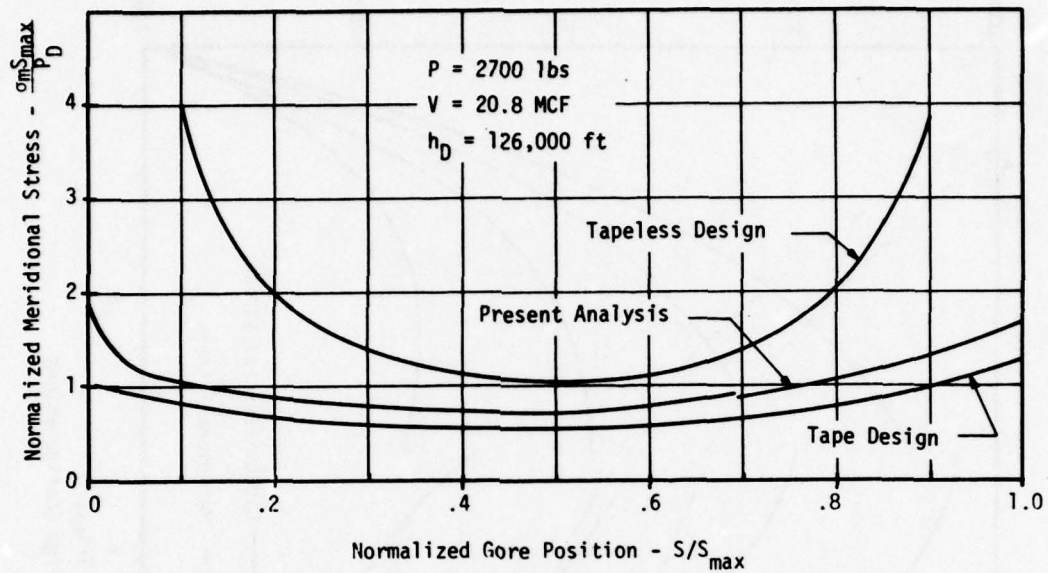


Figure 4. Meridional Stress Distributions

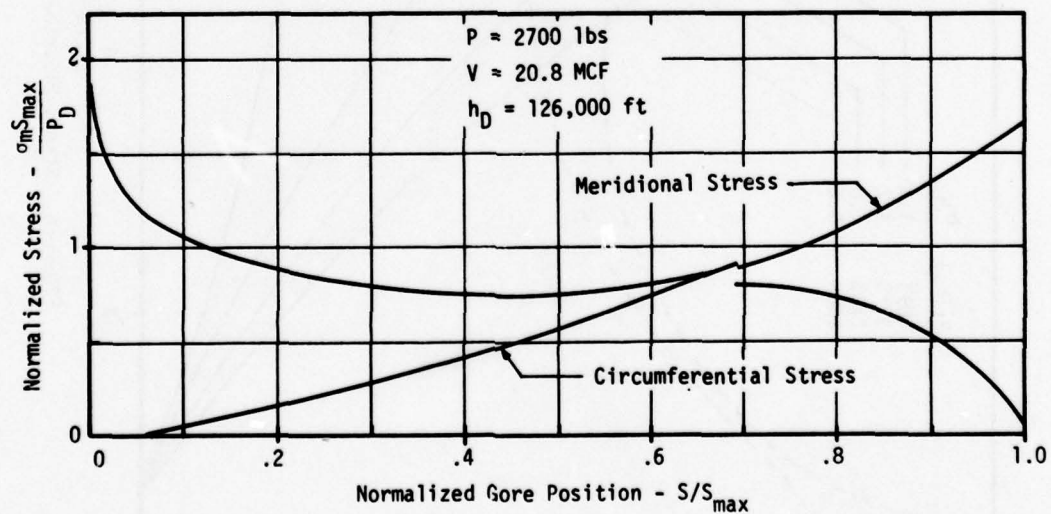


Figure 5. Stress Distributions at Design Altitude

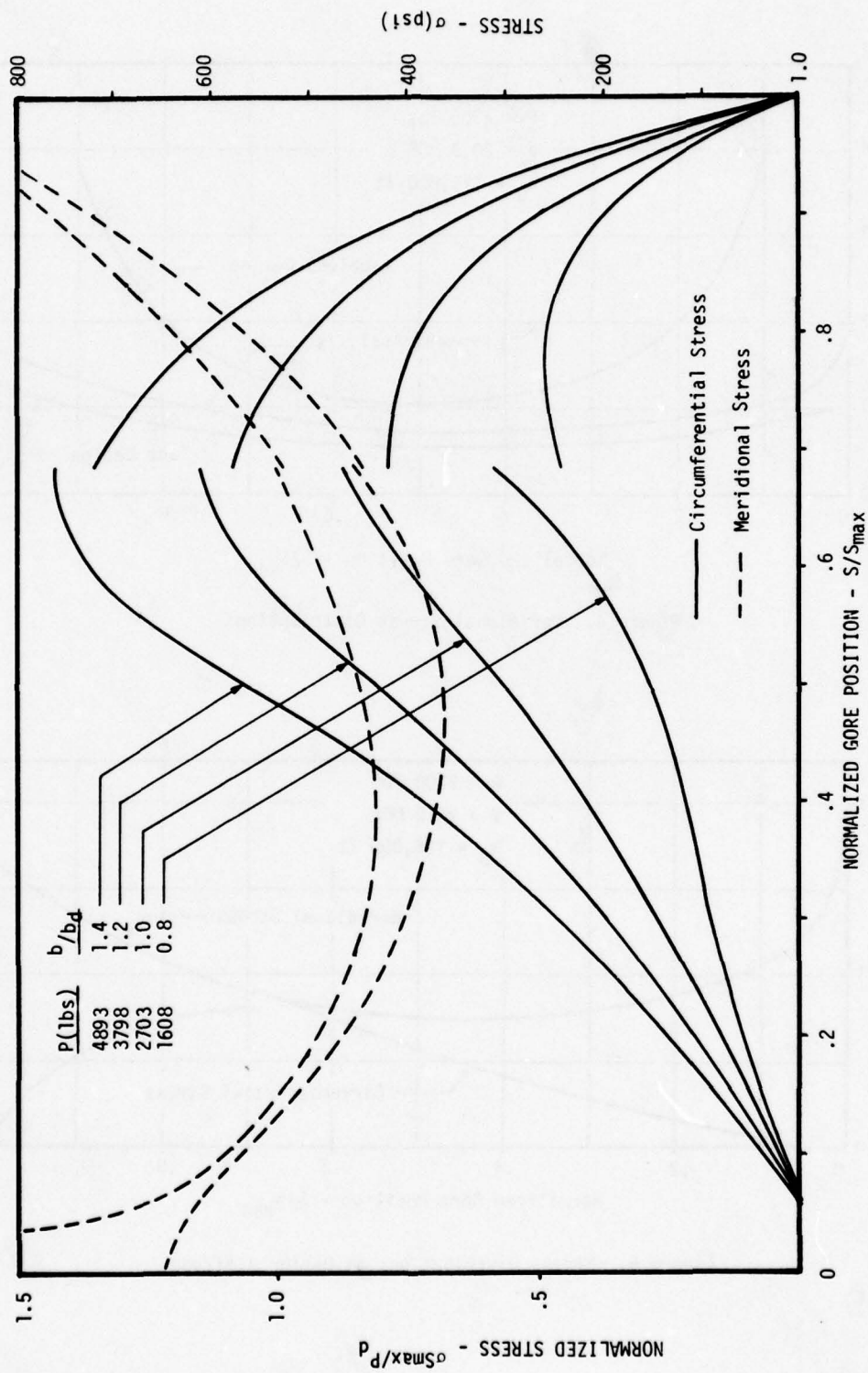


Figure 6. Stress Distributions in Off-Design Configurations

ABSTRACT

ON DETERMINING POISSON'S RATIO FOR THIN PLASTIC FILMS

Keith H. Hazlewood
Winzen Research, Inc.
Fleming Field
So St Paul, MN 55075

A closed form method for determining the in-plane Poisson's ratio for thin plastic films as a function of strain is presented. The calculations are made from data taken electronically during uniaxial testing. An analysis of the theoretical limits of Poisson's ratio for transversely isotropic materials is treated along with a discussion of Poisson's ratio for the thickness direction. Preliminary experimental results are promising and a recommendation is made that Poisson's ratio be included in the characterization of balloon films.

A NEW THERMAL ANALYSIS MODEL FOR HIGH ALTITUDE BALLOONS

Leland A. Carlson*
Texas A&M University
College Station, Texas

Abstract

Recent detailed flight data obtained by NSBF** indicates that lifting gas and balloon film temperatures are not the same during the daytime. *This phenomenon has been investigated and a new simplified engineering thermal model suitable for the prediction of equilibrium float temperatures has been developed. This paper reviews these efforts and shows the application of the model to flights for which data is available. These flights include zero pressure and superpressure cases, mylar and polyethylene films, and clear and overcast skies.*

1. INTRODUCTION

In the past several years, the user community has expressed considerable interest in the development of a balloon capable of lifting a reasonable payload to a constant float altitude for sixty to ninety days. Such a long duration balloon platform not only would permit the scientist to conduct long term experiments at altitude but also should greatly reduce the cost per data point. Several concepts, such as the superpressure, supported film superpressure, and Skyanchor (Rand, 1976; Carlson and Nelson, 1976), have been proposed for the design of such a balloon system. However, successful design with each of these concepts requires an accurate knowledge of the balloon gas and film temperatures.

*Associate Professor, Aerospace Engineering Department

**National Scientific Balloon Facility

For example, the daytime gas temperature, $T_{He,day}$, determines the amount of superpressure, Δp , and hence the film loads, since

$$\Delta p = p_a \left[\frac{T_{He,day}}{T_a} (1 + F) - 1 \right] \quad (1)$$

where p_a and T_a are the ambient pressure and temperature and the free lift, F , is

$$F = \frac{\text{Free lift at Launch}}{W_{\text{payload}} + W_{\text{gas}} + W_{\text{balloon}}} \quad (2)$$

On the other hand, since the amount of altitude loss at night should be minimum and since experience indicates that balloons which go slack at night usually fail within a few days, the night superpressure, Δp_{night} , should remain positive on even the coldest night. From Eq. (1), it can be seen that $\Delta p_{\text{night}} > 0$ requires that

$$F > \frac{T_a}{T_{He,night}} - 1 \quad (3)$$

Thus, $T_{He,night}$ determines the amount of gas required to prevent altitude loss at night; and thru the free lift it strongly influences the daytime superpressure and film loads.

Finally, the balloon wall temperature strongly affects the film material properties and hence the film strain, modulus, and design allowable stress. The influence of temperature on the stress-strain behavior of a typical balloon film is shown on Figure 1; and as can be seen, over the temperature range which may be encountered in a typical flight, the film modulus and design allowable stress can vary up to an order of magnitude.

From this discussion, it is obvious that the design of a successful long duration balloon requires an accurate knowledge and understanding of balloon gas and wall thermal behavior. As a consequence, researchers at NSBF and TAMU have conducted a series of theoretical and experimental investigations designed to improve the understanding of balloon thermal behavior. This paper will review these efforts, propose a new balloon thermal analysis model suitable for engineering estimates, and indicate those areas requiring further investigation.

2. ORIGINAL BALLOON THERMAL MODEL

During the 1960's several balloon flights were conducted for ONR which measured balloon gas and film temperatures (Lucas and Hall, 1967, 1968; Lucas, Hall, and Allen, 1970) at the relatively low float altitudes of 24.38 km (80,000 ft.) Subsequently, NSBF sponsored the development of an analytical model to predict the

performance of high altitude balloons (Kreith and Kreider, 1974; Kreider, 1975). While this model was primarily directed towards balloon transient behavior, it did include a very detailed thermal analysis model. Thus, it was used for the initial part of the present study.

This model is schematically represented on Figure 2, and it is formulated on the assumption that the lifting gas is radiatively totally transparent. In other words, the gas is assumed to neither emit nor absorb any radiation, and the only heat transfer mechanism associated with the gas is convection with the balloon film. Thus, for the steady state conditions of float, the gas temperature, T_{He} , and film temperature, T_{wall} , will be the same, and the governing steady state equations are

$$T_{He} = T_{wall} \quad (4)$$

and

$$q_{solar} + q_{albedo} + q_{c,a} + q_{IR} - q_{emit} = 0 \quad (5)$$

where

$$\begin{aligned} q_{solar} &= G \epsilon_{w,eff} F_1 = \text{direct solar flux on balloon} \\ q_{albedo} &= G \epsilon_{w,eff} r_e F_2 = \text{solar flux on balloon due to reflection off earth and clouds} \\ q_{c,a} &= CH_{air} A (T_a - T_{wall}) = \text{convective heating to balloon film by ambient air} \\ q_{IR} &= \sigma \epsilon_{w,eff} A T_{BB}^4 = \text{IR flux to balloon due to earth and atmosphere} \\ q_{emit} &= \sigma \epsilon_{w,eff} A T_{wall}^4 = \text{IR emission by balloon film} \\ F_1 &= 0.25A = \text{Balloon Shape Factor} \\ F_2 &= 0.50A = \text{Shape Factor (approximate) for albedo-radiation} \\ A &= \text{Balloon surface area} \\ G &= \text{Solar Constant} \\ \sigma &= \text{Stefan - Boltzman Constant} \\ T_{BB} &= \text{Black Ball temperature} \\ CH_{air} &= \text{Convection Coefficient film to air} \end{aligned} \quad (6)$$

In this model, the earth-atmosphere IR input is modeled using the equivalent black-ball concept (Kreith and Kreider, 1974) where $T_{BB} = 214.4^\circ K$ for clear skies and $194.4^\circ K$ for overcast skies. The factor, r_e , is the earth reflectivity and ranges from 0.18 for clear skies to 0.57 for overcast skies.

Now, since balloon films are semi-transparent any radiation to or from the balloon film will be partially transmitted, and then partially transmitted and

reflected off the opposite wall an infinite number of times. By taking into account these multiple reflections it can be shown that the effective solar emissivity, α_{eff} , and IR emissivity, ϵ_{eff} , of the wall or balloon film are

$$\alpha_{eff} = \alpha_s \left(1 + \frac{\tau_s}{1-r_s} \right) \quad (7a)$$

$$\epsilon_{eff} = \epsilon_{IR} \left(1 + \frac{\tau_{IR}}{1-r_{IR}} \right) \quad (7b)$$

where

- α_s = absorptivity of film in the solar spectrum
- τ_s = transmissivity of film in the solar spectrum
- r_s = reflectivity of film in the solar spectrum
- ϵ_{IR} = emissivity of film in the IR
- τ_{IR} = transmissivity of film in the IR
- r_{IR} = reflectivity of film in the IR

With these Eq. (5) reduces to

$$G_{w_{eff}}^{\alpha} \left(\frac{1}{4} + \frac{r_e}{2} \right) + CH_{air}(T_a - T_{wall}) + \sigma \epsilon_{w_{eff}} T_{BB}^4 - \sigma \epsilon_{w_{eff}} T_{wall}^4 = 0 \quad (8)$$

where it is obvious that the balloon skin temperature depends primarily upon the film effective radiative properties, $\alpha_{w_{eff}}$ and $\epsilon_{w_{eff}}$.

Consequently, NSBF had the NASA Johnson Spacecraft Center measure the radiative properties of several typical balloon films. These measurements, which are extremely difficult for highly transparent materials, were conducted carefully and were subsequently reduced at TAMU. The results are shown on Figure 3 along with some values previously obtained from NASA Langley (Smith, 1973). It is believed that these results are indicative of the accuracy available in the laboratory and that they reflect variations due to experimental error and different film samples. Unfortunately, as can be seen on Figure 3, the results contain a high degree of scatter.

At about the same time, August 1975, NSBF flew a 2 million cubic feet 1 mil Stratofilm[®] balloon which floated at 33.52 km (110,000 ft.). This balloon was instrumented with two helium thermistors, two ambient air thermistors, and a black ball. During the night ascent, helium temperatures below -90°C were recorded in the troposphere, but after sunrise the gas temperature stabilized at an average value of -16.8°C. Since accurate data was available from this flight, it was decided to use the thermal model and the newly acquired α and ϵ values to see if the flight measurements could be reproduced; and the results are shown on Figure 4.

As can be seen, the predicted daytime gas temperatures, which range from 0°C to -23°C, are very sensitive to the α and ϵ values. Similar results were obtained for night values, and it was concluded that laboratory values of α and ϵ contained too much scatter to be of value. Instead, it was decided to utilize the flight data to deduce the film radiative properties.

By substituting measured night temperatures into Eq. (8) with G equal to zero, a value for ϵ_{weff} was obtained. With this result and daytime temperature Eq. (8), with $G \neq 0$, then yielded estimate for ϵ_{weff} . These results are shown on Figure 4 under the heading "TAMU Estimate", and in general they yielded excellent estimates for both day and night steady state temperatures.

At this point it was believed that the thermal problem was understood and that it was only necessary to conduct a series of instrumented flights with various films and under various cloud conditions. It was felt that such data not only would verify the model but also would yield accurate radiative property estimates. As will be seen in the next section, this belief was premature.

3. NEW FLIGHT MEASUREMENTS

From August 1975 thru October 1976, five instrumented balloon flights were conducted by NSBF which measured balloon film and gas temperatures. Tables 1 and 2 summarize the results of these flights, and the temperatures shown are steady state average values. The two superpressure flights, Boom V and VII, were part of the Long Duration Platform development program; while the three zero-pressure balloon flights were NSBF engineering flights designed particularly to investigate balloon film and gas temperatures.

The two superpressure flights yielded results that were essentially indistinguishable, and the night measurements supported the thermal model assumption that the wall and gas temperatures are the same. The daytime values were, however, quite surprising. They showed a 10°C difference between the balloon and gas temperatures with the helium being warmer. This difference was too large to be attributed to measurement error, but lacking any other flight verification no conclusions were deduced at the time.

Now as alluded to previously, the presence of a cloud deck below a balloon greatly affects its thermal environment. Basically the solar albedo heating is increased by about a factor of three, while the earth-atmosphere IR radiation is significantly decreased due to shielding by the cloud deck. (T_{BB} drops to about 194.4°K) In general, the daytime heating is increased causing higher temperatures; while the night heating is decreased leading to very cold temperatures. In order to verify this expectation and to obtain some idea of the magnitude of the phenomena,

RAD II was launched just prior to the passage of a frontal system. As a result, it floated both before and after sunrise over a solid overcast.

As can be seen on Table 2, the night gas and film temperatures were considerably colder than those experienced on RAD I, although the altitude was lower. The day-time gas temperature, however, was higher and again significantly warmer than the wall temperature. Quite obviously some previously unaccounted for mechanism was heating the lifting gas during the daytime.

To verify this observation a third zero pressure balloon was launched in August 1976. This flight was identical to RAD II but for clear rather than cloudy skies. As expected, the night temperatures were warmer and the day gas temperature was colder. The average wall temperature, however, while essentially unchanged from RAD II, was still considerably colder than the gas temperature.

Based upon the data obtained from these flights, it was apparent that the gas was somehow being externally heated during the daytime. It was believed that this heating was primarily due to solar radiation since RAD II and III showed a definite sensitivity to the amount of albedo radiation. While helium is considered radiatively transparent and its absorptivity is small, it is not zero; and thus, solar absorption could still be significant. Consequently, it was decided to develop a new balloon thermal analysis model.

4. NEW BALLOON THERMAL ANALYSIS MODELS

Theoretically, in developing a model that includes gas emission and absorption, the integral equations associated with radiative gas dynamics should be utilized. The complexity of these equations and the lack of knowledge of the radiative properties of helium at the temperatures of interest made this approach, however, extremely difficult. In addition, it was desired to develop a simple engineering model; and, thus, it was decided to retain the effective area concept previously used in the original model.

The phenomena included in this new model are schematically represented on Figure 5. Notice that the gas is permitted to absorb radiation in both the solar and IR spectra, but that because of its low temperature it is assumed to emit only in the IR. In addition, IR radiative exchange and convection between the film and the gas is permitted. The latter is included because the convection coefficient of helium is about six times that of air; and thus, it might be significant, particularly in the superpressure case.

For these mechanisms, the governing steady state equations are:

Gas

$$q_{g,solar} + q_{g,albedo} - q_{g,interchange} - q_{c,gw} - q_{g,emit} + q_{g,IR} = 0 \quad (9)$$

Wall

$$q_{w,solar} + q_{w,albedo} + q_{w,interchange} + q_{c,gw} + q_{c,a} - q_{w,emit} + q_{w,IR} = 0 \quad (10)$$

Upon considering the multiple pass effect the equations become:

Gas

$$\frac{1}{4} G \alpha_{g,eff} + \frac{1}{2} G r \epsilon_{g,eff} - \epsilon_{int} (T_g^4 - T_w^4) - CH_g (T_g - T_w) - \epsilon_{g,eff} \sigma T_g^4 + \epsilon_{g,eff} \sigma T_{BB}^4 = 0 \quad (11)$$

Wall

$$\frac{1}{4} G \alpha_{w,eff} + \frac{1}{2} G r \epsilon_{w,eff} + \epsilon_{int} (T_R^4 - T_w^4) + CH_g (T_g - T_w) + CH_w (T_a - T_w) - \epsilon_{w,eff} \sigma T_w^4 + \epsilon_{w,eff} \sigma T_{BB}^4 = 0 \quad (12)$$

where

$\alpha_{g,eff}$ ~ effective solar absorptivity of the gas

$\epsilon_{int} = \frac{\epsilon_g \epsilon_w}{1 - r_w (1 - \epsilon_g)}$ ~ effective interchange IR emissivity

$\epsilon_{g,eff} = \frac{\epsilon_g}{1 - r_w (1 - \epsilon_g)}$ ~ effective IR emissivity of gas

$\alpha_{w,eff}$ ~ effective solar absorptivity of the wall

$\epsilon_{w,eff} = \epsilon_w \left[1 + \frac{\tau_w (1 - \epsilon_g)}{1 - r_w (1 - \epsilon_g)} \right]$ ~ effective IR emissivity of wall

ϵ_g ~ actual IR emissivity of gas

ϵ_w ~ actual IR emissivity of wall

r_w ~ actual IR reflectivity of wall

τ_w ~ actual IR transmissivity of wall

(13)

Initially, the radiative film properties measured in the laboratory were utilized in these equations along with estimates for the gas properties. Unfortunately, none of the property data sets reproduced the flight measurements. In addition, since the amount of flight data was less than the number of unknown radiative properties, the technique used in the original model to evaluate the radiative properties could not be utilized. Subsequently, many attempts were made to estimate these properties; but no single set of parameters was found to accurately predict all the flight data. Number sets could be constructed which could reproduce the results of one flight, say RAD III, but this same set would yield erroneous values for the other flights,

RAD I and RAD II.

As a result, a more basic approach was taken which attempted to only include the dominant effect -- namely, that the helium appeared to be completely transparent to IR radiation, i.e., $\epsilon_g = 0$, and to lose and gain heat only through solar emission-absorption and convection with the balloon wall. While not theoretically complete, this approach greatly simplified Eqs. (11) and (12) and led to the following equations:

Day:

Gas

$$\frac{1}{4} G_{g,eff} + \frac{1}{2} r e_{g,eff} - CH_g(T_g - T_w) - \alpha_{g,eff} T_g^4 = 0 \quad (14)$$

Wall

$$\frac{1}{4} G_{w,eff} + \frac{1}{2} Gr e_{w,eff} + \frac{2}{3} CH_g(T_g - T_w) + CH_w(T_a - T_w) - \epsilon_{w,eff} \sigma T_w^4 + \epsilon_{w,eff} \sigma T_{BB}^4 = 0 \quad (15)$$

Night:

Gas

$$T_g = T_w \quad (16)$$

Night

$$CH_w(T_a - T_w) - \epsilon_{w,eff} \sigma T_w^4 - \epsilon_{w,eff} \sigma T_{BB}^4 = 0 \quad (17)$$

where a two-thirds factor is used on the gas-wall convection term in the wall equation to account for the thermal transition region between the gas and the wall.

Notice that with these simplified equations the flight data can be utilized to obtain the effective radiative properties. Equation (17) yields $\epsilon_{w,eff}$, and then Eq. (14) yields $\alpha_{g,eff}$ and Eq. (15) gives $e_{w,eff}$. Unfortunately, Eq. (17) is usually too sensitive to give accurate values for $\epsilon_{w,eff}$, and so it must be estimated. Nevertheless the model is considerably simpler than before and contains the important phenomena.

This simplified model requires the solution of a nonlinear set of algebraic equations and includes nonlinear functions, CH_g and CH_w , of temperature. Thus, the equations have been programmed and are solved by a simple Newton iteration scheme. A typical case requires about 1 millisecond on an Amdahl V/6.

Figure 6 shows results obtained with the model for a mylar superpressure balloon. Notice that the wall radiative properties, $\alpha_{w,eff}$ and $\epsilon_{w,eff}$, used are identical to those obtained by NASA/JSC for 1 mil mylar. As can be seen, the predictions fall essentially near the center of the values measured on flights Boom V and VII.

Results for the three zero pressure balloons are portrayed on Figure 7. Unlike the detailed model, the simple model did utilize a consistent set of radiative property values that yielded good predictions for all three flights. However, this data set was not in total agreement with any values determined from laboratory measurement. Nevertheless, the only apparent difficulty is that the clear night predicted temperatures are always slightly colder, which is conservative, than the actual values. The critical design values (i.e., cloudy day and cloudy night temperatures, see RAD II) are predicted, however, very accurately.

At this point, it should be noted that the helium absorption coefficient, $\alpha_{g,eff}$, for mylar balloons is different from the value deduced for polyethylene balloons. While there are several possible explanations, this difference is most likely associated with either oversimplification in the model or with the multiple pass effect and different film transmissivities. However, until a more detailed model and more extensive flight data are obtained, no explanation will be attempted.

When the present model is applied to a variety of conditions, some interesting phenomena are observed which may have an effect on current programs. In general, as shown on Tables 3 and 4, as balloon float altitude increases, its day wall temperature remains relatively constant while its daytime gas temperature will increase. This increase occurs because with increased altitude balloon size increases and balloon gas density decreases, and both trends decrease the effective convection between the gas and the wall. Since the solar energy input to the gas is essentially independent of altitude, the gas temperature increases. The wall temperature, on the other hand, remains relatively constant since the gas and ambient air convection effects are small compared to the radiative input and emission. These phenomena not only are predicted by the model but also have been observed experimentally as shown on Table 3.

The variation in gas temperature could have a significant effect on super-pressure vehicles and their skin stresses. It would also affect the Skyanchor concept. At 130,000 ft. (39.62 km) the predicted temperature excursion from cloudy day to cloudy night of the polyethylene balloon would be from 9.4°C down to -71.8°C. This 81.2°C difference would, of course, require the system to utilize a larger ballast balloon in order to prevent a significant altitude drop at night.

Finally, the present model could be further verified, extended, and improved if additional flight data were obtained. In particular, detailed data at higher altitudes are needed since the present experimental results are for 110,000 ft. (33.53 km) and below. Such flights should contain instrumentation not only for measuring gas and wall temperatures but also for determining albedo coefficient and black-ball temperatures. In addition, accurate records of weather conditions, cloud cover, and time of day are required.

Also, it would be beneficial to perform or obtain additional radiative property measurements for typical balloon films and lifting gases.

5. CONCLUSIONS

Based upon the results presented in this paper, it is believed that the following conclusions can be stated:

- (1) The equilibrium gas and wall temperatures for a balloon at float during the day are not the same. The gas temperature is higher than the wall temperature and increases with altitude. The wall temperature, however, is relatively insensitive to altitude.
- (2) Accurate equilibrium temperatures can be predicted for mylar-like super-pressure balloons at float.
- (3) The night minimum and day maximum temperatures can be predicted for polyethylene balloons at float.
- (4) Day equilibrium float temperatures for polyethylene balloons can be predicted for a variety of weather conditions.
- (5) More information is required before more detailed balloon thermal analysis models can be developed.

Acknowledgments

The information upon which this report was based was obtained while performing consulting research for the University Corporation for Atmospheric Research which is sponsored by the National Science Foundation. UCAR's technical representatives for the work herein are Mr. Alfred Shipley, manager, National Scientific Balloon Facility, and his delegated representative, Mr. Steve Smith, Head of the Engineering Department. The author also acknowledges the support of Winzen Research, Inc. who, as part of a grant to Texas A&M University, provided the funds for the preparation and presentation of this paper.

References

- Carlson, L.A. and Nelson, J.R. (1976) Supported film superpressure balloons, in Proc. 9th AFGL Scientific Balloon Symposium, G. F. Nolan, Ed., AFGL-TR-76-0306.
- Kreider, J. F. (1975) Mathematical modeling of high altitude balloon performance, AIAA Paper 75-1385.
- Kreith, F. and Kreider, J. F. (1974) Numerical prediction of the performance of high altitude balloons, NCAR-TN/STR-65.
- Lucas, R.M. and Hall, G. H. (1967) The measurement of high altitude balloon gas temperature, in Proc. 4th AFCRL Scientific Balloon Symposium, J.F. Dwyer, Ed., AFCRL-67-0075.
- Lucas, R.M. and Hall, G. H. (1968), The measurement of balloon flight temperatures through sunset and sunrise, in Proc. 5th AFCRL Scientific Balloon Symposium, AFCRL-68-0661.
- Lucas, R.M., Hall, G. H., and Allen, B. M. (1970) Experimental balloon gas and film temperatures, in Proc. 6th AFCRL Scientific Balloon Symposium, L.A. Grass, Ed., AFGL-70-0543.

Rand, J. L. (1976) Long duration balloons, in Proc. 9th AFGL Scientific Balloon Symposium, G. F. Nolan, Ed., AFGL-TR-76-0306.

Smith, D. M. (1973) Tinting of balloon fabrics to increase their solar absorptivity, in Proc. 7th AFCRL Scientific Balloon Symposium, G. F. Nolan, Ed., AFCRL-TR-73-0071.

Table 1. Superpressure Flight Data

Boom V (Oct. 1975) and VII (Oct. 1976)	
1.5 mil Celenar balloon at 96,000 ft.	
Clear Skies	
<u>Day</u>	<u>Night</u>
$T_a = -50^\circ\text{C}$	$T_{\text{gas}} = -59^\circ\text{C}$
$T_{\text{gas}} = -30^\circ\text{C}$	$T_{\text{wall}} = -59^\circ\text{C}$
$T_{\text{wall}} = -40^\circ\text{C}$	

Table 2. Zero Pressure Flight Data

RAD I ~ Aug. 75; Stratofilm^R; 110,000 ft.; Clear skies

<u>Day</u>	<u>Night</u>
$T_a = -35.7^\circ\text{C}$	$T_{\text{gas}} = -47.4^\circ\text{C}$
$T_{\text{gas}} = -16.8^\circ\text{C}$	

RAD II ~ June 76; X-124, Cloudy skies

<u>Day</u>	<u>Night</u>
Altitude = 97,300 ft.	Altitude = 85,000 ft.
$T_a = -40^\circ\text{C}$	$T_a = -50^\circ\text{C}$
$T_{\text{gas}} = -10^\circ\text{C}$	$T_{\text{gas}} = -71^\circ\text{C}$
$T_{\text{wall}} = -36.5^\circ\text{C}$	$T_{\text{wall}} = -71^\circ\text{C}$

RAD III ~ Aug. 76; x-124; Clear Skies

<u>Day</u>	<u>Night</u>
Altitude = 97,300 ft.	Altitude = 95,000 ft.
$T_a = -41^\circ\text{C}$	$T_a = -46^\circ\text{C}$
$T_{\text{gas}} = -22^\circ\text{C}$	$T_{\text{gas}} = -47^\circ\text{C}$
$T_{\text{wall}} = -37.5^\circ\text{C}$	$T_{\text{wall}} = -47^\circ\text{C}$

Table 3 - Clear Day Results

Altitude (ft)	T_{He}		$T_{wall} (^{\circ}C)$		Flight
	Theory	Flight	Theory	Flight	
80,000	-29.1	-32	-40.5	-39	Lucas-Hall
97,300	-22.1	-22	-36.7	-37	RAD III
109,000	-16.0	-16.9	-35.3	--	RAD I
130,000	-9.50	--	-36.2	--	----

Table 4 - Cloudy Day Results

Altitude (ft)	T_{He}		T_{wall}		Flight
	Theory	Flight	Theory	Flight	
97,300	-11.3	-10	-37.0	-36.5	RAD II
130,000	9.4	--	-37.0	--	----

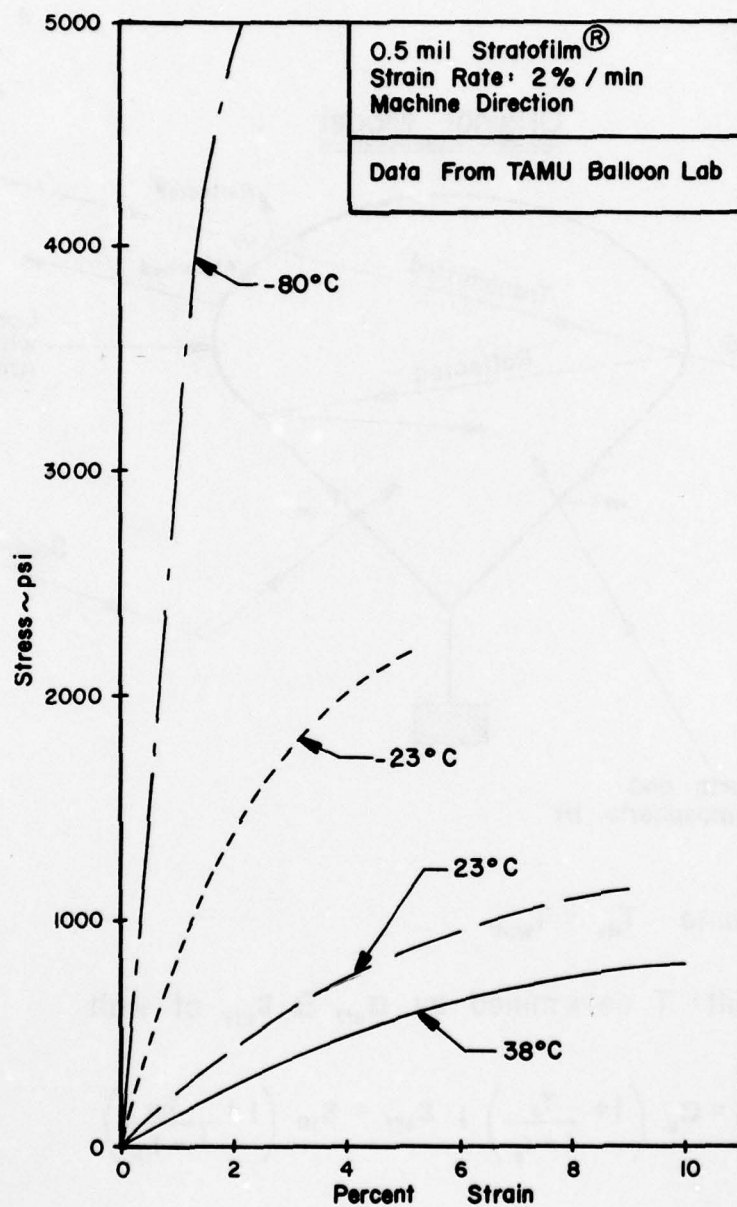
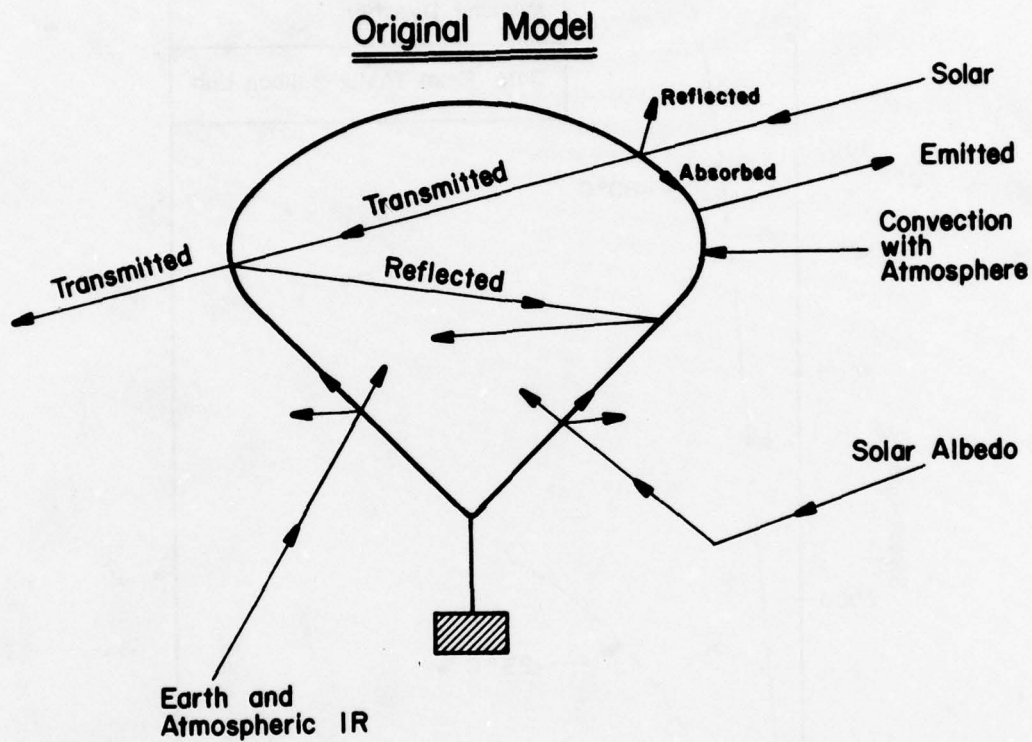


Figure 1. The Influence of Temperature on the Stress-Strain Behavior of Stratofilm.®



Assume : $T_{H_0} = T_{Wall}$

Result: T determined by α_{eff} & ϵ_{eff} of wall

$$\alpha_{eff} = \alpha_s \left(1 + \frac{T_s}{1 - r_s} \right) ; \epsilon_{eff} = \epsilon_{IR} \left(1 + \frac{T_{IR}}{1 - r_{IR}} \right)$$

Figure 2. Original Balloon Thermal Model (Schematic).

α_{eff} & ϵ_{eff} Measurements

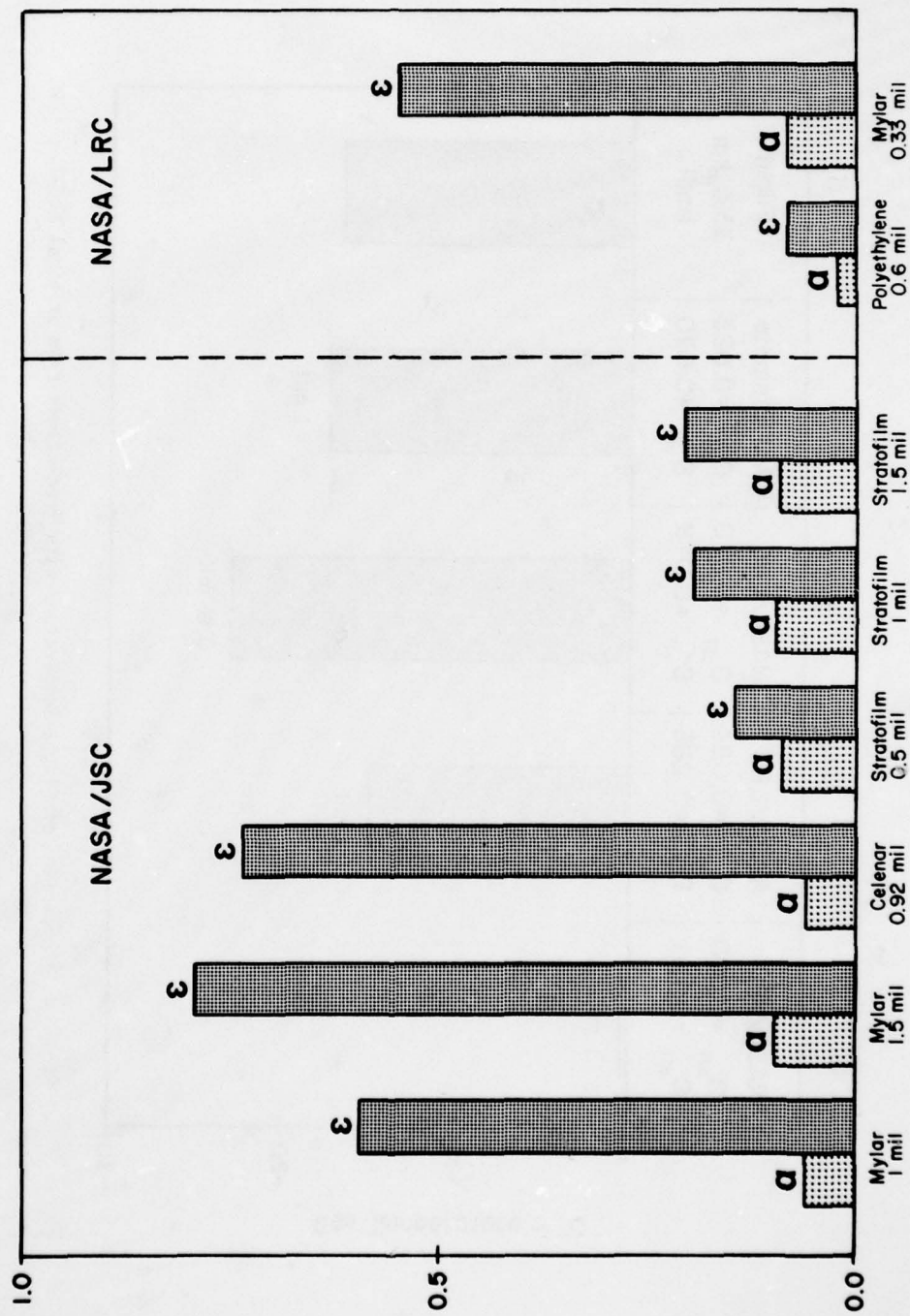


Figure 3. Absorptivity and Emissivity Measurements for Balloon Films.

AD-A074 469

AIR FORCE GEOPHYSICS LAB HANSCOM AFB MA
PROCEEDINGS OF THE AFGL SCIENTIFIC BALLOON SYMPOSIUM (10TH) HEL--ETC(U)
MAR 79 C L RICE
AFGL-TR-79-0053

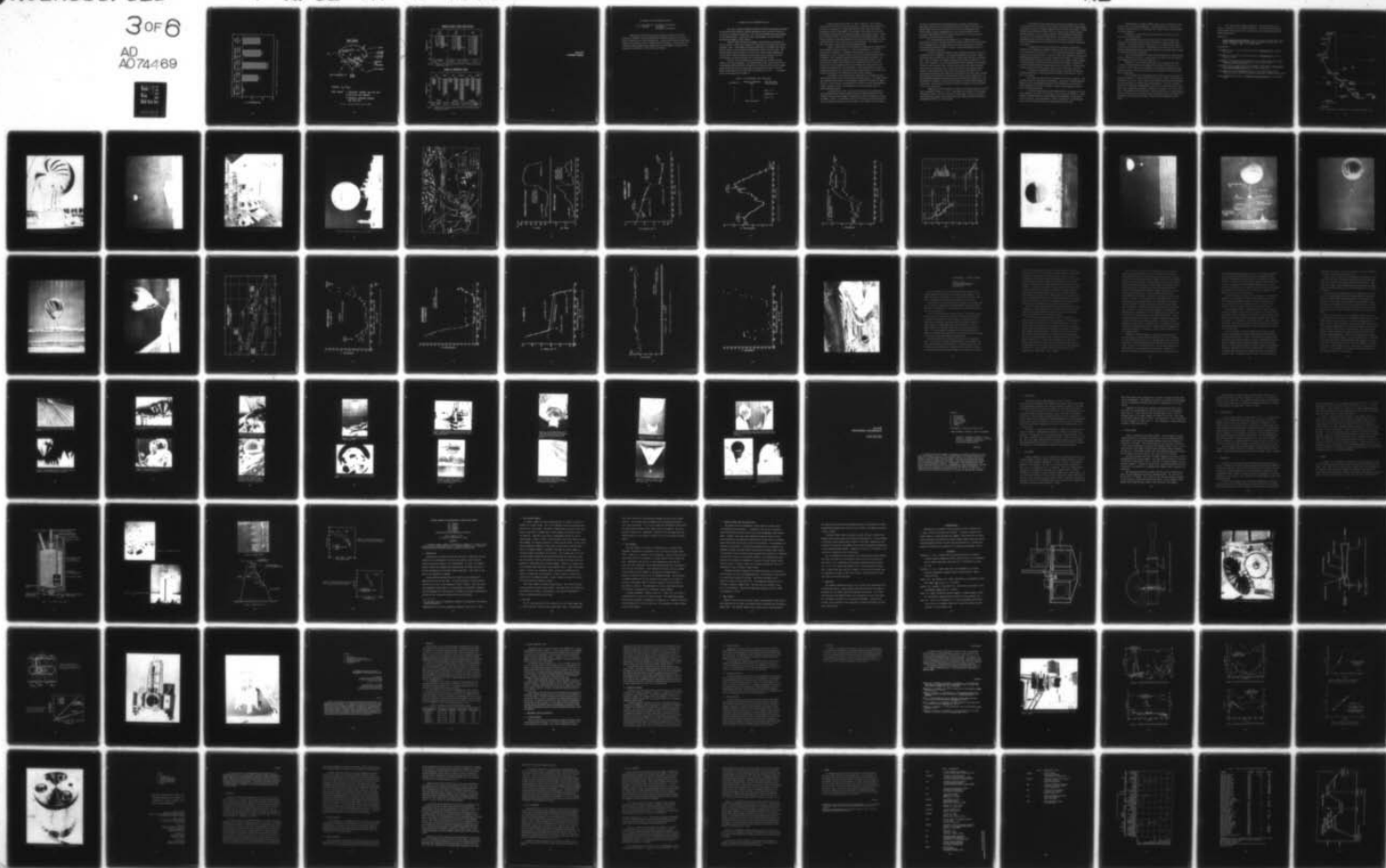
F/G 1/3

UNCLASSIFIED

NL

3 OF 6

AD
A074469



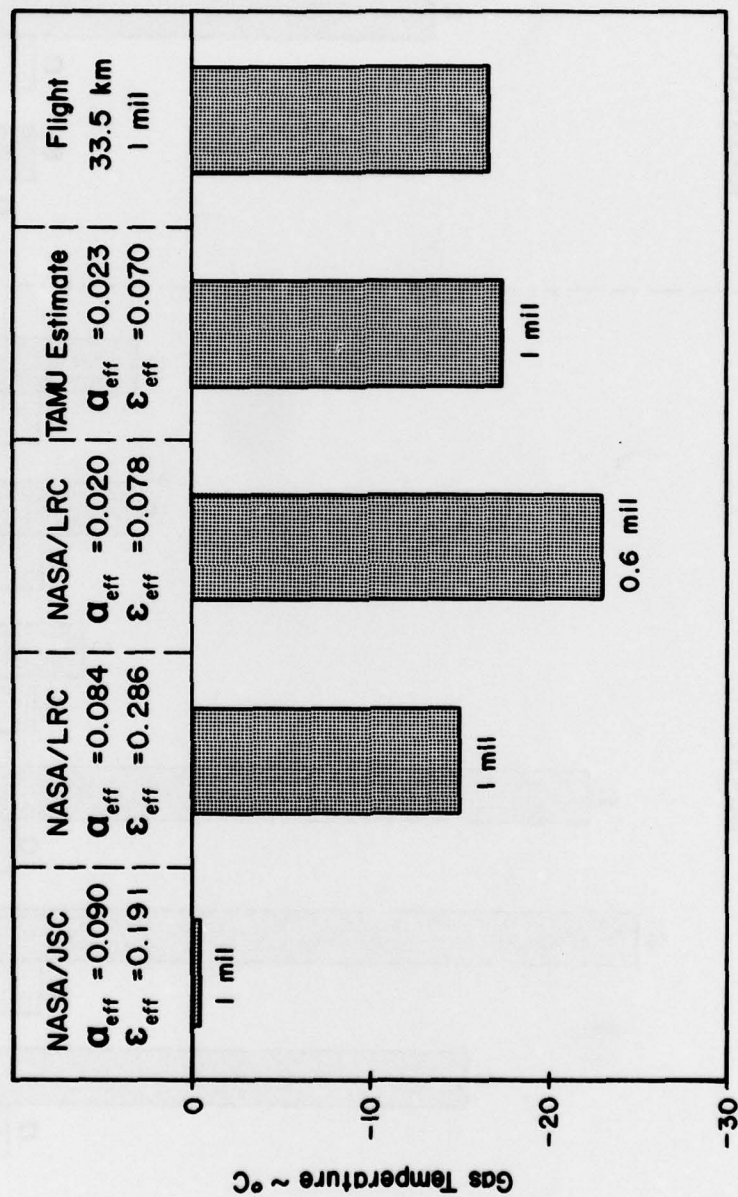
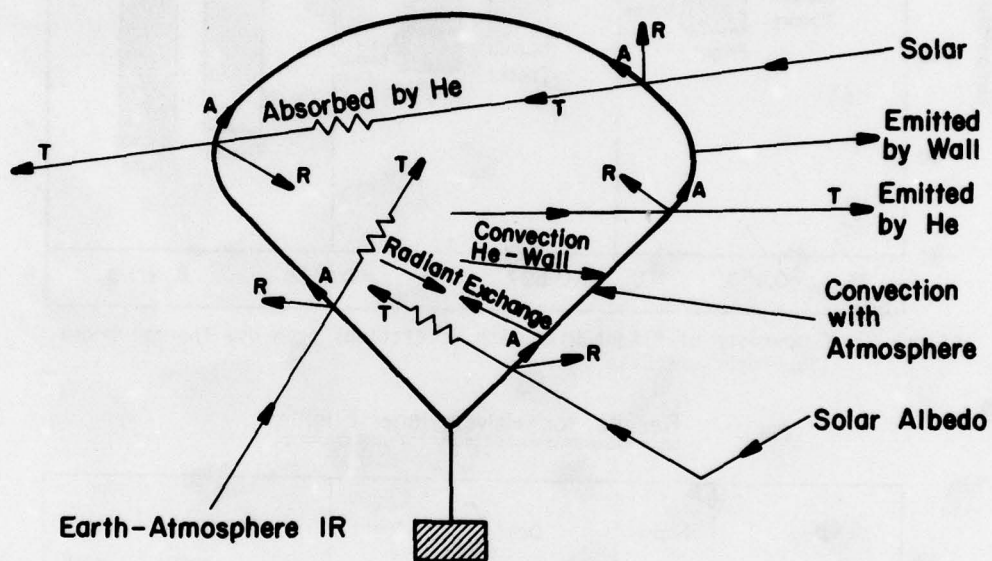


Figure 4. Comparison of Flight Temperature with Predictions from Original Model.

New Model



Assume : $T_{He} \neq T_{Wall}$

- New Effects:
1. Convection between gas and wall.
 2. Gas emits and absorbs.
 3. Radiation exchange between gas and film.

Figure 5. New Balloon Thermal Analysis Model.

Results for Mylar Flights Boom V & VII

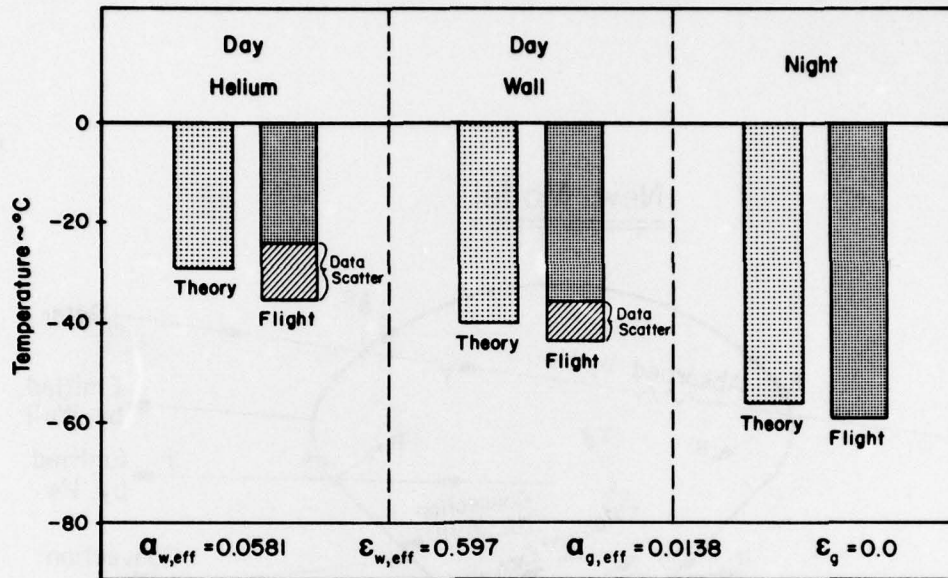


Figure 6. Comparison of Flight Data with Predictions from New Thermal Model, (Superpressure Case).

Results for Polyethylene Flights

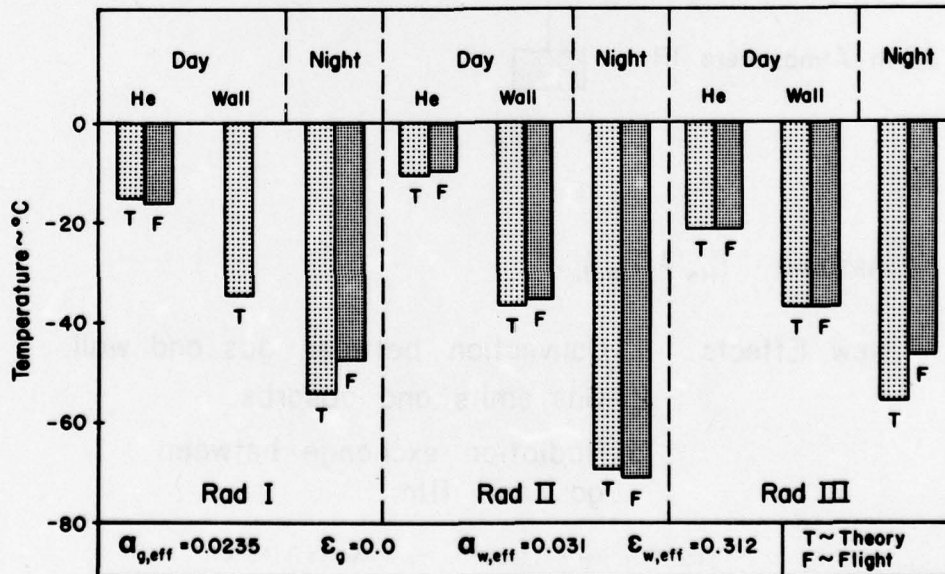


Figure 7. Comparison of Flight Data with Predictions from New Thermal Model, (Zeropressure Cases).

Session II
MANNED FLIGHTS

An Update on the ATMOSAT Project

T. F. Heinsheimer - Aerospace Corporation
P. C. Neushul - Consultant,
Aerospace Corporation

This paper will describe progress made and lessons learned in flying the ATMOSAT manned superpressure balloon system since the last report presented to the AFGL Symposium. The four, air-pollution monitoring flights in New Mexico and Los Angeles will be discussed. Future plans for continued manned flights and consideration of an ATMOSAT concept for the exploration of MARS in 1985/86 will be presented.

An Update on the ATMOSAT Project

The three manned ATMOSAT flights described in the paper presented at the Ninth AFGL Scientific Balloon Symposium have produced a series of contracts for pollution monitoring. The four air-pollution monitoring flights are described below. Trajectory maps, photographs, and data collected during these flights are also shown.

Flight 4 lifted off from Farmington, New Mexico on December 8, 1976 at 5:14 p.m. MST and terminated 7 hours and 16 minutes later outside Blanding, Utah. This flight primarily proved that a free flight drift can be flown in order to track a plume in mountainous terrain even at night. The balloon flight characteristics are such that accurate altitude adjustments can be made so that the balloon can join itself to any stratum of interest and maintain a constant buoyancy for extended periods of time.

The fact that the balloon was manned gave an excellent backup system to the grab sampling. The observations of the crew that there was a sulfurous smell (olefactory threshold for average persons being 0.5 ppm) assured them that they had been with the plume up to 36 miles from the point of emission and were still with it at least out to 75 miles as indicated by the grab samples (see Table 1).

Table 1. Grab Sample Cook-off Results

Sample No.	Distance Downwind, miles	SO ₂ Detection, chart divisions
1	7	
2	12	trace, 2.0
3	36	significant, 3.2
4	75	trace, 2.0
5	108 (on ground)	0

Flight 5 lifted off at 6:30 a.m. PDT on June 27, 1977 and was terminated at 12:30 p.m. PDT the same day. This flight was made by The Aerospace Corporation in cooperation with the South Coast Air Quality Management District (SCAQMD). The purpose of the flight was to track air pollutants during a day of significant smog from Orange County, across the Los Angeles basin, into Riverside and San Bernardino Counties. This flight primarily proved that pollution levels can be monitored with an ultraviolet photometer that measures ozone concentrations. The flight crew also were able to gather several NO₂ measurements.

Flight 6, also made by The Aerospace Corporation in cooperation with SCAQMD, lifted off at 8:09 a.m. PDT on September 8, 1977 from Long Beach, California. The flight terminated at 5:20 p.m. PDT on September 8, 1977 at western edge of the San Bernardino National Forest. In addition to the standard communication and navigation equipment, the gondola was equipped with ambient air monitoring instruments. These consisted of a Dasibi model 1003-AH for measuring ozone; a YSI Tele-thermometer for measuring ambient and balloon-skin temperature; two Tyland mass flowmeters, two air pumps, a spectrophotometer, and the peripheral hardware for measurement of nitrogen dioxide via the Saltzman method; and bags for the collection of hydrocarbon samples.

In addition to measuring ozone continuously, the flight also provided periodic data on the concentrations of hydrocarbons. The hydrocarbon data indicated that methane concentrations changed little during the flight, but that, as with ozone, concentrations of the more reactive hydrocarbons, ethane, propane, butane, and isopentane decreased sharply above the (pollution) mixing layer.

During October 1977, the City of Long Beach was preparing an Environmental Impact Report (EIR) regarding a planned facility for off-loading crude oil being brought by supertankers from the pipeline terminus at Valdez, Alaska. An important issue to be evaluated in the EIR was the effect of tanker emissions on the air quality of the South Coast Air Basin.

The City of Long Beach contracted with The Aerospace Corporation (developer and owner of the ATMOSAT system) to organize and conduct a balloon flight to trace the direction of the air mass originating in the Santa Barbara Channel shipping lanes about ten miles south of Point Conception and to follow that air mass to determine if it moves on shore anywhere in the South Coast Air Basin.

The requirements for this flight were: the balloon had to be launched at sea from a preselected point 10 miles south of Point Conception in the shipping lanes, the flight had to last at least 24 hours (or until the air mass being monitored came on shore), and all preparations had to be completed within two weeks.

In order to launch the balloon from a position off-shore, one of two methods had to be employed. The uninflated balloon and a helium trailer containing some 20,000 cubic feet of gas could be ship-carried to the launch site. Once on station, the balloon would be inflated and weighed off on the ship, then released. A second method would involve inflation of the balloon on shore, then towing it to sea using a much smaller ship and releasing it upon arrival at the launch site. It was clear that the first option would require a large and costly vessel and more significantly would require operational procedures that could not be perfected in the short time available between the initial request for the mission and the expected flight date. As the ATMOSAT program had already acquired considerable experience in the inflation of the balloon at remote sites on land, the second option appeared preferable. The decision was made to inflate the balloon on shore and then tow it to the launch site.

Flight seven of the ATMOSAT "America" started on October 10, 1977 and concluded on October 11, 1977. This flight was made by The Aerospace Corporation under contract to the Port of Long Beach, with the scientific and operational support of the South Coast Air Quality Management District (SCAQMD) and the U.S. Coast Guard.

The balloon moved southeastward along the shipping lane at about seven knots for the first hours of the flight, then stagnated overnight, finally arriving on the beach at Oxnard approximately 26 hours after launch. Flight altitude was maintained at 200 to 250 feet, typical of the height of tanker emission plumes. The resulting analysis by the SCAQMD of flight data, concurrent meteorological measurements, and historical wind statistics suggest that such a result (in which the air mass does not move directly from the shipping lane into the South Coast Air Basin) would be found most of the time.

A proposal has been made (by the Jet Propulsion Laboratory, Pasadena, CA) using the ATMOSAT design as part of a mission for possible future exploration of Mars (Ref. 1). The "Roving Ball Planetary Explorer" would be an instrument-laden, reinforced-fabric ball capable of inflating and deflating automatically or on remote command from Earth. Driven by the high winds known to prevail on Mars' surface, any number of these balloons or bouncing balls could roam the surface almost at random, conducting scientific experiments and measurements over a vast area. Or they could be powered and steered by an inner drive system, much like a bicycle.

If a pause for additional study of an area is needed, the ball can partially deflate like a child's punctured kickball, and lose most — if not all — of its bounce.

The "bouncing ball" has the advantages of low cost, long life, and extended traverse of the planet's landscape. It was felt it should provide a payload of 20 to 30 kilograms (about 44 to 66 pounds) with a traverse of 100 to 200 kilometers (60 to 120 miles), and be strong enough to survive any of the Martian terrain.

A Mars mission using the giant balls would be to deploy several of them ranging in size from 3 to 10 meters (10 to 33 feet) in diameter. Each would be equipped with commanded inflation and deflation, an adjustable center of gravity, pressurization by a blower using Mars' carbon dioxide (CO_2), and the instrument payload suspended within each ball.

Fully inflated, the balls would be blown across the surface by the Martian wind, much like tumbleweed. Partially deflated, with the center of gravity lowered close to the flattened "foot" thus formed, the ball would be fixed in position.

If powered, a ball would require only about 10 watts to travel 1 meter per second (2 mph).

By manipulating the pressure and center of gravity within each ball, its motion could be started and stopped under any prevailing wind condition. By sensing wind direction and force, the ball could be maneuvered over the Martian surface. Adjustment of the pressure and center of gravity would allow the ball to surmount obstacles of a height equal to about one-third the diameter of the ball.

The two Viking Landers, still gathering information on the Martian surface, showed the terrain — at least in the area under their surveillance — to be rugged and strewn with large boulders.

Ultimately, the scientists and technicians working on the effort concede, the ball would become trapped by an obstacle too large to be overcome. This, they say, would likely be a location of special scientific interest because of the great accumulation of wind-blown Martian material also trapped there.

The ATMOSAT manned superpressure balloon system has demonstrated the ability to remain stable in a parcel of air without perturbing air chemistry in any way. Such a system has allowed the precise determination of air trajectories over many miles of land and sea. The use of trained observers on board has facilitated the collection of atmospheric data: ozone, NO_x , SO_2 , temperature gradients, turbulence, and other. It is also a low cost, recoverable vehicle that neither contaminates the air by any propellant fumes, nor agitates it by propeller wash, thus gathering accurate data and providing a new dimension in today's multifaceted air pollution control effort.

The "Roving Ball Planetary Explorer" concept presents a new avenue of research for the ATMOSAT system. The progress and developments toward this concept will be reported on at the next AFGL Scientific Balloon Symposium.

References

1. Mars Program Vehicle Options, 720-14, For Presentation to the Mars Science Working Group, Jet Propulsion Laboratory, Calif. Inst. of Tech., Pasadena, Calif. (11-13 May 1978).

Bibliography

"ATMOSAT 6 and 7 - One by Land One by Sea," Ballooning 10 (6), 14 (Nov-Dec 1977).

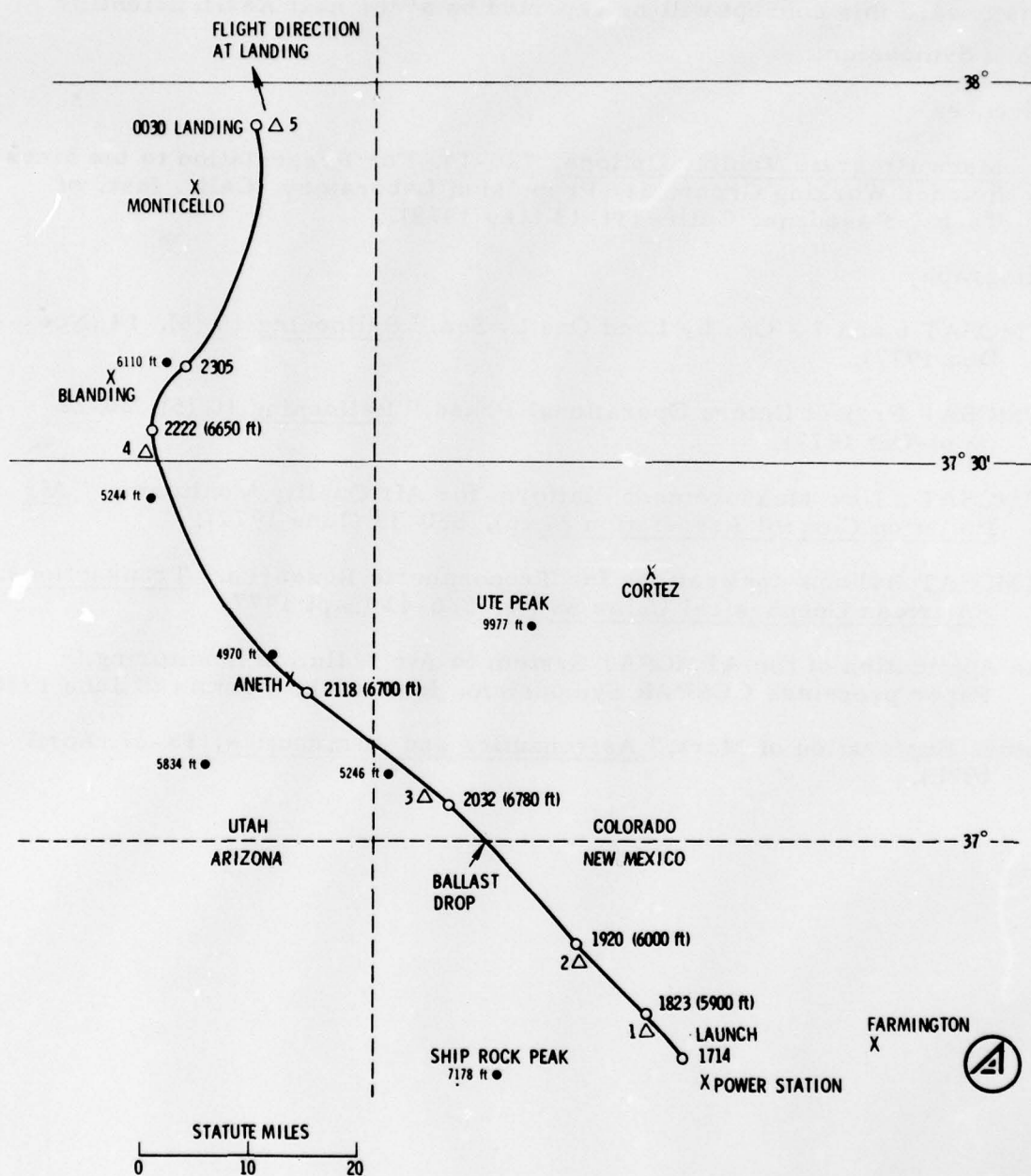
"ATMOSAT Project Enters Operational Phase," Ballooning 10 (5), 20-22 (Sept-Oct 1977).

"ATMOSAT a New Measurement Platform for Air Quality Monitoring," Air Pollution Control Association 27 (6), 530-33 (June 1977).

"ATMOSAT Balloon Applications for Tropospheric Research," Transactions, American Geophysical Union 58 (9), 836-43 (Sept 1977).

"The Application of the ATMOSAT System to Air Pollution Monitoring," Paper presented COSPAR Symposium, Innsbruck, Austria (8 June 1978)

"Future Exploration of Mars," Astronautics and Aeronautics, 18-27 (April 1978).



Δ GRAB SAMPLES

Figure 1. ATMO SAT IV, 8-9 December 1976. All times in MST (GMT - 7 hr)



Figure 2a. Balloon Inspection and Patching Operations Prior to Flight 5

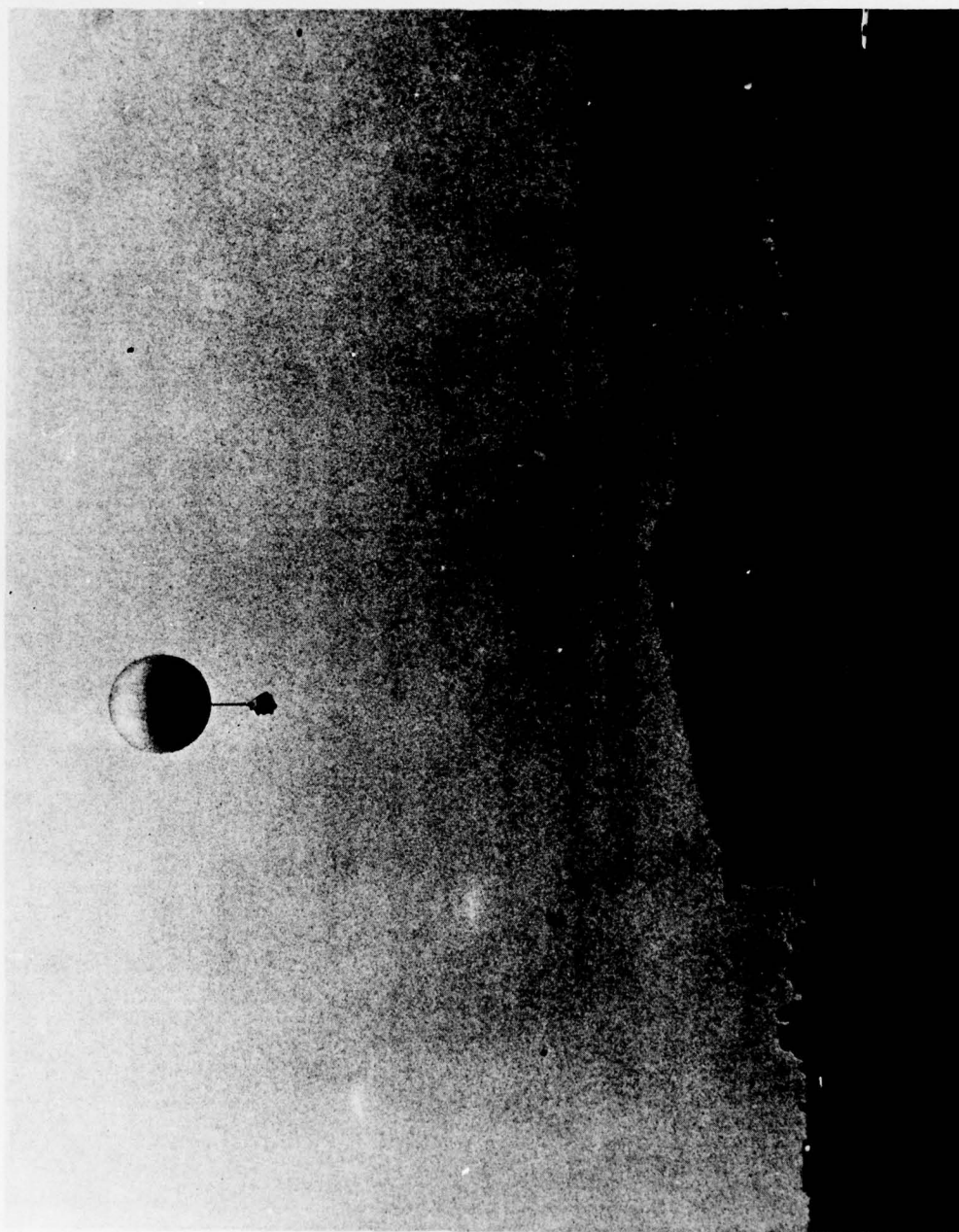


Figure 2b. Liftoff—Flight 5

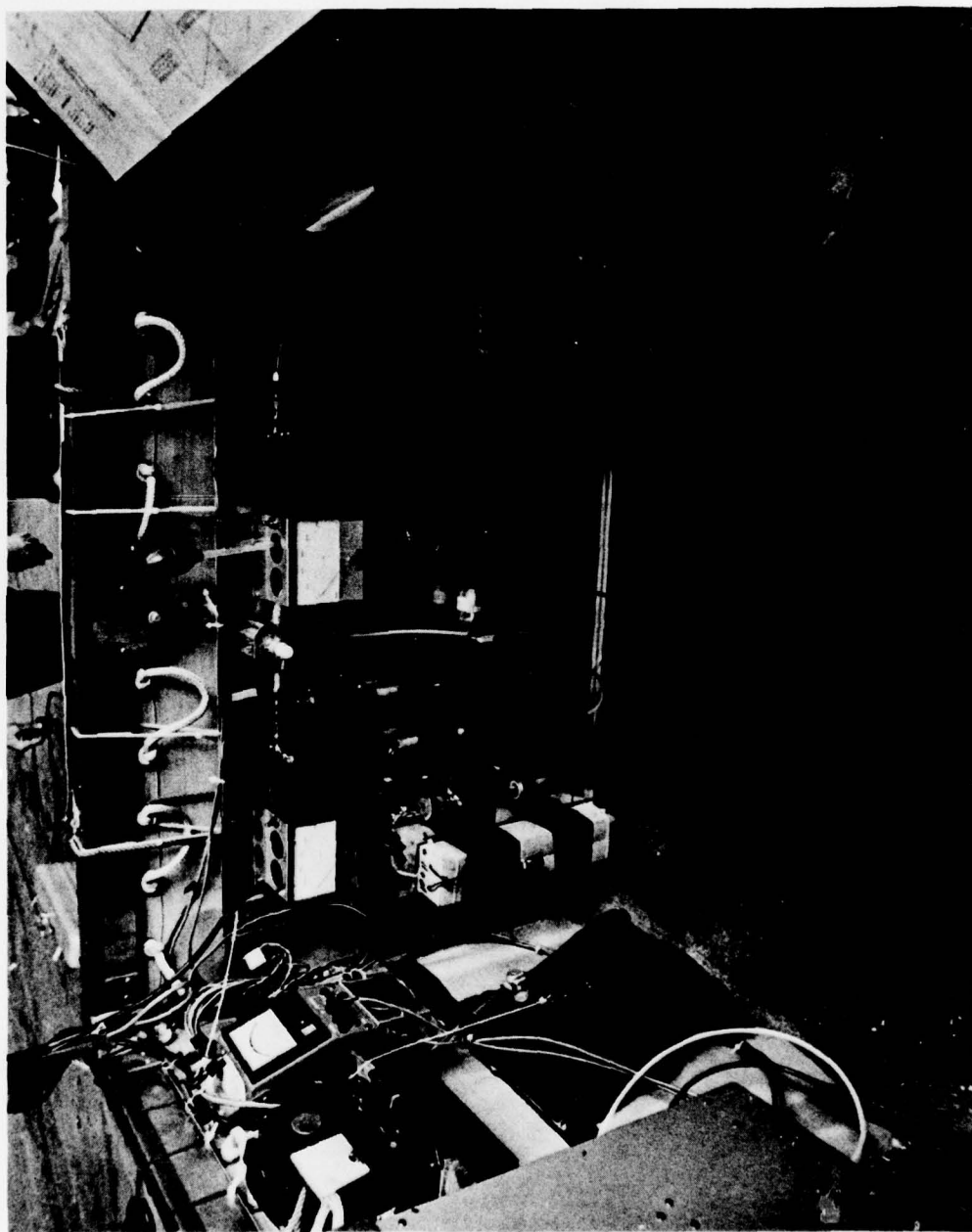


Figure 2c. NO_2 Experiment Used During Flights 5 and 6

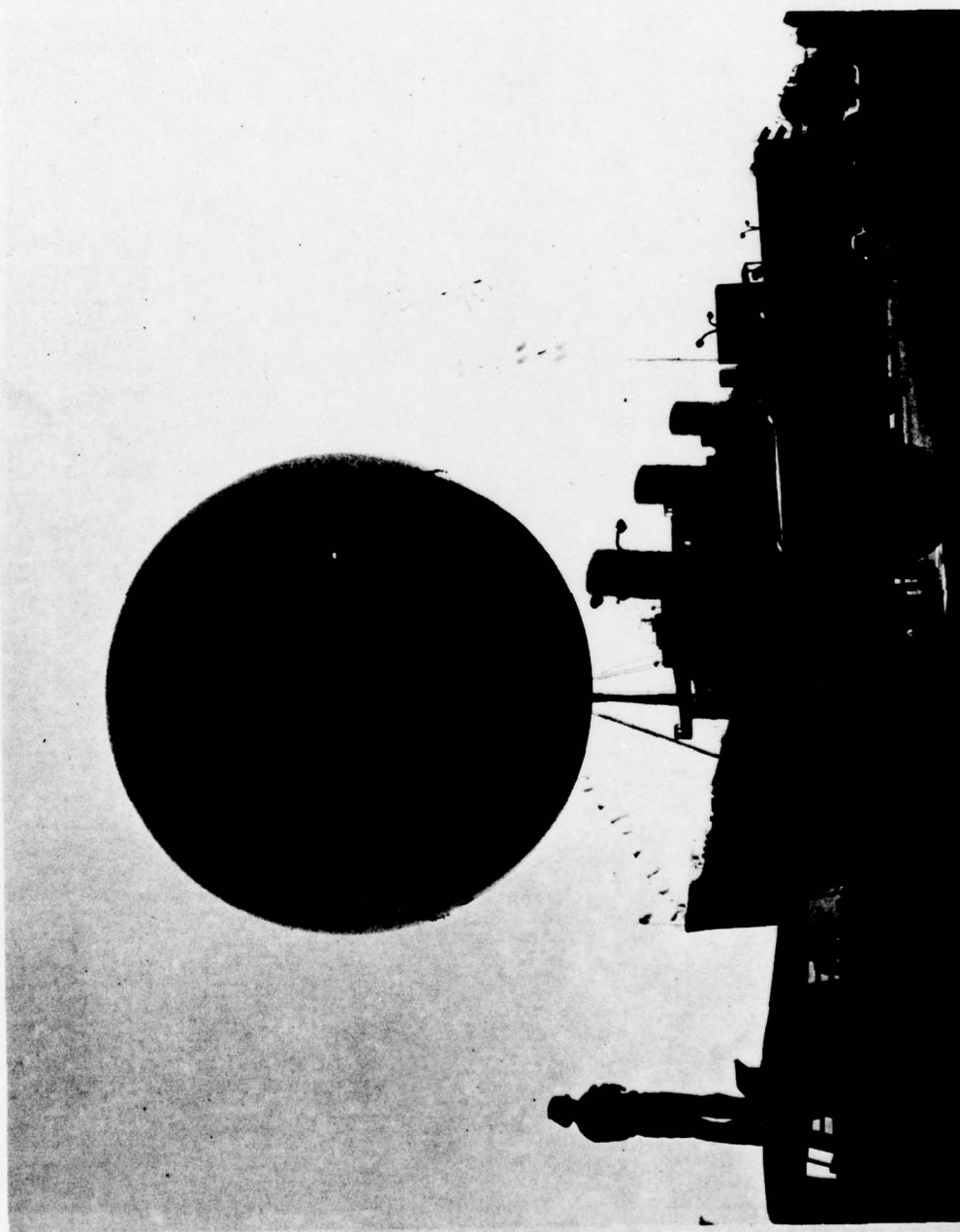
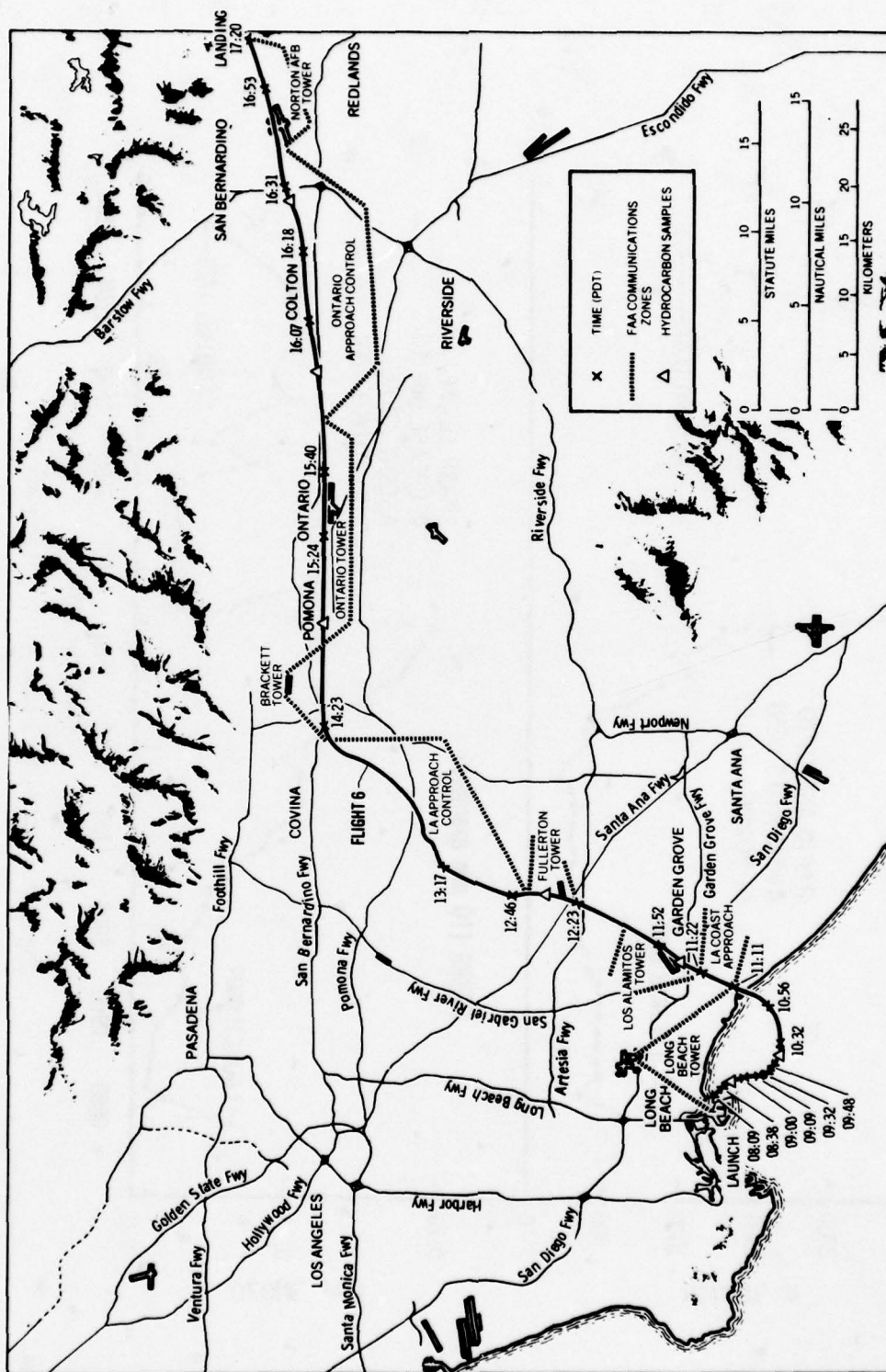


Figure 3a. Final Checkout Prior to Launch—Flight 6



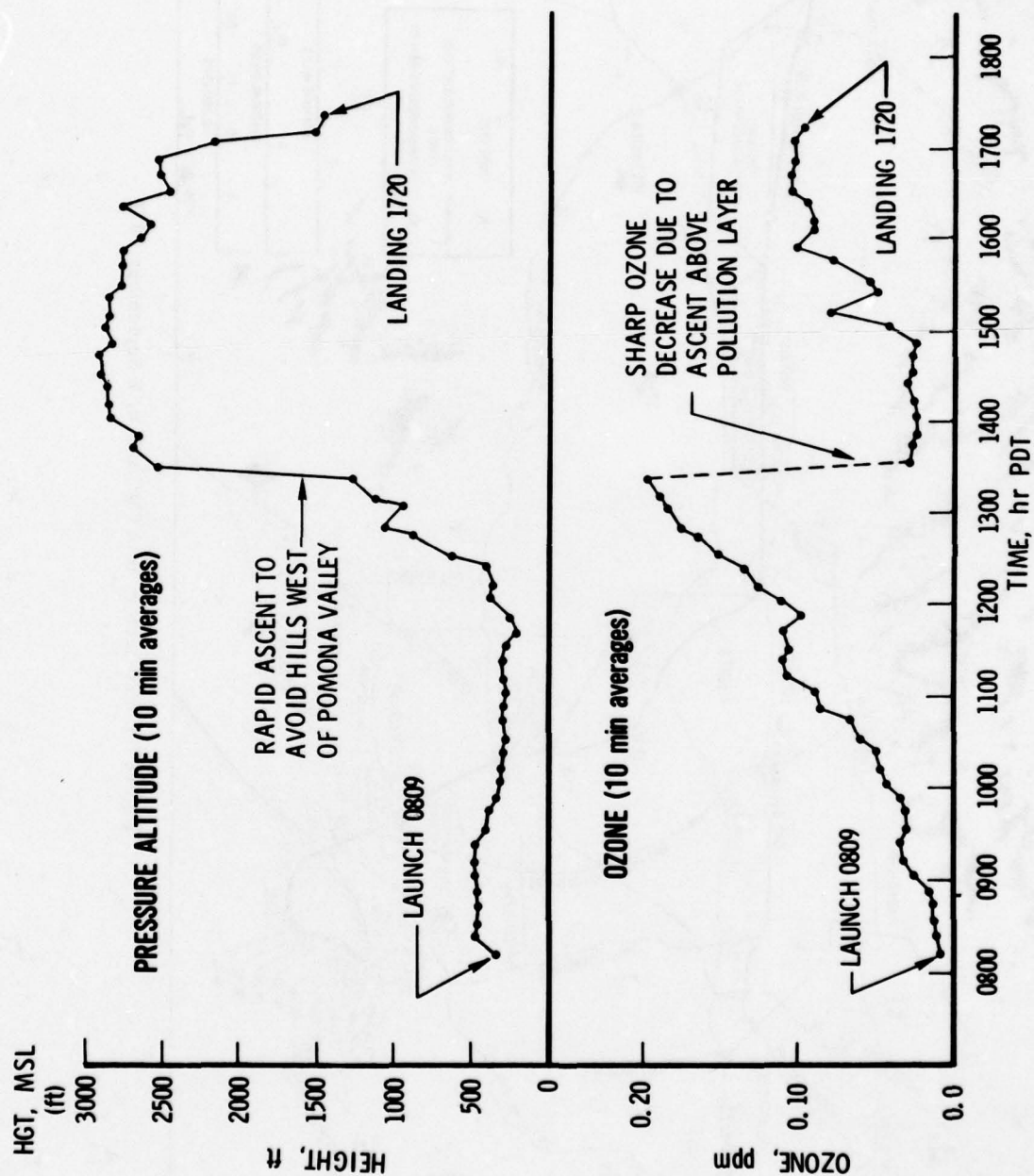


Figure 3c. ATMOS-6 Flight Data, 8 September 1977

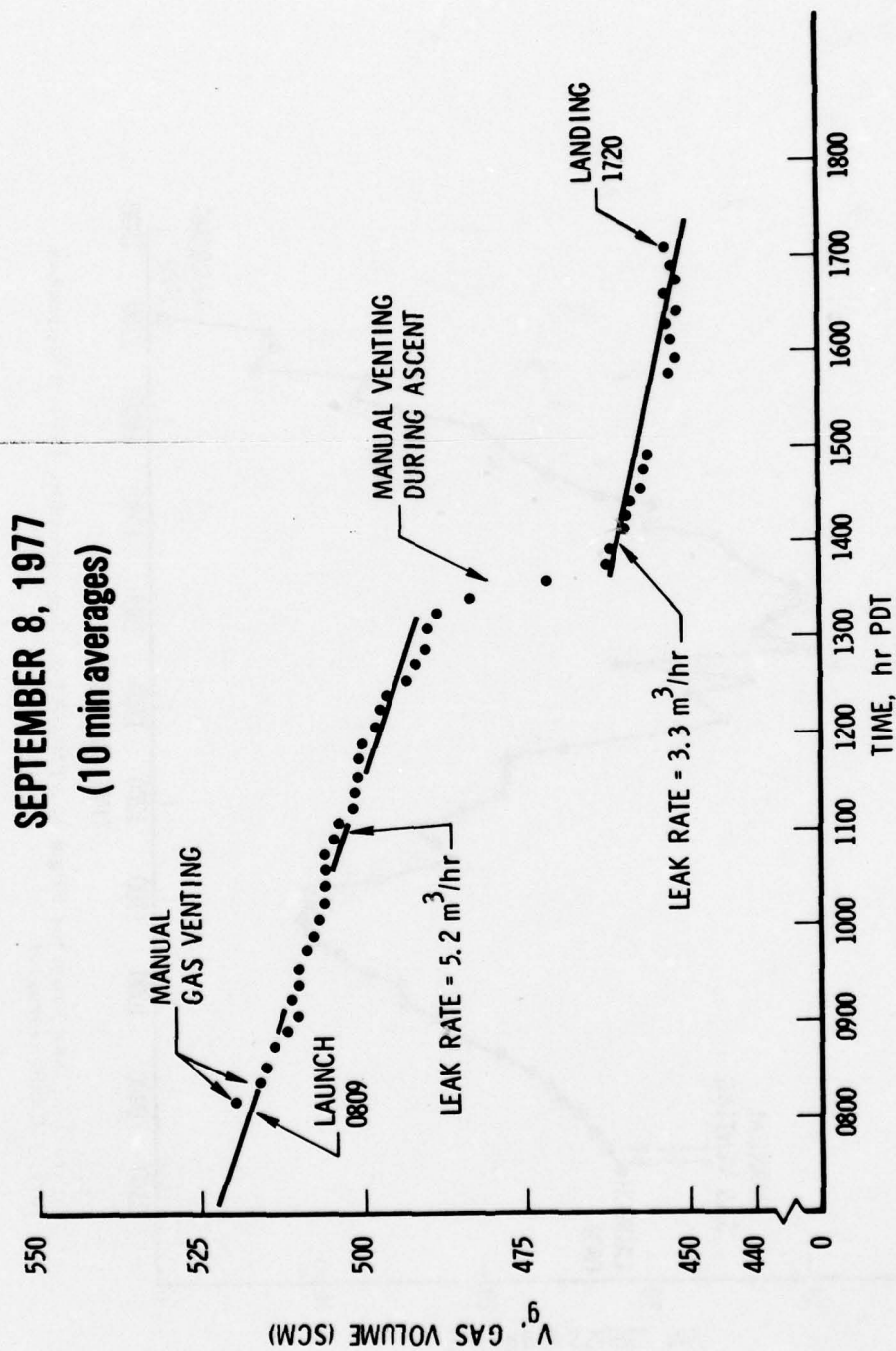


Figure 3d. ATMOSAT-6 Flight Data, Gas Volume (standard cubic meters), 8 September 1977 (10 min averages)

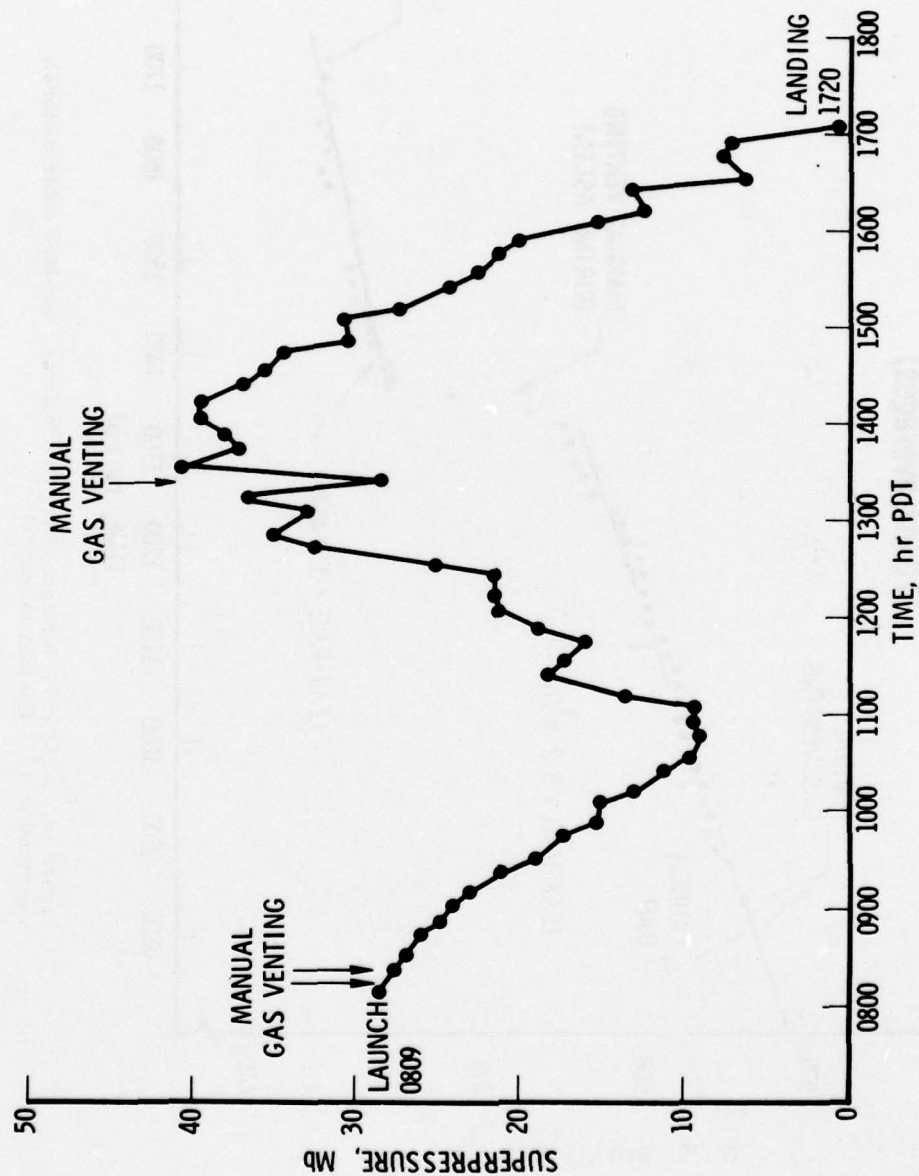


Figure 3e. Data From the Flight of ATMOSA T-6, Superpressure (ΔP), 8 September 1977, (10 min averages)

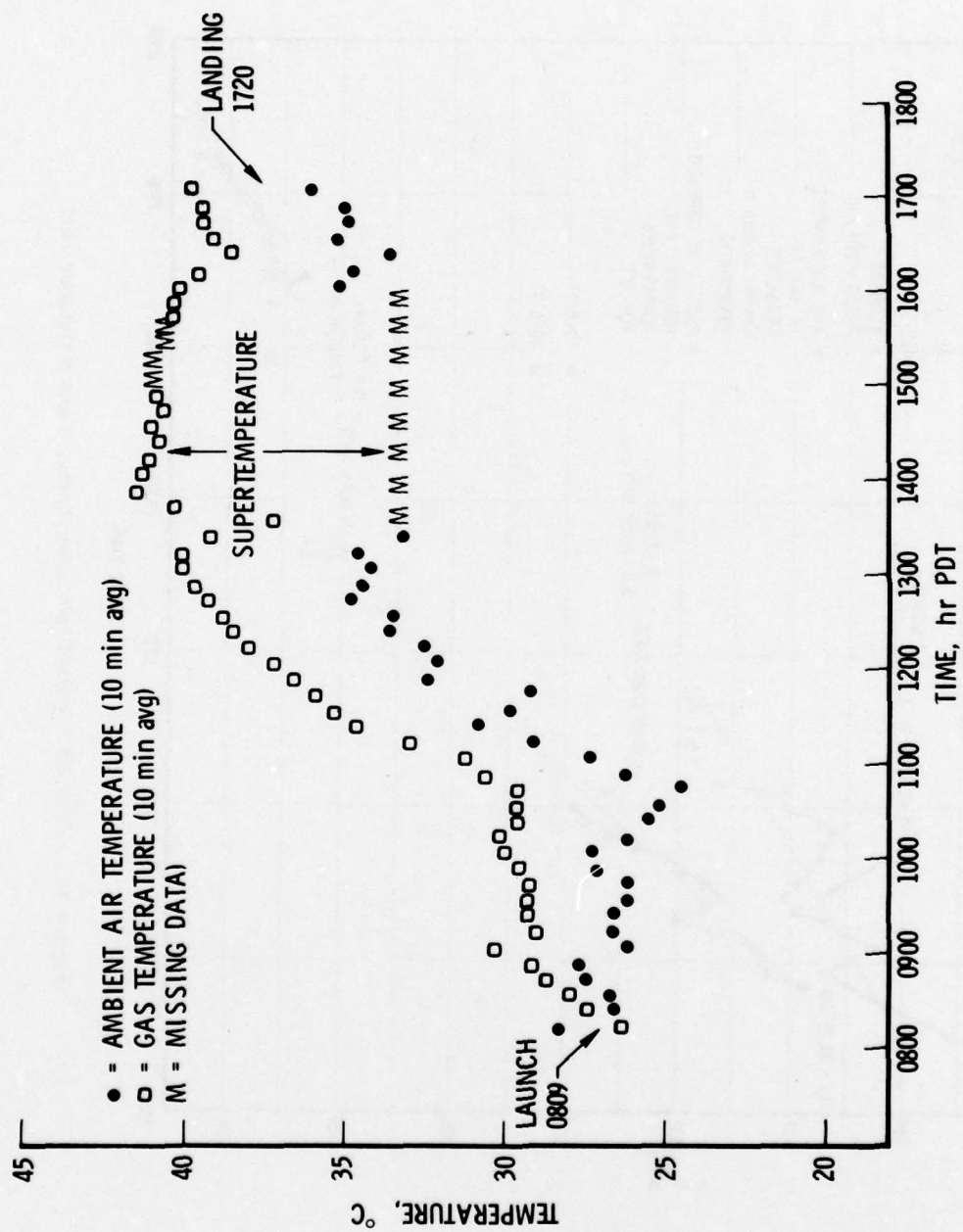


Figure 3f. ATMOSAT 6 Flight Data, Automatically Recorded Air and Gas Temperatures, 8 September 1977 (10 min averages)

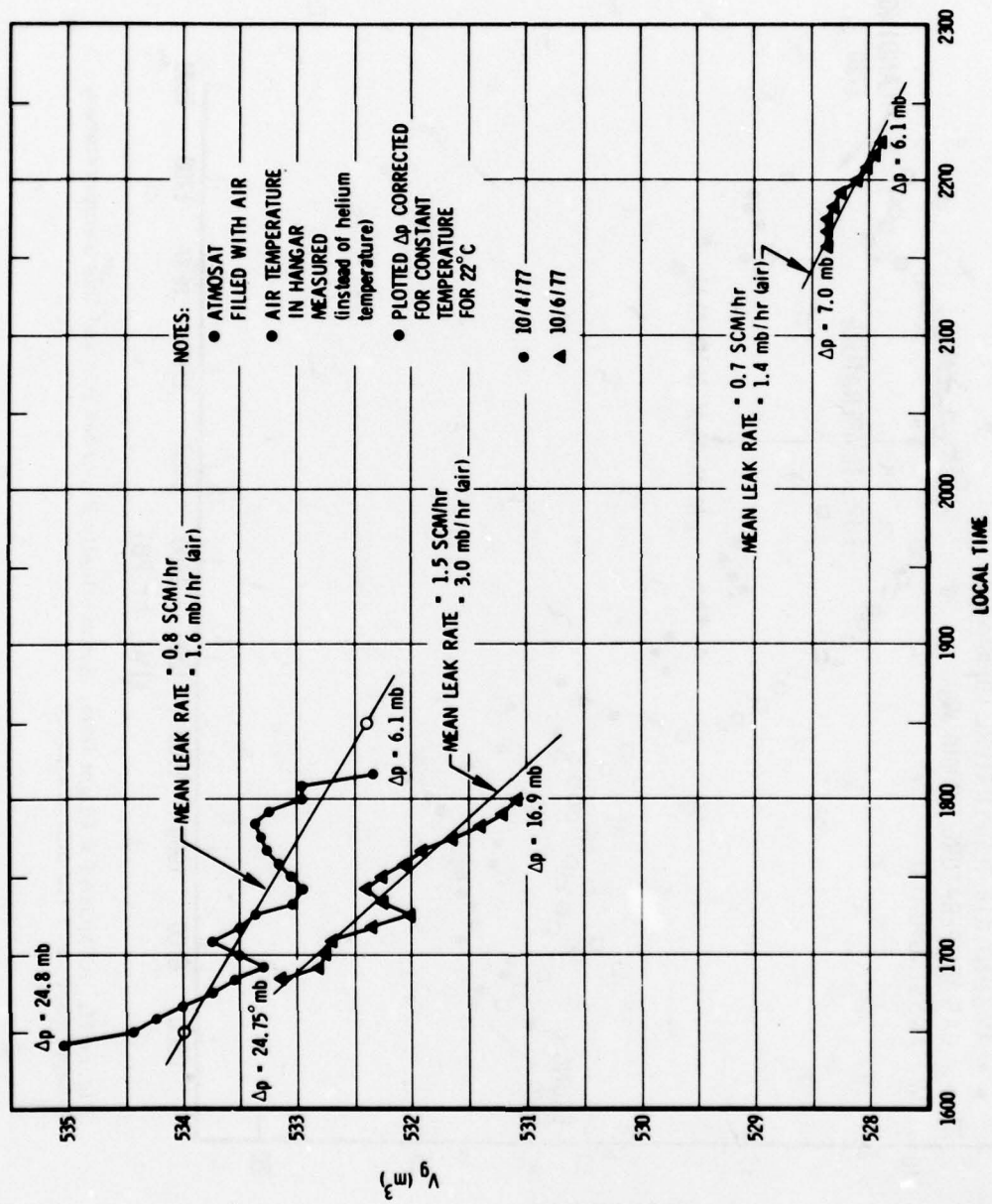


Figure 4a. ATMOSAT-7 Preflight Leak Tests, 4 and 6 October 1977

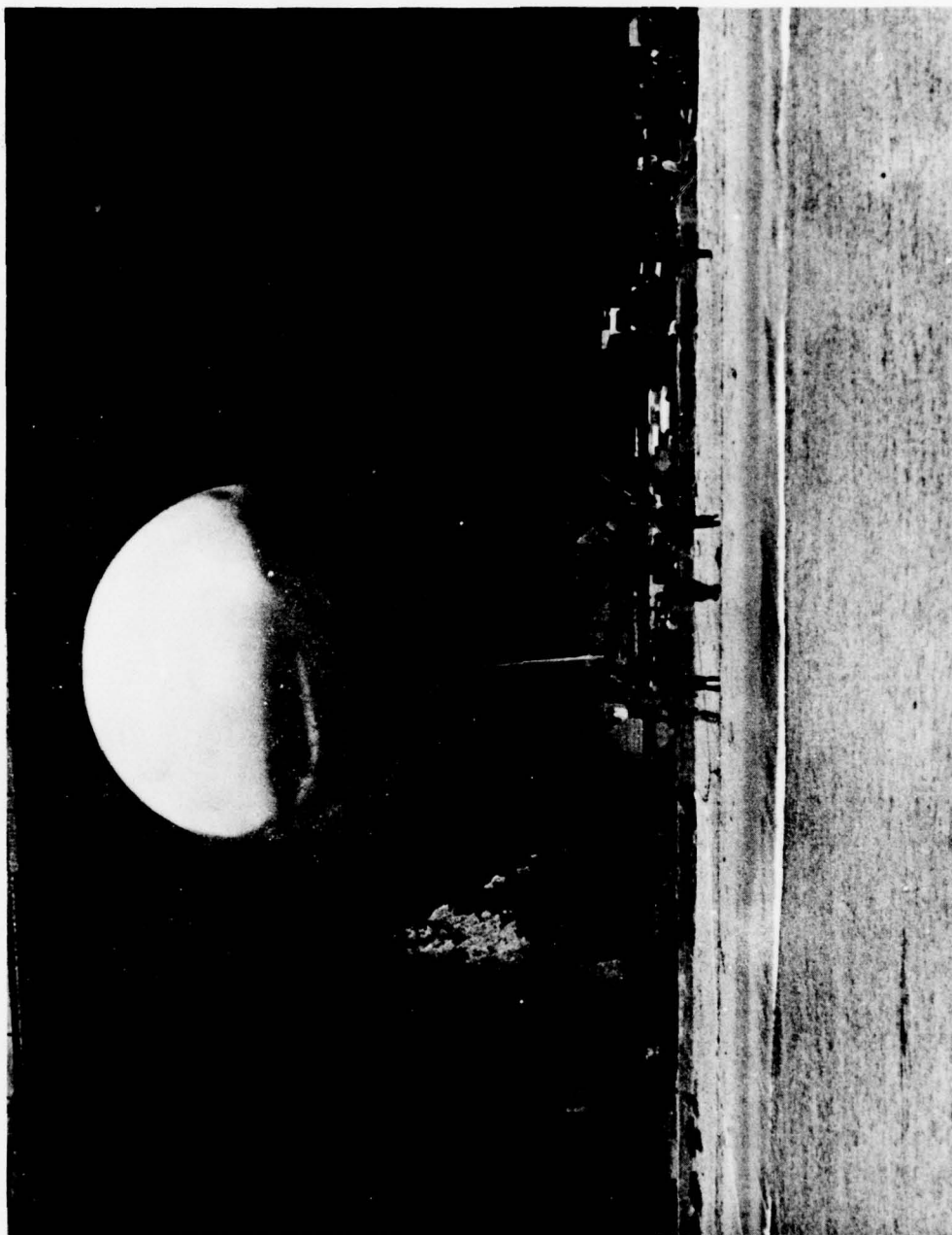


Figure 4b. Liftoff From Gaviota Beach—Flight 7

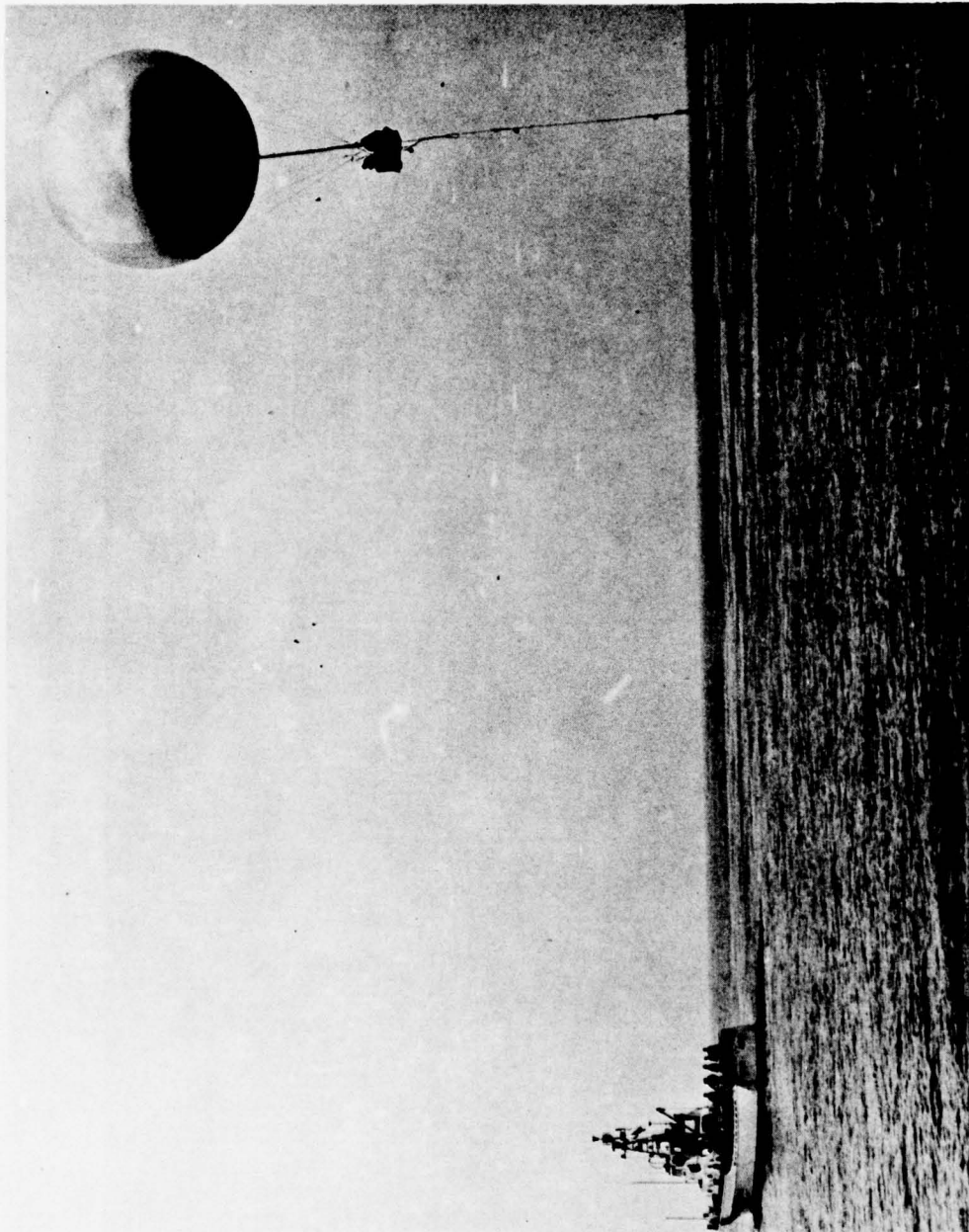


Figure 4c. Towing to Launch Site—Flight 7

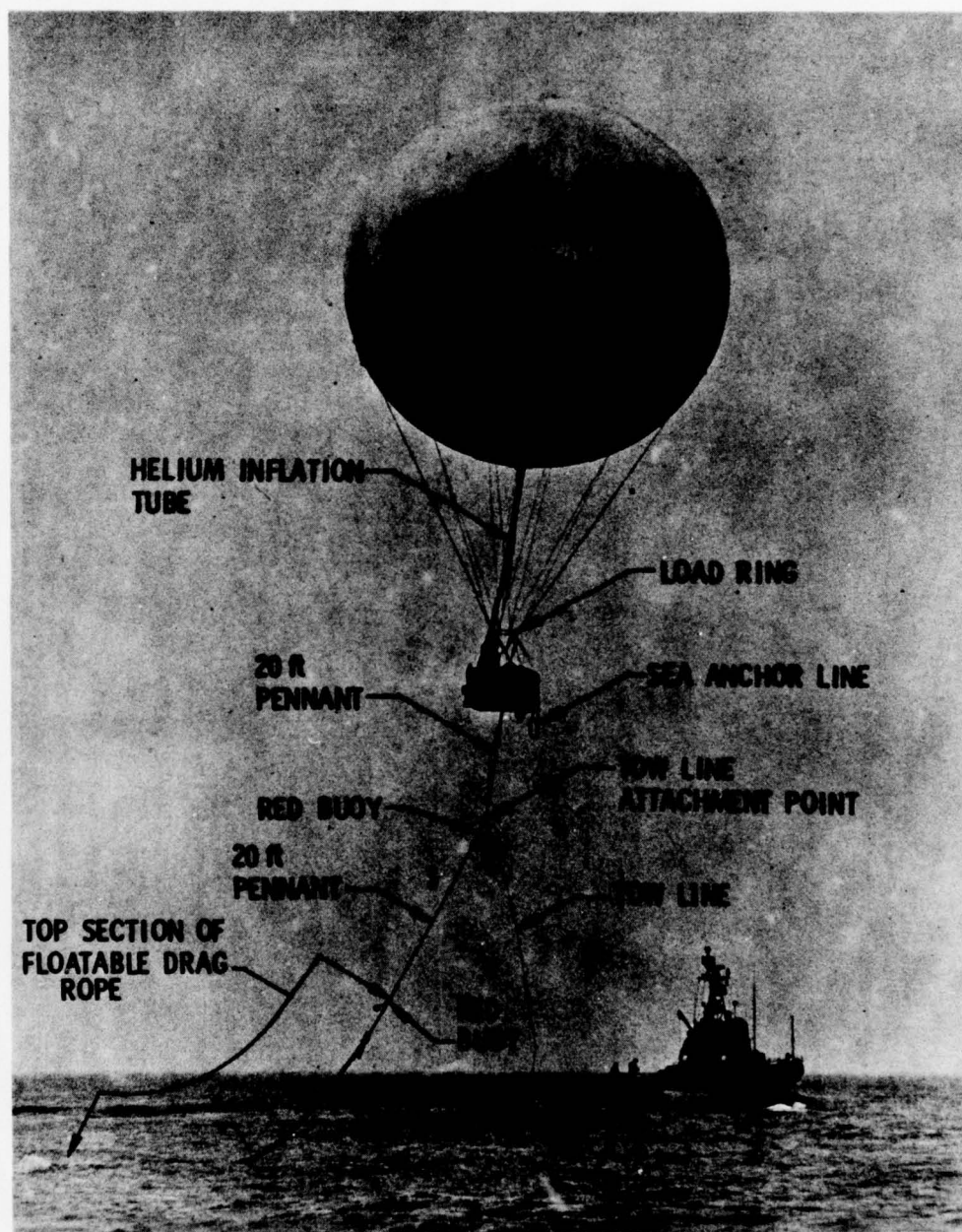


Figure 4d. Rigging Lines in Operation—Flight 7

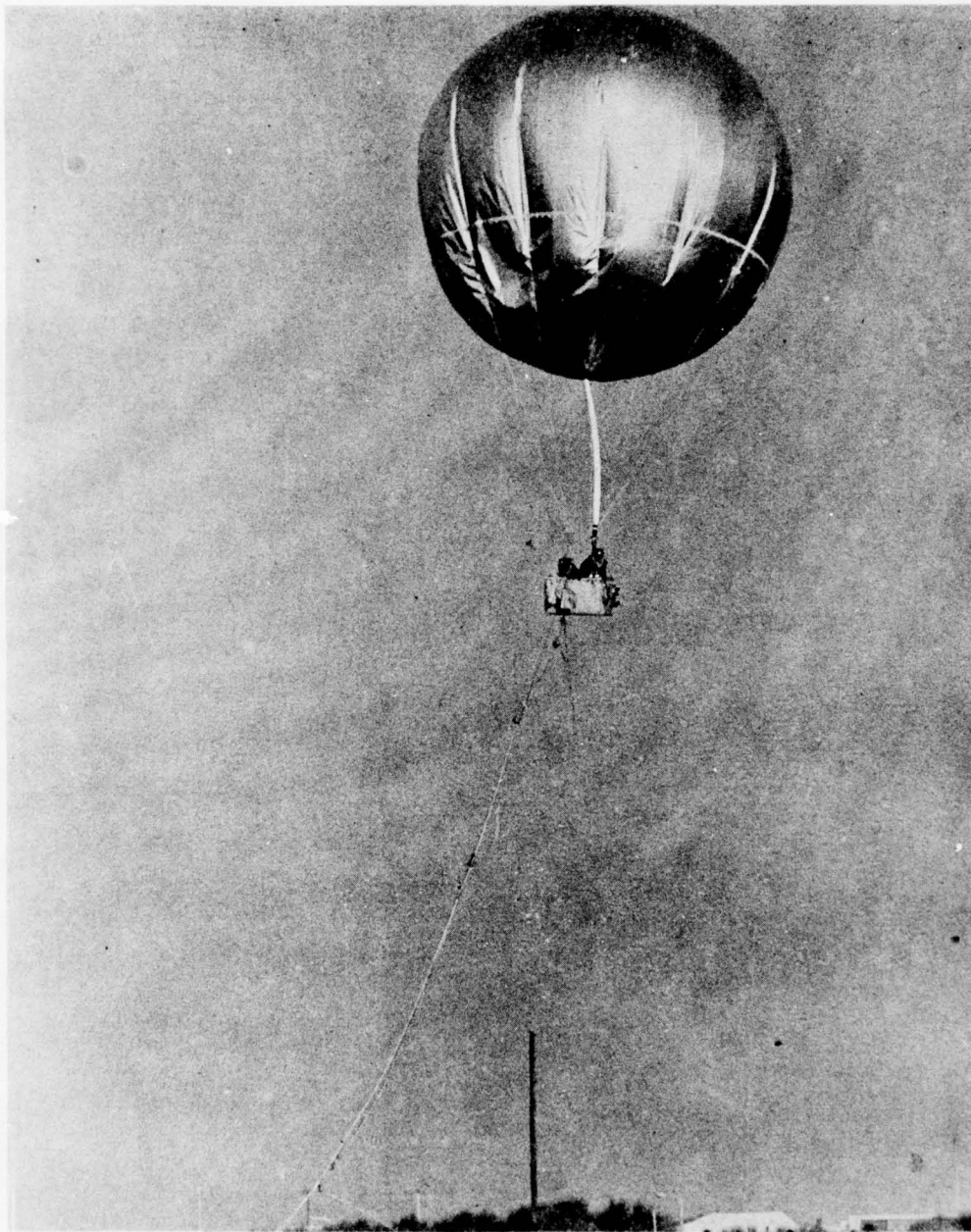


Figure 4e. Balloon Deflating Due to Helium Venting by Crew—Flight 7

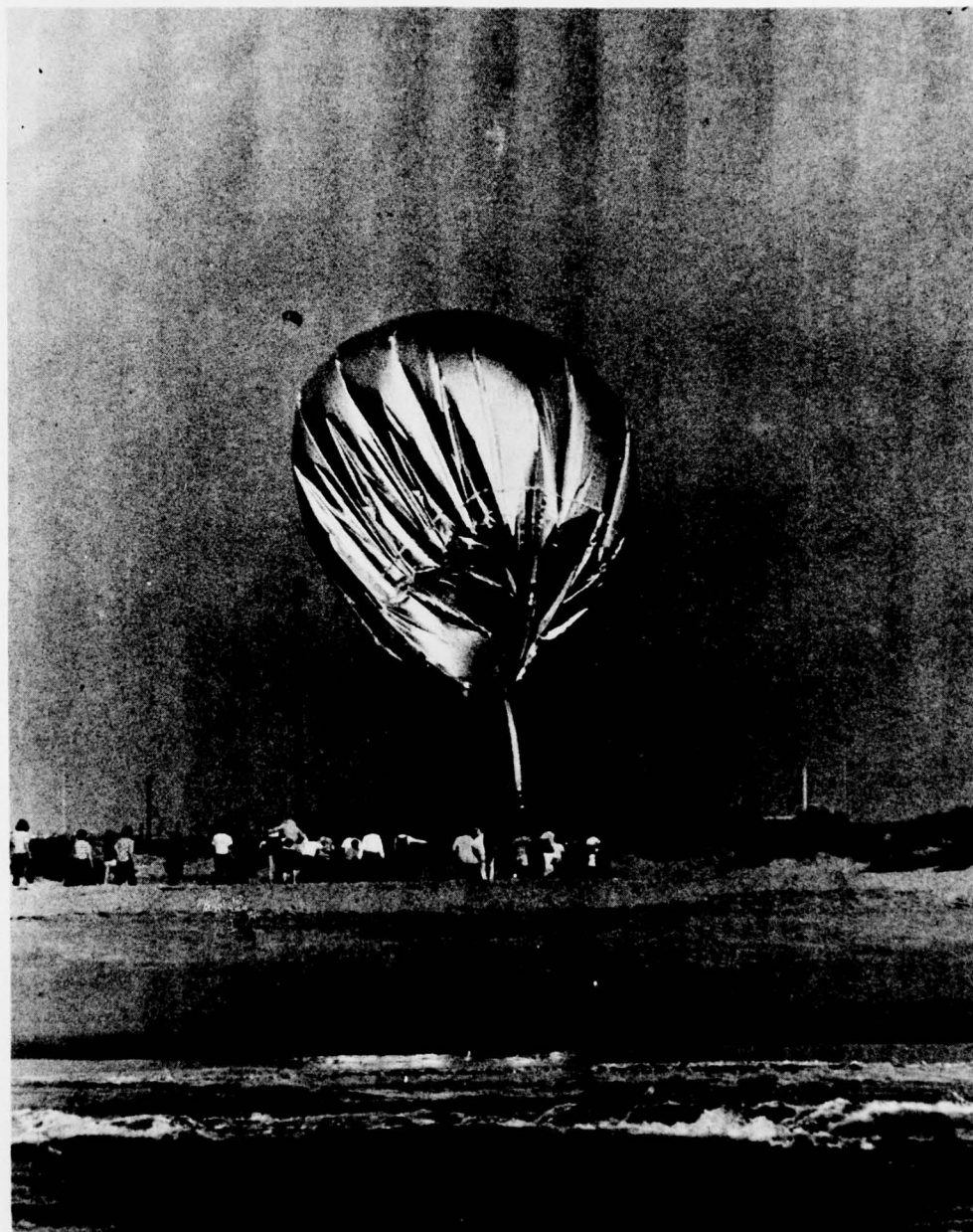


Figure 4f. Touchdown at Oxnard Shores—Flight 7

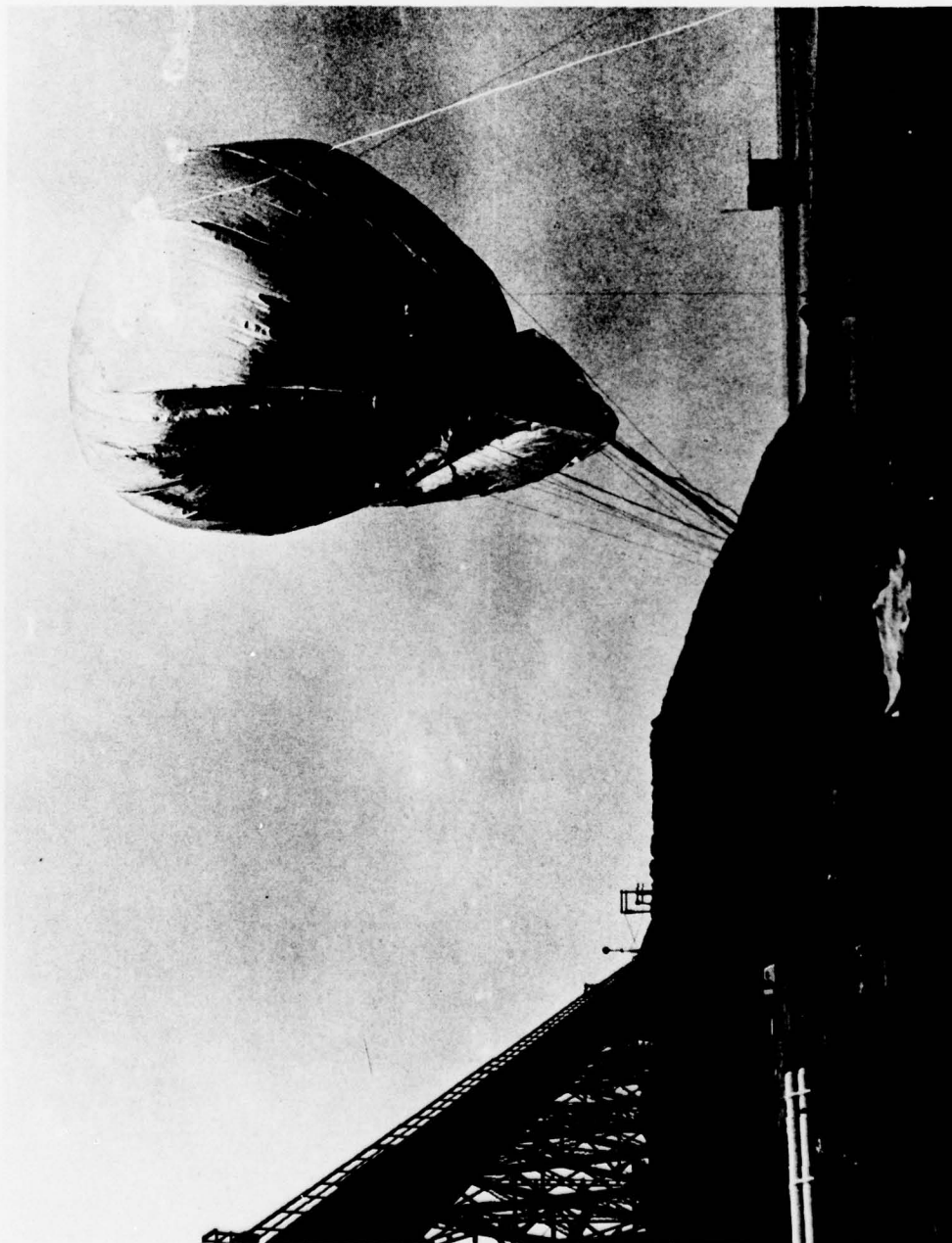


Figure 4g. Inflation of ATMOSAT—Flight 7

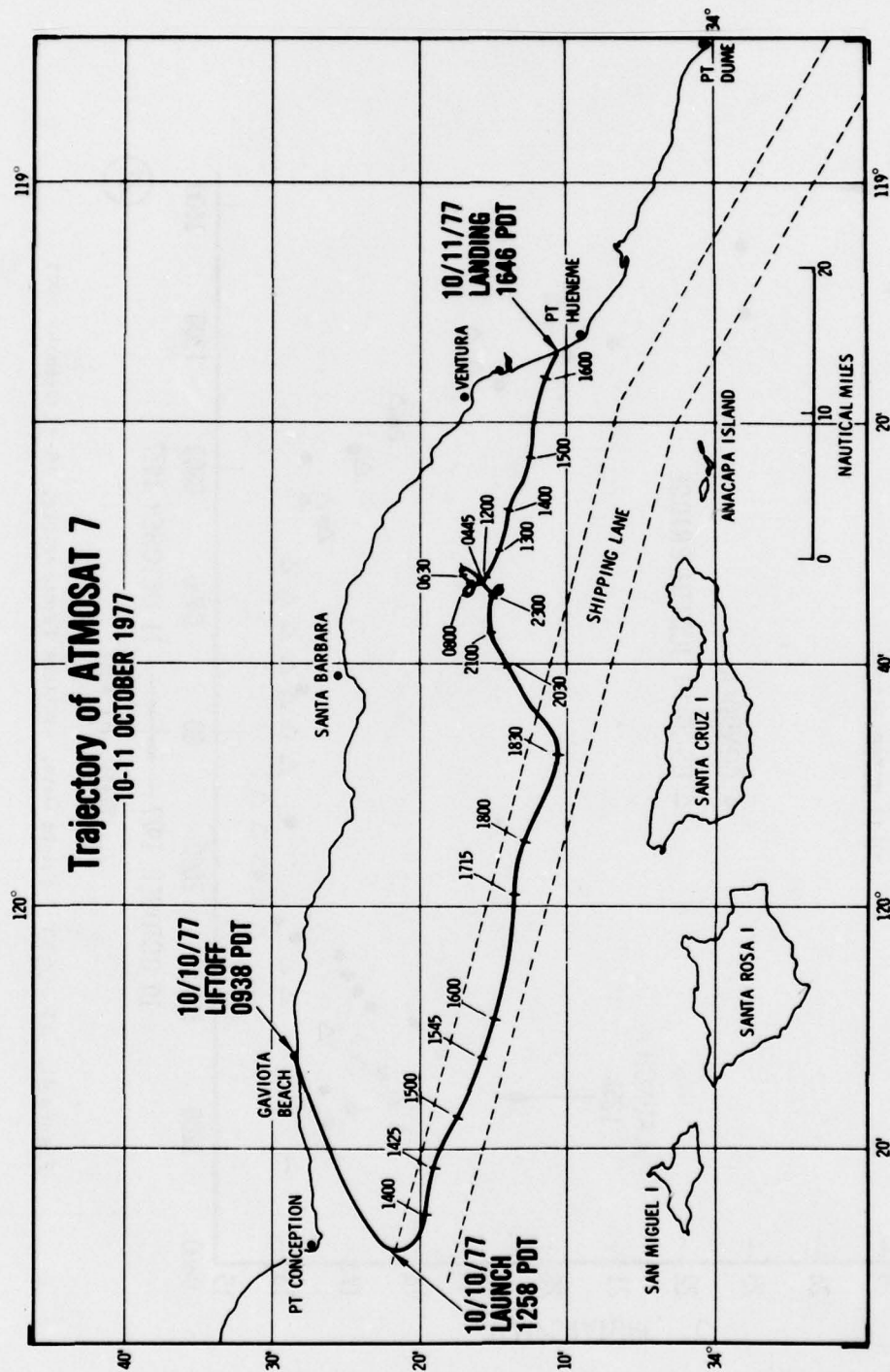
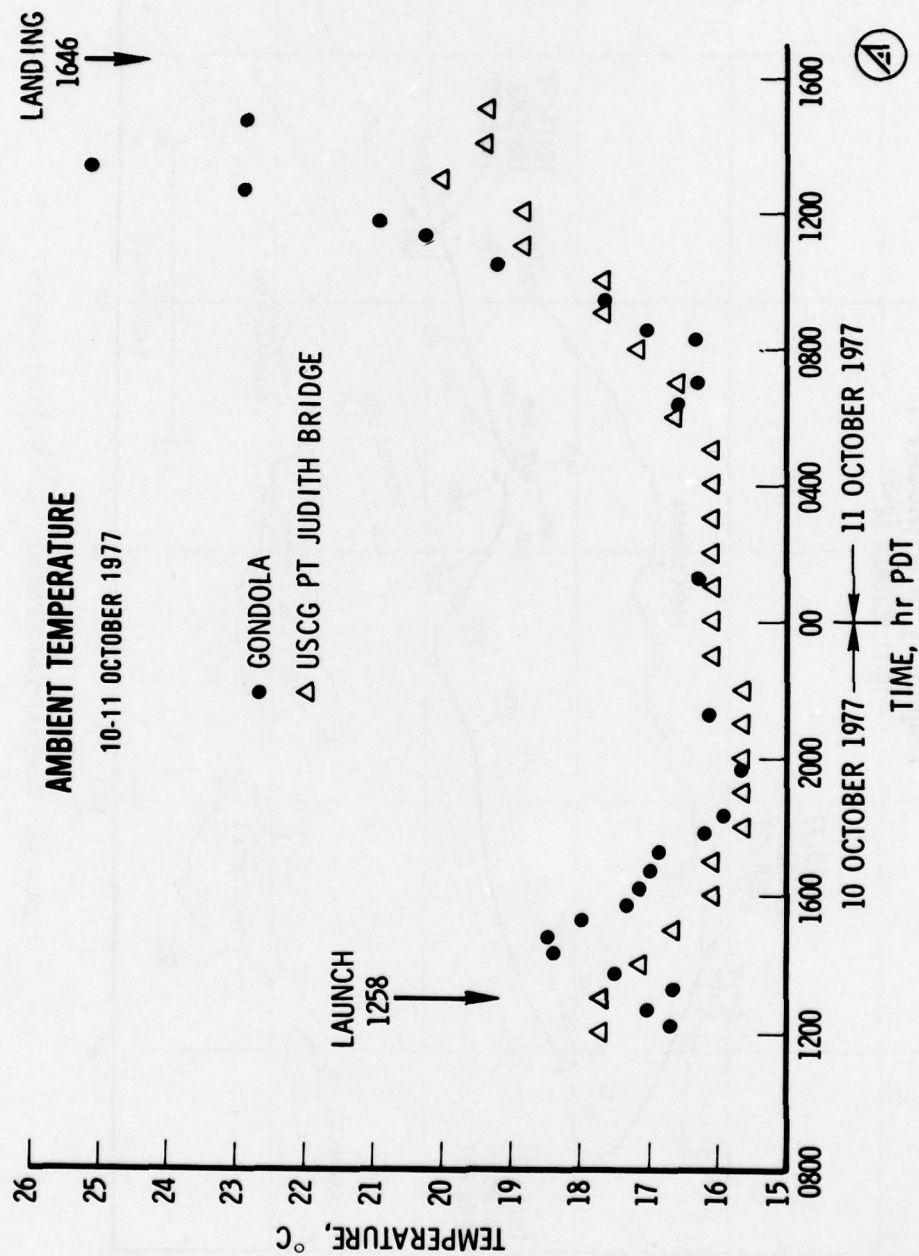
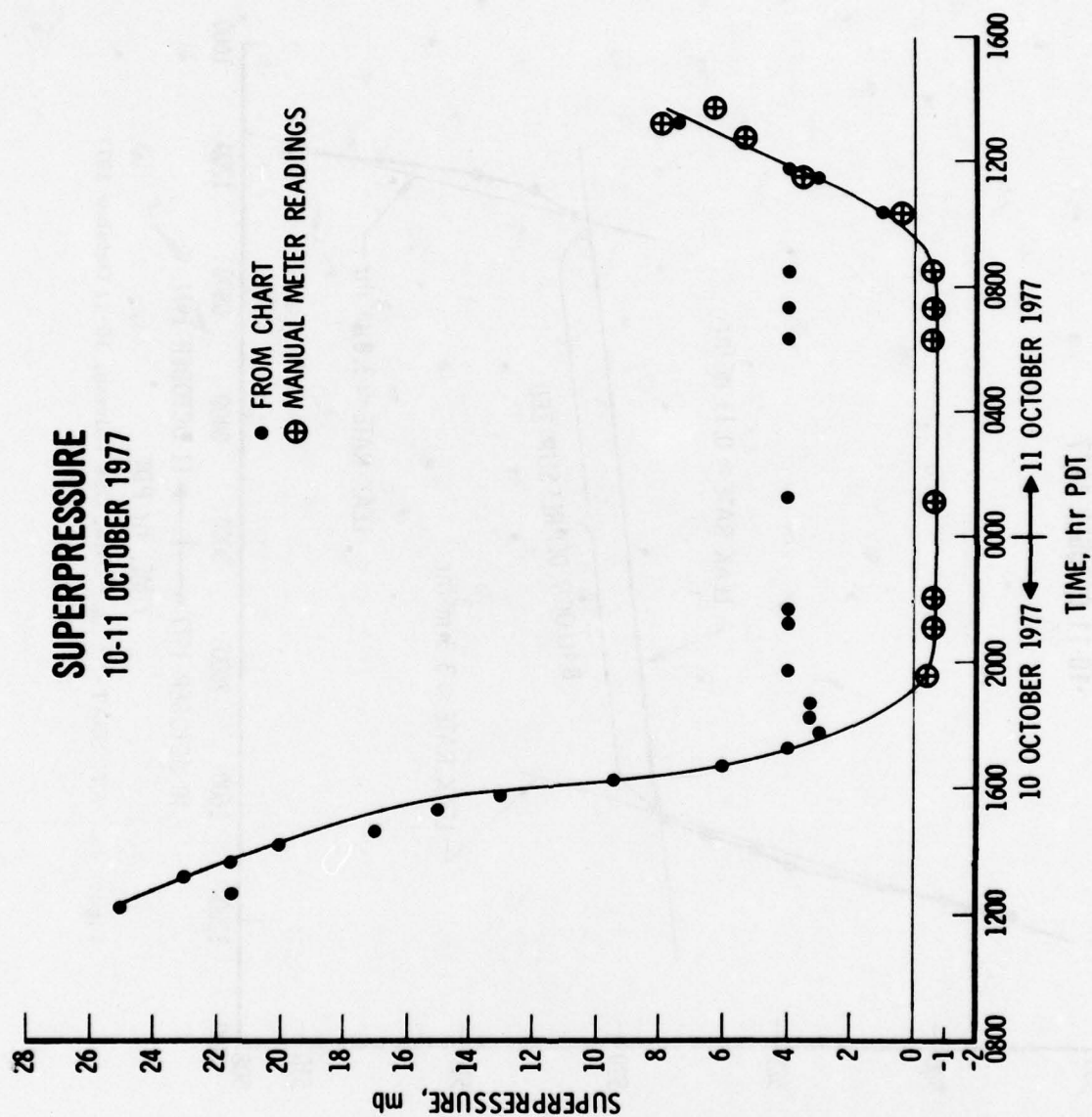


Figure 4h. Trajectory of ATMOSAT 7, 10-11 October 1977





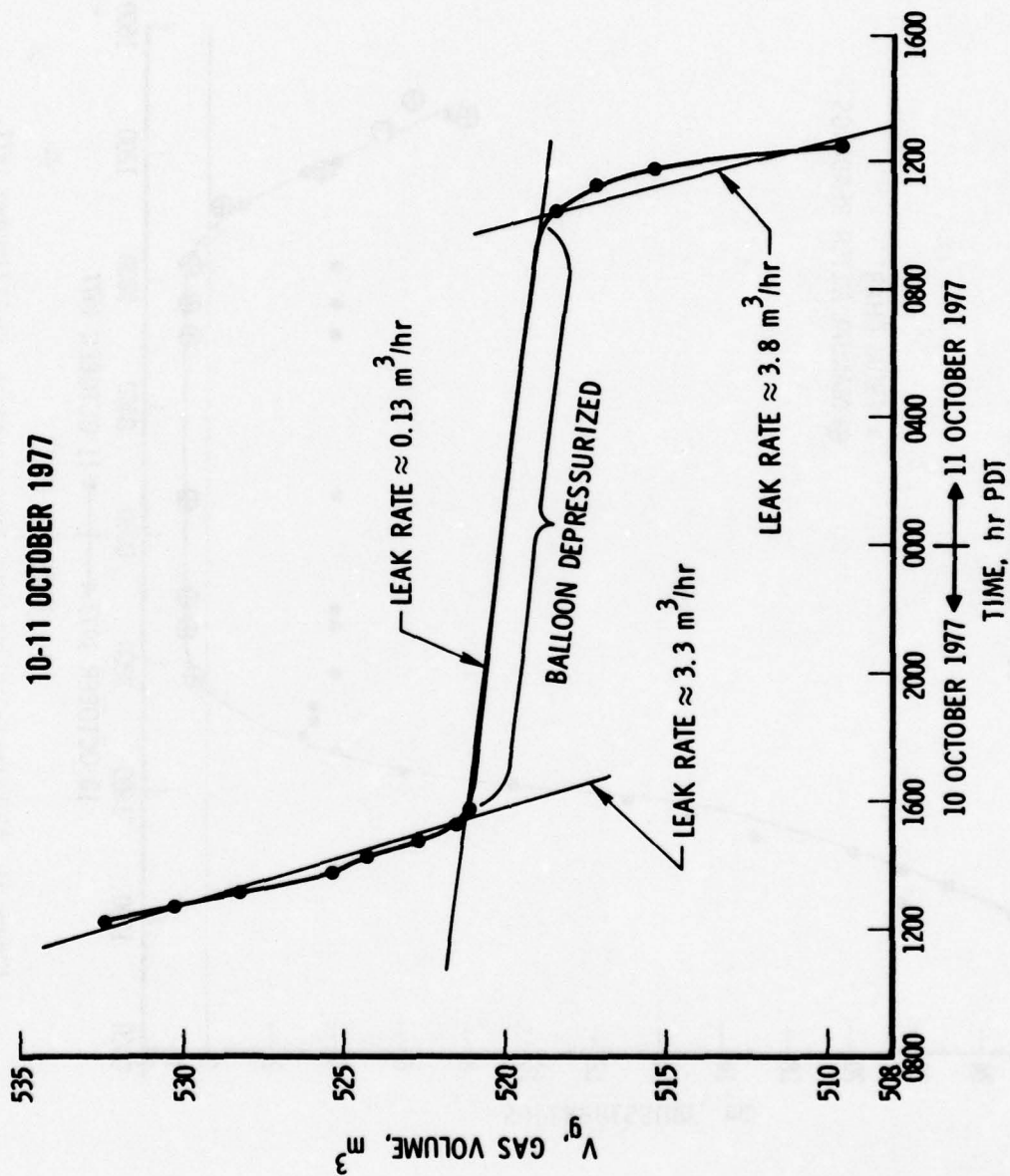


Figure 4k. ATMOSAT-7 Flight Data, Gas Volume, 10-11 October 1977

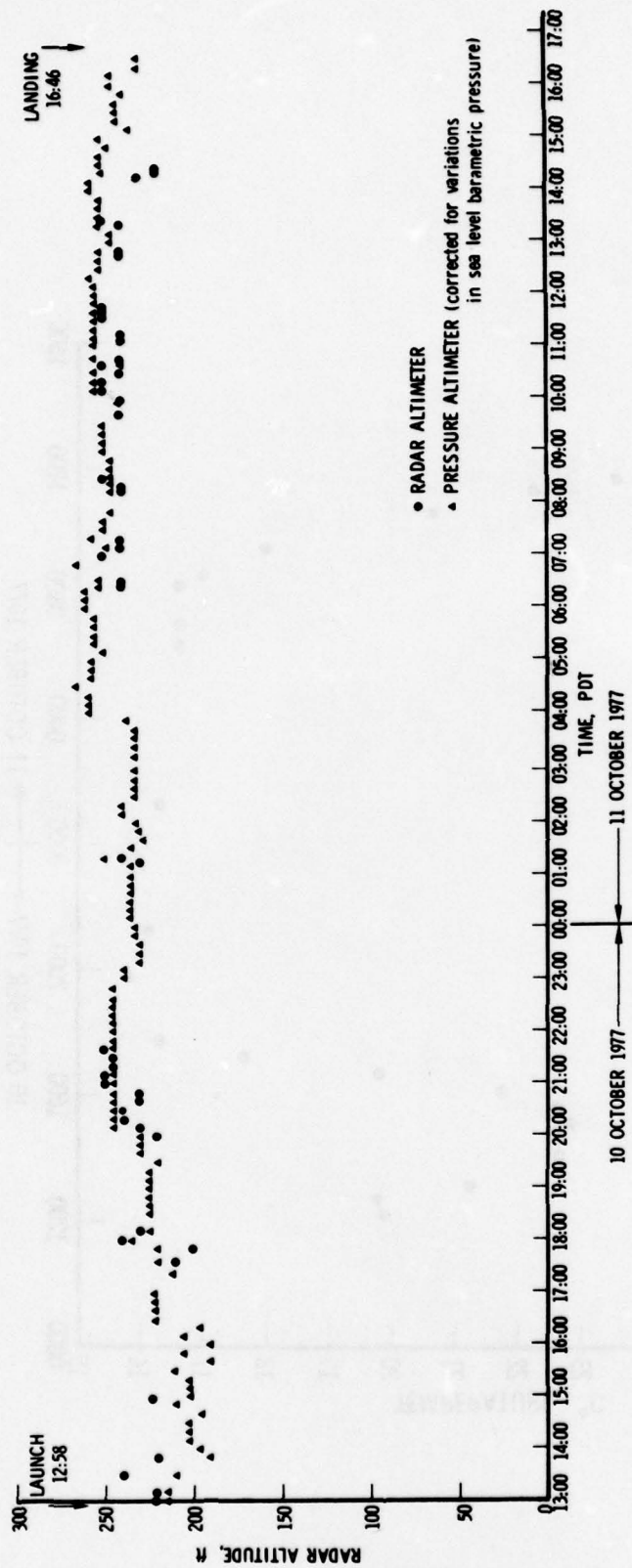


Figure 41. ATMOSAT-7 Altitude Profile, 10-11 October 1977

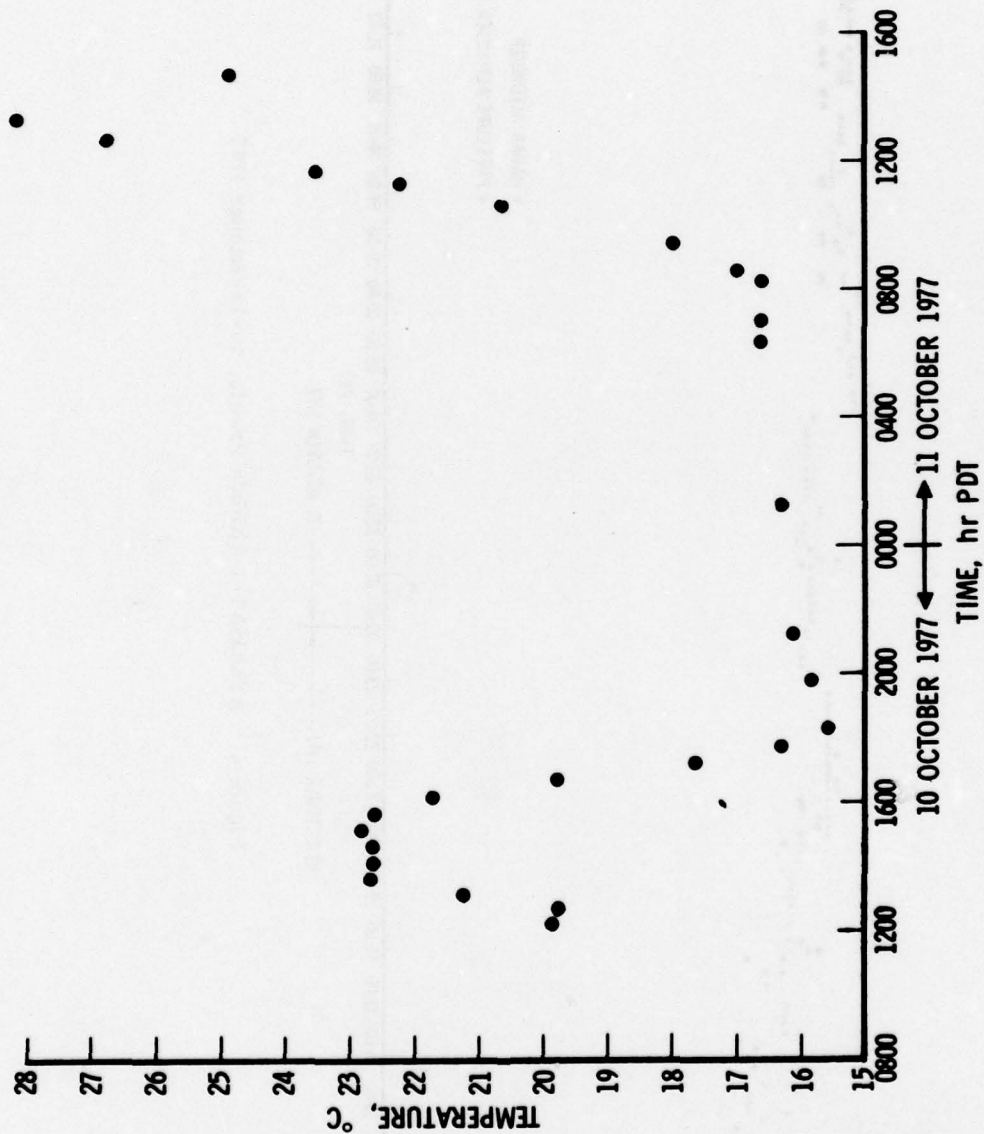


Figure 4m. ATMOSAT-7 Flight Data, Gas Temperature, 10-11 October 1977



Figure 5. Artist Concept—Roving Ball on Mars

SPORT BALLOONING - A SCIENTIFIC APPROACH

Julian R. P. Nott
The Hot-Air Balloon Company Ltd.
14-16 Great Pulteney Street
London W1R 4AR

By way of introduction, there is no doubt that most sport balloonists are woefully ignorant of the activities of the scientific balloon community. I don't know if the reverse is true and even if it is, I don't know if it matters. Nonetheless, I hope that what follows may be of interest, if not of direct use.

In many respects, I feel I should remain in the audience as I have largely been a user of the sort of information this symposium produces, rather than providing basic data. On the other hand, I have been involved in a variety of projects over the last six or seven years.

For me, one of the attractions of these activities is that they have involved being an end user of a wide variety of sciences. The range is from basic physics and chemistry, through materials science, combustion, aerodynamics and statics, communication and navigation, aviation medicine and life support systems and of course a great deal of meteorology. Current sport ballooning can, I feel, be compared somewhat to the position of light aviation in the late 1920's and early 1930's. It is still possible for individuals to put new technical ideas into practice in a relatively short space of time, and at the sort of price it is possible to beg, steal or borrow from advertisers and other sponsors.

With that introduction, it seems simplest to take projects in chronological order. In 1972, we made a crossing of the Sahara Desert by hot-air balloon. The pilots were Don Cameron, Felix Pole and myself. To be honest, most of the 2,500 mile crossing was in landrovers and a truck and we flew at the oases! As you can see the project produced some amazing photographs, but one important event was that

Felix Pole and I made a flight to 20,000 ft. in a 2400 m³ balloon. This was not very exceptional in itself. At that time the altitude record for a hot-air balloon had been pushed to over 31,000 ft. by Karl Stefan, one of the most scientific balloonists ever to have been in sport flying, and Chauncey Dunn. But, a physicist called Bob Bradshaw had written a computer model to predict the optimum rate of climb for a hot-air balloon. Our flight to 20,000 ft. showed that the model worked reasonably. It showed that by climbing at the rates indicated by the model, rather faster than had been used in the past, it was possible to climb using relatively little fuel which meant valuable weight saving. Since we had made the flight in Africa together, Felix Pole was a little annoyed when I set out to break the record myself! I managed to get to 36,000 ft. in a 2400 m³ balloon, while Karl Stefan had used a 3000 m³ balloon. This was the first successful use we made of mathematical modeling in hot-air ballooning, and it has proved very useful ever since.

In 1973, Felix and I got together again to fly over the Alps with a Swiss pilot, Ernst Krauer, in a conventional gas balloon. We made a direct crossing to Italy, a perfect crossing being complemented by landing in a grass field five hundred yards from an autostrada exit so our retrieve was instant!

In 1974, Felix and I again combined forces to make a new attempt on the altitude record for a hot-air balloon. This time we hoped to fly to over 50,000 ft. and accordingly built the first ever hot-air balloon pressure cabin. The total structure weight was only about 95 lbs. The cabin shell was made of glass fibre, the floor and hatch of honeycomb board and the whole 'tied together' with reinforcing bands of parallel stranded carbon fibre. The windows were three layers of clear Mylar (Melinex) laminated by Sheldahl in their UK plant. One of the windows was very large to allow rapid parachute escape. (Before construction we made a cardboard mock-up to confirm this). It could be cut out completely by an explosive tape around its edge. This tape is used to shatter jet-canopies before pilot ejection. The light weight of the window material and the large cut-out for them helped reduce the total weight. Fuel was carried in racks on the outside and the cabin was completed with a 6" sponge rubber 'sole' for landing.

From a short list of several sites with suitable weather and air traffic, we chose to make the flight in India, for a variety of reasons, not the least the romantic/photogenic ones because we hoped to make money from film rights. We hoped to be able to insulate ourselves from what one might call the lack of infrastructure, but this was not entirely possible! The whole project turned into quite an adventure and got more and more behind schedule, mainly for logistic and bureaucratic rather than technical reasons. One important miscalculation concerned retrieving the balloon. We had estimated that even landing at random we would never be more than about one mile from a made-up road. What was overlooked was that in Europe, because farming is so mechanized, it is possible to reach almost any point at least by tractor. In India, it is only possible to reach many fields on foot. Twice, it took 36 hours to move the balloon less than a mile from landing to a made-up road. In the end, after four test flights, we made it to 46,000 ft. the actual flight going rather smoothly. Incidentally, we used mathematical modeling in two valuable ways: as before, it was used to estimate fuel consumption, and in addition Bob Bradshaw produced a 'handling model'. This was important, because we were not sure if we could even fly the balloon because of its large volume (10,200 cm). At this time the largest modern hot-air balloon was Tracey Banes' 5600 cm solar balloon, and the largest balloon I had ever flown was only 4000 cm. Interestingly, although mathematically rather simple (e.g. pressure was taken to vary linearly with altitude) it turned out that balloon pilots could 'fly' the model neatly to a 'landing' while others could not without a lot of practice. Even at a volume of 10,200 m³ it was still reasonably flyable.

Although not so technically complex, one of the most interesting projects I have been involved in, was the 'Flight of the Condor' at Nazca in Peru. The object was to fly a manned balloon at Nazca, site of the famous desert lines in Peru, made from materials it could be proved would have been available to the pre-Inca civilization. The lines are only visible from the air. Eric von Daniken (Chariots of the Gods) maintains this is because spacecraft arrived at Nazca. The project was organized by Jim Woodman of International Explorers Society to demonstrate an alter-

native way flight might have occurred at Nazca. The I.E.S. design was supposed to be to an authentic pre-Inca blueprint but did seem to owe something to modern balloons! The balloon was built by Raven and my only contribution was actually to pilot it. The project was started as much as anything to generate publicity for the I.E.S.; yet although I started out completely skeptical about the theory of pre-historic flight at Nazca, I was completely satisfied, both by what the expedition did and by what I saw in museums, that the pre-Inca Peruvians could have flown. Whether they did or not is a different matter.

The most interesting fact is that in 1709, three-quarters of a century before Montgolfier, a Brazilian-born Jesuit who had traveled through what is now Peru was summoned to the Portuguese court and flew a model hot-air balloon for the king. Although everyone 'knows' Montgolfier was first, in recent years many balloonists have come to accept the Jesuit's as the first balloon flight.

The circumstantial evidence is interesting. Hot-air ballooning is difficult enough in most climates, even when you know it is possible. It seems more likely that it might have been discovered in a place like Nazca, which has uniquely suitable conditions in my experience, which includes flying at supposedly ideal sites on five continents. As I understand it, the conditions at Nazca - endless sunshine and calm mornings - depend only on the constancy of the trade-winds and so are unlikely to have altered with the moderate changes in global climate that may have occurred in the last 2,000 years.

It was very striking, how everything needed would be available at Cawachi, within easy walking distance of the most interesting markings (the Nazca Plains are actually 25 Km from Nazca). Cawachi is a fascinating and virtually untouched site with the roofs of houses sticking out of the sand. Wherever graves have been robbed, the abandoned corpses are invariably wrapped in cotton shrouds tied up with rope - the basic materials needed for a balloon (I brought back some fragments for dating). Having been on the 1972 Sahara Balloon Project, I was continuously worried about where we would get poles to support the balloon for inflation, as I expected no trees. Yet although the climate is arid, a river runs through Nazca

(and Cawachi) from the Andes, and we got two slender 30 ft. tree trunks immediately after we arrived, and used local timber for the fire.

Finally, I was most struck by how little can be seen from the ground. Driving on the road to Nazca you can see nothing, although the road cuts straight through a great number of lines and marks which are clearly visible from the air. Human vanity makes me wonder: would the mastermind who must have organized large numbers of people to make the marks have done so if he had been unable to see the finished work properly?

In recent years I have become heavily involved in commercial hot-air balloon operations in partnership with Colin Prescott, whose background is in advertising. Most of our activities involve flying for advertising. All the balloons are specially built and of course, if well designed, can be very spectacular. Among the fourteen or so balloons we operate are two made of metalized fabric, one gold and one silver, and a lamp-bulb shaped balloon operated for GEC in the UK. We have even flown this balloon at night, illuminated from inside, with most spectacular results.

Coming up to date with our projects; in the Autumn last year, Colin Prescott and I tried to cross the North Sea in a hot-air balloon. Sadly, we failed to take-off, trying to make the flight in strong winds. We are currently waiting for decent weather to make the crossing and hopefully break the hot-air balloon distance record. In fact, taking off from Edinburgh, if we reach almost any point in Europe we shall succeed in setting a new hot-air balloon distance record. This might seem rather optimistic; however, the balloon has a number of innovations which have all been well tested as was demonstrated by a flight which successfully broke the endurance record for class AX-6 hot-air balloons. (AX-6 is the 1600 m³ FAI class). Innovations include weight saving using a carbon-fibre gondola, Kevlar rigging and the like and in particular, the use of kerosene in place of the normal propane fuel. Kerosene not only gives a valuable weight saving as it can be carried in light-weight plastic containers, it is also convenient as the containers can easily be discarded. We hope to make that flight in the next few weeks.

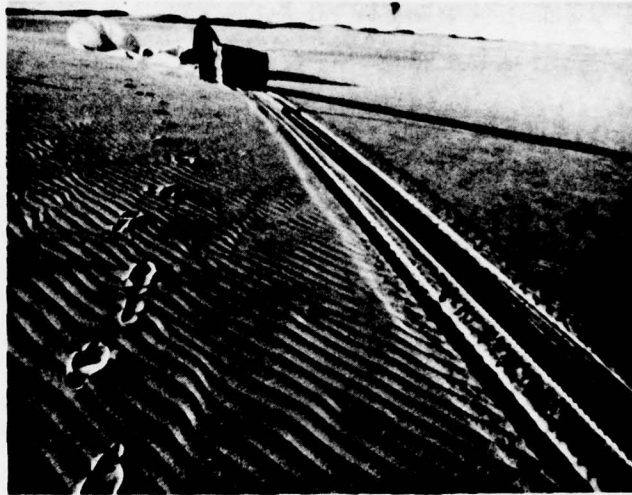


Figure 1. Crossing the Sahara. Flying without weather forecasts



Figure 2. Crossing the Sahara. As always, domestic animals upset, and their owners even more



Figure 3. Crossing the Sahara. Bilma Fort, inspiration for 'Beau Geste'



Figure 4. Crossing the Sahara. Nott (r) and Pole capture the British altitude record



Figure 5. Over the Alps to Italy.
Pole (l) and Nott before takeoff (1972)



Figure 6. After Take-Off From
Stechleberg (near Interlaken Bernese
Oberland). The balloon is already
nearly 3000 ft above its takeoff point



Figure 7. "En Plein Vol" Over the Highest Alps (1973)



Figure 8. Pole (l) and Nott Inside the Cabin at 46,000 ft (1974)



Figure 9. Night in the Open After the Record Breaking Flight. Balloon retrieval in India proved even worse than expected (1974)

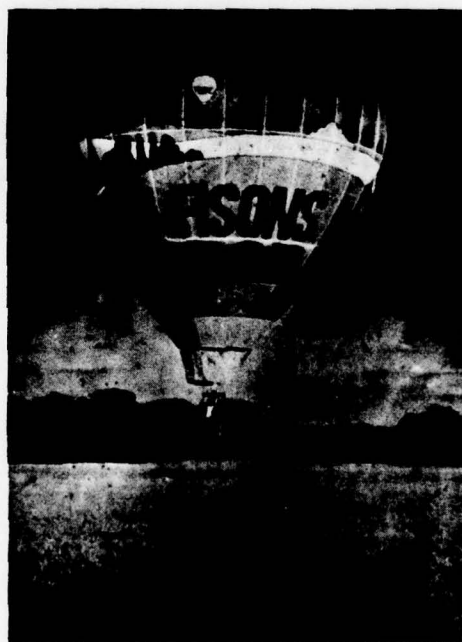


Figure 10. Fisons B25. Operated by the Hot Air Balloon Company, a typical contemporary hot air balloon used for advertising (1977)

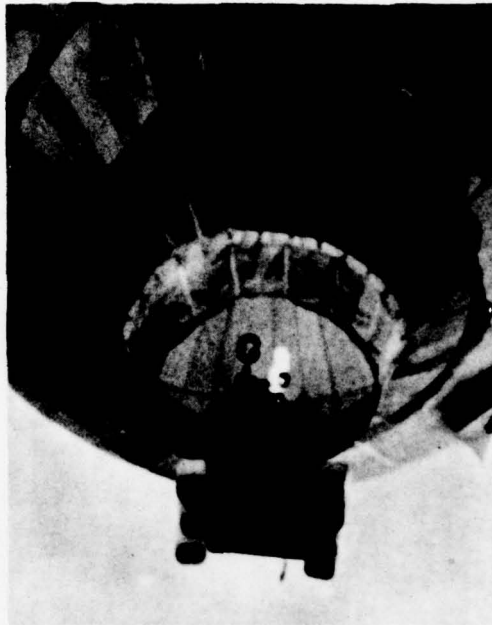


Figure 11. Fisons B25 During a Trial Flight Before Successfully Capturing the World AX6 Endurance Record. Note kerosene fuel and black carbon fibre gondola



Figure 12. Nazca, Peru (1975). Eric Von Daniken (Chariot of the Gods) thinks those runways indicate pre-historic visitations from outer space



Figure 13. "It Flies". Piloted by Nott, Woodman is carried aloft in "Condor"

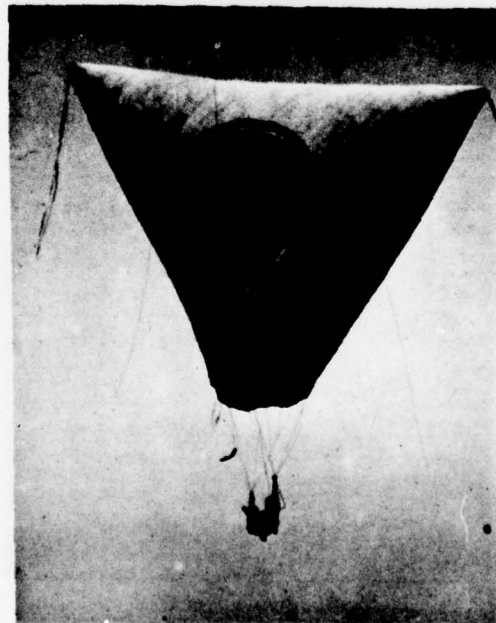


Figure 14. "Condor" in Flight, Built Exclusively From Materials Available in Pre-Inca Peru



Figure 15. Nott Received Royal Aero Club (of UK) Bronze Metal (1977) Becoming the First Pilot to Win Gold, Silver, and Bronze

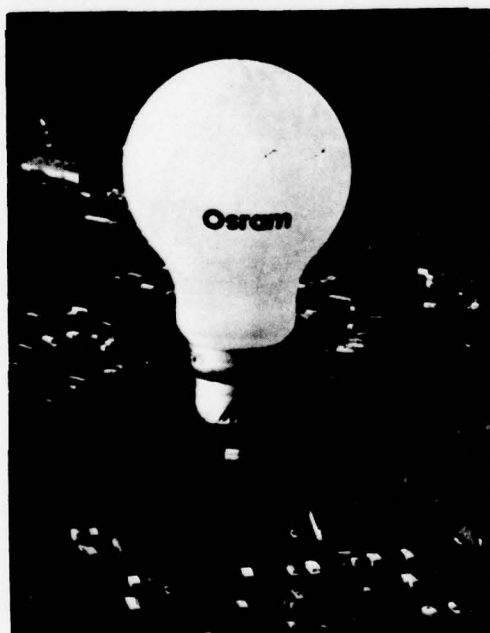


Figure 16. Another Advertising Balloon Operated by the Hot Air Balloon Company



Figure 17. Unsuccessful Take-off From Dunbar in Scotland (1977). Nott and Prescott were standing by to attempt the flight again at the time of presentation

Session III
STRATOSPHERIC MEASUREMENTS

Chairman, Thomas J. Gross
U.S. Govt., Dept. of Energy

Contents

1. Introduction
2. Tri-Sampler
3. Flight Package
4. Flight Profile
5. Diagnostics
6. Summary

Stratospheric, Trace Gas Studies Using

A Balloon-Borne, Cryogenic, Whole Air Sampler

Charles C. Gallagher, Robert V. Pieri,
Charles A. Forsberg and Gerard A. Faucher,
Air Force Geophysics Laboratory,
Hanscom AFB, Massachusetts

ABSTRACT

A liquid helium cooled sampler is designed to capture and freeze one mole, whole air samples at each of three altitude ranges on a single balloon flight. Sampling is accomplished during a descending mode as the balloon package is stepped through the three altitude ranges. The retrieved samples are warmed and then analyzed, immediately, for nitric oxide and nitrogen dioxide content using a chemiluminescent analyzer. Subsequently, concentrations of nitrous oxide and fluorocarbons 11 and 12 are measured on a gas chromatograph. Balloon flights have been conducted at four latitudes from Panama to Alaska and samples have been obtained at altitudes of 12, 15, 18, 20, 25 and 30 km, thus providing gas concentration profiles as a function of altitude and latitude.

1. INTRODUCTION

Various gas species, anthropogenic in origin, are injected into the stratosphere and, subsequently, either directly or through their photochemical products react with and destroy a portion of the ozone layer which protects the earth from harmful solar ultraviolet radiation.

This concerns the Air Force in two ways, first and primarily in the potential effects of exhaust emissions, such as the oxides of nitrogen, from the F15, F16 and other aircraft which operate in the stratosphere. A second concern is the diffusion of chlorofluoromethanes from the troposphere. Such species normally find wide use in electronics and other ground-based Air Force activities, in addition, of course, to the widespread use in the civilian sector.

Our task is to measure the stratospheric composition of several trace gases of interest. Measurements are made as a function of altitude and latitude. The approach is to use a balloon-borne cryogenic sampler to obtain three, one-mole whole air samples per flight at altitudes from 12 to 30 km. The large sample quantities permit extensive analysis of each sample. The retrieved samples are warmed to room temperature and 700-800 mm pressure for analysis on a chemiluminescent analyzer and gas chromatograph.

2. TRI-SAMPLER

Flights commenced in 1975, and samples were obtained alternately with a single chamber cryogenic sampler and by grab-sample techniques. Flights since 1977 have employed tri-samplers. Figure 1 contains a cross-section drawing of a tri-sampler. The unit is of stainless steel construction and is 50 in. in height and 18 in. in diameter. Each of the three sample cylinders is in contact with the same 42 l. of liquid helium. Thermal shielding is provided by a liquid nitrogen chamber and a vacuum region. The air sample tube leading to each cylinder is designed to permit laminar air flow at a rate such that a one-mole sample should be gathered in 60 minutes. Laboratory tests of the completed tubes reveal that the actual sampling time to obtain a one-mole sample averages 65 minutes.

Thus, each intake tube is designed for a specific altitude although tubes can be interchanged. The sampled air exists as a cryofrost on the cylinder wall at a temperature slightly above the 4° K temperature of the liquid helium.

Sampling is initiated by a remotely activated motor-driven valve. The three such systems appear as the top projections in the tri-sampler photo (Fig. 2). Below these are the cylinder pumpout valves joined by bellows tubing to one common pumping port shown at the right. This pump-out system is removed prior to flight. For perspective, a full length photo of the tri-sampler is shown in Fig. 3. The tri-sampler, as shown, including cryogenics, weighs about 380 lbs.

3. FLIGHT PACKAGE

Figure 4 illustrates the flight package. The tri-sampler and associated electronics are mounted on the base of a six foot diameter gondola. The gondola is constructed from welded aluminum tubing and is spherical except for a flat base. This factor, along with the low center of gravity in the flight configuration, results in the gondola coming to rest in an upright position after impact with the ground following flight termination. In this way, no appreciable cryogen loss occurs between impact and recovery. Ballast hoppers are also located in the lower half of the gondola.

Various precautions are taken to prevent sampling of air that could be contaminated by the flight package. Poly dust might be expected to come off the balloon surface, and so a 200 ft. load line is inserted between the parachute and gondola. A special, nitrogen blown, chlorofluoromethane free foam is used for all locations in the gondola where exposed foam is required for cushioning.

The principal precautions, however, are the use of an external sampling tube and sampling only during a descending mode. The inlet tube or duct is 20 ft. in length. Air is drawn up the tube and through the bodies of the valves by a fan mounted beyond the valves. Only a portion of this laminar flow, drawn from the center of the airstream, gets sampled.

Suspended payload weight ranges from about 1100 to 1600 lbs. depending on the amount of ballast carried. A $2.9 \cdot 10^6$ cu. ft. balloon is used for the 30 km flights. The command and TM electronics, the remainder of the flight package and the launch and recovery operations are provided by the Aerospace Instrumentation Division of AFGL.

4. FLIGHT PROFILE

A typical flight profile is illustrated in Fig. 5. A uniform ascent occurs to an altitude about 1 km higher than the ceiling of the first sampling range in order to provide an increment for adjustment to the desired descent rate through valving and ballasting. As previously indicated, sampling during descent greatly reduces the chances of sampling air contaminated by the flight package. The fan is turned on several minutes prior to sampling, and no sampling occurs within 5 minutes subsequent to any required dropping of the glass bead ballast. Two tri-samplers exist. The so-called high altitude unit provides the 30, 25 and 20 km samples. The low altitude unit provides samples from a second flight at 18, 15 and 12 km. The actual altitude increment, per sample, is seen to be 1.8 km.

Fourteen flights were conducted between June 1975 and June 1978, including six tri-sampler flights, and samples have been obtained on every flight. Latitudes studies have ranged from 9° N (Panama) to 64° N (Alaska).

5. DIAGNOSTICS

Following the termination, parachute descent, impact and recovery sequence, the samples are warmed to room temperature and allowed to expand into evacuated stainless steel spheres such that the final pressure is about 700-800 mm. Sphere surfaces are either gold plated or passivated with hexamethyldisilazane (HMDS) to prevent sticking or absorption of trace gas components on the surface. Use of HMDS was initiated by NOAA in their grab sampling program.

Portions of the samples are then analyzed immediately on a Thermo Electron Corp. Model 12A chemiluminescent analyzer for NO and NO₂ content. The remaining portions are then returned to the laboratory for analysis on

a Perkin Elmer Model 3920 gas chromatograph with Ni^{63} detector. Principal measurements to date are of N_2O , CFCl_3 (F11) and CF_2Cl_2 (F12). A 12 ft., 1/8" diameter, 80/100 Porasil C column is used. Initial measurements were made using stainless steel column tubing but with more recent measurements made with nickel tubing to reduce peak tailing.

Results to date will serve as baseline values against which any future changes in composition can be compared. Detailed papers on these results are in preparation; however, from representative data, the predicted upswelling of some trace gas components into the stratosphere in tropical regions and their subsequent gradual diffusion to higher latitudes is borne out by the following. In Figure 6, nitrous oxide 1977 data from New Mexico (33°N) and California (40°N) were not too different and were averaged. Values for Panama are obviously higher at each altitude compared. Those for Alaska are less convincing but lower. The newer Alaska data (June 1978) extends to 30 km and reinforces the conclusions. Similar conclusions are drawn for CF_2Cl_2 as shown in Figure 7. The tri-sampler was incorporated into the system prior to the Panama measurements, but was not used because international air space restrictions prevented sufficient flight times for gathering of all 6 of the desired samples.

6. SUMMARY

In summary, the stratospheric composition of 5 trace species of interest have been measured over a wide range of latitudes and stratosphere altitudes. These will serve as baseline values against which future changes can be compared. Other species of interest will also be investigated from future flights, and sufficient quantities of samples remain from most previous flights to permit investigation of other stable species contained therein.

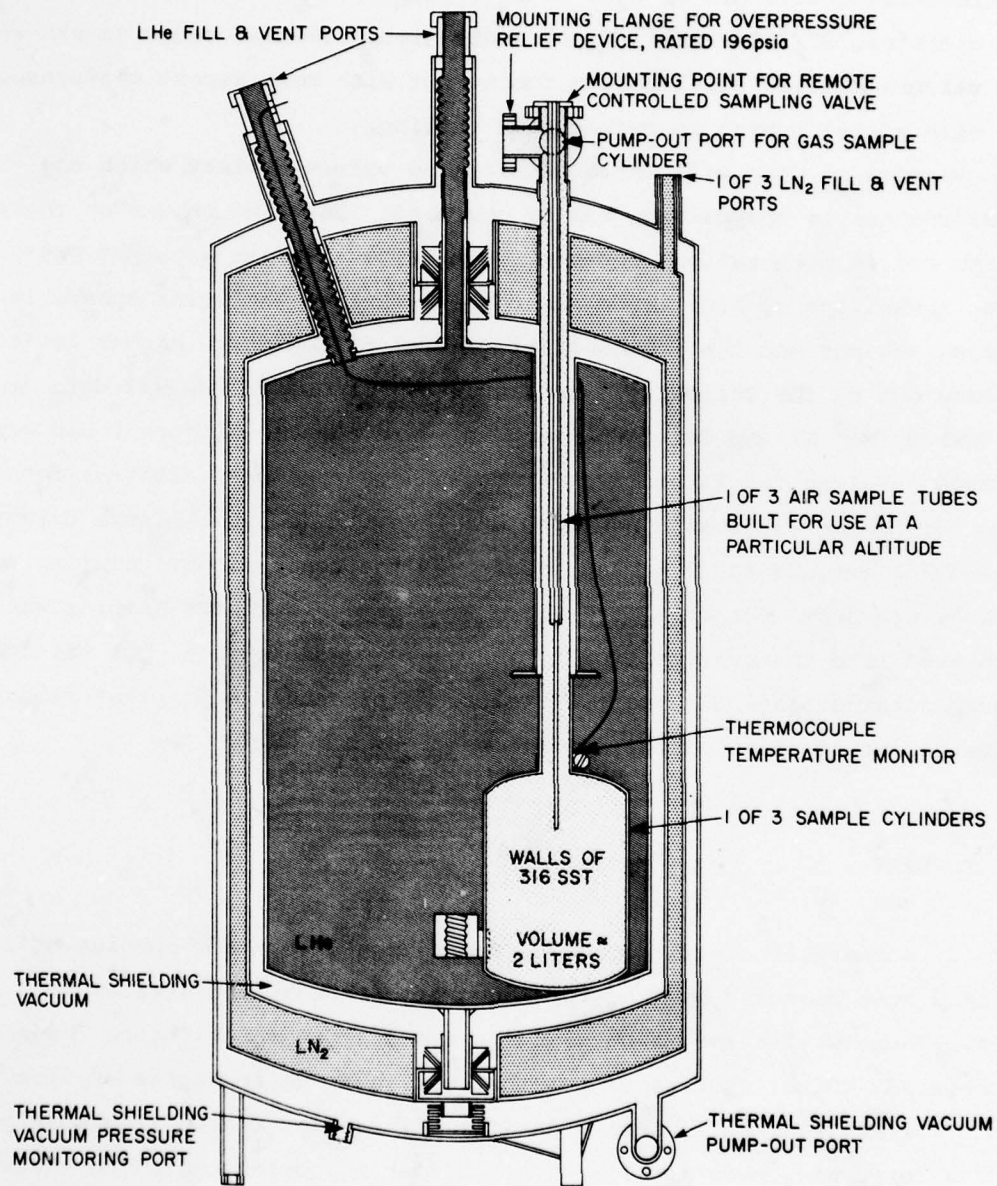


Figure 1. Tri-Sampler Cross Section

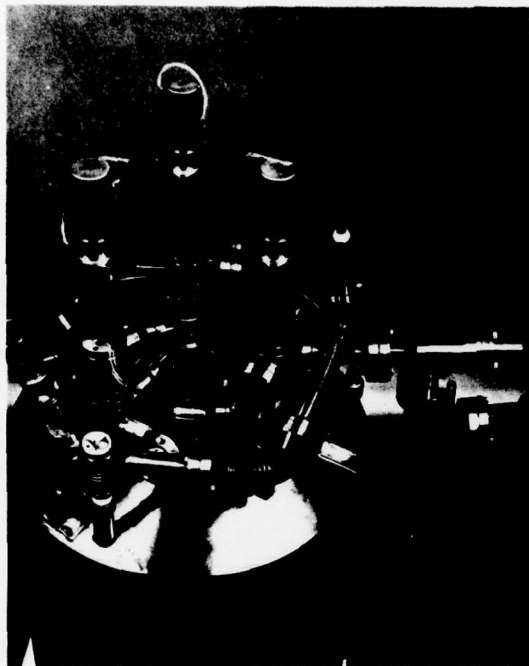


Figure 2. Tri-Sampler Top View

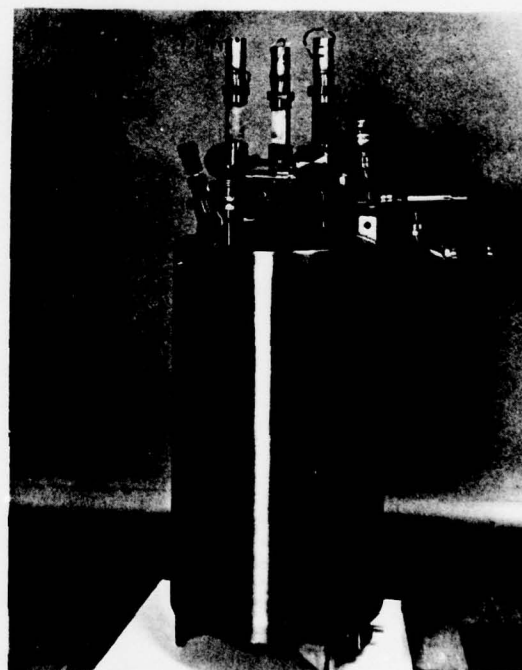


Figure 3. Tri-Sampler Full Length View

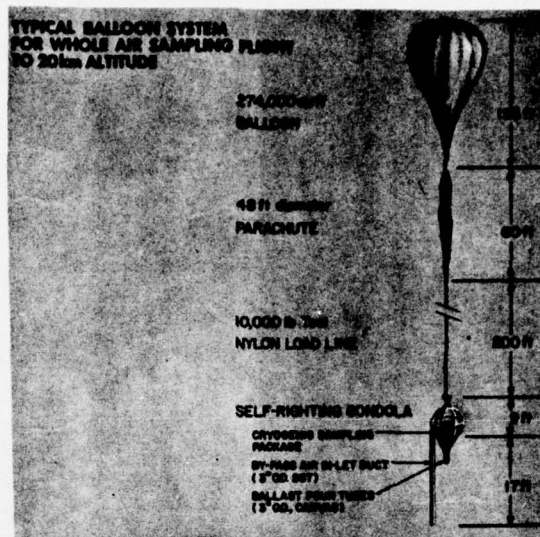


Figure 4. Flight Package

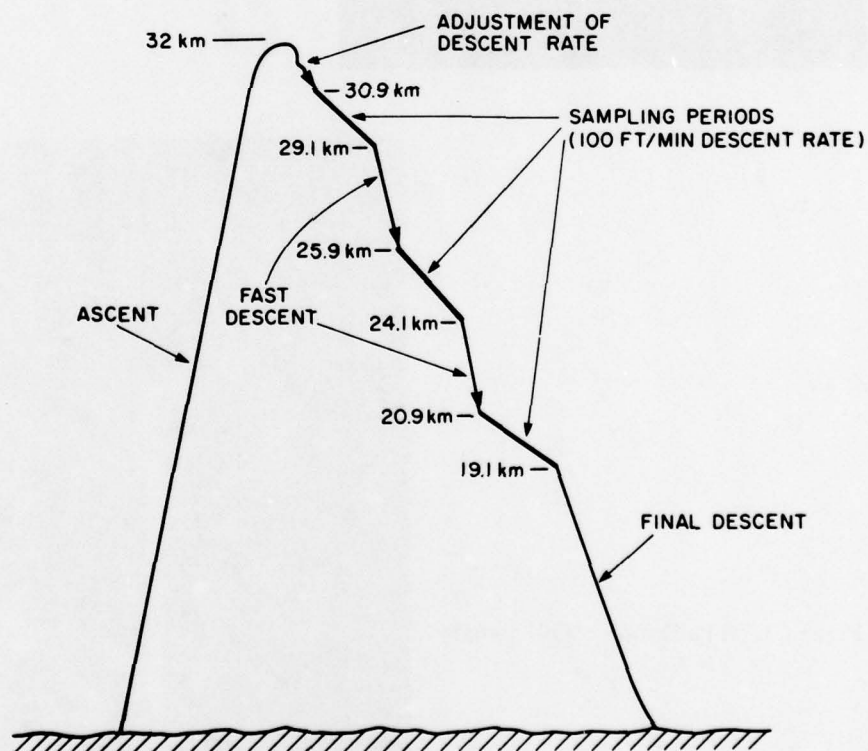


Figure 5. High Altitude Profile

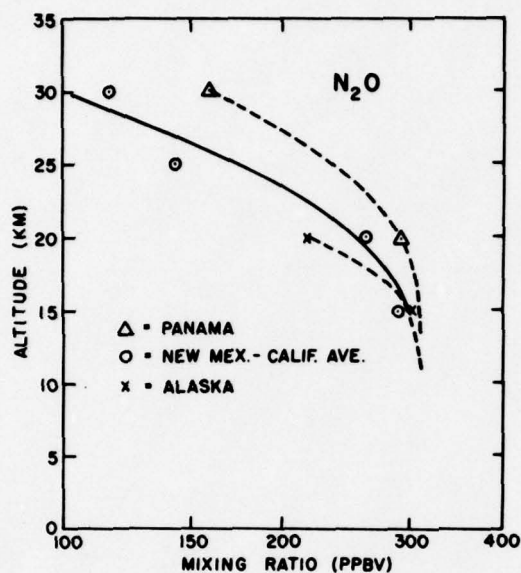
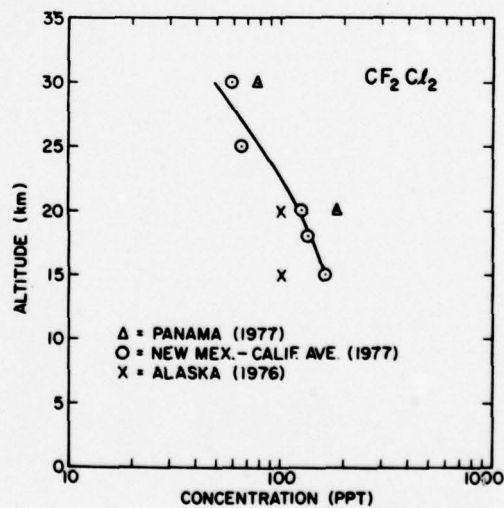


Figure 6. Nitrous Oxide Concentration as a Function of Altitude and Latitude

Figure 7. Chlorofluoromethane 12 Content as a Function of Altitude and Latitude



CASSETTE SAMPLER FOR STRATOSPHERIC AEROSOLS AND VAPORS

B.W. Gandrud

A.L. Lazrus

B.D. Lambdin

P.H. Johnson

L.W. Beaman

National Center for Atmospheric Research*

R.H. Cordella, Jr.**

Air Resources Laboratories, NOAA

ABSTRACT

A cassette sampler capable of gathering 20 samples on a single balloon flight has been designed and tested. Integrated samples over a selected altitude range are obtained during valve down of the balloon.

1. INTRODUCTION

NCAR has been involved over the past few years in obtaining vertical profiles of the concentration of nitric acid vapour, acidic chloride vapour, and aerosols present in the stratosphere. To obtain the samples, balloon flights and equipment were obtained from the former Division of Biology and Medicine of the Atomic Energy Commission. That group is now part of the Department of Energy.

Project Ash Can involves floating a balloon at an altitude and sampling for three to four hours. In order to obtain a vertical profile from 36 km to 21 km, it was necessary to have 5 flights. This was costly and consumptive of man power so it was decided to see whether a sampler could be designed that would allow us to obtain the vertical concentration profiles of the constituent desired with just one flight.

* The National Center for Atmospheric Research is sponsored by the National Science Foundation.

**Employed by the Air Force Geophysics Laboratory until July 31, 1978.

2. THE CASSETTE SAMPLER

A cassette sampler has been constructed that is capable of taking 20 samples on a single flight. The 15.5 cm diameter filters are spaced evenly every 18° in a large drum. The drum is rotated with an electric motor that drives a gear which is meshed with a chain located on the outside rim of the cassette. Indexing of the drum is accomplished through the use of microswitches. Figure 1 shows a cross sectional view of the cassette itself. Upon command, the cassette rotates to a filter and the filter is then lifted into the sampling chamber by an arm which is driven by an electric motor. Once in the sample chamber, a pneumatic seal made of silicon rubber is inflated around the perimeter of the filter. This ensures that all of the air being pumped through the system passes through the filter medium and that the filters stored in the cassette do not come into contact with the sampled air except when they are being sampled. Figure 2 is another view of the sampler which shows more of the sampling train. After a sufficient sample is taken on an individual filter, the seal is deflated and the filter is placed back in the cassette. Another filter is selected and inserted into the sampling stream. Figure 3 shows the inside of the cassette with the filter holders in place.

The filter holders are made of polypropylene. The filters are held in place between stainless steel screens. The space where the filters are held between the screens is adjustable so that various thicknesses of filter or absorbing medium can be used.

3. THE PUMP

Air is drawn through the filter medium with an air ejector pump that is used by the AEC in the Ash Can program (Wood, 1964). The pump works

by an axial ejection of high pressure nitrogen gas into the air stream. Figure 4. The nitrogen imparts momentum to the surrounding molecules and a flow is obtained. It is a nice system for stratospheric work because few moving parts and very little battery power are required. The high pressure nitrogen, 200 atmospheres, required to run the pump during the sampling portion of the flight is carried in a 63.5 cm diameter titanium sphere.

4. THE FLOWMETER

The flow through the filters is determined with a propeller-type anemometer developed for stratospheric use in the Ash Can program (Wood, 1965). Figure 5 is a schematic of the flowmeter. Figure 6 shows that the revolutions/second of the blades is a linear function of the volume flow rate. Experiments with the air at lower temperatures show that the curves are valid regardless of the temperature, provided that the bearings are virtually frictionless. The volumetric flow versus the rps response of the flowmeter can be changed to accommodate individual needs by changing the angle of the pitch of the anemometer blades. The difference in response between 60° and 30° (measured with respect to the plane of rotation of the blades where 90° would be parallel to the air flow) is also shown in figure 6. The temperature of the air being drawn through the flowmeter is measured with a thermistor, Fenwal UUB31J1.

A thermal anemometer, Thermal System, Inc., model 1610, was tried as a flowmeter but its use has not been continued. This temperature-compensated thermal anemometer is responsive to changes in ρv , density x velocity. It functioned well at 15 and 27 km, but at 36 km changes in ρv had no effect on the voltage output.

5. SAMPLER CONTROL AND DATA ACQUISITION

The sampler has four independent control functions (seals, pump, load mechanism and drum step). A laboratory test set or a relatively large balloon-borne control system could easily accommodate these requirements. However, the initial test flight was under the control of the second generation instrumentation developed for Project Ash Can (Cordella, March 1978) which had only two control lines available. To accommodate the sampler's four functions, a fairly straightforward cyclical sequencer was designed to accept two input signals and provide the proper output signals. Its alternating input interlock design precluded the possibility of advancing the drum with a filter in the sampling chamber. This sequencer was incorporated in the sampler and enabled it to accept two input controls while leaving the four original input ports directly available for use in the laboratory or with a different flight system.

Information directly supporting the sampling mission is contained in the altitude, flow rate, and temperature data. The accuracy of the altitude is a logarithmic function of altitude. The poorest accuracy, ± 167 m, (± 505 ft.) occurs at 40 km (120 k ft). Its resolution varies from 10 to 33 meters (Cordella, January 1978). The flow data are accurate to $\pm 2\%$ with $\frac{1}{4}$ rps resolution. Worse case temperature accuracy is $\pm 2^{\circ}\text{C}$ at -80°C ; its resolution is 0.1°C .

6. TEST FLIGHTS

Figures 7 and 8 show the cassette sampler being readied for the initial test flight, and on the flight line before launch at Holloman AFB, New Mexico, respectively. The cassette sampler has now been flown on three occasions.

Two flights have been made from Holloman AFB and one from Palestine, Texas. Although some problems have occurred on all flights, the sampler has proven itself a success.

A typical flight involves an ascent to float altitude, around 36 km. Sampling starts during float and continues during descent. A valved descent is used with a rate varying from 30 m/min. to 152 m/min. depending on the altitude of the balloon, the pumping rate, and the anticipated concentration of the constituent being sought. Selection of filters to be sampled is controlled via a telemetry link to the ground.

Due to problems with the flow data, the concentration profile obtained for nitric acid vapor on the Palestine flight is not of the accuracy we desired but it is in agreement with previously published values (Lazrus, A.L., et al, 1972; Lazrus and Gandrud, 1974). The concentration varies from 0.3 ppbv (parts per billion by volume) in the 35-33 km altitude range to a maximum of 4.7 ppbv at the 23-20 km range. These values for nitric acid vapor are accurate with $\pm 50\%$.

7. CONCLUSION

The cassette sampler has proven to be a success even though minor difficulties have arisen. These problems have been solved and the sampler is scheduled for 3-4 flights during the remainder of the year. Two flights from Palestine will provide ground truth information on nitric acid vapor for the Nimbus G satellite to be launched in September. Flights from Holloman will be devoted to the measurement of aerosol and acidic chloride vapor concentration.

ACKNOWLEDGMENTS

Appreciation is extended to the following for their contributions: T. Gross of DOE for providing test flights; T. Danaher of AFGL for providing access to a high altitude test chamber; John Ground and the launch crews at Holloman and Palestine for their efforts during launch and flight; the NCAR machine shop for its labors during fabrication; T. Ashenfelter, formerly of NOAA but now retired, for his experience, knowledge, and wit.

REFERENCES

- Cordella, Jr., R.H., (January 1978) An Autoranging Balloon Altimeter: A Single Pressure Transducer Monitors Altitude from 0 to 44 Kilometers with 30 Meters Resolution; AFGL-TR-78-0023 Instrumentation Papers No. 262.
- Cordella, Jr., R.H., (March 1978) About the Development of a Second Generation Atmospheric Sampler Control and Data System: SCADS-2. AFGL-TR-78-0065.
- Lazrus, A.L., and Gandrud, B.W. (1974) Distribution of Stratospheric Nitric Acid Vapor, JAS, 31 (No. 4): 1102-1108.
- Lazrus, A.L., Gandrud, B., and Cadle, R.D. (1972) Nitric Acid Vapor in the Stratosphere, JAM 11 (No. 2): 389-392.
- Wood, R.C. (1964) Air Ejector Particle Sampler, A Progress Report, Report No. C00-401-105, Applied Science Division of Litton Systems, Inc.
- Wood, R.C., Graf, L.R., and Nelson, L.V. (1965) Development and Calibration of the PR-3 Flowmeter, Report No. 00-401-118, Applied Science Division of Litton Systems, Inc.

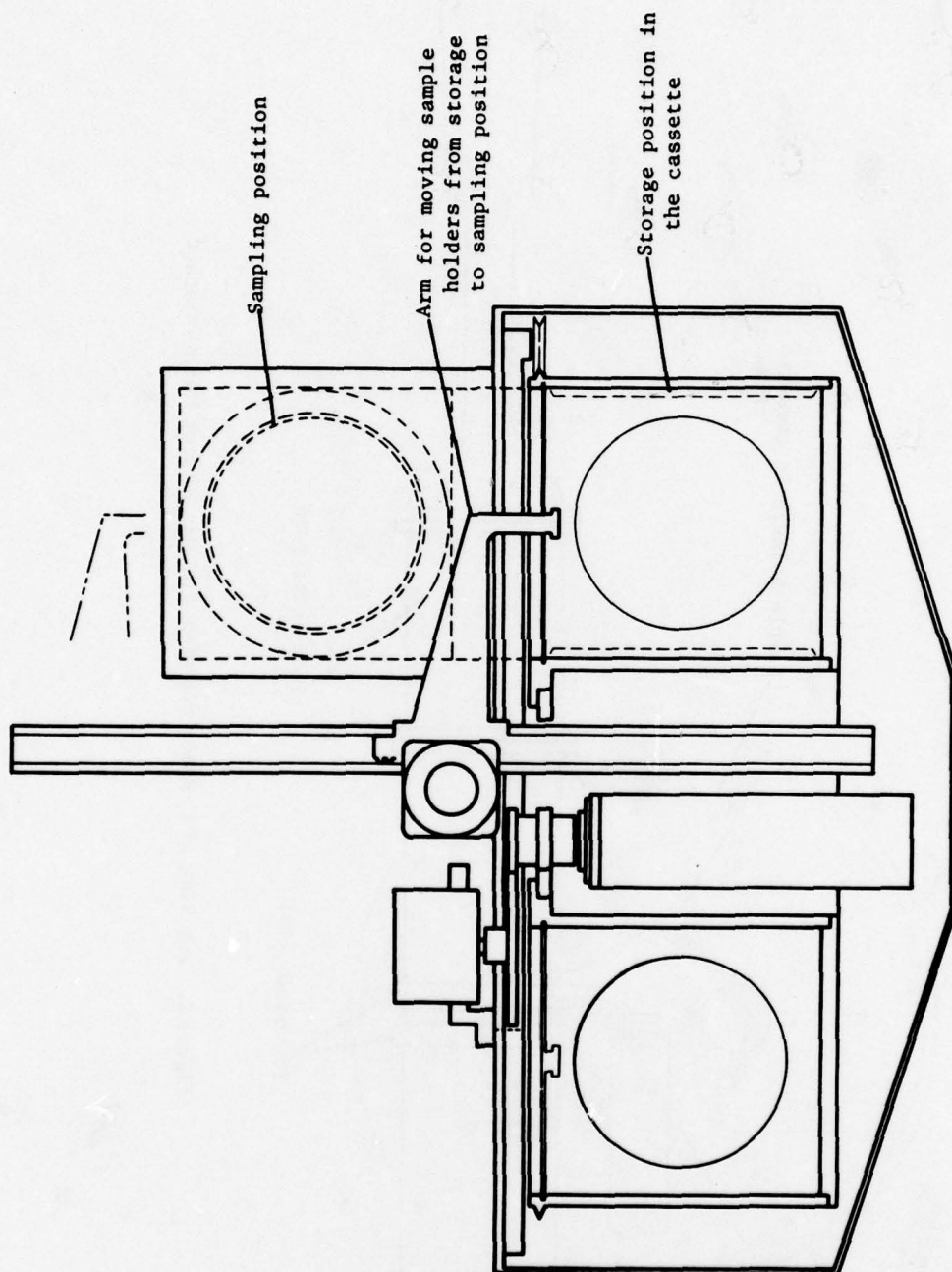


Figure 1. Cross Sectional View of Cassette Sampler

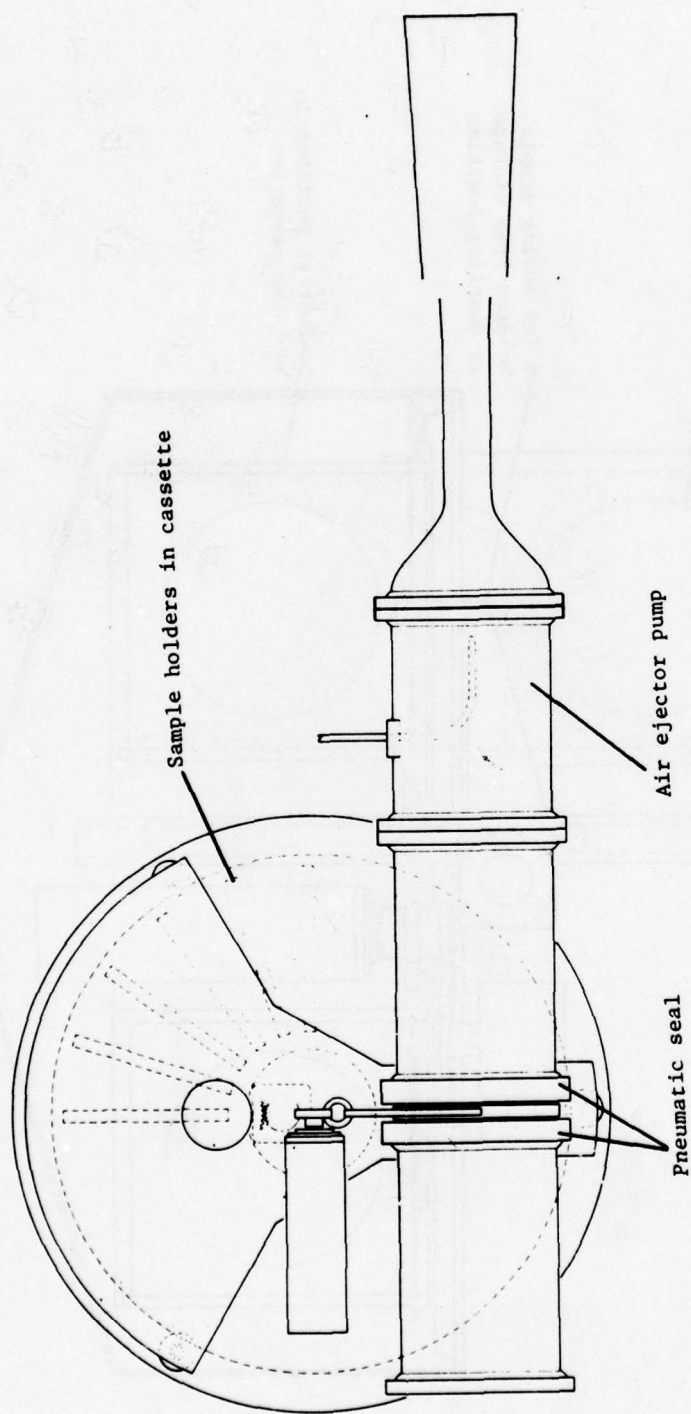


Figure 2. Top View of Cassette Sampler With Air Ejector Pump Attached

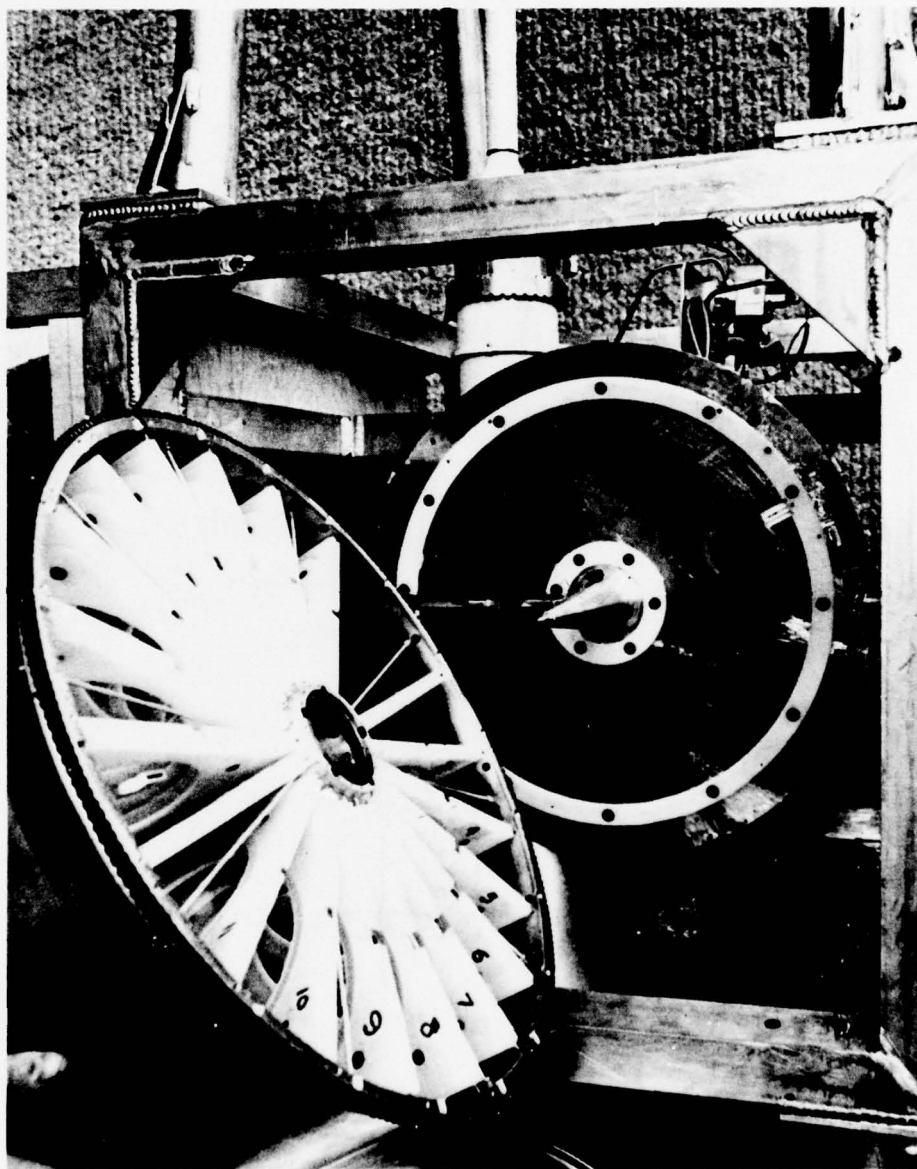


Figure 3. Cassette With Sample Holders

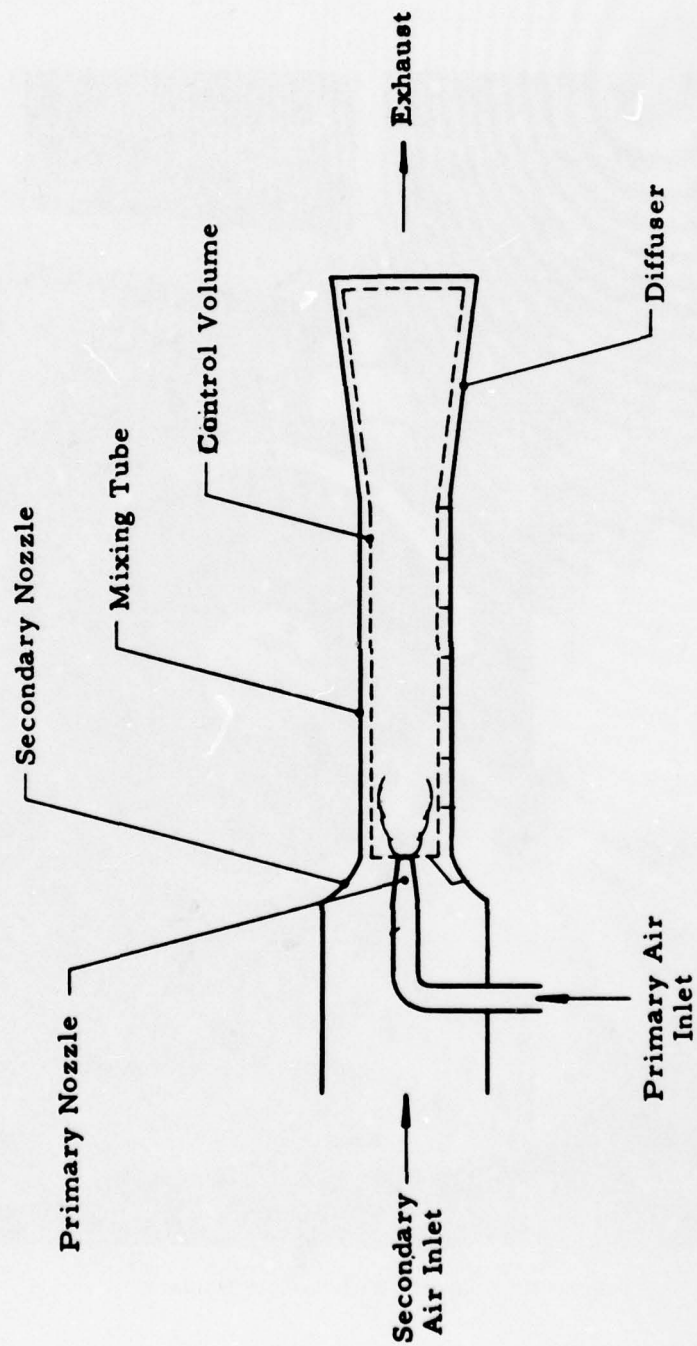


Figure 4. Schematic Diagram of a Constant Area Mixing Air Ejector Adapted From Figure 1. in Wood, 1964

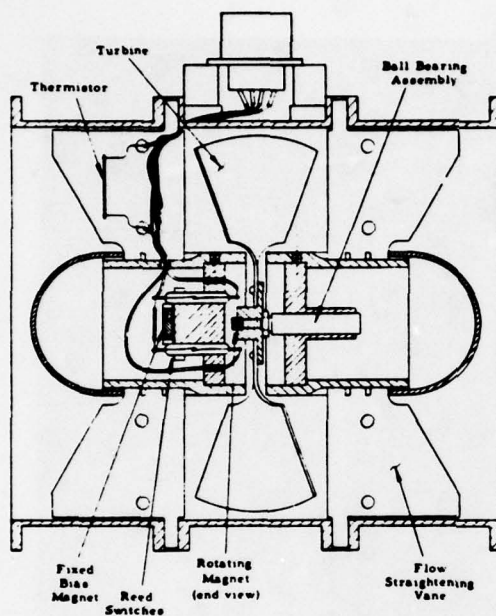
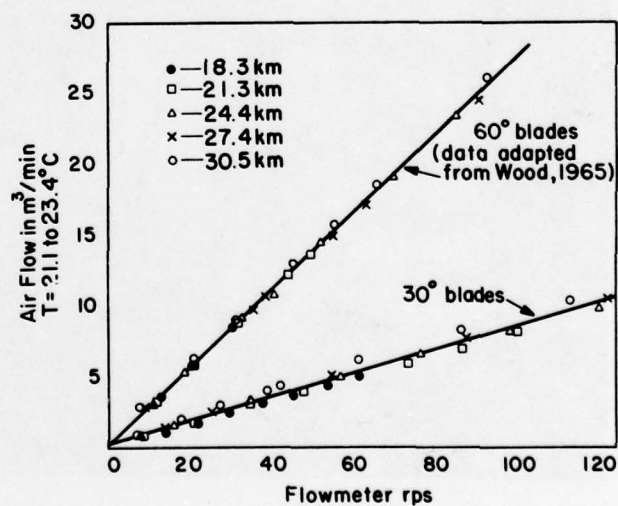


Figure 5. Sectional View of PR-3 Flow Sensor Taken From Figure 4 in Wood, 1965

Figure 6. Flowmeter Output as a Function of Volume Flow (18.3 to 30.5 km altitude)



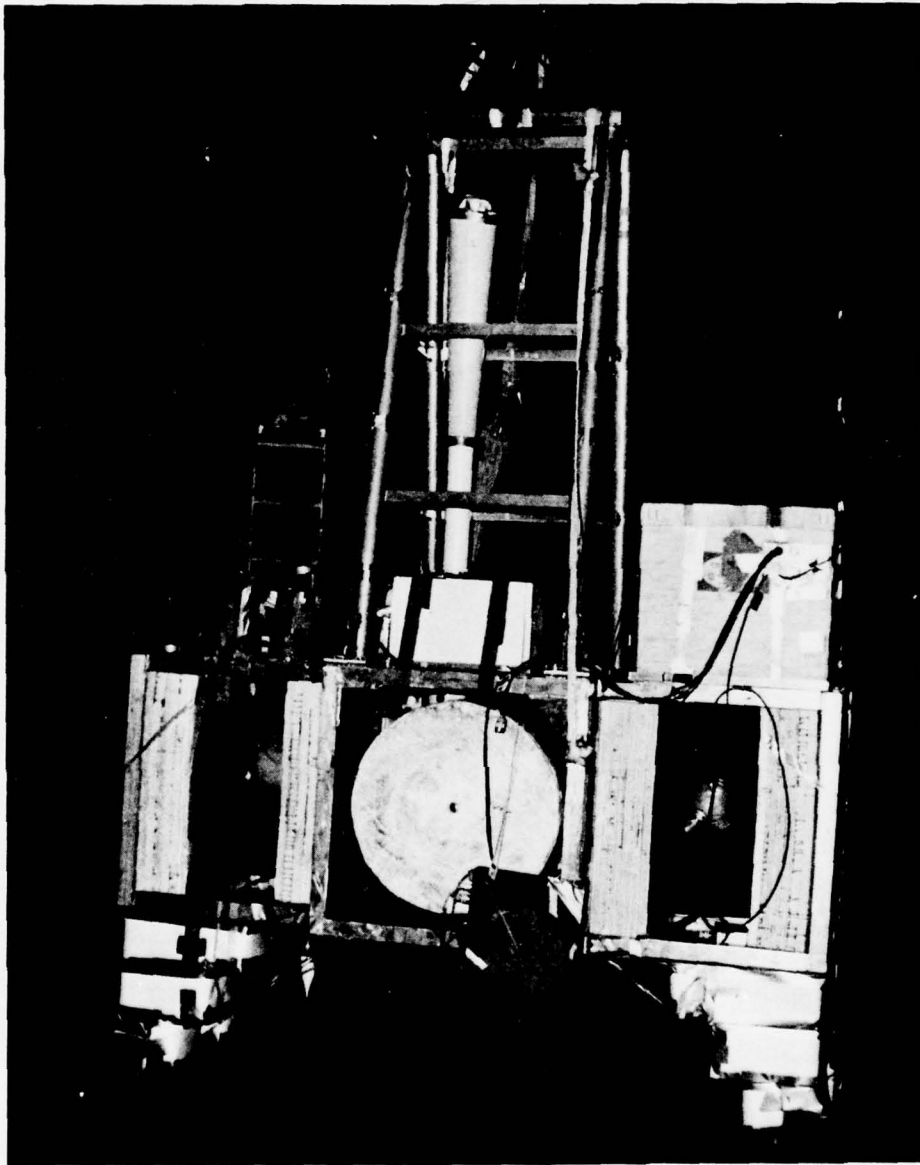


Figure 7. Assembled Sampler for Balloon Flight

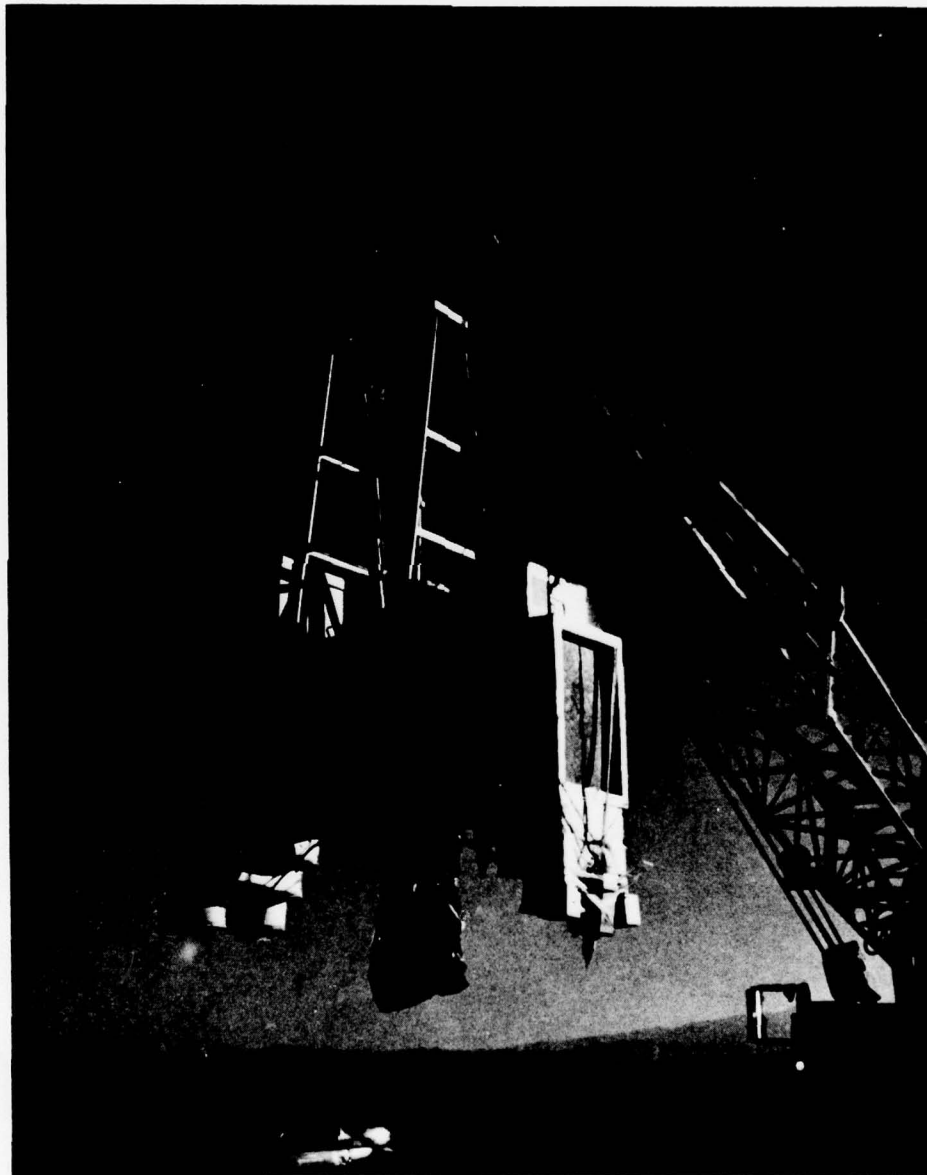


Figure 8. Cassette Sampler on Flight Line Before Launch

Contents

1. Introduction
2. Electrical Conductivity Data
3. Stratospheric Electrical Conductivity
4. A Future Experiment
5. Conclusions

STRATOSPHERIC ELECTRICAL CONDUCTIVITY MEASUREMENTS BY BALLOON-BORNE BLUNT PROBES

J. D. Mitchell
Electrical Engineering Department
The University of Texas at El Paso
El Paso, Texas 79968

L. C. Hale and C. L. Croskey
Ionosphere Research Laboratory
The Pennsylvania State University
University Park, Pennsylvania 16802

Abstract

Blunt probes for measuring electrical conductivity were flown with six of the STRATCOM balloon experiments. The conductivity data obtained from different probe configurations indicated that it is preferable to position the probe at some nominal distance from the main package, thus reducing the effects other instruments might have on the collection of charged particles. To supplement the balloon results, rocket-launched, parachute-borne blunt probe experiments were conducted during four of the balloon flights. The agreement between the data obtained from the two different launch systems was quite good. Useful information about stratospheric electrical conductivity and its variations with respect to altitude and temperature and during sunrise was obtained from these scientific balloon experiments.

1. INTRODUCTION

The blunt probe is a two-electrode instrument for measuring electrical conductivity [Hale (1967); Hale, Hoult and Baker (1968)]. Although originally designed for flight with rocket systems, the instrument was recently flown on balloon platforms as part of an integrated experiment package to measure stratospheric parameters. In particular, a blunt probe was flown on six of the STRATCOM (Stratospheric Composition) series of balloon experiments. These scientific balloon experiments measured various neutral constituents, solar fluxes and meteorological and ionization parameters in the stratosphere [Ballard, Izquierdo, McDonald and Whitacre (1976)].

A picture of the probe configuration used on the more recent flights (STRATCOM V to VIII) is shown in Figure 1. The blunt probe is located on the right with its collector directed vertically downward. Also shown in the figure is a Gerdien condenser (on the left) for measuring electrical conductivity and a krypton discharge lamp (positioned between the two probes). The lamp radiated at 1236 \AA and was used on ground command as an ionization source for the probes. This particular instrument configuration was placed approximately one meter from the rest of the scientific package, thus reducing the effects other instruments might have on the probe's collection of charged particles.

For the STRATCOM III and IV flights, a blunt probe was positioned below the instrument package and in relatively close proximity to it, resulting in noticed wake effects on the probe during ascent. A hydrogen discharge lamp (1216 \AA) was included as an ionization source with the blunt probe.

The launch parameters for the particular STRATCOM balloon flights on which a blunt probe was flown are listed in Table 1. The STRATCOM III flight concentrated on the measurement of upper stratospheric parameters, while the STRATCOM IV and V flights were limited to the lower stratosphere. The measurement region for the most recent three experiments was primarily in the middle stratosphere. All of the STRATCOM balloon flights were launched from Holloman Air Force Base, New Mexico with the exception of STRATCOM IV, which was launched from Palestine, Texas.

Table 1. Parameters for the STRATCOM Balloon Flights

Balloon Experiment	Launch Date	Launch Time	Flight Period	Peak Altitude
STRATCOM III	Sept. 18, 1972	0304 MST	6 hours	48 km
STRATCOM IV	Oct. 20, 1973	0348 CST	15 hours	28 km
STRATCOM V	May 22, 1974	0122 MST	24 hours	28 km
STRATCOM VI	Sept. 23, 1975	2257 MST	34 hours	39 km
STRATCOM VII	Sept. 28, 1976	0729 MST	27 hours	39 km
STRATCOM VIII	Sept. 29, 1977	0607 MST	31 hours	41 km

2. ELECTRICAL CONDUCTIVITY DATA

Stratospheric electrical conductivity data from the STRATCOM III, V, VI and VII experiments are shown in Figures 2, 3, 4 and 5, respectively. For the STRATCOM III and V data, the plus and minus signs represent measured positive and negative conductivity values, respectively. The dots in Figure 3 indicate positive and negative conductivity measurements which are comparable in value. Straight line segments connect the time-averaged conductivity values. The balloon's altitude is shown by the upper curve in these figures.

The additional notation in Figure 2 (e.g., "0-2" at 0439 MST) indicates the number of independent conductivity measurements observed to be negligible in value. These particular measurements occurred only during the balloon's ascent and are thought to demonstrate the wake effects of the balloon package on the probe's collection of ions. The nonzero conductivity measurements during ascent correspond to periods during or after which the hydrogen discharge ionization lamp was operating. In Figure 3, the conductivity values measured above 5×10^{-14} mho cm^{-1} correspond to ionization resulting from a krypton discharge lamp.

Figure 4 shows time-averaged values for positive and negative electrical conductivity connected by straight line segments, while in Figure 5 the data points represent five-minute, time-averaged values for electrical conductivity. The data in both of these figures were obtained for periods when the krypton discharge ionization lamp was turned off. The upper curve shows the balloon's altitude as a function of time.

Rocket-launched, parachute-borne blunt probe experiments were conducted from nearby White Sands Missile Range, New Mexico in conjunction with the STRATCOM V to VIII balloon flights. These particular experiments provided information about the altitude structure of electrical conductivity, thus supplementing the balloon conductivity data. Conductivity data obtained in conjunction with the STRATCOM VII balloon flight are shown in Figure 6. In this figure, the plus and minus signs represent positive and negative conductivity measurements, respectively, and the dots indicate measurements for which the positive and negative conductivity values are comparable.

3. STRATOSPHERIC ELECTRICAL CONDUCTIVITY

3.1 ALTITUDE DEPENDENCE

Electrical conductivity in the stratosphere is observed to decrease in value with decreasing height (see Figures 2 to 6), which is largely attributed to the altitude dependence of ion mobility. This is further demonstrated in Figure 7

where the positive conductivity data obtained during the slow descent phase of the STRATCOM VII flight (1100 to 1800 MST) are plotted with the corresponding positive conductivity measurements from the rocket experiment (launched at 1230 MST). (The descent phase of the balloon flight is preferable from a measurement standpoint since the air flow is directed against the probe's downward-oriented collector.) In the region of overlap, very good agreement is observed between the data obtained from the two different launch systems. The altitude dependence for positive conductivity in this region is approximately inversely proportional to that for neutral number density. This may be explained with a simple lumped-parameter ion chemistry model by a three-body, ion-ion loss process [Mitchell and Hale (1973)].

It should be noted that anomalous effects were observed during the ascent phases of some of the flights, presumably associated with the probe's flow geometry. For example, the wake effects on the STRATCOM III blunt probe, which was positioned just below the instrument package, resulted in negligible conductivity measurements during ascent except when a hydrogen discharge lamp was operating. Also, for the STRATCOM VI flight, the negative conductivity values were typically a factor of 2 to 3 larger than the corresponding positive conductivity values during ascent and when the balloon was floating. The negative-to-positive conductivity ratio reduced to a more expected range of values (1.3 to 1.5) during descent.

3.2 TEMPERATURE DEPENDENCE

Variations in the time-averaged positive conductivity values at float altitude in Figures 2 and 3 generally correspond to changes in air temperature, also measured by the balloon's instrument package. The temperature dependence of positive conductivity is thought to at least partly reflect the dependence of ion mobility on temperature, possibly associated with ion clustering processes in the stratosphere [Chesworth and Hale (1974)].

A positive conductivity temperature coefficient of approximately 25%/°K was deduced from the STRATCOM III float altitude data ($Z = 48$ km), while the temperature coefficient for the STRATCOM V float altitude data ($Z = 28$ km) was in the range of 1 to 2%/°K. This latter value is consistent with observations from midday rocket conductivity data [Cipriano, Hale and Mitchell (1974)]. It also is expected that the temperature coefficient for positive conductivity would be larger at 48 km; however, the balloon value is approximately six times larger than the corresponding value deduced from rocket experiments. If the relatively smaller STRATCOM III positive conductivity values at float altitude do reflect the presence of generally less mobile ions (possibly caused by clustering with outgassed water vapor from the balloon package), it would appear that the ion mobilities of these species are even more temperature dependent than for those ions collected by the rocket instruments.

3.3 SUNRISE VARIABILITY

Enhancements in positive conductivity have been observed above 30 km from recent midlatitude rocket experiments flown during sunrise, with the largest build-up (at least an order of magnitude) occurring between 45 and 50 km [Mitchell, Sagar and Olsen (1977)]. Corresponding increases in ion mobility during this period suggest the presence of an early morning photodissociation process resulting in the formation of lighter, more mobile ions.

A similar observation is made from the STRATCOM VI conductivity data, where a build-up is observed between 0630 and 0800 MST at a float altitude of 39 km. Unfortunately, photoemission from the collector of the STRATCOM III probe and the relatively low altitudes (below 30 km) of the other balloon flights at sunrise resulted in no further observation of this particular phenomenon.

3.4 IONIZATION LAMP EFFECTS

A hydrogen discharge lamp (1216 Å) flown with the STRATCOM III and IV experiments and a krypton discharge lamp (1236 Å) with the STRATCOM V to VIII experiments provided an additional source of ionization which could be detected by the blunt probe. The lamp's conductivity effects were shown in the data of Figures 2 and 3, but were not included in Figures 4 and 5. In general, enhancements in both positive and negative conductivity were observed when the lamp was operating, with the increased negative conductivity values being typically larger than the respective positive conductivity values. The lamp's ionization effects in the stratosphere will be further investigated, as described in the following section.

4. A FUTURE EXPERIMENT

It has been observed that ionizing radiation from krypton discharge lamps in the stratosphere, where such radiation does not normally penetrate, creates much more ionization than predicted by models which include only oxides of nitrogen as ionizable constituents. A payload is being prepared which uses lamps of several different wavelengths to identify the ionization potential and electron affinity thresholds of these species (see Figure 8). A ring of lamps will flash in sequence, with a blunt collector used to measure the relative increases in charged particle concentration caused by the different lamps. The first payload will use hydrogen, krypton and xenon discharge lamps, and also three incandescent visible lamps. The hydrogen and krypton lamps are both capable of ionizing oxides of nitrogen, but appear to produce inexplicably different effects on previous nonsimultaneous flights. The xenon lamp will produce somewhat longer wavelength radiation and the visible lamps will probably only ionize or detach electrons from aerosol particles.

5. CONCLUSIONS

In summary, blunt probes were successfully flown on six of the STRATCOM series of scientific balloon experiments. The instrument measured stratospheric electrical conductivity and its associated variability with altitude and temperature and during sunrise. Good agreement was observed between the balloon data and measurements from corresponding rocket experiments. Finally, stratospheric ionization effects associated with ultraviolet lamps were studied using balloon-borne blunt probes, and further experiments of this kind are planned for the near future.

Acknowledgments

The authors gratefully acknowledge Mr. Harold N. Ballard of the Atmospheric Sciences Laboratory at White Sands Missile Range and Mr. Miguel Izquierdo of the Electrical Engineering Department of The University of Texas at El Paso, who contributed much to the STRATCOM program of balloon experiments. The assistance of Mr. K. J. Ho in reducing the data is also very much appreciated. Engineering and launch support were provided by personnel of The University of Texas at El Paso, Atmospheric Sciences Laboratory, Sandia Laboratories and Air Force Geophysics Laboratory.

This research was supported by the Atmospheric Sciences Laboratory under Contract No. DAAD07-74-C-0263 and by the U. S. Army Research Office under Grant No. DAHC04-75-G-0031.

References

- Ballard, H. N., Izquierdo, M., McDonald, C., and Whitacre, J. (1976) Temperature measurements in the stratosphere from balloon-borne instrument platforms, 1968-1975, Electronics Command Tech. Rep. No. ECOM-5808.
- Chesworth, E. T., and Hale, L. C. (1974) Ice particulates in the mesosphere, Geophys. Res. Lett. 1 (No. 8): 347-350.
- Cipriano, J. P., Hale, L. C., and Mitchell, J. D. (1974) Relations among low ionosphere parameters and A3 radio wave absorption, J. Geophys. Res. 79 (No. 15): 2260-2265.
- Hale, L. C. (1967) Parameters of the low ionosphere at night deduced from parachute borne blunt probe measurements, Space Res. VII: 140-151.
- Hale, L. C., Hault, D. P., and Baker, D. C. (1968) A summary of blunt probe theory and experimental results, Space Res. VII: 320-331.
- Mitchell, J. D., and Hale, L. C. (1973) Observations of the lowest ionosphere, Space Res. XIII: 471-476.
- Mitchell, J. D., Sagar, R. S., and Olsen, R. O. (1977) Positive ions in the middle atmosphere during sunrise conditions, Space Res. XVII: 199-204.

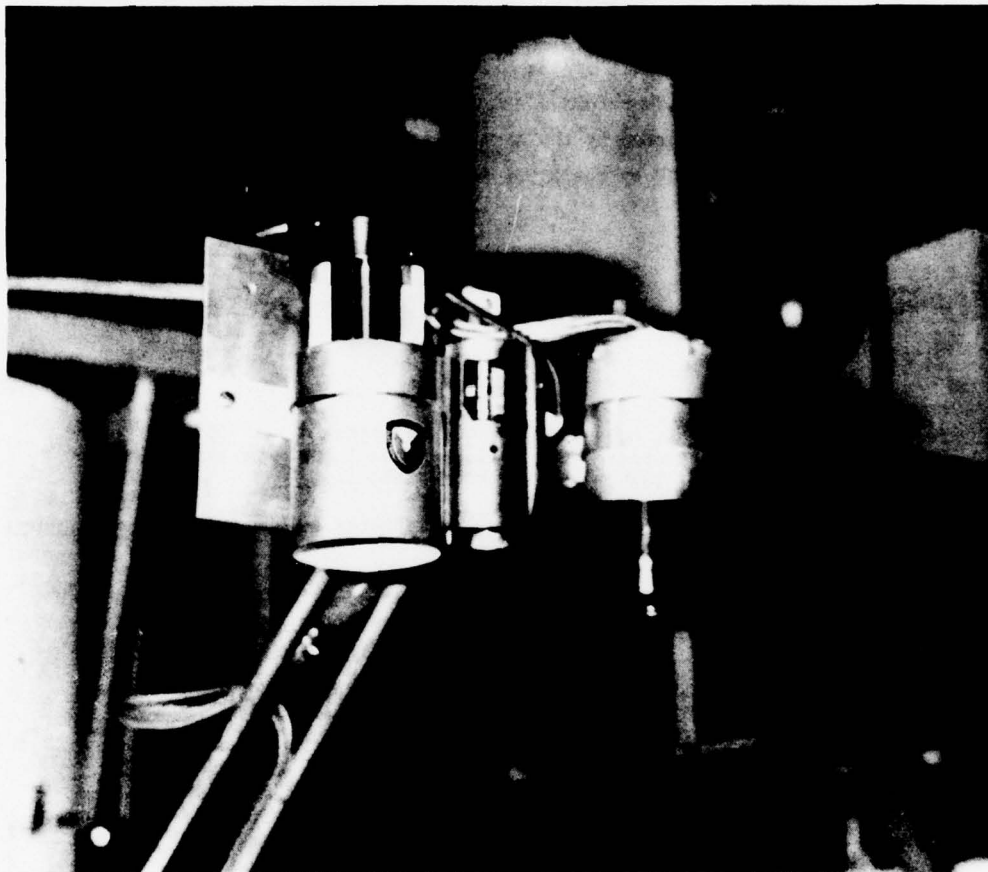


Figure 1. Blunt Probe Instrument Configuration for the STRATCOM V to VIII Balloon Flights

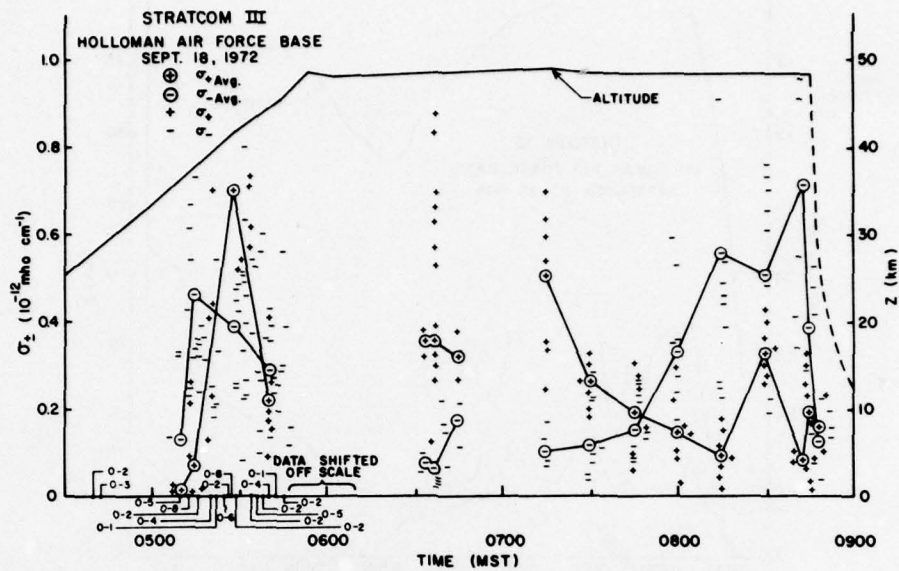


Figure 2. STRATCOM III Electrical Conductivity Data

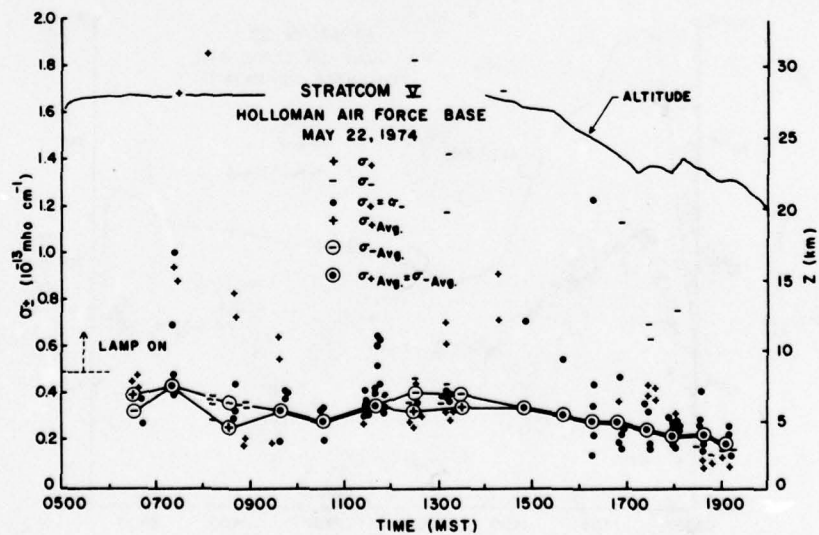


Figure 3. STRATCOM V Electrical Conductivity Data

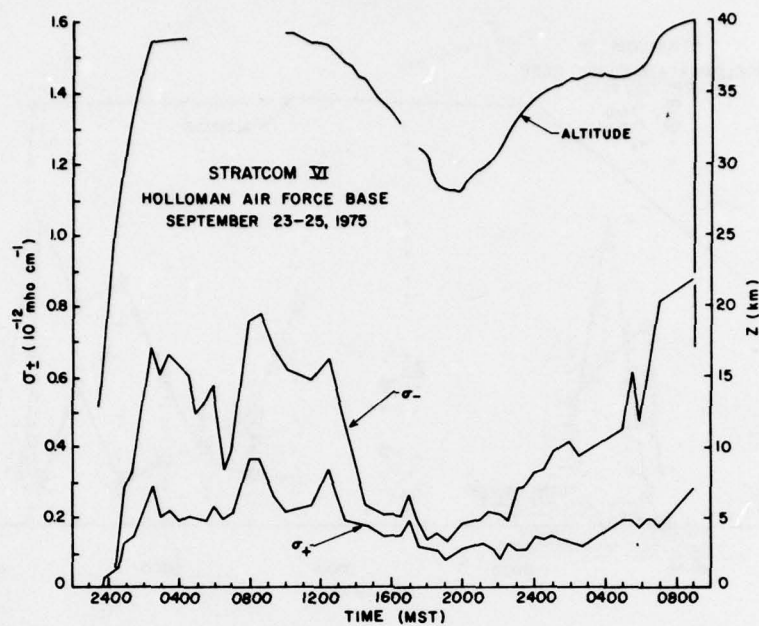


Figure 4. STRATCOM VI Electrical Conductivity Data

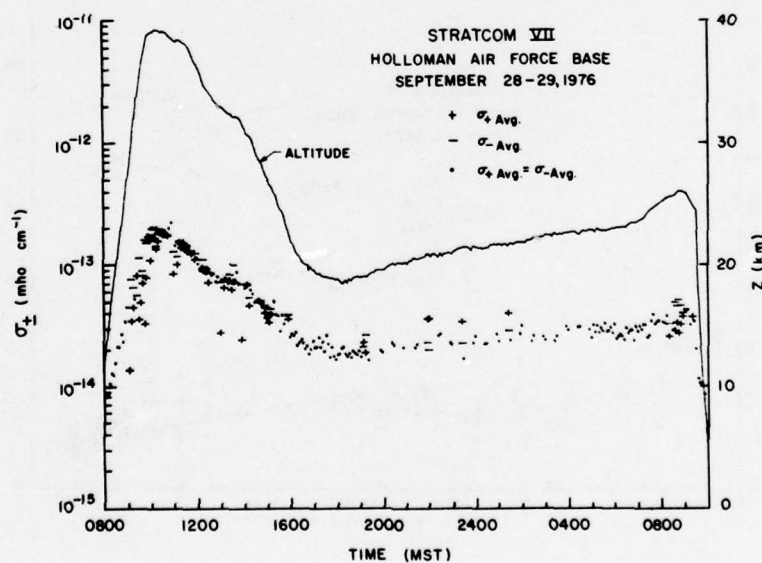


Figure 5. STRATCOM VII Electrical Conductivity Data

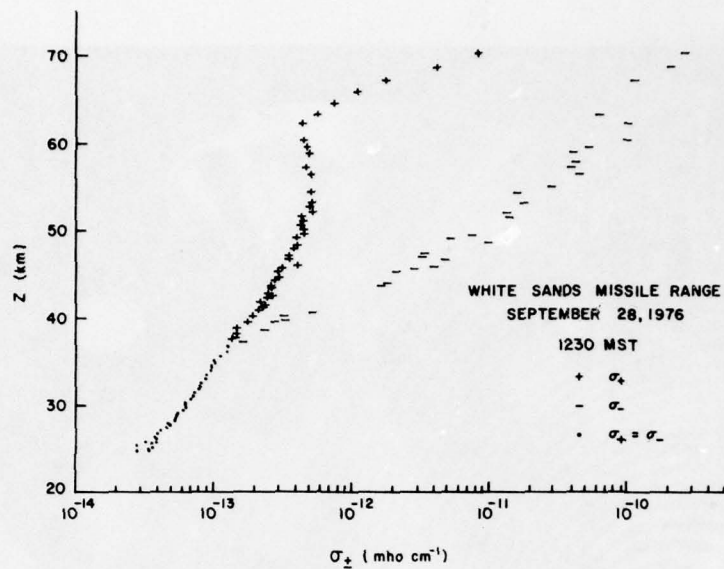


Figure 6. Rocket-Launched, Parachute-Borne Blunt Probe Electrical Conductivity Data_a

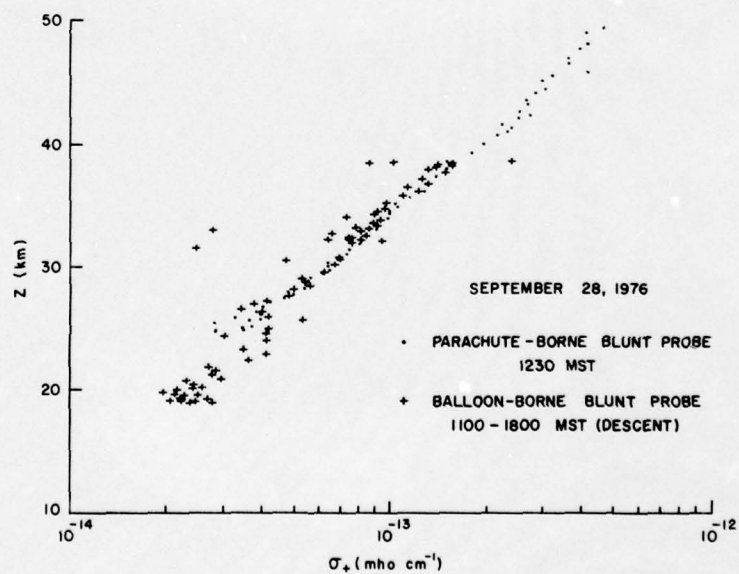


Figure 7. Balloon and Parachute-Borne Blunt Probe Electrical Conductivity Data

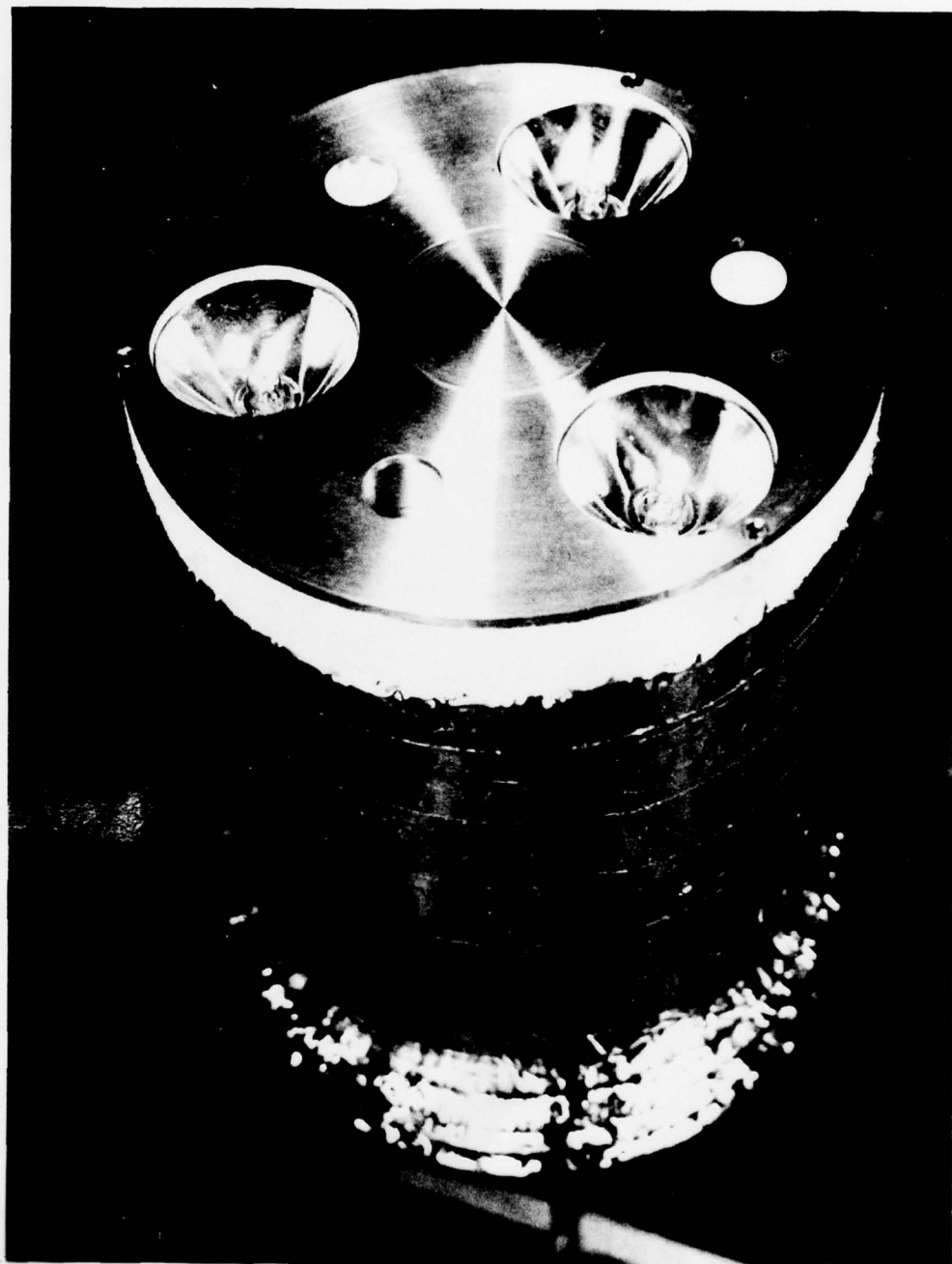


Figure 8. Future Ionization Lamp—Blunt Probe Experiment

Contents

1. Introduction
2. Scientific Objectives
3. Experiment Description
4. The VIII-b Experiment
5. The VIII-a Experiment
6. Summary

STRATOSPHERIC COMPOSITION BALLOON, AIRCRAFT, AND
ROCKET-BORNE EXPERIMENTS, 28-30 SEPTEMBER 1977
(STRATCOM VIII). (SYSTEMS, INSTRUMENTS, TRAJEC-
TORIES, SUPPORTING MEASUREMENTS)

Harold N. Ballard
Atmospheric Sciences Laboratory
US Army Electronics Research and Development Command
White Sands Missile Range, New Mexico

Miguel Izquierdo
Department of Electrical Engineering
University of Texas at El Paso
El Paso, Texas

Arthur Korn
Aerospace Instrumentation Division
Air Force Geophysics Laboratory
Lawrence G. Hanscom Field
Bedford, Massachusetts

David Murcray
Department of Physics
University of Denver
Denver, Colorado

William Page
NASA Ames Research Center
Moffett Field, California

ABSTRACT

The eighth experiment in the STRATCOM (STRATospheric COMposition) series, dating back to the first in 1968, was conducted at 32°N latitude in the period 28-30 September 1977. It was an integrated, correlated stratospheric parameter measurement experiment related to composition, thermodynamic structure, and radiative balance. Three airborne platforms in the form of two large balloons and a U-2 aircraft carried some 35 in situ and remote sensors to obtain 32 hours of interrelated data within the 20-41 km altitude interval. Complementary measurements were made in the earth-surface to 70 km interval by instruments launched on small balloons and rockets on 29 and 30 September. Scientific objectives and experiment description are presented.

1. INTRODUCTION

By 1968 balloon technology had progressed so that it was possible to launch to an altitude of 50 km a constant-altitude balloon carrying an atmospheric-parameter sensing payload of 60 pounds. Data concerning stratospheric winds, gathered by the Meteorological Rocket Network (MRN) over a period of ten years, made possible the prediction of the ensuing balloon trajectory. These two factors, since 1968 to the present, have led to eight, integrated-experiment balloon flights into the stratosphere under the name, Stratospheric Composition experiments. After the first in 1968, additional balloon flights were conducted in September 1969, September 1972, October 1973, May 1974, September 1975, September 1976, and September 1977, and were entitled STRATCOM II - STRATCOM VIII, respectively.

The original objective of the STRATCOM experiments, as related to the study of atmospheric tidal variations, was addressed during each flight. However, requirements by the Department of Defense for information concerning stratospheric composition and thermal structure as related to nuclear defense, and measurements of interest which are related to the possible pollution of the stratosphere by the Super Sonic Transport and by the Chlorofluorocarbons, gradually modified and increased the number, types and complexity of measurements conducted during each successive experiment (this made possible through the characteristics of large zero-pressure balloons). The number and types of instruments on each successive flight were increased so as to give additional information concerning the relationship existing among the various atmospheric parameters, through their simultaneous measurements at successive points in space and time along the various balloon trajectories. This was made possible in

the indicated timeframe only through the participation of other laboratories, and their associated research personnel, with existing atmospheric research capabilities.

Presented in that which follows are the various STRATCOM VIII experiment participants, instruments and corresponding atmospheric parameters measured, instrument payload configurations, balloon trajectories and supporting measurements. Details of the STRATCOM VIII scientific objectives and mission organization, as well as the initial results obtained by the various participating scientists from this stratospheric sounding experiment are available in two publications entitled, "STRATCOM VIII Scientific Objectives and Mission Organization", NASA Goddard Space Flight Center Preprint X-624-77-261, October 1977 and "STRATCOM VIII, Data Workshop April 13-14, 1978", NASA Conference Publication 2043, respectively. These two publications were diligently compiled and edited by Edith I. Reed of NASA Goddard Space Flight Center who served as NASA observer (and participant) for the eighth in the series of STRATCOM experiments. The authors wish to acknowledge that this comprehensive experiment would not have been possible without the funding provided by the Upper Atmosphere Research Office of NASA Headquarters and the knowledge and participation of the scientists from the various agencies, laboratories, and organizations listed in Table 1. In this same regard, the authors wish to acknowledge particularly the efforts and contributions of Dr. Frank P. Hudson of the Department of Energy, who was co-initiator of the STRATCOM program and now serves as consultant for the development of a chemical kinetic model of the stratosphere, which the STRATCOM series of measurements (as well as others) serve to validate.

2. SCIENTIFIC OBJECTIVES

The prime objective of the STRATCOM VIII effort was the study of stratospheric photochemistry, with emphasis on the ozone- NO_x -ultraviolet flux reactions, but also including members of the chlorine, water vapor, and carbon-containing families. Secondary objectives included the study of the balloon environment, comparison of independent measurements of ozone and NO , development of new sensor systems and some measurements for exploratory purposes.

3. EXPERIMENT DESCRIPTION

Initial planning for the experiment was conducted in January 1977 with the actual fabrication of the two large balloon-borne payloads beginning in April 1977. Integration of the various atmospheric parameter-sensing instruments into these two

payloads proceeded from this time with each payload being transported on 13 September to the launch site of the Balloon Branch of the Aerospace Instrument Division of the Air Force Geophysics Laboratory (AFGL) at Holloman Air Force Base. The Electrical Engineering Department of the University of Texas at El Paso was responsible for the fabrication and integration of the payload designated as VIII-a while the Department of Physics of the University of Denver was responsible for the fabrication and integration of the payload designated as VIII-b.

NASA Ames Research Center at Moffett Field, California was responsible for the preparation of the instruments carried aboard the U-2 aircraft. Within the same April-September 1977 time period, detailed plans were made with White Sands Missile Range personnel for the support of the STRATCOM VIII experiment with FPS-16 and Nike-Hercules radars, rocket and small balloon launches, ground-based measurements, and data acquisition telemetry. Table 2 presents a listing of parameters to be measured vs the measuring instruments and corresponding responsible organizations. Also indicated are the platforms on which each instrument was supported, i.e., VIII-a, VIII-b, U-2 aircraft and ground-based.

It was planned that the experiment would be conducted as indicated in Figure 1. On the first day, near the time of earth surface sunrise (0700-0730 MDT; 0600-0830 MST), the VIII-a balloon and payload were to be launched and would ascend at the indicated rate and reach a maximum altitude of at least 40 km. At an altitude of approximately 38 km the Utah State University (USU) NO payload was to be released from the principal VIII-a payload and thence float downward on a parachute. The release of the USU NO dropsonde was to be followed approximately 12 minutes later with the release on a parachute of the Penn State University NO dropsonde (10 1b). The balloon and VIII-a payload were then to float for approximately one hour near 40 km. During this time interval the H₂O sensor of Panametrics Inc. was to be released from the VIII-a payload and float downward while supported by parachute. The balloon was then to begin a slow descent at approximately 140 ft/min. The slow descent was for the purpose of permitting the cryogenic sampler of NCAR to obtain approximately 10 distinct atmospheric samples within the 40-25 km altitude interval.

During this time interval the VIII-b balloon and payload were to be launched so as to be floating at an altitude of 40 km at the time of sunset. The U-2 aircraft was to fly at an altitude of approximately 20 km, with the instruments aboard making measurements which complemented those being made aboard the two balloon-borne payloads. The VIII-b instruments were to make measurements through the time of sunset,

when the VIII-b flight would then be terminated.

The instruments aboard the VIII-a payload were to make measurements near 25 km for a period of 2.5 hours, as indicated in Figure 1, and then balloon VIII-a was to begin an ascent to 40 km, reaching that altitude one hour prior to the time of sunrise. It was to float for a period of three hours at 40 km, when a slow descent at a rate of 140 ft/min would be initiated, this procedure again being for the purpose of obtaining additional atmospheric samples with the cryogenic sampler of NCAR. The VIII-a flight was then to be terminated. Adverse weather conditions caused postponement of the VIII-a and VIII-b balloon launches on 26 and 27 September. Conflict with the Aim-9 (high priority) project for WSMR support caused postponement of the VIII-a flight on the morning of 28 September. It was evident from the WSMR support schedule that this would be a continuing situation. The decision was made to launch the VIII-b balloon and payload on the afternoon of 28 September when there was no conflict with range support, with the launching of the VIII-a balloon and payload to take place on the morning of 29 September. Thus, conflict for WSMR support precluded having both the VIII-a and VIII-b payloads aloft at the same time as indicated in the experiment plan of Figure 1.

4. THE VIII-b EXPERIMENT

Balloon VIII-b ($11.6 \times 10^6 \text{ ft}^3$) carrying a solar-pointing, grating infrared spectrometer, two CO_2 thermal emission radiometers, and two in-situ air temperature sensors (1000 lbs total payload weight) was launched at 1251 MST on 28 September 1977 from Holloman AFB (32°N) to float at an altitude of 39 km from 1521 MST, with the instruments making measurements at that altitude through the time of sunset at 1822 MST. Figure 2 shows the VIII-b payload and balloon just prior to the time of launching. Figure 3 shows the projection of the VIII-b balloon trajectory onto the earth's surface. The balloon floated eastward during the time of ascent and then westward after reaching its float altitude of 39 km. After the time of sunset the VIII-b mission was terminated. The recovery of the payload was not successful. There was a partial failure of some portion of the parachute suspension system. The expected descent time of the parachute and payload was 38 minutes; however, the payload descended from approximately 30 km to the earth's surface in 11 minutes and impacted in very rough terrain at four to five times its normal impact speed. The payload was destroyed by the impact and resulting fire.

The NASA U-2 aircraft flew under the VIII-b balloon and payload at an altitude of 20 km near the time of sunset and along an optical path to the west of the balloon.

5. THE VIII-a EXPERIMENT

Figure 4 shows the VIII-a payload on the east-west runway at Holloman AFB during the time of its preparation for launching on 29 September. Figure 5 shows the USU NO dropsonde (150 lbs) on the east-west runway before it was integrated into the VIII-a payload frame, while Figure 6 is a view from beneath the VIII-a payload showing the USU NO dropsonde, Penn State NO dropsonde (10 lbs) and Panametrics Inc. H₂O dropsonde (10 lbs). Figure 7 shows the complete VIII-a principal payload when it was suspended on the arm of the launching crane. Figure 8 corresponds to Figure 7, with Figure 8 indicating the location of the various instruments on the payload frame. The payload consisted of four UV filter photometers, two UV spectrometers, two chemiluminescent ozonesondes, Dasibi ozone monitor, 14 tube cryogenic samplers, two aluminum oxide H₂O sensors, four air temperature sensors, atmospheric pressure sensor, infrared and visible pyranometers, downward-looking camera (visible), blunt krypton lamp-Gerdien condensor probe, three-component anemometers and three parachute-borne dropsondes.

Figure 9 shows the apex-plate package consisting of ambient temperature thermistor, balloon-skin temperature sensors, pyranometer, carbon element H₂O sensor, aluminum oxide H₂O sensor, power supply, and telemetry transmitter. Figure 10 is the apex-plate payload atop the inflated bubble just prior to the time of balloon VIII-a launching. Figure 11 is a photograph of the complete VIII-a balloon and payload system just prior to the time of launching.

The balloon volume was 21.6×10^6 ft³. The principal payload was reeled downward a distance of approximately 650 feet beneath the balloon immediately after the balloon and payload were launched. This reel-down distance of 650 ft was the maximum permissible with the 920 pound principal payload weight.

Figure 12 is a photograph of the balloon fully expanded at its designed float altitude near 40 km. A close examination of the figure will show the principal payload suspended approximately 650 ft beneath the large balloon. After release at 0507 MST the balloon reached a maximum altitude of 41 km near 0900 MST, with measurements being made by the various instruments from the time of launching, and subsequently in the 41-30 km interval until shortly after the time of sunrise (0540 MDT) on 30 September. The three dropsondes were released successfully in the 0815-0945 time interval, 29 September.

Figure 13 presents the actual flight profile of the STRATCOM VIII-a system vs time, on 29 and 30 September. A comparison of Figure 13 with Figure 1 shows a

marked difference after 1200 MST in the actual profile relative to the one planned. It was established at 1200 MST that it was not possible to valve helium from the VIII-a balloon. It was later established that ballast could not be released. With the system unable to valve helium or drop ballast, the flight profile of Figure 13 resulted solely from changes in heat flux on the balloon. Indicated on Figure 13 are the time sequence of events of consequence from the time of balloon launching to the time of flight termination. They are balloon launching, release on a parachute of the USU NO sensor (35 km), release on a parachute of the Penn State University NO sensor (38 km), initial float altitude of 41 km, release of the Panametrics Inc H₂O sensor (41 km), slow descent of VIII-a to the time of sunset, more rapid descent to 30 km until the time of sunrise on 30 September followed by ascent to near 40 km and subsequent flight termination. Also indicated are the times of soundings of the atmosphere with sensors aboard small rockets and balloons which were launched in support of the VIII-a experiment. The NASA U-2 aircraft flew near 20 km just north of the balloon when the VIII-a balloon was floating at 41 km.

Figure 14 is the projection onto the earth's surface of the trajectory of the VIII-a balloon corresponding to the vertical profile of Figure 13. Indicated times are MST. The balloon and payload moved eastward over the Sacramento Mountains during ascent, followed by a generally westerly movement as it floated in the 41-39 km interval on 29 September. This westerly movement continued until the balloon reached the San Andreas mountains which are immediately west of WSMR. At this point the balloon began an abrupt movement northward directly along the line of the San Andreas Mountains. This apparent following of the San Andreas Mountain ridge continued through the day into the night when the balloon moved southward and eastward, until it abruptly changed direction to the west and crossed over the San Andreas Mountains quite readily. A study of the meteorological conditions that could have produced this somewhat erratic balloon motion is being conducted by the Institute for Storm Research of the University of St. Thomas.

Figure 15 is a photograph of the VIII-a payload on the earth's surface in the vicinity of Truth or Consequences, New Mexico, approximately 100 miles north and west of its launch site at Holloman AFB. No damage was suffered by any instrument aboard the payload.

Table 3 gives a listing of soundings of the atmosphere in time sequence beginning on 22 September 1977 and ending 30 September 1977. These soundings were conducted during the course of the STRATCOM VIII experiment.

6. SUMMARY

The STRATCOM VIII effort took place at Holloman Air Force Base and White Sands Missile Range, New Mexico on 28-30 September 1977. The prime emphasis of the experiment was on the study of stratospheric photo chemistry involving ozone, with secondary objectives including a study of the balloon environment, comparison of independent techniques for the measurement of O_3 and NO , and the development of new sensor systems. More than forty sensors were included on two large balloons, a U-2 aircraft, and several rockets and small balloons, in addition to meteorological balloons and rockets. A majority of the systems performed as expected, with the material presented by the various experimenters at STRATCOM VIII Workshop of 13-14 April 1978 indicating that data are available to achieve most of the planned scientific and engineering objectives of the experiment.

REFERENCES

- STRATCOM VIII Scientific Objectives and Mission Organization, Edith I. Reed, Preprint X-624-77-261, Goddard Space Flight Center, Greenbelt, Maryland, October 1977, 104 pages.
- STRATCOM VIII, Data Workshop, April 13-14, 1978, compiled by Edith I. Reed, NASA Conference Publication 2043, 108 pages.

Table 1. Organizations

AFGL	Air Force Geophysics Laboratory Hanscom Air Force Base, Massachusetts 01731
AFGL/HAFB	Detachment 1, Balloon Branch Air Force Geophysics Laboratory (AFCS) Holloman Air Force Base, New Mexico 88330
ASL	Atmospheric Sciences Laboratory US Army Electronics Command White Sands Missile Range, New Mexico 88002
CSU	Department of Atmospheric Sciences Colorado State University Fort Collins, Colorado 80523
DOE	Environmental Research Department of Energy Washington, D. C. 20545
NASA/ARC	Space Sciences Division Ames Research Center Moffett Field, California 94035
NASA/GSFC	Goddard Space Flight Center Greenbelt, Maryland 20771
NASA/LARC	Langley Research Center Hampton, Virginia 23065
NASA/WFC	DO-PMOB-PYS (ASRP) Wallops Flight Center Wallops Island, Virginia 23337
NCAR	National Center for Atmospheric Research P. O. Box 3000 Boulder, Colorado 80303
NOAA/ERL	Atmospheric Physics and Chemistry Laboratory NOAA Environmental Research Laboratories Boulder, Colorado 80303
Pan	Panametrics, Inc. 221 Crescent Street Waltham, Massachusetts 02154
Penn	Ionosphere Research Laboratory Pennsylvania State University University Park, Pennsylvania 16802
PSL	Physical Sciences Laboratory New Mexico State University Las Cruces, New Mexico 88001
Sandia	Division 9226 Sandia Laboratories Albuquerque, New Mexico 87115

THIS PAGE IS BEST QUALITY FRAGMENT
FROM COPY FURNISHED TO JDC

Table 1. Organizations (Cont)

SenTran	SenTran Company 2705 de la Vina Street Santa Barbara, California 93105
UDenver	Department of Physics and Astronomy University of Denver Denver, Colorado 80208
UTEP	Electrical Engineering Department University of Texas at El Paso El Paso, Texas 79968
UST	Institute for Storm Research University of St. Thomas Houston, Texas 77006
USU	Center for Research in Aeronomy Utah State University Logan, Utah 84322
WSMR	White Sands Missile Range New Mexico 88002

[illegible]

Table 3. Times of Launch and Other Significant Events

Platform	Time(MDT)	Date (1977)	Location
Balloon radio sonde	0700	Sept. 22	HAFB
Loki data sonde	1215*	"	SMR
Loki data sonde	1200*	23	"
Balloon radio sonde	0030	24	HAFB
Balloon radio sonde	0635	"	"
Loki data sonde	1100*	"	SMR
Balloon radio sonde	0001	25	HAFB
Balloon radio sonde	0600	"	"
Loki data sonde	1100*	"	SMR
Balloon radio sonde	0001	26	HAFB
Balloon radio sonde	0700	"	HAFB
Loki data sonde	1000*	"	SMR
Balloon radio sonde	1200	27	HAFB
Loki data sonde	1205*	"	SMR
Balloon radio sonde	0900	28	HAFB
Balloon radio sonde	1300	"	"
Balloon VIII-b	1351	"	"
Super-Loki data sonde	1427*	"	SMR
U-2 aircraft in vicinity	1845	"	"
Termination of Balloon VIII-b		"	"
Balloon radio sonde	2100	"	HAFB
Balloon radio sonde	0200	29	"
Mast ozone sonde	0230	"	SMR
Balloon radio sonde	0615	"	HAFB
Balloon VIII-a	0707	"	"
Parachute drop no. 1 #	0915	"	"
Parachute drop no. 2	0932	"	"
ECC ozone sonde	1025	"	SMR
U-2 aircraft in vicinity	1045	"	"
Parachute drop no. 3	1045	"	"
Balloon radio sonde	1200	"	HAFB
ARCAS ozone sonde (ASL) #	1207*	"	SMR
Super-Loki ROCOZ	1222*	"	"
Mast ozone sonde #	1230	"	"
Super-Loki data sonde	1330*	"	"
Super-Loki blunt probe	1445*	"	"
ARCAS Gerdien condenser #	1519*	"	"
ARCAS ozone sonde (ASL)	1620*	"	"
Balloon radio sonde	1800	"	HAFB
Loki data sonde	2010*	"	SMR
Balloon radio sonde	0600	30	HAFB
Loki data sonde	0702*	"	SMR
Mast ozone sonde	0800	"	SMR
Loki data sonde	1200*	"	"
Termination of Balloon VIII-a	1330	"	"

Notes:

*A balloonradio sonde was simultaneously launched at the Small Missile Range.

#Performance of vehicle or payload was seriously substandard.

HAFB - Holloman Air Force Base

SMR - Small Missile Range

The Balloon radio sondes and the Loki/Super-Loki data sondes are for meteorological data.

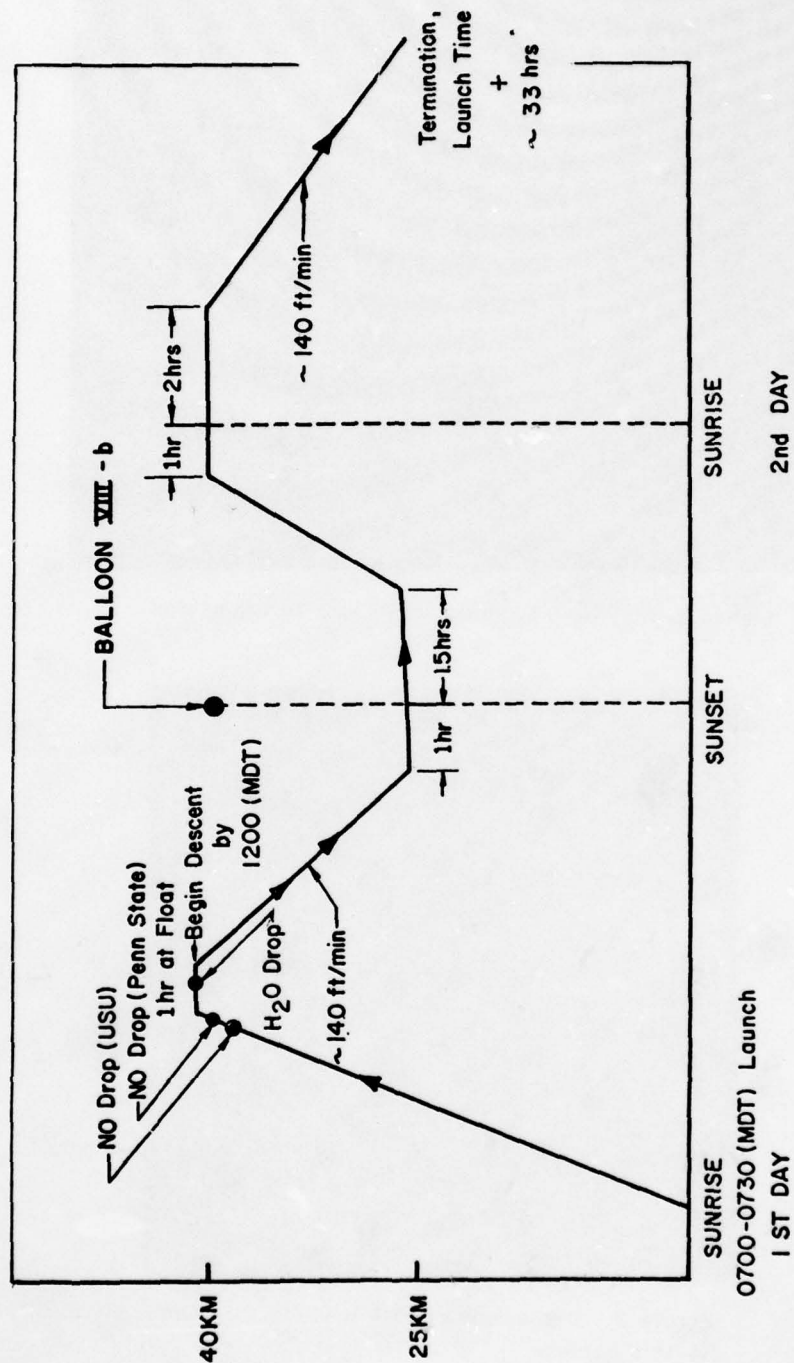


Figure 1. STRATCOM VIII-a Flight Profile (Planned)

AD-A074 469

AIR FORCE GEOPHYSICS LAB HANSCOM AFB MA
PROCEEDINGS OF THE AFGL SCIENTIFIC BALLOON SYMPOSIUM (10TH) HEL--ETC(U)
MAR 79 C L RICE

F/G 1/3

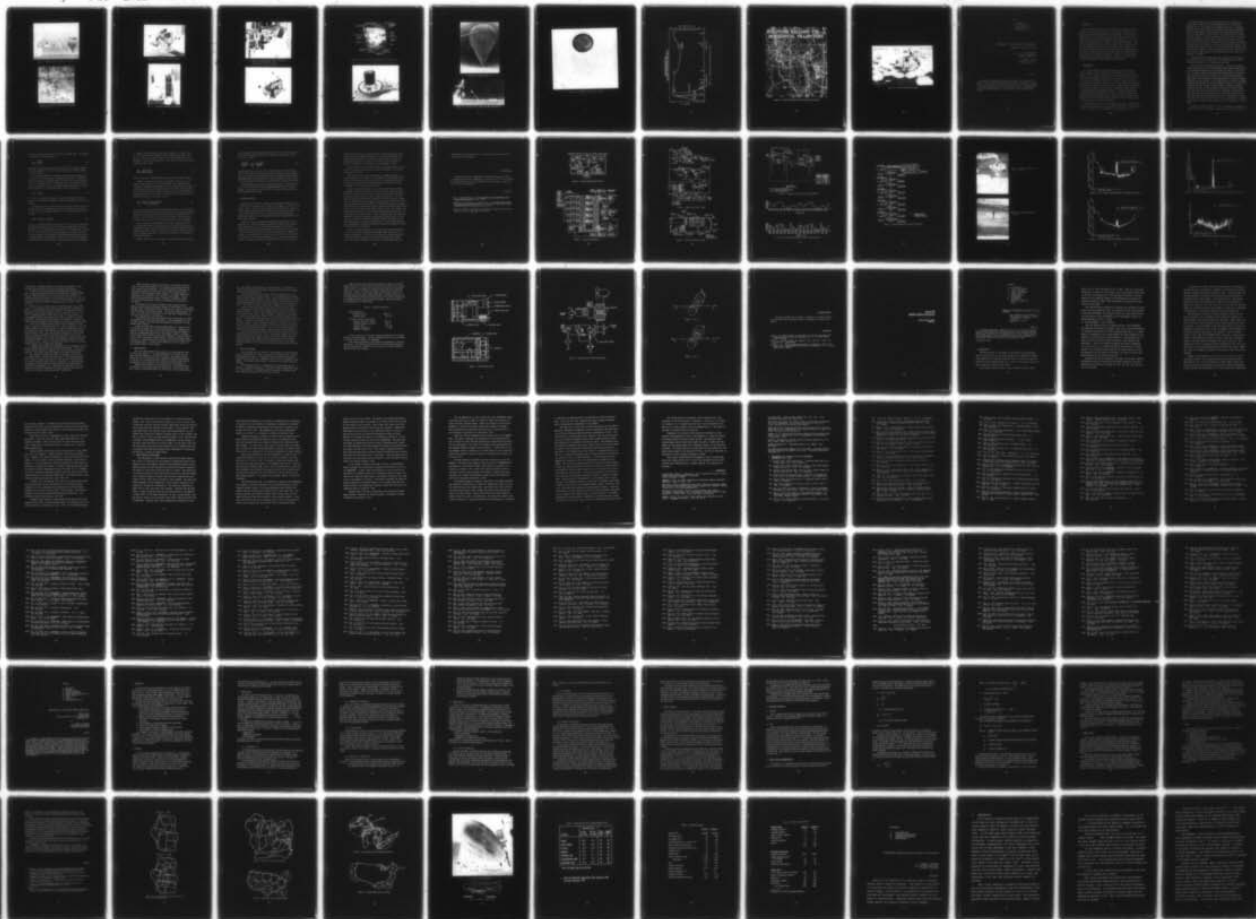
UNCLASSIFIED

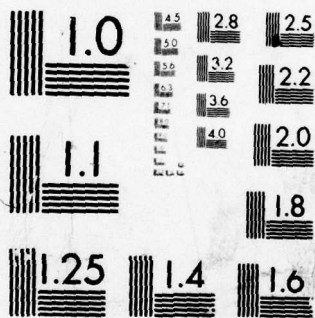
AFGL-TR-79-0053

NL

4 OF 6

AD
A074-469





MICROCOPY RESOLUTION TEST CHART
NATIONAL BUREAU OF STANDARDS-1963-A

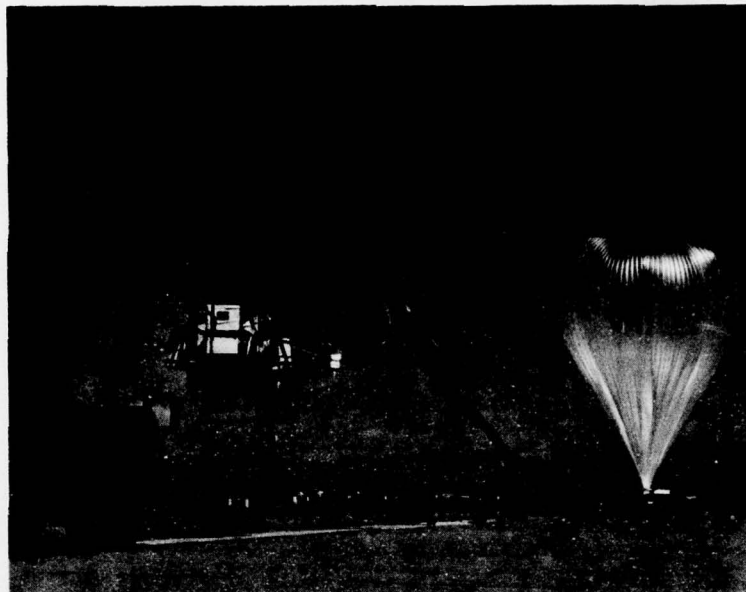


Figure 2. VIII-b Payload Just Prior to Launching

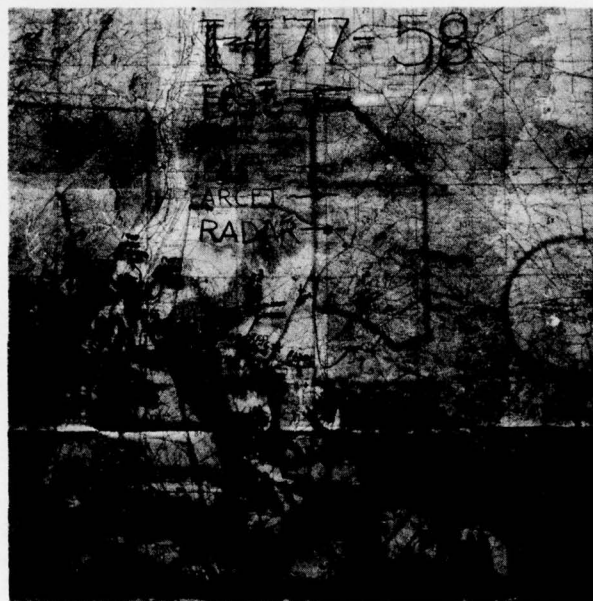


Figure 3. Projection of VIII-b Trajectory Onto Earth's Surface

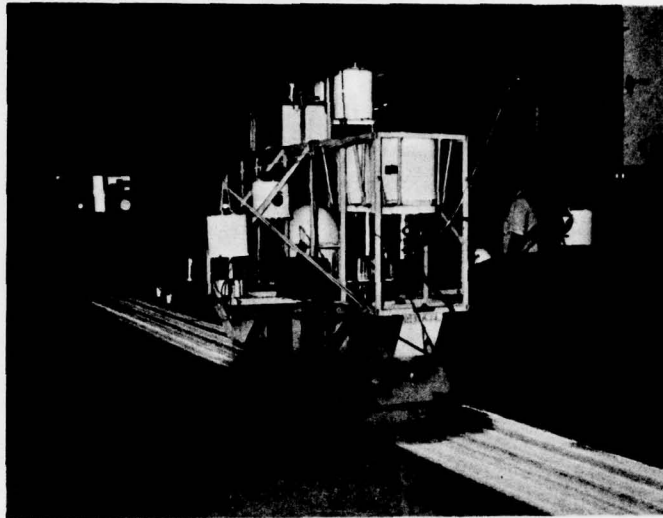


Figure 4. VIII-a Payload on HAFB Runway

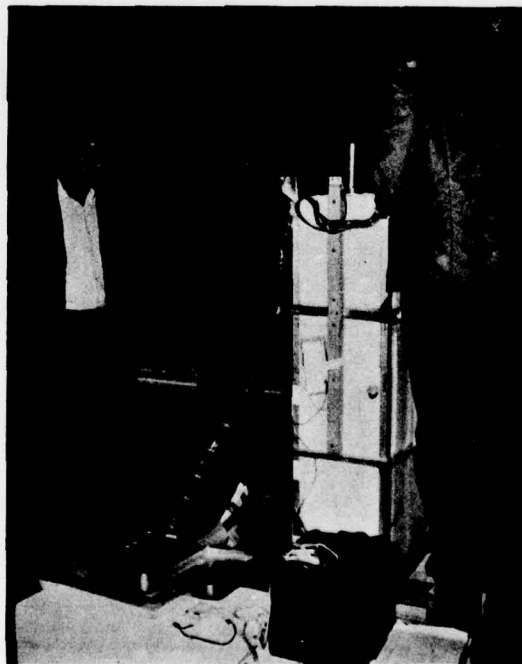


Figure 5. Utah State University NO Dropsonde

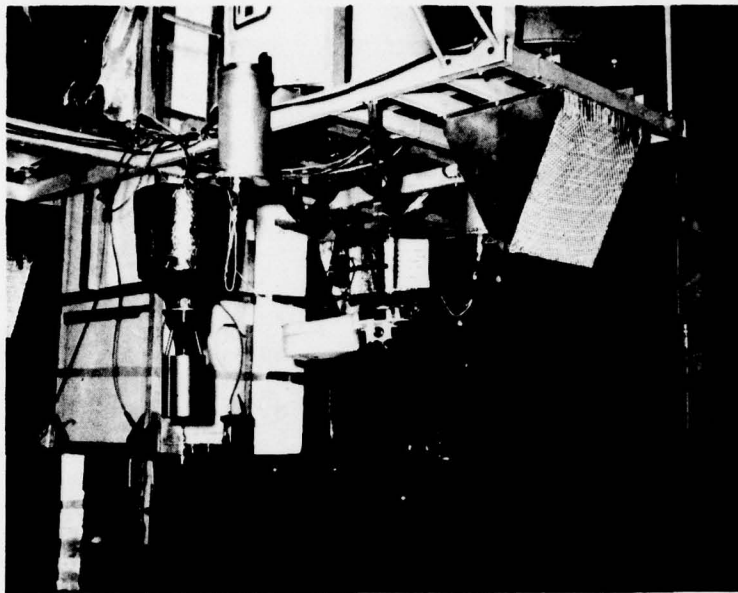


Figure 6. VIII-a Payload—USU NO Dropsonde, Penn State NO Dropsonde, and Panametrics, Inc. H₂O Dropsonde

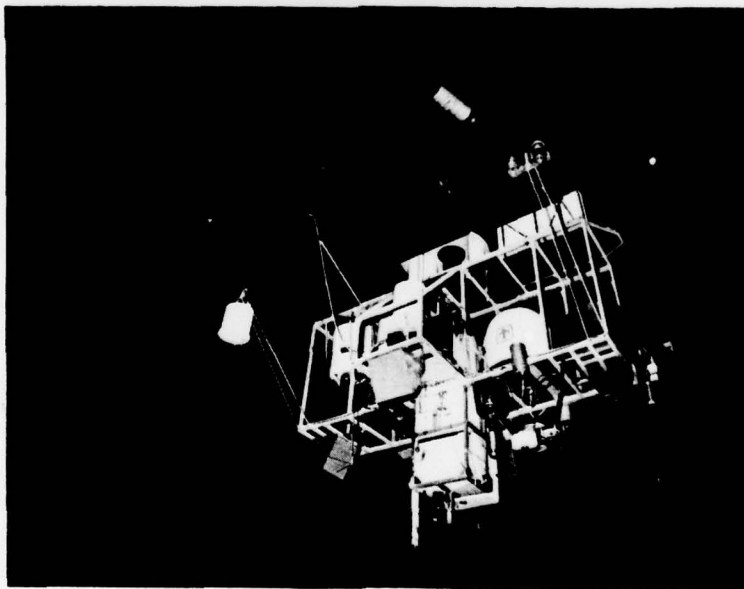


Figure 7. VIII-a Payload Suspended on Launching Crane

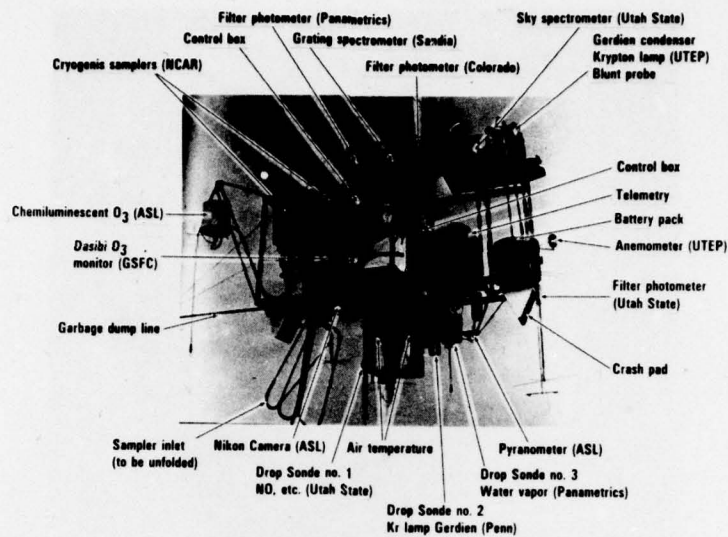


Figure 8. Location of Various Instruments on VIII-a Payload

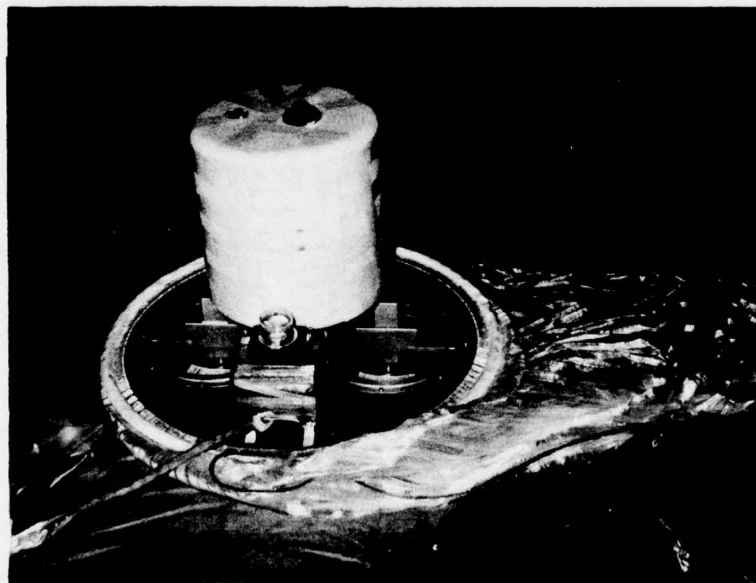


Figure 9. Balloon VIII-a Apex-Plate Payload

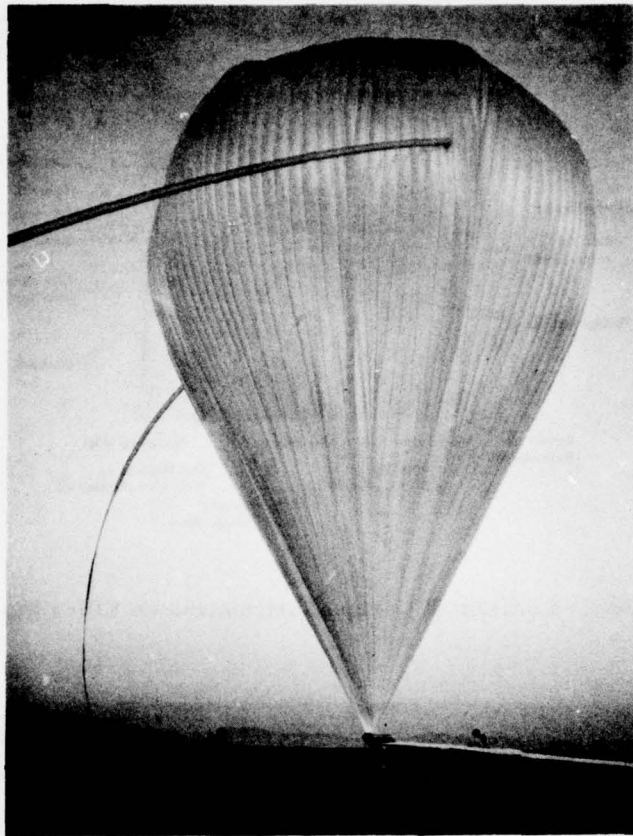


Figure 10. Inflated Bubble

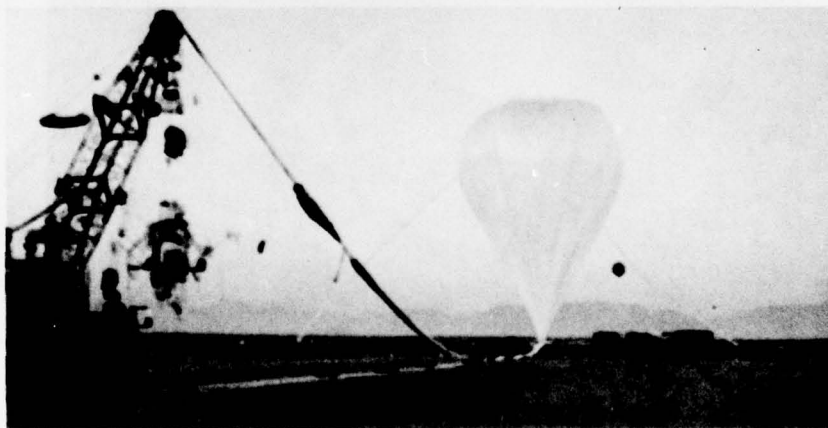


Figure 11. Complete VIII-a Balloon and Payload Systems

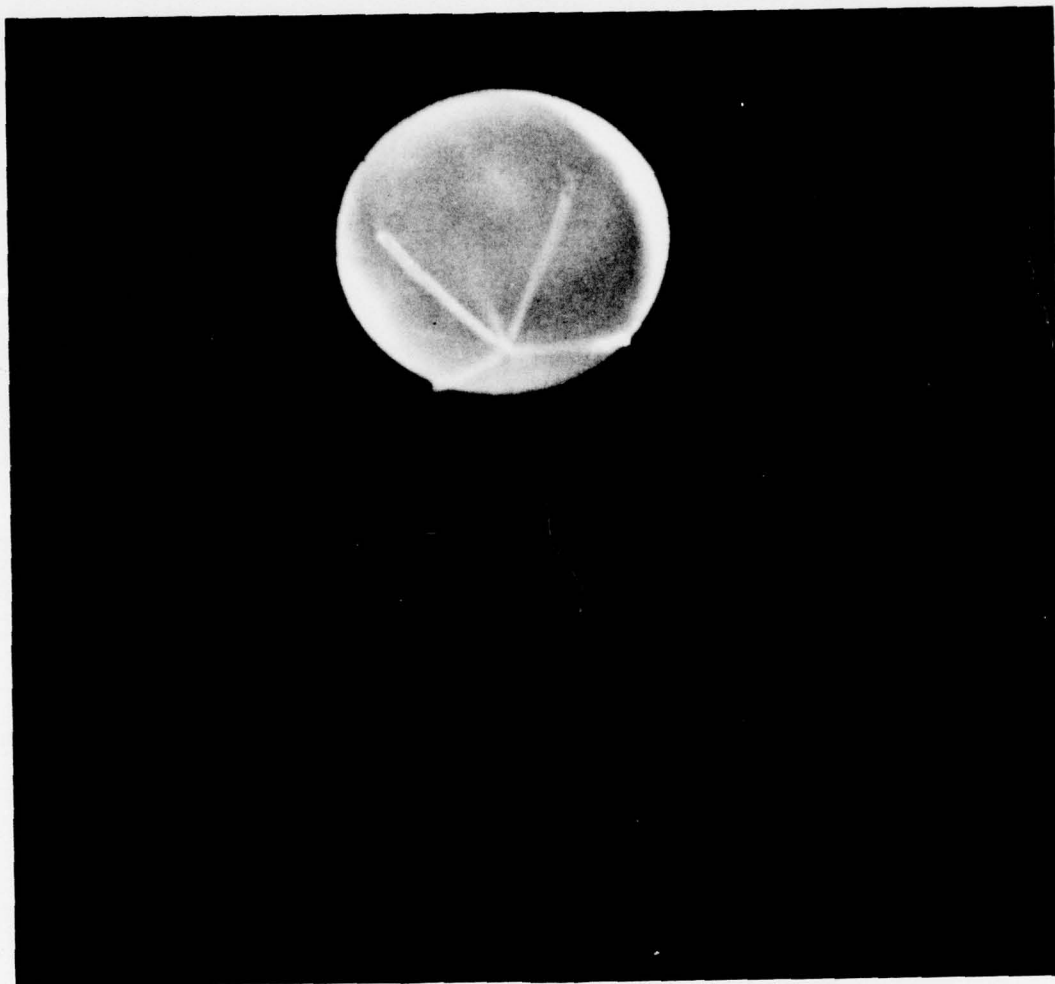


Figure 12. Balloon Fully Expanded Near 40 km

STRATCOM BALLOON VIII-A HOLLOMAN AIR FORCE BASE, NEW MEXICO

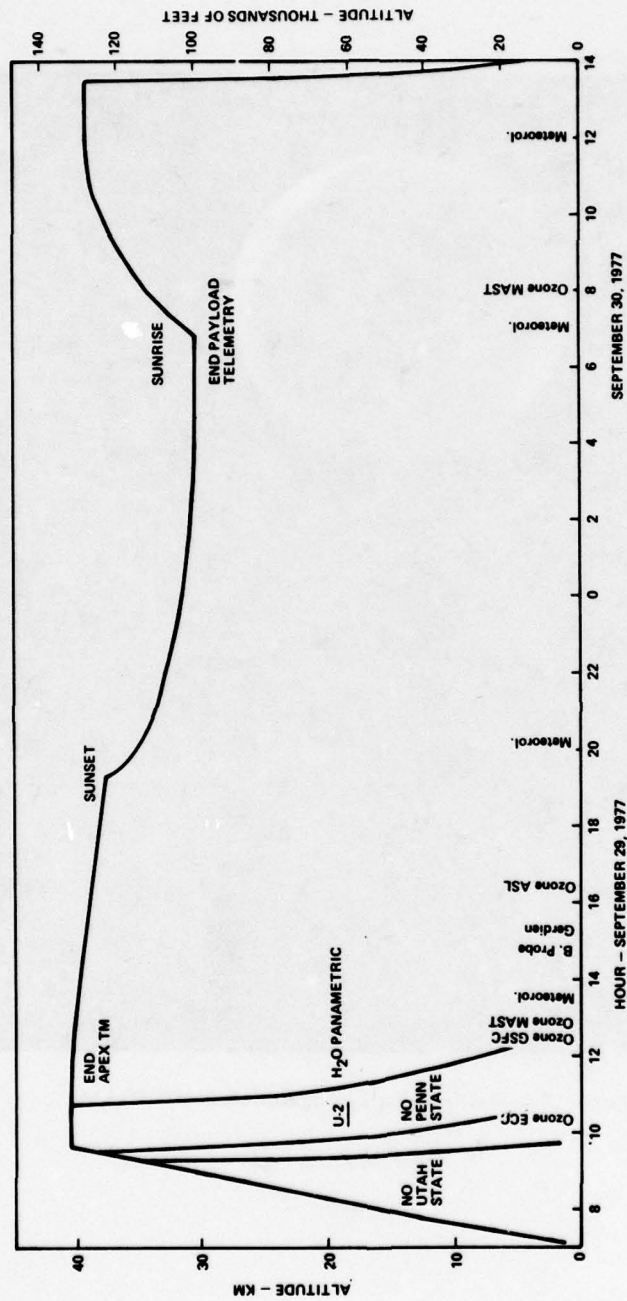


Figure 13. STRATCOM VIII-a Flight Profile (Actual)

STRATCOM BALLOON VIII—A HORIZONTAL TRAJECTORY

313

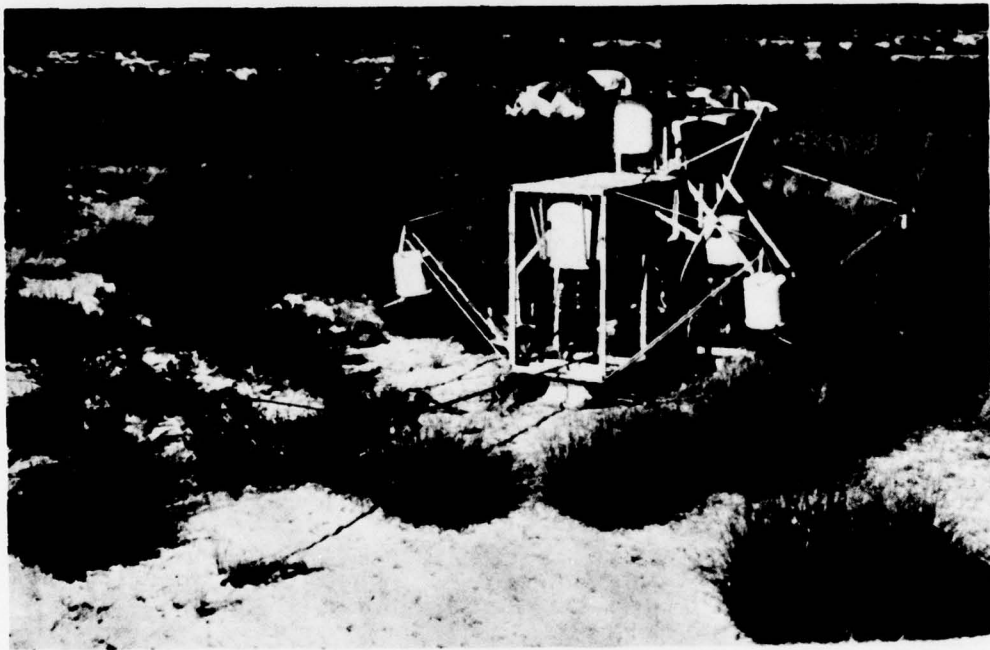


Figure 15. VIII-a Payload After Flight

Contents

1. Introduction
2. Instrumentation
3. Theory of Nephelometer Measurements
4. Experimental Results

THE MEASUREMENT OF OPTICAL SCATTERING FROM ATMOSPHERIC

AEROSOLS AS A FUNCTION OF ALTITUDE

Frank W. Gibson
Air Force Geophysics Laboratory
Bedford, Massachusetts

Norman C. Poirier
Northeastern University
Boston, Massachusetts

Abstract

Balloonborne instrumentation has been used to determine the altitudinal variability in angular scattering and polarization parameters of atmospheric particles. These in situ measurements provide new data on the vertical distribution of aerosols to an altitude of 26 Km. In view of the wide dynamic range of signals encountered, a unique gain-switching capability was developed which provides ground-command control of the telemetered signal intensity and thus optimum information transmission.

1. INTRODUCTION

When an atmospheric volume element is illuminated by a light beam, the scattered radiation, detected at various angles, gives information about the aerosol particles and air molecules contained in the volume element. In particular, suspended particles with radii greater than about $.1\mu\text{m}$ scatter more of the light in a forward direction, while the molecules and very small particles (i.e. less than $.1\mu\text{m}$) cause the same amount to be scattered in the forward and backward directions with a minimum amount at an angle of 90° with respect to the incident beam. Moreover, the wavelength and polarization of the scattered light are dependent upon such physical properties as particle size, shape, refractive index and composition. The intensity of the scattered light is also proportional to the number densities or concentration of the aerosols and molecules. Therefore, the investigation of angular scattering provides data of quantitative value and significance relative to atmospheric properties and their variability with altitude.

2. INSTRUMENTATION

An instrument, generally called a polar nephelometer, which measures the angular dependence of light, was constructed at AFGL (Gibson, 1971) and Northeastern University (Rocheffort, 1976) to facilitate balloon-borne investigations and thereby determine atmospheric optical properties as a function of altitude. The first figure gives a schematic diagram of the instrument. Because the particle concentration drops perhaps to values of less than one particle/cm³, the illuminated volume element must be sufficiently large to give an adequate signal-to-noise level. This requirement in addition to that of a well collimated source beam resulted in an experimental payload of approximately 1200 lbs. The gondola with dimensions (3.15mx1.63mx0.61m) is completely enclosed, except for the top and bottom of the measurement region where entrance and exit airducts are located. The ducts have a baffled construction that provides sunlight shielding while they conjunctively permit the unobstructed vertical flow of ambient air.

The balloon-borne system consists of three major subsystems: The Data Acquisition System, the Telemetry System and the Command Receiver System. These are shown in Figure 2. However, I will be high-lighting the Data Acquisition System.

The primary component in the Data Acquisition System is the light source, a 150 watt short-arc Xenon lamp, the collimated beam from which is mechanically chopped at 22.5 Hz. This provides intensity modulation so that a.c. synchronous detection of the scattered radiation may be used to suppress unwanted background light. The power supply for the lamp (Fig. 3) must provide two basic functions. The first is the ignition or starter function. A 15 to 20 Kilovolt pulse through an external trigger wire initiates ionization of the gas in the tube. After this initial ionization path is established, a sustainer circuit provides a 350 volt pulse across the two electrodes in the lamp until the arc is completely established. The second function of the power supply is to provide a continuous constant current through the lamp to maintain the arc. A current of approximately 7.5 amperes at 20 volts provides the 150 watts of power at which the lamp is rated. These values can vary from lamp to lamp and provisions have been made to adjust the supply to the rated power of the lamp.

The power supply was designed to automatically repeat the starting sequence until the constant current is established. The starting functions will also be reinitiated in the event the arc extinguishes during flight.

The circuitry for the lamp operates as follows: If the current through the current sensing resistor is less than two amperes (lamp extinguished) relays K_1 and K_2 are energized by comparators CP_1 and CP_2 through relay drivers. These relays turn on the power to the DC to DC converters which produce 400 volts and 350 volts each. The outputs of the DC to DC converters are connected through diodes to a common output; thus the sensing and high voltage supplies are completely redundant. The 400 volts is used to charge a 1.0 microfarad capacitor, C_1 , which is discharged by SCR1 through the primary of a step-up transformer to produce a 15 to 20 kilovolt pulse across the lamp. The 350 volt source charges up C_2 which can discharge through the lamp after the high voltage pulse establishes the initial ionization path. The constant current section consists of a comparator, CP_3 , which monitors the voltage across the current sensing resistor, R_1 , and gates, on and off, the series pass regulators Q_1-Q_2 and Q_3-Q_4 at such a rate as to maintain this voltage equal to the "set current" voltage. Energy is stored in the inductor, L_1 , and this stored energy is released during the time the series pass regulators are in the off state.

As shown in the payload schematic (Fig. 1), five photometers are mounted on an optically rigid frame so as to measure the scattered light at 15° , 30° , 50° , 100°

and 150° from a defined volume (about 250 cm^3) of atmosphere. The typical photometer is shown in Fig. 4. This is essentially a telescope with an f/2 objective lens focussed at the center of the nephelometer unit. A 2.5 cm square aperture serves as the field stop and provides a field-of-view of 6° . A pair of aspheric condenser lenses behind the stop images the objective lens onto an EMI 9558 photomultiplier, which has an S-20 spectral response. An eight-position filter wheel is mounted adjacent to the field aperture and spectral filters at $0.475\mu\text{m}$, $0.515\mu\text{m}$, $0.660\mu\text{m}$, and $0.745\mu\text{m}$ are used. The filter wheel is rotated stepwise so as to provide a sampling period of 3 sec/filter. In addition the $0.475\mu\text{m}$ and the $0.660\mu\text{m}$ filter have linear polarizers laminated to their surfaces, for the 50° , 100° , and 150° units, so that the perpendicular and parallel polarization of the scattered light is sequentially analyzed.

The outputs of the photometers are fed initially to Princeton Applied Research (PAR) Model 120 lock-in amplifiers, fixed-tuned to the 22.5 Hz chopper frequency, and then to sync insertion circuits to add spectral-filter channel and frame synchronization signals.

The amplifiers were modified to allow remote gain switching during a balloon flight. This modification is shown in Figure 5. The modification was achieved with the addition of three Reed relays and does not affect normal operation of the unit. Access to the relays in the amplifier is through a Winchester M-5S connector located in the rear of the amplifier housing and the relays are operated via ground-command. The range of remote gain control is from 1 mv to 50 mv full-scale in six steps. During the flight the manual gain control is set initially in the 50 mv full-scale position and as the signal intensity is monitored at the ground-command facility the amplifier sensitivity may be changed via the command system to optimum levels. The individual gain setting for each amplifier is also telemetered along with the measured intensity data to provide a record of the specific gain level at a particular time during the flight.

A typical signal waveform from the output of the synchronous amplifier is shown in Figure 6. The output is similar to an eight channel pulse amplitude commutator; however, the commutation is done by the filter-wheel rotation increments during which each spectral filter is inserted into the optical path of light detected. To facilitate computerized data reduction, synchronization signals were inserted into the data channels. Since the filter changing mechanism is relatively slow (i.e., $\sim 3 \text{ sec}$) it was possible to sense the filter position by simply using Reed switches

and magnets.

Figure 6 also illustrates the addition of the synchronization pulses to the data. The frame sync pulse occurs between channel eight and channel one, and the channel sync pulses occur at the center of each channel. The circuitry for inserting the synchronization pulses is shown in Figure 7. There are ten identical circuits, two for each photometer, and each is used to drive the five subcarrier oscillators in the main system as well as the five subcarrier oscillators in the spare system. The CA3130 amplifier facilitates limiting the signal data at 4.5 volts and ground (i.e., 0-volts) so that the synchronization levels of -1.25 volts and 5.00 volts are not reached by the data. These synchronization voltage levels are inserted when the sync inputs from the Reed switches are grounded. This saturates transistors Q_1 and Q_2 and overrides the amplifier output to the synchronization levels.

The Telemetry System consists of commutators, subcarrier oscillators, transmitters and antennas. It is configured as a standard S-Band FM/FM telemetry system as specified by the Inter-Range Instrumentation Group (IRIG). These components are connected to provide two identical transmission links as shown in Figure 2. Only one transmission link is active at a time and this selection is made via the ground-command system to the airborne command receiver.

The Command Receiving System uses an onboard FM receiver operating at 430 MHz, a tone decoder and output relays. The corresponding ground equipment included a two-watt transmitter, tone oscillators and a steerable antenna. This equipment was located in the telemetry room of the control center and there was immediate access to the command system while monitoring incoming data. As previously noted, the command system was used to change the gain of the onboard signal amplifiers and to sequence the telemetry system.

The next two figures (Fig. 8 and 9) show the entire experimental package during launch procedures at Holloman AFB, N.M.

3. THEORY OF NEPHELOMETER MEASUREMENTS

The polar nephelometer is used fundamentally to measure the angular volume scattering function, $\beta(\theta)$. This quantity simply represents the fraction of the light incident on an atmospheric volume, $V(\theta)$, that is scattered in the direction θ by the

aerosol particles and air molecules contained in the defined volume. This parameter is expressed in the following manner:

$$\beta_{\lambda}(\varphi) = \frac{I_{\lambda}(\varphi)}{E V(\varphi)} \quad (1)$$

where $\beta_{\lambda}(\varphi)$ is angular volume scattering function ($\text{cm}^{-1} \cdot \text{sr}^{-1}$), $I_{\lambda}(\varphi)$ is radiance at scattering angle φ (w sr^{-1}), E is incident light intensity (w cm^{-2}), and $V(\varphi)$ is scattering volume.

The scattering volume $V(\varphi)$ is fixed for a particular scattering angle by the intersection of the source beam and the photometer field-of-view. A photometer calibration technique is used which relates all quantities on the right hand side of Eq. (1) that depend upon the instrumentation, to a single constant factor for a particular photometer. That is, the measured analog signal voltage, or response of the instrument, is directly related to $\beta(\varphi)$ so that the response is

$$W(\varphi_s) = K \beta_{\lambda}(\varphi_s) \quad (2)$$

Thus, when K is determined by calibration, $\beta_{\lambda}(\varphi_s)$ can be computed in absolute quantities from the measured voltages, for a specific wavelength, λ , and scattering angle, φ_s .

The measurement volume is small enough such that primary scattering occurs (i.e., multiple scattering is negligible) and the aerosol and molecular contributions to the total intensity are separable and additive. The scattering function can then be written

$$\beta_{\lambda}(\varphi_s) = \sigma_{R\lambda} P_R(\varphi_s) + \sigma_{A\lambda} P_A(\varphi_s) \quad (3)$$

where $\sigma_{R\lambda}$ is the Rayleigh scattering coefficient (cm^{-1}), $P_R(\varphi_s)$ is the normalized Rayleigh phase function (sr^{-1}), $\sigma_{A\lambda}$ is the aerosol scattering coefficient (cm^{-1}), and $P_A(\varphi_s)$ is the normalized aerosol phase function (sr^{-1}). Because the first additive term involves only molecular scattering, $P_R(\varphi_s)$ is a well-known function of the scattering angle, φ_s , and $\sigma_{R\lambda}$ can be determined reasonably accurately from the Standard Atmosphere or radiosonde data. Consequently the aerosol term $\sigma_{A\lambda} P_A(\varphi_s)$ is extractable from the scattering function $\beta_{\lambda}(\varphi_s)$ as measured with the nephelometer.

However, Rayleigh or molecular scattering is symmetric with respect to φ_s , a fact which gives additional information on the scattering from aerosols. When Eq. (3) is written for two symmetric angles (e.g., 30° and 150°) and the ratio is determined, it follows that the turbidity, or the relative concentration of aerosols to molecules takes the form

$$\frac{\sigma_{A\lambda}}{\sigma_{R\lambda}} = \frac{P_R(\varphi_1) (R-1)}{P_A(\varphi_1) - R P_A(\varphi_2)} \quad (4)$$

where R is the ratio of forward-to-backscatter intensities for symmetric angles.

Perhaps the parameter most sensitive to atmospheric particle size is the degree of linear polarization of the scattered light. When unpolarized light illuminates an atmospheric volume element, the air molecules and very small particles cause the scattered light to be highly polarized at $\varphi_s = 90^\circ$. Thus a measurement of the vertical and horizontal polarization intensities gives another signature for the amount of aerosols in the volume. It can be shown that a relationship exists between the polarization ratio and the turbidity:

$$\frac{\sigma_{A\lambda}}{\sigma_{R\lambda}} = \frac{P_{RV}/P_{AH} - (I_V/I_H) (P_{RH}/P_{AH})}{I_V/I_H - P_{AV}/P_{AH}}, \quad (5)$$

where I_V is the vertically polarized scattered intensity and I_H is the horizontally polarized scattered intensity and the V and H subscripts on the Rayleigh and aerosol phase functions simply refer to the vertical and horizontal components of these functions. In Eqs. (4) and (5) the only unknown variable is the aerosol phase function $P_A(\varphi)$, since the ratio R and I_V/I_H are measurable and $P_A = (P_{AV} + P_{AH})/2$.

Thus, in principle, these equations can be solved simultaneously by best-fitting an assumed theoretical function $P_A(\varphi)$ for a particular altitude region. As a consequence, values of σ_A/σ_R as a function of altitude may be determined. Additionally, a best-value of $P_A(\varphi)$, which provides the solution to these two equations, defines the angular scattering characteristics of the aerosols in the atmospheric volume under examination.

However, another useful fact, from empirical data on scattering from aerosols,

is that at $\phi_s = 50^\circ$ the molecular and aerosol phase functions are linearly related to their respective scattering coefficients for aerosol size distribution found in clear air. This means

$$\frac{\beta_{A\lambda}(50^\circ)}{\beta_{R\lambda}(50^\circ)} = C \frac{\sigma_{A\lambda}}{\sigma_{R\lambda}} = \frac{\beta_{Total}(50^\circ)}{\beta_{R\lambda}(50^\circ)} - 1 \quad (6)$$

and the constant C when the visibility is 30 km or better. This relationship implies that the total intensity at the 50° scattering angle provides an approximation to the turbidity since the Rayleigh factors can be determined from standard measurement data as previously mentioned. Equation (6) together with Eqs. (4) and (5) provide quantitative information on the distribution of aerosols with altitude.

The nephelometer data thus provides the valuable feature of self-consistency. This is Eqs. (4), (5), and (6) provide independent determinations of the same quantity. Further details of this utilization of angular scattering data is presented elsewhere (Gibson, 1976).

4. EXPERIMENTAL RESULTS

We have had five successful flights with this experimental package and I will illustrate some of the salient data. Perhaps the most spectacular results occurred during a flight in June 1974. Figure 10 depicts the altitude profile of $\beta(\phi)$ at 15° and $.515\mu\text{m}$ and shows the strong forward scattering from aerosol particles. The initial spike at ground level is due to exhaust smoke from the launch crane. Aerosols are evident in the 3-7 km region and the intensity dropped sharply in the next kilometer interval.

Above an altitude of about 8 km the measurement volume was relatively free of large particles. The signal enhancement which begins at about 17 km is the well-known Junge aerosol layer. At 25 km the payload encountered a rare event, a nacreous cloud, over the San Andres mountains. The very strong intensity increase is a result of the combination of the large size of the particles - probably ice crystals - and the higher particle concentrations characteristic of a stratified cloud structure. The experimental package was still in the cloud at peak altitude of 26.6 km. Moreover, the cloud was at least 50 km in horizontal extent because

the balloon had traversed this distance relative to the ground before the strong signals ceased as the package was descending. The intensity then dropped to the signal levels observed prior to penetrating the cloud. High cirrus clouds were apparent at about 10.6 km on descent and it should be noted that the peaks in intensity are comparable to those observed for the stratospheric clouds.

The next Figure (11) shows the 50° data and the angular variability in scattering which is evident from the reduction in intensity as compared to the extreme forward scattering at 15° .

Figure 12 depicts the forward-to-backscatter or dissymmetry parameter. This provides a measure of the variability in the atmospheric scattering phase function. The plot illustrates the effect of particle size on the angular scattering and clearly outlines regions of significant concentrations of aerosols, by virtue of the asymmetry in their angular scattering pattern.

Figure 13 shows the polarization ratio at 100° scattering angle and $.475\mu\text{m}$ wavelength. A qualitative assessment of the range of particle sizes contributing most to the polarization can be inferred from the plot. The launch crane smoke is indicated by a ratio of about 1.25, that is, about 10% polarization. The ratio begins to increase with altitude from a value of 4.4 at 5 km to a maximum of about 7.5 in the region of 9 km, even though the scattering functions were still indicating relatively high turbidity between 5 and 6 km. The polarization maximum corresponds to 76% polarization of the scattered light and suggests the presence of high concentrations of very small aerosol particles because aerosol-free air (i.e., molecular scattering) would require a ratio of 14.4, nearly twice the maximum observed value. The ratio decreases to a minimum of about 1 in the stratospheric cloud layer in much the same manner as the launch crane smoke and thus, shows the dominance of the larger particles. The profile is essentially repeated on descent and the high cirrus is indicated by a drop in polarization at about 10.6 km. The polarization maximum at 9 km is reproduced on the down-leg even though the experimental package had traveled over 200 km relative to the ground.

The last two figures show some of the more recent data but the data reduction is still in a preliminary stage and the gain change evident at about 13 km is not accurately represented. This was in fact an automatic gain reduction achieved via a transducer on-board the payload and necessitates employing further computer analysis techniques. Nevertheless, the instrument was descending through high

thunderclouds and precipitation when this occurred and the relative difference in signal structure is informative.

Acknowledgments

The authors would like to acknowledge the invaluable assistance of W. Thorn of Northeastern University, M. Daddario and J. Essex of AFGL as well as the personnel at the Balloon R&D Test Facility, Holloman AFB, N.M., without whom the experiments could not have been accomplished.

References

- Gibson, F.W. and Dearborn, F.K. (1971) Atmospheric Optics Measurements with a Balloon-borne Nephelometer, AFCRL-71-0455.
- Rocheft, J.S., O'Connor, L.J. and Poirier, N.C. (1976) Signal Processing and Data Transmission from Space Vehicles, AFGL-TR-76-0120, Final Report, Contract AF19628-73-C-0148, Northeastern University, Boston.
- Gibson, F.W. (1976) In Situ Photometric Observations of Angular Scattering from Atmospheric Aerosols, Appl. Opt., 15: 2520-2533.

SCHEMATIC DRAWING OF BALLOON-BORNE NEPHELOMETER

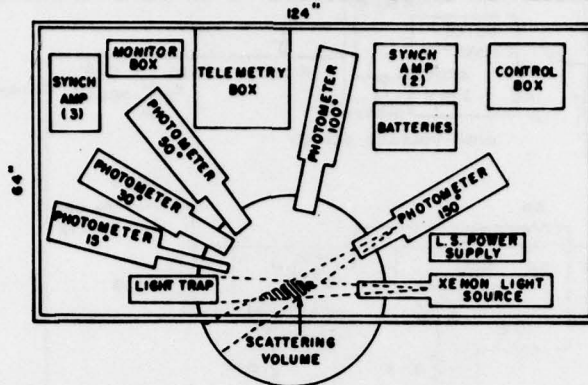


Figure 1. Balloon Experimental Payload

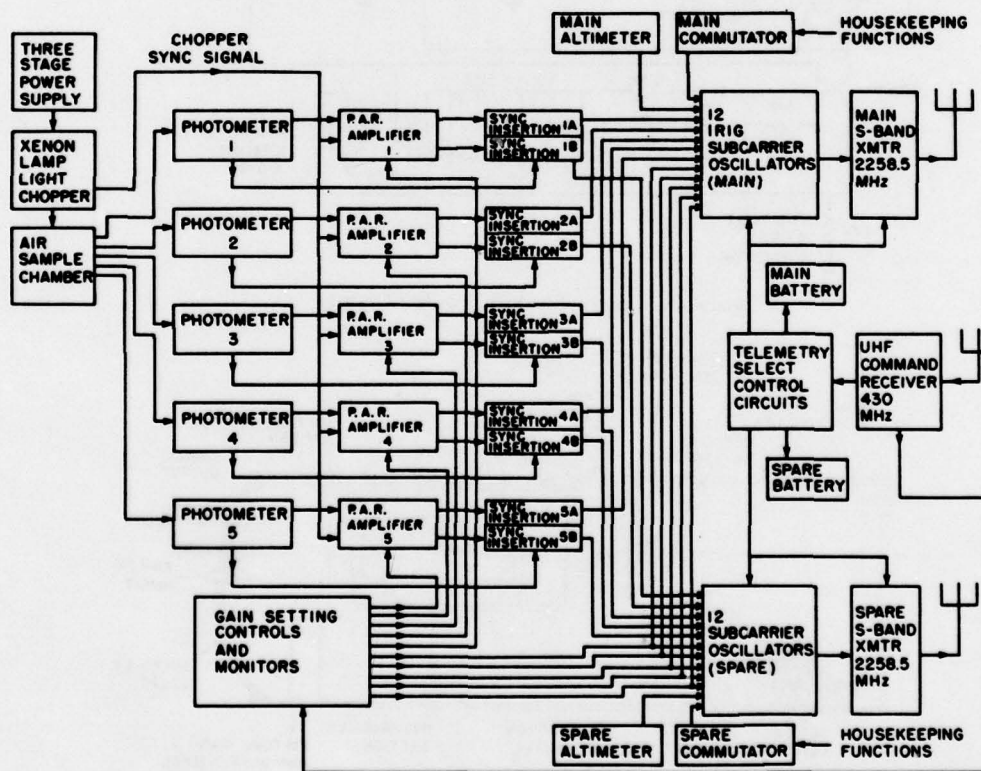
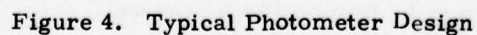
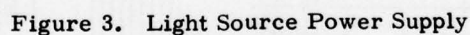


Figure 2. System Block Diagram



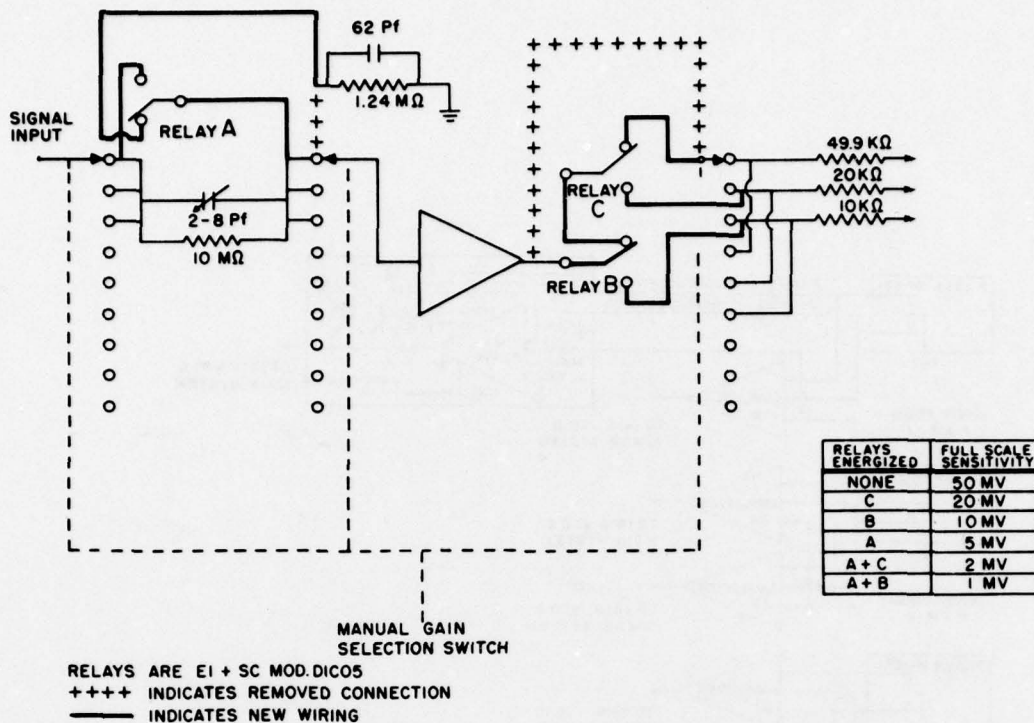


Figure 5. Amplifier Remote Gain Switching Diagram

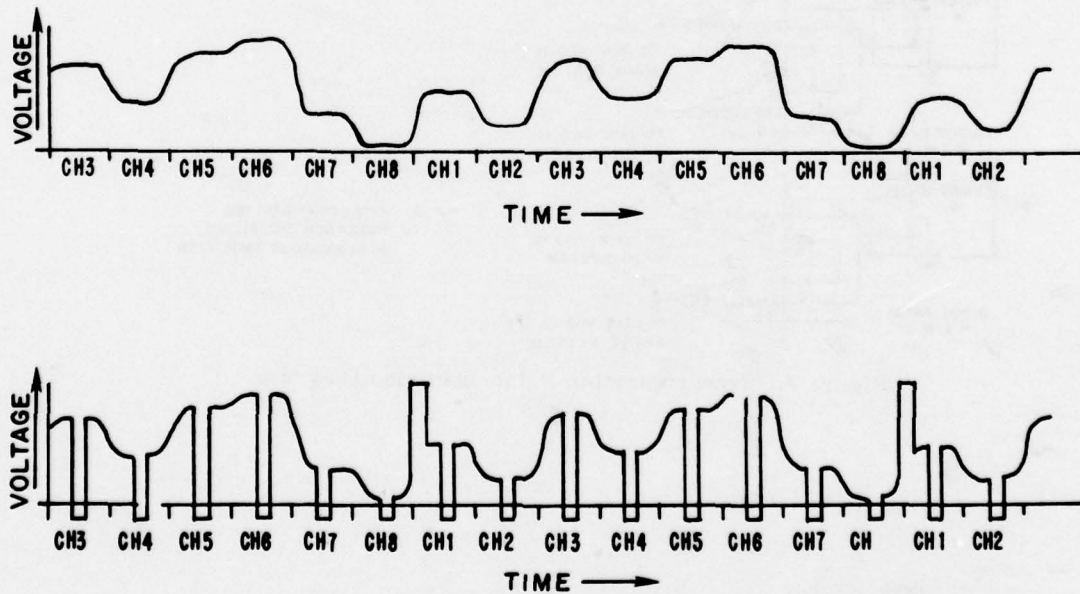


Figure 6. Typical Signal Output and Synchronization Pulses

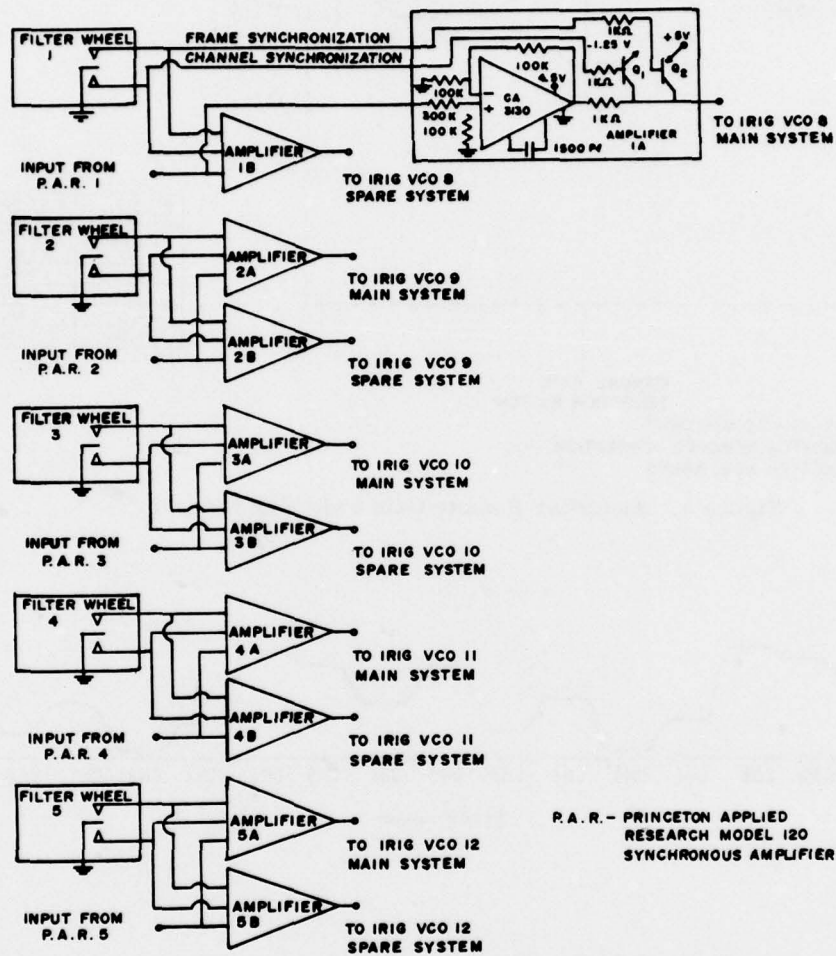


Figure 7. Synchronization Pulse-Insertion Diagram

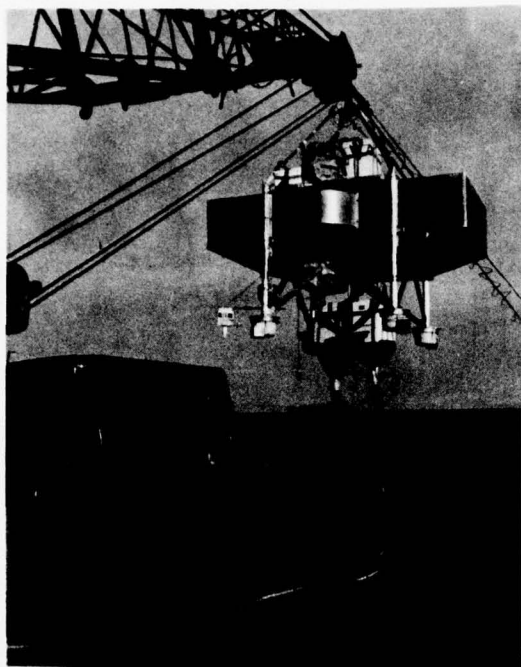


Figure 8. Experimental Payload
Prior to Launch



Figure 9. Experimental Payload
at Launch

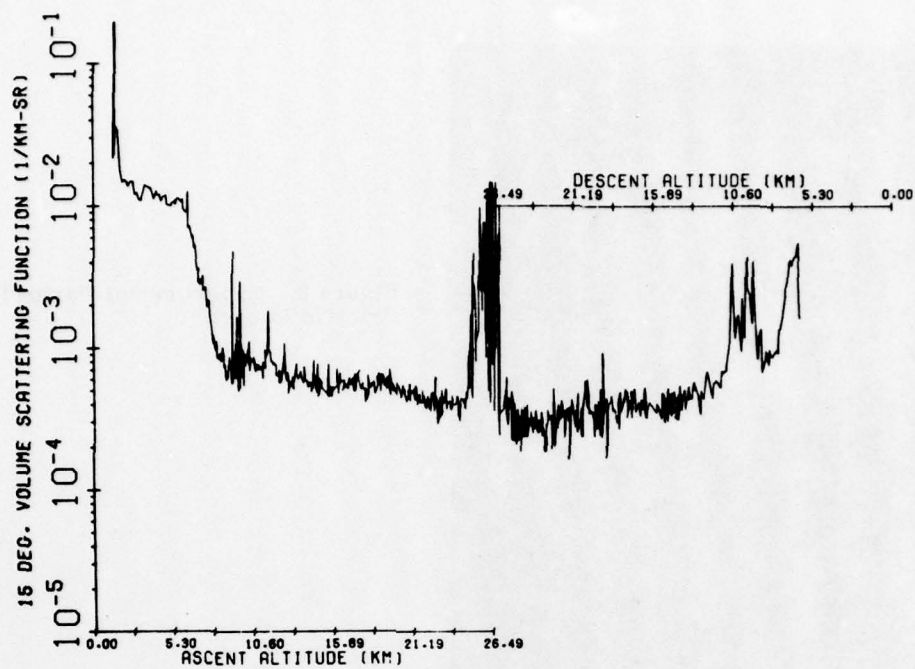


Figure 10. 15° Volume Scattering Function vs Altitude at 0.515 μm

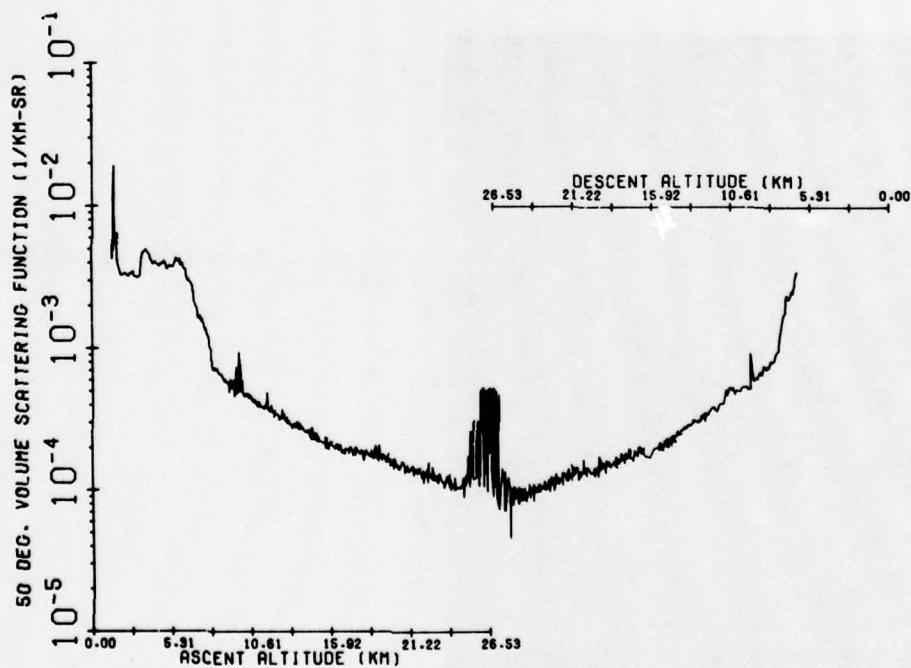


Figure 11. 50° Volume Scattering Function vs Altitude at 0.515 μm

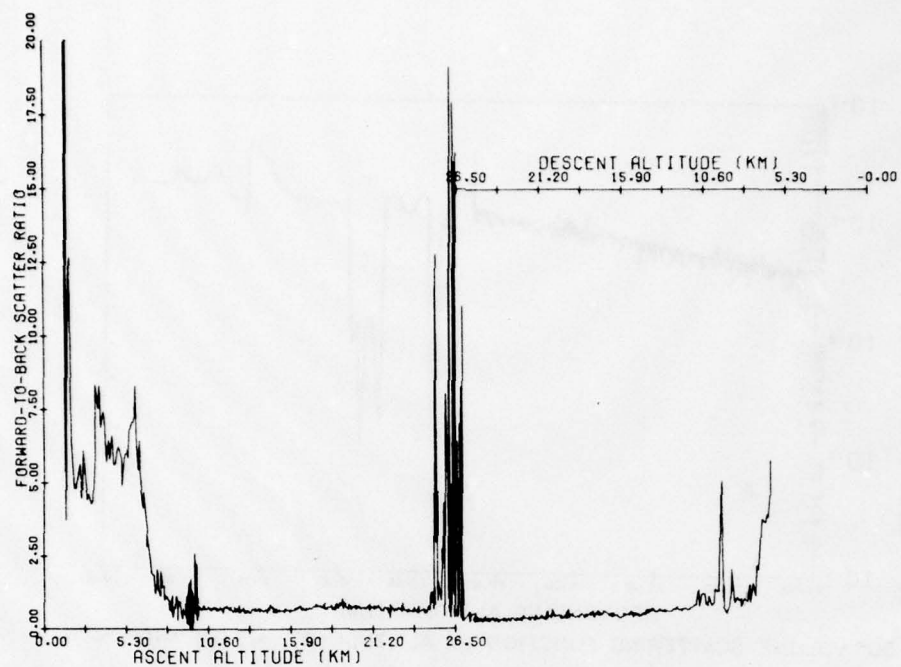


Figure 12. Forward-to-Backscatter (Dissymmetry) Ratio vs Altitude at $0.515 \mu\text{m}$

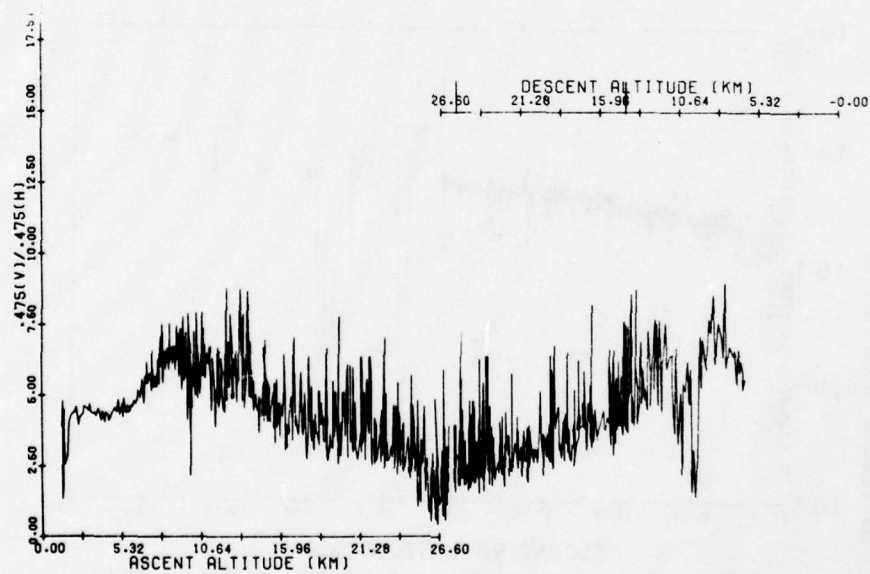
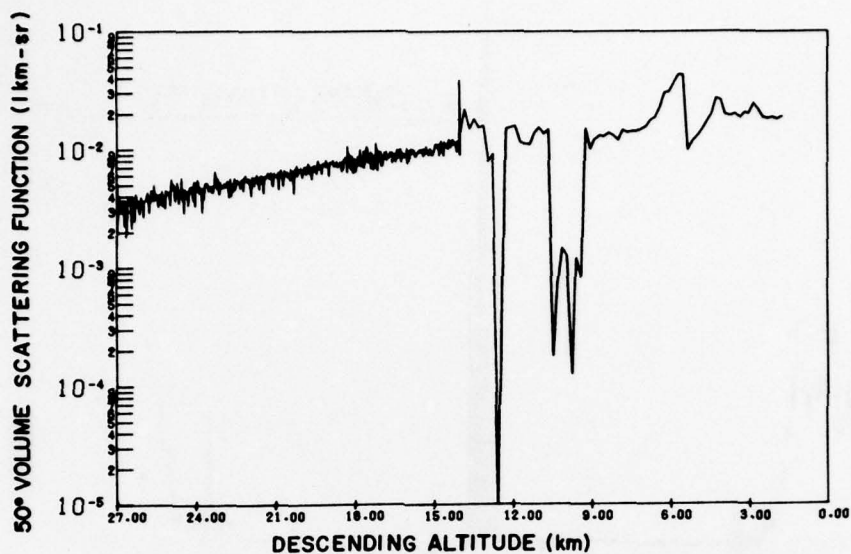
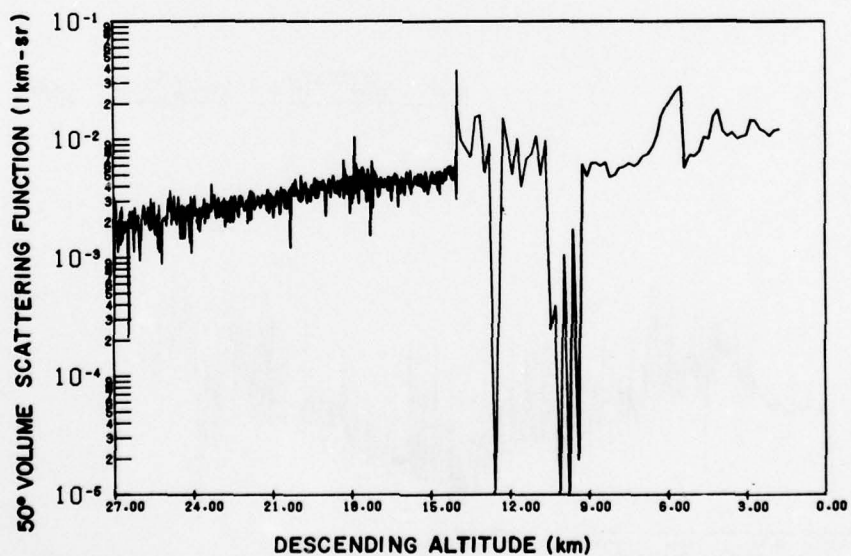


Figure 13. 100° Polarization Ratio vs Altitude at $0.475 \mu\text{m}$



50° VOLUME SCATTERING FUNCTION vs. ALTITUDE AT .475(V) MICRON

Figure 14. 50° Volume Scattering Function vs Altitude
(14 September 1976 Flight)



50° VOLUME SCATTERING FUNCTION vs. ALTITUDE AT .475(H) MICRON

Figure 15. 50° Volume Scattering Function vs Altitude
(14 September 1976 Flight)

AUTOMATIC LOW TENSION INHAUL WINCH SYSTEM
FOR SLACK LINE ABATEMENT

Wm. C. Lane
Otis Engineering Corp.
Dallas, Texas

ABSTRACT

The Special Products Department of Otis Engineering Corporation, OEEO, has developed a high speed automatic inhaul winch system for prevention of slack line in balloon tethering systems. Automatic inhaul begins when line tension drops below a preselected actuation tension. The winch will accelerate as required to maintain this tension. Inhaul ceases as line tension returns to an acceptable value. The system consists of a constant torque storage drum and an overrunning clutch. The paper discusses the system background, its operation, and the predicted performance.

1. BACKGROUND

With the current advancements in balloon and aerostat technology, supporting systems are tasked with keeping pace. Diverse types and sizes of tethered lighter than air vehicles have necessitated many distinct winching systems. Severe operating environments in remote locations demand rugged reliable support equipment resistant to corrosion

and abrasion. Winching systems have become more powerful, faster, and more sophisticated to meet growing operational demands.

Recently the potential value of using special winching systems to counteract balloon flight problems has been studied by OECO. The two flight problems felt to be most suited for correction by winching systems were excessive line tension and slack line. In the first instance the winch must relieve the line of energy. Slack line presents the opposite problem of requiring the winch to do work on the line.

Excessive line tension carries the obvious threat of a broken tether. It is generally the result of rapid lateral or upward movement of air masses surrounding the balloon. The solution to this problem is also obvious; outhaul line to relieve the tension. This can be accomplished with a brake that slips at a given tension, or a transmission which resists motion but does not prohibit it under high loads. Either method can be made to be automatic. Several systems are being examined by OECO engineers for future winch applications.

Slack line conditions result from violent atmospheric disturbances or aerostat operational problems. Loss of buoyancy or lift can cause a sudden loss of line tension. In some instances rain water on the aerostat skin has added sufficient weight to cause dramatic descents (Mertens, 1975). One such incident resulted in a rain soaked aerostat plunging earthward at 1000 fpm and landing tail down in a nearby lagoon (Masch, 1972, Flight Test Summary). Recovery operations included dismembering trees to free the entangled tether as the balloon began to rise. While on the ground the tether cable was severely chafed (Masch, 1972, Flight Test Incident).

Although line abrasion and entanglement are the primary villains, another problem may result from slack line conditions. If the line tension returns suddenly an impulse load can occur when the slack is taken up. This might result in damage to the tether and balloon.

One method of solving the slack line problem is to inhaul at low tension before the line can become slack. This winching requirement is more stringent than relief of high tension since work must be done by the winch rather than by the balloon. In some incidents the operator reaction time and winch response were insufficient to cope with line becoming slack. Therefore, an effective slack line abatement system must automatically inhaul rapidly when tension becomes too low without requiring operator interaction.

OECO performed a feasibility study for one balloon winch customer in January and February of 1978 aimed at precluding possible line tension related problems. The study examined retrofitting existing OECO winches with automatic high tension relief and high speed low tension automatic inhaul systems. A reworked hydrostatic transmission was proposed as the tension relief system. This required an automatic brake release, secondary transmission pumps, and increased transmission cooling to dissipate the work input to the winch.

The proposed low tension automatic inhaul system involved adding a second drive transmission capable of high speed at low torques. The main drive transmission would be isolated by a clutch to avoid overspeeding during the automatic inhaul. Low tension would initiate inhaul. The power would be diverted to the high speed transmission as the main transmission is clutched out.

The proposed solutions required extensive winch rework to obtain the automatic features and higher speeds. OECO recommended that the customer consider a new winch system designed specifically to accommodate these features.

Since the study OECO has begun development of a series of modular winches primarily for balloon tethering systems. Concurrently, systems to abate high tension and slack line were studied further in hope of incorporating them into the new modular winches. Although several high tension relief systems were promising, a simple solution to the slack line problem seemed elusive. Finally after many design iterations, a simple system was formulated which could preclude slack line automatically. It could also be added as a bolt on option to the proposed modular winch systems.

2. SYSTEM CONCEPT

The basic OECO Modular Winch consists of a spooling unit and a traction unit (Figure 1). A powered pumping unit located near the winch provides hydraulic power for the winch. An automatic inhaul system for low line tensions can be added with minimal modifications. It consists of a storage drum with a constant spooling torque and an overrunning clutch located in the capstan drive line (Figure 2).

During normal operation the balloon exerts a strong pull F_B on the capstan in the outhaul direction (Figure 3). The resulting capstan torque is balanced primarily by the capstan drive system reaction

T_R . The storage drum maintains a constant torque. This results in a relatively constant low spooling tension F_D pulling on the capstans toward the inhaul direction.

The overrunning clutch can only transfer torque loads in one direction and slips for reverse loads. It is oriented in the capstan drive system to engage against outhaul torque loads exclusively. Therefore when the balloon tension is normal ($F_B > F_D$), the clutch acts as a rigid coupling, transmitting torque from the capstans to the brake and motor. The winch can inhaul and outhaul normally in this condition.

However, when the balloon line tension drops below the drum spooling tension ($F_B < F_D$) the net capstan torque is in the inhaul direction (Figure 4). The clutch disengages automatically as it cannot hold capstan inhaul loads. This arrangement allows the storage drum to inhaul line through the capstans past the capstan brake and drive motor. The drum accelerates as required to maintain its preset spooling tension. Therefore, the balloon line tension is held near the drum spooling tension. Small differences between the balloon line tension and the spooling tension are expected due to gear box resistance and system inertia during acceleration. This automatic inhaul retards and ceases as the balloon line tension rises above the spooling tension.

With this system the capstan brake and motor are isolated during automatic inhaul by the clutch. Thus the automatic inhaul can be activated during normal inhaul, outhaul, or neutral (braked) operation. Manual control of the storage drum spooling tension and the storage drum brake provide overrides for the automatic system. The inhaul actuation tension can be selected by varying the storage drum spooling tension.

3. SYSTEM PERFORMANCE

The performance of the system is constrained by the drum maximum speed, capstan gear box speed, inertia of the rotating parts, and the spooling tension limits. In the OECO Modular Winches the drums are balanced and the drum drive components can be sized to accommodate high speeds. The maximum capstan speed is limited by the capstan gear box bearings.

The actuation tension is bounded by the storage drum spooling tension. The minimum tension is a function of cable composition, stiffness, and diameter. The maximum actuation tension is dependent upon the structural integrity of the drum and levelwind.

Table I presents the predicted performance limits of one OECO Modular Winch for 1/2 inch steel cable with the automatic low tension inhaul feature. Although winch characteristics vary with component selection, the data presented represents the maximum line pull configuration. Other 1/2 inch cable units exhibit higher normal performance speeds with lower maximum tensions. Overrunning speeds can be increased above 1000 fpm by placing the clutch within the gear box to isolate the first stage reduction bearings. This would require special gearing to be fabricated.

Table 1. Predicted Performance

Normal Operation	
Maximum tension	30000 lb.
Maximum speed	700 fpm
Automatic Inhaul (bare drum)	
Maximum actuation tension	2000 lb.
Minimum actuation tension	500 lb.
Maximum speed	900 fpm
Maximum acceleration (2000 lb. tension)	7 fps ²

Field testing of the system is awaiting completion of the OECO Modular Winch development. Actual performance data will be collected as various modular winches are completed.

This system represents a cost effective advancement in balloon protection. Its simplicity should lead to an excellent reliability and maintainability. Therefore, it is felt to be a viable answer to balloon slack line problems.

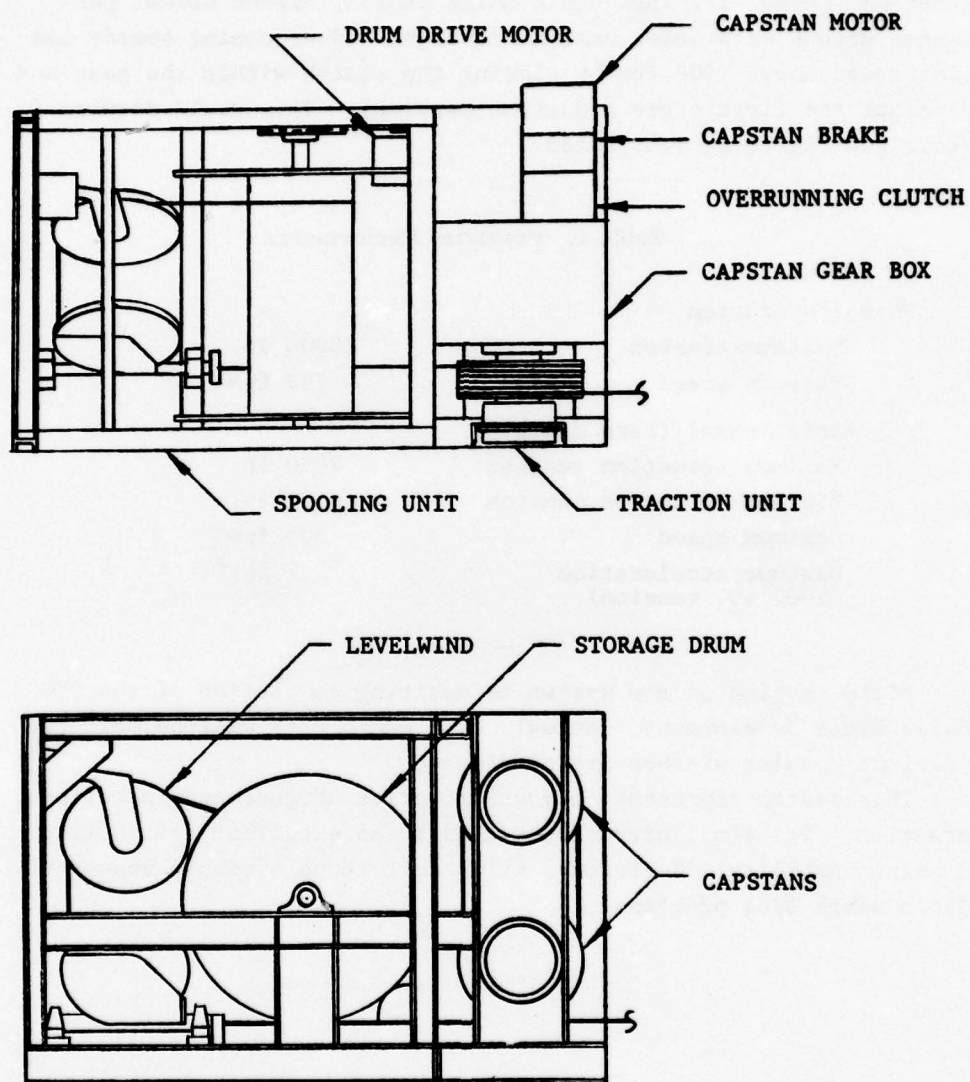


Figure 1. OEKO Modular Winch

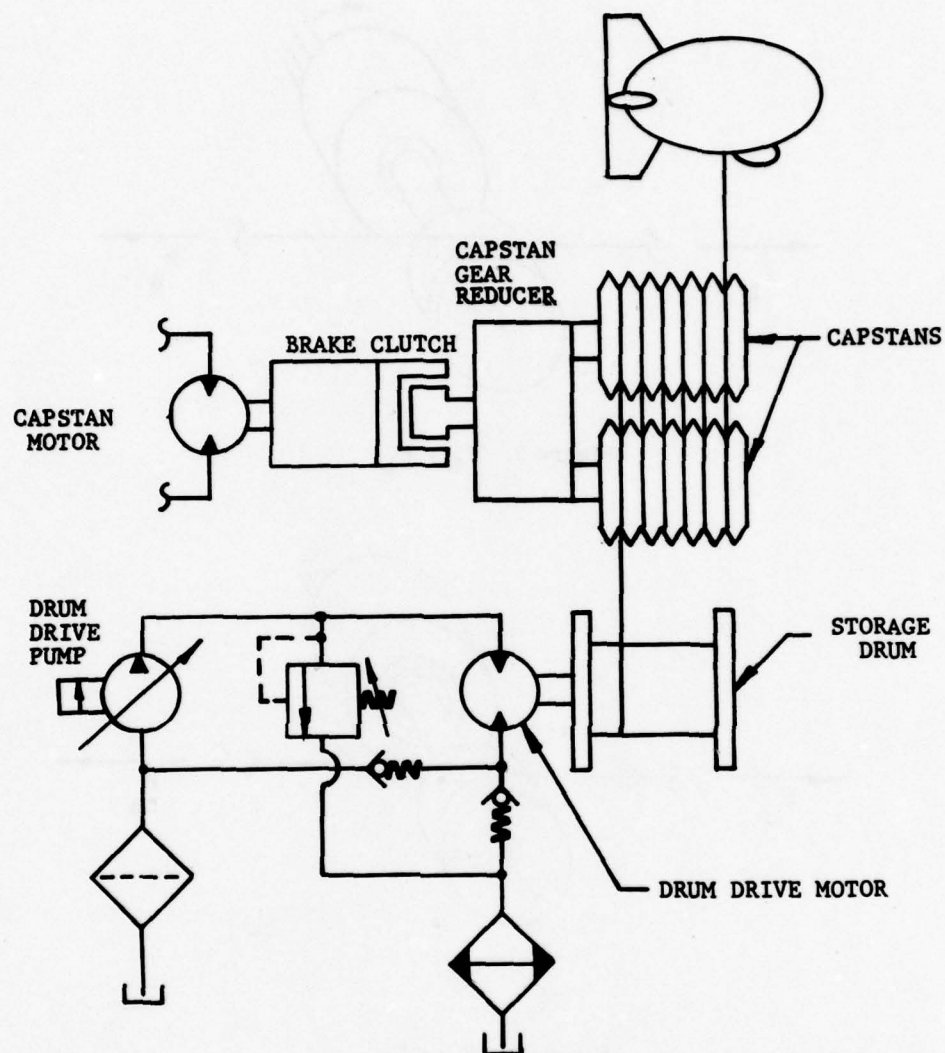


Figure 2. Automatic Low Tension Inhaul System

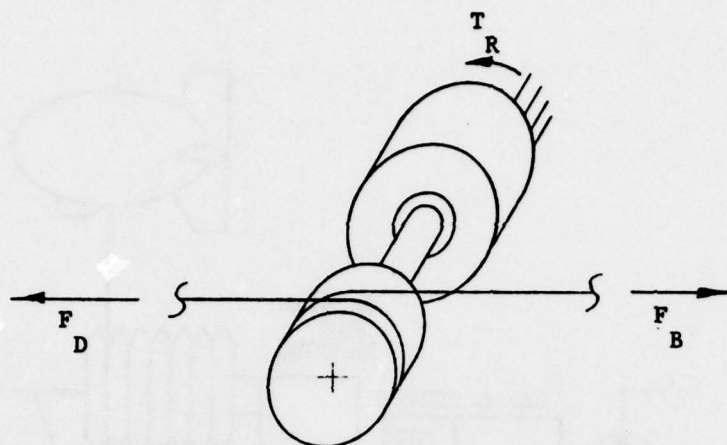


Figure 3. $F_B > F_D$

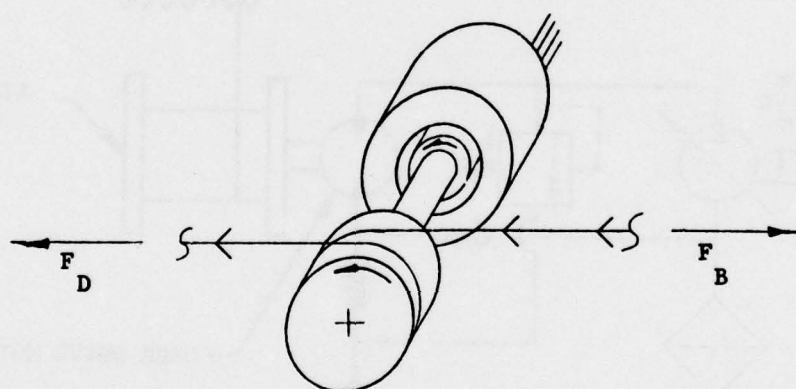


Figure 4. $F_B < F_D$

ACKNOWLEDGMENTS

The author would like to thank Lt. Colonel A. L. Calton, Patrick Air Force Base, for the timely release of documents to support this effort.

REFERENCES

- Masch, H. D. (1972) Flight test incident, Test 201-44, 28 August 1972. Unpublished RCA internal correspondence to R. P. Murkshe, TELTA project manager.
- Masch, H. D. (1972) Flight test summary, Flight test no: 201-44, 28 August 1972. Unpublished.
- Mertens, L. E. (1975) Thunderstorm encounter - Flight no: 206-37, 20 August 1975. Unpublished RCA internal correspondence to R. P. Murshe, TELTA project manager.

Session IV
AIRSHIP DESIGN CONCEPTS

Chairman, Norman J. Mayer
NASA Hqs.

Contents

1. Introduction
2. U.S.S. LOS ANGELES
-Hull Structure
3. U.S.S. LOS ANGELES
-Outer Cover
4. Water Recovery
Development
5. References
6. Memorandum Tests of
A&R Dept., Eng. Div.,
LNAS

RECORDS OF MAINTENANCE AND REPAIR OF RIGID AIRSHIPS

*

D.E. Woodward and H. Walker, Jr.
Association of Balloon & Airship
Constructors (ABAC)
P.O. Box 7
Rosemead, CA 91770

Abstract

This paper provides a summary text of state-of-the-art development of rigid airship hull structures, outer cover and water ballast recovery from exhaust gases as experienced by the United States Navy in the 1920's and 1930's. An extensive bibliography listing applicable Serial Reports of the Assembly and Repair (A&R) Department of the Lakehurst Naval Air Station is also provided. (GEW)

*Directors, ABAC

1. INTRODUCTION

The main purpose of this paper is to present its bibliography, which lists about 80% of the Serial Reports of the Assembly and Repair (A&R) Department of Lakehurst Naval Air Station. These are from the collection of Mr. Hepburn Walker, Jr., as are all but one or two of the other references which have been used.

The highest numbered report in this collection is #443, which

dates to 1939, while the lowest is #7, of 1922. There are 343 serials listed here, so about 100 are missing. All of the reports listed, both in the main bibliography and in the additional references, have been copied into the Technical Library of the Association of Balloon and Airship Constructors (ABAC); this association has supported the preparation of this paper.

The following short discussions illustrate the usefulness of these reports in three technical areas: the longevity of the hull structure of the USS LOS ANGELES; (the longest-lived of all rigid airship hulls); the outer cover of the LOS ANGELES; and the development of water recovery apparatus in the U. S. Navy.

2. USS LOS ANGELES -- Hull Structure

When the Zeppelin LZ-126 (to become the ZR-3, USS LOS ANGELES) was delivered from Germany in October, 1924, only a very limited amount of technical information on its hull structure came with it. (A great amount of information in the Design Reports and other documents of the Inspector of Naval Aircraft, Friedrichshafen -- LCDR Garland Fulton -- does not seem to have been readily available to the Lakehurst A&R Department.) One of the technical documents delivered, "Behandlung der Gerippekonstruktion" gives brief general instructions on girder repairs, with illustrated specifications for channel splices, as well as examples of initial shear wire tensions, and those of the car suspension cables and the wiring of the fins.

Because of the scant information furnished, the A&R Dept. devoted considerable efforts to testing the structural elements of the ship. These tests are reported in Serials 197, 198, 200, 202, 203, 208, 222, 235, 287, and 288.

In the Winter of 1924, calcium chloride was used as antifreeze in the ballast water, and wherever it spilled on the duralumin structure, serious corrosion was evident by February, 1925. (The German Navy had the same problem in the Winter of 1917, when alcohol and glycerine antifreeze were in short supply.) This corrosion led to many girder channels and joints being removed for tests, which are reported in Serials 221, 228, 230, 232, 234, 243, 271, 273, 274, and 295; Schmidt's report on corrosion protection also applies. During 1925, a wholesale reconstruction of the keel and adjacent structure was required.

When delivered, the ship's structure showed no concern for corrosion protection, so the immediate areas around keel hatches, the climbing shaft, and the valve hoods were varnished. These areas, however, continued to show occasional mild corrosion caused by the entry of moisture. As various parts of the ship were worked on, during replacement of gas bags or outer cover, for example, the accessible girders and wiring were painted with spar varnish. After the Panama flight of 1928, when the LOS ANGELES spent some time in tropical rainstorms at the PATOKA mast during the return, there was a remarkable spread of serious corrosion throughout the entire structure. This appeared to be due to excessive moisture absorption by the cover, and retention by it and the gasbags where they contacted the cover. Report 345, which is a summary of structural history up to 1930, covers this episode.

Report 345 was prepared in conjunction with a Board of Inspection and Survey in April, 1930; reports 344, 346, 347, and 348 also refer. Beginning in 1927, it was the practice to remove sample channels and lattices from the ship annually, for test by the Bureau of Standards. A very extensive set was removed at the time of this BIS, and additional

samples were supplied to the Aluminum Company of America and to Good-year-Zeppelin. (Both Dr. Durr, the constructor of the LOS ANGELES, and Dr. Arnstein, her structural designer, assisted in this inspection.) Report 346 shows the locations from which specimens were removed, and 348 illustrates the unexpected collapse of a keel side-brace girder which then occurred, and discusses the steps taken to replace it.

After LOS ANGELES was decommissioned in 1932, structural records are scanty. She was inspected by quarterly (later annual) hull boards, and the annual submission of girder test specimens to the Bureau of Standards continued.

After the loss of the MACON in 1935, it was proposed to cut down the LOS ANGELES by removing the three largest amidship bays and the two forward engine cars, and replacing the passenger quarters and bridge by a MACON-type control car. It was considered that the ship was only half as strong as required for gust encounters, and cutting-down would alleviate this potential weakness.(439)

The final BIS of January, 1939, found that there was obvious corrosion in girder channels in which dirt could collect and retain moisture, and where the lay of the cover against the girders had the same effect. However, the 1939 report of the Bureau of Standards (quoted in the BIS report) concluded, "Whatever increase in corrosion or change of strength may have taken place in these channels and lattices during the last seven years is not great enough to be shown by the tests." The corrosion was mainly superficial, and the BIS concluded, "Inspections and tests indicate that the aluminum alloy structure of the ship is generally sound."

Another aspect of the A&R Department's work was on the ship's wiring. On the very first ZR-3 flights there had been broken bulkhead

wires, and these continued to break throughout the ship's life. (344) Investigation showed that failure was always where the wire bent in forming the loop over the cast saddle in the transverse girder joint, and appeared to be due to a lack of quality control at Friedrichshafen. Many of the loops were two or three times as long as they should have been. By the 1939 BIS, virtually all of these original German bulkhead wire eyes had been replaced by a design which the Naval Aircraft Factory had developed for the SHENANDOAH, and gave no more trouble. In order to make such replacements and other wire repairs, data were developed on the physical characteristics of German wire in comparison with American, optimum geometry of splices, and fluxes compatible with both kinds of wire and not corrosive to either structure or fabric work. These investigations are in Reports 206, 269, 276, 277, 279, 344, 376, and 397.

The BIS of 1939 concluded that the shear and bulkhead wiring was in fair condition, although a considerable amount of rusting was apparent where the wires were in contact with the gas cells. Some irregular slackness in the shear wires was thought to be caused by the practice of keeping the ship always in a static hogging condition. Tests showed, however, that the wiring all participated in resistance to shear loads, and returned properly to its original tension when the loads were removed.

3. USS LOS ANGELES -- Outer Cover

We are fortunate that Mr. Walker's collection included Design Report #26 of INA Friedrichshafen, which deals in great detail with the design, construction, and application to the ship of the outer cover. After delivery to Lakehurst, a few modifications were made. For example, the covers between Longitudinals 5 and 6, on both sides, had been put

on in 45 meter lengths. To improve the tailoring and help maintain tautness of the cover, extra circumferential lacing wires were provided around the tops of several main frames to divide these long covers into 15 meter (one bay) panels. (345)

There were occasional replacements of small areas with new American panels. (240) The top of the ship, above Longitudinals 3, was redoped in November, 1926, and the entire old cover two years later. (345) These coats of nitrate dope were, of course, put on over the German acetate dope.

The A&R reports record many tensile strength tests of the German cover over its lifetime. A major overhaul of the ship in November, 1930- January, 1931, gave an opportunity to test the German cover thoroughly, and it was found to be in excellent condition, with three exceptions: - (1) the extreme bow, which was subjected to high dynamic air pressures and severe rain impact; (2) areas of particularly heavy traffic, such as along #6 Longitudinal and in the lower fin; (3) mildewed spots, which resulted from contact between the cover and the gas cells, causing moisture to be retained between them. The German cover at this time was nearly seven years old. (370, 370A, 375)

In April 1931, and January 1932, some of the light German fabric (which covered most of the ship except for the bow and fins) was replaced; it was in generally fair condition for tensile strength, although the fill was noticeably weaker than the warp. This was considered to be caused by overstretching during installation. Tear strength, however, was very low. (393, 395)

In March, 1932, panels of heavy German fabric near the bow were removed which showed (in some scattered areas, not generally) very low tensile strength, particularly in fill. (401) In the following month,

considerable deterioration was also reported in lightweight German panels. (406) There was also much flaking of the two (or more) coats of American dope away from the original German dope, which was noted as still having excellent adhesion to the fabric. And by October, 1932 eight years after the delivery flight from Friedrichshafen, all the German cover panels were reported as having very low tear strength, and poor (in fill) to fair (in warp) tensile strength. (417) By this time, of course, the LOS ANGELES was out of commission, and the history of the outer cover from then on is poorly known. By the time of the 1939 BIS, the entire cover was in poor condition due to slackness and loss of strength, and would have required total replacement in overhauling the ship for a return to flight status.

4. WATER RECOVERY DEVELOPMENT

The development of water ballast recovery from engine exhaust gas in the U.S. Navy was for the purposes of maintaining static equilibrium as fuel was consumed, without valving expensive helium, and of gaining ballast for such emergencies as gas-cell deflation, replacing the weight of fuel ballast available early in flight. The possibility of recovering ballast in this way arises from the fact that the combustion of gasoline yields an exhaust gas containing substantially more weight of water vapor than the weight of fuel consumed. The exact proportion depends on fuel composition, fuel/air ratio, humidity of the intake air, and details of combustion. The limits for gasoline are about 135% to 150%, with 145% a fair average. Although this may seem ample, it must be realized that the relative humidity of the exhaust, at some 1600°F, is far below saturation, so that a large volume of hot gas must be cooled to its dew point, about 125°F, before any water can be condensed. Whatever water vapor saturates the exhaust gas at the

final discharge temperature and pressure is necessarily lost overboard, so cooling to as near ambient air temperature as possible is required. At 80°F gas temperature, approximately 100% recovery is possible, and as much as 127% at 60°F. Gas temperatures have usually approached ambient air within 10 - 15 degrees in coolers of practical size.

Perhaps suprisingly, recovery of 100% of the fuel weight has not been difficult, provided the weather was cool, the apparatus didn't leak, and internal soot and oil didn't interfere too drastically with heat transfer. It takes only a thin layer of carbon inside the condenser to reduce the flow of heat dramatically, and ease of cleaning therefore proved to be essential to the efficient operation of water recovery.

After some false starts, the first apparatus to recover water in flight was designed by the Bureau of Standards and flown in the Army non-rigid D-3, in 1920 - 1922. To achieve a large heat transfer area with low weight and back pressure, the condenser was made of 3 banks of 50 thin-walled aluminum tubes, each 1 inch in diameter and 20 feet long. This condenser easily handled the exhaust from two 125 hp engines without excess back pressure, and recovered 80% of the fuel burned, with some leakage apparent. Its weight was 450 pounds, about 1.8 pounds per horsepower.

For rapid availability, it was decided to equip the USS SHENANDOAH with copies of the Army condensers, with such modifications as would overcome apparent faults. The long, unsupported tubes vibrated and sagged, and were mechanically awkward to rig to the engine cars. The entire condenser was therefore "folded" into a 5-foot cube, with 45 tubes running back and forth between 14 cast aluminum headers. A separator was also fitted to the condenser outlet, with zig-zag plates to remove water droplets from the cool gas; this increased the water

recovery by as much as a third. The weight of the apparatus showed a modest increase to about 470 pounds, or 1.6 lb/hp at the 300 hp rating of the Packard 1A-1551 engines. Early flight test results with this apparatus gave a recovery of 110% of the fuel consumed. Temperature measurements at many points in the condenser showed it to have too much cooling capacity and therefore unnecessary weight and drag. Redesign to cut down the number of tube banks was undertaken, but had not been completed before the loss of the SHENANDOAH. The soot problem showed up dramatically after the ship's transcontinental flight; the three condensers fitted had weighed an average of 471 pounds before the flight, and 520 after. (210) (The airship's Commanding Officer also mentioned operational problems caused by decreasing water recovery during the leg from Puget Sound to San Diego.) Small corroded holes in the tubes were also discovered when bubbles of "gum" were blown through them by the exhaust pressure. (219)

In an attempt to reduce both weight and drag, an experimental fabric condenser was constructed at Lakehurst and fitted to Car #5 of the SHENANDOAH. A small steel tube precoolers on top of the car was connected to a condenser formed of a rectangular duralumin frame, covered on the sides with doped fabric, and mounted in place of the outer cover in four panels of the hull. This fabric condenser was effective and was unharmed by the exhaust gases, but it leaked fumes into the ship's interior, and drummed and vibrated so badly that the ship's C.O. refused to keep it installed. (362)

Another false trail was an experiment with passing the exhaust gases through a container of calcium chloride. The amount of water recovered was negligible. (153)

The LOS ANGELES was at first fitted with spare SHENANDOAH condensers which were soon cut down to 8 banks of tubes, and had side curtains and winter shutters added. These were adequate for the 400 hp Maybach VL-1 engines with which the ship was originally equipped. When the engines were uprated to the VL-2 type, of about 525 hp, it was necessary to increase to 10 tube banks. (238)

Tests with fabric condensers were no better than in the SHENANDOAH. The fabric condenser was replaced with an all-duralumin flat box, of which the outer side had longitudinal corrugations protruding into the windstream. This "Mark III" apparatus was incorporated into the Goodyear-Zeppelin proposals for the ZRS-4/5. Flight tests in the LOS ANGELES, however, resulted in the welded seams of the corrugations opening and leaking so much gas that very unsatisfactory recovery was realized. (362)

Further separator development was also carried out on the LOS ANGELES. The baffle-type separator inherited from the SHENANDOAH was superseded by a centrifugal "Hagen" type, similar in principle to a cyclone air cleaner. (355) There was a distinct increase in water recovered, and this type remained the standard, although tests were also made on a counter-flow separator based on gas drying apparatus used in the Lakehurst helium plant. (408)

The Goodyear-Zeppelin apparatus installed in the AKRON and MACON had condensers consisting of 14 panels of longitudinal tubes fitted in the mainframe above each engine room. The tubes which first took the hot exhaust were steel; heavy, medium, and light-gauge aluminum was used as the gases cooled. These tubes fitted over elbows welded to headers within the cover, to reduce drag. The tubes were coated internally with Bakelite to prevent corrosion and soot adhesion; if scratched

or punctured, the Bakelite had to be recoated by a tedious hand process. (R11, 415, 416, 420) (Cleaning the water recovery condensers was an "administrative punishment" on the MACON.)

The high point of Navy water recovery development was the Mark IV apparatus, developed at Lakehurst from an unsuccessful experiment made at the British non-rigid engineering base, Kingsnorth, in 1917. This consisted of a cross-flow gas-to-air radiator, with the exhaust gases led into a plenum surrounding numerous short aluminum tubes through which ambient air was forced by the ship's speed. The Kingsnorth unit had gummed up hopelessly after only a short trial, but it was believed at Lakehurst that more modern engines and fuels would be easier to deal with. The condenser was in the shape of a streamlined strut cut off at its leading and trailing edges, forming surfaces into which the air tubes were set in a hexagon pattern. Flight trials on the LOS ANGELES were promising. (384) The development continued with the AKRON. The original condensers had been fitted with internal baffles to lead the gases back and forth across the tubes, but these proved to be ineffective and also rubbed against the thin aluminum tubes and in time would cut through them. It was found necessary to increase the heat transfer area by adding precoolers, similar in design to condensers. The entry part of the precooler was stainless steel to take the heat, the remainder duralumin. Each Mark IV condenser saved about a third of the weight of the Goodyear-Zeppelin panels (740 lbs to 1152 lbs.), had lower back pressure, and gave greater recovery. They also were easier to clean; less soot collected, and the outboard side plate of the condenser was hinged to open for cleaning access. The AKRON progressively received Mark IV apparatus as overhaul periods allowed; by the time of the ship's loss, all but one engine had been fitted. (409)

The "MACON Operation and Upkeep" report commented that, operationally, it would be possible to maintain a "one week out, two weeks in" schedule, but if problems with the water recovery apparatus were solved (or if water recovery could be dispensed with), a "one week out, one week in" schedule might be achieved.

Subsequent to the period of the Lakehurst A&R Reports, water recovery was developed for LZ-130, Graf Zeppelin II, which was planned for helium inflation and used Diesel engines. The apparatus used a cooling system that the Navy had thought too heavy, a water-tube condenser for the exhaust gases with a separate radiator to cool the cooling water. The weight came out at 2200 pounds for each engine car; the normal rated output of the engine was 900 hp. No data are available on the amount of water actually recovered in flight.

Still later, proposed Navy developments of water recovery apparatus for K-ships and the ZPG-2's would have followed the LZ-130 gas-to-water heat transfer system. Neither, however, was actually constructed.

5. REFERENCES

Luftschiffbau-Zeppelin, "Behandlung der Gerippeskonstruktion" (1924?) (German with partial English translation)
13 pp. including 7 plates

Schmidt, K. (Lt., CC, ULN) "Protection of Duralumin against Corrosion" Lakehurst, March 23, 1925. 2 pp.

Navy Dept., Board of Inspection and Survey, "Report of Material Inspection of U.S.S. LOS ANGELES (ZR-3) Held 6 January 1939", ZR3/F3-1 (967-S), 27 May 1939, 14 pp. plus Appendixes A-G.

Inspector of U.S. Naval Aircraft Friedrichshafen a/B, Germany (G. Fulton) "Design Report #26, Outer Cover", 18 August 1923 (with Supplements to 18 July 1924), 45 pp. including illustrations.

Fravel, Lt. Col. Ira F. (AAS), "Water Balast (sic) Recovery for Airships", Aviation, November 19, 1923, pp. 625-6.

U.S. Navy Dept., "Rigid Airship Manual 1927", pp. VIII - 42-47.
University Microfilms, Ann Arbor, 1963.

Aero Engine Lab. Serial No. AEL-84, "Test of Water Recovery Apparatus for U.S.S. SHENANDOAH", Naval Aircraft Factory, 19 Sept. 1924.
63 pp. including curves, photos, data sheets.

Aero. Engine Lab. Serial No. AEL-85, "Flight Tests of Water Recovery Apparatus on U.S.S. SHENANDOAH", Naval Aircraft Factory, 20 Sept. 1924.
14 pp. including curves and photos.

Parker, H. P., "Installation and Flight Tests of Water Recovery Apparatus on Aft Centerline Car of U.S.S. SHENANDOAH" D-5-ZR-1-4926,
11 June 1924. 3 pp.

Bureau of Aeronautics, Material Division Progress Reports, Vol. IV,
No. 1, July - Sept. 1924, p. 23.

Goodyear-Zeppelin Co., "Operation Manual U.S.S. MACON", 1933,
pp. 81-82.

U.S. Naval Air Station Sunnyvale, "U.S.S. MACON - Doctrines and Policies for Operation and Upkeep", April 1935. University Microfilms,
Ann Arbor, 19 .

6. MEMORANDUM TEST REPORTS OF THE A&R DEPARTMENT,
ENGINEERING DIV., LNAS.

- #7 18 Oct. 1922, Fleet Airship ZR-1 Rubberized Tape used in securing wires, 1 pg., R.D. Weyerbacher
- #10 13 Nov. 1922, Fleet Airship ZR-1 - Test of Fuel Tanks between frames 97½ and 100. 2 pp. J.M. Kangeter
- #13 24 Nov. 1922, Gas Bag Test, Nov. 23, 1922, between frames 100 and 110, position 11. 2pp. J.M. Kangeter
- #16 28 Nov. 1922, Fleet Airship ZR-1 - Air Test of Gas Cell #11. 2 pp. plus 2 pp. Report of Wire Tensions. R.D. Weyerbacher.
- #19 20 Dec. 1922, Fleet Airship ZR-1 - Duralumin Rivets, Test of. 2 pp. J.M. Kangeter.
- #25 Jan. 8 1923, Springs for Controls, Minor, on ZR-1, Test of. 3 pp. J.M. Kangeter.
- #28 Jan. 24, 1923, ZR-1 Varnish Evaporation -- Test to determine percentage of evaporation.. 2 pp. J.M. Payne (Weight Office)
- #29 Jan. 27, 1923, ZR-1 Report on Dope Evaporation based on (2) Experimental Panels installed on ship at this station. 3pp. J.M. Payne (Weight Office)
- #30 Feb. 3, 1923, Test of Defective Duralumin Rivets. 3 pp. plus 1 print. C.C. Tripolitis

- #31 7 Feb. 1923, Exhaust Trunks - Weight of. 1 p. C.D. Tripolitis
- #32 7 Feb. 1923, Contract #54084 - Water Ballast Bags for Fleet Airship ZR-1 - Ordinary and Emergency Bags (Test of). 3pp. T. M. Ramsay
- #33 Feb. 10, 1923, Fleet Airship ZR-1 - Water Ballast Bags, Contract 54084. 2 pp. R.D. Weyerbacher
- #34 Feb. 16, 1923, Fleet Airship ZR-1 - Report of Test on Outer Cover Experimental Panels installed between frames #80, #120, and longitudinalinals C, E, and C' E'. 11 pp. J.M. Kangeter
- #38 March 2, 1923, Report of tests made on maneuvering valve with Gas Cell No. 11 inflated with helium. 1 p.
- #40 March 5, 1923, Fleet Airship ZR-1 - Test with Helium of Gas Cell #11, Feb. 19 to March 3, 1923. 19 pp. J. Work
- #45 Feb. 16, 1923, Report of Test made on Slipping Device for Slip Fuel Tanks. 1 p. T.M. Ramsay
- #46 March 14, 1923 Fleet Airship ZR-1 - Slip Tank Release Fittings. 1 p. R.D. Weyerbacher.
- #48 March 27, 1923, Test with Helium of Gas Cell No. 11 - Correction of Weights Applied during Test. 2 pp. C.D. Tripolitis
- #51 April 6, 1923, Test of Duralumin Rivets April 6, 1923, 1 p. J.H. Kangeter
- #53 April 11, 1923, Fleet Airship ZR-1 - Axial Cable, Test of. 2 pp. C.D. Tripolitis.
- #56 April 13, 1923, Fleet Airship ZR-1 - Test of Wire Grommets for Docking and Handling Ship at Frames #30 to #180 inclusive. 1 p. J.H. Kangeter
- #58 April 16, 1923, Helium Data obtained on recent Cell Test of ZR-1. 2 pp. R.D. Weyerbacher.
- #64 May 9, 1923, Test of Duralumin Rivets. 1 p. P.E. Ward
- #65 May 17, 1923, Test of 1/16" F.S. Covered Cable, Roebling, as used on ZR-1 Exhaust Gas Trunks. 2 pp. P.E. Ward
- #66 May 16, 1923, Fleet Airship ZR-1 - Tests of Fuel Line Valves with Shellaced Gaskets - effect of gasoline, alcohol mixture upon. 2 pp. P.E. Ward
- #68 May 23, 1923, Test of Fuel Line Valves with 1/16" thick, No. 6, Vellumoid Gaskets. 2 pp. P.E. Ward
- #71 May 26, 1923, Fleet Airship ZR-1 - High Potential Bonding Test on Structure and Attachments. 2 pp. J.H. Kangeter.

- #75 June 11, 1923, Test on Landing Clamp and Landing Spider. 1 p.
A. Heinen
- #80 Aug. 21, 1923, Strength of Car Struts. 1 p. C.D. Tripolitis
- #85 Sept. 4, 1923, Fleet Airship ZR-1 - Launching Report. 11 pp.
C.D. Tripolitis
- #87 Sept. 10, 1923, Fleet Airship ZR-1 - First Trial Flight Weights.
1 p. C.D. Tripolitis
- #101 June 18, 1923, Test of Major Control Sheave Feet. 1 p.
C.D. Tripolitis
- #102 June 5, 1923, Axial Cable Fittings. 1 p. plus 1 plan.
C.D. Tripolitis
- #103 June 11, 1923, Monthly Test of Duralumin Rivets. 1 p.
C.D. Tripolitis
- #104 June 13, 1923, Serving of No. 14, Galvanized Steel Wire. 1 p.
C.D. Tripolitis
- #105 June 14, 1923, Tool Steel - Strength of. 1 p. C.D. Tripolitis
- #106 June 6, 1923, Test of Fuel System with 50 lbs. air pressure.
1 p. P.E. Ward
- #107 June 15, 1923, Vibration Test of Welds and Method of Securing
1" Manifolds used on Fuel System of ZR-1. 2 pp. P.E. Ward.
- #108 June 29, 1923, Test of Fastenings on Maneuvering Valve Cables to
Control Box. 1 p. C.D. Tripolitis
- #109 July 3, 1923, Shackle for External Fin Wiring at Frame No. 0.
1 p. C.D. Tripolitis
- #110 July 12, 1923, Test of Serving of 1/16" Flexible Cable. 1 p.
C.D. Tripolitis
- #111 July 18, 1923, Test of Serving of 1/8" Galvanized Flexible Cable.
1 p. C.D. Tripolitis
- #112 July 16, 1923, Fleet Airship ZR-1 - Tests on Horizontal Fins and
Elevators. 10 pp. J. Work
- #113 July 21, 1923, Test of Turnbuckle, Standard Stock No. 34335-6.
1 p. C.D. Tripolitis
- #114 July 26, 1923, Fleet Airship ZR-1 - Test on and Adjustment of
Transverse Reinforcement for Mooring Point, Frame No. 180. 2 pp.
J. Work
- #115 July 26, 1923, Fleet Airship ZR-1 - Tests on Rudder Controls.
2 pp. J. Work

- #116 July 27, 1923, Fleet Airship ZR-1 - Outer Cover Doping - Evaporation. (Weight Office). 2 pp. J.H. Payne
- #117 July 27, 1923, Test of Vent Arrangement of Fuel System. 4 pp. C.D. Tripolitis
- #118 July 27, 1923, Test of Gasoline Tank for External Pressure. 1 p. C.D. Tripolitis
- #119 July 30, 1923, Fleet Airship ZR-1 - Final Test on Fuel Line with Gasoline. 2 pp. P.E. Ward
- #120 July 30, 1923, Fleet Airship ZR-1 - Proof Loading of Axial Cable Units. 2 pp. P.E. Ward
- #121 Aug. 6, 1923 Test of Snap Hooks for Suspension Bridles. 1 p. C.D. Tripolitis
- #122 Aug. 16, 1923, Periodic Test of Duralumin Rivets. 1 p. C.D. Tripolitis
- #123 Jan. 10, 1924, Wind Resistance of Car Suspension Cables. 4 pp. C.D. Tripolitis
- #124 Jan. 2, 1924, Test of Main Mooring Point Frame #180. 2 pp. C.D. Tripolitis
- #125 Jan. 24, 1924, U.S.S. SHENANDOAH - Final Report on Fuel System, including all previous Tests. 11 pp. P.E. Ward & R.D. Weyerbacher
- #126 April 18, 1924, Walkway Girder at A - investigation and strength of same. 2 pp. S.H. Phillips
- #127 Jan. 18, 1924, U.S.S. SHENANDOAH - Wind Resistance of External Fin Wires. 2 pp. S.H. Phillips
- #128 Aug. 18, 1924, U.S.S. SHENANDOAH - Mechanical Telegraphs for Airships. 3 pp. S.H. Phillips
- #129 Jan. 2, 1924, Test of Hand Rails of Control Car and Power Car #1. 1 p. C.D. Tripolitis
- #130 Oct. 29, 1923, Design Memo. No. 127, Stresses observed in the seventh trial flight of airship ZR-1 (Lakehurst to St. Louis and return) Oct. 1 to 3, 1923, and in shed bending tests. 6 pp. + 7 tables. C.P. Burgess.
- #131 Aug. 29, 1923, Test of Anchor Shackle, Navy Stock No. 12-S-59. 1 p. C.D. Tripolitis
- #132 Jan. 2, 1924, Test of Trolley Attachment Points at Frames #40 and #170. 1 p. C.D. Tripolitis
- #133 Sept. 20, 1923, Test of Defective Turnbuckles. 1 p. C.D. Tripolitis

- #134 Oct. 17, 1923, U.S.S. SHENANDOAH - Shed Test of Bow Mooring Equipment. 2 pp. C.M. Bolster.
- #135 Sept. 28, 1923, Test on Mooring Ship Cone. 1 p. P.E. Ward.
- #136 Sept. 28, 1923, Test on Handle for Gasoline Hand Pump. 1 p. P. E. Ward.
- #137 Nov. 5, 1923, U.S.S. SHENANDOAH - Stresses Indicated by Electrical Strain Meters on Flight of Oct. 27th, 1923. 1 p. J. Work.
- #138 Nov. 6, 1923, U.S.S. SHENANDOAH - Stresses Indicated by Electrical Strain Meters on Flight of Nov. 5, 1923. 1 p. J. Work.
- #139 Nov. 8, 1923, Kite Balloon Winch, Test of. 2 pp. C.C. Tripolitis.
- #140 Nov. 26, 1923, Proof Loading of Strut Shanks. 1 p. C.D. Tripolitis.
- #141 Dec. 1, 1923, U.S.S. SHENANDOAH - Stresses Indicated by Electrical Strain Meters on Flight of 16 Nov. 1923. 1 p. J. Work.
- #142 Nov. 28, 1923, U.S.S. SHENANDOAH - Stresses Indicated by Electrical Strain Meters on Flight of 20 Nov. 1923. 1 p. J. Work.
- #143 Dec. 6, 1923, Test of Steel Plate for Tension. 1 p. C.D. Tripolitis.
- #144 Jan. 3, 1924, Fabric Tension Meter, Model #1 - Test of. 5 pp., 1 chart, 1 sketch. S.H. Phillips.
- #146 Jan. 4, 1924, Test of Bow Mooring Equipment. 1 p. C.D. Tripolitis.
- #147 Jan. 5, 1924, U.S.S. SHENANDOAH - Stresses Indicated by Electrical Strain Meters on Flights of Dec. 15, 18, and 19, 1923. 1 p. J. Work.
- #148 Jan. 14, 1924, Kite Balloon Winch, Second Test of. 1 p. C.D. Tripolitis.
- #149 Feb. 8, 1924, U.S.S. SHENANDOAH - Test of Voice Tube from Frame No. 165 to Crew's Quarters. 1 p. P.E. Ward.
- #150 Feb. 15, 1924, U.S.S. SHENANDOAH - Investigation of Mooring Spindle, Installation and Damages to same on Jan. 16, 1924. 2 pp. J. Work.
- #151 Feb. 18, 1924, Test of Special Steel for Physical Properties. 1 p. C.M. Yater
- #152 Feb. 27, 1924, Test of Slack Adjuster Winch, U.S.S. SHENANDOAH. 2 pp. C.D. Tripolitis.
- #153 Feb. 27, 1924, Calcium Chloride Water Recovery System - Investigation of. 3 pp. S.H. Phillips.

- #154 March 10, 1924, Test of Tinned Aircraft Wires. 1 p.
C.D. Tripolitis.
- #155 March 3, 1924, U.S.S. SHENANDOAH - Keel Walkway, Investigation
and Test. 5 pp., including sketches. S.H. Phillips.
- #156 Feb. 21, 1924 U.S.S. SHENANDOAH - Bending Stresses During Flight
No. XXVIII of Jan. 16-17, 1924. 6 pp. + 1 graph. C.D. Tripolitis.
- #157 March 27, 1924, Moisture Test on Mahogany Wood. 1 p.
C.D. Tripolitis.
- #158 March 18, 1924, U.S.S. SHENANDOAH - Test of Turnbuckle To Be Used
In Connecting Axial Cable To Frame #194.75. 1 p. C.C. Tripolitis.
- #159 March 25, 1924, U.S.S. SHENANDOAH - Test of Dundee "A" Friction
Tape Used In. 2 pp. P.E. Ward & R.D. Weyerbacher.
- #160 March 22, 1924, Alignment of Rudder and Elevator Bearings after
Flight of. Jan. 16, 1924. - U.S.S. SHENANDOAH. 1 p. P.E. Ward.
- #161 March 25, 1924, Test for Compression of Special Angle for Cruci-
form Girder - U.S.S. SHENANDOAH. 1 p. C.D. Tripolitis.
- #162 March 25, 1924, U.S.S. SHENANDOAH - Corrosion Test of Unvarnished
Structure and Wires. 2 pp. P.E. Ward.
- #163 April 4, 1924, Test of Wire Terminal (Steel) Pad Fitted to .047"
Duralumin Plate, U.S.S. SHENANDOAH. 1 p. C.D. Tripolitis.
- #164 April 10, 1924, Test of 1/8" Flexible Cables and No. 9 Gauge
Steel Wire. 1 p. C.D. Tripolitis.
- #165 April 7, 1924, U.S.S. SHENANDOAH - Test of Fabric Tension Meter,
Model #1 and Tension in Outer Cover. 4 pp. + 3 charts.
S. H. Phillips.
- #166 May 9, 1924, Test of Specimin of Steel Furnished by Machine Shop.
1 p. C.D. Tripolitis.
- #167 May 6, 1924, U.S.S. SHENANDOAH - Tabulation of Weights and Pre-
liminary Calculations for Launching of. 3 pp. 1 table, 1 chart.
C.D. Tripolitis.
- #168 May 10, 1924, U.S.S. SHENANDOAH - Test on Fuel System After Repairs.
1 p. P.E. Ward.
- #169 May 20, 1924, U.S.S. SHENANDOAH - Calibration of Carbon Pile Bow
Weighing Device. 1 p., 1 graph, 1 sketch. S.H. Phillips.
- #170 May 21, 1924, U.S.S. SHENANDOAH - Test of Trail Rope Hatches as
Redesigned. 1 p. P.E. Ward.
- #171 June 3, 1924, U.S.S. SHENANDOAH - Test of Slip Release for Yaw
Line Cables and Main Mooring Cable, Frame 175. 2 pp. P.E. Ward.
- #172 June 3, 1924, U.S.S. SHENANDOAH - Test of 9/16", 6 x 37, Mooring
Cable. 1 p. C.D. Tripolitis.

- #173 May 17, 1924, U.S.S. SHENANDOAH - Report of Launching on 15 May, 1924. 14 pp. C.D. Tripolitis.
- #174 June 14, 1924, U.S.S. SHENANDOAH - Fabric Tension Meter, Calibration Chart for use with Grade "A" Fabrics and Tension of Bow Fabric. 3 pp., 2 charts, 1 photo. S.H. Phillips.
- #175 June 27, 1924, U.S.S. SHENANDOAH - Strength of Officers and Crew's Space Stiffening Girders as Manufactured Against a Substitution of Tubing. 2 pp. S.H. Phillips.
- #176 July 26, 1924, Test of Aluminum Alloy Castings. 1 p. C.D. Tripolitis.
- #177 Aug. 5, 1924, Kite Balloon Winch - Test of Brakes. 2 pp. S.H. Phillips.
- #178 Aug. 11, 1924, U.S.S. SHENANDOAH - Test of Droque Cable Stopper. 5 pp., 1 drawing, 2 photos. S.H. Phillips.
- #179 Oct. 21, 1924, U.S.S. SHENANDOAH - Test of Coupling for Mooring and Nose Steadying Guy Wires. 2 pp. S.H. Phillips.
- #180 Aug. 16, 1924, U.S.S. SHENANDOAH - Trim of, Due To Inter-change of Power Cars Nos. 2 and 3 with 4 and 5. 1 p. C.C. Tripolitis.
- #181 Aug. 28, 1924, U.S.S. SHENANDOAH - Test of Fuel System. 1 p. P.E. Ward.
- #182 Sept. 16, 1924, U.S.S. SHENANDOAH - Shear and Bending Moments in the Light Condition. 1 p., 3 tables, 1 graph. S.H. Phillips.
- #183 Sept. 23, 1924, U.S.S. SHENANDOAH - Test of Porcelain Insulator. 1 p. S.H. Phillips.
- #185 Sept. 23, 1924, Test of Cargo Trip Hooks Obtained from Thomas Laughlin & Co., Portland, Me. 1 p. S.H. Phillips.
- #186 Sept. 24, 1924, U.S.S. SHENANDOAH - Flexible Steel Wire (Tinned), 1/4" dia. 7 x 19 Strand, for use in Major Control System. 1 p. S.H. Phillips.
- #187 Sept. 30, 1924, U.S.S. SHENANDOAH - Tensile Strength of Fabrics Comprising Outer Cover in way of Insignia Paint. 3 pp. S.H. Phillips.
- #188 Sept. 27, 1924, U.S.S. SHENANDOAH & ZR-3 - Tensile Strength of Close Link Crane Chain for One Ton Direct Differential Hoist Used in Service Docking Operations. 2 pp. S.H. Phillips.
- #189 Sept. 24, 1924, U.S.S. SHENANDOAH - Investigation into the Redesign of Clapper Gear for E.R. Telegraphs. 3 pp. S.H. Phillips.
- #190 Oct. 2, 1924, U.S.S. SHENANDOAH - Flexible Steel Wire (Galvanized) 1/4" dia., 7 x 19 strand, for use in Major Control System. 1 p. S.H. Phillips.

- #191 Oct. 3 1924, ZR-3 - Forged Galvanized Steel Swivel Hook for 3/8" wire For Use in Docking Under Total Deflated Conditions. 1 p. + 1 sketch. S.H. Phillips.
- #192 Sept. 30, 1924, Modification in Connection With Holding Reflecting Mirror Fitted to the "Byrd" Sextant. 2 pp. S.H. Phillips.
- #193 Sept. 30, 1924, Report on Manufacture and Test of Differential Resistance Thermometer for Measuring Superheat. 4 pp. + 8 plates. R.M. Parsons, BuAer.
- #194 Oct. 9, 1924, Test of Steel for Physical Properties For Use In The Manufacture Of The Mooring Rope Couplings. 1 p. S.H. Phillips.
- #195 Oct. 10, 1924, U.S.S. SHENANDOAH & ZR-3 - Wood Strain Insulators for Service Docking Operations. 1 p. S.H. Phillips.
- #196 Oct. 18, 1924, U.S.S. SHENANDOAH - Test of Steel for Physical Properties for use in the Manufacture of the Mooring Couplings. 2 pp. S.H. Phillips.
- #197 Oct. 24, 1924, ZR-3 - Strength of Rivets in Shear. 3 pp., 1 graph. S.H. Phillips.
- #198 Oct. 23, 1924, ZR-3 - Strength of Solid Drawn Wires. 2pp., 1 graph. S. H. Phillips.
- #199 Oct. 28, 1924, U.S.S. SHENANDOAH - Flexible Steel Wire (Galvanized) Contract #61, with Roebling & Sons, 1/4" dia. 7 x 19 strand for use in Major Control System. 1 p. S.H. Phillips.
- #200 Nov. 4, 1924, ZR-3 - Strength of German Solid Drawn Steel Wire (Oval Section). 1 p. + 1 graph. S.H. Phillips
- #201 Nov. 4, 1924, ZR-3 - Strength of Ramie Cord used in Gasbag Nets. 1 p. S.H. Phillips.
- #202 Nov. 11, 1924, ZR-3 - Strength of Turnbuckles. 3 pp. S.H. Phillips
- #203 Nov. 12, 1924, ZR-3 - Strength of Lattices. 3 pp. + 7 diag. S.H. Phillips.
- #204 Nov. 15, 1924, U.S.S. SHENANDOAH - Sheet Steels for Exhaust Manifolds. 1 p. S.H. Phillips.
- #205 Nov. 25, 1924, U.S.S. SHENANDOAH - Steel Sheet for the Manufacture of Exhaust Manifolds. 1 p. S.H. Phillips.
- #206 Jan. 12, 1925, Test of Soldered Wire Loops, using different fluxes on German Steel Tape Wire 6 m/m x 3 m/m. 2 pp. + 1 diag. S.H. Phillips.
- #207 Nov. 25, 1924, U.S.S. SHENANDOAH - Tests of Steel for Physical Properties for use in the Manufacture of the Mooring Couplings. 1 p. S.H. Phillips.

- #208 Dec. 1, 1924, ZR-3 - Shed Test of Bow Mooring Equipment. 3 pp. J. Work.
- #209 Dec. 12, 1924, U.S.S. SHENANDOAH - Proof Loading of Coupling for Main Mooring Cable. 1 p. S.H. Phillips.
- #210 Jan. 30, 1925, U.S.S. SHENANDOAH - Carbon Contents of Water Recovery Condenser Units. 2 pp. S.H. Phillips.
- #211 Dec. 8, 1924, U.S.S. SHENANDOAH - Flexible Steel Wire (Galvanized) Contract #61350 with MacWhite, 7 x 19 strand for use on Major Control Systems, 1/4" dia. 1 p. S.H. Phillips.
- #212 Dec. 8, 1924, U.S.S. LOS ANGELES - Test of German Steel Flexible Cable. 3 pp. S.H. Phillips.
- #213 Dec. 19, 1924, U.S.S. LOS ANGELES - Test of Wind Driven Pump. 1 p. P.E. Ward.
- #214 Jan 20, 1925, U.S.S. LOS ANGELES and U.S.S. SHENANDOAH - German Trail Ropes. 2 pp. S.H. Phillips.
- #215 Dec. 27, 1924, U.S.S. SHENANDOAH - Flexible Steel Wire (Gal.) Contract #61350 with MacWhite 7 x 9 strand, 7/16" dia. for use on Yaw Wires. 1 p. S.H. Phillips.
- #216 Feb. 16, 1925, Test of Aluminum Sheet for Physical Properties. 1 p. S.H. Phillips.
- #217 Feb. 2, 1925, U.S.S. LOS ANGELES - Test of Main Control Cables. 2 pp. S.H. Phillips.
- #218 Jan. 12, 1925, U.S.S. SHENANDOAH - Test of Couplings for Nose Steadying Guy Wires. 1 p. S.H. Phillips.
- #219 Feb. 13, 1925, U.S.S. SHENANDOAH - Water Recovery Apparatus - Deposits on Condenser Tubes. 1 p. S.H. Phillips.
- #220 Feb. 13, 1925, Improved Plow Steel Rope 1/16" diameter, 7 x 7, (Tru-Lay). 2 pp. S.H. Phillips.
- #221 March 17, 1925, U.S.S. LOS ANGELES - Duralumin Channel Removed, Showing Corrosion due to Calcium Chloride Deposits. 2 pp. S.H. Phillips.
- #222 March 9, 1925, U.S.S. SHENANDOAH and U.S.S. LOS ANGELES - Strength of Materials used on - American and German Equivalents. 9 pp. + 3 pp. sketches. S.H. Phillips.
- #223 March 11, 1925, Improved Plow Steel Rope 1/4" diameter, 7 x 19, Tinned. 1 p. S.H. Phillips.
- #224 March 14, 1925, U.S.S. SHENANDOAH - Strength of Main Mooring Cable. 2 pp. S.H. Phillips.
- #225 March 24, 1925, Periodic Test of Duralumin Rivets. 1 p. S.H. Phillips.

- #226 March 28, 1925, U.S.S. LOS ANGELES - Strength of Lattice Palms.
2 pp. + 8 sketches. S.H. Phillips.
- #227 March 28, 1925, U.S.S. SHENANDOAH and U.S.S. LOS ANGELES -
Weight Comparison of. 7 pp. + 2 fig. C.D. Tripolitis.
- #228 March 31, 1925, U.S.S. LOS ANGELES - Reinforcing Channel Removed
from Apex of Keel Walkway Girder, Frame 27.5. 1 p.
S.H. Phillips.
- #229 April 20, 1925, Film Cement for Attaching Fabric to Cellon.
4 pp. S.H. Phillips.
- #230 April 2, 1925, U.S.S. LOS ANGELES - Duralumin Material Removed
from Ridge Girder Car #1 2 pp. S.H. Phillips.
- #231 March 31, 1925, U.S.S. LOS ANGELES - Flax Cordage - 5/32" dia.
4 ply. 1 p. S.H. Phillips.
- #232 April 2, 1925, U.S.S. LOS ANGELES - Reinforced Channel Removed
From Apex of Keel Walkway Girder. 1 p. S.H. Phillips.
- #233 April 2, 1925, 3 ply Rubberized Fabric. 2 pp. S.H. Phillips.
- #234 April 7, 1925, U.S.S. LOS ANGELES - Duralumin Channel Joint Plate
Removed from Frame 25, port side at #1/2. 1 p. S.H. Phillips.
- #235 April 3, 1925, U.S.S. LOS ANGELES - Tensile Strength of Material
Used in Rolled Shapes. 1 p. S.H. Phillips.
- #236 April 29, 1925, U.S.S. SHENANDOAH - U.S.S. LOS ANGELES - Flash-
lights for use on. 3 pp. + 2 photos. S.H. Phillips.
- #237 April 15, 1925, U.S.S. LOS ANGELES - Strength of German Steel
Flexible Wire for Handling Lines. 2 pp. S.H. Phillips.
- #238 April 16, 1925, U.S.S. LOS ANGELES - Condenser for Water Recovery,
Test of. 2 pp. P.E. Ward.
- #240 May 16, 1925, U.S.S. LOS ANGELES - Tension of New Outer Cover
Panel. 5 pp. + 2 charts. S.H. Phillips.
- #241 July 14, 1925, U.S.S. LOS ANGELES - Force Indicator for Bow
Mooring. 2 pp. + 5 illus. S.H. Phillips.
- #243 July 2, 1925, U.S.S. LOS ANGELES - Duralumin Material Removed Due
to Corrosion by Calcium Chloride. 3 pp. + 5 figs. S.H. Phillips.
- #244 May 28, 1925, Periodic Test of Heat Treated Duralumin Rivets.
2 pp. C.D. Tripolitis.
- #245 July 3, 1925, U.S.S. SHENANDOAH - U.S.S. LOS ANGELES - Main
Mooring Coupling - Proof Loading of. 2 pp. S.H. Phillips.
- #246 June 25, 1925, U.S.S. LOS ANGELES - Test of Water Ballast Bag
(Ordinary Type) with Recovered Water. 2 pp. P.E. Ward.

- #247 June 23, 1925, Water Proofing for Gas Cell Fabric used in Rigid Airships - Exposure Tests. 3 pp. S.H. Phillips.
- #248 June 12, 1925, U.S.S. SHENANDOAH - Tensions of Outer Cover Panels. 5 pp. + 1 fig. S.H. Phillips.
- #250 July 15, 1925, Physical Tests of Duralumin Sheet. 2 pp. S.H. Phillips.
- #251 June 15, 1925, U.S.S. LOS ANGELES - Tensions of Outer Cover between Longitudinals 5 & 6, Port and Starboard. 2 pp. + 1 nomogram. S.H. Phillips.
- #252 July 14, 1925, U.S.S. LOS ANGELES - Strength of Main Mooring Cable. 1 p. S.H. Phillips.
- #253 July 7, 1925, Periodic Test of Heat Treated Duralumin Rivets. 1 p. P.E. Ward.
- #254 July 29, 1925, Fabrics Wrongly Graded in Technical Stores. 2 pp. S.H. Phillips.
- #255 July 31, 1925, U.S.S. LOS ANGELES - Tensions of Outer Cover Panels. 2 pp. + 1 nomogram S.H. Phillips.
- #257 Aug. 5, 1925, Inspection Report on Solid Aircraft Wire. 1 p. P.E. Ward.
- #258 Aug. 10, 1925, Periodic Test of Heat Treated Duralumin Rivets. 1 p. P.E. Ward.
- #260 Aug. 8, 1925, Elastic Limit of Bronze supplied by Mogul Corp. 1 p. + 1 curve. S.H. Phillips.
- #261 Nov. 6, 1925, U.S.S. SHENANDOAH - Tension of Outer Cover Panels. 2 pp. S.H. Phillips.
- #262 Aug. 28, 1925, U.S.S. SHENANDOAH - Calibration of Distance Type Thermometer. 1 p. S.H. Phillips.
- #263 March 24, 1926, German Gas Cell Fabrics with Reference to Strength of Seams, Using Hide Glue. 7 pp. + 4 tables. S.H. Phillips.
- #264 Sept. 14, 1925, U.S.S. LOS ANGELES - Test of Fabric Buckets for Handling Recovered Water. 2 pp. + 2 fig. P.E. Ward.
- #265 Jan. 3, 1924, Test of Rudder and Elevator Controls. 2 pp. C.D. Tripolitis.
- #266 Jan. 3, 1924, Test of all Hatches and Hatch Controls. 2 pp. C.D. Tripolitis.
- #267 Oct. 22, 1925, Periodic Test of Heat Treated Duralumin Rivets. 1 p. P.E. Ward.
- #268 Sept. 16, 1925, U.S.S. LOS ANGELES - Test of Water Ballast Bag (Ordinary Type) with Recovered Water. 2 pp. P.E. Ward.

- #269 Oct. 21, 1925, U.S.S. LOS ANGELES - Clamping strength of Zeppelin type and proposed type shear wire clamps. 1 p. T.M. Ramsay.
- #270 Oct. 28, 1925, Test to determine average force per man on the handling lines. 2 pp. C.D. Tripolitis.
- #271 Nov. 5, 1925, The effect of anti-freeze agents used in ballast water on duralumin and on rubber contained in ballast bags. 6 pp., 6 photos, 1 graph. S.H. Phillips.
- #272 Nov. 11, 1925, Periodic Test of Heat Treated Duralumin Rivets. 1 p. P.E. Ward.
- #273 Nov. 19, 1925, U.S.S. LOS ANGELES - Duralumin Channel Joint Plate Removed from Frame 175, Starboard side at Joint #1. 1 p. S.H. Phillips.
- #274 Nov. 25, 1925, U.S.S. LOS ANGELES - Duralumin Channel Removed From Apex of Keel Girder "O". 3 pp. incl. 3 figs. S.H. Phillips.
- #275 Nov. 28, 1925, The Effect of Anti-freeze Agents on Rubberized Fabric used in the Manufacture of Water Ballast Bags. 3 pp. S.H. Phillips.
- #276 Jan. 6, 1926, Test of German Steel Wire 3 x 6 mm. 1 p. W.E. Snyder.
- #277 Dec. 1, 1925, Method of Splicing German and American Aircraft Wire - Test of. 2 pp. + 1 photo. P.E. Ward.
- #278 Nov. 30, 1925, Test of Liquid for Treating Ground Cloths for Prevention of Mildew. 2 pp. P.E. Ward.
- #279 Dec. 4, 1925, Test of German and American Design Shear Wire Clamps for Slippage. 2 pp. P.E. Ward.
- #280 Dec. 14, 1925, Test of deposit on sample piece of outer cover lacing cord from U.S.S. LOS ANGELES. 1 p. R.R. Bottoms.
- #281 Dec. 14, 1925, Wire gauze as a base for the outer covers of Airships. 2 pp. W.E. Snyder.
- #282 Dec. 15, 1925, Periodic Test of Heat treated Duralumin rivets. 1 p. P.E. Ward.
- #283 Jan. 6, 1926, Test of Deposits removed from ship. 1 p. R.R. Bottoms.
- #284 Jan. 18, 1926, Periodic Test of Heat Treated Duralumin Rivets. 1 p. P.E. Ward.
- #285 Jan. 20, 1926, Analysis to ascertain calcium chloride content of specimens of fabric. 1 p. R.R. Bottoms.

- #286 Jan. 20, 1926, Test of Boiler Feed Water. 2 pp. R.R. Bottoms.
- #287 Jan. 27, 1926, Test of Channel from Los Angeles. 1 p. W.E. Snyder.
- #288 n.d., Tests of Strength of specimens from walkway base plate - U.S.S. LOS ANGELES. 1 p. W.E. Snyder.
- #289 Feb. 13, 1926, Periodic Test of Heat Treated Duralumin Rivets. 1 p. P.E. Ward.
- #290 March 11, 1926, U.S.S. LOS ANGELES - Test of Springs for Automatic Valves of. 2 pp. + 1 graph. C.D. Tripolitis.
- #291 March 15, 1926, Periodic Test of Heat Treated Duralumin Rivets. 1 p. P.E. Ward.
- #292 April 28, 1926, U.S.S. LOS ANGELES - Bow Mooring Force Indicator - Test of. 3 pp. + 1 graph, C.D. Tripolitis.
- #293 May 12, 1926, Periodic Test of Heat Treated Duralumin Rivets. 1 p. P.E. Ward
- #294 May 27, 1926, U.S.S. LOS ANGELES - Main Mooring Pendant - Proof Loading of. 2 pp. P.E. Ward.
- #295 Oct. 14, 1926, Corrosion Tests on American and German Duralumin. 4 pp. W.E. Snyder.
- #296 Sept. 8, 1926, Test of 10 inch Pelican Hook. 1 p. C.D. Tripolitis.
- #297 Sept. 22, 1926, Test of mushroom anchor ring similar to those embedded in concrete at three point mooring. 1 p. C.D. Tripolitis.
- #298 Nov. 15, 1926, U.S.S. LOS ANGELES - Bow Mooring Force Indicator - Test of. 2 pp. + 1 graph. C.D. Tripolitis.
- #299 Nov. 23, 1926, Periodic Test of Heat Treated Duralumin Rivets. 1 p. P.E. Ward.
- #300 Nov. 22, 1926, U.S.S. LOS ANGELES - Fuel Tank - Slipping Device. 2 pp. P.E. Ward.
- #300 Dec. 13, 1926, Periodic Test of Heat Treated Duralumin Rivets. 1 p. P.E. Ward.
- #301 Dec 30, 1926, Mechanical Handling Arrangement - Proof Loading of Trolley Rings. 1 p. P.E. Ward.
- #302 Jan. 11, 1927, U.S.S. LOS ANGELES Weight Increase during the calendar year 1926. 2 pp. C.D. Tripolitis.

- #303 Jan. 31, 1927, Periodic Test of Heat Treated Duralumin Rivets. 1 p. P.E. Ward.
- #304 Feb. 16, 1927, Test of tractor Cletrac - 20-K. 3 pp. C.D. Tripolitis.
- #305 March 15, 1927, Test of Hangar Gasoline Supply Pumps. 2 pp. + 2 figs. C.D. Tripolitis.
- #306 Oct. 16, 1926, Moisture absorption - Outer Cover Fabric. 5 pp. + 1 curve. G.S. Worthington.
- #307 March 25, 1927, Hydrostatic Test on Fabric Covered Gasoline Hose. 2 pp. P.E. Ward.
- #308 April 5, 1927, U.S.S. LOS ANGELES - Automatic Gas Valves - Test for leakage. 2 pp. + 2 encl. P.E. Ward.
- #309 April 23, 1927, Periodic Test of Heat Treated Duralumin Rivets. 1 p. P.E. Ward.
- #310 June 21, 1927, Pressure Test on Rubber Gasoline Hose. 2 pp. + 2 tables. P.E. Ward.
- #311 June 28, 1927, Gas Cell Fabric Diffusion Test. 2 pp. P.E. Ward.
- #312 May 24, 1927, Periodic Test of Heat Treated Duralumin Rivets. 1 p. P.E. Ward.
- #313 June 28, 1927, Periodic Test of Heat Treated Duralumin Rivets. 1 p. P.E. Ward.
- #314 July 27, 1927, Test for physical properties of wood taken from timber used as stub mast. 2 pp. C.D. Tripolitis.
- #315 Oct. 5, 1927, Pressure Test on Rubber Gasoline Hose. 2 pp. P.E. Ward.
- #316 Jan. 9, 1928, Artillery Tractor for Mechanical Handling - Speed of. 1 p. P.E. Ward.
- #317 Jan. 13, 1928, Holding Power of Standard Railroad Spikes - Test of. 1 p. P.E. Ward.
- #318 Jan. 9, 1928, Test of 1/4 inch diameter eyelets for anti-flutter ties. 2 pp. P.E. Ward.
- #319 Jan 20, 1928, Comparison of Lime and Navy Standard Boiler Compound. 3 pp. R.E. Davenport.
- #320 Feb. 7, 1928, Heat tests on oil used in motors of Los Angeles. 3 pp. R.E. Davenport.

- #321 April 14, 1928, U.S.S. LOS ANGELES Weight Increase during the calendar year 1927. 2 pp. C.D. Tripolitis.
- #324 Feb. 18, 1929, Test to determine consumption and anti-knock value of Domestic Aviation Gasoline and Texaco Aviation Gasoline. 4 pp. + 1 curve. B.J. Rodgers.
- #325 May 9, 1929, Non-Rigid Airship Mooring and Handling Cable Junction Plates and Fittings: Redesign and Replacement. 2pp. O. Loeser Jr.
- #326 Mar. 25, 1929, Test of Aluminum Solder - (Trade Name Soldalume). 2 pp. P.E. Ward.
- #327 April 12, 1929, U.S.S. LOS ANGELES - Experimental Decking for Keel Walkway. 2 pp. P.E. Ward.
- #328 May 10, 1929, Test of U.S.S. LOS ANGELES handling line swivel - dural. 2 pp. O. Loeser Jr.
- #329 May 11, 1929, Test of relative output and performance of U.S.S. LOS ANGELES air driven membrane fuel pumps. 2 pp. O. Loeser Jr.
- #330 June 25, 1929, Test of Swivel Shackle for Non-Rigid Field Mooring. 2 pp. P.E. Ward.
- #331 June 14, 1929, Test on Modified Snap for Parachute Harness. 2 pp. + 1 print. P.E. Ward.
- #332 Nov. 4, 1929, Main Mooring Mast - Remote Control for Waterbury Speed Gear-Link on Sheave Block - Test for Strength of Link. 1 p. P.E. Ward.
- #334 Jan. 27, 1928, Non-rigid Airship Hand Blower - Test. 2 pp. + table. P.E. Ward.
- #335 Jan 6, 1930, Test Venturi designed for measuring output of Maybach engine water pump. 3 pp. + 1 curve. T.M. Ramsay.
- #336 Jan. 30, 1930, Inspection Trip (Jan. 20, 1930) - Bellanca Aircraft Corp. 4 pp. + 19 figs. J. M. Allison and R. H. Shepard.
- #337 Oct. 14, 1929, Mechanical docking trolley - Releasing hook - investigation for redesign. 2 pp. P.E. Ward.
- #338 Jan. 27, 1930, U.S.S. LOS ANGELES - Trail Ropes - Test of Manila Rope from Boston Navy Yard. 2 pp. P.E. Ward.
- #339 March 7, 1930, Notes on Inspection Trip Through Curtiss Airplane Factory, Garden City, L.I. - Feb. 11, 1930. 3 pp. O.E. Loeser.

- #340 March 8, 1930, 1 - American Legion Aircraft Show. 2 - Inspection Trip through Curtiss Plant, Garden City. 3 - Aeronautical Meeting ASME - NYC. 10 pp. incl. 14 figs. J.M. Allison & R.L. Creel.
- #341 Oct. 19, 1929, U.S.S. LOS ANGELES - Mechanical Handling Arrangement - Test of. P.E. Ward.
- #342 Nov. 22, 1929, Oil Immersion Heater - Comparative Tests. 3 pp. P.E. Ward.
- #343 Nov. 22, 1929, Oil Immersion Heater, 750 Watt Thermo-Pete Service Test. 2 pp. T.M. Ramsay.
- #344 Feb. 11, 1930, Memorandum Report relative to NAS Lakehurst practice on rigid airship hard wire terminals and splices. 3 pp. P.E. Ward.
- #345 n.d. Report of structural inspections of the U.S.S. LOS ANGELES conducted by and under the direction of Chief Inspector covering the period from October 1924 to December 1929. 10 pp. + 8 pp. encls. P.E. Ward.
- #346 March 13, 1930, U.S.S. LOS ANGELES - Test Specimens Removed from Ship. 1 p. + Encl. A - F. P.E. Ward.
- #347 March 17, 1930, Memorandum Report on Visit of Board of Investigation and Survey. 3 pp. P.E. Ward.
- #348 March 21, 1930, Collapse of and Repairs to Kingpost Strut Frame 160. 1 p. + 2 photos. T.M. Ramsay.
- #349 March 24, 1930, Test of 25 Liter Aluminum Air Starting Flasks for Maybach Engines. 2 pp. T.M. Ramsay.
- #350 March 16, 1930, Notes on Inspection Trip Through the Fairchild Airplane Manufacturing Co. Plant at Farmingdale, L.I., Mar. 10, 1930. 3 pp. O. Loeser.
- #351 March 18, 1930, Inspection Trip (March 3, 1930) Sikorsky Aviation Corp., Whittelsey Manufacturing Co., Engineers Aircraft Corp. 9 pp. + 39 f gs. R.H. Shepard & J.M. Allison.
- #352 n.d. ROEDER-L. DEVICE Airship Device for Training in Steering. 3 pp. + 1 print. J.D. Sandorf (Translator).
- #353 March 29, 1930, Motion Picture Reels of Lighter-Than-Air Activities Available at this Station. 13 pp. T.M. Ramsay.
- #354 Wire Tensions in Flight. P.E. Ward.
- #355 April 28, 1930, Comparative Test Between Hagan and Baffle Separator. 5 pp. + 2 photos. T.M. Ramsay.

- #356 June 26, 1930, Tests Conducted on Torpedo Release for Los Angeles Docking Bridles. 3 pp. P.E. Ward.
- #357 April 23, 1930, Comments on Metalclad Airship MC-38 by Engineering Division. 15 pp. M.Q. Corbett.
- #359 April 4-5, 1930, Flight Tests of Tube Cooled Oil Tank Installation, Power Car #5, U.S.S. LOS ANGELES. 4 pp. M.Q. Corbett.
- #360 Jan. 20, 1930, Experimental Crankcase Ventilation. 3 pp. T.L. Blakemore.
- #361 May 9, 1930, Comparison of LOS ANGELES and GRAF ZEPPELIN Cooling Systems. 5 pp. T.M. Ramsay.
- #362 March 10, 1930, Study of Water Recovery Apparatus. 24 pp. M.Q. Corbett.
- #363 May 29, 1930, Study of Wind Break Revolving Type for Non-Rigids. 1 p. + 1 print. M.Q. Corbett.
- #365 June 16, 1930, Construction of the ZRS-4 at Goodyear-Zeppelin Corp. Plant, Akron, Ohio. 10 pp. incl. 13 figs. R. H. Shepard.
- #366 n.d., A.S.M.E. AERONAUTICAL MEETING, Dayton, Ohio, May 19-23, 1930. 8 pp. J.M. Allison.
- #367 May 15, 1930, NEW YORK AERONAUTICAL SHOW, May 3-10, 1930. 17 pp. J.M. Allison & R.H. Shepard.
- #368 Aug. 26, 1930, Experimental Covering for Plywood Walkways. 2 pp. P.E. Ward.
- #369 Aug. 21, 1930, Superheat Meter for ZMC-2. 9 pp. W.G. Brombacher & H.C. Sontag.
- #370 Oct. 14, 1930, Test of German Outer Cover Fabric removed from port horizontal and lower vertical fin of U.S.S. LOS ANGELES. 2 pp. P.E. Ward.
- #370A Oct. 28, 1930, Test of German Outer Cover Fabric Used as Lower Vertical Fin Covers on U.S.S. LOS ANGELES. 3 pp. P.E. Ward.
- #371 October 14, 1930, Test for Strength of Envelope and Ballonet Fabric removed from Envelope El95 - J3 Non-Rigid. 5 pp. P.E. Ward.
- #372 Nov. 25, 1930. Wind Driven Gear Pump Proposed for Water Recovery Distribution. 3 pp. + 1 graph. T.M. Ramsay & M.Q. Corbett.

- #373 Oct. 29, 1930, Tensile Test of 3/8" Telephone Center Kite Balloon Cable. 2 pp. P.E. Ward.
- #374 Nov. 11, 1930, U.S.S. LOS ANGELES, Procedure in case of deflated gas cell. 7 pp. (Signature illegible.)
- #375 Dec. 29, 1930, U.S.S. LOS ANGELES - Outer Cover Panels, Strength of. 8 pp. incl. tables. P.E. Ward.
- #376 Dec. 18, 1930, U.S.S. LOS ANGELES - Inspection of Shear Wire Clamps and Shear Wires. 2 pp + 1 dwg. P.E. Ward.
- #378 Feb. 10, 1931, Visit to Naval Aircraft Factory, Observations on (1) Parachute Dummy Release Box. (2) Application of Metal Cloth. 3 pp. T.M. Ramsay.
- #379 Jan. 22, 1931, ZMC-2 Repairs and Removal of Test Specimens from Hull. 6 pp. + 2 figs. P.E. Ward.
- #380 Jan. 8, 1931, Cord-Hemp, Blocking, Submitted by Ludlow Sales Corp. 3 pp. P.E. Ward.
- #381 March 31, 1931, Inspection of Cellophane Gas Cell, Position #2. 4 pp. P.E. Ward.
- #382 March 17, 1931, Stress Analysis of Stern Handling Beam, ZRS-4. 6 pp. J. Gertz.
- #383 Jan. 2, 1931, Intake and Exhaust Cams Maybach Engines VL-1, VL-2. 19 pp. J.C. Sandorf.
- #384 April 2, 1931, Trial Flight Test of Mark IV Water Recovery Condenser, U.S.S. LOS ANGELES. 27 pp. incl. plates. T.M. Ramsay & M.Q. Corbett
- #386 June 1, 1931, Quick Cable Coupling for ZRS-4. 3 pp. P.E. Ward.
- #387 July 14, 1931, Blackmer #50 Gasoline Pump at Mooring Site No. 1. 2 pp. T.M. Ramsay.
- #388 July 21, 1931, RAE Rpt. #E3218 "Experiments on Flame Extinction in Hydrogen Air Mixtures" 9 pp. Sqd. Ldr. W. Helmore.
- #389 July 30, 1931, Construction of 80 Ft. Anemometer Mast. 3 pp. J.M. Allison.
- #390 Sept. 1, 1931, Loads Required to Compress Springs for Ram on Mooring Mast (Rail Type) for Mooring U.S.S. AKRON. 4 pp. P.E. Ward.
- #392 Sept. 15, 1931, Description of Askania Distance Recording Meteorograph Designed by Prof. Moltchanoff. 6 pp. E.B. Yassin (Translator)
- #393 Jan. 5, 1932, German Outer Cover Fabric Removed from U.S.S. LOS ANGELES. 2 pp. P.E. Ward.

- #394 Jan. 21, 1932, Inspection and Maintenance of Resiliency Devices on Bulkhead Wiring of U.S.S. AKRON. 2 pp. T.M. Ramsay.
- #395 April 28, 1931, U.S.S. LOS ANGELES - Outer Cover Fabric, Strength of. 3 pp. P.E. Ward.
- #397 Feb. 11, 1932, Wire Netting Eyelets on U.S.S. LOS ANGELES. 2 pp. P.E. Ward.
- #398 Feb. 25, 1932, Stainless Steel as used by Goodyear-Zeppelin Corp. 3 pp. T.M. Ramsay.
- #399 March, 1932, Cables Removed from U.S.S. AKRON and Stern Handling Beam After Failure of Feb. 22, 1932. 3 pp. P.E. Ward.
- #400 Feb. 4, 1932, Condition of Cable Drums of Airplane Trapeze for U.S.S. LOS ANGELES. 2 pp. + 5 photos. P.E. Ward.
- #401 March 8, 1932, U.S.S. LOS ANGELES - Outer Cover Panels, Strength of. 5 pp. P.E. Ward.
- #403 April 22, 1932, Served and Soldered Splices on Tinned Aircraft Wire for U.S.S. AKRON. 4 pp. P.E. Ward.
- #404 May 13, 1932, Steel Rings for Handling Line Spiders for U.S.S. AKRON. 6 pp. P.E. Ward.
- #405 May 26, 1932, Modified Trail Rope Spider Snatch Block. 4 pp. T.M. Ramsay. (plus Addendum, 2 pp. + 1 photo.)
- #406 May 17, 1932, German Outer Cover removed from U.S.S. LOS ANGELES. 7 pp. P.E. Ward.
- ~~#407~~ April 1, 1932, Suspension of ZMC-2 in Non-Rigid Hangar. 12 pp. I.B. Yassin.
- #408 June 28, 1932, New Type Separator Test on U.S.S. LOS ANGELES Flight of June 8, 1932. 4 pp. G.C. Calnan.
- #409 Aug. 4, 1932, Trial Flight Test of Mark IV Water Recovery Installation on U.S.S. AKRON. 20 pp. + Appendixes A-L. M.Q. Corbett.
- #410 July 27, 1932, Observations Made on 17 Gal. Air Cooled Oil Tanks on U.S.S. AKRON under Operating Conditions. 4 pp. T.M. Ramsay.
- #411 Aug. 2, 1932, Repairs to Maybach Engine Cylinder Water Jackets (on U.S.S. LOS ANGELES). 5 pp. T.M. Ramsay.
- #412 March 25, 1932, 2nd Inspection of Cellophane Gas Cell, Position No. 2, U.S.S. LOS ANGELES. 3 pp. P.E. Ward.

- #413 May, 1932, Tests of 12" Snatch Block (Wellman Eng. Co.) for Side Handling Equipment U.S.S. AKRON. 3 pp. + 3 photos. P.E. Ward.
- #413A May, 1932, Tests of 12" Snatch Block (Montgomery & Co.) for Side Handling Equipment U.S.S. AKRON. 3 pp. + 3 photos. P.E. Ward.
- #414 Sept. 21, 1932, Spray Gun Equipment Demonstrations by Competing Bidders. 9 pp. P.E. Ward.
- #415 July 27, 1932, Comparative Effects of Service Exposure on Special Treated Aluminum Tubes on Water Recovery Drain Lines of U.S.S. AKRON. 3 pp. P.E. Ward.
- #416 Aug. 22, 1932, Protective Treatment for U.S.S. AKRON Water Recovery Condenser Panels. 2 pp. T.M. Ramsay.
- #417 Oct. 17, 1932, Strength of Outer Cover Panels of U.S.S. LOS ANGELES. 6 pp. P.E. Ward.
- #418 Nov. 8, 1932, Transfer of Pyrofax Gas from Commercial to Ship Cylinders. 2 pp. T.M. Ramsay.
- #419 Dec. 15, 1932, Instructions Covering the Procedure in Unloading Helium Tank Cars at Expeditionary Masts. 2 pp. J.H. Severyns.
- #420 Jan. 30, 1933, Goodyear-Zeppelin Experimental Water Recovery Panel for Positon #4. 8 pp. P.E. Ward.
- #422 Feb. 16, 1933, Le Courtenay Co. Centrifugal Pump Data. 12 pp.
- #424 March 27, 1933, LeCourtenay 3 Stage Centrifugal Water Pump on R.R. Mast. 3 pp. T.M. Ramsay.
- #439 Jan. 10, 1936, The Investigation of the Static Shear and Bending Moments, and the Bending Moment at a Gust of 30 ft./sec. on the Cut Down LOS ANGELES Airship. 10 pp., tables. F.M. Bondor.
- #443 April 21, 1939, Expeditionary Operations Non-Rigid Airship K-2. 8 pp. + 6 plates. D.M. Mackey.

Unserialized items from A&R Serials:

Feb. 7, 1925, Notes on Flying, Gas Cells, and Valves (ZR-3), and Engineering Notes, Maybach Motors type VL. 1, 400 P.S. Saamt and Knorr. 4 pp.

Revision to General Specification for Navy Airship ZRS-4, Covering Change Order No. 1. Gas Cell Fabric. 1 p.

Revision to General Specification for Navy Airship ZRS-4,
Covering Change Order No. 6, Gas Cell Fabric. 2 pp.

17 Jan. 1924, Memorandum to Chief Engineer, Subject: U.S.S.
SHENANDOAH - Resistance of Car Suspension Wires. 2 pp. S.H. Phil-
lips.

D-5-ZR-1-4926, 11 June 1924. Installation and flight tests
of water recovery apparatus on aft centerline car of U.S.S. SHEN-
ANDOAH. H.F. Parker, 3 pp.

4 Sept. 1924. Test of Swarthout 3/4" Horizontal Type Com-
pressed Air Separator. C.M. Bolster. 2 pp.

D-5-ZR-3, 20 Oct. 1924, Fuel Test, Gasoline from ZR3. 1 p.
R.R. Bottoms.

D-5-ZR-3-998, 8 Dec. 1924, Slip Release Devices - Testing
of. 1 p. H.M. Dietzman.

March 23, 1925, Protection of Duralumin against Corrosion.
2 pp. K. Schmidt (Lt, CC).

Contents

1. Introduction
2. Missions
3. Present Technology
4. Operating Requirements
5. Vehicle Size and Characteristics
6. General Concept
7. Costs
8. Discussion
9. Summary and Conclusions

NASA STUDIES OF A HIGH ALTITUDE POWERED PLATFORM (HAPP)

Norman J. Mayer
LTA Consultant
National Aeronautics and Space Administration
Washington, D.C.

and

Harvey C. Needleman
NASA Wallops Flight Center
Wallops Island, Virginia

Abstract

A concept for a geostationary high-altitude remotely-controlled airship powered by microwave beams was studied by NASA for use as a telecommunications platform and for remote sensing. The vehicle was studied to determine its general feasibility and system costs. The payloads were examined to identify their characteristics and the types of missions most applicable. Results showed that a non-rigid airship design using a low pressure envelope was feasible and capable of supporting payloads from 130 to 720 kg when operating at 70,000 feet altitudes. The use of a low pressure envelope reduced gas losses and minimized material problems. Annual operating costs were estimated at approximately \$0.5 million. The mission-payload analysis showed that there were several applications possible in remote sensing, but costs benefits were uncertain. The telecommunications application was by far the most effective use. Further studies were recommended.

1. INTRODUCTION

Several proposals have been advanced for a high altitude aerial platform to function similar to a geosynchronous satellite for use in communications, earth surveillance, etc. One of the more recent recommendations involved the use of a vehicle powered by microwave energy beamed from the ground. This high altitude powered platform (HAPP) would be a remotely piloted airship or airplane capable of long endurance flight and functioning primarily as a telecast station.

The HAPP vehicle was postulated on the basis that it would offer lower costs and significant new applications compared to space systems or ground systems. Among these advantages would be such improvements as:

1. Cost reduction through use of less complex systems which would not have to endure the high loads of a spacecraft launch, could be recovered for refurbishing and maintenance, have lower power requirements, and of course, eliminate the high cost of the launch vehicle.
2. Smaller surface coverage allowing more discrete telecasts and conservation of the frequency spectrum and the use of very narrow spot beams.
3. Direct competition with ground stations and cable systems.
4. Possible links with satellite systems.
5. Direct broadcast for medical, educational, social services, teleconferences, and data and telephone trunks.

The achievement of these goals is highly dependent on the vehicle and system reliability. NASA in-house studies and contracted efforts by Battelle Columbus Laboratories (Ref. 1) and the Stanford Research Institute (Ref. 2) were performed to explore the various technical aspects of the mission. Both heavier-than-air and lighter-than-air vehicles were studied. Each offers some advantages. This paper discusses the aerostat approach.

2. MISSIONS

The mission/payload applications for the HAPP concept - a high-altitude, remotely-piloted, station-keeping platform - have been examined to determine its economic and scientific utility. Various areas of applications, including communications, surveillance, remote sensing, and in-situ measurements are potential candidates for this type of platform. The recent studies concentrated their investigation in those areas which were felt to have the most payoff when comparing mission effectiveness and system capabilities. In particular, the disciplines of communications and remote sensing were singled out

as being the two prime consideration areas. For these applications the HAPP would play the role of a near-earth (21 kilometers) geostationary satellite and compete primarily with satellites, airplanes and ground systems.

2.1 Communications

By virtue of its mission design altitude - 21 kilometers - the HAPP provides a unique coverage capability in the broadcast sense. Since, at almost all frequencies, the higher the antenna the better the reception, the HAPP, with its unobstructed line-of-sight in excess of 500 kilometers, can provide coverage of better than five times the range (25 times the area) of a typical 300-meter antenna tower. On the other hand, compared to the geosynchronous satellite, the HAPP has a very small coverage capability, but this facilitates the adaptability to regional broadcast uses where wide satellite coverage may limit local stations or where point-to-point communications is desired within the limited frequency bands available. Obviously, the HAPP concept does not provide a solution to all communications situations, but it can provide capabilities that can complement existing methods and provide more effective and unique capabilities in some cases.

In examining the communication applications in terms of the HAPP concept, certain mission examples were identified which were felt to exhibit the concept's capabilities and to be representative of the application requirements. Three specific mission types were selected for detailed study. These were representative of the following general communication missions:

- Educational T.V.
- Communication Experiments
- Direct Broadcast

In addition, the areas of two way communications and nationwide television distribution were addressed but not in detail.

2.1.1 Educational T.V.

To illustrate and examine the effectiveness of the HAPP concept with the educational T.V. area the Rocky Mountain States Education Experiment was investigated. This experiment, part of the Health/Education Telecommunication (HET) experiment program, which is conducted with the ATS-6 satellite, was chosen because it highlights the comparison of HAPP with satellites for communications.

In the Rocky Mountain States Education Experiment television material was to be relayed to high schools and public broadcast stations in an eight state area known as the Federation of Rocky Mountain States. To compete directly with the satellite somewhere between two and fifteen HAPPs would be required - the actual number being a

function of the actual topological features. With an unobstructed field the minimum number of two is obtained and for a worst case assumption the number required was fifteen. Figure 1 illustrates the coverage extremes. The result of this analysis was that where a small number of channels are required/or a large number of HAPPs, a satellite is less expensive. However, since the HAPP costs are much less sensitive to payload weight a system providing a large number of channels to a limited area would be quite competitive.

2.1.2 Communications Experiments

The use of a HAPP as a communication experiment platform was chosen to illustrate its capability as a platform for new experiments/hardware or ideas which might ultimately be used on other mission vehicles such as satellites. The HAPP in this mode can provide a low cost, flexible method for experiment payloads by providing the capability of retrieval for repair, modification or replacement. For this evaluation two types of experiment platforms, a large and small payload, were chosen and compared on a satellite to HAPP basis. The results indicate that the HAPP is considerably less expensive than the equivalent satellite platform with costs being somewhere between .2 and .5 for shuttle launched experiments.

2.1.3 Direct Broadcast

The effectiveness of a HAPP as a direct broadcast element was examined by comparing it to a typical UHF television station (Figure 2). In this application the HAPP would provide extended broadcast coverage, acting basically as a large antenna and replacing various components used in the local station's broadcast operation. The advantage offered by using the HAPP concept is approximately 4 to 1 in favor of HAPP. That is, using the HAPP system's broader coverage, the replacement of the conventional system would cost one-fourth that of a conventional system.

Another aspect of direct broadcast is that of broadcast from satellite. In this case the use of a HAPP is over two orders of magnitude less expensive than the satellite system.

2.1.4 National T.V. Distribution

Because of the favorable results in direct broadcasting, two applications of national T.V. distribution were studied to determine their potential as HAPP applications.

1. For these applications it was assumed that there would be 13 HAPPs required for complete coverage of the contiguous United States (Figure 3). For

examination purposes both HAPP-to-HAPP relays as well as HAPP-to-satellite relays were considered. First the potential of HAPP in Public Broadcasting Service (PBS) was examined. Here the results indicate that more capability at less than one-half the cost could be provided by HAPP when compared to the existing PBS network.

2. The HAPP nationwide system was compared to commercial distribution. When compared to the cable television industry the HAPP network, as analyzed, was able to provide eight channel service for one-sixth the cost and still be an attractive investment.

2.2 Remote Sensing

Here, as in the case of the communication field, the application of the HAPP concept was felt to provide capabilities - long-endurance, station-keeping, wide or specific coverage - that would enhance and complement existing platforms as well as provide new techniques in a cost effective manner. The HAPP concept should be capable of meeting the specific requirements of the remote sensing community - endurance, coverage capability, resolution, etc. - as the existing platform inventory including airplanes, balloons (tethered and free flight), rockets, and satellites are doing. Many opportunities in this discipline exist; however, for the purposes of the studies conducted, in-depth analysis in only three specific applications were performed. The selection of which ones to pursue was based on a preliminary screening of a comprehensive list of candidates. Those selected were felt to have the best potential from a return standpoint keying on coverage capability.

The specific applications examined in detail in these studies were:

- Forest Fire Detection
- Ice Mapping on the Great Lakes
- Enforcement in the 200 Mile Fisheries Zone

Though specific in detail, these were felt to be representative of the broad range of applications within the HAPP concept capability.

2.2.1 Forest Fire Detection

Based upon the HAPP's long-duration capability and its wide-angle coverage the surveillance of forest fires was selected as a prime remote-sensing application. In this role the HAPP would compete with aircraft surveillance. To assess the HAPP's effectiveness in this use, the potential savings that would be realized with the continuous HAPP surveillance was determined and compared to the noncontinuous aircraft detection system now employed. Results of this comparison indicate that there are cost benefits to be realized if the HAPP capabilities were concentrated in areas of high timber

values. However, for wide use of the HAPP concept only marginal benefits may be achieved.

2.2.2 Ice Mapping

The use of the HAPP concept as an aid to winter navigation was analyzed. By providing maps of ice conditions of the major waterways, economic as well as safety advantages would be realized. The specific system examined for evaluation of the HAPP platform was the Great Lakes Reconnaissance Program. In this mission three radar-equipped HAPPs and a ground control station to monitor and control the radars would be required. In comparison, the existing ICE WARN system utilizes aircraft for its surveillance. Figure 4 presents comparisons of the coverage for project ICE WARN. It was concluded that for equivalent costs the HAPP could provide continuous coverage in comparison to the four times per day coverage of the aircrafts. Further advantages using the HAPP system could also be found in its use as a marine traffic monitor (requiring only a shipboard beacon) and search and rescue aid.

2.2.3 200-Mile Fisheries Zone

The enforcement of the 200-mile fisheries zone was the third remote-sensing candidate examined for use with the HAPP. For this application determination of the location of all fishing vessels, the size and type of equipment used as well as the size of catch are some of the key problems involved in this enforcement duty. Through the use of remote-sensing techniques some of the most basic data can be provided - in particular, ships within the zone, their location and their course. Here it was shown that a HAPP system composed of six HAPP platforms could provide continuous coastal zone coverage for about a third of the cost of an aircraft system providing only four times daily observations. Figure 5 presents the required coverage for the 200-mile limit.

As is apparent from the three discussions, comparisons were made with aircraft for determining HAPP effectiveness. This has been done because of the unusually high frequency of coverage requirement that exists in all these examples. To provide the needed coverage from orbit geosynchronous satellites would be needed, which in turn reduce resolution capabilities or increase costs considerably. Specific satellites, however, were examined and in all cases, based upon present or near-term satellite systems technology, the HAPP systems were superior in either cost, coverage or both.

In general, the results of these recently completed studies indicate that remote sensing application opportunities for the HAPP concept do exist but, the benefits are not totally conclusive. Obvious capabilities exist with the systems, as examined here, but the costs and returns associated with the concept are not established firmly enough to weigh its effectiveness. On the other hand, the results of the communication

applications appear to be much more attractive at this juncture, due to the magnitude of the comparison differences between the HAPP and existing systems.

Two studies are presently being performed to further examine the HAPP concept in terms of potential user applications. These studies' objective is to identify applications, primarily for the experimenter community, to identify potential users within the various application disciplines, and determine requirements of the users in terms of mission requirements (platform design) and sensor requirements (instrument design). Specifically, one study is aimed at the ocean/coastal zone scientific requirements while the other is more broad based and will be evaluating applications in terms of platform capability and effectiveness.

3. PRESENT TECHNOLOGY

High altitude flight with balloons is a well established technique used to conduct scientific experiments and test various space components. The extreme altitudes (above 170,000 feet) are achieved only by minimizing balloon weight and using designs which allow the stresses to be well distributed. These features also result in very fragile structures which are easily damaged during all phases of the operation from manufacture to float altitude. The accommodation of the expansion of an initially small volume of gas requires the balloon envelope to carry its own weight and the payload in a constantly changing variety of configurations. Balloon flights are usually of short duration (less than 1 day) although some have been flown at high altitudes as long as 4-5 days. This is usually the limit due to gas loss and ballasting constraints for zero pressure balloons.

Great endurance has been achieved through the application of the superpressure principle wherein no gas is sacrificed and virtually no balloon volume changes are permitted once the operating altitude is achieved. Since balloons using this approach operate at high pressures, they are heavier and therefore less effective than zero pressure types for reaching high altitudes and are limited to smaller sizes and lower altitudes.

A remotely-controlled long-endurance aerostat platform must combine the features of scientific balloons, both zero pressure and superpressure types, and airships. An existing program which attempts to do this is the HASPA (High Altitude Superpressure Powered Aerostat) - Figure 6. This is a Navy project involving development of a surveillance vehicle. It has not achieved flight status and has experienced several problems which are currently being explored for solution. This vehicle was designed to fly at a nominal altitude of 70,000 feet in minimal winds for periods up to 30 days. It employs on-board power derived from various combinations of fuel cells, batteries, and solar photo-voltaic cells. It is propelled by a stern-located (axial) propeller driven by two electric motors with a maximum total output of 5 H.P. This program has

been described extensively in various papers and reports (Ref. 3, 4, and 5). Certain pertinent details of this system are contained in Appendix A.

An examination of the HASPA shows two major areas where penalties were experienced due to design characteristics. One of these is the use of a superpressure envelope and the other is the use of a heavy propulsion system. Some compensation was made for the superpressure penalty by choosing a more slender envelope shape.

The HASPA concept incorporates many of the characteristics that a high altitude vehicle must have. The difficulties encountered thus far are good examples of the kinds of problems which must be solved prior to achieving success in a HAPP vehicle. Some of these problems may be circumvented by using different design approaches.

4. OPERATING REQUIREMENTS

4.1 Duration

A civil communications vehicle is presumed to be on station 24 hours a day and all year. In practice, this requirement could be met by having dual systems in a ready status with one on standby and one flying.

4.2 Wind

Initial studies examined vehicle size for altitudes up to 100,000 feet. An examination of wind data shows that practical aerostat operation may be feasible only in the stratonull region where minimum velocities are encountered between the tropospheric easterlies over a range of 20-30 km. (66-98,000 feet). Data for a density altitude of 50 mb. (about 68,000 feet) show only one instance of a wind speed in excess of 50 knots in one location (Table 1). The maximum and average wind velocities vary with both altitude and season at any given location. These data show that a 95 percentile probability could be met by a 50 knot maximum vehicle speed for all U. S. locations except a few northern border points at altitudes between 60-72,000 feet. If a 100 percent case is desired, the design velocity would have to be 75-80 knots. For the HAPP study, a 50 knot maximum velocity was assumed at a normal operating altitude of 70,000 feet. A more complete discussion of upper atmosphere wind characteristics can be found in Ref. 5.

5. VEHICLE SIZE AND CHARACTERISTICS

The vehicle size is determined by the total mass of the system which can be broken down as the weight of the lifting gas (W_g), the structural weight (W_s), propulsion

system weight (W_{ps}), and the payload (W_{pl}). A method of representing these relationships as percentages of total displacement (D) was first developed by Burgess (Ref. 6) for airship size estimating. This approach was used with certain modifications to arrive at a preliminary size estimate for the HAPP where:

$$D = W_g + W_s + W_{ps} + W_{pl}$$

$$W_g = \frac{\rho H_e}{\rho_a} D$$

$$W_s = k_1 D$$

(k_1 = structural weight fraction)

$$W_{ps} = (w_p \text{ H.P.}) D$$

(w_p = unit weight of propulsion system)

W_{pl} is specified.

The weight of helium will range between 0.14D and some higher value, depending on degree of purity, moisture content, etc. For this analysis, a value of 0.17D was chosen.

The vehicle structural weight (W_s) is assumed to vary linearly with D and depends on the design approach and other factors. The HASPA vehicle showed a k_1 value of 0.46 for its envelope, fins, patches, and lines. As noted previously this was a superpressure design. For envelopes of the same proportions, a low pressure design could be built for about one-third the weight. If it is assumed that the control (or stabilizing) surfaces represent 25 percent of the total structural weight, then the low pressure envelope design (including fins) equals 0.23D. This leaves 0.6D for propulsion and useful load weight.

The propulsion system weight, W_{ps} , includes all components associated with the system installation and is assumed to vary with the power required. The power required is a function of vehicle drag, airspeed, and propulsion efficiency and can be expressed as:

$$\text{H.P.} = \frac{D^{2/3} \rho v^3}{fk}$$

$$\text{Where } \rho = \text{air density at altitude (slugs)} = \frac{\rho_h}{32.3} = .000139$$

$$= \rho_h = \text{air density at altitude (lb./ft.}^3\text{)}$$

$$v = \text{maximum speed (ft./sec.)} = 84.45$$

$$f = 550 / \left(\frac{1}{\rho_h} \right)^{2/3} = 14.93$$

$$k = \text{propulsive coefficient}$$

$$\text{H.P.} = \left[\frac{.000139 \times (84.45)^3}{14.93 \times 33} \right] D^{2/3} = .17 D^{2/3}$$

Later analysis by SRI indicated that a k value of 23 may be more applicable. This gives a H.P. equivalent to $.246 D^{2/3}$.

The unit weights of the propulsion system components can be expressed as:

$$w_p = w_s [w_m + w_r + w_{pr} + w_w]$$

Where w_s = weight of structure required to support various components (assumed as 5%)

w_m = motor weight

w_r = microwave receiving antenna and power converting system (rectenna)

w_{pr} = propeller weight

w_w = electrical conductors, etc.

According to Brown, (Ref. 7), rectenna weight (w_r) could be as low as 0.1 - 0.5 lb./kW using printed circuits on thin films. If this becomes feasible, it could be ideally suited for the HAPP application. For these preliminary studies, a more conservative assumption was made using unit weights derived from an actual experimental system flown on an airplane. A total unit weight of 0.26 lbs./ft.² was assumed with a maximum power handling capacity of 100 W/ft.²

The total rectenna size is dependent on the beam density. Initial calculations

assumed a value of about 100 mw/cm^2 , but the later (SRI) analysis used a value of about 10 mw/cm^2 . Because the aircraft will not necessarily be aligned with the antenna with regard to polarity, dual rectenna elements were assumed to be required.

Electric motor weight (w_m) is another variable. Small electric motors can weigh as little as 0.25 lb./H.P. . In the Stanford analysis, a unit weight of 1 lb./H.P. was assumed with an additional weight of 0.5 lbs./H.P. for speed reductions.

Electrical conductor weight (w_w) is a critical item. On HASPA this amounted to 49.2 lbs./H.P. . This seems high and exceeded initial estimates by a factor of 5. The NASA initial analysis assumed a unit weight of 25 lbs./H.P. . This was later modified to about 1 lb./H.P. , based on assumed proximity of components.

Propeller weight (w_{pr}) also contributes to the determination of total power and volume requirements, since large diameter propellers are required. Studies show that a 20 - 1 variation is possible.

A range of 22.74 - 40.66 was used in the NASA studies for values of w_p . This range resulted from the use of different assumptions and design approaches for power plant unit weight and location.

Two payload values were specified by Battelle and used by SRI to size the vehicle. These were 130 kg. (286 lbs.) with a 720 watt power requirement, and 720 kg. (1584 lbs.) with a 595 watt power requirement. The two sizes of airships resulting from these payloads were 500,000 cu. ft. and 1,300,000 cu. ft. Other characteristics are listed in Table 2.

6. GENERAL CONCEPT

Figure 7 shows a concept for the HAPP vehicle. It would use a low pressure envelope. Propulsion would be located on a car-like structure near the bottom center of the envelope possibly using long outriggers to achieve some steering control. Surfaces would be used for stabilizing and control in pitch and yaw. A ballonnet air pressure system would be used to maintain envelope shape and control pressure. It would also assist in maintaining static turn. The airship would be flown dynamically heavy or light to maintain altitude when positive or negative superheat effects alter the lift.

This general approach was used to size the airship. Other systems and design approaches, however, were not ruled out as either necessary or desirable.

All studies of the microwave power system were based on using transmitting frequency of 2.45 GHz. This is the only frequency currently recommended by the CCIR for microwave power transmission, and is relatively insensitive to atmospheric and weather attenuation. Considerable technology and power transmission hardware development exists for the use of the 2.45 GHz frequency. Lower frequencies produce lower

efficiencies. However, while higher frequencies are more efficient, attenuation is also a problem. The indications are that first generation vehicles, at least, would operate at 2.45 GHz, but because of the benefits of smaller antenna size (transmitting and receiving), future systems would likely use higher frequencies.

Power densities of 10 mw/cm^2 are a present U. S. standard for commercial microwave equipment. Higher densities would result in smaller transmitting and receiving antennas, but in higher costs. Considering the safeguards which could be used and the limited areas involved, they could be a future possibility.

A combined collection and rectification efficiency of 82 percent has been demonstrated. Slightly higher efficiencies were used in the analysis.

Transmission of the power can be accomplished by either a retrodirective array or a steerable dish antenna. Although retrodirective array technology is not as advanced as the steerable dish, it promises to produce a considerable cost saving over the steerable dish. In either case, the beam must be slewed through a $1\text{-}2^\circ$ angle to compensate for aircraft maneuvers. These angles have an important bearing on the efficiency of the antenna since as the beam is steered off boresight, the peak power density is attenuated. This factor has an influence on the design of the aircraft and selection of its maneuvering characteristics.

7. COSTS

Costs for the two sizes of airships selected are shown in Table 3. These are based on the following assumptions:

1. Envelope costs - \$100/lb.
2. Nonrecoverable envelope
3. Recoverable rectenna and propulsion system
4. No payload capitalization or operating costs included
5. No developmental costs

It can be noted that microwave power costs are over eight times the vehicle costs. There are large uncertainties associated with all of these estimates, but the microwave system is obviously a target for development and more accurate assessment.

One large item in the annual costs is the replacement of an envelope and rebuilding the rectenna. This was based on the deterioration of the envelope material by U. V. and on the difficulty of recovery without irreparable damage. If the envelope life is extended to two years, a 12-25 percent annual cost reduction could be made.

It was estimated that development of an operational HAPP vehicle could run between \$6.5 - 13M.

8. DISCUSSION

A lighter-than-air vehicle would seem to be well suited to the HAPP mission. It offers the stability and the low inertial environment required to achieve the advantages discussed in the early part of this paper. There are, however, several key problems which need to be solved prior to assuming the readiness of the technology. These are as follows:

8.1 Type of Airship

A superpressure design assures reasonable altitude control. The use of a superpressure envelope increases size and power, produces much more severe requirements for materials, and increases the rate of gas loss. If a design can be produced to compensate for temperature and pressure changes by other means, there is a probability that these problems can be alleviated or avoided. Some of the possibilities include:

1. Operating heavy or light using ballonets (as assumed in the SRI study)
2. Heating the gas
3. Compressing and storing the gas
4. Combinations of (1), (2), and (3) with each other or with partial superpressure
5. Use of evaporating-condensing (compound) gas systems

8.2 Materials

The development of a long-life, gas-tight envelope material is another key to achieving the long endurance needed for the mission. The type of performance required seems to be attainable in present day superpressure balloons, but balloon flight conditions are probably less severe than the HAPP would experience.

The size of the vehicle is highly sensitive to any weight increase so the development of a satisfactory envelope material is more complex than equating film thickness to permeability rates. Superheat control, for example, is related to the material selection. If a low-pressure envelope is used, some of the weight saving could be sacrificed for improved material performance, in terms of durability and gas retention. Research and development on reliable high quality thin films and methods of fabrication is needed to assure a reliable envelope fabric.

8.3 Propulsion

It is obvious from the analysis that propulsion weight has an important bearing on the overall system size and complexity. Lightweight electric motors and lightweight propellers are a prime ingredient for keeping this weight to a reasonable value. The

other part of this system is the conduction of power from the power source. As noted for HASPA, this element accounted for a large segment of the total propulsive weight. A possible solution is to use AC power conduction and locate components close to the rectifying system, as was assumed in the SRI study.

8.4 Launching and Recovery

The launching of the HAPP system is the most difficult part of the operation. No specific means for doing this was assumed. Balloons have survived the launch environment even in winds, although failures in this phase are not uncommon. Launching a completely inflated vehicle has been considered and may be possible, but loading conditions, atmospheric turbulence, and the low initial wind velocity at launch could preclude this as a practical solution. Since the airship needs to be equipped with a large rectenna, this component may have to be launched as a rigid or foldable structure if a balloon type launch is used. Several other possibilities exist, such as balloon assisted launches. This aspect interfaces with the baseline design and also requires experimental development to assure success.

8.5 Operating Environment

Although various science programs over the years have yielded a vast amount of data on the upper atmosphere, there may not be sufficient detail available to characterize wind velocity, direction, and turbulence to satisfy requirements for system design. More thorough analysis of existing data is also needed. Determination must be made on the reality of selecting a maximum flight velocity of 50 knots. The rate of velocity and direction change have an important bearing on the selection of control response, sizing of control surfaces, and probably the characteristics of the microwave power system.

9. SUMMARY AND CONCLUSIONS

In conclusion, the HAPP concept in a mission role provides a highly capable and effective aerial platform. Cost advantages of almost an order of magnitude and improved geographical coverage have been shown for certain mission scenarios. As a near earth geosynchronous satellite the line-of-sight capability coupled with point to point and regional coverage capability makes it an excellent communications platform. This communication application can apply to not only mass broadcasting but accessibility to otherwise remote points in the ocean or in underdeveloped areas. The surveillance aspect of HAPP with continuous monitoring capability for shipping in coastal areas for traffic

control, for enforcement of fishing regulations and boundaries, navigation, and detection of forest fires presents an application opportunity which must be further explored.

Research applications exist including the testing of new instruments for spacecraft and for acquiring data to evaluate and perfect data reduction methods. The HAPP could provide precursor evaluation of remote sensing targets to enhance satellite effectiveness by determining frequency ranges for best coverages and best times to perform the monitoring, and at the same time provide continuous truthing information. Finally the area of in-situ sampling not addressed in the previous studies could be effectively supported by the HAPP vehicle. Here a long duration platform could perform atmospheric measurements over specific sites to determine processes that have only been samples on a very limited basis for very short durations.

Microwave power systems have experienced sufficient development that it is possible to predict with assurance that a power supply system of this type can be built. The greatest uncertainty is cost.

Achievement of a dependable operational vehicle is less of a certainty, since a number of technological problems exist which must be resolved. More detailed studies involving specific design approaches and technology development programs in materials, propulsion, and launch and recovery methods will be required to assure success.

References

1. Kuhner, M. B. et al, "Applications of a High Altitude Powered Platform (HAPP)," Battelle Columbus Laboratories, Report No. BCL-OA-TFR-77-5, Sept. 1977.
2. Sinko, James W., "High Altitude Powered Platform Cost and Feasibility Study," Stanford Research Inst. Report, Oct. 1977.
3. Lagerquist, D. and Keen, L. B., "Structural Design of a High Altitude Superpressure Powered Aerostat," AIAA Paper 75-933, July 1975.
4. Petrone, F. J. and Wessell, P. R., "HASPA Design and Flight Test Objectives," AIAA Paper 75-294, July 1975.
5. Hill, M. L. et al, "Station Keeping Analysis of the HASPA Vehicle in the Northern Hemisphere," AIAA Paper 77-1191, Aug. 1977.
6. NACA, TN 194
7. Brown, W. C., "Technology Forecast for Free-Space Power Transmission by Microwave Beam," Paper No. 4-19766, I.E.E.E. MIT International Microwave Symposium.

Optimistic - 2 HAPPS



Pessimistic - 15 HAPPS

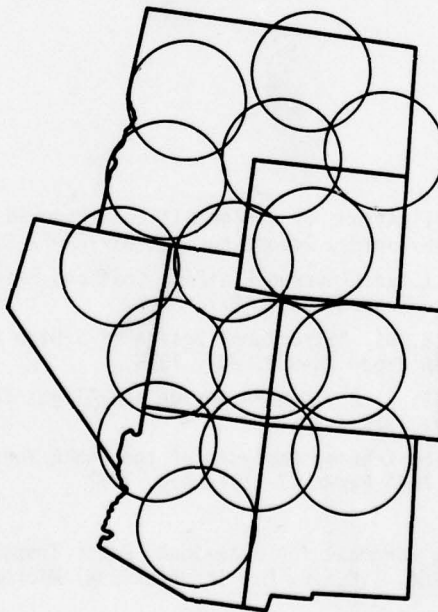


Figure 1. Coverage Extremes for Rocky Mountain States Education Experiment

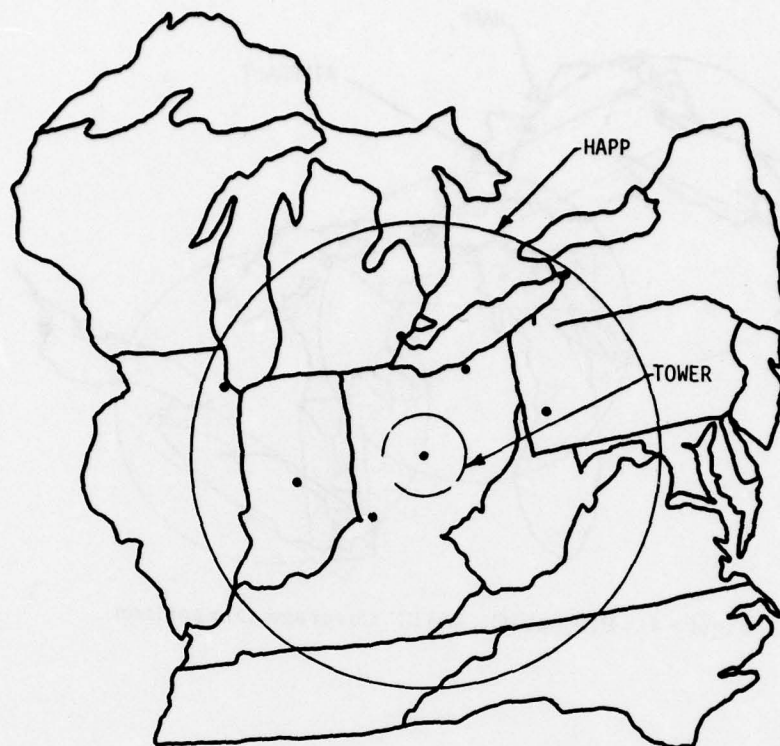


Figure 2. Broadcast Coverage Comparison

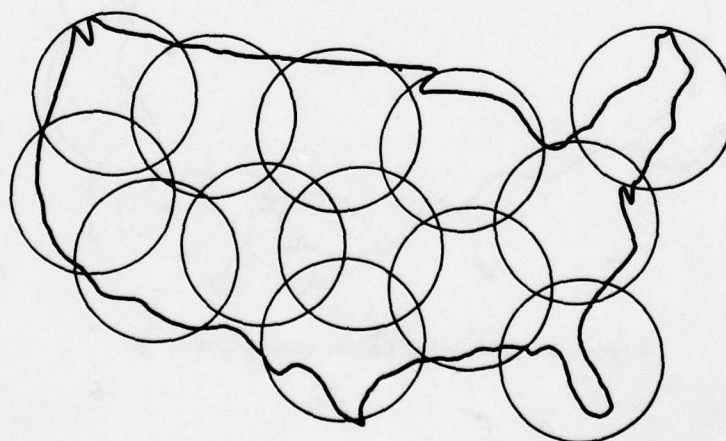


Figure 3. Continental United States Coverage

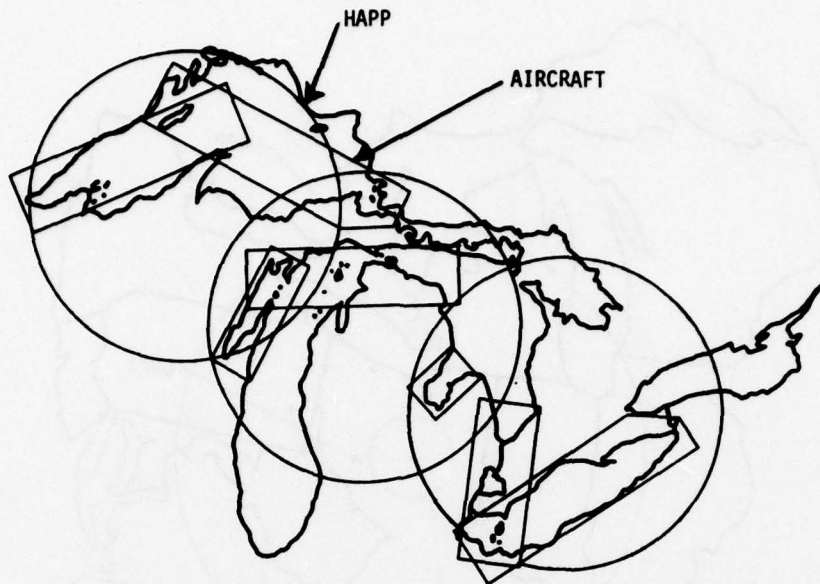


Figure 4. Project ICE WARN Coverage Comparison



Figure 5. 200-Mile Enforcement Coverage

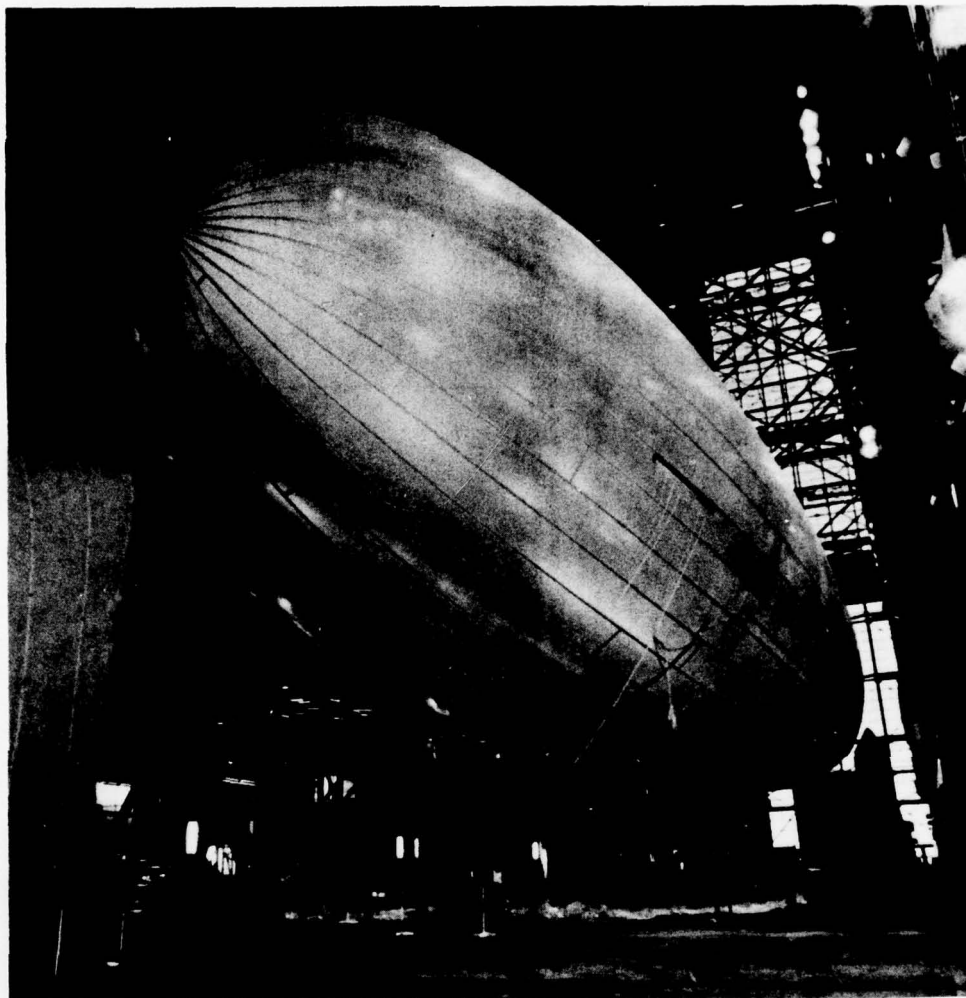


Figure 6. HASPA Balloon

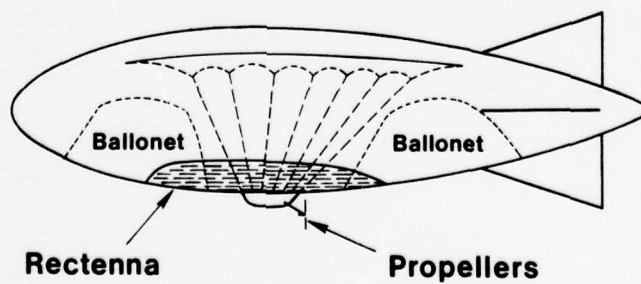


Figure 7. Ballonet Airship Design

Table 1. Wind Speeds at 50 mb (Approximately 68 Kft)

Location	Percent over:		Max mps	Speed Kts
	15 mps (29 Kts)	20 mps (39 Kts)		
Tampa	13.0	2.1	23	45
Lake Charles	8.1	0.3	22	43
El Paso	5.0	0.3	22	43
Oakland	0.3	0	19	37
Portland, ME	7.6	1.7	24	47
International Falls	6.7	1.9	31	60*
Quillayute, WA	1.0	0.3	26	50

* Only recorded speed over 50 Kts

- 1200 and 2400 GMT Radiosonde data December 1969 through November 1970

Table 2. Airship Parameters

	<u>Mission 1</u>	<u>Mission 2</u>
Volume (ft. ³)	500,000	1,300,000
Hull weight (lbs.)	515	1,340
Car weight (lbs.)	150	250
Rectenna weight (lbs.) (.26 lbs./ft. ²)	611	1,156
Motor, propeller, wiring (lbs.)	172	271
Parachute for payload retrievals (lbs.)	50	100
Batteries (lbs.)	50	75
Payload (lbs.)	287	1,587
Control electronics (lbs.)	<u>22</u>	<u>22</u>
Total Weight	1,857	4,801
C _{DV}	0.06	0.05
Propeller efficiency	0.75	0.75
Power (two motors)	42 HP	62 HP
Propeller diameters (ft.)	15	24
Rectenna efficiency	0.85	0.85
Motor, gear reduction efficiency	0.86	0.86

Table 3. Airship Costs (in \$1000)

<u>Vehicle Costs</u>	<u>Mission 1</u>	<u>Mission 2</u>
Rectenna (\$50/ft ²)	115	220
Airframe (\$100/lb)	51	130
Motors (\$1000 + 100/HP)	6	9
Propeller(s)	10	10
Controls/Telemetry	25	25
Helium	<u>5</u>	<u>11</u>
	210	410
 <u>Microwave Power Costs</u>		
Transmitter/Antenna	1,600	1,400
Annual Electricity Cost (@ 2.6¢/KWH)	62	56
Annual Repairs	40	40
Auxilliary Power System	30	30
 <u>Annual Costs</u>		
10% of Capital Costs (2 vehicles)	190	190
Launch and Recovery (yearly)	30	50
Operations	30	30
Replacement, Repairs	110*	220*
Electricity	<u>62</u>	<u>56</u>
Total Annual Costs	420	550

* Replace hull, rebuild rectenna each year

Contents

1. Introduction
2. Fastcom Description
3. Simulation Results
4. Conclusions

A Predictive Steering Control System for Dirigibles

Ralph O. Hookway
Martin Marietta Corp.
Denver, Colorado

Abstract

Results of the simulation of a predictive type of dirigible heading control system are presented. The objective of the system is to increase the speed of dirigible response by optimum use of control torques. This concept is an adaptation of techniques that have been well developed in the process control industry but are unique in airship design. Simulation results show that the predictor system improves the airship's response to pilot commands.

1. INTRODUCTION

Pilot control of manned airships tends to be complicated by the fact that most airships are unstable over an angle of attack range of about ± 10 degrees (in pitch and yaw) and have been inherently stable at larger angles of attack (Freeman, 1932). On the other hand, pilot control tends to be simplified by the very slow response of the airship to control-surface deflections. In other words, airship response is primarily a low-frequency (approximately 0.05 rad/s) phenomenon and is well within the 12-rad/s bandwidth of the pilot (Muckler, 1962). However, turning accelerations of typical airships are quite small (in the range of 0.04 rad/s^2) and are just about at the detection threshold (1.3 deg/s^2 or 0.02 rad/s^2) of the semicircular canals in the human ear (BuAer, 1954). Therefore, pilot detection of turning must be augmented by visual cues obtained from the view out-the-window and/or instruments. Without these added cues, the pilot-airship system operates as an open loop system part of the time, and precision control becomes very difficult.

Thus, flight response of a manually controlled airship is apt to be oscillatory depending on the fin configuration, available control torques, and the ability of the pilot to provide the proper dynamic compensation to the system. This problem is typified by data measured on the ZPG-2W (1956), shown in Figure 1.

From a more qualitative standpoint, impressions of the airship control problem were reported by Ernest Gann (1974):

" . . . I am fascinated by the amount of movement required of the rudder pedals for every course change. It is as though the pilot were walking to our destination.

"There are moments when I am not at all sure who is in charge up here . . . When Columbia wants to go down, she lowers her snout steeply; when she wants to go up, the reverse occurs. I roll the great elevator wheel smartly to minimize the action . . . but the immediate result is hardly satisfying. Likewise, rudder control, with either leg fully extended, continues to suggest that within certain limits Columbia does what she damn well wants to do. If you experienced such limited management of an airplane, the only solution would be to resign immediately and bail out.

"I have flown some headstrong flying machines in my time, but nothing to compare with a blimp."

Thus, early dirigibles were typified by slow response, non-linear aerodynamic characteristics, and relatively low control torques. Also, the pilot is in the very-low frequency part of his bandwidth. He therefore has difficulty maintaining proper control because the effects of control inputs are not immediately apparent to him. Thus, pilot-induced oscillations are easy to generate.

Fargel and Ulbrich (1963) point out that ". . . Any system whose response is a slow and complex function of the input signal and not easily describable by the operator should gain from predictive control. There are a number of real systems with such characteristics, particularly in vehicular control and navigation, where the human operator is still considered indispensable."

The dynamics of the LTA manual control problem has led us to consider two types of manual control-system configurations, as shown in Figures 2 and 3. In Figure 2, the pilot is inside the control loop and is part of the dynamic system. In Figure 3, the pilot is outside the control loop, where he functions as system commander. The system we are considering here is of the type shown in Figure 3, where the predictive logic is included in the flight controls computer.

Chestnut et al discussed (1961) predictive control-system applications, pointing out that predictive control is attractive to minimize the time required to accomplish a change in system state by optimum use of the maximum available control torque. Figure 4 shows Chestnut's approach, and an operational overview is given in the error phase plane portrait, Figure 5. For the aircraft landing problem considered by Chestnut (altitude versus ground range to a desired touchdown point), a typical phase plane trajectory could begin in the third quadrant (aircraft too high, rate of descent too low) with the application of down elevator. As the real-time trajectory enters the

AD-A074 469

AIR FORCE GEOPHYSICS LAB HANSCOM AFB MA
PROCEEDINGS OF THE AFGL SCIENTIFIC BALLOON SYMPOSIUM (10TH) HEL--ETC(U)
MAR 79 C L RICE
AFGL-TR-79-0053

F/G 1/3

UNCLASSIFIED

NL

5 OF 6

AD
A074469



fourth quadrant, predictions are made of when the control torque should be reversed so the trajectory will reach the origin. The predicted trajectories (dashed lines) are in fast time. Control torque is reversed when the prediction shows that the ensuing real-time trajectory after control torque reversal will reach the origin (i.e., the desired touchdown point on the runway).

Chestnut's approach has several attractive features:

- 1) The system can handle time-varying references;
- 2) It tends to reduce an error and its derivative to zero in minimum time;
- 3) It will work successfully for wide variations in knowledge of the controlled vehicle dynamics.

However, the bang-bang or nonlinear characteristics of the concept lead to limit cycling near synchronization.

Predictive control has been studied for control of sluggish industrial processes (Lefkowitz and Eckman, 1959), airplane landing control (Chestnut et al, 1961), submarines (Kelley, 1962), and spacecraft (Fargel and Ulbrich, 1963).

The balance of this paper will consider application of a predictive control system (similar to that in Figures 4 and 5) to manual steering of dirigibles.

2. FASTCOM DESCRIPTION

Figure 6 is single-axis block diagram of a predictive control system for dirigibles adapted from the Chestnut's (1961) airplane landing system. We call our dirigible predictive control system Fastcom (Fast-time-computation).

Assume that, from his PDI cues, out-the-window cues, or both, the pilot decides to change heading. He selects a new heading by rotating a knob on a scale calibrated in degrees of desired heading change, and with another knob selects the desired turn rate. These commands are then processed by the control logic both in real time and in fast time.

The control logic compares the output of the displacement and rate gyros with the commanded heading change and turn rate, and determines whether the displacement and rate errors are of the same or opposite signs. If the initial signs of heading error (ψ_e) and rate of change of heading error ($\dot{\psi}_e$) are the same, the rudder will be deflected to make its sign the same as the sign of the displacement error and thus drive the trajectory to the new heading as rapidly as possible (Figure 7).

The signs of either ψ_e or $\dot{\psi}_e$ change when the phase plane trajectory crosses into the next quadrant and, if nothing is done to the rudder position, ψ_e and $\dot{\psi}_e$ will continue to move away from the origin. Thus, the sign of rudder deflection should be changed at the value of ψ_e and $\dot{\psi}_e$ that will force the trajectory to the origin. The computer determines when the control torque

should be switched by using the present value of ψ_e and $\dot{\psi}_e$ to enter the fast-time predictor at the proper state values and determine the future values of the input. Dirigible response is simultaneously predicted in fast time, $(\psi_e)_{tf}$ and $(\dot{\psi}_e)_{tf}$ are calculated, and the rudder deflection will be switched when

$$(\psi_e)_{tf} = (\dot{\psi}_e)_{tf} = 0.$$

The bang-bang nature of the Fastcom control logic is advantageous because of its maximum use of available control torques, but it causes limit cycling after completion of the basic maneuver. To eliminate limit cycling, we switch from the bang-bang predictive operation to conventional linear control at values of ψ_e and $\dot{\psi}_e$ that are less than a preset threshold.

Dirigible response is modeled by using linearized perturbation side-force and yawing-moment equations. Simultaneous solution of these equations leads to the following transfer function for a typical dirigible with a volume of 800,000 cubic feet:

$$\begin{aligned} \frac{\Delta \psi}{\Delta \delta} &= \frac{\Delta \text{ heading}}{\Delta \text{ control effector}} \\ &= \frac{0.0264 (10.93s + 1)}{s(30.4s + 1)(8.84s + 1)} \\ &= \frac{0.0264}{s(30.4s + 1)} \end{aligned}$$

In Figure 8, the time response of the two degree-of-freedom linearized equations is compared to the time response obtained from a six degree-of-freedom non-linear model when both are commanded to turn from an initial dirigible heading of +90 degrees to a final heading of -90 degrees. The two responses agree closely, so it is considered valid to use the two degree-of-freedom model for this study.

The slow response of dirigibles to turning commands is exemplified by this case in which the maximum turning rate achieved with full rudder is 0.66 deg/s. Therefore the heading angle is not able to keep up with the heading command and it takes approximately 540 seconds to complete the 180 degree turn. The slow turning rate is caused both by the small available control torque and by the nature of the control law. The linear control law used in this example is $\delta = 1.0 (\psi_{\text{ref}} - \psi_b) - 75 (\dot{\psi}_{\text{ref}} - \dot{\psi}_b)$. With this control law the rudder initially goes hard over to establish the commanded turn rate. When the turn rate command returns to zero, the gimballed propeller (acting as the rudder) slowly returns to neutral. No opposite rudder is used. Thus a deadbeat heading response results, but it takes 540 seconds to complete the turn. The effect of increased control torques on the ability of the dirigible to turn more rapidly is also shown in Figure 8.

3. SIMULATION RESULTS

A single-axis Fortran simulation of Fastcom was programmed and used to evaluate Fastcom's potential usefulness.

The yaw moment and side-force equations were used to represent dirigible response in real time and in the fast-time scale model. The simulation is diagrammed in Figure 9.

Fast-time calculations were made at the maximum speed of the laboratory facility, i.e., much faster than the 1-second intervals between calculations of the real-time dirigible state. In other words, the time scaling is $\gg 100:1$. Time scaling of 100:1 has been found satisfactory in submarines and aircraft problems and should be applicable to dirigibles.

The simulation program included the following nonlinearities:

- 1) Rudder gimbal limit = 25 deg
- 2) Rudder gimbal rate limit = 4 deg/s

A simulation of HASPA* with its linear control law is shown in Figure 10 to provide a basis for comparison with Fastcom. The linear control law is $\delta = 1.0 (\psi_{\text{ref}} - \psi_b) + 75 (\dot{\psi}_{\text{ref}} - \dot{\psi}_b)$. In this case the maximum commanded turn rate is 0.6 deg/s which is within the vehicle capability of 0.66 deg/s and the time to turn through 178 degrees is 540 seconds.

Figure 11 shows the error phase plane portrait of the response of the same vehicle as it recovers from initial heading and heading rate errors of 20.28 deg and -0.28 deg/s respectively with the Fastcom control law in operation. The initial response is full rudder

*HASPA - High Altitude Superpressured Aerostat

deflection, but when reverse control is required to stop the turning acceleration, Fastcom sends the rudder hard over in the opposite direction, taking maximum advantage of the available control torque. With Fastcom, the time to reach the phase plane origin is approximately 74 seconds.

Dashed lines in the fourth quadrant of Figure 11 show the operation of the predictive function, i.e., they represent the forecast of where the phase plane trajectory would terminate for control reversal at the noted time.

Limit cycling around the origin is shown in Figure 11. To minimize limit cycling after acquisition, we switch from bang-bang control to linear control when rate and displacement error have been reduced to acceptably small values such as $\psi_e = 0.2$ deg and $\dot{\psi}_e = 0.2$ deg/s.

The sensitivity of Fastcom to various shapes of turn commands was studied briefly. The results are shown in Figures 12, 13 and 14. In each figure the real time trajectory is the solid line and the fasttime predicted trajectories are shown as dashed lines. In Figure 12, the leading and trailing edge of the rate command is a step. This type of command caused large rate errors at the beginning and end of the command. In Figure 13, two smaller steps were used in the leading and trailing edges of the turn commands and although the maximum rate errors were reduced significantly, they were still quite large. The best results obtained are shown in Figure 14 in which the turn rate command was applied and removed as a ramp over

a period of 30 seconds. In each case, to minimize limit cycling after synchronization, the bang-bang Fastcom was switched out and linear control switched in as described above. With Fastcom and the input command of Figure 14, the time to turn 178 degrees was reduced to about 340 seconds, or only 63 percent of the time taken by the linear system.

4. CONCLUSIONS

The Fastcom dirigible control concept greatly increases the speed of dirigible heading response by making more efficient use of available control power. The control logic required can be easily mechanized within a dedicated flight control computer or as part of an overall data-handling and control computer. The system does not require the pilot's direct participation in the control loop, thus reducing his task load and making it possible for him to manage other functions.

Acknowledgment

With great appreciation, the author acknowledges the help of Mr. D. B. Roberts who programmed and ran the simulations included here and who contributed many helpful suggestions.

References

- Freeman, H. B. (1932) Force Measurements on a 1/40 - Scale Model of the U.S. Airship Akron, NACA TR-432.
- Muckler, F. A., Hookway, R.O., and Burke, H. H. (1962) Manned control of large space boosters, Proceedings of 7th Symposium on Ballistic Missiles and Space Technology.
- Anon, (1954) The Human Pilot, BuAer Report AE 61-4 III prepared by Northrop Aircraft, Inc.
- Steffen, E. W. (1956) Performance, Stability and Control, and Miscellaneous Tests Phases, Model ZPG-2W-Report No. 3.

References

- Gann, E. K. (1974) Love Affair with a Fat Lady, Flying May, 1974.
- Fargel, L. C. and Ulbrich, E. A., (1963) Predictor Displays extend manual operation, Controls Engineering, August 1963
- Chestnut, H., Sollecito, W. E., Throatman, P. H. (1961) Predictive - control system application, A.I.E.E. Transactions, Pt. II, Applications and Industry, pp 128 - 139.
- Lefkowitz, I., Eckman, D. P. (1959) Application and analysis of a computer control system, Journal of Basic Engineering, December 1959.
- Kelley, C. R. (1962) Predictor instruments look into the future, Control Engineering, March 1962

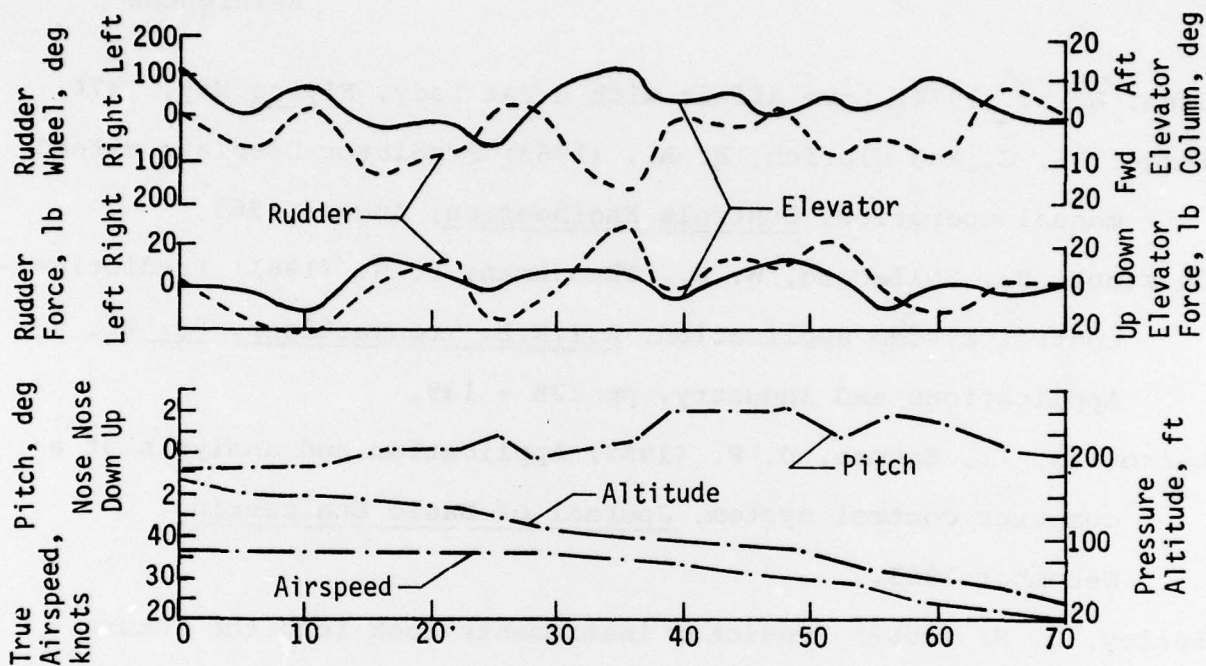


Figure 1. ZPG-2W Control Forces, Normal Landing (Power Boost in Use)

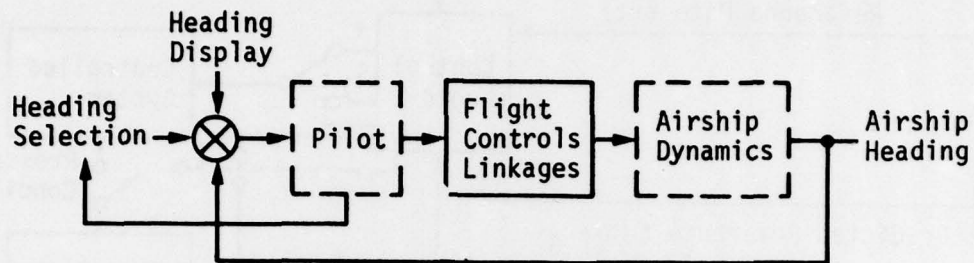


Figure 2. Pilot Inside Control Loop Must Select Desired Headings and Continuously Generate Commands to Control Effectors (surfaces, engine gimbals)

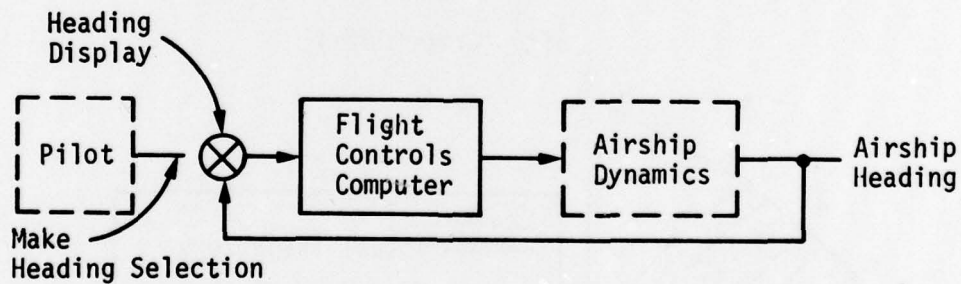


Figure 3. Pilot Outside Control Loop Functions as Commander by Selecting Heading and Letting Autopilot Generate Commands to Control Effectors

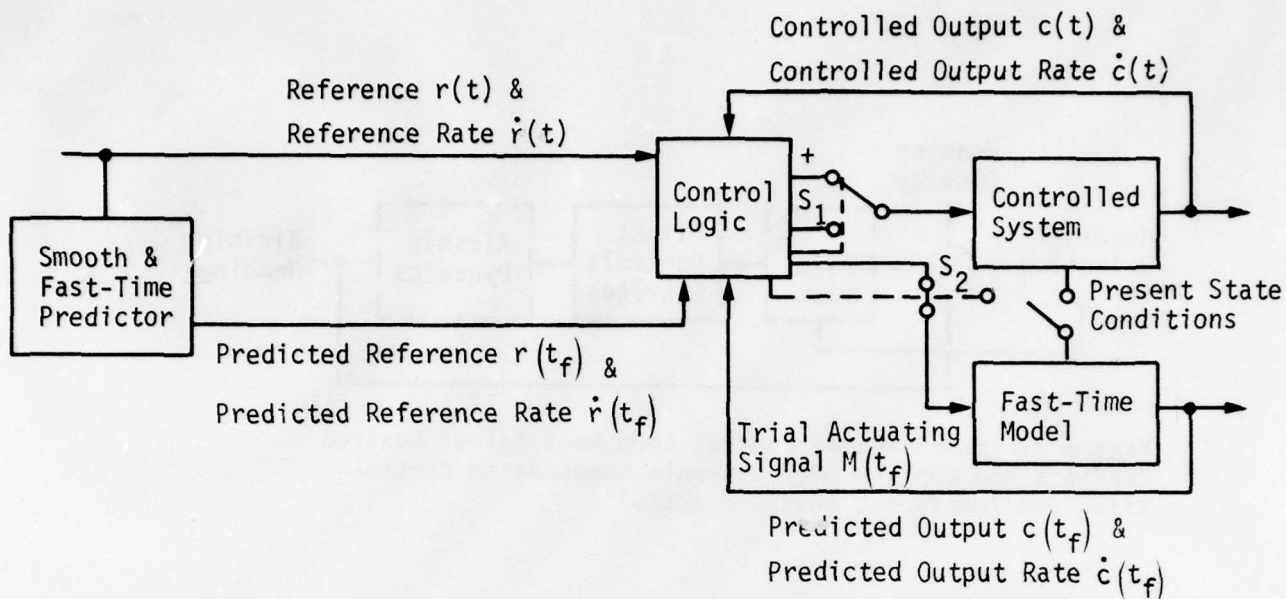


Figure 4. Block Diagram of Predictive Control System [from Chestnut (1961)]

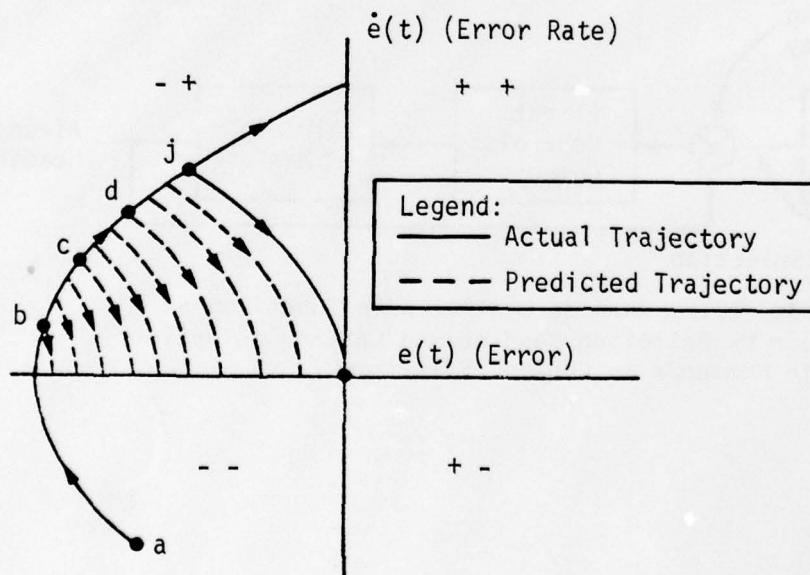


Figure 5. Phase-Plane Portrait for Aircraft Landing [from Chestnut (1961)]

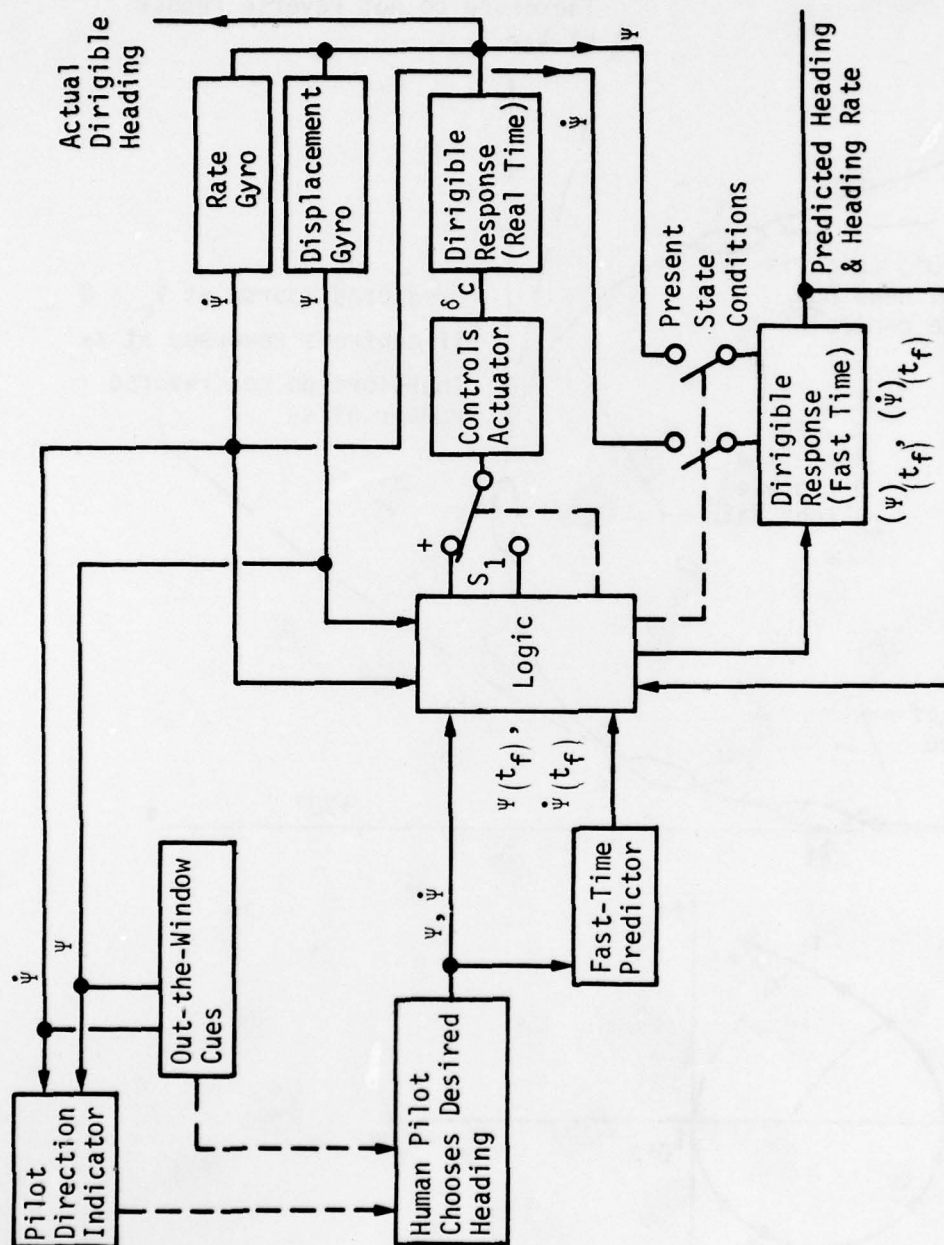


Figure 6. Fastcom Dirigible Heading Control

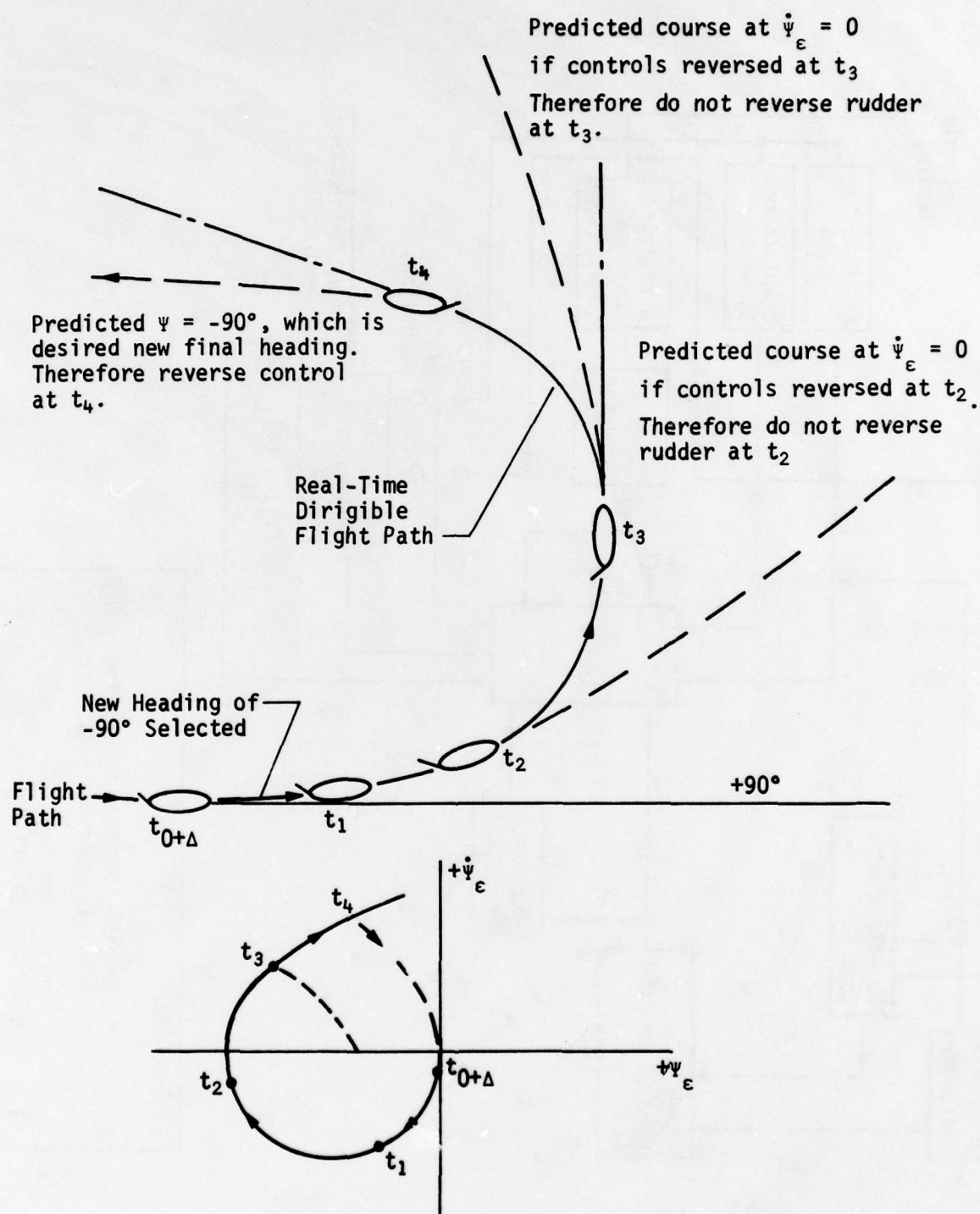


Figure 7. Fastcom Dirigible Steering

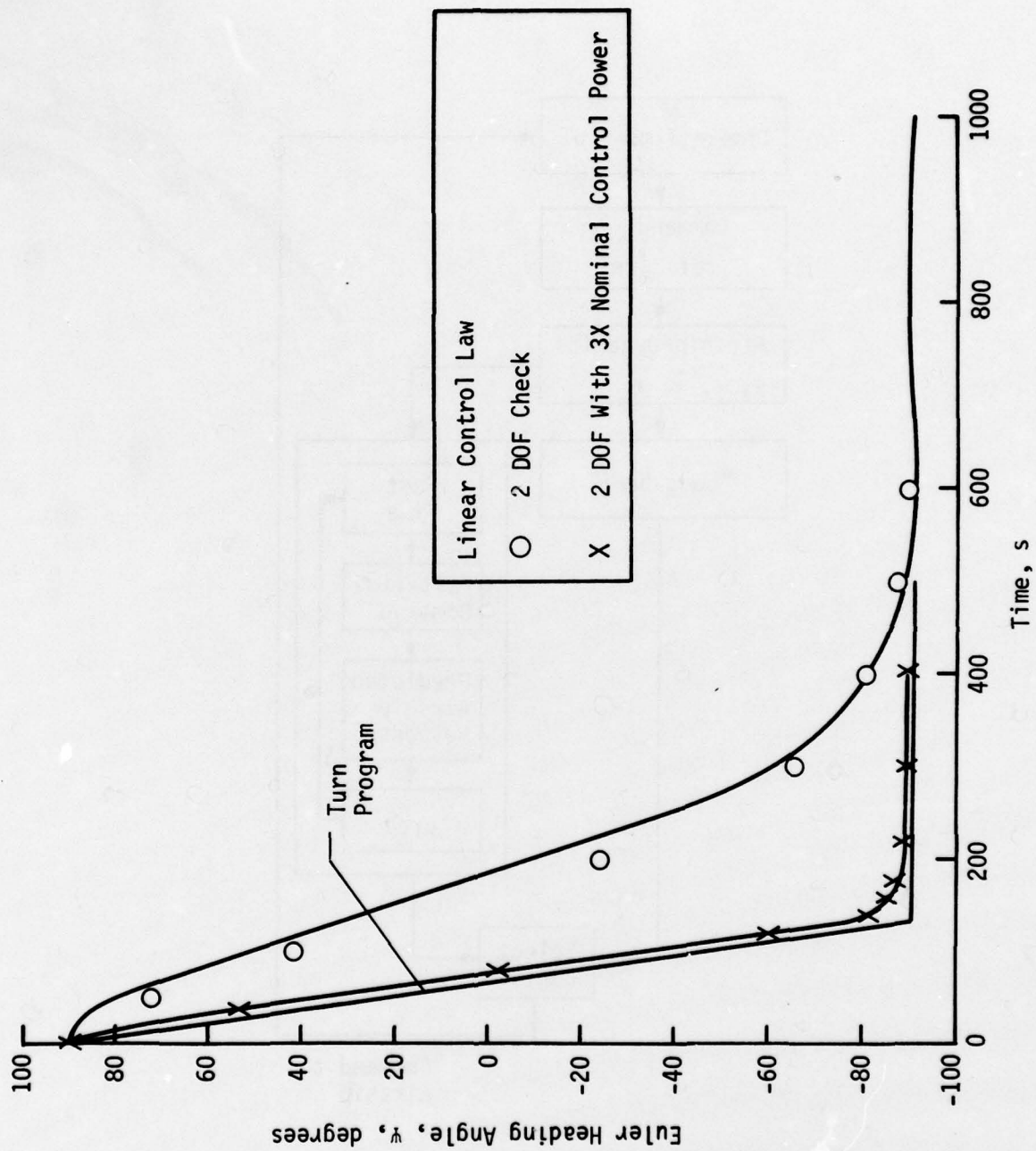


Figure 8. 6-DOF Nonlinear Simulation Time Responses for 180° Turn Program

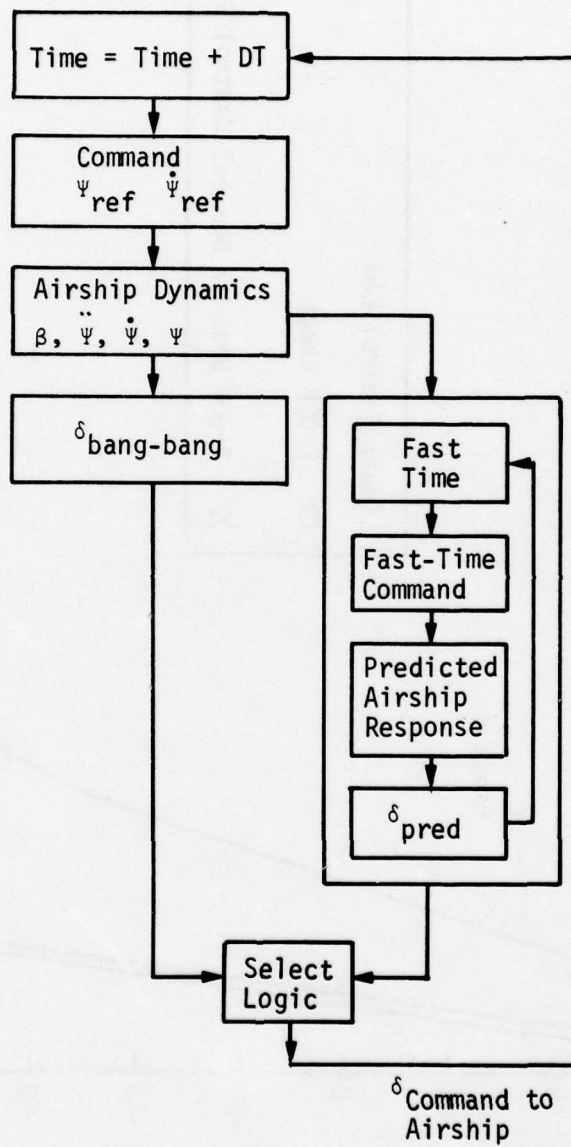


Figure 9. Fastcom Simulation

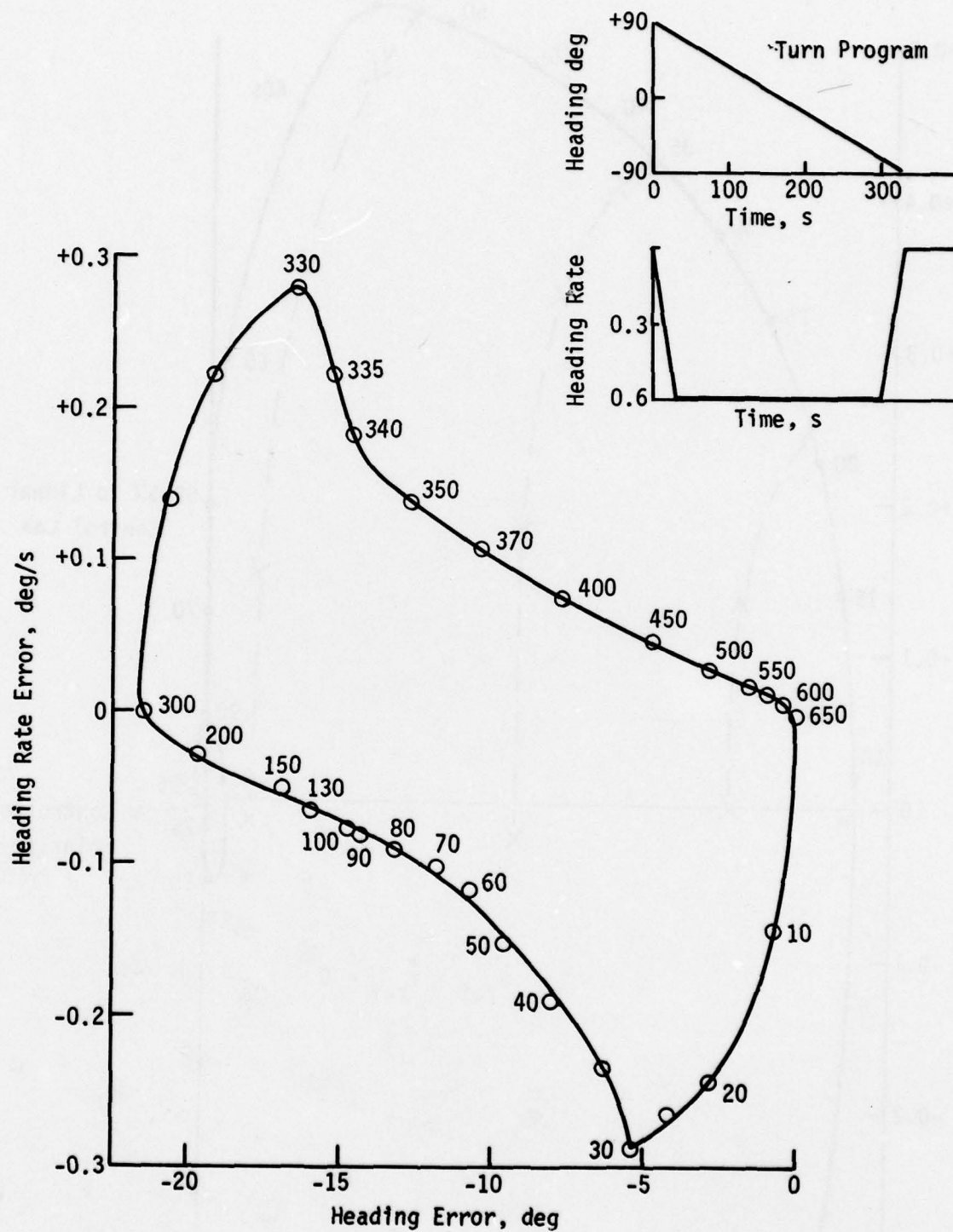
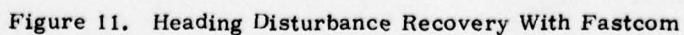


Figure 10. Phase Plane for Linear Control Law



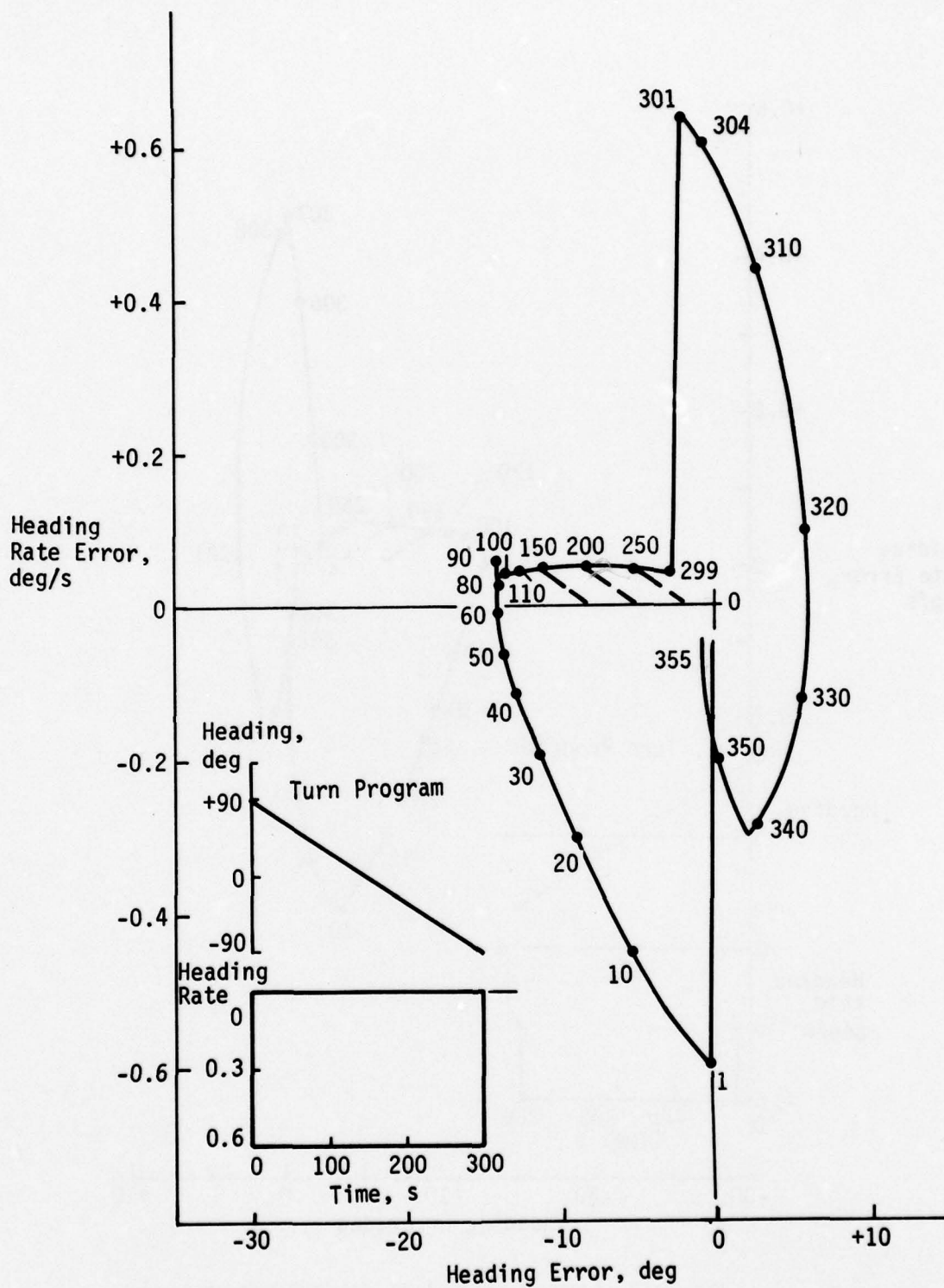


Figure 12. Fastcom Response to Step Turn Program

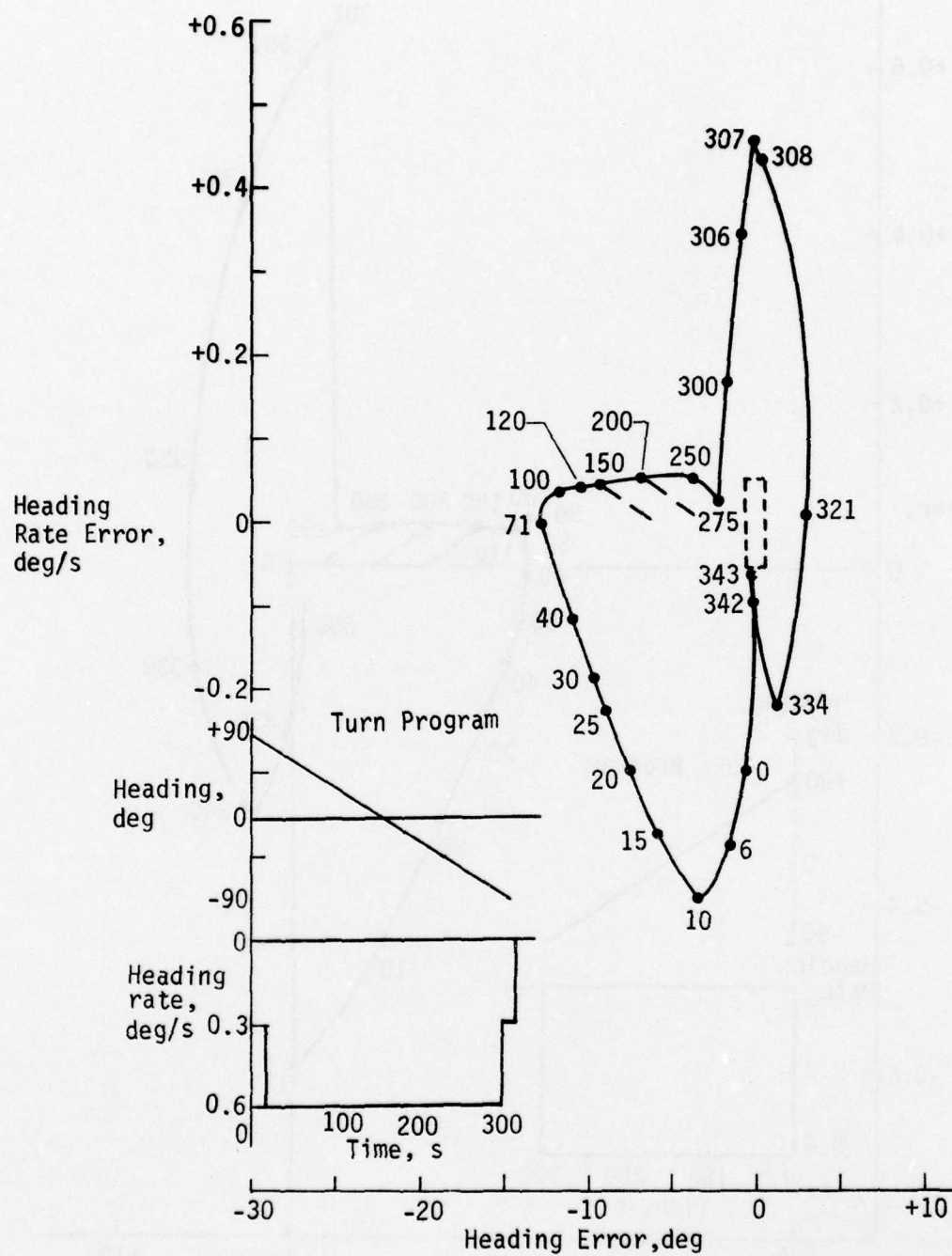


Figure 13. Fastcom Response to Two-Step Turn Program

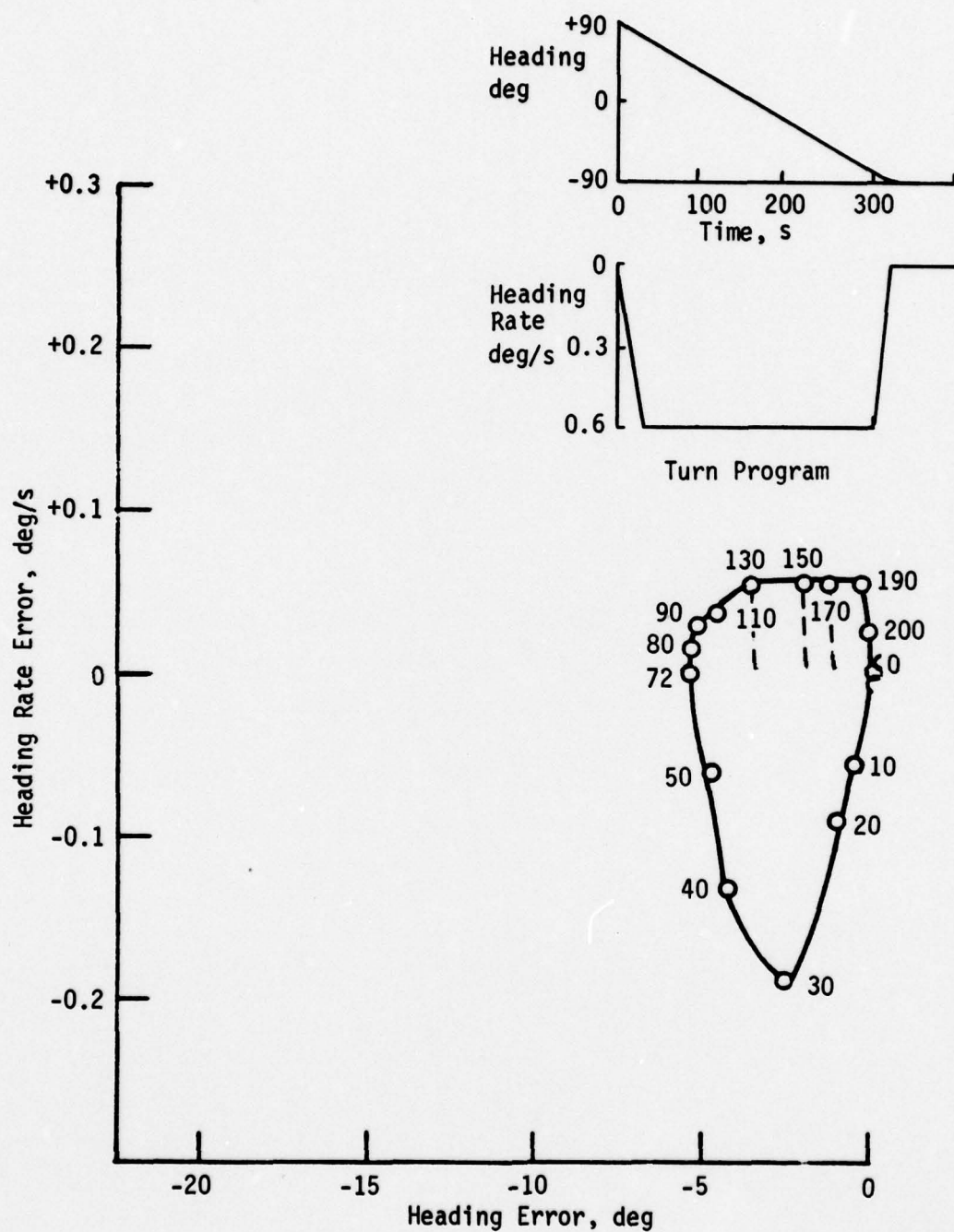


Figure 14. Fastcom Response to Ramp Turn Program

APPLICATIONS FOR A HIGH ALTITUDE RESEARCH DIRIGIBLE (HARD)

Kurt R. Stehling
National Oceanic and Atmos-
pheric Administration
Rockville, MD 20852

High altitude balloons, ascending to 100,000 ft (33,000 m) or more are an established means for studying the upper atmosphere, cosmic rays, and certain astronomical phenomena. They are routinely launched, are mostly reliable and their payloads are generally recovered, more or less intact, by parachute.

The virtues of balloons are offset by several factors listed in order of decreasing importance - or annoyance:

- a. An experimenter may have to wait for propitious weather conditions (low winds, no storms) at his launch site and in many cases, his anticipated payload recovery site. Weather delays may infringe upon the "experiment time window" for certain transient phenomena such as solar emanations; the delay of course always means extra costs for scientists and supporting institutions.
- b. The mission is a "one shot" event. If all goes well the experimenter will have from a few hours to a day or two to gather data. (Certain superpressure balloon long-duration flights and transoceanic - Sicily-U.S.- trips are occasional exceptions.
- c. The cost of the flight has to be amortized over this short time period. The number of launch sites is limited by local winds and weather, launch facilities, ground crew support, tracking and payload recovery. This puts a damper on the dependent missions performable by balloons. For example, much data from total solar eclipses, of great interest to astronomers and other scientists, can best be gotten from high altitude observations. However, the eclipses are rarely gracious enough to occur in geographically convenient areas. The National Aeronautics and Space Administration has made an aircraft available for eclipse expeditions. This can operate around 40,000 feet and can move with the eclipse shadow. However, the aircraft is altitude-limited (for UV/IR etc. observation) and the scanning and detector instruments are limited by available space and most must peer through windows.

d. The unmanned balloons and payloads are operated or controlled via telemetry. While this is a standard and mostly reliable and proven practice and works best for single-purpose experiments, it does not have the flexibility and versatility of manned operations.

The foregoing are some of the more obvious limitations of unmanned, high-altitude balloon missions. Nevertheless, balloons do work and much good and even advanced and new scientific work has been accomplished. So long as nothing better (mostly "cheaper") is available, aerological, cosmic ray and astronomical workers will, and should, continue to use them, especially in the region between 90,000 and 150,000 feet.

But that doesn't mean that other non-rocket vehicles couldn't complement and improve on what balloons could do at "medium" high altitudes. One possibility is an LTA vehicle which, in one system, combines the low-cost lift capacity provided by buoyancy with self-powered mobility and manned on-site experiment manipulation as well as good payload capacity, including astronomical optics with long optical paths.

A manned, high-altitude dirigible is suggested as a candidate that could do the following:

- Operate as high as 85,000 feet (28,000 m).
- Have a cruising radius of about 3,000 miles (5,000 km).
- Have airborne endurance, aloft, of 10-20 days, at reduced or idling propulsion power.
- Have living, operating, and laboratory space for about 8 crew and 10 scientists/technicians.
- Carry about 10 tons of instruments, including:
 - solar telescopes and a coronagraph;
 - x-ray, gamma-ray, IR and UV detectors;
 - conventional high resolution diffraction-limited astronomical telescopes;
 - very high resolution earth and ocean scanners;
 - cosmic ray "telescopes" and other cosmic ray detectors;
 - various microwave instruments including a 1mm (or less) radio telescope;
 - aerological/meteorological instruments.

This vehicle would combine at once the scientific functions and purposes of many higher altitude balloons, while providing the scientist with long duration viewing and detection of phenomena without intervention of a sealing window, some laboratory space for emulsion preparation, instrument check-out and maintenance and calibration -- and computer and data management facilities.

Some of the phenomena which could be peculiarly well observed from the 85,000 ft altitude include:

- most electromagnetic radiation normally absorbed or scattered by the atmosphere; far UV, x- and gamma-ray flux would be, however, at best, quite low, but still detectable;

- some cosmic ray primaries and first-stage showers; detector emulsions could be prepared and stacked with less stray or unwanted radiation fogging than accrues from the normal groundlevel (where scattered radiation is high); preparation of photoemulsions for balloon payloads, other detectors, such as geiger scintillation or spark, or even a smaller bubble or cloud chamber might be used;
- solar disk details revealed from viewing in other than normal visible wavelengths;
- corona details not normally even visible in ground coronagraphs, due to scattering and absorption;
- oceanographic/atmospheric manifestations (waves, currents, temperature turbulence, under-water features, etc.) not readily detectable from spacecraft. The vehicle could linger for days or hover, unlike an aircraft or non-synchronous spacecraft, over a particularly interesting ocean region and do a variety of water and atmosphere scanning and other missions. An example of such a region would be the hurricane "womb" in the Caribbean or S. Atlantic where detailed examination of the ocean surface temperatures, air temperature and humidity, wind vectors and cloud formations (observable by visible, IR and microwave and even laser scanner means as well as by surface data from small buoys dropped by the dirigible) air pressure, electrical activity, etc., might reveal the conception and birth mechanism of young hurricanes. The dirigible would have the great advantage over surface ships by being able to have a simultaneous overview over a large area of ocean and by being able also to examine and analyze the large superimposed atmospheric volume. The vehicle could also track or follow the hurricane.

A wide variety of other ocean/atmosphere, astrophysical and astronomical and earth resource missions suggest themselves. Much of the data gained from the vehicle's activities could be analyzed for "quick-look", or even more penetrating treatment, and the attendant scientist could make needed changes or adjustments to his apparatus.

If the principle of a high altitude, manned, roving science platform can be accepted, what might it look like? Obviously, it would be streamlined and probably cylindrical (instead of a delta shape for aerodynamic lift) and have all the appurtenances of a dirigible: control cabins, engines and engine pods, aerodynamic controls, etc. In other words, the vehicle would look much like a "classical" dirigible - but with certain important modifications resulting from its high altitude design.

It must be remembered that the buoyant gas of an LTA vehicle such as a balloon expands with altitude in order to adjust to ambient pressure. A rubber toy balloon will rise until it bursts, as did latex meteorological balloons. A dirigible, as a "powered balloon", must be able to accommodate expanding lifting gas - say, helium - either by shrinking or contracting air-pressurized "balloonets" within its volume in proportion to the expanding lifting gas, or, it must have under-inflated gas balloons inside its volume which can be allowed to expand with altitude, just as a meteorological balloon does.

Since an ascent from sea-level to just over 80,000 feet means at least a

20-fold expansion of the buoyant gas, it is apparent that the gas must have the requisite volume into which to expand. For example: if the vehicle takes off with 1,000,000 cu ft of helium (which can lift about 33 tons) then that volume of helium will expand to 20,000,000 cu ft at high altitude, and still, of course, be able to lift the 33 tons or so of total weight.

Since we postulated 10 tons of scientific gear, we have only 23 tons left for hull, empennage, cabins, engine(s), etc. That is "slim pickins" for a 20,000,000 cu ft vehicle. Extraordinary design elegance and innovation would be necessary to produce, for example, a strong but light-weight hull, at least 800 feet long and 200 feet diameter. Presumed here is a "monocoque" (eggshell) hull made of very thin ($1/32$ or less) fiber-reinforced composite material, able to contain the leak-prone helium and have enough self-rigidity not to wrinkle or collapse if the interior gas pressure should drop. Also, the hull must serve to embody the science laboratories or cubicles, living and control quarters, communication and data center and engine fuel cells. This is a tall order, but not beyond late 1970's technology. If the hull and cabins and observing "blisters" then weighed 23 tons, we have 10 tons left for personnel, engine(s) and fuel and rear propulsion (ducted) rotor. That, again, would need almost magical (but not impossible) improvements in weight reductions (including crew!) with moderate "breakthroughs" necessary in, especially, engine packaging and weight.

Since aerodynamic drag is very low at these high altitudes, propulsion requirements, at least in terms of fuel consumption, would be low - about 800 lb/day at 20 kt speed. If we allocate five tons to propulsion, of which four tons are fuel, then the vehicle could stay aloft for about eight days, not ten days as the bare arithmetic shows, since fuel consumption from launch to altitude, and descent, would be high, and equivalent to two days of cruising consumption.

The design details, cost, etc., of the vehicle are too complicated, and the concept is too advanced, to permit more than a casual treatment here. It is sufficient to note that light-weight aeronautical structures technology, high-altitude turbo-prop - or ducted rotor technology and high altitude aerodynamic design as well as dirigible technology, as shown in NASA studies, are moving along fast enough to permit at least the suggestion of the concept.

Such a vehicle would not lessen the need for ocean- or weather-scanning satellites, or for most high altitude balloon flights above 90,000 feet, or for the 40,000 ft, or so NASA "flying observatories". Each of these classes of platforms has a special use for specific missions. The HARD would supplement or complement these platforms and would introduce a new dimension into earth scanning and astronomical experiments.

Session V
METHODS AND MODELS

Chairman, Dr. James DeLaurier
University of Toronto

Improved Method for Predicting Attitude of Balloon Gondolas

N. J. Nigro, Associate Professor
Mechanical Engineering Dept.
Marquette University
Milwaukee, Wisconsin 53233

P. Nimityongskul, Graduate Student
Mechanical Engineering Dept.
Marquette University
Milwaukee, Wisconsin 53233

D. E. Hinton, Project Engineer
Langley Research Center, NASA, ESR Branch
Hampton, Virginia 23665

ABSTRACT

The purpose of this paper is to present a method for predicting the attitude (orientation) of research platforms which form a part of many balloon systems used to conduct experiments in the earth's atmosphere. In many cases, where the instruments for conducting the experiments include a radiometer or telescope, it is necessary to first determine the orientation of the research platform to which the instruments are mounted. The attitude determination method described in this paper is completely general and, moreover, has the advantage that it does not require the user to develop a detailed system model (i.e., only the general form of the model is required). This is significant since it is extremely difficult to develop a system model which has a high degree of reliability. The method is a modification of one developed in previous work⁽¹⁾.

1. INTRODUCTION

Balloon systems have been used many times over the past years as a means for conducting experiments in the earth's atmosphere. In some instances the experiments are conducted with instruments which include a radiometer to sense and measure concentrations of selected atmospheric trace constituents or a telescope for high resolution spectroscopy on celestial objects. These instruments are usually mounted on a research platform (gondola) which is attached to the balloon tether via a ball and socket (or ring and clevis) connector. In experiments involving these instruments it is essential to stabilize the platform or predict its orientation in order to determine the direction of the line of sight of the instrument.

Feedback control systems have been employed in the past to stabilize gondolas weighing over one ton to within 30 arc seconds⁽²⁾. Such systems, however, are usually extremely complex and costly. An alternate approach is to permit the platform to swing freely from its suspension point and then predict its orientation (as a function of time) by employing the output of certain attached sensors (e.g., gyroscopes or angular accelerometers). This method was employed previously^(1,3,4) to determine the attitude of the research platform of the LACATE balloon system which will be described in the next section. In this paper, an improved method for determining attitude will be presented.

2. LACATE EXPERIMENT

The LACATE (Lower Atmosphere Composition and Temperature Experiment) mission was a high altitude balloon platform test which employed an infrared radiometer to sense vertical profiles of the concentrations of selected atmospheric trace constituents and temperatures. The constituents were measured by inverting infrared radiance profiles of the earth's horizon. The radiometer line-of-sight was scanned vertically across the horizon at approximately $0.25^\circ/\text{second}$. The relative vertical positions of the data points making up the profile had to be determined to approximately 20 arc seconds.

The balloon system for accomplishing the mission is shown in Fig. 1. It consisted of (a) a 39 million cubic feet (zero pressure) balloon, (b) a load bar containing the balloon control equipment, (c) a package containing additional balloon control electronics with gondola recovery parachute, and (d) a gondola containing the research payload. The balloon was designed to lift the payload to a float altitude of approximately 150,000 feet. Instrumentation to determine attitude consisted of 2 magnetometers and 3 orthogonally oriented precision rate gyros. The magnetometers and rate gyros were flown with the research payload on the instrumentation platform, and their output was telemetered to ground operations for recording and real time data reduction and display. The three rate gyros were employed to obtain an accurate time history of the angular velocity components of the research platform for subsequent data reduction and attitude determination.

An important problem in the LACATE experiment was to determine the orientation (i.e., the attitude) of the instrumentation platform with

respect to a local vertical. Moreover, this orientation had to be determined with high precision. Once this was known, the direction of the line-of-sight of the radiometer could be determined since its relative motion with respect to the platform was prescribed.

3. DEVELOPMENT OF EQUATIONS

The attitude of any research platform can be determined as a function of time if (a) a method for predicting its motion is available and (b) its initial state is known. The motion can be predicted once the math model is determined. The initial state can be obtained by fitting the system motion (as measured by sensors) to the corresponding output predicted by the mathematical model. In the case of the LACATE experiment the sensors consisted of the three orthogonally oriented rate gyros and magnetometers all mounted on the research platform. Thus, the initial state can be determined by fitting the platform rates determined from the gyro output to the corresponding rates predicted from the solution of the math model. All of the necessary equations for accomplishing this will be developed in this section.

The LACATE system was idealized as shown in Fig. 2 in order to develop the form of the system math model. The balloon subsystem was treated as an equivalent rigid body and the mass of the entire system was lumped at the center of gravity of the balloon and positions 1, 2 and 3 as shown in this figure. The ring and clevis connectors at positions 1 and 2 were assumed to be ideal ball and socket joints which permit three dimensional rotation. Twelve generalized coordinates were chosen to specify the system configuration. These consisted of three translational coordinates to locate the mass center of the balloon, three Eulerian angles to specify the orientation of the balloon, and three Eulerian angles to specify the orientation of each of the remaining subsystems (sections).

Several sets of Euler angles are possible for fixing the orientation of each subsystem. The set selected for this study is shown in Fig. 3.

This set was chosen so that, in the case of small motion, the angles θ_i and ψ_i measure pendulation in two mutually perpendicular planes. The pendulation angles in the θ plane are shown in Fig. 4.

A lumped parameter system model was then developed for the balloon system by employing Lagrange's equations and the details for this development can be found in reference 3. A first order form of this model, which involves only the pendulation angles (θ_i, ψ_i) is given as follows:

$$\ddot{\bar{\theta}} + A\bar{\theta} = \bar{0}, \quad (1)$$

$$\ddot{\bar{\psi}} + A\bar{\psi} = \bar{0}, \text{ where} \quad (2)$$

$$\bar{\theta} = \begin{bmatrix} \theta_1 \\ \theta_2 \\ \theta_3 \end{bmatrix}, \quad \bar{\psi} = \begin{bmatrix} \psi_1 \\ \psi_2 \\ \psi_3 \end{bmatrix},$$

θ_i, ψ_i = pendulation angles in the two orthogonally oriented planes, and

$$A = (a_{ij}) \quad i, j = 1 \dots 3$$

It is important to note that, for the particular set of Euler angles chosen in this study, equations (1) and (2) describe the form of the model for a general balloon system with any number of subsystems separated by ball and socket connectors.

The relationship between the platform motion $(\theta_3, \dot{\theta}_3, \psi_3, \dot{\psi}_3, \phi_3$ and $\dot{\phi}_3)$ and the platform angular velocity components $(\omega_1, \omega_2, \omega_3)$ is obtained through the application of the Euler angle transformations. These transformation equations are given below for the system platform which is shown in Fig. 5.

$$\omega_1 = \dot{\theta}_3 \cos \psi_3 \cos \phi_3 + \dot{\psi}_3 \sin \phi_3, \quad (3)$$

$$\omega_2 = -\dot{\theta}_3 \cos \psi_3 \sin \phi_3 + \dot{\psi}_3 \cos \phi_3, \text{ and} \quad (4)$$

$$\omega_3 = \dot{\theta}_3 \sin \psi_3 + \dot{\phi}_3, \text{ where} \quad (5)$$

$\omega_i (i = 1, 2, 3)$ = angular velocity components of the platform
along \bar{e}_i direction,

θ_3 = Platform (pendulation) angle in the $\bar{e}_2 \bar{e}_3$ plane,

ψ_3 = Platform (pendulation) angle in the $\bar{e}_1 \bar{e}_3$ plane, and

ϕ_3 = Platform (spin) angle about the \bar{e}_3 axis.

Eqs. (3-5) enable one to determine the platform angular velocity components relative to an axis fixed in the earth. The revised linearized form of the equations, corrected for earth rate, are given below:

$$\omega'_1 = \dot{\theta}_3 \cos \phi_3 + \dot{\psi}_3 \sin \phi_3 + \omega_E \cos \lambda \cos \phi_3, \quad (6)$$

$$\omega'_2 = \dot{\theta}_3 \sin \phi_3 + \dot{\psi}_3 \cos \phi_3 - \omega_E \cos \lambda \sin \phi_3, \quad (7)$$

$$\omega'_3 = \dot{\phi}_3 + \omega_E \sin \lambda, \text{ where} \quad (8)$$

λ = latitude of location,

ω_E = earth's rate, and

$\omega'_i (i = 1, 2, 3)$ = angular velocity components (along \bar{e}_i
direction) relative to an inertial reference
axis.

The above equations are inverted to obtain $\dot{\theta}_3$, $\dot{\psi}_3$ and $\dot{\phi}_3$ as a function of ω'_i and ϕ_3 ; this yields:

$$\dot{\theta}_3 = \omega'_1 \cos \phi_3 - \omega'_2 \sin \phi_3 - \omega_E \cos \lambda, \quad (9)$$

$$\dot{\psi}_3 = \omega_1^i \sin \phi_3 + \omega_2^i \cos \phi_3 , \quad (10)$$

$$\dot{\phi}_3 = \omega_3^i - \omega_E \sin \lambda . \quad (11)$$

Once the initial state ($\theta_3(0)$ & $\psi_3(0)$) is known, then the orientation (attitude) of the research platform can be obtained by integrating Eqs. (9-11) where ω_1^i is given from the gyros ($\hat{\omega}_1$).

4. SOLUTION OF EQUATIONS

The solution to Eq. (1) can be obtained by assuming the following form for $\bar{\theta}$; i.e.,

$$\bar{\theta} = \bar{X} \sin \Omega t. \quad (12)$$

Substitution of Eq. (12) into Eq. (1) yields the following eigenvalue problem,

$$A\bar{X} = \Omega^2 \bar{X}, \text{ where} \quad (13)$$

$$\bar{X}_i = \begin{bmatrix} X_{1i} \\ X_{2i} \\ X_{3i} \end{bmatrix} \text{ are the eigenvectors } (i = 1, 2, 3) \text{ and}$$

$\Omega_i (i = 1, 2, 3)$ are the respective eigenvalues which correspond to the natural frequencies of the system.

The solution to Eq. (2) can be obtained in the same manner and leads to the identical eigenvalue problem.

The closed form solution for the platform rates ($\dot{\theta}_3, \dot{\psi}_3$) can now be written as follows:

$$\begin{aligned} \dot{\theta}_3 = & \Omega_1 (C_1 \cos \Omega_1 t - C_2 \sin \Omega_1 t) \\ & + \Omega_2 (C_3 \cos \Omega_2 t - C_4 \sin \Omega_2 t) \\ & + \Omega_3 (C_5 \cos \Omega_3 t - C_6 \sin \Omega_3 t), \text{ and} \end{aligned} \quad (14)$$

$$\begin{aligned} \dot{\psi}_3 = & \Omega_1 (C_7 \cos \Omega_1 t - C_8 \sin \Omega_1 t) \\ & + \Omega_2 (C_9 \cos \Omega_2 t - C_{10} \sin \Omega_2 t) \\ & + \Omega_3 (C_{11} \cos \Omega_3 t - C_{12} \sin \Omega_3 t) \end{aligned} \quad (15)$$

It should be noted that Eqs. (14-15) can be easily generalized for the balloon system with n subsystems.

From Eqs. (14) & (15) it is clear that the evaluation of the initial platform state ($\theta_3(0)$, $\psi_3(0)$) requires the determination of the twelve constants $C_1 \dots C_{12}$. These constants, however, are not independent since the initial rates computed from Eqs. (14) and (15) must be equal to those computed from Eqs. (9) and (10). This results in two constraint equations which relate the twelve constants.

The solution for the platform spin angle (ϕ_3) is obtained by integrating Eq. (11) with ω_3^i set equal to the gyro rate ($\tilde{\omega}_3^i$). This yields

$$\phi_3 = \phi_3(0) + \int_0^t (\omega_3^i - \omega_E \sin \lambda) dt \quad (16)$$

where the initial spin angle $\phi_3(0)$ can be obtained from the magnetometers.

5. ATTITUDE DETERMINATION METHOD

As stated earlier, this method for predicting the attitude of the research platform is a modification over the one presented in reference (1). A flow chart illustrating the new method is given in Fig. 6. With this method:

- (a) The unknown parameters are determined by fitting over the platform rates ($\dot{\theta}_3, \dot{\psi}_3$) instead of the platform angular velocities ($\omega_1, \omega_2, \omega_3$),
- (b) The platform orientation ($\theta_3(t), \psi_3(t)$) is determined by integrating the angular velocities obtained from the gyros instead of predicting it from the closed form solution of the system math model, and
- (c) The system natural frequencies are determined along with the initial state parameters instead of obtaining them from the solution to the system math model.

As a result of the above modifications, this new method has several advantages over the one presented earlier. First, by retaining the system frequencies (Ω_i) as additional unknown parameters it is no longer necessary to develop a detailed system model; only its general form is required. This is important since it is extremely difficult to develop a detailed system model which has a high degree of reliability. Second, by fitting over the platform rates, the optimization problem becomes uncoupled and this results in a reduction in the number of parameters to be determined at one time. The method for determining these parameters is discussed in the next section.

6. PARAMETER DETERMINATION METHOD

The object of the parameter determination method is to enable one to determine the unknown constants $\Omega_1 \dots \Omega_3, C_1 \dots C_{12}$ such that the rates $\dot{\theta}_3(t)$ and $\dot{\psi}_3(t)$ predicted from Eqs. (14-15) fit (over some time interval $0 \leq t \leq T$) those predicted from Eqs. (9-10) with $\omega_i^!$ obtained from the gyros. For the purpose of this work these constants were determined by minimizing a function Φ , where

$$\Phi = \sum_{i=1}^N (\dot{\theta}_i - \dot{\hat{\theta}}_i)^2 + (\dot{\psi}_i - \dot{\hat{\psi}}_i)^2, \quad (17)$$

N = number of data points in the interval $0 \leq t \leq T$,

$\dot{\theta}_i, \dot{\psi}_i$ = platform rates computed from Eqs. (14-15), and

$\dot{\hat{\theta}}_i, \dot{\hat{\psi}}_i$ = platform rates computed from Eqs. (9-10).

It is important to note that the above optimization problem becomes uncoupled once the frequencies (Ω_i) are specified since the constants $C_1 \dots C_6$ do not enter into the expression for $\dot{\psi}_3$ nor do $C_7 \dots C_{12}$ enter into the expression for $\dot{\theta}_3$. Without this coupling, the parameters $C_1 \dots C_{12}$ could be determined by solving the following optimization problems:

$$\min \Phi_1 = \sum (\dot{\theta}_i - \dot{\hat{\theta}}_i)^2, \text{ and} \quad (18)$$

$$\min \Phi_2 = \sum (\dot{\psi}_i - \dot{\hat{\psi}}_i)^2, \text{ where} \quad (19)$$

$$\Phi = \Phi_1 + \Phi_2. \quad (20)$$

In order to take advantage of this property, a method was devised to search for the unknown constants in three separate stages. A flow chart illustrating this search method is presented in Fig. 7. In addition to reducing the number of unknowns to be determined at any one stage, the

method also has the advantage that the constants $C_1 \dots C_6$ and $C_7 \dots C_{12}$ are now obtained by solving linear equations. This results in a considerable saving of computer time.

7. RESULTS AND CONCLUSIONS

In order to obtain verification of the accuracy, precision and convergence of the proposed method, a test problem was developed by simulating the LACATE balloon system. The equations for the simulated system were identical to those developed in the previous sections; the constants (e.g., λ , Ω_i , etc.) corresponded to those of the actual system. The testing process consisted of the following steps: (a) values were assigned to the unknown parameters $\Omega_1 \dots \Omega_3$, $C_1 \dots C_{12}$, (b) the platform rates ($\dot{\theta}_3$ and $\dot{\psi}_3$) were computed from Eqs. (14-15), (c) the corresponding values of $\omega_1' \dots \omega_3'$ were generated from Eqs. (6-8)* and (d) the latter were employed (as input) with the method to recover the values of the unknown parameters. Results obtained from several test cases are presented in table 1; the results demonstrate that the method is capable of recovering both the system frequencies and the initial platform state with good precision.

The method was also employed in conjunction with the gyro data obtained from the LACATE system. Values of the platform rates ($\dot{\theta}_3$, $\dot{\psi}_3$) were obtained and typical values are shown plotted (against the actual values predicted from the gyro data) in Figs. 8-9. The corresponding plots of θ_3 and ψ_3 are presented in Fig. 10. The predicted values of $\Omega_1 \dots \Omega_3$ are presented in table 2 along with the values obtained in earlier work⁽⁴⁾ from a solution of the system math model.

Values for the initial platform state ($\theta_3(0)$, $\psi_3(0)$) were also obtained by employing several different time intervals in order to test the consistency of the results. These values are presented in table 3.

*For purposes of the test problem, $\dot{\phi}_3$ was taken as a constant.

In general the results obtained thus far indicate that the method may have considerable merit for determining the attitude of balloon borne research platforms. However, further tests must be conducted to determine the sensitivity of the results to errors in gyro and magnetometer data. This will be the subject of future research.

References

1. N. J. Nigro, A. F. Elkouh, et. al., "Attitude Determination of the LACATE Balloon System", Proc. Ninth AFGL Scientific Balloon Symposium, 20: 239-262.
2. L. N. Haser, "Dynamics and Attitude Control of the IM IR-Telescope Balloon Gondola", Proc. Ninth AFGL Scientific Balloon Symposium, 20: 263-274.
3. N. J. Nigro, A. F. Elkouh, et. al., "Attitude Determination of a High Altitude Balloon System; Part I. Development of the Mathematical Model", NASA Report CR-142193, 1975.
4. N. J. Nigro, A. F. Elkouh, et. al., "Attitude Determination of a High Altitude Balloon System; Part II. Development of the Parameter Determination Process", NASA Report CR-145958, 1976.

Table 1. Results from Test Problem

Unknown Parameters	Case Study #1		Case Study #2		Case Study #3	
	Actual Values	Predicted Values	Actual Values	Predicted Values	Actual Values	Predicted Values
α_1	3.0	3.0	3.0	3.0	3.0	3.0
α_2	0.7	0.7	0.7	0.7	0.7	0.7
α_3	0.1	0.1	0.1	0.1	0.1	0.1
$\theta_3(0)$	3.84×10^{-3}	3.84×10^{-3}	4.60×10^{-3}	4.60×10^{-3}	1.49×10^{-4}	1.43×10^{-4}
$\psi_3(0)$	-1.11×10^{-3}	-1.11×10^{-3}	-2.73×10^{-3}	-2.73×10^{-3}	1.77×10^{-4}	1.74×10^{-4}

Table 2. Results for Natural Frequencies of LACATE System

Ω_i	Values Obtained from Improved Method	Values Calculated from System Math Model, Reference (4)
Ω_1	3.00	3.04
Ω_2	0.70	0.71
Ω_3	0.04	0.13

Table 3. Values of Initial Platform Angles Obtained With Different Time Intervals

Initial Platform Angle (radians)	T = 40 sec	T = 50 sec	T = 60 sec	T = 70 sec
$\theta_3(0)$	2.0×10^{-3}	3.1×10^{-3}	3.2×10^{-3}	3.9×10^{-3}
$\psi_3(0)$	-1.1×10^{-3}	-1.2×10^{-3}	-0.6×10^{-3}	-0.8×10^{-3}

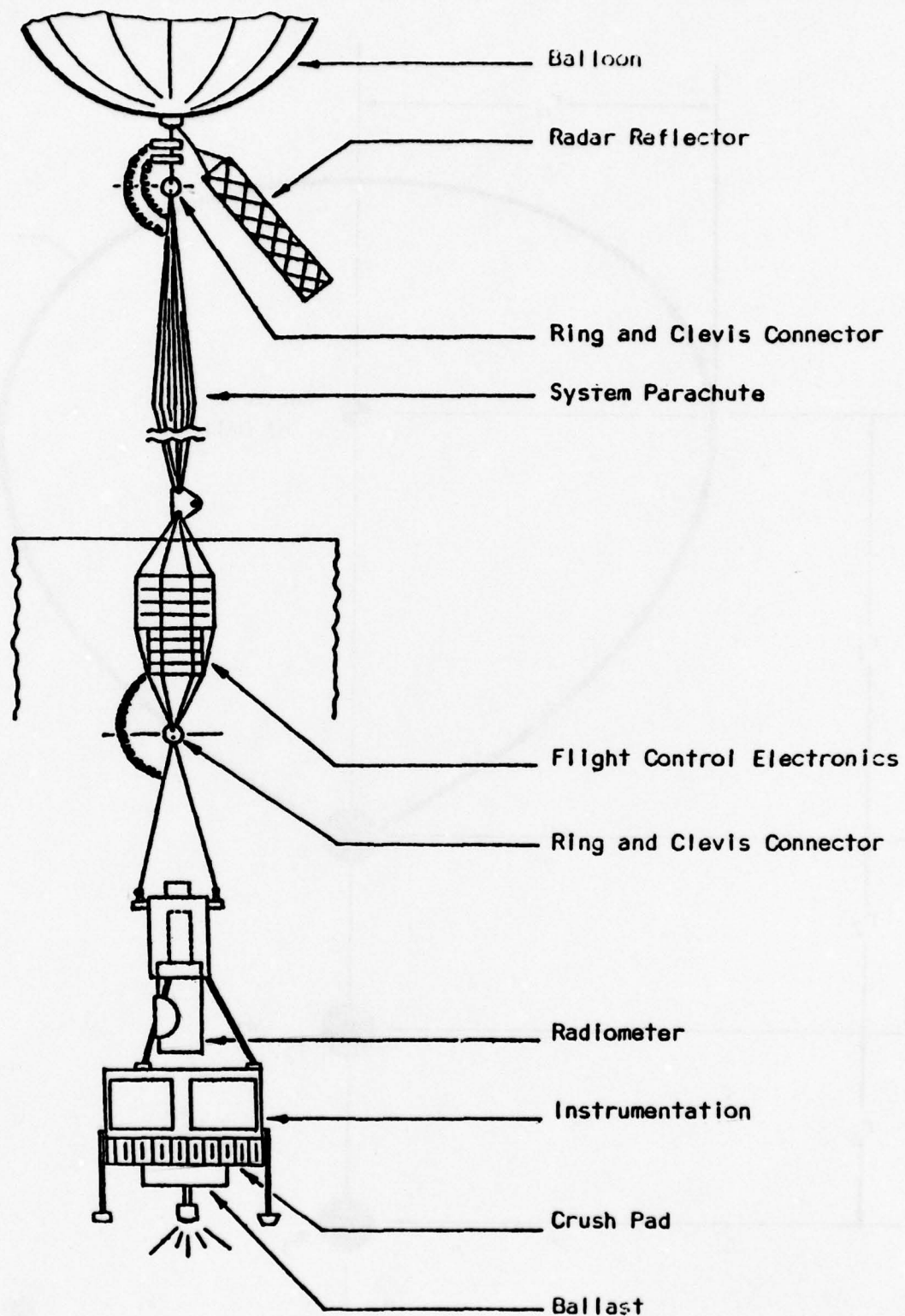


Figure 1. LACATE Balloon System

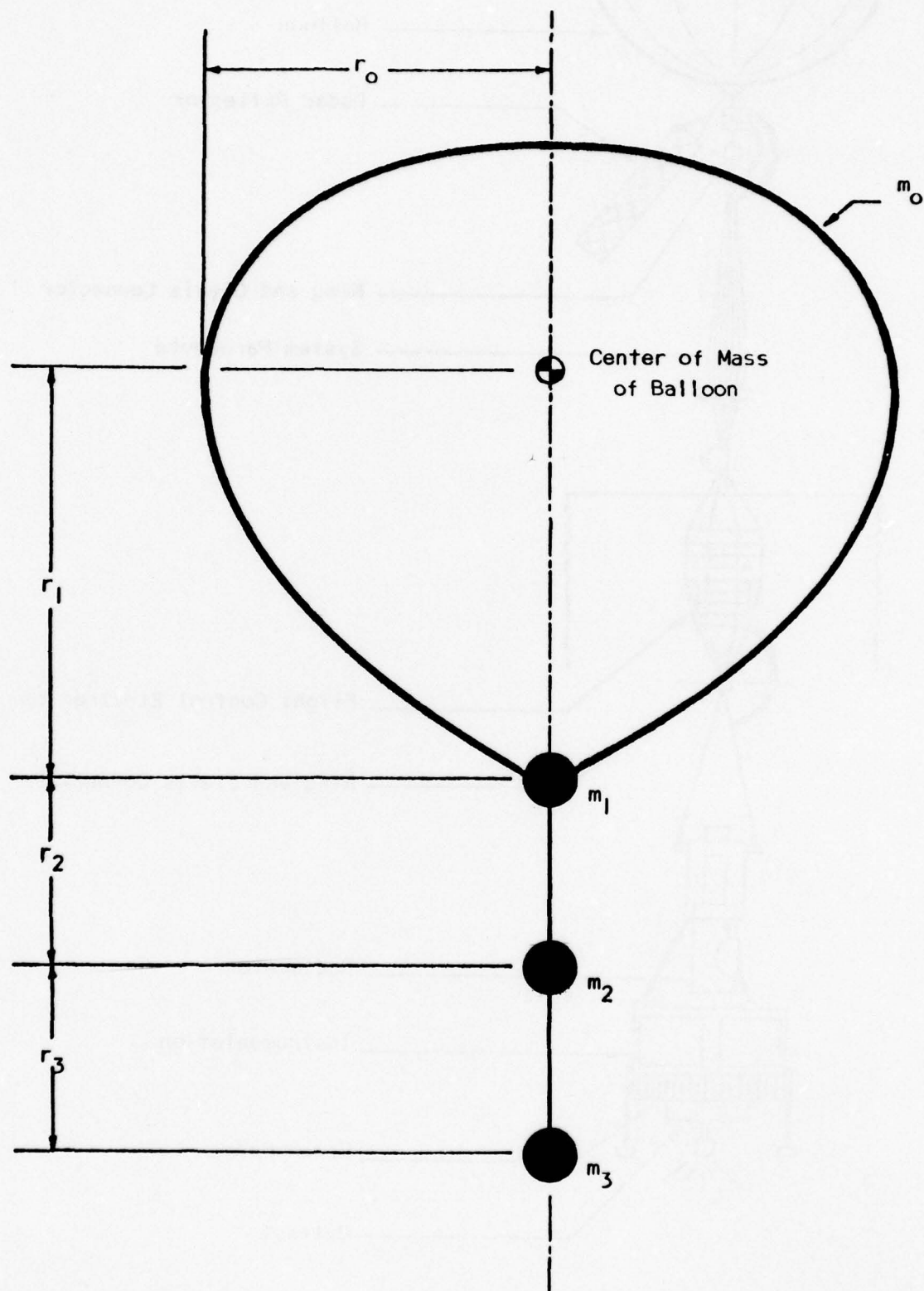
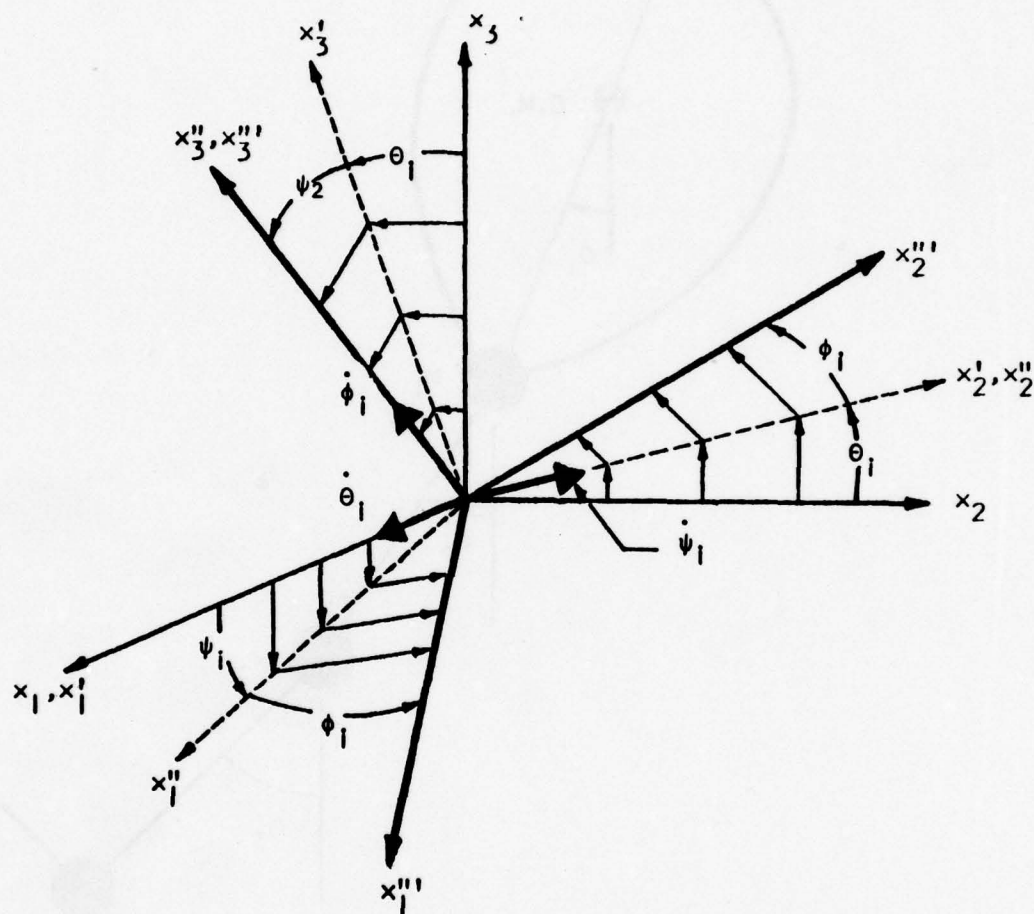


Figure 2. Idealized LACATE System



- (1) $\dot{\theta}_1$ about x_1 axis
- (2) $\dot{\psi}_1$ about x_2' axis
- (3) $\dot{\phi}_1$ about x_3'' axis

Figure 3. Rotations Defining Eulerian Angles

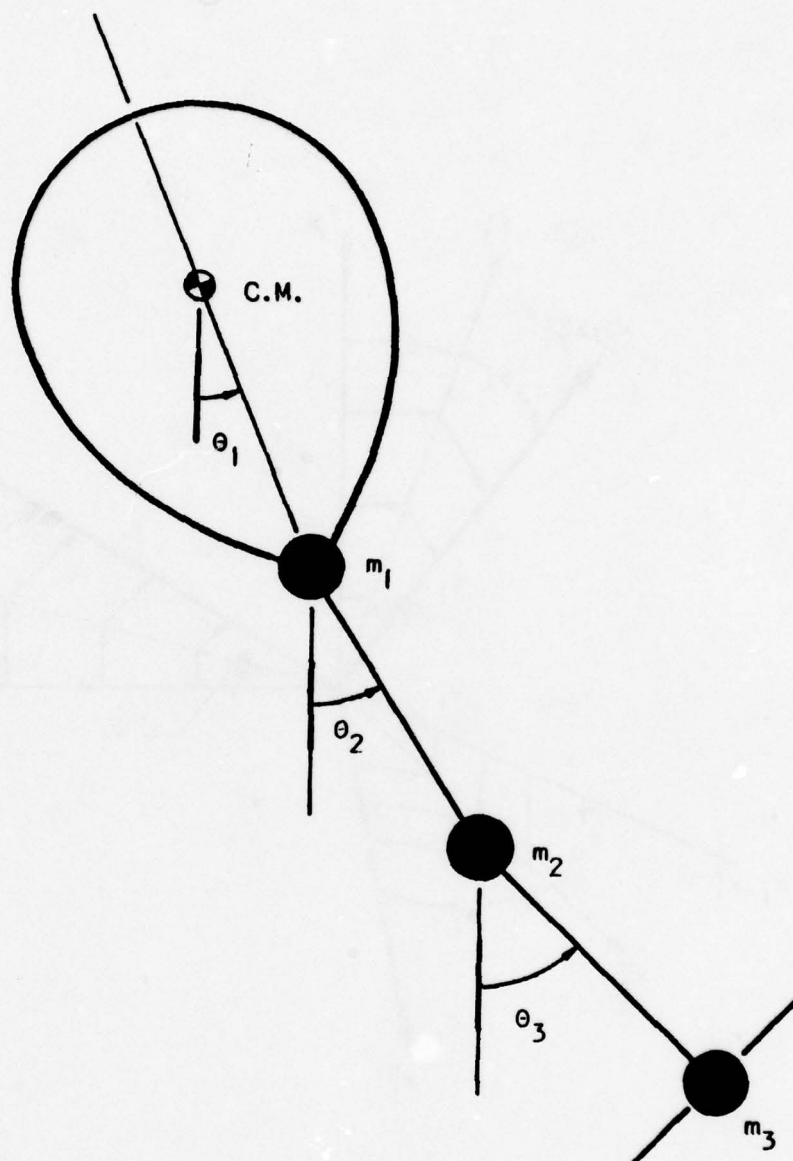


Figure 4. Pendulation Angles in $X_2 X_3$ Plane

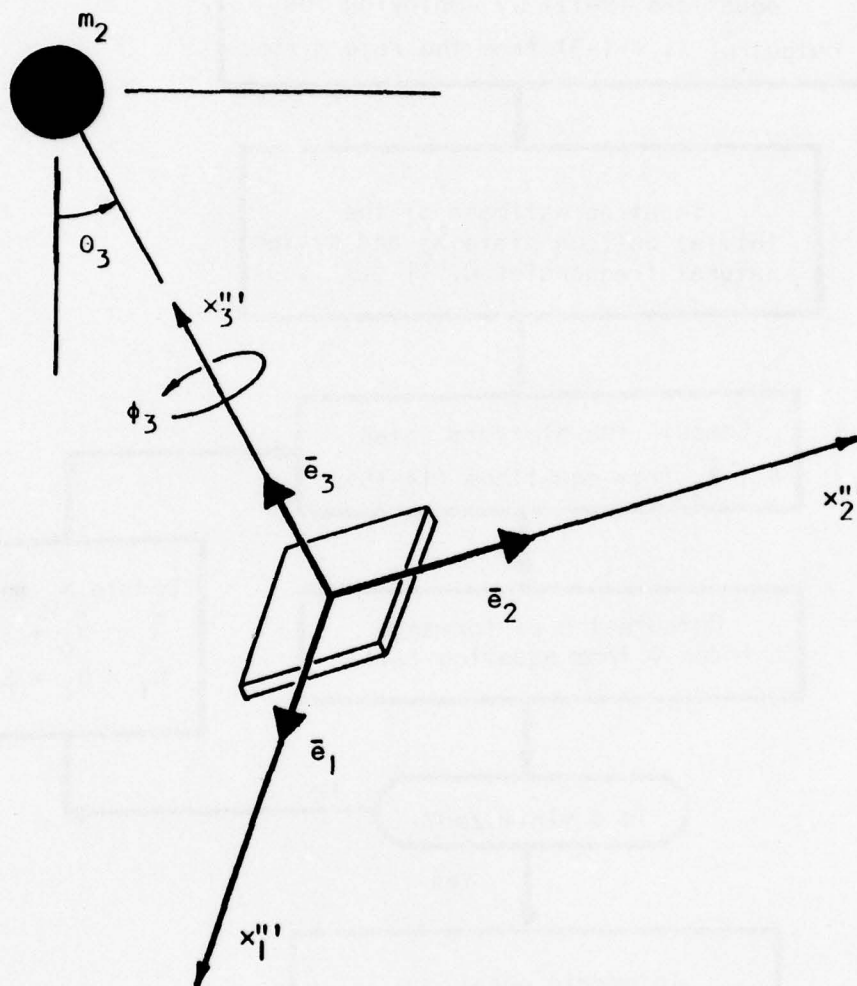


Figure 5. Platform Axes

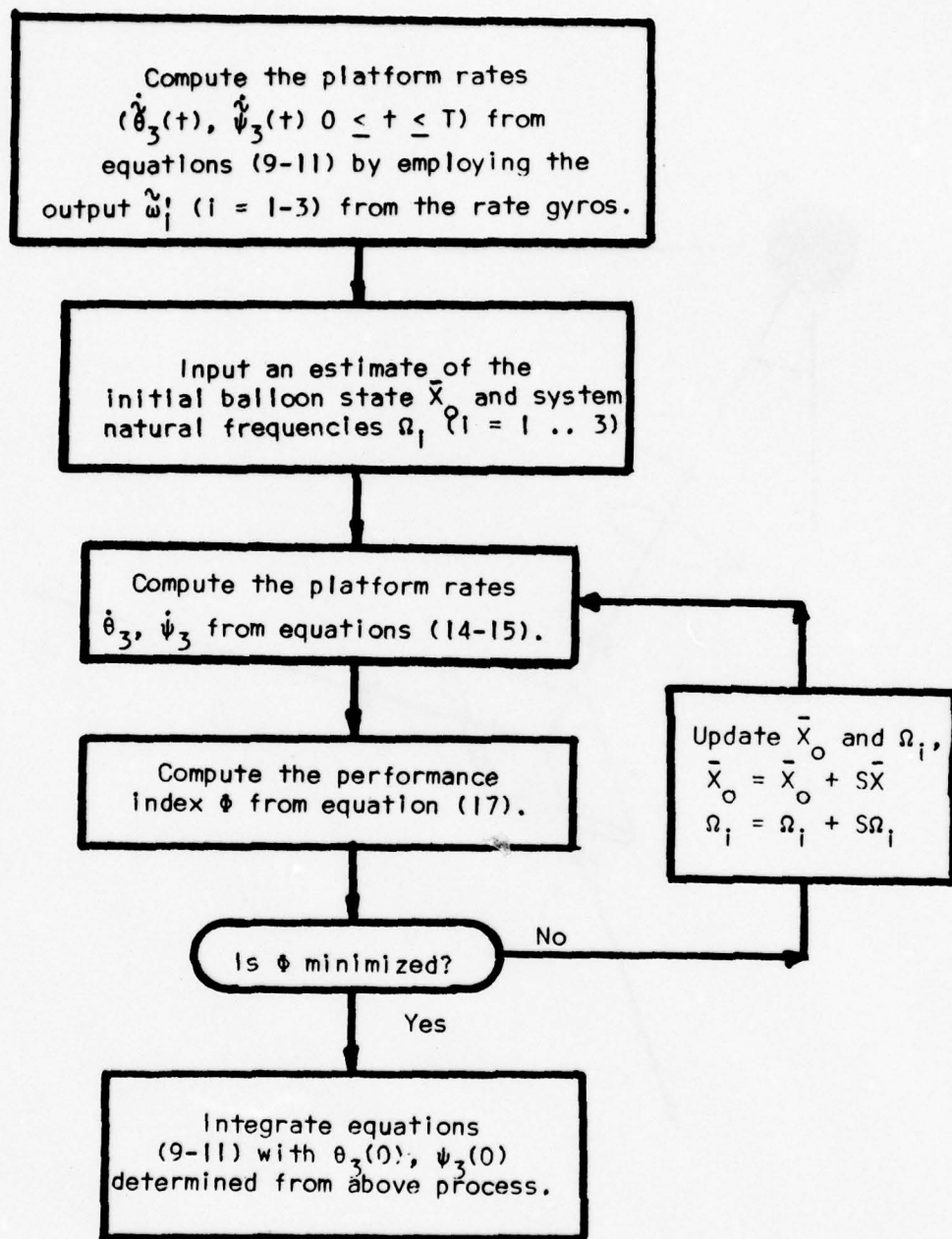


Figure 6. Method for Attitude Determination

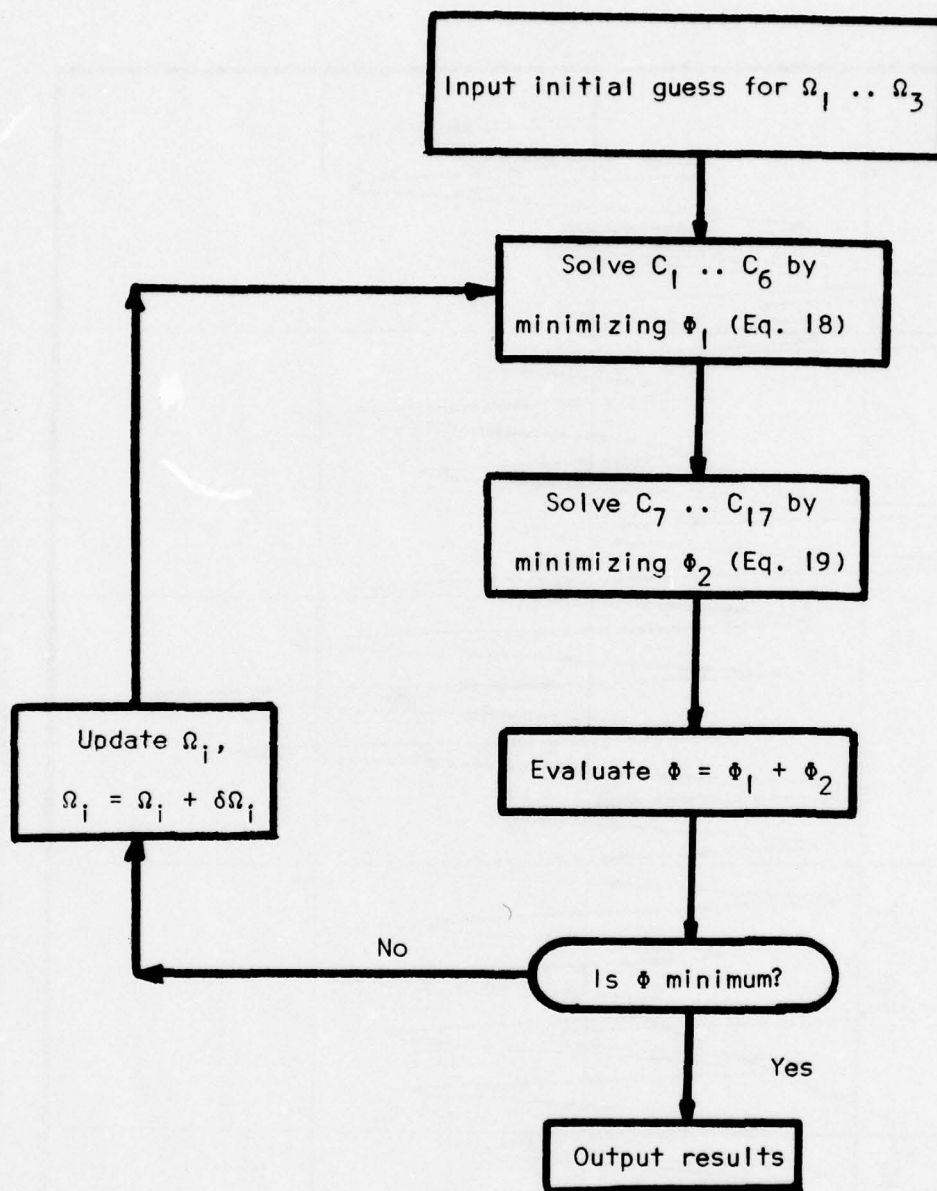


Figure 7. Parameter Determination Process

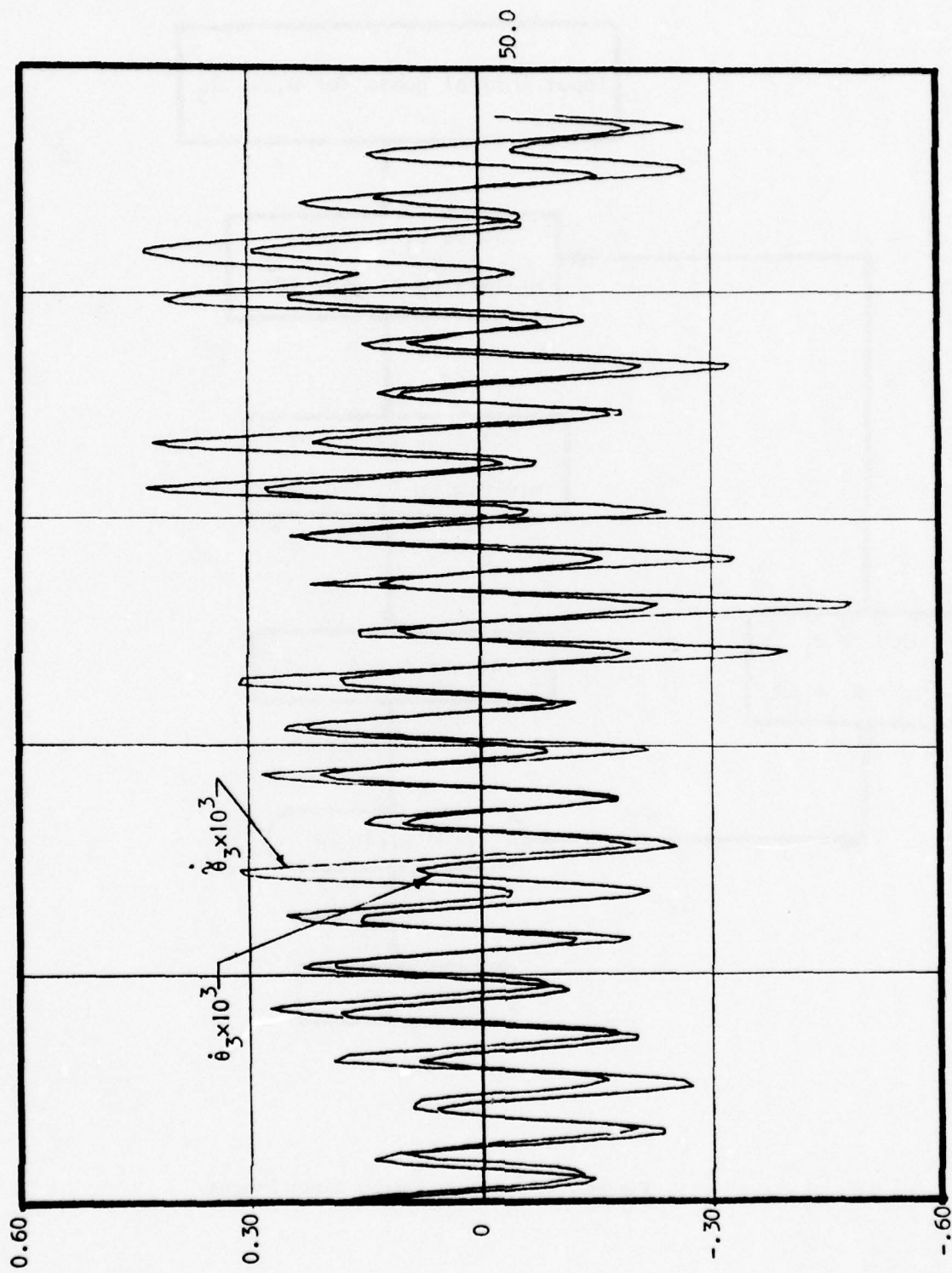


Figure 8. Plots of Predicted Platform Rate ($\dot{\theta}_3$) and Actual Platform Rates ($\dot{\theta}_3$) vs Time

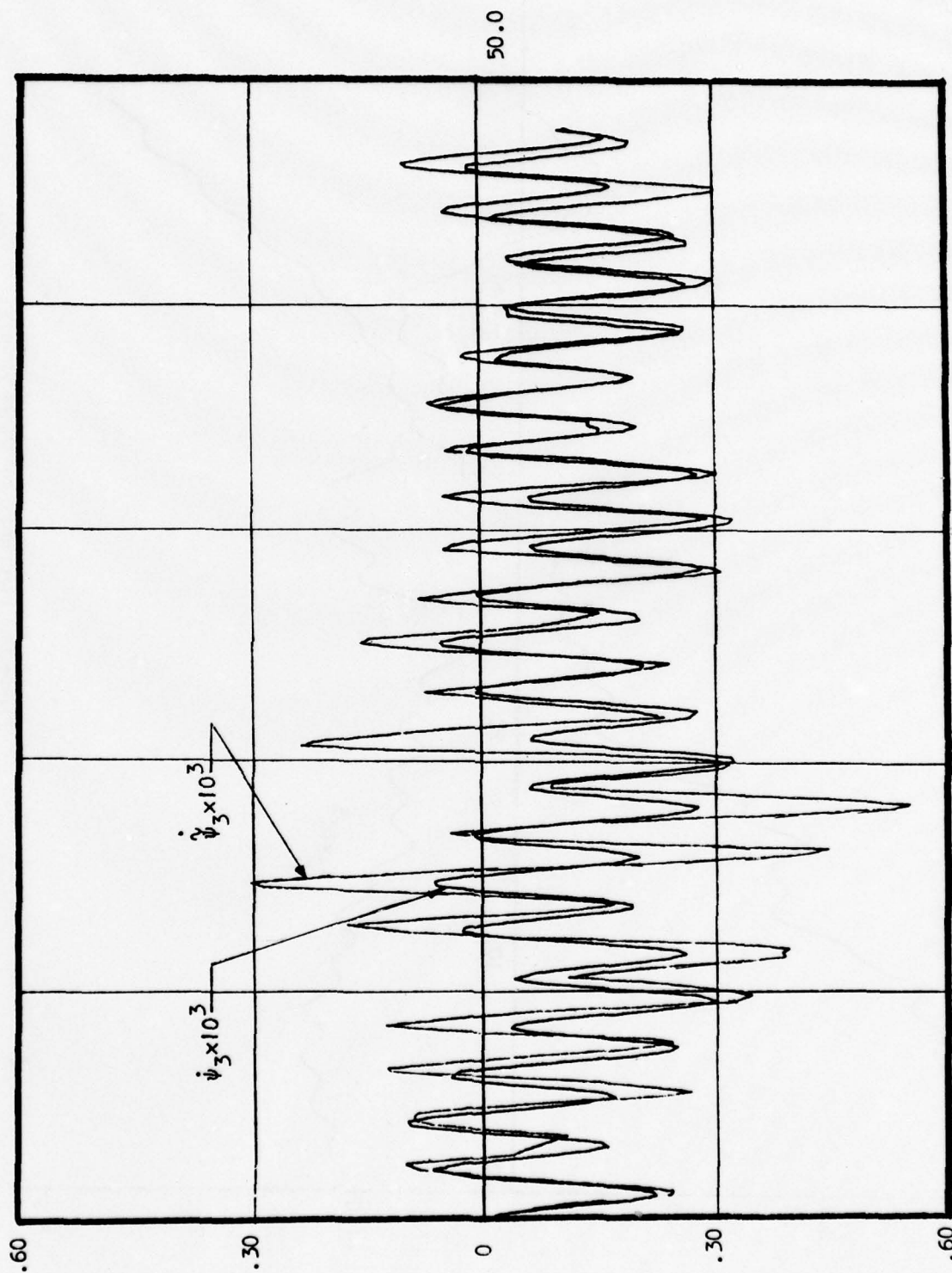


Figure 9. Plots of Predicted Platform Rate (ψ_3) and Actual Platform Rate ($\dot{\psi}_3$) vs Time

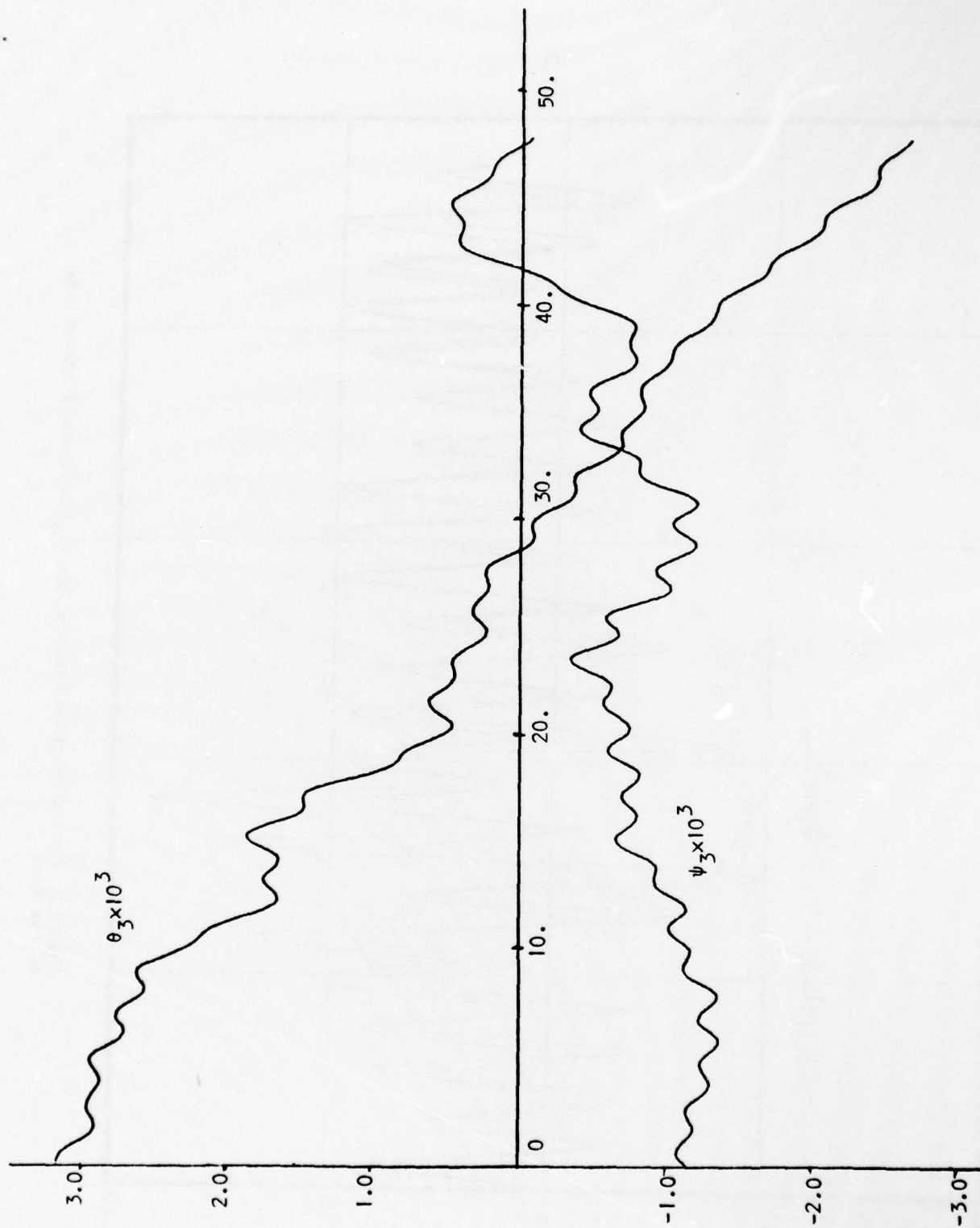


Figure 10. Plots of θ_3 and ψ_3 vs Time

A SEMI-EMPIRICAL METHOD FOR ESTIMATING THE SUBSONIC
AERODYNAMIC CHARACTERISTICS OF FINNED AXISYMMETRIC BODIES

James DeLaurier and Stefan Podleski
Institute for Aerospace Studies
University of Toronto

ABSTRACT

Modern interest in airships has generated a requirement for accurate estimates of the normal forces and moments of finned axisymmetric bodies. The "piecemeal" methods of the past were generally inaccurate, especially for stability-derivative estimations; and the current finite-element methods are rarely cost effective for initial design purposes. Hence, a semi-empirical method has been developed which promises to be a convenient and reasonably-accurate design tool.

The essence of the method is that the hull's normal forces are provided by Munk's slender-body theory up to the station where the fins begin. From that point, the fin's normal force is given by lifting-surface theory, where it is assumed that the fins effectively "carry through" the hull with constant chord (root chord). There are two parameters which modify these forces: a constant, K , for the Munk force, and an efficiency constant, η , for the fin force. These parameters are assumed to be functions of another parameter, λ , which is determined by the configuration's geometry. Wind-tunnel data on various airships have been used to obtain values of η vs. λ and these plot out in a regular and well-behaved fashion; hence it is felt that this method is suitable for application to a fairly wide range of finned-axisymmetric bodies.

Also, this analytical model has been applied to the calculation of the turbulence forcing functions on airship configurations. With the assumption of a frozen-field spectral-component model for atmospheric turbulence, distributed loads, as well as their integrated force and center-of-pressure values may be obtained as functions of the characteristics of the spectral component.

INTRODUCTION

The flight-dynamic and performance analysis of an airship requires accurate estimates of the aerodynamic normal forces and moments on the vehicle as functions of its motions with respect to the air. The purpose of this research has been to develop a simple, but accurate, method for calculating these forces and moments on airship-type finned-axisymmetric bodies; and this work has been motivated by the fact that other methods have either lacked sufficient accuracy, or have been excessively time consuming and expensive.

Previous techniques have included the time-honored "piece-meal" methods from airplane analysis, such as described by Roskam (1977). Briefly, the vehicle is assumed to be composed of distinct aerodynamic components, each with their particular lifts, moments, and aerodynamic centers. The total aerodynamic characteristics are assumed to be the sum total of those due to the components, with appropriate correction factors for mutual interference. As applied to airships, this method has usually assumed components consisting of the fins alone, with an assigned effective planform (as described by Redd, Bennett, and Bland, 1973), and the complete hull without fins. The fin's normal force and aerodynamic center are found from finite-wing theory, but the hull's force and moment are usually obtained from empirical curves such as shown in Figures 1 and 2. These empirical data are required because the hull's normal force is due to a region of separated flow, and it is this fact which imposes the greatest limitation to the accurate application of this piece-meal method.

First of all, the extent of the separated region is dependent

on the influence of the fins; and for certain cases, the fins may so change the aft-hull flow that the separated region is effectively suppressed, thus greatly modifying the hull's contribution to the aerodynamics of the complete vehicle. Second, an unreferenced technique that the first author has encountered in industry is a method which estimates the hull's contributions to the rotary stability derivatives by assuming that the hull's aerodynamic force is concentrated at the center of the separated region, and that it is a function of the local induced flow angle at that point (hence, the hull is acting like a fin whose aerodynamic center is located at the center of the separated region). It will be shown that this gives erroneous and generally unconservative results.

A more accurate method is obtained from slender-body analysis as applied by Nielsen (1960) to missile aerodynamics. The components, as before, are the body and fins; but an essential difference is that the body's force and moment are integrated values of theoretically-determined normal forces along the hull, which are functions only of the local geometry and cross-flow conditions. Further, if the fins have sufficiently low aspect ratios, the slender-body analysis may be extended to provide values for their aerodynamic contributions. Although this analytical model is over-extended for larger fin aspect ratios, Nielsen proposes a generalization to the method: namely, the aerodynamic characteristics of the fins alone are obtained by whatever method is appropriate, and then added to the hull's characteristics after being multiplied by interference factors obtained from the slender-body analysis. Nielsen states that static measurement results from tests on various missile configurations have compared well with those obtained from his

analysis, and it may be expected that similar accuracy would be obtained if his analysis were applied to certain of the slender small-finned airships of the past, e.g., the ZR-1, "Shenandoah". Indeed, Regan (1974) uses this method for obtaining the stability derivatives for a somewhat similar airship. However, modern configurations which propose lower fineness ratios and larger relative fin sizes would exceed the limitations of the analytical model, which essentially envisioned slender missile-type shapes.

These limitations may be overcome with a finite-element source/vortex model such as developed by Hess and Smith (1967), where the body is aerodynamically modelled by a number of adjacent panels, each with constant source strength, over the body's surface; and the fins are aerodynamically modelled by a number of bound "horseshoe" vortices distributed over their mean (zero-thickness) surface. Further, fin thickness effects may be accounted for, if required, by introducing sources on the fins. The flow field produced by each of these elements must interact with that produced by the others to satisfy the boundary conditions over the entire vehicle. Hence, mutual interference effects among all components are accounted for, in principle.

To all appearances, the finite-element method is the most comprehensive and exact way to obtain the non-viscous aerodynamic properties of configurations in non-separated low-speed flow; and in fact, the source-panel method has been successfully applied to the pressure-coefficient calculations on the hull of the Family-II tethered balloon, as shown in Figures 3 and 4. However, the correct matching of the finite elements between the fins and the hull is more of an "art" than most practitioners

of this method are willing to admit. This is especially true when the fins must join a rapidly-tapering body. In principle, this problem can be overcome, and the elements can be matched and extended in a proper fashion, e.g., vortices may be extended from the fins into, or on, the hull; but in practice, considerable numerical experimentation may be required, and the method may be far from being time or cost effective for initial design studies.

In 1951, Hopkins proposed a method for estimating the static normal force and moment of an axisymmetric body by assuming that Munk's (1936) slender-body theory applied along the hull to the point of separation, from which point 2-dimensional viscous cross-flow forces took over. When the theory was compared with experiments, the results matched reasonably well, and it was interesting to note that the normal force was not due so much to the viscous cross-flow as to the non-closure of the potential-flow region, which gave an effective "base area". The present authors noted that the assumed separation region on the body, alone, was always aft of the point where fins began on nearly every airship design considered, so it was conjectured that Hopkin's method could be applied up to that point, and modified lifting-surface theory could be applied beyond that. Based on this, a semi-empirical method has been developed, which is described in the balance of this paper.

METHOD OF ANALYSIS

The analytical model is schematically represented in Figure 5, where, aerodynamically, it is divided into two distinct regions: the hull which extends from the nose to the point where the fins intersect the hull, l_h , and the fins, which continue from that point to their

trailing edge. The distributed loads on the hull are assumed to be given by Munk's equation from slender-body theory, which, for $\hat{\alpha} \ll 1$ is given by

$$\frac{dL_h}{d\xi} = \rho U_o^2 K \frac{dA}{d\xi} \hat{\alpha} \quad (1)$$

where

L_h = hull lift force

ξ = axial coordinate, measured from the nose

ρ = density of the air

U_o = mean velocity through the air

K = modification coefficient for bodies with finite fineness ratios (given by Munk as $K_2 - K_1$)

A = local cross-sectional area

$\hat{\alpha}$ = local angle of attack of the flow

Also, the load on the fins is assumed to be concentrated at their aerodynamic center and is expressed as

$$L_f = \frac{\rho U_o^2}{2} S_f \eta (CL_{\alpha})_f \hat{\alpha}_f \quad (2)$$

where

S_f = the fin's surface area, defined in Figure 6

L_f = the fin's lift force, acting at the aerodynamic center of S_f

η = the fin-efficiency factor accounting for the interference between hull and fins

$(CL_{\alpha})_f$ = the fin's lift-curve slope, found from finite-wing theory and based on the planform defined by S_f

$\hat{\alpha}_f$ = local angle of attack at the fin's aerodynamic center

Therefore, at a uniform angle of attack

$$\hat{\alpha} = \hat{\alpha}_f = \alpha$$

the vehicle's total lift is given by

$$L = \rho U_o^2 \left[K A_h + \frac{S_f \eta}{2} (CL_\alpha)_f \right] \alpha \quad (3)$$

where A_h is the hull's cross-sectional area at l_h

Similarly, the vehicle's pitching moment about its nose ($\xi = 0$) at uniform α is given by

$$M^{\text{nose}} = - \rho U_o^2 \left\{ K \int_0^{l_h} \xi \frac{dA}{d\xi} d\xi + \frac{S_f \eta}{2} l_f [(CL_\alpha)_f + (CD_o)_f] \right\} \alpha, \quad (4)$$

where

$(CD_o)_f$ = the drag coefficient of the entire tail

l_f = the axial distance to the fin's aerodynamic center (Figure 5).

Now, the fin-efficiency factor, η , is assumed to be a function of a nondimensional geometrical parameter, λ , given by

$$\lambda \equiv \frac{1}{f} \frac{1}{AR} \frac{S_h}{S_f} \frac{S_{fh}}{S_f} \frac{\bar{C}}{\bar{C}_f}, \quad (5)$$

where

f = hull's fineness ratio (based on total hull length)

AR = the fin's aspect ratio, based on S_f

S_h = the hull's total volume taken to the 2/3 power

S_{fh} = the area of S_f buried in the hull (Fig. 6)

\bar{C} = reference length (total hull length)

\bar{C}_f = mean aerodynamic chord of the fins, based on the S_f planform.

The functional relationship between η and λ is empirically determined by adjusting η to provide a match between the theoretical lifts and

moments given by (3) and (4) with those given by experiments on various configurations. In particular, (3) and (4) are nondimensionalized to give

$$C_L = CL_\alpha \alpha, \quad (Cm)^{nose} = (Cm_\alpha)^{nose} \alpha, \quad (6)$$

where

$$CL_\alpha = 2K\hat{A}_h + \eta(CL_\alpha)_f \hat{S}_f, \quad (7)$$

$$(Cm_\alpha)^{nose} = -2K \int_0^{\hat{l}_h} \frac{\hat{d}\hat{A}}{\hat{d}\hat{\xi}} d\hat{\xi} - \eta[(CL_\alpha)_f + (CD_o)_f] \hat{S}_f \hat{l}_f \quad (8)$$

$$\hat{A}, \hat{A}_h, \hat{S}_f \equiv \frac{A, A_h, S_f}{S_h}, \quad \hat{\xi}, \hat{l}_f, \hat{l}_h \equiv \frac{\xi, l_f, l_h}{\bar{C}}$$

At $\alpha = 0$, K and η are found by matching the theoretical and experimental CL_α and Cm_α values; and at other α values, K is assumed to be constant, and matching is achieved between the C_L values only. The moment coefficients could also have been used, but it was assumed that the wind-tunnel lift measurements were generally more accurate. However, in all cases considered, the differences between the moments were less than 13%. Also, a certain number of cases were rerun using moment matching, and the resulting η values varied by less than 10%.

NUMERICAL CALCULATIONS

The specific experimental data used for calculating the η vs λ dependence come from wind-tunnel tests on models of the Sheldahl Family-II and Family-IIS aerostats (Haak, 1976), the Goodyear GAC No. 1649 aerostat (Myers and Vorachek, 1971), the Univ. of Washington "Class C Balloon" (Peters, Lysons, and Shindo, 1973), the airship ZR-4 "Akron" (Freeman, 1932), the British airships R-100 and R-101, and the German airships LZ-126 "Los Angeles", LZ-127 "Graf Zeppelin", and LZ-129 "Hindenburg" (Schirmer, 1942). Table 1 summarizes the λ values for the configurations,

along with the calculated η and K values, and the η values are plotted vs. λ in Figure 7. Notice that these follow a general trend, with high efficiencies for those configurations with relatively large fins (low λ), and decreasing efficiencies with decreasing relative fin size (increasing λ). However, beyond $\lambda = 1.6$, the η values begin to increase. It is felt that this was due to the use, by the authors, of lifting-line theory for the calculation of $(CL_\alpha)_f$. In fact, the configurations beyond $\lambda = 1.4$ are characterized by having extremely low aspect-ratio highly-swept fins for which a slender-wing theory would have, perhaps, been more appropriate. Up to that point, however, an empirical η vs λ curve may be identified, and the authors propose the one plotted in Figure 7.

Also shown in Table 1 are the theoretical values of Munk's fineness ratio parameter, $K_2 - K_1$, based on total hull length, \bar{C} . For all cases, the average difference between K and $K_2 - K_1$ is less than 17%. Therefore, when this semi-empirical method is applied, it is suggested that K be set equal to $K_2 - K_1$ for the configuration in question.

In order to assess the effect of angle of attack on fin efficiency, η vs. α was calculated from the experimental data. These results are summarized in Figure 8, which shows a generally increasing η with angle of attack. The reason for this is that in all cases (except the GAC balloon) the experimental CL_α increased with increasing α . Since the hull contribution to CL_α has been assumed to be constant (Eq. (7)), the increase in CL_α had to come from an increase in fin efficiency, η . It is felt that this is physically realistic for the lower λ cases, where the nonlinear contributions of viscous cross flow and hull-vortex lift are second-order for the angle-of-attack range considered (less than 10°).

However, hull-vortex lift becomes increasingly important with increasing λ values, and it is felt that the η values would not increase so rapidly with α if this contribution was accounted for.

STABILITY-DERIVATIVE CALCULATIONS

This analytical model readily lends itself to the calculation of the vehicle's static and rotary stability derivatives. For example, Eq. (7) may be transformed to the body-fixed Z-force direction (Ashley, 1974) to give

$$Cz_{\alpha} = (Cz_{\alpha})_h + (Cz_{\alpha})_f, \quad (9)$$

where

$$(Cz_{\alpha})_h = -2K\hat{A}_h, \quad (Cz_{\alpha})_f = -\eta\hat{S}_f[(CL_{\alpha})_f + (CD_o)_f]$$

Also, Cz_q and Cm_q may be obtained from (1) and (2) by noting that pitching angular velocity, q , about the vehicle's mass center gives

$$\hat{\alpha} = q \frac{(\xi - l_{cm})}{U_o}, \quad \hat{\alpha}_f = q \frac{(l_f - l_{cm})}{U_o} \quad (10)$$

where l_{cm} is the axial location of the mass center (Figure 5). When the resulting equations are nondimensionalized, one obtains

$$Cz_q = (Cz_q)_h + (Cz_q)_f, \quad (11)$$

$$Cm_q = (Cm_q)_h + (Cm_q)_f, \quad (12)$$

where

$$(Cz_q)_h = - 2(Cz_\alpha)_h l_{cm}/\bar{C} + (Cz_q)_h^{nose}, \quad (13)$$

$$(Cz_q)_f = - 2(Cz_\alpha)_f (l_{cm} - l_f)/\bar{C} + (Cz_\alpha)_f \bar{C}_f/\bar{C}, \quad (14)$$

$$(Cm_q)_h = - (Cz_q)_h l_{cm}/\bar{C} - (Cz_q)_h^{nose} l_{cm}/\bar{C} + (Cm_q)_h^{nose}, \quad (15)$$

$$(Cm_q)_f = - (Cz_q)_f (l_{cm} - l_f)/\bar{C} - (\pi/4) \hat{S}_f (\bar{C}_f/\bar{C})^2, \quad (16)$$

$$(Cz_q)_h^{nose} = - 4K \int_0^{\hat{l}_h} \hat{\xi} \frac{d\hat{A}}{d\hat{\xi}} d\hat{\xi}, \quad (17)$$

$$(Cm_q)_h^{nose} = - 4K \int_0^{\hat{l}_h} \hat{\xi}^2 \frac{d\hat{A}}{d\hat{\xi}} d\hat{\xi}. \quad (18)$$

Also, note that the last terms in equations (14) and (16) account for the aerodynamic force and moment generated by the chordwise variation of $\hat{\alpha}$, produced by q .

The lateral stability derivatives may be calculated in a similar fashion. However, the resulting expressions are somewhat more complicated in that the vertical displacement of the mass center, h_{cm} (see Fig. 5), and the vehicle's equilibrium angle of attack are accounted for.

Example values were calculated for the SN 204 Family-II aerostat, whose properties are described by DeLaurier (1975). For $l_{cm}/\bar{C} = .514$ and $h_{cm}/\bar{C} = .079$ the results are

	hull	fins	total
Cz_α	-0.342	-1.572	-1.914
Cm_α	0.588	-0.716	-0.128
Cz_q	1.177	-1.868	-0.691
Cm_q	-0.362	-0.899	-1.261

Notice that the hull's contribution to the derivative Cz_q is positive. This is considerably different from the $(Cz_q)_h$ that would have been calculated by the piecemeal method described in the INTRODUCTION, which would be negative. Therefore, the present method gives stability-derivative values which could significantly improve the predictions of airship dynamic behavior.

TURBULENCE FORCING-FUNCTION CALCULATIONS

The normal forces and moments on a finned axisymmetric body due to a spectral component of frozen atmospheric turbulence (Etkin, 1966) may also be calculated with this analytical model. Figure 9 illustrates the situation considered, where the spectral component produces an variation given by

$$\hat{\alpha} = w_g/U_o = \Gamma \exp(i\omega t - i\omega x/U_o), \quad (19)$$

$$\hat{\alpha}_f = (w_g)_f/U_o = \Gamma \exp(i\omega t - i\omega l_{ff}/U_o), \quad (20)$$

where

w_g = vertical gust velocity component (Figure 9)

Γ = maximum $\hat{\alpha}$ amplitude of the spectral component

ω = time frequency of the spectral component

t = time

l_{ff} = the axial distance from the nose to the midchord location of \bar{C}_f (see Fig. 9).

These may be nondimensionalized by

$$\omega \equiv \frac{2U_o}{\bar{C}} k, \quad t \equiv \frac{\bar{C}}{2U_o} \hat{t}, \quad l_{ff} \equiv \bar{C} \hat{l}_{ff} \quad (21)$$

to give

$$\hat{\alpha} = \Gamma \exp(ikt - 2ik\hat{\xi}), \quad (22)$$

$$\hat{\alpha}_f = \Gamma \exp(ikt - 2ik\hat{\ell}_{ff}). \quad (23)$$

Further, note that in addition to the hull lift given in Eq. (1), one must account for an "apparent-mass" effect produced by the time rate of change of w_g at any given section on the body. This is expressed as

$$\left(\frac{dL_h}{d\xi} \right)_a = \rho A K_2 \frac{\partial w_g}{\partial t}, \quad (24)$$

where K_2 is an apparent-mass coefficient obtained from Munk (1936). Therefore, the total lift on the hull is given by

$$\frac{dL_h}{d\xi} = \rho U_o^2 K \frac{dA}{d\xi} \hat{\alpha} + \rho U_o K_2 A \frac{\partial \hat{\alpha}}{\partial t}. \quad (25)$$

Also, the lift produced by the fins is given by

$$L_f = \frac{\rho U_o^2}{2} S_f \eta(CL_{\alpha})_f H(k_f) \hat{\alpha}_f \quad (26)$$

where $H(k_f)$ is the lift-attenuation function for finite aspect-ratio wings (Filotas, 1971), which is a function of

$$k_f \equiv \frac{\omega \bar{C}_f}{2U_o} \approx \frac{\bar{C}_f}{\bar{C}} k \quad (27)$$

When L_h and L_f are transformed into the body-fixed Z-force direction and nondimensionalized, one obtains

$$C_z = Gz_{\gamma} \Gamma \exp(ikt), \quad (28)$$

where

$$Gz_{\gamma} = (Gz_{\gamma})_h + (Gz_{\gamma})_f \quad (29)$$

$$(Gz_\gamma)_h = -2K \int_0^{\hat{l}_h} \frac{d\hat{A}}{d\hat{\xi}} \exp(-i2k\hat{\xi}) d\hat{\xi} - i4kK_2 \int_0^{\hat{l}_h} \hat{A} \exp(-i2k\hat{\xi}) d\hat{\xi}, \quad (30)$$

$$(Gz_\gamma)_f = (Gz_\alpha)_f H(k_f) \exp(-i2k\hat{l}_{ff}). \quad (31)$$

A similar procedure may be used to find the pitching-moment coefficient about the nose,

$$(Cm)^{nose} = (Gm_\gamma)^{nose} \Gamma \exp(ikt), \quad (32)$$

where

$$(Gm_\gamma)^{nose} = (Gm_\gamma)_h^{nose} + (Gm_\gamma)_f^{nose}, \quad (33)$$

$$(Gm_\gamma)_h^{nose} = -2K \int_0^{\hat{l}_h} \hat{\xi} \frac{d\hat{A}}{d\hat{\xi}} \exp(-i2k\hat{\xi}) d\hat{\xi} + i4kK_2 \int_0^{\hat{l}_h} \hat{\xi} \hat{A} \exp(-i2k\hat{\xi}) d\hat{\xi}, \quad (34)$$

$$(Gm_\gamma)_f^{nose} = \hat{l}_f (Gz_\gamma)_f \quad (35)$$

With Gz_γ and $(Gm_\gamma)^{nose}$, one may define a pressure center where the net resultant turbulence force acts:

$$\hat{l}_{cp} = (Gm_\gamma)^{nose} / Gz_\gamma$$

Note that by virtue of the complex-number representation of the spectral component (Eqs. (19) and (20)), Gz_γ , $(Gm_\gamma)^{nose}$, and \hat{l}_{cp} are, in general, also complex. The interpretation of a complex pressure center may seem strange, but it can be understood, as with the other terms, by noting that it has an amplitude and phase with respect to the reference turbulent input,

$$\gamma = \Gamma \exp(ikt) \quad (36)$$

For use of these results in a vehicle's flight-dynamic equations, it is often convenient to obtain the moment about the mass center. This is done with the following equation:

$$Gm_{\gamma} = (\hat{\ell}_{cp} - \hat{\ell}_{cm})Gz_{\gamma} \quad (37)$$

In a similar fashion, the equations for lateral turbulent forcing may be expressed in terms of a spectral force and pressure center. However, as with the lateral stability derivatives, the vertical location of the mass center, h_{cm} , and the vehicle's equilibrium angle of attack must be accounted for in order to correctly obtain yawing and rolling moments about the mass center.

Figures 10 and 11 show example values of Gz_{γ} and $\hat{\ell}_{cp}$ for the Family-II aerostat. It is seen that for $k = 0$ (infinite spectral wavelength) Gz_{γ} equals Cz_{α} and $\hat{\ell}_{cp}$ equals the steady-state pressure-center location, as one would expect. However, as k increases, the magnitudes and phases change significantly. For example, note that the maximum magnitude of Gz_{γ} is twice that of Cz_{α} and occurs at $k \approx \pi$, which corresponds to a spectral wavelength equal to \bar{C} . Since the \bar{C} values of the great airships were nearly equal to the wavelengths of the most energetic components of atmospheric turbulence (≈ 300 m), one could speculate that their flight-loads may have been generally higher than those calculated from steady-state analysis.

Also seen from Figure 11, is that the magnitude of $\hat{\ell}_{cp}$ increases dramatically at k values ≈ 5 . However, the resulting moment change is not as extreme as one would expect because, as Figure 10 shows, the magnitude of Gz_{γ} goes nearly to zero.

As k further increases, the curves continue to spiral around near the origin. However, it should be noted that these results are based on the assumption of a one-dimensional ("washboard") model for turbulence. If a two-dimensional model is chosen, there will be significant variations in w_g normal to the ξ axis, for the higher k values. This means that the magnitude of Gz_y would decrease much more rapidly at $k > 5$ than shown in Figure 10.

CONCLUDING REMARKS

It should be clear, from the previous development, that there are several limitations to the analytical model. First of all, the hull-force equation (1) is obtained from slender-body theory. Even with Munk's corrections for finite fineness ratios, the model still assumes that the distributed loads are dependent only on local geometry and flow conditions. Also, finite fineness-ratios should affect the calculation of the rotary derivatives in that yawing and pitching rates generate components of axial velocity varying in a direction normal to the hull's longitudinal axis. This contribution could be significant for hulls with lower fineness ratios.

Another limitation to the analytical model is that viscous effects are not accounted for, such as the influence of the boundary layer on the fins' efficiency, and separation effects on the fins and hull. It has been assumed that the boundary layer is very thin compared with the vehicle's dimensions, and that the flow is attached over the vehicle's entire surface. These assumptions would most likely be exceeded by the higher- λ configurations at any significant angle of attack, where hull viscous cross-flow and vortex-lift contributions become important.

Other limitations arise from the calculations for the fin-efficiencies, η , in that they are not only based on the analytical model, but are also dependent on the accuracy of the experimental data. Although the data chosen was the best available, in no cases were error estimates given, and in only two cases were force and moment coefficients tabulated (Haak, 1976, and Freeman, 1932).

Within the spirit of this simple semi-empirical method, there are several ways in which it may be improved. First of all, the lift-curve slope for the lower aspect-ratio fins (less than 2) should be more accurately calculated by methods similar to those described by Putnam (1977). In particular, the non-linear vortex-lift contributions of highly-swept leading edges should be accounted for. Also, it might be possible to account for boundary-layer effects if the definition of λ were extended to include the hull's boundary-layer thickness at the fins, represented, perhaps, by a Reynolds no. to a power appropriate for turbulent flow. And finally, the calculation of η would be best served by drawing on a large body of test data specifically planned to cover a predetermined range of λ values. Such data would provide not only a larger number of points in Figure 7, but it would also provide a means for refining the definition of λ .

Subject to the limitations noted, the authors of this article feel that the analytical model represents, with reasonable accuracy, configurations with λ values below 1.4 and angles of attack below 5° . Within these constraints, this should be a useful, cost-effective, and convenient method for estimating the normal forces and moments of finned-axisymmetric bodies.

Table 1. Calculated Values of Airship Parameters for Zero Angle-of-Attack

AIRSHIP	λ	η	K	K_2-K_1
Family-II	0.1235	0.8529	0.7974	0.6223
Family-IIS	0.1544	0.8249	0.8745	0.7160
GAC 1649	0.2279	0.8131	0.9311	0.6819
U. of W. "C"	0.3602	0.7178	0.7472	0.7369
LZ 129	1.089	0.3900	0.6681	0.8719
ZR-4	1.094	0.3683	0.8296	0.8703
R 100	1.265	0.3725	0.6904	0.8554
LZ 127	1.431	0.2760	0.7312	0.9120
LZ 126	2.231	0.3607	0.8343	0.9059
R 101	2.465	0.4952	0.8249	0.8587

ACKNOWLEDGEMENTS

This work has resulted from an ongoing study of the dynamics and aerodynamics of LTA flight vehicles which is supported by a Research Grant from the National Research Council of Canada and a Research Contract from Transport Canada. Also, the finite-element geometry and pressure coefficients in Figures 3 and 4 were obtained from computer programs developed by Mr. Brian Kroeker while he was a Research Associate at the U. of T. Institute for Aerospace Studies.

REFERENCES

- Roskam, Jan (1977) Methods for Estimating Stability and Control Derivatives of Conventional Subsonic Airplanes, The University of Kansas, Lawrence, Kansas.
- Redd, L. T., Bennett, R. M. and Bland, S. M. (1973) Experimental and Analytical Determination of Stability Parameters for a Balloon Tethered in a Wind, NASA Technical Note D-7222.
- Nielsen, Jack N. (1960) Stability Derivatives, Missile Aerodynamics, McGraw-Hill, New York: 349-420.
- Regan, Frank J. (1975) The Planar Dynamics of Airships, Proceedings of the Interagency Workshop on Lighter Than Air Vehicles, J. F. Vittek, Ed., MIT Flight Trans. Lab. Rept. R75-2: 177-186.
- Hess, J. L. and Smith, A.M.O. (1967) Calculation of Potential Flow About Arbitrary Bodies, Progress in Aeronautical Sciences, 8, D. Kuchemann, Ed., Pergamon Press, Oxford: 1-138.
- Hopkins, E. J. (1951) A Semi-Empirical Method for Calculating the Pitching Moment of Bodies of Revolution at Low Mach Numbers, NACA Research Memorandum A51C14.
- Munk, Max M. (1936) Aerodynamics of Airships, Aerodynamic Theory, 6, W. F. Durand, Ed., Julius Springer, Berlin: 2-48.

- Haak, E. L. (1976) Private Communication.
- Myers, Philip F. and Vorachek, Jerome, J. (1971) Definition of Tethered Balloon Systems, AFCRL-71-0213.
- Peters, P. A., Lysons, H. H. and Shindo, S. (1973) Aerodynamic Coefficients of Four Balloon Shapes at High Attack Angles, Proceedings, Seventh AFCRL Scientific Balloon Symposium, AFCRL-TR-73-0071: 19-47.
- Freeman, Hugh B. (1932) Force Measurements on a 1/40-Scale Model of the U.S. Airship "Akron", NACA Technical Report No. 432.
- Schirmer, M. (1942) Aerodynamic Model Tests With German and Foreign Airship Designs in the Wind Tunnel of the Zeppelin Airship Works at Friedrichschafen, ZWB Report F.B. No. 1647 (U.K. Ministry of Supply Translation No. GDC.10/1381T).
- Ashley, Holt (1974) Equations of Motion for Rigid Flight Vehicles, Engineering Analysis of Flight Vehicles, Addison-Wesley, Reading, Mass.: 27-50.
- DeLaurier, J. D. (1975) Refinements and Experimental Comparisons of a Stability Analysis for Aerodynamically-Shaped Tethered Balloons, AIAA Paper 75-943.
- Etkin, B. (1966) Flight in Turbulent Air, Dynamics of Flight (No. 5) Wiley, New York: 320-328.
- Filotas, L. T. (1971) Approximate Transfer Functions for Large Aspect Ratio Wings in Turbulent Flow, Journal of Aircraft, 8 (No. 6): 395-400.
- Putnam, William F. (1977) Aerodynamic Characteristics of LTA Vehicles, AIAA Paper No. 77-1176.

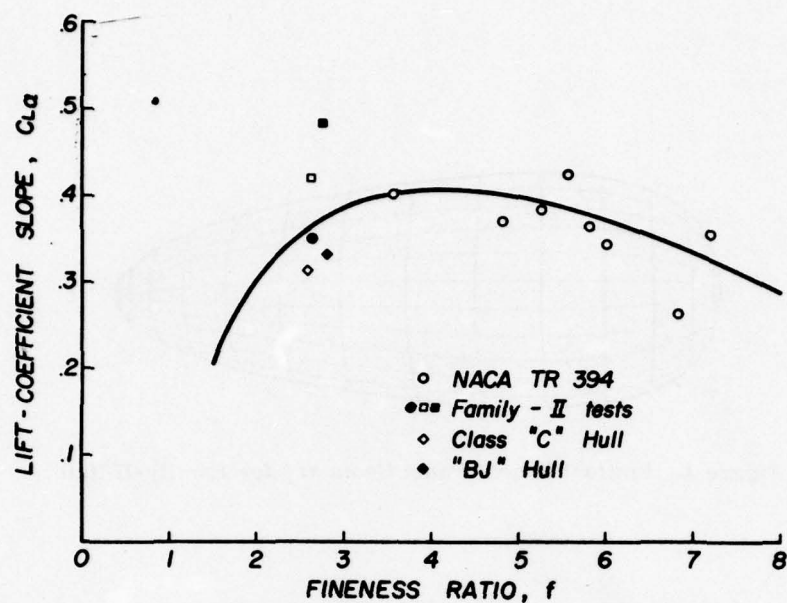


Figure 1. Hull Lift-Curve vs Fineness Ratio

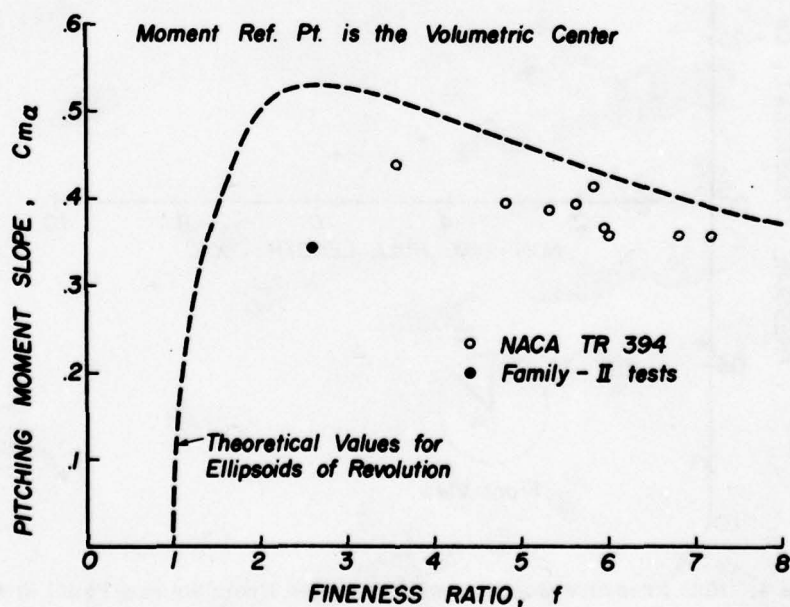


Figure 2. Hull Pitching-Moment Slope vs Fineness Ratio

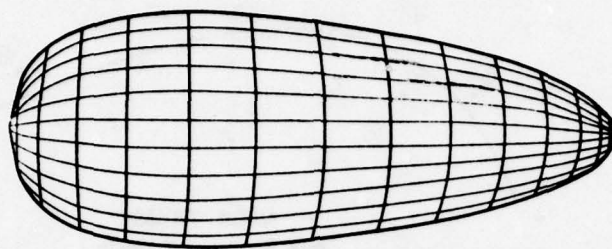


Figure 3. Finite-Element Panel Geometry for Family-II Hull

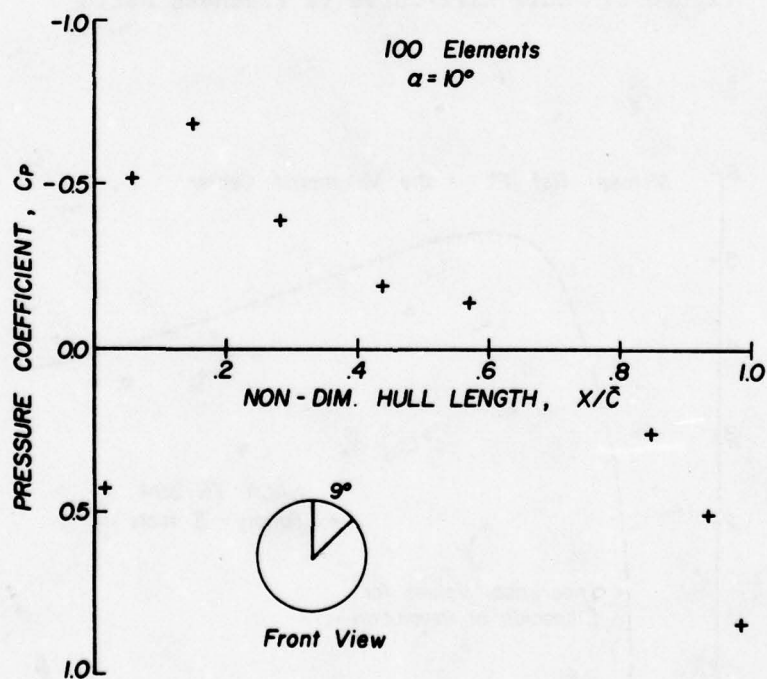


Figure 4. Hull Pressure Coefficients Calculated From Source-Panel Method

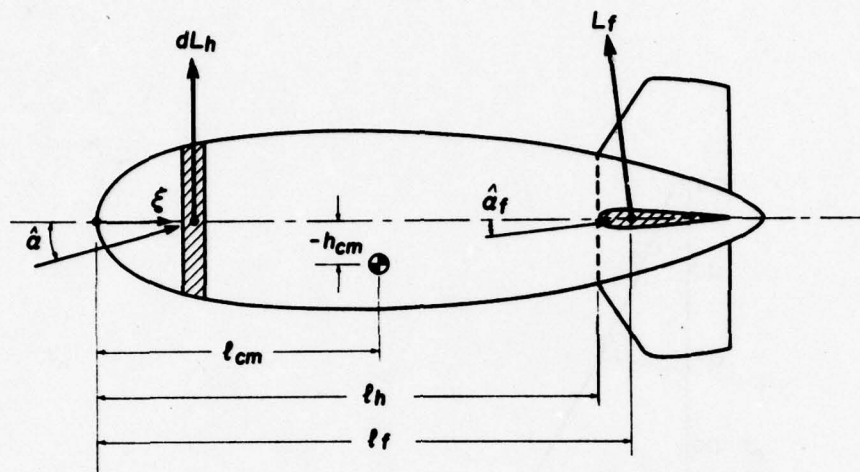


Figure 5. Schematic of Analytical Model

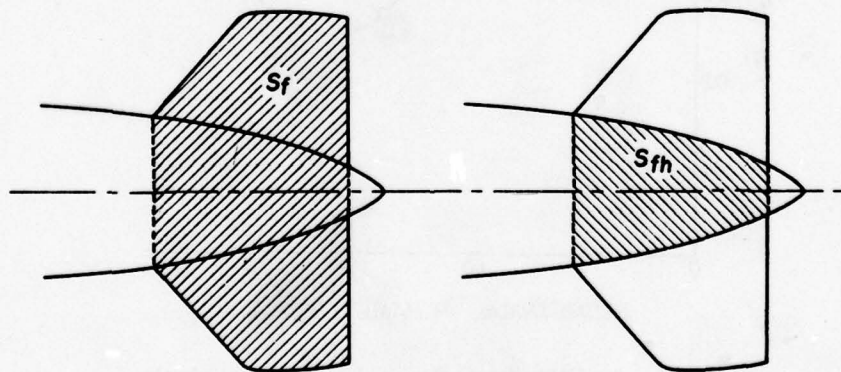


Figure 6. Fin Planform Definitions

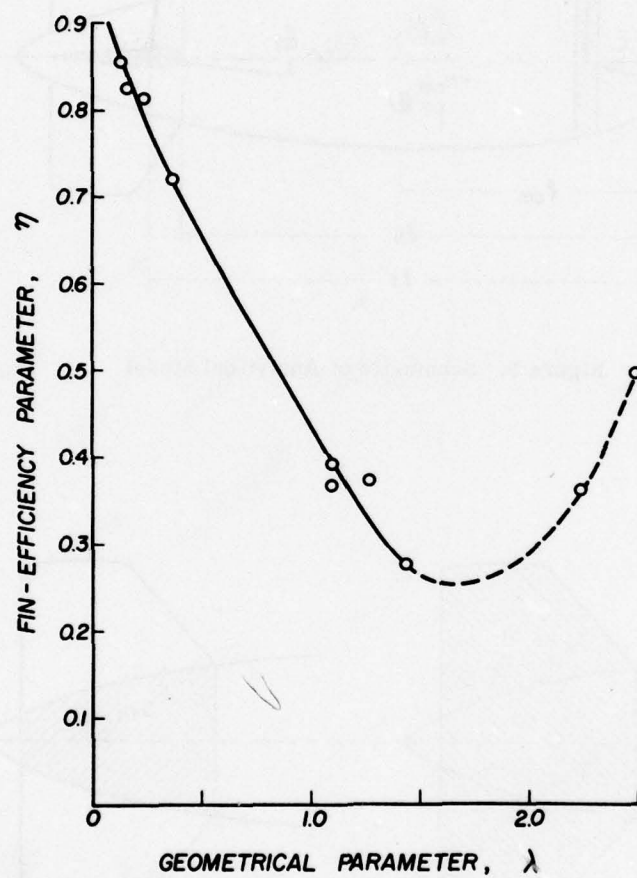


Figure 7. Fin-Efficiency Parameter, η , vs Vehicle Configuration Parameter, λ

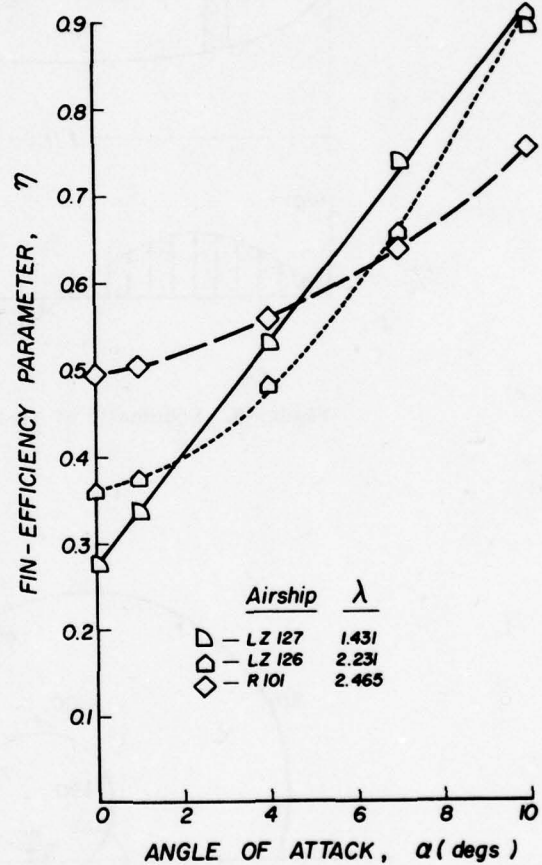
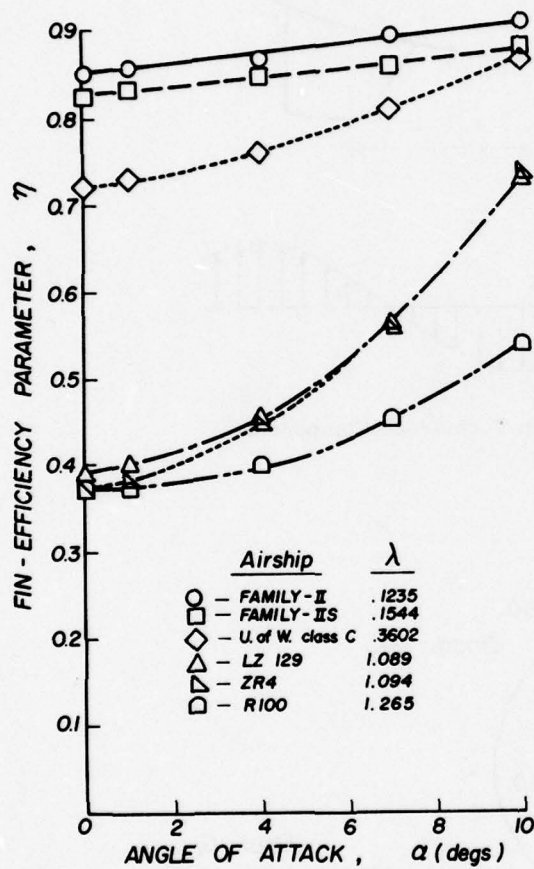


Figure 8a, b. Fin-Efficiency Parameter, η , vs Vehicle Angle-of-Attack, α

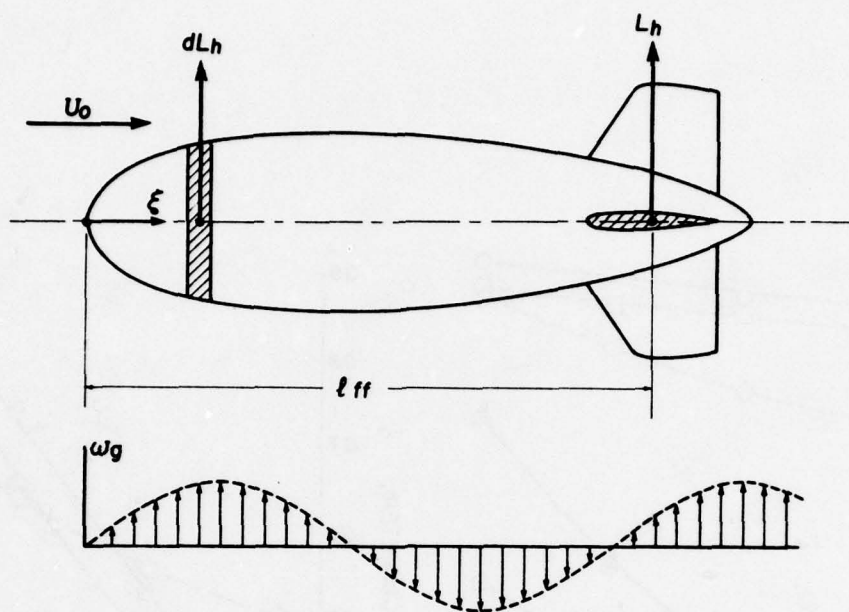


Figure 9. Schematic of Airship in Turbulence Component

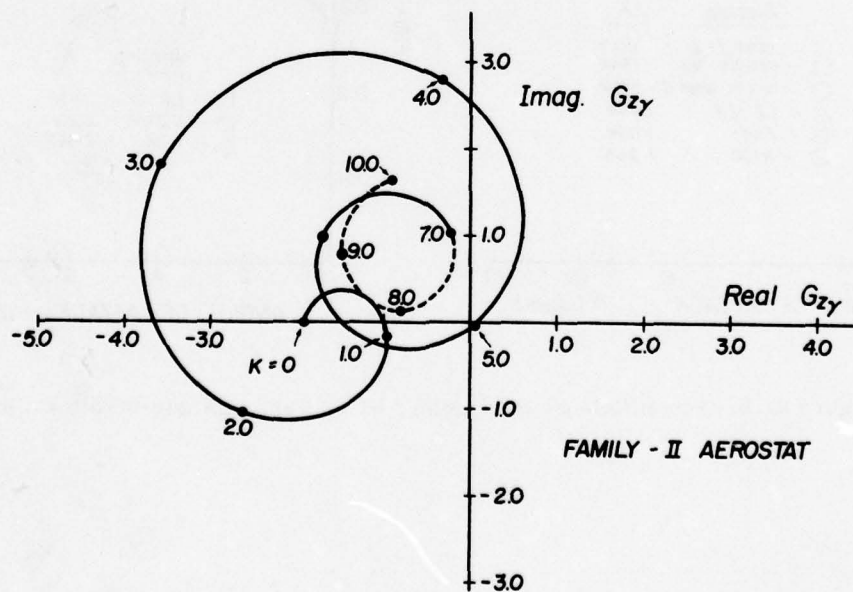


Figure 10. Turbulence Forcing Function for Family-II Configuration

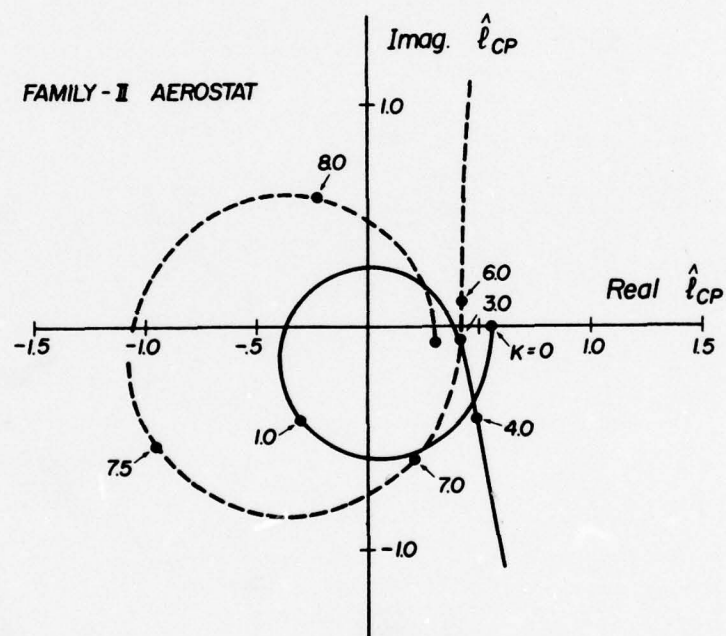


Figure 11. Pressure Center of Turbulent Force for Family-II Configuration

Contents

1. Introduction
2. Theory
3. Some Approximations
4. Computations
5. Summary and Conclusions

COMPUTATION OF TETHERED AEROSTAT PITCH ANGLE AND VENT CEILING FROM STANDARD CURVES

S. P. Jones
TCOM Corporation
Columbia, Maryland

Abstract

The computation of static pitch angle of a tethered aerostat is complicated by the relationship of center of buoyancy to pitch angle and ballonnet air volume. The latter is a function of density ratio, superheat, superpressure and helium impurity including its moisture content. The aerodynamic pitching moment is also a function of pitch angle. A simplified method of computing pitch, taking into account all of these factors, makes use of curves of trim angle and the derivative of the gravitational moment with respect to angle for a standard configuration of the aerostat in a standard atmosphere. Based on a model of the atmosphere, an equivalent altitude in the standard atmosphere, the "virtual altitude," is computed and corrections are made for other factors which affect pitch including moments due to superheat, superpressure, changes in weight and balance and dynamic pressure. The method, programmed on a hand-held calculator, is in use at TCOM operational sites.

The model of the atmosphere is also used to derive an equation for vent ceiling and a set of approximations or "rules of thumb" for estimating the virtual altitude and vent ceiling.

1. INTRODUCTION

Large tethered aerostats carrying communications payloads at 10,000 ft msl or higher are now flown operationally at sites in various parts of the world. Since this service is most often provided to developing nations, the sites are invariably remote from technical facilities such as digital computers. Thus, there is a need to provide field engineers with generalized flight characteristics and simplified methods, requiring no more than a hand-held, programmable calculator for computing static pitch angle, vent altitude and other operational parameters.

Several computer programs which determine pitch angle have been developed by Wright (1976). These, however, have not dealt in any detail with the influence of ballonnet fullness or the significant effects of hull pressure differential (super-pressure) and temperature differential (superheat). Myers (1969) has estimated the effect of the latter on lift but not on pitch angle or vent ceiling. There seems to have been no serious attempt to take into account the effect of meteorological conditions such as lapse rate and surface temperature and pressure on the density ratio and thus ballonnet fullness affecting pitch angle and vent ceiling. These factors are of daily concern to the operator of a commercial aerostat communication system.

The method to be presented is based upon a mathematical model of the aerostat and the atmosphere embodied in a large general-purpose computer program developed at the TCOM Corporation. By means of simplifications and approximations it is possible to program the computation of pitch, taking into account all of the significant variables, on a Hewlett Packard HP-67 calculator having 224 program steps and 26 storage registers. However, the program requires look-up data from two supplementary figures. In addition, vent ceiling can be obtained by the application of a few simple "rules of thumb."

For purposes of illustration the TCOM CBV365A, a 390,000 ft³ aerostat, will be used. A description of this aerostat is given in Table 1.

The principal difficulty in the computation of pitch arises from the variability of the center of buoyancy or centroid of the helium, which is a function of both helium volume (or ballonnet air volume) and pitch angle. This relationship for the reference aerostat, is shown in Figure 1. These curves were generated by a computer integration of the ballonnet shape as a function of air volume and pitch angle with the assumption, verified by observation, that the ballonnet curtain interface of helium and air is level, material fullness permitting. A reasonably accurate mathematical description of the curves requires four, fifth degree polynomials each for the longitudinal and vertical coordinates of the center of buoyancy, giving a grand total of 48 coefficients. While this presents no problem for a small computer, it is well beyond the capability of portable, programmable calculators without considerable mathematical simplification.

Table 1. TCOM CBV365A Aerostat

Hull Volume	390,200 ft ³
Empennage Volume	34,200 ft ³
Hull Length	196 ft
Overall Length	223 ft
Maximum Diameter	58.7 ft
Aerostat Weight*	6,440.7 lb
Payload Weight	5,009.7 lb
Total Weight	11,449.7 lb
Confluence Point Location:	
X (Length From Soft Nose)	60.6 ft
Z (Down From Center Line)	58.7 ft
Nominal Buoyant Lift of Helium	17,000 lb
Power Source	Electric via Tether

*Includes rigging and housekeeping hardware.

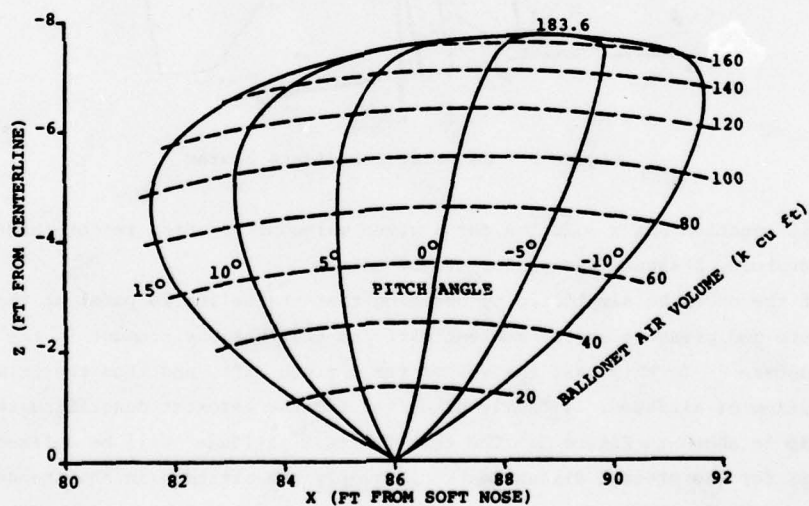


Figure 1. Center of Buoyancy or Centroid of the Helium for the CBV365A Aerostat, Showing the Relationship to Ballonet Air Volume and Pitch Angle

2. THEORY

2.1 The Standard Case

Consider an aerostat of a specified weight, W , and center of gravity, (X_W, Z_W) , referenced to the body coordinate system shown in Figure 2. Let the aerostat contain a gross lift of helium, B , with a center of buoyancy located at $X_B(V, \alpha)$ and $Z_B(V, \alpha)$, where V and α are the helium volume and pitch angle, respectively. For static analysis it is most convenient to take the moments about the confluence point, which is the origin of our coordinate system. Denoting by α_0 the trim angle (pitch in the absence of wind), the pitching moment equation is,

$$M_\alpha = W(X_W \cos \alpha_0 + Z_W \sin \alpha_0) - B(X_B \cos \alpha_0 + Z_B \sin \alpha_0) = 0 \quad (1)$$

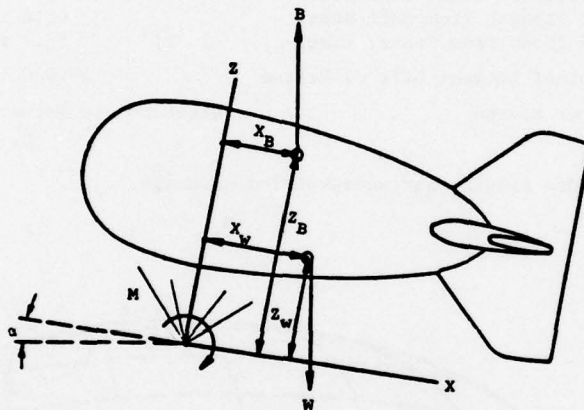


Figure 2. Aerostat Coordinate System

This equation has a solution for a given value of V , which is determined by the temperature, pressure and purity of the helium.

Let the model be simplified by assuming that the helium is pure, at the same temperature and pressure as the ambient air, and that the environment is the Standard Atmosphere.* In this case the volume for a given lift, and thus the trim angle, is a function of altitude. A family of curves for the aerostat describing this relationship is shown in Figure 3. The term "virtual altitude" will be defined subsequently; for the present discussion it is simply the altitude in the Standard Atmosphere.

Note the broken line in Figure 3 labeled "vent." This is the vent ceiling, or altitude at which the ballonnet is empty. Any further increase in altitude will cause the pressure to rise and open the helium valves.

*U.S. Standard Atmosphere, 1962, U.S. Government Printing Office, December 1962.

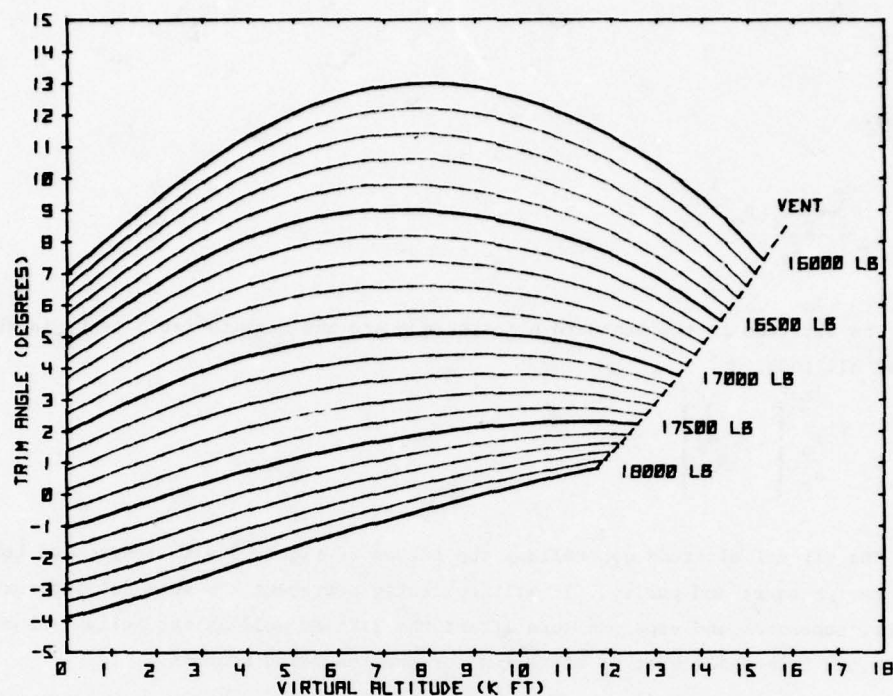


Figure 3. Trim Angle vs Virtual Altitude with Gross Lift of Helium as a Parameter for the CBV365A Aerostat

2.2 Equivalent Altitude

If the conditions do not conform to the ideal case described above it is possible to compute an equivalent altitude; e.g., an altitude in the Standard Atmosphere for the ideal case where the helium volume is the same as in the actual case. This will be termed the "virtual altitude." For pure helium in the absence of superheat and superpressure, that altitude will be the density altitude.

Denoting by R_ρ the density ratio, ρ/ρ_0 , and by λ_0 the specific lift of helium under standard conditions, the helium volume will be,

$$V = \frac{B}{\lambda_0 R_\rho} \quad (2)$$

After List (1951), the temperature, T , pressure, P , and air density, ρ , at any altitude, H , can be computed from the hydrostatic equation if the lapse rate, a , is constant and the conditions at the surface, T_s and P_s , are specified.

$$\frac{dP}{dH} = -\rho g \quad (3)$$

$$T = T_s - aH \quad (4)$$

where,

$$R_v = \frac{f_g T_o P_g}{T_g P_o} \quad (11)$$

The altitude in the Standard Atmosphere where the density ratio is R_v is the virtual altitude, H_v .

$$H_v = \frac{T_o}{a_o} \left[1 - \frac{1}{R_v} \right] \quad (12)$$

The virtual altitude generalizes the curves of Figure 3 with respect to temperature, pressure and purity. It will correctly represent the vent ceiling curve; however, superheat and superpressure affect the lift as well as the helium volume, so that the trim angle must be corrected for the resulting moments.

2.3 Pitch Angle

Changes in configuration from the "standard" represented in Figure 3, as well as superheat and superpressure, will introduce moments affecting the trim angle. In order to correct for these moments, consider Eq. (1) to be linear in the region of α_o and denote by α_r , the reference or uncorrected trim angle.

$$M_\alpha = A - I\alpha_r = 0 \quad (13)$$

$$\alpha_r = \frac{A}{I} \quad (14)$$

The slope, I , is derived from Eq. (1) and, for lack of a better term, is referred to as the "pitch index."

$$I = - \frac{\partial M_\alpha}{\partial \alpha_r} \quad (15)$$

Like the trim angle, it is a function of gross lift and virtual altitude. The family of curves for the aerostat is presented in Figure 4.

The solution to equations (3) and (4) with the boundary conditions at the surface is,

$$\frac{P}{P_s} = \left(\frac{T}{T_s} \right)^n \quad (5)$$

where,

$$n = \frac{\rho_o g T_o}{P_o a} \quad (6)$$

It follows that,

$$\frac{\rho}{\rho_s} = \left(\frac{T}{T_s} \right)^m \quad (7)$$

where $m = n - 1$.

Up to 20,000 feet these equations produce negligible error due to the assumption that the geometric altitude is equal to the geopotential.

For the Standard Atmosphere,

$$a = a_o = 0.0035662 \text{ } ^\circ\text{F/ft}$$

$$n = n_o = 5.2558$$

The density ratio can be written in terms of the temperature and pressure or, by expanding Eq. (7), the density altitude, H_ρ .

$$R_\rho = \frac{P T_o}{P_o T} = \left(1 - \frac{a_o H_\rho}{T_o} \right)^{m_o} \quad (8)$$

$$H_\rho = \frac{T_o}{a_o} \left[1 - R_\rho^{\frac{1}{m_o}} \right] \quad (9)$$

In the general case the helium volume will be affected by the purity, f_g , the superheat, ΔT , and superpressure, ΔP . Let $T_g = T + \Delta T$ and $P_g = P + \Delta P$ represent the actual temperature and pressure of the helium.

$$V = \frac{B}{\lambda_o R_v} \quad (10)$$

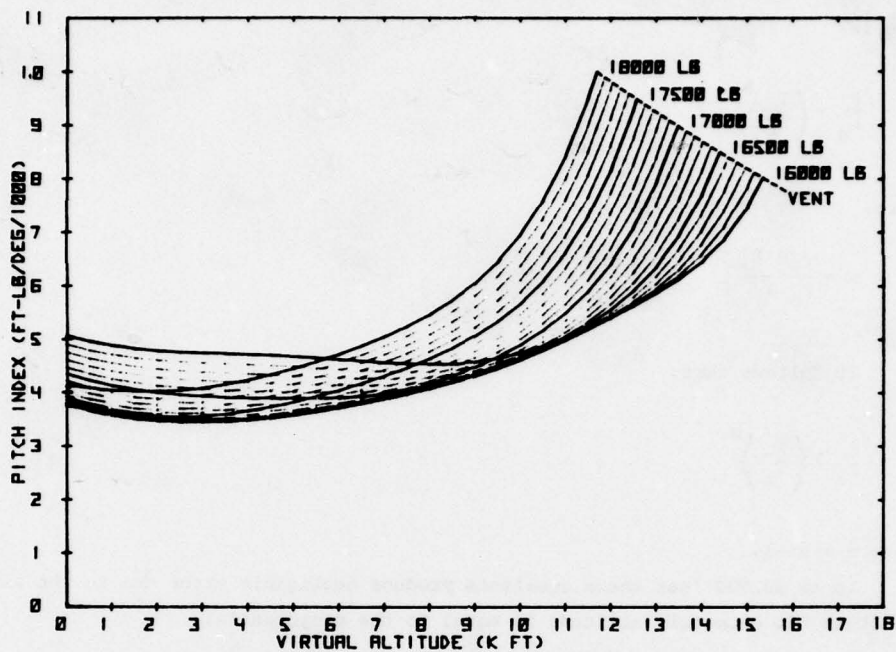


Figure 4. Pitch Index vs Virtual Altitude with Gross Lift of Helium as a Parameter for the CBV365A Aerostat

Let there be a change in the static moments produced by a vertical force, ΔF , acting at (X, Z) in the body coordinate system. This will produce the moments,

$$\Delta M_x = - X \Delta F \quad (16)$$

$$\Delta M_z = - Z \Delta F \quad (17)$$

Making use of Eq. (13), the moment equation is now,

$$A - I \alpha_o + \Delta M_x \cos \alpha_o + \Delta M_z \sin \alpha_o = 0 \quad (18)$$

Division by I and substitution of Eq. (14) yields,

$$\alpha_r - \alpha_o + (\Delta M_x \cos \alpha_o + \Delta M_z \sin \alpha_o) / I = 0 \quad (19)$$

If the angles are small and α_o is expressed in degrees, a close approximation of the solution is,

$$\alpha_o = \frac{\alpha_r + \Delta M_x / I}{1 - \pi \Delta M_z / 180 I} \quad (20)$$

2.3.1 Moments due to Superheat and Superpressure

In order to arrive at the moments due to superheat and superpressure, assume that the temperature and pressure are uniform throughout the envelope, including the inflated empennage. In that case the force resulting from the change in density of the gases in the envelope (helium plus ballonnet and fin air) acts at the centroid, (\bar{X}, \bar{Z}) . Denoting by Ψ' the volume of the envelope, the moments are,

$$\Delta M_x = \bar{X} \rho g \Psi' \left(\frac{\Delta P}{P} - \frac{\Delta T}{T} \right) \quad (21)$$

$$\Delta M_z = \bar{Z} \rho g \Psi' \left(\frac{\Delta P}{P} - \frac{\Delta T}{T} \right) \quad (22)$$

2.3.2 Moments due to Weight and Balance

The standard configuration, to which the curves of Figures 3 and 4 apply, has a weight, W , and center of gravity, (X_w, Z_w) , resulting in the reference moments, $M_{rx} = WX_w$, and $M_{rz} = WZ_w$. Let the configuration change to the weight W' at (X, Z) . The change in gravitational moments is,

$$\Delta M_x = W'X - M_{rx} \quad (23)$$

$$\Delta M_z = W'Z - M_{rz} \quad (24)$$

The corrected trim angle can be computed from Eq. (19) or (20).

2.3.3 Aerodynamic Pitching Moment

In the presence of wind the aerodynamic pitching moment acts to change the angle from α_0 to the pitch angle, α . Let C_{mc} be the pitching moment coefficient transformed to the confluence point and denote by q the dynamic pressure,

$$q = \frac{1}{2} \rho u^2 \quad (25)$$

From Eq. (13) the pitching moment equation is,

$$A - I\alpha + q \Psi'^{2/3} \bar{C}_{mc}(\alpha) = 0, \quad (26)$$

which reduces to,

$$\alpha_0 - \alpha + q \Psi'^{2/3} \bar{C}_{mc}(\alpha) = 0 \quad (27)$$

where,

$$q' = \frac{q}{I}$$

(28)

The coefficient, C_{mc} , is a function only of α and usually can be expressed to a close approximation by a quadratic or cubic polynomial. The pitch angle, therefore, is a function only of α_0 and q' . Curves of pitch angle as a function of q' are shown in Figure 5 for various trim angles. The latter, of course, is the ordinate value when $q' = 0$.

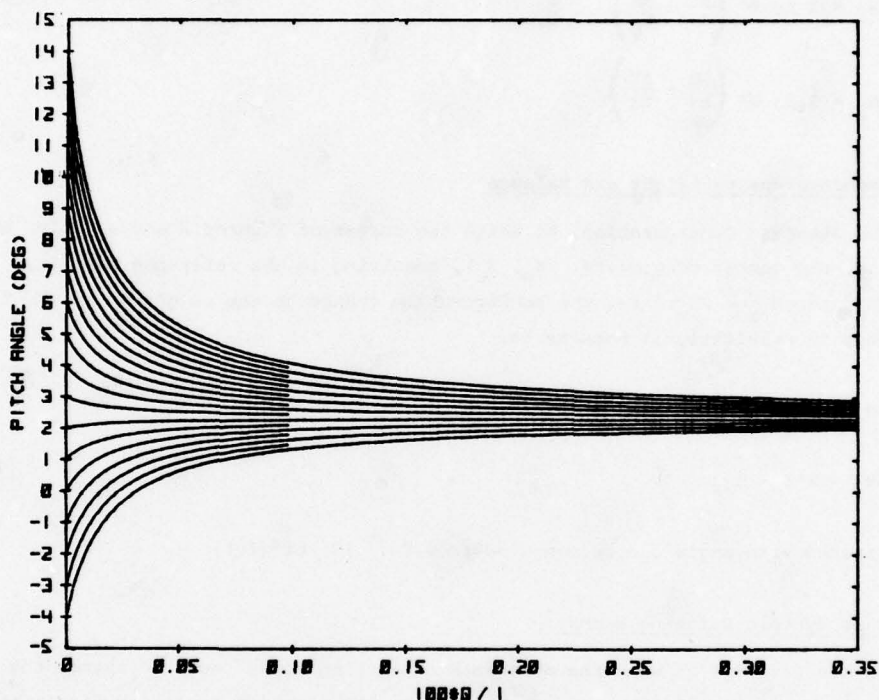


Figure 5. Pitch Angle as a Function of Dynamic Pressure Divided by Pitch Index (q') with Trim Angle as a Parameter for the CBV365A Aerostat. Values of the Abscissa are Multiplied by 100.

2.4 Effect of Humidity

Meyer (1969) has pointed out that the lifting gas contains water vapor which slowly approaches equilibrium with the water vapor pressure in the surrounding air. We have confirmed this fact by measuring the water vapor content of the helium inside the aerostat and by laboratory measurements on the water vapor transmissivity of the hull material. Whereas the material is an excellent barrier for helium, water vapor is transmitted with relative ease, apparently by a chemical diffusion process. Initially dry helium will approach the same relative humidity as the outside air at an initial rate of about 2 percent per day.

In hot, humid climates, water vapor will have a significant effect on helium volume since it occupies space in the helium chamber. If the water vapor pressure is the same in the helium as in the outside air, there will be no effect on buoyant lift. Although the latter condition will not prevail exactly most of the time, there would seem to be no practical alternative but to ignore the effect of humidity on lift.

Let the relative humidity in the helium-air mixture be ϕ , measured at the temperature T_s . Denote by p_v the water vapor pressure and by $P_v(T)$ the saturation vapor pressure. Initially the partial pressure of water vapor in the helium will be,

$$p_{v0} = \phi P_v(T_s) \quad (29)$$

Since the diffusion process through the hull is slow, assume the system to be closed for periods of time of the order of the duration of a flight. In that case the partial pressure (but not the relative humidity) will remain constant at p_{v0} until the temperature reaches the dew point, below which water will condense and the partial pressure will be the saturation vapor pressure,

$$p_{v1} = P_v(T) \quad (30)$$

Thus p_v will be p_{v0} or p_{v1} , whichever is smaller.

An approximation for the saturation vapor pressure, sufficiently accurate over the range of interest for the present purposes, is the following:

$$P_v = C e^{-k/T} \quad (31)$$

where

$$C = 4.9049 \times 10^7 \text{ (in Hg)}$$

$$k = 9540 \text{ (}^\circ\text{R)}$$

The effect of water vapor on the virtual altitude can be taken into account by considering P_g to be the partial pressure of the helium-air mixture.

$$P_g = P + \Delta P - p_v \quad (32)$$

This will give the correct density ratio in Eq. (11) and the correct volume and virtual altitude in Eqs. (10) and (12), respectively. Thus, the partial pressure of water vapor has an effect on virtual altitude similar to superpressure but opposite in sign. Its magnitude can be much larger than the usual superpressure.

Neglecting the buoyant lift effects due to differences in water vapor content of the helium and ambient air, there is no change in the moment resulting from superpressure. All the gases in the hull are compressed and the change in density relative to the outside air is unaffected by the presence of water vapor.

Another effect of humidity must be mentioned. Eqs. (3) through (7) were developed with the assumption of dry air. If the air contains moisture the virtual temperatures and lapse rate must be used. The virtual temperature, $T_v(T, P, \phi)$, is the temperature dry air must be at the pressure, P , in order to have the same density as moist air at the temperature, T , pressure, P , and relative humidity, ϕ . Tables of virtual temperature as a function of the arguments above are given by List (1951). For the present purposes the error resulting from the use of actual temperatures and lapse rate is small and will be ignored.

2.5 Vent Altitude

At the vent altitude the helium volume, V , is equal to the hull volume, Ψ . Thus, from Eq. (10),

$$R_v = \frac{B}{\lambda_o \Psi} \quad (33)$$

In view of Eqs. (5) and (31) we note that P , p_v , and thus R_v are functions of T , which is a function of altitude.

$$f(T) = R_v - \frac{B}{\lambda_o \Psi} = 0 \quad (34)$$

$$H = \frac{T_s - T}{a} \quad (35)$$

The root of Eq. (34) can be found by numerical methods. A form of R_v in terms of the boundary conditions can be derived from Eqs. (7) and (11).

$$R_v = \frac{f_q T_o P_s C_p}{T_s P_o C_T} \left(\frac{T}{T_s} \right)^m \quad (36)$$

where,

$$C_p = 1 + (\Delta P - p_v)/P \quad (37)$$

$$C_T = 1 + \Delta T/T \quad (38)$$

By rearranging Eq. (34) we have,

$$T = T_s \left(\frac{B T_s P_o C_T}{\lambda_o \Psi f_g T_o P_s C_p} \right)^{\frac{1}{m}} \quad (39)$$

Although C_p and C_T are functions of T , their values are near unity and T can be found by the method of successive substitution. Assume an initial estimate of T and compute P , P_v , C_p , C_T and the right-hand side of Eq. (39) to obtain a better estimate of T . About three iterations of this process will give a sufficiently accurate result. The vent altitude is then obtained from Eq. (35).

3. SOME APPROXIMATIONS

Of particular interest to the field engineer, who has little time for elaborate calculations, are approximations which permit rough but reasonably accurate estimates. A number of such approximations can be formulated with respect to density altitude and virtual altitude by taking the partial derivatives of Eq. (12) with R_v expressed in the form of Eq. (36). Expressed as "rules of thumb," these approximations are especially valuable in estimating the vent ceiling.

Let the conditions be the Standard Atmosphere, with pure helium and no superheat or superpressure. The partial derivatives with respect to each of the variables will give the effect of deviations from these conditions.

$$\frac{\partial H_v}{\partial P_s} = - \frac{T}{a_o m_o P_o} \quad (40)$$

$$\cong - 1100 \text{ (ft/in. Hg)}$$

The virtual (and density) altitude will decrease by about 1100 ft for every inch of mercury change in barometric pressure above 29.92.

$$\frac{\partial H_v}{\partial T_s} \cong \frac{1}{a_o m_o} - \frac{n_o H}{m_o T_o} \quad (41)$$

$$\cong 66. - 2.4 H/1000 \text{ (ft/}^\circ\text{F)}$$

The increase in virtual (and density) altitude per $^\circ\text{F}$ increase in surface temperature is about 66 feet less 2.4 feet per 1000 feet of altitude. Thus at 10,000 feet altitude the density altitude changes 42 feet per $^\circ\text{F}$ change in surface temperature.

$$\frac{\partial H_v}{\partial f_g} = - \frac{T}{a_o m_o} \quad (42)$$

$$\cong - 330 \text{ (ft/\%H}_e\text{)}$$

The virtual altitude decreases about 330 feet for every percent increase in helium purity. Conversely, it increases 330 feet for every percent air impurity.

$$\frac{\partial H_v}{\partial \Delta T} = \frac{1}{a_o m_o} \quad (43)$$

$$\cong 66 \text{ (ft/}^\circ\text{F)}$$

The virtual altitude increases approximately 66 feet for every $^\circ\text{F}$ increase in superheat

$$\frac{\partial H_v}{\partial \Delta P} \cong - \frac{T_o}{a_o m_o P_o} - \frac{H}{P_o} \quad (44)$$

$$\cong - (1140 + 33H/1000) \text{ (ft/in. H}_g\text{)}$$

$$\cong - (84 + 2.4H/1000) \text{ (ft/in. water)}$$

The virtual altitude decreases about 1140 feet plus 33 feet per 1000 feet of altitude for ever inch of mercury increase in hull pressure differential. It increases by the same amount per inch of mercury partial pressure of water vapor. At 10,000 feet the virtual altitude decreases about 100 feet per inch of water superpressure.

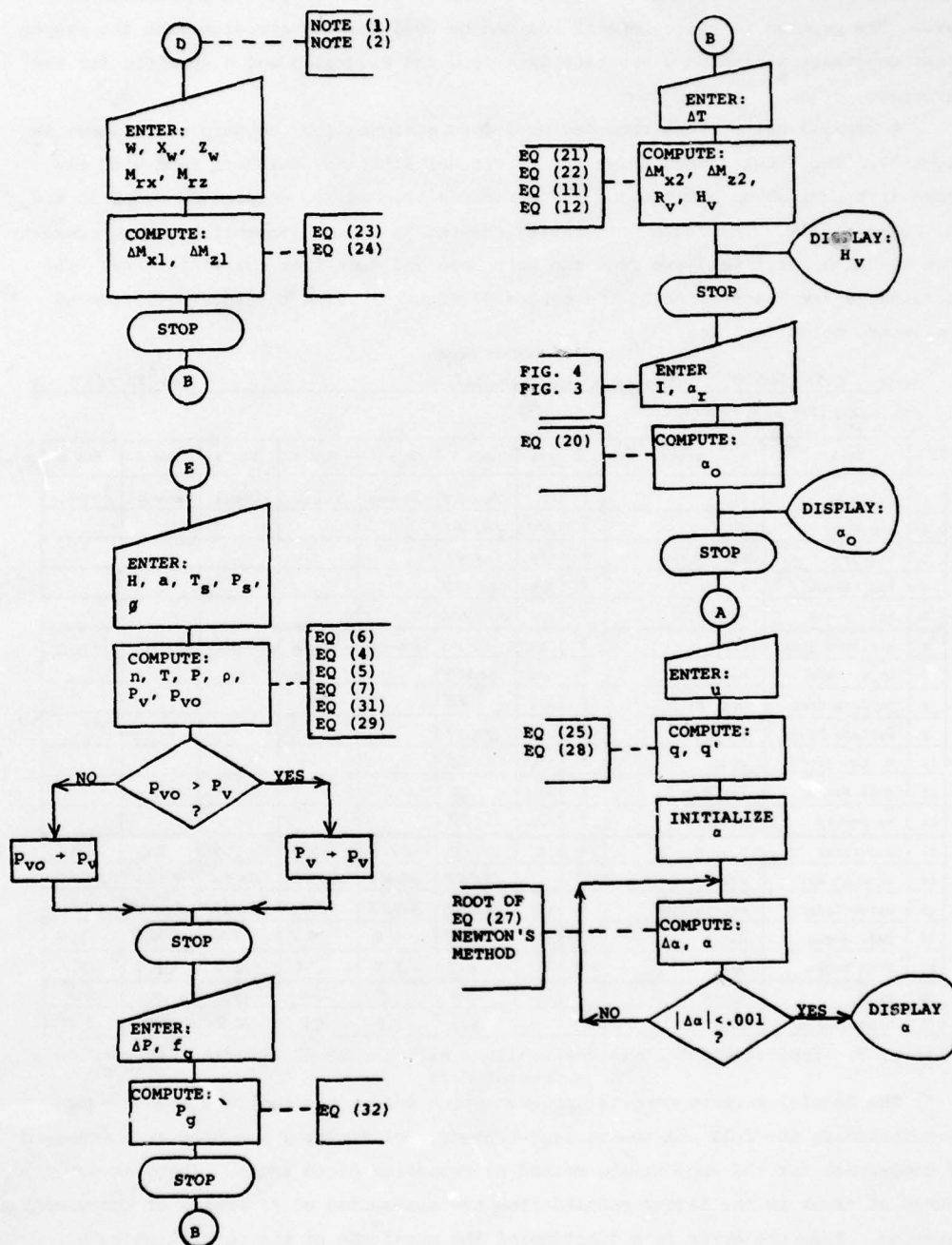
These rules can be applied in reverse (e.g., with opposite sign) to estimate the true vent ceiling from the virtual vent altitude shown in Figure 3.

4. COMPUTATIONS

Using the "rules of thumb" developed above, a Standard Atmosphere table, Figures 3, 4 and 5, and a little diligence, pitch angle and vent ceiling can be estimated to a reasonable approximation. The preferred alternative is to program the equations of Section 2 on a calculator such as the Texas Instruments TI-59 or the Hewlett Packard HP-67, both of which have magnetic card storage of program and data. We have used the latter calculator.

The flow chart for the computation of pitch angle on the HP-67 is shown in Figure 6. In this program pitch angle is found by taking the root of Eq. (27) in

HP-67 PROGRAM PITCH



NOTE (1) CONNECTOR LETTERS CORRESPOND WITH SPECIAL FUNCTION KEYS ON HP-67 CALCULATOR.
NOTE (2) CONSTANTS AND DEFAULT VALUES LOADED FROM MAGNETIC DATA CARD.

Figure 6. Program Flow Chart for Computation of Pitch Angle with the HP-67 Calculator

AD-A074 469

AIR FORCE GEOPHYSICS LAB HANSCOM AFB MA
PROCEEDINGS OF THE AFGL SCIENTIFIC BALLOON SYMPOSIUM (10TH) HEL--ETC(U)
MAR 79 C L RICE
AFGL-TR-79-0053

F/G 1/3

UNCLASSIFIED

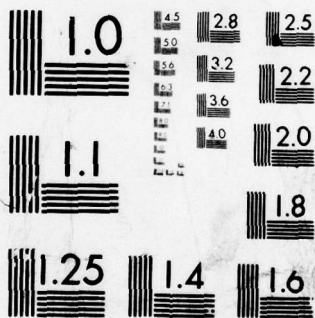
NL

6 OF 6

AD
A074469



END
DATE
FILMED
10-79
DDC



MICROCOPY RESOLUTION TEST CHART
NATIONAL BUREAU OF STANDARDS-1963-A

which C_{mc} is expressed as a third degree polynomial. The coefficients of the latter and other constants relating to the CBV365A aerostat are stored on a magnetic data card. The program is quite general and can be used for any aerostat with the proper input constants stored on a separate data card and Figures 3 and 4 specific for the aerostat.

A typical set of runs recorded on a form designed for the purpose is shown in Figure 7. The first output (Step 14) is virtual altitude, which is used with the gross lift to look up pitch index and reference trim angle, entered in Steps 15 and 16, respectively. The center of gravity entered is in the conventional body coordinates measured positively aft from the soft nose and down from the centerline. The coordinates are transformed to the system of Figure 2 using the internally stored confluence point location.

HP-67 PROGRAM PITCH

TITLE CBV 365 A Sample Computation DATE 7/17/78

STD. GROSS LIFT = 17000 Lb.

	DATA	UNITS	I/O	KEY	RUN 1	RUN 2	RUN 3	RUN 4	RUN 5	RUN 6
1	Gross Wt.	Lb.	↑	D	11449.7	Same	Same	Same	Same	Same
2	X-C.G.	Ft.	↑	R/S	101.31					
3	Z-C.G.	Ft.	↑	R/S	16.48					
4	Ref. X-Mom.	Ft.-Lb.	↑	R/S	466117					
5	Ref. Z-Mom.	Ft.-Lb.	↑	R/S	483406					
6	Altitude (AGL)	Ft.	↑	E	100	Same	Same	Same	Same	Same
7	Lapse Rate	Deg. F/Ft.	↑	R/S	.00357					
8	Surface Temp	Deg. F	↑	R/S	85					
9	Surface Press	In. Hg.	↑	R/S	29.51					
10	R. Humidity	Frac.	↑	R/S	.80					
11	Hull Press.	In. H ₂ O	↑	R/S	2					
12	He Purity	Frac.	↑	R/S	.98					
13	Superheat	Deg. F	↑	B	0	21.8	7.9	3.9	2.6	1.6
14	Virtual Alt.	Ft.	→		3848	5148	4326	4085	4006	3995
15	Pitch Index	Ft.-Lb/Deg	↑	R/S	3450	3650	3550	3500	3500	3500
16	Ref. Angle	Deg	↑	R/S	4.3	4.8	4.5	4.4	4.4	4.4
17	Trim Angle	Deg	→		6.1	-3.8	1.6	3.7	4.9	5.1
18	Wind	Knots	↑	A	0	0	10	20	30	50
19	Pitch Angle	Deg	→		6.1	-3.8	1.9	2.8	2.7	2.5

Figure 7. Typical Pitch Angle Computations with the HP-67 Program, Recorded on a Special Form

The general purpose computer program which solves the complete moment equation including the full polynomial representation of Figure 1 was used as a standard of comparison for the approximate method of computing pitch angle. The greatest source of error in the latter results from the assumption of linearity of the moment equation. Thus the error is a function of the magnitude of the correction to α_x . The error as compared with the computer program is shown in Figure 8 as a function

of the correction to α_r . This is, of course, a function of the particular aerostat and its configuration including the confluence point location. For the CBV365A, the error is greatest at large positive corrections which result from high negative values of superheat such as would be encountered in a dead calm at night. Over the range of practical application the error is a few tenths of a degree. We refer, of course, to the mathematical error in the approximate method of computation as compared with the more exact solution. Whether the mathematical model accurately represents the aerostat and its environment is a matter still under investigation.

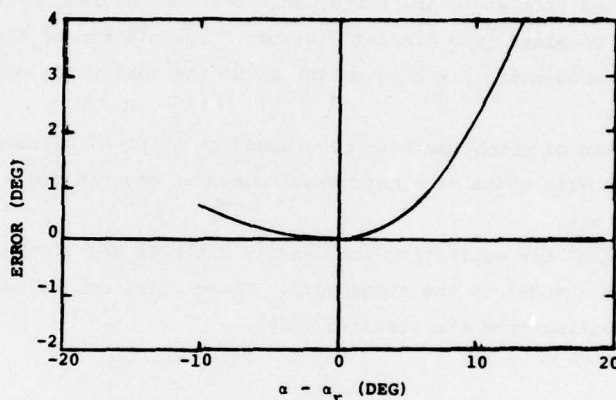


Figure 8. Approximate Mathematical Error in the Simplified Method of Computing Pitch Angle as a Function of the Correction to α_r

The programming of vent ceiling is straightforward from Eqs. (39) and (35). This can be done on the HP-67 with sufficient memory left for a Standard Atmosphere table of temperature, pressure and air density as a function of altitude from Eqs. (4), (5) and (7) which are accurate for this purpose up to about 20,000 feet.

5. SUMMARY AND CONCLUSIONS

A simplified method of computing pitch angle and vent ceiling altitude of a tethered aerostat has been developed. The method is based upon use of a standard configuration of the aerostat containing pure helium in a Standard Atmosphere. For this ideal or "standard" case the trim angle and the vent ceiling are functions only of the altitude and gross lift of helium. For a real case, pitch angle is computed by making corrections for deviations from the standard.

The corrections involve first computing an equivalent or "virtual" altitude, taking into account the surface temperature and barometric pressure, lapse rate,

helium purity, superheat, superpressure and water vapor content of the helium. The virtual altitude is the altitude in the Standard Atmosphere where the standard case has the same helium volume as the actual case. This altitude is used to obtain from standard curves a "reference" trim angle and "pitch index." The latter is the negative slope of the pitching moment equation for that helium volume, gross lift and standard weight and balance at the reference trim angle.

Making use of the pitch index, the reference trim angle is corrected for the moments produced by superheat, superpressure and deviations of weight and center of gravity from that of the standard configuration.

The pitch angle in the presence of wind is shown to be approximately a function of the corrected trim angle and the dynamic pressure divided by the pitch index. Pitch can be obtained from standard curves by solution of the moment equation in which the aerodynamic pitching moment about the confluence point is expressed as a polynomial.

The computation of pitch has been programmed on an HP-67 calculator. The results when compared with those of a more exact computer program are sufficiently accurate for field use.

"Rules of thumb" for estimating the density altitude and virtual altitude have been developed from a model of the atmosphere. These rules can be used for estimation of the vent ceiling from the standard curve.

References

- Wright, John B. (1976) Computer Programs for Tethered-Balloon System Design and Performance Evaluation, AFGL-TR-76-0195
- Myers, Philip F. (1969) Tethered Balloon Handbook, Goodyear Aerospace Corp. Report GER14142 (AFCRL-69-0017)
- List, Robert J. (1951) Smithsonian Meteorological Tables, Smithsonian Institution Washington, D.C.

Glossary

a	= lapse rate ($^{\circ}\text{F}/\text{ft}$)
a_o	= Standard lapse rate = $0.0035662(^{\circ}\text{F}/\text{ft})$
A	= a constant in the linear moment equation (ft lb)
B	= buoyant lift in the absence of superheat and superpressure (lb)
\bar{c}	= hull length (ft)
C	= a constant in Eq. (31) = 4.9049×10^7 (in. Hg)
C_{mc}	= coefficient of aerodynamic pitching moment about the confluence point (non-dimensional)
C_p	= correction factor for superpressure and water vapor defined in Eq. (37) (non-dimensional)
C_T	= correction factor for superheat defined in Eq. (38), (non-dimensional)
f_g	= helium purity expressed as volumetric fraction of helium (non-dimensional)
g	= gravitational constant = 32.174 (ft/sec ²)
H	= geometric altitude above the ground (ft)
H_p	= density altitude (ft)
H_v	= virtual altitude (ft)
I	= pitch index defined in Eq. (15) (ft lb/deg.)
k	= a constant in Eq. (31) = 9540 ($^{\circ}\text{R}$)
m	= exponent of temperature ratio in Eq. (7) (non-dimensional)
m_o	= m for the Standard Atmosphere = 4.2558
M_a	= pitching moment about the confluence point (ft lb)
M_{rx}	= gravitational moment in the x direction for the standard or reference configuration (ft lb)
M_{rz}	= gravitational moment in the z direction for the standard or reference configuration (ft lb)
n	= exponent of temperature ratio in Eq. (5), defined in Eq. (6) (non-dimensional)
n_o	= n for the Standard Atmosphere = 5.2558
P_v	= partial pressure of water vapor (in. Hg)
P_{vo}	= initial partial pressure of water vapor (in. Hg)
P_{vl}	= partial pressure of water vapor below the dew point (in. Hg)
P	= pressure (in. Hg)
P_g	= pressure of the lifting gas or partial pressure of the helium-air mixture (in. Hg)
P_o	= standard pressure = 29.921 (in. Hg) = 2116.22 (lb/ft ²)
P_s	= barometric pressure at ground level (in. Hg)
P_v	= saturation vapor pressure of water (in. Hg)
q	= dynamic pressure (lb/ft ²)
q'	= q/I (deg/ft ³)
R_p	= density ratio (non-dimensional)

R_v	= virtual density ratio defined in Eq. (11) (non-dimensional)
T	= temperature ($^{\circ}R$)
T_o	= Standard temperature = $518.76^{\circ}R$
T_g	= temperature of the lifting gas ($^{\circ}R$)
T_s	= air temperature at ground level ($^{\circ}R$)
T_v	= virtual air temperature ($^{\circ}R$)
u	= wind speed (ft/sec)
V	= volume of the lifting gas (ft ³)
v	= hull volume (ft ³)
v'	= volume of the envelope including ballonnet air and empennage (ft ³)
W	= gross weight of the aerostat (lb)
W'	= modified gross weight (lb)
x	= longitudinal coordinate in the body system (ft)
x_B	= longitudinal coordinate of the center of buoyancy (ft)
x_w	= longitudinal coordinate of the center of gravity (ft)
\bar{x}	= longitudinal coordinate of the centroid of the envelope (ft)
z	= vertical coordinate in the body system (ft)
z_B	= vertical coordinate of the center of buoyancy (ft)
z_w	= vertical coordinate of the center of gravity (ft)
\bar{z}	= vertical coordinate of the centroid of the envelope (ft)
α	= pitch angle (deg)
α_o	= trim angle or pitch angle in the absence of wind (deg)
α_r	= reference trim angle; eg, for the standard configuration in the Standard Atmosphere (deg)
ΔF	= incremental force (lb)
ΔM_x	= moment in the x direction for an incremental gravitational force (ft lb)
ΔM_z	= moment in the z direction for an incremental gravitational force (ft lb)
ϕ	= relative humidity (non-dimensional)
λ_o	= specific lift of helium under standard conditions (lb/ft ³)
ρ	= air density (slugs/ft ³)
ρ_o	= air density under standard conditions (slugs/ft ³)
ρ_s	= air density at ground level conditions (slugs/ft ³)

Contents

1. Background
2. The Elastic Catenary Model
3. Definition of Spring Constants in the Elastic
4. Computation of Spring Constants through Position Displacement
5. Computation of Spring Constants through Force Displacement
6. Sensitivity Analysis

MATHEMATICAL MODEL OF AN ELASTIC TETHER WITH CATENARY FOR STATIC AND STABILITY ANALYSIS

N. A. Dresner and S. P. Jones
TCOM Corporation
Columbia, Maryland

Abstract

Stability Analysis of tethered aerostats requires that the boundary conditions of the restoring forces of the tether on the aerostat be represented by a set of equivalent linear springs. A mathematical model of an elastic tether subjected to aerodynamic and gravity forces is presented. A methodology for deriving the equivalent linear springs is also presented and analyzed.

1. BACKGROUND

The tethered aerostat stability model developed by Redd (1973) has been used as a basis for our own dynamic model, which includes a number of modifications and additions applicable to TCOM aerostats. Among these is the inclusion of the dynamic effects of ballonet air, ignored in Redd, and a tether model which takes into account the elasticity of the cable. The latter is the subject of the present paper.

The tether model employed by Redd is that developed by Neumark (1961), which includes a number of assumptions that serve to simplify the numerical computations. Foremost among these is the simplification that the tether is inelastic. The Neumark procedure leads to a simple analytical model of a set of equivalent linear springs that represent the restoring force on the aerostat due to the catenary when the upper end is given an infinitesimal displacement as represented by

$$dF_x = k_{xx} dx + k_{xz} dz \quad (1a)$$

$$dF_z = k_{zx} dx + k_{zz} dz \quad (1b)$$

$$dF_y = k_{yy} dy \quad (1c)$$

However, for a typical TCOM aerostat deployment, the Neumark formulation yields spring constants that are similar in magnitude to the elasticity of the tether, and hence the elastic effects cannot be ignored. Additionally, because of the high spring constants, a (vertical) mode is predicted with a very short period; i.e., 0.1 second. Under some conditions, the accelerations in this mode produce highly unrealistic results. These have been largely ignored, but the complex couplings in the model dynamics probably lead to inaccurate results in other modes as well.

In early 1977, TCOM developed an alternative tether model which included the elasticity of the tether, but neglected the effects of the catenary. This approximation is accurate enough for low altitude and/or low wind speed cases in which the tether is essentially straight. This model is called the Rigid Elastic Rod.

A new tether model has been developed which includes both the elastic and catenary effects. This model, called the Elastic Catenary, is described and analyzed in this report.

2. The Elastic Catenary Model

In the stability model for the aerostat, the dynamic modes are derived assuming small (infinitesimal) displacements about the equilibrium position.* Thus the tether model requires that:

- (a) the equilibrium position be computable and
- (b) the restoring forces due to a small displacement of the upper end of the tether be computable.

The Elastic Catenary Model treats the tether as a linear, longitudinal spring and modifies the Neumark aerodynamic force equations to act on the stretched tether. Figure 1 shows the coordinate system for the model.

The differential equations for the tether are written in parametric form, with the parameters being the length along the unstretched tether measured from $s=0$ at the point (x_1, y_1, z_1) . Because the tether is assumed to be a linear spring, the elongation can be expressed as

$$\frac{dL}{ds} = 1 + \frac{T}{k} \quad (2a)$$

where L = length of stretched tether,

k = elastic "spring constant,"

and T = scalar tension on the tether.

* A true equilibrium position exists because the model requires a constant, homogeneous windfield.

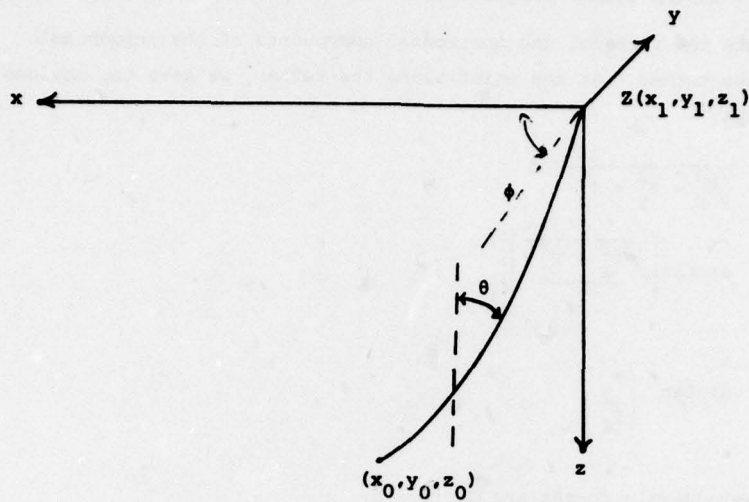


Figure 1. Coordinate System for Tether Models

The equations for the equilibrium position then become:

$$\frac{dz}{ds} = \left(1 + \frac{T}{k}\right) \cos\theta \quad (2b)$$

$$\frac{dx}{ds} = \left(1 + \frac{T}{k}\right) \sin\theta \cos\phi \quad (2c)$$

$$\frac{dy}{ds} = \left(1 + \frac{T}{k}\right) \sin\theta \sin\phi \quad (2d)$$

The model is completed by specifying the changes in the vector tension along the tether to allow computation of the scalar tension, T , and the tether angles. The equations are:

$$\frac{dT_x}{ds} = F_{\text{drag},x} (T, x, z, s, \theta, \phi) \quad (2e)$$

$$\frac{dT_z}{ds} = -\mu - F_{\text{lift}} (T, x, z, s, \theta, \phi) \quad (2f)$$

$$\frac{dT_y}{ds} = F_{\text{drag},y} (T, x, z, s, \theta, \phi) \quad (2g)$$

Here, μ is the linear weight density of the unstretched tether, and F_{lift} and F_{drag} are the vertical and horizontal components of the aerodynamic forces on the tether. At any point along the tether, we have the obvious relationships:

$$T = \sqrt{T_x^2 + T_y^2 + T_z^2} \quad (3a)$$

$$\theta = \arctan \left(\frac{\sqrt{T_x^2 + T_y^2}}{T_z} \right) \quad (3b)$$

$$\phi = \arctan \left(\frac{T_y}{T_x} \right) \quad (3c)$$

The aerodynamic forces are defined by

$$F_{\text{lift}} = \frac{1}{2} \rho V^2 d_c (C_{Dc} \cos^2 \theta \sin \theta) \left(1 + \frac{T}{k}\right) \quad (3d)$$

$$F_{\text{drag}} = \frac{1}{2} \rho V^2 d_c (C_{Dc} \cos^3 \theta + \eta) \left(1 + \frac{T}{k}\right) \quad (3c)$$

where

ρ = air density*

V = wind velocity*

d_c = tether diameter

C_{Dc} = tether drag coefficient**

η = tether drag coefficient**

The differential Eqs. (2) together with the relationships in Eqs. (3) constitute the Elastic Catenary Model.

The simplest application is to provide, as initial conditions, the components of the tension*** at the aerostat confluence point, $x_1(0) = y_1(0) = z_1(0) = L(0) = 0$, and to integrate the equations to find:

*We make the common assumption that: (a) the wind field is constant in direction, and (b) the dynamic pressure $1/2 \rho V^2$ is a constant. While these assumptions are not strictly valid, there is currently insufficient data to support a more detailed model. In Neumark's model, these assumptions are necessary to allow integration of the equations analytically. When reliable data becomes available, it can be included easily into the TCOM Elastic Catenary model by addition of a variable V and modification of the associated aerodynamic force equations.

- (a) the tether shape $x(s)$, $y(s)$ and $z(s)$
- (b) the aerostat's altitude z_0 and downdraft displacement x_0
- (c) the stretched length of the tether****
- and (d) the tether tension T_0 and angles θ_0 and ϕ_0 at the bottom.

These equations are not analytically integrable, but standard numerical methods provide excellent approximations to the solution.

3. Definition of Spring Constants in the Elastic Catenary Model

To determine the equivalent linear springs (after Neumark), one makes small, independent changes in the aerostat's position, dx , dy and dz , and, from the resulting change in the forces, the spring constants are defined by

$$\begin{aligned} k_{xx} &= \frac{\partial T}{\partial x_1} & k_{xz} &= \frac{\partial T}{\partial z_1} \\ k_{zx} &= \frac{\partial T}{\partial x_1} & k_{zz} &= \frac{\partial T}{\partial z_1} \\ k_{yy} &= \frac{\partial T}{\partial y_1} \end{aligned} \quad (4)$$

where

(a) dT is the change in the upper tension (ref. Figure 2) required to provide an equilibrium cable from $(x_1 + dx_1, y_1 + dy_1, z_1 + dz_1)$ to (x_0, y_0, z_0) ,

and (b) the derivatives are evaluated at the static equilibrium position $x_1 = y_1 = z_1 = 0$ (ref. Figure 1)

4. Computation of Spring Constants Through Position Displacement

Figure 2 illustrates the basic process of displacing the end of the tether through the infinitesimal distance and observing the new upper tension,

**The use of the two constants allows one to treat both McLeod's model in which the normal force on the tether is $1/2 \rho V^2 C_{DC} \cos^2 \theta$ and Hoerner's model which differs from McLeod's in that it includes a residual drag component even when the tether is parallel to the wind. For the TCOM tether $C_{DC} = 1.12$, $\eta = 0$ in McLeod's model; $C_{DC} = 1.1$, $\eta = .02$ in Hoerner.

***In equilibrium, the tension of the confluence point is equal to the vector sum of the aerostat's reserve buoyancy and the aerodynamic forces on the aerostat.

****The variable L is not necessary for the solution of the equations, but it is included for the additional information provided.

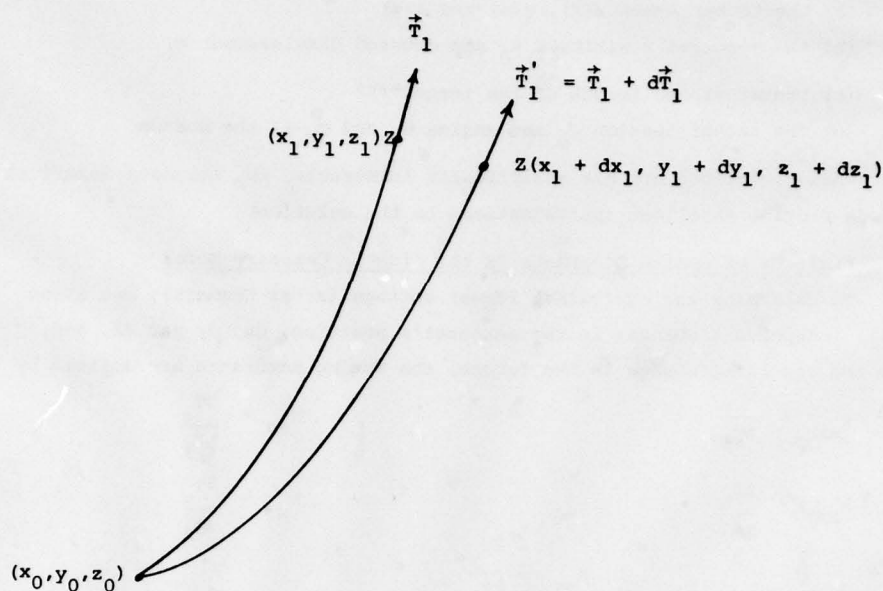


Figure 2. Derivation of Spring Constants Through Infinitesimal Displacement of the Upper End of the Tether

T'_1 , required for equilibrium with unchanged lower end point (x_0, y_0, z_0) . The restoring force used in Eqs. (4) is the difference $\vec{T}'_1 - \vec{T}_1$.

Unfortunately, the process of finding the upper tension, \vec{T}'_1 , resulting from the displacement is not an explicit process since the initial tension at the upper end point is required as part of the initial conditions of the differential Eqs. (2). The process of finding the upper tension can be formulated as follows:

- Consider the Elastic Catenary Model as a vector function of the upper tension, T_1 , and position (x_1, y_1, z_1) whose values are the position of the lower end point, $(T_1, x_1, y_1, z_1) = (x_0, y_0, z_0)$
- Solve, the implicit equation, $(T'_1, x_1 + dx_1, y_1 + dy_1, z_1 + dz_1) = (x_0, y_0, z_0)$ for the upper tension, T'_1 .

For technical reasons, it has been found easier to implement the model if the upper end point is always at $(x_1, y_1, z_1) = (0, 0, 0)$. This is accomplished, in the displacement method, by a linear translation of the coordinate system through (dx_1, dy_1, dz_1) . We then define the implemented

model function $S(T_1) = \mathcal{S}(T_1, 0, 0, 0)$ and reformulate the problem as

* Solve, for T_1 , the equation $S(T_1') = (x_0 + dx_1, y_0 + dy_1, z_0 + dz_1)$ (5)
which is equivalent to

$$S_x(T_1') = x_0 + dx_1 \quad (6a)$$

$$S_y(T_1') = y_0 + dy_1 \quad (6b)$$

$$S_z(T_1') = z_0 + dz_1 \quad (6c)$$

For ease of computation of the derivatives in Eqs. (4), three applications of Eqs. (6) are employed; with

$$(dx_1, dy_1, dz_1) = (\delta, 0, 0), (0, 0, \delta), \text{ and } (0, \delta, 0)$$

It was found that the values of the spring constants depended on the size of the displacement δ . Figure 3 illustrates this variation for one aerostat deployment. Figure 4 gives the spring constant values for various δ 's and estimates of the spring constants at $\delta = 0$ by various methods.

Investigation has shown:

The loss of precision using values of δ considerably smaller than $\sim .1$ foot leads to gross inaccuracies in the estimates of the spring constants.

Use of the method of sensitivity analysis described in Section 6, below, provides sufficiently accurate estimates of the derivatives at $\delta = 0$ from an average of two symmetrical displacements of $\pm \delta$ using $\delta \sim 1/8$ foot.

This then, requires six solutions of equations : i.e., for (dx_1, dy_1, dz_1) equal to $(\delta, 0, 0)$, $(-\delta, 0, 0)$, $(0, 0, \delta)$, $(0, 0, -\delta)$, $(0, \delta, 0)$, and $(0, -\delta, 0)$.

4.1 Computational Considerations Using Position Displacement*

The root finding algorithm used to solve Eqs. (6) is the inverse Jacobian method. The Eqs.(6) are transformed into an equivalent problem.

Find the roots T and θ of:

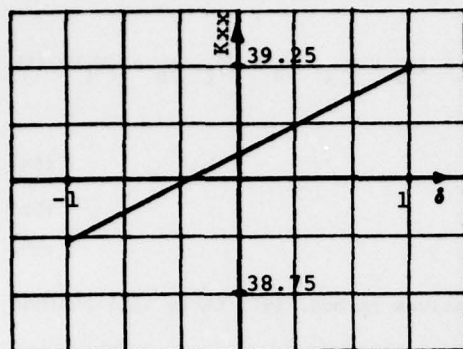
$$E_x(\vec{T}, \theta) = S_x(T_1') - (x_0 + dx_1) = 0 \quad (7a)$$

$$E_z(\vec{T}, \theta) = S_z(T_1') - (z_0 + dz_1) = 0 \quad (7b)$$

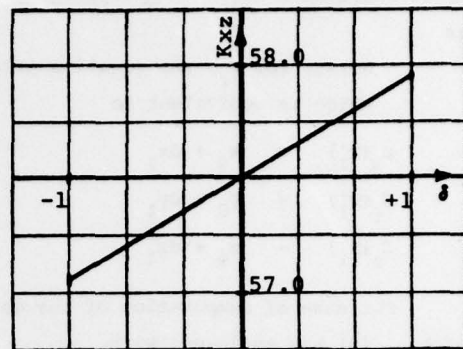
where

$$T_{1x}' = T_1' \sin \theta \quad \text{and} \quad T_{1z}' = T_1' \cos \theta$$

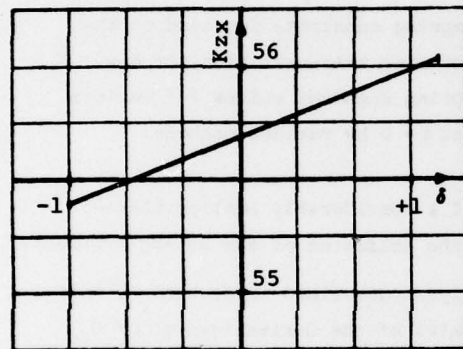
*For convenience, this section is written for the two dimensional problem, i.e., with the lateral effects ignored.



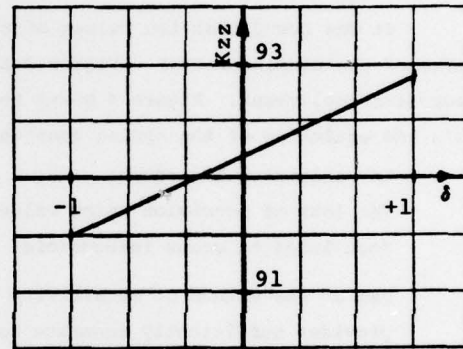
(a) Kxx



(b) Kxz



(c) Kzx



(d) Kzz

Figure 3. Examples of Variation of Computed Spring Constant With Unipolar Displacement Using the Position Displacement Method

Starting with the current, i -th, approximation $T^{(i)}$ and $\theta^{(i)}$, a first-order Taylor Series approximation is made:

$$E_x(T^{(i)} + dT, \theta^{(i)} + d\theta) = E_x(T^{(i)}, \theta^{(i)}) + \frac{\partial E_x}{\partial T} dT + \frac{\partial E_x}{\partial \theta} d\theta \quad (8a)$$

$$E_z(T^{(i)} + dT, \theta^{(i)} + d\theta) = E_z(T^{(i)}, \theta^{(i)}) + \frac{\partial E_z}{\partial T} dT + \frac{\partial E_z}{\partial \theta} d\theta \quad (8b)$$

We then set the right-hand side of each of the Eqs. (8) to zero to get:

displ.
+1
Kxx = 39.2409081
Kzz = 92.9160343
Kzx = 56.0263075
Kxz = 58.0071396

displ.
+1/2
Kxx = 39.1493624
Kzz = 92.5778852
Kzx = 55.8927290
Kxz = 57.7998184

displ.
+1/8
Kxx = 39.0808874
Kzz = 92.3252304
Kzx = 55.7928040
Kxz = 57.6448844

displ.
-1/8
Kxx = 39.0853120
Kzz = 92.1571888
Kzx = 55.7263000
Kxz = 57.5418278

displ.
-1/2
Kxx = 38.9670901
Kzz = 91.9058526
Kzx = 55.6267394
Kxz = 57.3876585

displ.
-1/8
Kxx = 38.8763540
Kzz = 91.5719925
Kzx = 55.4943197
Kxz = 57.1828357

Figure 4a. Calculated Values of Spring Constants for Various Unipolar Displacements. Displacements are in feet and spring constants in pounds per foot

Method	Kxx	Kxz	Kzx	Kzz
Lagrange Interpolation				
Order: 2	39.057817	57.592497	55.759151	92.239736
3	39.058098	57.593346	55.759545	92.241194
4	39.058093	57.593334	55.759541	92.241173
5	39.058092	57.593332	55.759540	92.241168
6	39.058091	57.593331	55.759540	92.241166
2-Pt Average				
: <u>+1/8</u>	39.058100	57.593356	55.759552	92.241210
<u>+1/2</u>	39.058226	57.593738	55.759734	92.241869
<u>+1</u>	39.058631	57.594988	55.760314	92.244013

Figure 4b. Estimates of Spring Constants at Equilibrium Position Using Various Methods (spring constants in pounds per foot)

$$\frac{\partial E_x}{\partial T} dT + \frac{\partial E_x}{\partial \theta} d\theta = -E_x(T^{(1)}, \theta^{(1)}) \quad (9a)$$

$$\frac{\partial E_z}{\partial T} dT + \frac{\partial E_z}{\partial \theta} d\theta = E_z(T^{(1)}, \theta^{(1)}) \quad (9b)$$

If the values of the partial derivatives in equations (9) are known, we can solve them for the changes dT and $d\theta$ in the estimates of the roots. In matrix form we have:

$$\begin{pmatrix} dT \\ d\theta \end{pmatrix} = - \begin{pmatrix} \frac{\partial E_x}{\partial T} & \frac{\partial E_x}{\partial \theta} \\ \frac{\partial E_z}{\partial T} & \frac{\partial E_z}{\partial \theta} \end{pmatrix}^{-1} \begin{pmatrix} E_x(T^{(i)}, \theta^{(i)}) \\ E_z(T^{(i)}, \theta^{(i)}) \end{pmatrix} \quad (10a)$$

and

$$\begin{pmatrix} T^{(i+1)} \\ \theta^{(i+1)} \end{pmatrix} = \begin{pmatrix} T^{(i)} \\ \theta^{(i)} \end{pmatrix} + \begin{pmatrix} dT \\ d\theta \end{pmatrix} \quad (10b)$$

This process is repeated until some convergence criterion is satisfied. As implemented, $E_x^2 + E_z^2 < P$ was used, where P is the square distance limit ($P=10^{-10}$ ft² was the conventional value). Since the derivatives in (9) cannot be calculated exactly, they were estimated using a convenient step size. Values of

$$\frac{\partial E_x}{\partial T} \approx \frac{E_x(T + \Delta T, \theta) - E_x(T, \theta)}{\Delta T}, \text{ etc.} \quad (11)$$

ΔT and $\Delta \theta$ used to estimate the derivatives were 1 lb. and .001 degree, respectively. These values were found to provide a good balance between finite step-size errors and finite precision errors.

4.2 Computational Work in the Position Displacement Method

The Eqs. (6) are solved six times. Typically, each solution requires three iterations of the root finder, and each iteration of the root finder requires seven integrations of the differential equations, one to compute E_x, E_y, E_z for $T^{(0)}, \theta^{(0)}$ and $\phi^{(0)}$ and six to compute the five derivatives. Thus each application of the displacement requires (typically) 126* integrations of the model's equations.

*Observed limits of the number of iterations are 2 to 4. Thus the limits on the whole are 84 to 168 integrations.

This is an unacceptable amount of computational effort for general usage, but because this method corresponds so closely with the definitions of the spring constants, it was used to perform all initial investigations and to validate other methods.

5. Computation of Spring Constants Through Force Variation

In the method of position displacement, the change in force necessary to support a specified displacement in position is determined. In the method of force variation, the problem is inverted and the displacement in position caused by a specified variation in the force is computed.

Again, the defining equations (1) are used

$$\begin{aligned} dF_x &= k_{xx} dx + k_{xz} dz \\ dF_z &= k_{zx} dx + k_{zz} dz \\ dF_y &= k_{yy} dy \end{aligned} \quad (11)$$

but this time the tension at the upper end point is changed by dT and the resulting positional change (dx , dz , dy) is computed from *

$$dx = S_x(\vec{T}_1 + d\vec{T}) - S_x(T_1) \quad (12a)$$

$$dy = S_y(T_1 + dT) - S_y(T_1) \quad (12b)$$

$$dz = S_z(T_1 + dT) - S_z(T_1) \quad (12c)$$

The linear Eqs (12) are then solved for the spring constants.

In practice, since there are five spring constants, five equations must be solved. They are defined by applying Eq. (12) twice for two linearly independent force variations $dT^{(1)}$ and $dT^{(2)}$, yielding the equation, in matrix form,

$$\begin{pmatrix} \Delta x^{(1)} & \Delta z^{(1)} & 0 & 0 & 0 \\ 0 & 0 & \Delta x^{(1)} & \Delta z^{(1)} & 0 \\ \Delta x^{(2)} & \Delta z^{(2)} & 0 & 0 & 0 \\ 0 & 0 & \Delta x^{(2)} & \Delta z^{(2)} & 0 \\ 0 & 0 & 0 & 0 & \Delta y \end{pmatrix} \begin{pmatrix} k_{xx} \\ k_{xz} \\ k_{zx} \\ k_{zz} \\ k_{yy} \end{pmatrix} = \begin{pmatrix} F_x^{(1)} \\ F_z^{(1)} \\ F_x^{(2)} \\ F_z^{(2)} \\ F_y \end{pmatrix} \quad (13)$$

which is solvable by standard, elementary, numerical methods.

*Recall that the function S assumes $(x_1, y_1, z_1) = (0,0,0)$ by linear translation of the origin.

5.1 Computational Considerations Using Force Variation

As implemented, $\Delta F^{(1)} = (\delta, 0, 0)$, $F^{(2)} = (0, 0, \delta)$, and $F_y = (0, \delta, 0)$.

Additionally, for the same reasons described for the position displacement method, there is a variation of the solution, depending on the value of δ . To find the best estimate of the spring constants, the method is applied twice for each ΔF ; i.e., for $+\Delta F$ and for $-\Delta F$.

The final consideration is that δ be neither too large, causing finite step-size errors, nor too small causing finite precision errors. A value of δ in the range 1/2 pound to 2 pounds seems adequate and 1 pound has been chosen as the normal variation.

5.2 Computational Work in the Force Variation Method

The computation of the spring constants using the force variation method requires exactly seven integrations of the model's differential equations(2).^{*} Thus the force variation method requires an order of magnitude less computation than does the position displacement method.

6. Sensitivity Analysis

The values of the spring constants themselves provide a convenient analytical tool by which various methods can be compared. However, in practice, the spring constants themselves are unobservable. The spatial position (x_0, y_0, z_0) and tether tension T_0 are observable. Tension differences between the values obtained using the Neumark and Elastic Catenary Models are below the limits of measurability. Thus these two are "paper checks" which are valuable for some analyses but do not provide the required link to reality.

If, however, rather than using the results of the tether model directly, we use these results in the stability model, we find a completely different situation. The usable output from the stability model consists of a set of eigenvalues (frequencies and damping constants) and a set of modal (eigen) vectors relating to the amplitude and phase of the aerostat's motion in each mode.

Work is currently underway using spectral analysis techniques to validate the entire aerostat model against experimental data and will be reported later. However, it was decided that, based on the requirement of measurability, the results of the stability model would be used for analyzing the sensitivity of the Elastic Catenary Model to various techniques and parameter changes.

^{*} Once to compute (x_0, y_0, z_0) and one for each of the force variations.

6.1 Summary of Sensitivity Analysis Results*

- Regardless of the method used, a Runge-Kutta integration requires that the integration step size be generally not larger than 500 feet; e.g., 2 steps for a 1000 foot tether, 20 steps for a 10,000 foot tether. However, the use of less than two steps for tethers shorter than 1000 feet is not recommended.
- Using the position displacement method, the error criterion, P , must be on the order of 10^{-10} ft^2 . Smaller values for P provide no noticeable gain in accuracy. For most problems, $P=10^{-8}$ is equivalent to $P=10^{-10}$ since the sequence of E^2 is typically δ^2 , 10^{-5} , $10^{-11} (\text{ft}^2)$. Values of P as large as 10^{-6} ft^2 produce noticeable inaccuracies in some problems.
- Using either method, the averaging of symmetric displacements ($\pm \delta$) is necessary.
No observable differences are seen between the results obtained from the position displacement and force variation methods.
- Inclusion of lateral-longitudinal coupling constants; i.e., k_{xy} , k_{zy} , k_{yx} , and k_{yz} is not required. These spring constants are many (typically 6-8) orders of magnitude below the others.
- The assumption that the tether is a linear spring can be generalized to include nonlinear terms if sufficient data are available.

*Most of the sensitivity analysis, for convenience, was performed on the 2 - dimensional (i.e. x - z) model.

References

- S. Neumark (1961) "Equilibrium Configuration of Flying Cables of Captive Balloons and Cable Derivatives for Stability Calculations", Royal Aircraft Establishment (Farnborough) Report No. AERO. 2653
- L.T. Reed, S.R. Bland; and R.M. Bennett (1973) "Stability Analysis and Trend Study of a Balloon Tethered in a Wind, with Experimental Comparisons", NASA Technical Note NASA TND-7272

A COMPOUND AEROSTAT OF CONTROLLABLE ALTITUDE

R. M. Dunlap
Naval Underwater Systems Center
Newport, Rhode Island

Abstract

The concept is presented of a compound aerostat employing a primary lifting mixture of helium and methanol in one envelope and ammonia in a second envelope contained within the primary envelope. The methanol in the primary envelope gradually condenses as the altitude increases, yielding a decreasing lift with altitude up to the stratosphere to provide passive altitude stability to the system. An absorbent, metallic lithium is provided within a third container to controllably absorb the ammonia from the second envelope and thereby control the displacement of the secondary envelope. The process is reversible via the application of heat (e.g., propane combustion or solar heating). The use of other absorbents such as LiNO_3 , LiCl , and CaCl_2 is discussed. This controllable displacement system can compensate for solar super heat and snow and ice accumulation and facilitate long endurance flights, especially in the troposphere. The advantage of using ammonia rather than sand for ballast is also discussed.

1. INTRODUCTION

A previous method of maintaining a limp aerostat within the troposphere relies on the release of ballast by night and lifting gas by day. The altitude varies over a wide range. The flight endurance of this system is limited by the need to dump about 15 percent of the gas and ballast during each 24-hour period. An alternate method is to use a taut aerostat that seeks out an altitude where the atmospheric density equals that of the aerostat. This method requires strong fabric. Moreover, a pin-hole leak will result in considerable loss

of lift over a period of days and will result in flight termination. Ice accumulation can sink the aerostat even more rapidly. A mass-conservative, limp (not taut), constant-altitude aerostat system not having these deficiencies is described in this paper. The aerostat consists of two limp envelopes designated the primary and secondary envelopes. Figure 1 illustrates the system.

2. THE PRIMARY ENVELOPE

The primary envelope provides the principal source of lift and contains a mixture of about 90 percent helium and 10 percent methanol (CH_3OH). The helium is selected to provide the lift. The small amount of methanol, which is chosen because of its appropriate boiling point (64.7°C) and low formula weight (32.04) is just totally evaporated at sea level in the standard U. S. atmosphere. Its partial pressure in the mixture equals its saturation pressure at all times. As the altitude in the troposphere increases, the methanol gradually condenses out of the system onto the surface of the primary envelope causing the volume of air displaced to decrease; hence, a decrease in lift. Conversely, an altitude decrease causes the film or drops of methanol on the envelope to re-evaporate and increase the lift. Note from Figure 2, however, that above 9 km the methanol is destabilizing.

The saturation pressure for methanol (CH_3OH) as a function of temperature is given by the Antoine equation as quoted by Boublik, Fried, and Hala (1973):

$$\log_{10} P \text{ mmHg} = A - \frac{B}{t + C}, \quad (1)$$

where the constants $A = 9.2250$, $B = 2239$, and $C = 288.5$ are computed by fitting the Antoine equation to the data in Perry et al. (1963):

$t^\circ\text{C}$	$P \text{ mm}$
-6.0	20
2.1	60
34.8	200

$$(P\text{N/m}^2 = P \text{ mmHg} \times \rho_{\text{Hg}} g = 133.32 P \text{ mmHg})$$

The lift of this primary system is computed for 1 kg-mol of mixture in which the methanol is all vapor at a partial pressure equal to its saturation pressure at sea level; the balance of the mixture is helium.

Defining:

R = gas constant for air = $287.02 \text{ N-m/}^\circ\text{K} - \text{kg air}$,

g = acceleration of gravity = 9.807 m/sec^2 ,

γ = lapse rate of troposphere = $6.5^\circ\text{C km}^{-1}$,

L = lift,

X = mol fraction of methanol in gas mixture,

X_0 = mol fraction of methanol at sea level,

Z = mols of CH_3OH gas at altitude,

M = molecular weight, with subscripts as follows:

A = air	$M_A = 28.97,$
H = helium	$M_H = 4.00,$
C = condensible gas	$M_C = 32.04$ (methanol),

we may observe that the number of moles of helium at any altitude is $(1 - X_0)$ and

$$X = P_{\text{sat}}/P_{\text{atm}}, \quad (2)$$

where $P_{\text{atm}} = P_0 (T/T_0)^{g/R\gamma}$ according to Hess (1959), and

$$X = \frac{Z}{1 - X_0 + Z}, \quad (3)$$

so that

$$Z = (1 - X_0) (X^{-1} - 1)^{-1}. \quad (4)$$

The lift is then

$$L = (1 - X_0) (M_A - M_H) + Z M_A - X_0 M_C. \quad (5)$$

This standard atmosphere is plotted in Figure 4 together with the January and July atmospheres for 45°N (Valley, 1965). For the U. S. standard atmosphere, the lift L is computed for various altitudes and plotted in Figure 2 using the above equations, which are summarized below for convenience:

$$P_{\text{atm}} = 101325 [(t + 273.15)/288.15]^{5.2567} \text{ N/m}^2, \quad (6)$$

$$P_{\text{sat}} \text{ N/m}^2 = 133.32 \times 10^{(9.2250 - \frac{2239}{t + 288.5})}, \quad (7)$$

$$X = P_{\text{sat}}/P_{\text{atm}}, \quad X_0 = (P_{\text{sat}}/P_{\text{atm}}) \text{ sea level}, \quad (8)$$

$$L = (1 - X_0) [24.97 + 28.97(X^{-1} - 1)^{-1}] - 32.04X_0. \quad (9)$$

HAZARDS. It is estimated that this mixture of helium and methanol is not flammable. As shown in Figure 3, mixtures containing less than 70 percent methanol are not flammable with any proportion of air.

3. THE SECONDARY ENVELOPE

The secondary envelope, which is preferably contained within the primary envelope to reduce aerodynamic drag and handling problems during buffeting winds, contains a condensible lifting gas, anhydrous ammonia. The vapor pressure of ammonia as a function of temperature is given by Antoine's equation, as given by Boublik, Fried, and Hala (1973):

$$\log_{10} P \text{ mmHg} = A - \frac{B}{t + C}, \quad (10)$$

where $A = 7.4404$, $B = 954.19$, and $C = 242.63$. These constants are computed by fitting the equation to the following data in Perry et al. (1963):

$t^{\circ}\text{C}$	P mm
-77	47.8
-47	365.5
-20	1427.0

The formula weight of ammonia is 17.03; its boiling point at 760 mm is -33.35°C . Saturated ammonia pressures for various altitudes of the U. S. standard atmosphere are plotted in Figure 4.

HAZARDS: Ammonia is toxic but gives ample olfactory warning of its presence. Its flammability limits with air are from 16 to 26 percent NH_3 . It is difficult to ignite.

Ammonia is chosen for the secondary envelope because of its low molecular weight and its ability to be absorbed in large amounts by a variety of materials including water, calcium chloride, lithium chloride and nitrate, and pure lithium. Ammonia is a vapor under almost all conditions in the earth's atmosphere; the absorbents listed below when saturated and in temperature equilibrium with the atmosphere have vapor pressures less than ambient atmospheric pressure under virtually all natural conditions. The solution or combination of ammonia with these materials is accompanied by a release of heat. Conversely, the application of heat (from a propane burner, for example) will dissociate the ammonia from the material. Thus, the operation is easily reversible with simple apparatus and changes in displacement, hence, lift is easily accomplished. Below are listed the materials in order of their ability to absorb NH_3 :

<u>Material</u>	<u>Reference</u>	<u>Mass Per Unit Mass of NH_3</u>	<u>$t^{\circ}\text{C}$ ($P = 100$ mm)</u>
Lithium	Marshall and Hunt (1956); Johnson and Piskur (1933)	0.1132	+20.5
$\text{LiCl} \cdot 5\text{NH}_3$	Bonnefoi (1901); Biltz (1923)	0.4978	-49
$\text{CaCl}_2 \cdot 8\text{NH}_3$	Hüttig (1922); Linge (1929)	0.8147	-2
$\text{LiCl} \cdot 3\text{NH}_3$	Bonnefoi (1901); Biltz (1923)	0.8297	+23.5
$\text{LiNO}_3 \cdot 4\text{NH}_3$	Chinnapa (1961); Buffington (1931); Berestneff (1938)	1.012	---

Lithium is by far the best of these materials, absorbing about 9 grams of ammonia per gram of lithium with a sub-atmospheric vapor pressure in virtually all atmospheres. The solution formed is not a compound according to Kraus (1931) and Johnson and Piskur (1933). Garroway and Cotts (1973), however, show lithium to be solvated by four ammonia molecules. Most systems were used or proposed for refrigeration systems before the advent of reliable compressors, electric motors, and the fluorinated halocarbon refrigerants.

The important data for lithium-ammonia solutions are given below:

<u>t°C</u>	<u>P cmHg</u> (Marshall and Hunt, 1956)	<u>g Li/g NH₃ = B</u> (Johnson and Piskur, 1933)
-63.8	0.005	--
-63.5	--	0.10698
-45.4	0.055	--
-33.2	--	0.10866
-32.7	--	0.10895
-22.9	0.760	--
0.0	3.285	0.11319
21.3	10.390	--
40	25.1	--

(Conversion factor: $P \text{ N/m}^2 = 1333.2 P \text{ cmHg}$)

If we fit the equation

$$\log_{10} P \text{ cmHg} = A - \frac{B}{T} \quad (11)$$

to the two data points at 0 and 21.3°, we get

$$\log_{10} P_2/P_1 = -B\left(\frac{1}{T_2} - \frac{1}{T_1}\right), \quad (12)$$

and

$$B = -\log P_2/P_1 / \left(\frac{1}{T_2} - \frac{1}{T_1}\right) = 1888.3, \quad (13)$$

and

$$A = \log_{10} P_2 + \frac{B}{T_2} = 7.4296. \quad (14)$$

From the simplified Clausius-Clapeyron equation (which neglects the volume of the liquid solution and assumes NH₃ to be a perfect gas)

$$\Delta H \approx \frac{RT^2}{P} \frac{\Delta P}{\Delta T}, \quad (15)$$

we may compute in the vicinity of 0°C

<u>t°C</u>	<u>T°K</u>	<u>P cmHg</u>
-5	268.15	2.4414
0	273.15	3.2851
+5	278.15	4.3734

so that

$$H = \frac{8314}{17.03} \frac{\text{N-m}}{\text{kg NH}_3 \cdot ^\circ\text{K}} \frac{273.15^2}{10} \frac{(4.3734 - 2.4414)}{3.2851}$$

$$= 2.142 \times 10^6 \frac{\text{N-m}}{\text{kg} - \text{NH}_3},$$

since 1 kcal = 4190 J (1J = 1 N-m). $H = 511.2 \text{ kcal/kg NH}_3$. This is in agreement with Kraus (1908).

The quantity of propane (heat of combustion of 1 g mol = 530.7 kcal; MW $\text{C}_3\text{H}_8 = 44.11$; B. P. = -42.07°C) required to drive 1 kg of NH_3 from a lithium solution is

$$F = \frac{511.2 \text{ kcal}}{\frac{\text{kg NH}_3 \text{ gas } 530.7 \text{ kcal} \times 1000}{44.11 \text{ kg} - \text{C}_3\text{H}_8}} \quad (17)$$

$$= 0.0425 \text{ g C}_3\text{H}_8/\text{g NH}_3 \text{ gas.}$$

To avoid irreversible formation of lithium amide and hydrogen, care must be exercised to ensure that the solution is dry, clean, and especially free of heavy metals, including iron, and that it is not subjected to temperatures above 50°C to 60°C .

5. SYSTEM PROPORTIONS AND NET SYSTEM LIFT

For 1 mol of primary mixture consisting of helium and methanol, we need sufficient lift variation to accommodate the extra lift of solar superheat at one extreme and the extra weight of ice and snow at the other extreme.

Let us define:

Y = total number of mols of NH_3 ,

B = mass of Li required to absorb unit mass of $\text{NH}_3 = 0.1132$ (forms Li/NH_3 solution at 0°C),

S = superheat, $^\circ\text{C}$ above T ,

T = atmospheric temperature $^\circ\text{K}$,

M_A = MW air = 28.97,

M_M = MW mixture = 6.5985,

M_C = MW NH_3 = 17.03,

W = mass of ice,

P = payload,

X_0 = mols of methanol at sea level (all vapor) = 0.092666.

Observe that at altitude h we have $1 - X_0$ mols of helium and X mols of methanol gas. With solar superheat and no ice and no ammonia gas, the equation for lift equilibrium is

$$(1 - X_0 + X) \left(1 + \frac{S}{T}\right) M_A - M_M - Y M_C (1 + B) - P = 0. \quad (18)$$

With no solar superheat and with ice or snow present and all ammonia as gas, the equation for lift equilibrium becomes

$$(1 - X_o + X + Y) M_A - M_M - Y(1 + B) M_C - P - W = 0. \quad (19)$$

Subtraction and transposition yields

$$Y = \frac{W}{M_A} + (1 - X_o + X) \frac{S}{T}, \quad (20)$$

and

$$P = (1 - X_o + X) \left(1 + \frac{S}{T}\right) M_A - M_M - Y M_C (1 + B), \quad (21)$$

for $h = 2$ km, $T = 275.154^\circ\text{K}$, and if $S/T = 0.08$, $S = 22.01^\circ\text{C}$. If $W/M_A = 0.12$, then $W = 3.4764$ and $Y = 0.2$. At $h = 2$ km, $X = 0.055237$ and $P = 19.73$ kg/kg-mol of primary mixture. For a flight of n days, the total fuel requirement is $E = n F Y M_C = 0.145 n$. For $n = 10$ days, $E = 1.45$ units of mass.

6. ALTERNATE SYSTEMS

A single envelope filled with ammonia as the lifting gas together with the lithium absorbent to control displacement is inexpensive but will produce much less lift.

A single envelope containing helium and ammonia together with a lithium absorber will give more lift, but it is questionable that the partial pressure of ammonia will be sufficient to permit its absorption by lithium without gas compression. Moreover, the presence of helium will slow down the solution. On the other hand, the low partial pressure of ammonia in the envelope will promote the dissociation process.

A single envelope of ammonia and methanol (no lithium absorber) will provide a stable altitude system similar to the helium and methanol system. Since the components are condensed to a liquid at shallow sea water depths and since the liquid is less dense than water, we have a system which may be submarine launched, then float to the sea surface and rise to a stable altitude.

The system described in this paper probably can be controlled adequately without the methanol in the helium. This would result in a higher-lift, less-complicated system.

The lift of the helium system (with or without methanol) may be safely increased by the addition of up to 15 percent hydrogen based on extrapolation of the work of Zabetakis (1956) on hydrogen-steam-air flammability limits. (Zabetakis' diagram is reproduced herein as Figure 5.)

We might also consider here the use of ammonia rather than sand as ballast. If we carry sand as ballast we get 1 kg of lift by dropping 1 kg of sand. However, if we carry 1 kg of ammonia, we get

$$\frac{M_A}{M_C} = \frac{28.97}{17.03} = 1.701 \text{ kg} \quad (22)$$

of lift if we evaporate the ammonia and collect it in the lifting envelope. Obviously, ammonia is 70.1 percent better than sand as ballast. The ammonia could be carried in a Dewar flask or light steel tank.

7. FLIGHT DURATION

The flight duration in days may be computed by the following equation

$$(1 + ax)^n = 1 + y, \quad (23)$$

where

a = weight of ammonia yielding unit lift = 0.5878 for NH_3 (1/1.701), (1.00 for sand),

x = fractional daily lift change = 0.15 depending on extent of sunshine and rain, etc.,

y = initial ballast load carried for unit payload,

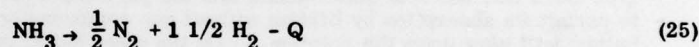
n = number of days of flight.

For example, using sand and $n = 5$ days, $y = 1.0114$; that is, the payload and ballast load are nearly equal. With this same value of y , but using ammonia as ballast

$$n = \ln(1 + y)/\ln(1 + ax) = 8.27 \text{ days}, \quad (24)$$

which is an increase of over 3 days in flight time. This shows the value of using ammonia as ballast. It makes especially good sense with this system to have a reserve of NH_3 on board.

As further aid in reducing ballast requirements, ammonia may be broken into its components with the addition of heat and in the presence of a catalyst at 500°C as shown by Hinshelwood (1925):



This reaction yields an "a" factor as defined above of

$$17.03/(1/2 + 1 \frac{1}{2}) 28.97 = 0.2939, \quad (26)$$

and a flight duration of $n = 16.20$ days. The hydrogen generated will introduce hazards, but the hydrogen will be diluted with the helium. Referring again to the Zabetakis flammability diagram, we can infer that the flammability limits with air will be very limited. The quantity of propane for effecting the decomposition is relatively minor.

8. SUMMARY OF PERFORMANCE OF SYSTEM SHOWN IN FIGURE 1

Primary lifting aerostat, 1 kg-mol mixture: 0.90733 mol helium (He), 0.09267 mol methanol (CH_3OH). Lift decreases with altitude due to gradual condensation of methanol as shown in Figure 2.

Secondary lifting aerostat: 0.2 mol ammonia (NH_3).

Ammonia absorbing system: 0.0556 atomic weights of lithium to form Li-NH_3 solution.

Propane fuel to provide heat for dissociation depending on flight duration.

Ballast: 0.5879 kg NH_3 — when evaporated displaces 1 kg air.

Payload: 19.73 kg/kg-mol of primary mixture.

Superheat accommodated: 22°C .

Ice and snow accommodated: 3.47 kg.

8. SUMMARY

A concept for an aerostat has been described that promises long endurance flight in both the troposphere and stratosphere under adverse conditions of solar superheating and ice and snow accumulation. It may be applied to meteorological survey, ocean surveillance, stratospheric communication relays, and sporting activity. Manned transatlantic and circumpolar flights in the troposphere appear probable with this system. The concepts described herein may permit exploration of the atmospheres of other planets.

The methanol condensation and the NH_3/Li solution processes described in this paper should be confirmed by testing. Also, the rate of absorption should be determined, as well as means of accelerating the absorption rate, if necessary.

REFERENCES

- Berestneff, A. A. (1938), Refrig. Eng., 35 (No. 5): 323.
- Biltz, W., and Hansen, W. (1923), Z. Anorg. Allg. Chem., 127:4.
- Bonnefoi, J. (1901), Ann. Chim. Phys., Series 7, 23:317.
- Boublik, T., Fried, V., and Hala, E. (1973), The Vapour Pressures of Pure Substances, Elsevier Scientific Publishing Co., Amsterdam.
- Buffington, R. M. (1931), U. S. Patent 1,792,628.
- Chinnappa, J. C. V. (1961), Solar Energy, 5 (No. 1): 1-18.
- Dunlap, R. M. (1977), NUSC TM 77-2181, Naval Underwater Systems Center, Newport, R. I.
- Fredholm, H. (1930), British Patent 358,844.
- Garroway, A. N., and Cotts, R. M. (1973), Physical Review A, 7 (No. 2): 635.
- Hess, S. L. (1959), Introduction to Theoretical Meteorology, Holt, Rhinehart, and Winston, New York, p. 83.
- Hinshelwood, C. N., and Burk, R. E. (1925), J. Chem. Soc. (Lond.), 127: 1105.
- Hüttig, G. F. (1922), Z. Anorg. Chem., 123: 31.
- Jander, J. H. G. (1966), Anorganischen und Allgemeine Chemie in Flüssigen Ammoniac, Vieweg und Sohn, Braunschweig, FRG/Wiley-Interscience, New York.
- Johnson, W. C., and Piskur, M. M. (1933), J. Phys. Chem., 37: 93.
- Jones, G. W. (1938), Chemical Reviews, 22: 1.
- Kraus, C. A. (1908), J. Am. Chem. Soc., 30: 653 and 1323.
- Kraus, C. A. (1931), J. Franklin Institute, 212: 537.

- Lepoutre, G., and Sienko, M. J., Eds. (1964), Solutions Metal-Ammoniac, Colloque Weyl, Lille, France, W.A. Benjamin, New York.
- Linge, K. (1929), Z. Ges. Kälte-Ind. Beihefte, Series 2 (No. 1): 1-69.
- Marshall, P. R., and Hunt, H. J. (1956), J. Phys. Chem., 60: 732.
- Mellor, J. W. (1922), A Comprehensive Treatise on Inorganic and Theoretical Chemistry, Vol. III, Longmans/Green, London-New York, p. 716.
- Perry, P. H., Chilton, C. H., and Kirkpatrick, S. D, Eds. (1963), Chemical Engineers Handbook, 4th Edition, McGraw-Hill, New York.
- Plank, R., and Heiss, R. (1938), Landwirtschaftliche Jahrbucher, Berlin, 85: 627-750.
- Ruff, O., and Geisel, E. (1906), Ber. Deutsche Chem. Gesell., 39: 828.
- Sidgewick, N. V. (1950), The Chemical Elements and Their Compounds, Vol. I, Oxford Press.
- Smith, H. F. (1931), U. S. Patent 1,791,515.
- Valley, S., Ed. (1965), Handbook of Geophysics and Space Environments, A. F. Cambridge Research Laboratory.
- Zabetakis, M. G. (1956), Research on the Combustion and Explosion Hazards of Hydrogen-Water Vapor-Air Mixtures, Final Report, Bureau of Mines, Division of Explosive Technology, Pittsburgh, Pa.; AECU-3327(3), Atomic Energy Commission, Technical Information Service Extension, Oak Ridge, Tenn.

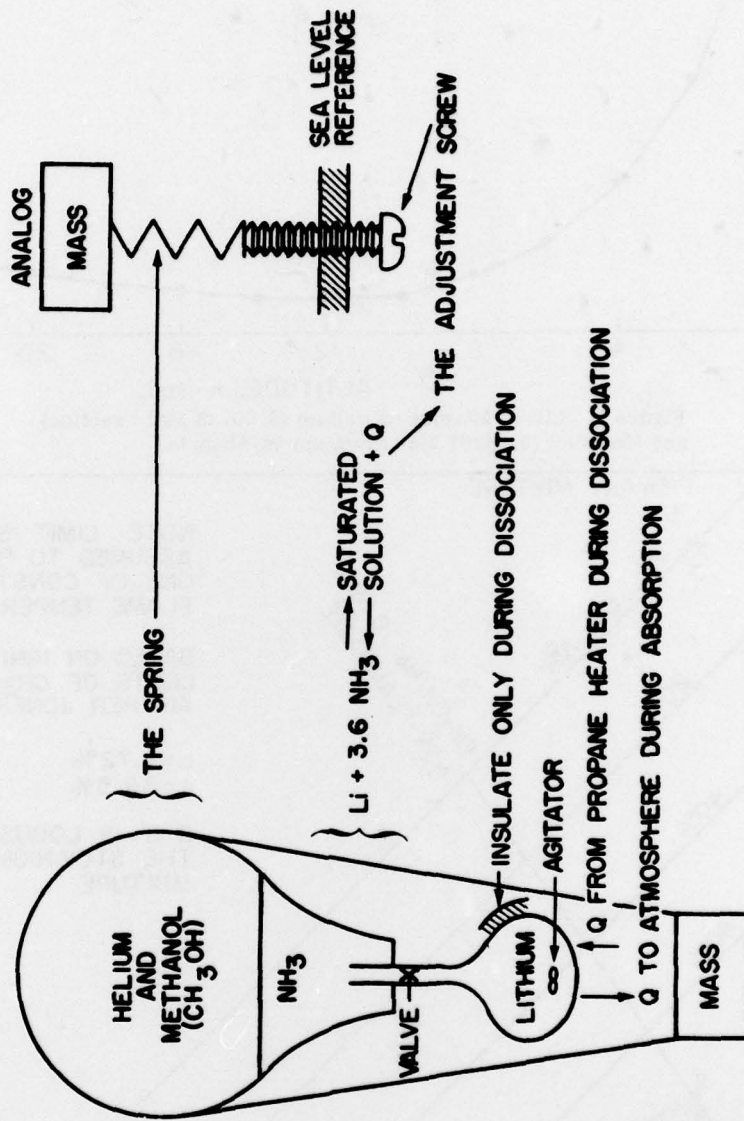


Figure 1. Controllable Altitude Aerostat

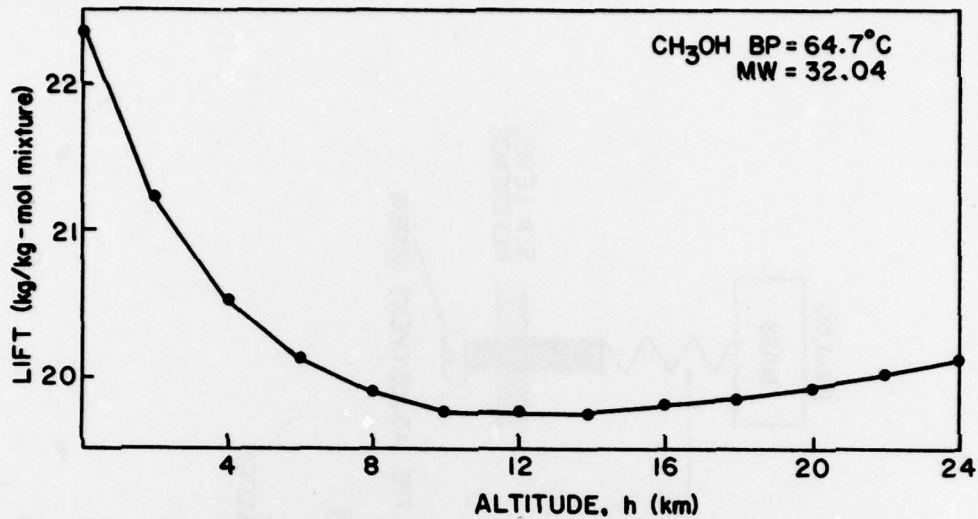


Figure 2. Lift of Mixture of Helium (0.90733 Mol Fraction) and Methanol (0.09267 Mol Fraction) vs Altitude

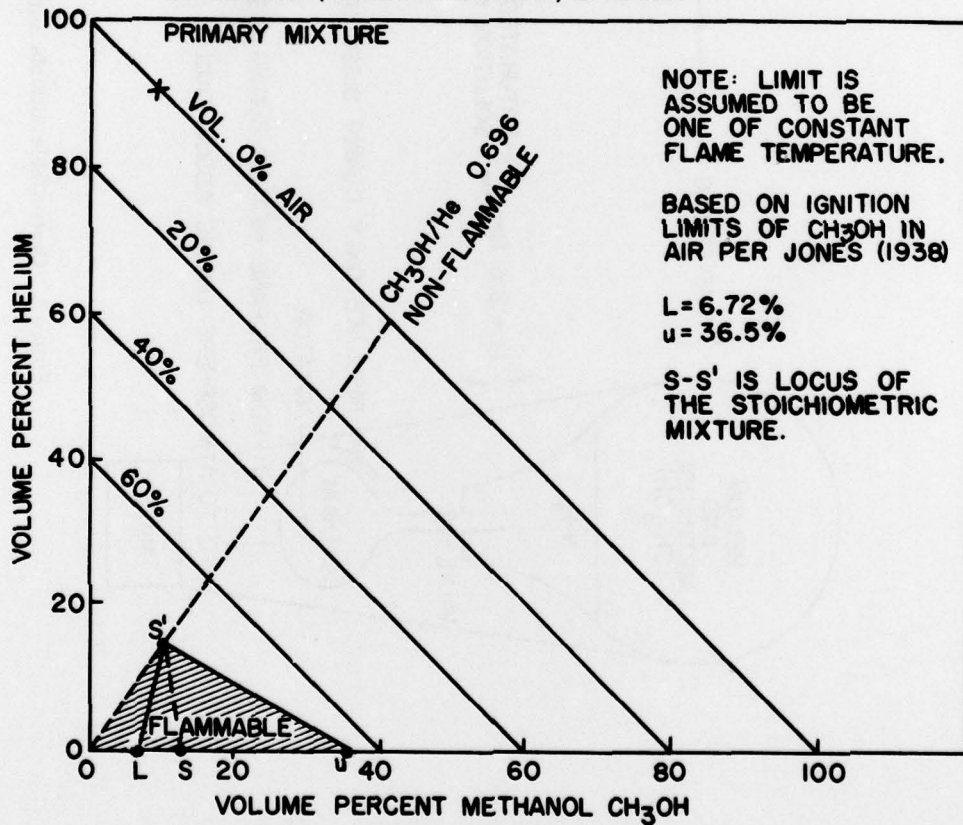


Figure 3. Computed Flammability Limits for Mixture of Methanol, Air, and Helium

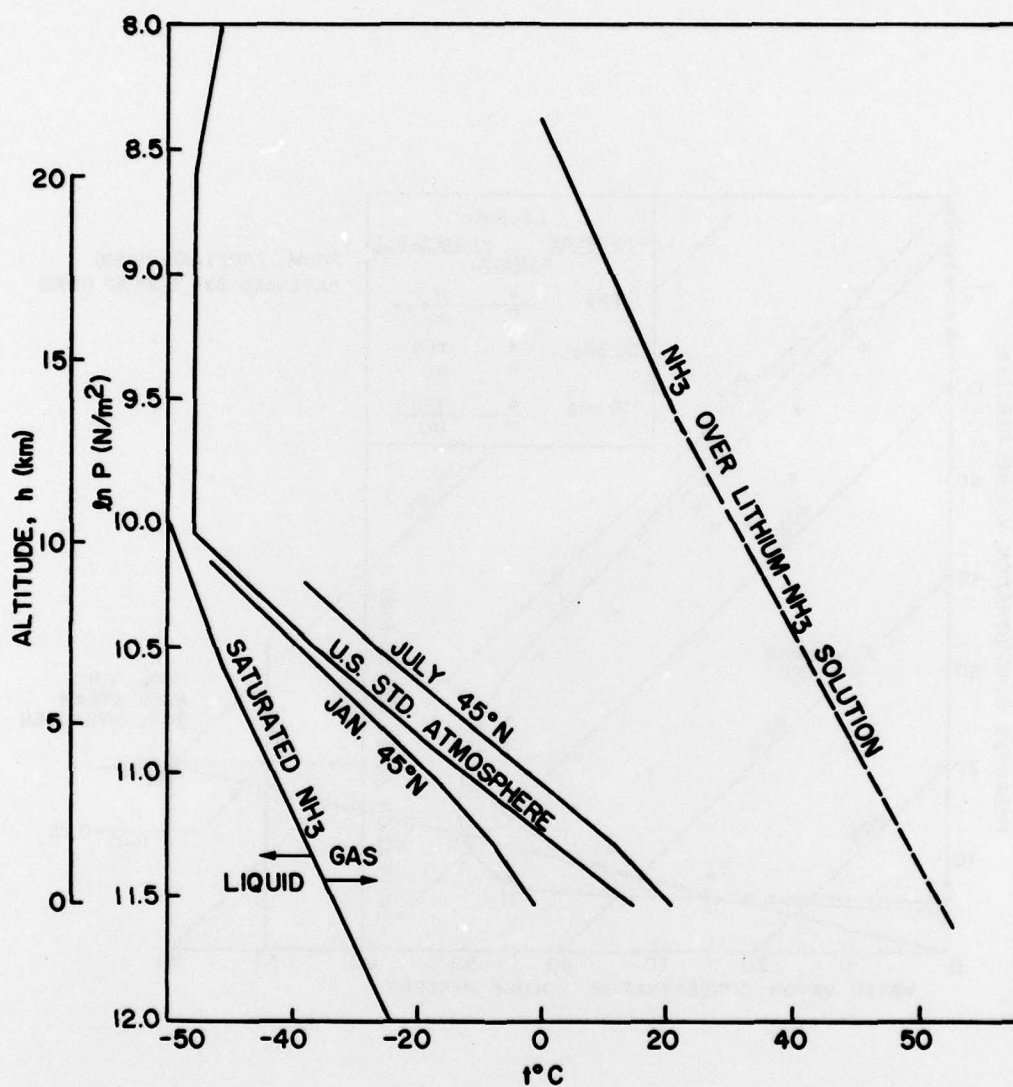


Figure 4. Pressure-Temperature Relationships for Saturated NH_3 and NH_3 Over Lithium Solution from Pure Metal to Approximately 4 Mols of NH_3 Per Atom of Lithium

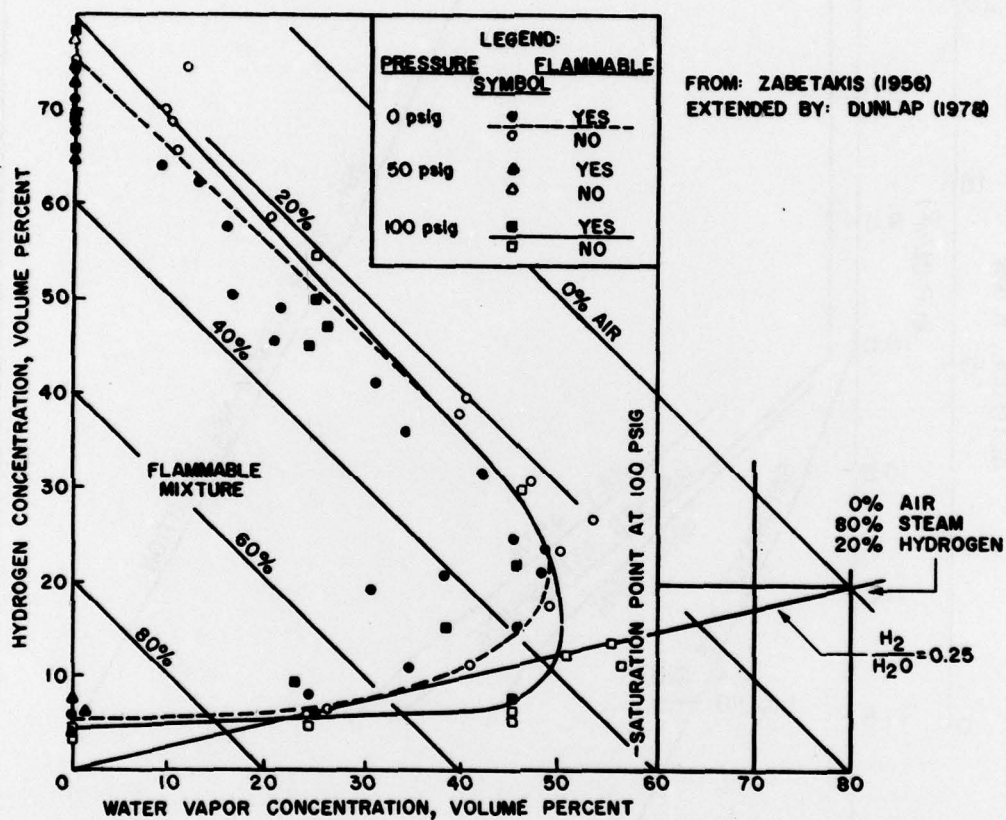


Figure 5. Limit-of-Flammability Test Data on Hydrogen-Water Vapor-Air Mixtures at $\sim 300^\circ\text{F}$

LIST OF REGISTRANTS

Lt Colonel T. Andrada
AFGL/OP
Hanscom AFB, MA 01731

Harold N. Ballard
Atmospheric Sciences Laboratory
White Sands Missile Range, NM 88002

G. O. Berringer
National Research Council of Canada
Ottawa, Ontario, Canada K1A 0R6

Wilson T. Botner
Sandia Laboratories
P. O. Box 5800
Albuquerque, NM 87115

Keith Browne
Loos & Co., CASTLOK Division
Pomfret, CT 06258

Leland A. Carlson
Texas A&M University
College Station, TX 77801

Andrew S. Carten, Jr.
AFGL/LCB
Hanscom AFB, MA 01731

T. S. Church
Sandia Laboratories
Division 9487
Albuquerque, NM 87185

Robert H. Cordella, Jr.
Air Resources Laboratories (R32)
8060 13th St.
Silver Spring, MD 20910

Rene V. Cormier
AFGL/XOP
Hanscom AFB, MA 01731

John Cramer
Boeing Aircraft
Box 344/Roof 2
Vashon, WA 98070

C. L. Croskey
Pennsylvania State University
Ionosphere Research Laboratory
University Park, PA 16802

William F. Cross
Office of Naval Research
Federal Bldg, Fort Snelling
Twin Cities, MN 55111

William F. Cuddihy
NASA Langley Research Center
Hampton, VA 23665

Colonel Chester G. R. Czepyha
AFGL/CV
Hanscom AFB, MA 01731

William S. Dalton
University of Massachusetts
Astronomy Research Facility
Amherst, MA 01003

Thomas J. Danaher
AFGL/LCA
Hanscom AFB, MA 01731

Frank K. Dearborn
AFGL/OPA
Hanscom AFB, MA 01731

D. Dechter
State of Israel
Ministry of Defence
Electronic-Development Division
P. O. Box 10248
Tel Aviv, Israel

James DeLaurier
Institute for Aerospace Studies
4925 Dufferin St.
Downsview, Ontario, Canada M3H 5T6

Louis J. Del Do
LTA International, Inc.
Valkaria Airport
Palm Bay, FL 32905

Harold Dewhirst
Naval Air Development Center
Warminster, PA 18974

Francis X. Doherty
AFGL/LC
Hanscom AFB, MA 01731

N. A. Dresner
TCOM Corporation
Ridgely Building
5575 Sterrett Place
Columbia, MD 21044

Richard M. Dunlap
U.S.N. Underwater Systems Center
Newport, RI 02840

George P. Durney
ILC-Dover
P. O. Box 266
Frederica, DE 19946

James F. Dwyer
AFGL/LCB
Hanscom AFB, MA 01731

L. Early
NASA Wallops Flight Center
Wallops Island, VA 23337

Robert Enderson
Raven Industries, Inc.
P. O. Box 1007
Sioux Falls, SD 57101

J. Craig Erickson
Physical Science Laboratory (PSL)
Box-3PSL
Las Cruces, NM 88003

Richard A. Formato
GTE Sylvania, Inc.
Electronic Systems Group
Communication Systems Division
189 "B" St.
Needham, MA 02194

Malcolm M. Fowler
Los Alamos Scientific Laboratory
P. O. Box 1663, CNC-11 MS 514
Los Alamos, NM 87545

Charles C. Gallagher
AFGL/LKD
Hanscom AFB, MA 01731

Walter A. Gallie
AFSC/DLS
Andrews AFB, DC 20334

Captain Gerald J. Geeser
AFGL/LCC
Hanscom AFB, MA 01731

Arthur A. Giannetti
AFGL/LCC
Hanscom AFB, MA 01731

Frank W. Gibson
AFGL/OPA
Hanscom AFB, MA 01731

CMSgt Harold W. Greenlee
AFGL/LCA
Hanscom AFB, MA 01731

Thomas J. Gross
Department of Energy
Environmental Programs/ Division of
Biomedical & Environmental Research
Washington, DC 20545

John R. Ground
New Mexico State University (PSL)
Box 3548
Las Cruces, NM 88003

Barry Handlin
Otis Engineering Corporation
1000 W. Crosby Road
Dallas, TX 75006

Zenon Hansen
Airship International Press
P. O. Box 1543
Bloomington, IL 61701

Jared F. Haren
ABAC-LTAS
807 S. James Road
Columbus, OH 43227

Jean C. Hartshorne
P. O. Box 319
3 Chestnut St.
Wakefield, MA 01880

Keith Hazlewood
Winzen Research Inc.
Fleming Field
South St. Paul, MN 55075

Ralph Hookway
Martin-Marietta Corporation
P. O. Box 179
Denver, CO 80201

John N. Howard
AFGL/CA
Hanscom AFB, MA 01731

Alvin H. Howell
Tufts University
Dept. of Elec. Eng'g.
Medford, MA 02155

2Lt Frank V. Hunsinger
AFGL/LCB
Hanscom AFB, MA 01731

A. F. Hutters
Sandia Laboratories/Div. 9487
Albuquerque, NM 87185

R. Ilgner
TCOM Corporation
Ridgely Building
5575 Sterrett Place
Columbia, MD 21044

Miguel Izquierdo
University of Texas at El Paso
El Paso, TX 79968

Lelan R. Jamison
Sheldahl, Inc.
North Highway 3
Northfield, MN 55057

Sam P. Jones
TCOM Corporation
Ridgely Building
5575 Sterrett Place
Columbia, MD 21044

Thomas W. Kelly
AFGL/LC
Hanscom AFB, MA 01731

Arthur O. Korn
AFGL/LCB
Hanscom AFB, MA 01731

Louis M. Kovach
Louis Airship Company
P. O. Box 25
Worthington, OH 43085

William C. Lane
Otis Engineering Corporation
1000 W. Crosby Road
Dallas, TX 75006

Jarvis C. Lehmann
National Scientific Balloon Facility
P. O. Box 1175
Palestine, TX 75801

Kenneth H. Lindenfelser
8 Park Avenue
Kearny, NJ 07032

Tangredo J. Maltacea
AFGL/SUO
Hanscom AFB, MA 01731

M. Mani
State of Israel
Ministry of Defence
Electronic-Development Division
P. O. Box 10248
Tel Aviv, Israel

Dennis L. Mann
Vitro Laboratories
14000 Georgia Avenue
Silver Spring, MD 20910

Hans Mark
Under Secretary of the Air Force
Washington, DC 20330

Tim Markhardt
Raven Industries Inc.
P. O. Box 1007
Sioux Falls, SD 57101

Walter F. Martin
Office of Naval Research/Code 465
800 N. Quincy St.
Arlington, VA 22217

Norman J. Mayer
Hq NASA/RWS-3
600 Independence S.W.
Washington, DC 20546

Carlos McDonald
University of Texas at El Paso
Elec. Engr. Department
El Paso, TX 79968

Frank G. McGuire
Editor, "Advanced Lighter-Than-Air Review"
Kimberly Communications Corporation
1067 National Press Building
Washington, DC 20045

John A. C. Morley
Loos & Co., CASTLOK Division
Pomfret, CT 06258

Walter Nagel
NASA Goddard Space Flight Center/Code 745.2
Greenbelt, MD 20771

H. Needleman
NASA Wallops Flight Center
Wallops Island, VA 23337

Robert Nock
NASA Wallops Flight Center
Wallops Island, VA 23337

George F. Nolan
AFGL/LCA
Hanscom AFB, MA 01731

Julian Nott
11 Campden House Close
London W8 7NU, England

James C. Payne
AFGL/LCB
Hanscom AFB, MA 01731

Norman C. Poirier
Northeastern University
360 Huntington Ave.
Boston, MA 02115

G. Duane Powers
Naval Weapons Center/Code 393
China Lake, CA 93555

James L. Rand
Texas A&M University
Dept. of Aerospace Engr.
College Station, TX 77843

Charles H. Reynolds
Bureau of Indian Affairs/Quarters#1092
Many Farms, R. Br. Chinle, AZ 86503

Catherine L. Rice
AFGL/LC
Hanscom AFB, MA 01731

J. S. Rochefort
Northeastern University
360 Huntington Ave.
Boston, MA 02115

Sidney Rosenthal
AFGL/SUM
Hanscom AFB, MA 01731

Michel Rougeron
CNES-Centre Spatial de Toulouse
18 Avenue Edouard Belin
Toulouse, France

Walter Salyer
ILC Dover
1050 Bay Area
Houston, TX 77058

E. Scala
Cortland Advanced Products
Cortland Line Company
P. O. Box 1362
Cortland, NY 13045

E. E. Sheppard
USAF Det 1 SAMTEC/TOETP
Technology Division
Patrick AFB, FL 32925

Rodney Simons
AIL Division of Cutler Hammer
Comac Road
Deer Park, NY 11729

Charles F. Sindt
National Bureau of Standards
Thermophysical Properties Division
Boulder, CO 80302

Dave Smith
Airship International Press
P. O. Box 1543
Bloomington, IL 61701

Dean Smith
Boeing Aircraft
Roofe 2, Box 344
Vashon, WA 98070

I. Steve Smith, Jr.
National Center for Atmospheric Research
National Scientific Balloon Facility
P. O. Box 1175
Palestine, TX 75801

Paul D. Stang
Sandia Laboratories
Division 9487
Albuquerque, NM 87185

Kurt R. Stehling
National Oceanic & Atmospheric Administration
Manned Undersea Science & Technology Office
Rockville, MD 20852

Edwin F. Strother
Florida Institute of Technology
Physics/Space Science Department
Melbourne, FL 32901

Donald A. Sumner
Winzen Research Inc.
Fleming Field
South Saint Paul, MN 55075

Charles D. Tangren
Southeastern Forest Experiment Station
Southern Forest Fire Laboratory
P. O. Box 5106
Macon, GA 31208

Fred Tausch, Jr.
P. O. Box 386
Lexington, MA 02173

Kenneth Tekrony
Raven Industries Inc.
P. O. Box 1007
Sioux Falls, SD 57101

Clayton L. Thomas
Balloon School of Mass., Inc.
Balloon Port at Dingley Dell
RFD #1
Palmer, MA 01069

Paul E. Tychsen, Jr.
Balloon Services Co.
19049 8th Ave., N.W.
Seattle, WA 98177

Hepburn Walker, Jr.
Rt. 2, Box 4-B
Vero Beach, FL 32960

D. R. Williams
Winzen Research Inc.
Fleming Field
South Saint Paul, MN 55075

James A. Winker
Raven Industries, Inc.
Box 1007
Sioux Falls, SD 57101

Donald E. Woodward
Assoc. of Balloon & Airship
Constructors
922 S. Patrick St.
Alexandria, VA 22314

Clifford H. Zierdt
General Electric (RESO)
3198 Chestnut St.
Philadelphia, PA 19101